

# Heterogeneous Catalytic Materials

Solid State Chemistry,  
Surface Chemistry and  
Catalytic Behaviour

**Guido Busca**



**ELSEVIER**

AMSTERDAM • BOSTON • HEIDELBERG • LONDON • NEW YORK • OXFORD  
PARIS • SAN DIEGO • SAN FRANCISCO • SINGAPORE • SYDNEY • TOKYO

Elsevier  
Radarweg 29, PO Box 211, 1000 AE Amsterdam, The Netherlands  
The Boulevard, Langford Lane, Kidlington, Oxford OX5 1GB, UK

First edition 2014

Copyright © 2014 Elsevier B.V. All rights reserved.

No part of this publication may be reproduced, stored in a retrieval system or transmitted in any form or by any means electronic, mechanical, photocopying, recording or otherwise without the prior written permission of the publisher.

Permissions may be sought directly from Elsevier's Science & Technology Rights Department in Oxford, UK: phone (+44) (0) 1865 843830; fax (+44) (0) 1865 853333; email: [permissions@elsevier.com](mailto:permissions@elsevier.com). Alternatively you can submit your request online by visiting the Elsevier web site at <http://elsevier.com/locate/permissions>, and selecting Obtaining permission to use Elsevier material.

#### **Notice**

No responsibility is assumed by the publisher for any injury and/or damage to persons or property as a matter of products liability, negligence or otherwise, or from any use or operation of any methods, products, instructions or ideas contained in the material herein. Because of rapid advances in the medical sciences, in particular, independent verification of diagnoses and drug dosages should be made

#### **British Library Cataloguing in Publication Data**

A catalogue record for this book is available from the British Library

#### **Library of Congress Cataloging-in-Publication Data**

A catalog record for this book is available from the Library of Congress

For information on all Elsevier publications visit our  
web site at [store.elsevier.com](http://store.elsevier.com)

Printed and bound in Poland

14 15 16 17 18 10 9 8 7 6 5 4 3 2 1

ISBN: 978-0-444-59524-9

		<p>Working together to grow libraries in developing countries</p>
<p><a href="http://www.elsevier.com">www.elsevier.com</a> • <a href="http://www.bookaid.org">www.bookaid.org</a></p>		

# Heterogeneous Catalysts

# 1

## CHAPTER OUTLINE

<b>1.1 Introduction</b> .....	1
1.1.1 On the merits of industrial chemistry as a production activity .....	1
1.1.2 Catalysis and its role in industrial chemistry .....	2
1.1.3 Why solid catalysts? .....	3
1.1.4 Industrial catalytic materials .....	5
<b>References</b> .....	7

## 1.1 Introduction

### 1.1.1 On the merits of industrial chemistry as a production activity

At the beginning of the third millennium, few disciplines such as industrial chemistry are in a difficult situation and, together, transformation with exciting prospects. Public opinion attributes to chemistry, and not without a few good reasons, the environmental degradation, with its harmful consequences.

However, the merits of chemistry as an industrial activity are actually largely unknown to people and neglected by experts that would know them. In fact, industrial chemistry is a service activity, allowing in particular the production of materials and molecules that are strictly needed by other activities to obtain their goals.

It is well evident, for example, that the exponential growth and improving of information and telecommunication technologies are largely dependent from the development of suitable materials made available by the product and process developments of industrial chemistry. It is sufficient to think about the number of chemical components (constituting conducting electrodes, insulating components, dyes, polymers) involved in the i-phone touch screens, and to understand how chemistry and industrial chemistry contributed to the development of electronic technologies.

By analogy, we can say that, without the past development of industrial chemistry and processes, the cars, aircraft, household electrical appliances and equipments, etc., of today would not be available.

Similarly, part of the development of medicine is due to the development, at the research level, of new active drug molecules as well as, at the industrial level, of efficient synthesis processes, allowing them to be obtained at moderate costs. Medicine

also takes advantage of instrumentations in part, based on chemical analytical techniques, as well as of materials and chemicals that become unique. An example is polyvinyl chloride, which is the main component of hospital wastes, proving its very large application in the medical equipment. Another example is that of sodium hypochlorite, which is universally considered today as a unique disinfecting agent. Both these chemical species have been the object of criticism due to safety and environmental concerns in their preparation and end-of-life destiny. However, both of them proved to have unique and irreplaceable behavior, while safety and environmental concerns have been addressed and largely (if not completely) resolved technologically.

Another important and disputed example is that of crop protection technology, which includes the developments of processes allowing the large scale production of pesticides, herbicides, insecticides, fungicides, etc. These chemical products help control the thousands of weed species, harmful insects and numerous plant diseases that afflict crops. The development of these molecules and of the processes for their production allowed millions of people to be fed and a number of lethal illnesses to be reset.

Chemical activities are usually considered to be responsible for environmental degradation. This is largely true, but it is quite evident that this is right as a result of the initial development of chemical technologies at their childhood level, mixed with (at times) a still poor knowledge of several natural phenomena and of some chemical phenomena too. A better knowledge of environmental chemistry and biochemistry reached in more recent years allowed to actually resolve most of environmental issues of chemical production technologies. Today, and sometimes also earlier, environmental problems arise from the lack of application of technologies that have been developed just to reduce and sometimes neutralize any environmental concern. On the other hand, it is evident that chemistry and industrial chemistry are leading actors in the environment remediation too.

In spite of the evident concerns associated with the environment degradation, it is without any doubt that industrial chemistry has been a major leading actor in the exponential technological development that occurred in the last 150 years, allowing a very high level of wealth reached today by most of the populations of the developed countries. It is certainly a pity, and a dishonor for our civilization, that this high level of wealth did not catch up with most of the populations of less developed countries and also with a large part of the inhabitants of our industrialized countries. But this is a matter of politics more than of that of science and technology.

### 1.1.2 Catalysis and its role in industrial chemistry

As first recognized by the Swedish chemist J.J. Berzelius in 1835, catalysis is a phenomenon allowing a chemical reaction occurring faster when a nonreactant species is present. In spite of the apparent limited interest of doing a reaction faster, catalysis gives rise to very relevant practical effects. In fact, the increase of the rate of a reaction can in practice result in many cases in its practical feasibility. The

acceleration of a desirable chemical conversion, in fact, frequently allows it to be realized instead of other competitive reactions, less desirable, being definitely slower. Thus, finding an appropriate catalyst to make the desired reaction faster than the competitive ones, as well as allowing it to perform with high efficiency, is crucial in developing industrial processes. Thus, since maybe 180 years (the contact process for sulfuric acid production was developed in 1831), heterogeneous catalysis is a keystone in industrial chemistry.<sup>1</sup> For this reason, catalysts are also important products of the chemical industry itself and their industrial production represents a big business, like 13 billion dollars per year.

### 1.1.3 Why solid catalysts?

In practice, a large majority of industrial chemical processes (likely 85%<sup>2</sup>) are catalyzed and most of them are catalyzed by solids. The main reasons to use catalysts are synthetically the following:

1. The catalyst allows the desired reaction to become faster than competitive reactions thus allowing the desired reaction to be actually realized.
2. For exothermic equilibrium reactions: the catalyst allows the reaction to be performed also at lower temperature, where it would be kinetically hindered without it. Thus, it allows the reaction to be realized in conditions where thermodynamics is more favorable.
3. For endothermic equilibrium reactions: the catalyst allows the reaction to be performed also at moderately high temperatures, where it would be kinetically hindered without it. Thus, it allows the reaction to be realized in conditions where thermodynamics is already quite favorable with lower energy waste and allowing cheaper materials to be used for the reactor.
4. For exothermic nonequilibrium reactions: the catalyst allows reactions less favored by thermodynamics and kinetics (without it) to be realized instead of more favored and otherwise faster reactions.
5. A better catalyst allows reactions to be performed in smaller flow reactors with the same performances, or with better performances and lower recycles of unconverted reactants in the same reactor, or even with shorter times in batch reactors.

Solid catalysts are usually preferred in the industry with respect to liquid catalysts because of their easier separation from the reaction fluid. On the other hand, solid catalysts are frequently more environmentally friendly than liquid catalysts and their manipulation far safer. A typical example is that of acid catalysts for refinery and petrochemistry. Protonic zeolites substituted for liquid acids catalysts in some important processes. In practice, dangerous corrosive liquids characterized by unsafe manipulation procedures, difficult regeneration and inappropriate disposal, like sulfuric acid, and  $\text{AlCl}_3$ -based Friedel Crafts type liquid acid, and very toxic and volatile acids like hydrofluoric acid have been substituted by environmentally friendly silicoaluminates. Additionally, catalyst performances have also been improved.

<b>Table 1.1</b> Summary of Some Most Relevant Families of Industrial Catalysts			
<b>Oxide Catalysts</b>		<b>Example Reaction</b>	
Bulk single oxide	Alcohol dehydration to olefins	$\gamma\text{-Al}_2\text{O}_3$	Lewis acidic catalyst
Bulk mixed oxide	Aldol condensation	MgO–Al <sub>2</sub> O <sub>3</sub> calcined hydrotalcite	Basic catalyst
	Propane to acrylonitrile	V/MoNb/Sb oxides	(Amm)oxidation
Oxide supported on oxide	<i>o</i> -Xylene to phthalic anhydride	V <sub>2</sub> O <sub>5</sub> –TiO <sub>2</sub>	Selective oxidation
	Isobutane to isobutene	K <sub>2</sub> O–Cr <sub>2</sub> O <sub>3</sub> /Al <sub>2</sub> O <sub>3</sub>	Dehydrogenation
Impregnated melt or liquid	SO <sub>2</sub> to SO <sub>3</sub>	K <sub>2</sub> SO <sub>4</sub> –V <sub>2</sub> O <sub>5</sub> /SiO <sub>2</sub>	Oxidation
	Olefin oligomerization	H <sub>3</sub> PO <sub>4</sub> /SiO <sub>2</sub> ("solid phosphoric acid")	Protonic acid catalyst
<b>Zeolite Catalysts</b>		<b>Example Reaction</b>	
Protonic zeolite	Benzene + ethylene to ethylbenzene	H-BEA	Protonic acid catalyst
Metal exchanged zeolite	N <sub>2</sub> O decomposition/reduction	Fe–MFI	Redox catalyst
<b>Metal Catalysts</b>		<b>Example Reaction</b>	
Bulk metals	Ammonia synthesis	Fe (CaO, K <sub>2</sub> O, Al <sub>2</sub> O <sub>3</sub> , SiO <sub>2</sub> promoters)	Hydrogenation
Metal gauzes	Ammonia oxidation to NO	Pt (Rh stabilizer)	Selective oxidation
Supported metal	Acetylene hydrogenation in ethylene	Pd/Al <sub>2</sub> O <sub>3</sub> (Ag promoter)	Preferential hydrogenation
	Car catalytic mufflers	Pt–Rh/Al <sub>2</sub> O <sub>3</sub> –CeO <sub>2</sub> –ZrO <sub>2</sub>	Combustion + NO red
	Alcohols to aldehydes	Pt/Carbon	Liquid phase oxidation
	Aromatization of paraffins	Pt/K-L zeolite	Dehydrogenation
<b>Sulfide Catalysts</b>		<b>Example Reaction</b>	
Bulk sulfide	Bituminous sands to oil fractions	MoS <sub>2</sub>	Hydrocracking
Supported sulfides	Gasoline treatment	NiS–MoS <sub>2</sub> / $\gamma$ -Al <sub>2</sub> O <sub>3</sub>	Hydrodesulfurization

### 1.1.4 Industrial catalytic materials

In Table 1.1, some examples of different kinds of catalysts actually used in the chemical industry are summarized.

The research in the field of heterogeneous catalysis is very active, as demonstrated by the relevant number of specialized international journals and book series covering the catalysis subject (Table 1.2). Catalysis journals are also characterized by significantly high impact factors, showing again the high activity characterizing this research field. As obvious, excellent catalysis research is also published in the most distinguished general chemistry journals, such as Nature, Science, Angewandte

<b>Table 1.2</b> Scientific Publications of Heterogeneous Catalysis Research			
<b>Series of Books Reporting High-level Reviews in Catalysis</b>			
1	Catalysis Reviews—Science and Engineering	Taylor and Francis	
2	Advances in Catalysis	Elsevier	
3	Catalysis—Specialist Periodical Reports	RSC	
<b>Series of Books Reporting Full Papers Coming from Conference Papers</b>			
	Studies in Surface Science and Catalysis	Elsevier	
<b>Specialistic Journals (Impact Factor 2012)</b>			
1	Applied Catalysis B: Environmental	Elsevier	5.825
2	Journal of Catalysis	Elsevier	5.787
3	ACS Catalysis	ACS	5.265
4	ChemCatChem	Wiley	5.181
5	Catalysis: Science and Technology	RSC	3.753
6	Applied Catalysis A: General	Elsevier	3.410
7	Journal of Molecular Catalysis A: Chemical	Elsevier	3.187
8	Catalysis Today	Elsevier	2.980
9	Catalysis Communications	Elsevier	2.915
10	Topics in Catalysis	Springer	2.608
11	Catalysis Letters	Springer	2.244
12	Catalysis Surveys from Asia	Springer	1.897
13	Chinese Journal of Catalysis	Science Press	1.304
14	Reaction Kinetics, Mechanisms and Catalysis	Springer	1.104
15	Kinetics and Catalysis	Maik	0.543
16	Open Catalysis Journal	Bentham	
17	Catalysis in Industry	Maik	

*Continued*

**Table 1.2** Scientific Publications of Heterogeneous Catalysis Research—cont'd**Other Journals Publishing Papers in the Catalysis and in the Catalysts Fields (Impact Factor 2012)**

1	ChemSusChem	Wiley	7.475
2	Green Chemistry	RSC	6.828
3	Journal of Physical Chemistry C	ACS	4.814
4	Applied Energy	Elsevier	4.781
5	Journal of Power Sources	Elsevier	4.675
6	Langmuir	ACS	4.187
7	International Journal of Hydrogen Energy	Elsevier	3.548
8	Chemical Engineering Journal	Elsevier	3.473
9	Microporous and Mesoporous Materials	Elsevier	3.365
10	Fuel	Elsevier	3.357
11	Fuel Processing Technology	Elsevier	2.816
12	Energy and Fuels	ACS	2.853
13	Chemical Engineering Science	Elsevier	2.386
14	Industrial and Engineering Chemistry Research	ACS	2.206

Chemie, while a number of high-level reviews can also be found in typical general chemistry-review publication journals such as Chemical Reviews (ACS) and Chemical Society Reviews (RSC).

Due to this enormous experimental work, a very big number of new catalysts or catalytic materials are prepared, characterized and tested in a number of different reactions. It is obvious that the large majority of them lack activity, selectivity,

**Table 1.3** Some Leading Catalyst Producers

1	Haldor Topsoe	Refining, petrochemicals	Denmark
2	UOP	Refining, petrochemicals	USA
3	Axens	Refining, petrochemicals	France
4	Johnson Matthey	Refining, petrochemicals	UK
5	Criterion	Refining	USA
6	Clariant (SüdChemie)	Refining, petrochemicals	Switzerland/Germany
7	Albemarle	Refining, petrochemicals	USA
8	Grace Davison	Refining	USA
9	BASF	Refining, petrochemicals	Germany
10	ExxonMobil	Refining, petrochemicals	USA



stability to arrive to optimization and industrial exploitation. In this book, really industrially applied catalysts will be considered with some detail. This is because in this case the good practical behavior is actually proven.

Besides the many papers published in open journals, information can also be found in patent literature and from data reported by the catalyst producer industries, some of them being reported in [Table 1.3](#). Indeed most of these companies reveal some information on their commercial catalysts in some excellent brochures available at their Websites.

---

## References

1. Armor JN. *Catal Today* 2011;**163**:3–9.
2. de Jong KP. In: de Jong KP, editor. *Synthesis of solid catalysts*. Wiley-VCH; 2009. pp. 3–11.

# Preparation of Solid Catalysts: A Short Summary

## CHAPTER OUTLINE

<b>2.1 Preparation of catalyst precursors</b> .....	<b>11</b>
2.1.1 Choice of the starting compounds .....	11
2.1.2 Dry preparation procedures.....	11
2.1.2.1 Thermal decomposition of precursors .....	11
2.1.2.2 Solid-state reaction.....	11
2.1.2.3 Flame hydrolysis of metal chlorides.....	11
2.1.2.4 Solid-state wetting .....	12
2.1.2.5 Solid-state ion exchange.....	12
2.1.2.6 Combustion synthesis methods.....	12
2.1.2.7 Preparation of fused catalysts .....	13
2.1.3 Wet catalyst preparations and other slurry-phase preparation methods ..	13
2.1.3.1 Precipitation and coprecipitation .....	13
2.1.3.2 Sol–gel preparations .....	14
2.1.3.3 Aerogel preparations (sol–gel chemistry followed by supercritical drying) .....	14
2.1.3.4 Direct sol–gel preparation in supercritical liquids .....	15
2.1.3.5 Microemulsion and reverse micelle methods .....	15
2.1.3.6 Hydrothermal and other solvothermal methods .....	16
2.1.3.7 The “polyol” technique.....	16
2.1.3.8 Template-driven hydrothermal preparation procedures of porous materials.....	17
2.1.3.9 Solution combustion synthesis .....	17
2.1.3.10 The citrate autocombustion method.....	17
2.1.3.11 Impregnation methods.....	18
2.1.3.12 Deposition/precipitation .....	18
2.1.3.13 Ion exchange and adsorption.....	18
2.1.3.14 Grafting.....	18
2.1.3.15 Plasma–chemical syntheses .....	19
2.1.4 Intermediate and final treatments in preparation chemistry .....	19
<b>References</b> .....	<b>20</b>

Although the primary property of a catalyst is its chemical composition, a number of properties of them depend on how the catalyst has been prepared, thus allowing optimal dispersion/agglomeration of the active components, surface area and morphology, etc. Many preparation techniques may be applied to the preparation of materials having the same composition. Many data can be found in the literature, published in the last 50 years, concerning catalyst preparation. To limit to the most recent ones, some exhaustive books<sup>1,2</sup> have been published while several reviews have been devoted to more specific topics such as the preparation of supported catalysts<sup>3</sup> and of nanoparticles.<sup>4</sup> A number of data can be found in the series of books reporting the Scientific Bases for the Preparation of Heterogeneous Catalysts, the most recent one being published by Elsevier in 2011.<sup>5</sup>

In the following, we will summarize shortly most of the common preparation procedures for solid catalysts.

Catalytic materials can be roughly divided into two families:

1. Bulk catalytic materials;
2. Supported catalytic materials.

Supported catalysts are mostly defined as those where a presynthesized carrier material is used to deposit on it a thin layer or the “active phase”, microcrystals, or nanoparticles or even, sometimes, isolated complexes or clusters or atoms. Supported catalysts are usually intended as those the nature of the support influences the morphological properties and, frequently, also the chemical properties of the supported phase, thus participating to the generation of the catalytic properties of the overall catalyst.

However, in the practical industrial work, low-surface area ceramic supports (such as corundum powders, carborundum powders, cordierite monolites) are sometimes used to support a bulk catalyst. In this case, where big particles or porous thick layers of a “bulk” catalyst are physically deposited on ceramic supports, the support plays a determinant role in heat transfer and flow-dynamics of the system, without exerting a definite role in the chemical–catalytic behavior of the material. Thus, the term “support” is somehow ambiguous.

Preparation procedures of catalyst powders may differ significantly for supported and unsupported bulk catalysts. However, for most sophisticated materials, several components can be included in catalyst formulations using techniques typical for both supported and bulk materials preparation.

In fact, in a typical list of catalytic materials, a number of components can be included. They are:

1. The active phase, supposed to be that mainly responsible for the rate determinant catalytic act;
2. The support, if needed to produce optimal activity of the active phase and optimal morphology and surface area, with optimization sometimes also of heat transfer and flow-dynamics aspects;
3. Promoters that can further improve the catalytic activity;

4. Stabilizers that stabilize the catalyst from a number of possible deactivation phenomena, such as stabilizers from sintering, from phase transformation, from coke deposits formation, from active phase volatilization, etc.

---

## 2.1 Preparation of catalyst precursors

### 2.1.1 Choice of the starting compounds

Supposing the chemical composition of the catalytic material is fixed (e.g., active phase and support, if any, together with additional promoter or stabilizing components), still room remains for the choice of a number of alternative techniques and precursor materials. The choice of the starting compounds for catalysts preparation is dictated, in the industry, largely from economics. In the academic research, instead, purity and simplicity are the most relevant choice parameters. As for example, sodium silicate is a typical starting compound for producing silica-based materials in the industry, while silicon alkoxides are mostly used in the academic investigations.

As it will be clear later on, another important factor is the chemistry of the compound and in particular of all moieties composing it. In particular, preparation of inorganic solids implies largely the use of salts, one of whose ions contains the desired element, usually a metal. Care must be taken to the chemistry of the other ion to reduce the risk of contamination of the final catalyst.

### 2.1.2 Dry preparation procedures

#### 2.1.2.1 *Thermal decomposition of precursors*

A number of inorganic solids can be prepared by thermal decomposition of precursors. This is usually the case of metal oxides prepared by decomposition of the corresponding hydroxides, sometimes of the corresponding nitrates, carbonates, hydroxy-carbonates or of other salts. Decomposition reactions sometimes occur at moderate temperature with breaking of the original structure allowing high surface area materials to be prepared.

#### 2.1.2.2 *Solid-state reaction*

A number of mixed oxides can be prepared by thermal treatment of the simple component oxides. As for example,  $\text{NiAl}_2\text{O}_4$  is easily prepared by heating  $\text{NiO}$  and  $\text{Al}_2\text{O}_3$  at  $1200^\circ\text{C}$ . This preparation method usually allows the preparation of well-crystallized complex solids with very low-surface area.

#### 2.1.2.3 *Flame hydrolysis of metal chlorides*

The reaction of volatile metal chlorides, such as  $\text{SiCl}_4$ ,  $\text{TiCl}_4$ ,  $\text{ZrCl}_4$ ,  $\text{CeCl}_4$ ,  $\text{AlCl}_3$  in a hydrogen–oxygen flame at high temperature  $>1000^\circ\text{C}$ , produces the corresponding metal oxides with very small nonporous oxide primary particles that tend to agglomerate in linear and branched chain-like structures.<sup>6</sup> This

method represents the commercial production of some alumina, silica and titania materials, useful as catalyst supports, such as the Aeroxide materials from Evonik.<sup>7</sup>

#### **2.1.2.4 Solid-state wetting**

Wetting is a method allowing the dispersion of some chemical species, mostly low melting point compounds, on the surface of a catalyst support. It has in fact been found that metal anhydrides such as  $V_2O_5$  and  $MoO_3$  can spread spontaneously over typical oxide carriers such as alumina, titania and zirconia when the support/supported oxide mixture is heated at a sufficiently high temperature.<sup>8,9</sup> Catalysts prepared by wetting have been reported to be as active as catalyst prepared by the more conventional wet impregnation technique.

#### **2.1.2.5 Solid-state ion exchange**

Ion exchanger solids, such as zeolites, can be exchanged not only with the usual liquid-phase ion exchange but also by a solid-state reaction. Similarly as above, when the mixture exchanger salt (such as a metal chloride)/protonic zeolite are heated at a sufficiently high temperature, cation exchange occurs and HCl is evolved. This can be applied e.g., to the preparation of copper/zeolites using  $CuCl_2$  as the starting salt and protonic zeolites.<sup>10</sup>

#### **2.1.2.6 Combustion synthesis methods**

Combustion synthesis, which is also known as self-propagating high-temperature synthesis, is a method to produce inorganic materials from exothermic combustion reactions.<sup>11</sup> In contrast to conventional solid-state synthesis methods characterized by a longtime heat-treatment at high temperatures, combustion synthesis can be finished in a short time and requires much lower energy consumption, because it uses the heat energy released in combustion reactions and no furnace is necessary. With these merits, combustion synthesis offers an efficient way for industrial production of many inorganic materials. For example, many kinds of refractory and hard materials have been prepared by combustion synthesis, including alloys, intermetallics, ceramics and cermets in a form of powders or consolidated bulks.

Among the several variants of this technique, carbon combustion synthesis of oxides is a novel and economical technology for production of micron and nanostructured particles of complex oxides for advanced device applications.<sup>12</sup> Pure carbon in the form of graphite or soot, or even carbon compounds, such as e.g., starch, is added to the reactant mixture to generate the desired heat (upon ignition). The mixture is placed in a reactor and exposed to gaseous oxygen. The high-temperature exothermic reaction between the carbon and oxygen generates a self-sustaining reaction in the form of a propagating temperature wave that causes a reaction among the reactants. The reaction proceeds rapidly following ignition, and the final product comprises simple and/or complex oxides of elements present in the oxide precursor(s). The high rate of  $CO_2$  release facilitates synthesis of highly porous (70%) powders having particle size in the range of 50–800 nm.<sup>13</sup>

### 2.1.2.7 Preparation of fused catalysts

A common preparation of iron ammonia synthesis catalysts consists in the fusion of the magnetite  $\text{Fe}_3\text{O}_4$  precursor above  $1400^\circ\text{C}$  with the promoters silica, alumina, potash calcium oxide, followed by melting, cooling and grinding.<sup>14</sup> A similar procedure can be used to prepare iron catalysts for Fischer–Tropsch reaction.<sup>15</sup>

## 2.1.3 Wet catalyst preparations and other slurry-phase preparation methods

A number of wet preparation methods are available for producing finely dispersed powders.<sup>16,17</sup> They start from classical procedures to a number of innovative “chimie douce” (soft chemistry) approaches.

### 2.1.3.1 Precipitation and coprecipitation

Most metal ions are largely soluble in acidic water solution while they precipitate, in the form of their hydroxides, in neutral and basic conditions. Thus, a typical preparation method of base metal oxides consists in the precipitation of the corresponding hydroxides or hydroxy-salts at the typical precipitation pH, usually slightly basic, followed by calcination to decompose the hydroxide/acid phases producing anhydrous oxides. Most of hydroxides decompose in the  $200\text{--}550^\circ\text{C}$  range.

The homogeneous coprecipitation of different base metal cations finally producing solid-solution type mixed oxides can be obtained sometimes easily because of the mutual solubility of some cations in some hydroxide phases (e.g., brucite-type hydroxides of bivalent metal cations, such as  $\text{Mg}^{2+}$ ,  $\text{Ni}^{2+}$ ,  $\text{Co}^{2+}$ ,  $\text{Zn}^{2+}$ , ..., or hydroxides and oxy-hydroxides of trivalent metals such as  $\text{Al}^{3+}$ ,  $\text{Ga}^{3+}$ ,  $\text{Fe}^{3+}$ ,  $\text{Cr}^{3+}$ , ...). On the other hand, the coprecipitation of trivalent and bivalent cations can be obtained by precipitating hydrotalcite-like layered mixed hydroxides,<sup>18</sup> in the form of hydroxy-carbonates, hydroxy-nitrates or hydroxy-chlorides.

One of the limits of the precipitation techniques is the need of a base to obtain the basic precipitation pH. Alkali metal hydroxides allow precipitation, but result normally in the contamination of the precipitate and of the final oxide product by alkali cations. Complex and tedious washing procedures of the precipitate with pure water are needed to limit contamination.

The use of ammonia or amines, urea, ammonium carbonate or bicarbonate are more appropriate for high purity oxides preparations, because these compounds easily desorb, decompose or burn upon calcination.

A similar problem may occur with the counter-ion of the metals to be precipitated. In this respect, nitrates, acetates, oxalates and alkoxides are the best, because they decompose/burn under calcination conditions. The use of chlorides or sulphates usually leads to significant contamination of the resulting metal oxide powders.

Semimetals and metals that produce amphoteric oxides or anhydrides are also soluble in strongly basic solutions but precipitate in neutral or acidic conditions. In this case, amorphous acids and/or anhydrides are mostly obtained,

which also may decompose to mixed oxides by calcination. Again, care must be given to the behavior of the counter-ion of the precipitating acid, to avoid contamination.

### **2.1.3.2 Sol–gel preparations**

A colloid is a liquid that contains, evenly distributed in a stable way, particles ranging between 1 and 1000 nm in diameter. A sol, or a colloidal suspension with solid particles in a liquid, arises from hydrolysis and polymerization of a precursor that is either a salt or an organometallic compound such as a metal alkoxide. The solvent is frequently an organic liquid or mixture of liquids to which some water is added. By completing the polymerization and removal of the solvent, the sol converts into a gel (xerogel). The removal is usually obtained by evaporation. This is the typical preparation method, e.g., of silica gel and silica-based materials,<sup>19</sup> but can be applied to a number of other oxides of industrial interest.<sup>20</sup>

The so-called sol–gel coordination chemistry is based on co-condensation, during the sol–gel preparation, of a complex or nanoparticle modified with terminal trialkoxysilane groups, with a silica source (such as tetraethoxysilane) and in the presence of an adequate surfactant giving rise to the preparation of hybrid materials.<sup>21</sup> The method can also be applied to prepare mixed oxides and to functionalise silica-based materials. The obtained materials are frequently still fully amorphous and may retain significant amounts of organic matter.

Nonhydrolytic (NH) or nonaqueous sol–gel routes have also been proposed, based on the reaction of various precursors (such as metal chlorides) with alcohols, ethers, esters, alkoxides, in the absence of water. A number of mixed oxides with very high interest in catalysis can be prepared by this way. Ionic liquids can also be used as solvents. The NHSG process offers simple, one-step syntheses of mixed oxides with well-controlled compositions and non-ordered mesoporous textures, avoiding the use of supercritical drying or templates.<sup>22,23</sup>

The advantages of sol–gel methods include: their high yield, low operation temperatures and low operation costs.

### **2.1.3.3 Aerogel preparations (sol–gel chemistry followed by supercritical drying)**

Drying the gel by evaporation under ambient pressure gives rise to capillary pressure that causes shrinkage of the network. Aerogels<sup>24</sup> are obtained by removing the solvent from a sol under supercritical conditions, thus avoiding capillary stress and associated drying shrinkage. Typical solvents for aerogels preparations are methanol, ethanol and CO<sub>2</sub>. Because of the fact that in a supercritical fluid a single phase exists, drying in SC conditions circumvents the liquid–gas interface during vaporization, hence preventing collapse of the solid network from capillary forces during the drying process, thus allowing the production of materials with very high surface areas.

The supercritical drying process consists of three steps: (1) pressurization combined with heating to attain SC conditions; (2) continuous flushing with fresh SC

fluid to remove the solvents; (3) depressurization is used to remove the fluid phase. Heating and depressurization must be slow enough to avoid shear stress and consequent cracks in the nanostructure.

Silica aerogels<sup>25,26</sup> are produced industrially and have application in insulation technologies.<sup>27</sup> In the catalysis field, a number of mixed oxide aerogels can be prepared, finding interesting catalytic properties, such as e.g., TiO<sub>2</sub> catalysts and photocatalysts,<sup>28</sup> WO<sub>3</sub>–ZrO<sub>2</sub> acid catalysts<sup>29</sup> and V<sub>2</sub>O<sub>5</sub>–TiO<sub>2</sub> oxidation catalysts for VOC abatement.<sup>30</sup>

#### **2.1.3.4 Direct sol–gel preparation in supercritical liquids**

Sol–gel chemistry can be performed directly in supercritical fluids (SCFs) such as CO<sub>2</sub> or water.<sup>24</sup> The use of higher temperatures and pressures may allow crystallization of the resulting materials. These SCFs are environmentally benign, and add ecological credits to the sustainability of the sol–gel process. Importantly, supercritical CO<sub>2</sub> has already been used as an established medium for industrial-scale polymerizations, as well as food and nutrition production. Other advantages of using SCFs as reaction media for sol–gel reactions lies in the fact that the resulting materials are readily dried after SCF venting, and that reaction kinetics can be fine tuned using both pressure and temperature, thus allowing some difficult sol–gel reactions to take place. Many crystalline metal oxides can be readily prepared in high temperature sol–gel SCF processes. This eliminates the heat-treatment step and further simplifies the manufacturing process.

The rapid reaction kinetics in supercritical water (SCW) makes it possible to prepare metal oxide nanoparticles using continuous reactors, which is more attractive for industrial-scale production. Other advantages of using SCW include: (1) the tunable dielectric constant of water provides an extra parameter for controlling the solubility of the solutes in addition to the SCF density; (2) the high crystallinity of the metal oxide products formed; and (3) lower temperatures for the formation of certain crystals in SCW.

#### **2.1.3.5 Microemulsion and reverse micelle methods**

In colloidal synthesis methods, surfactant molecules are used to limit particle growth. The microemulsions<sup>31,32</sup> consist of a combination of three kinds of components: an oil phase, a surfactant and an aqueous phase. They are transparent solutions consisting of small droplets of an immiscible phase dispersed in a continuous phase. Surfactants are added to lower the interfacial tension between the immiscible dispersed and continuous phases to stabilize the droplets.

Microemulsions may consist of oil-in-water or water-in-oil, depending on the concentration of the different components. By varying the concentration of the dispersed phase and the surfactant, it is possible to tailor the size of the droplets in the range 1–100 nm, approximately. Self-assembled structures of different types can be formed, ranging, for example, from (inverted) spherical and cylindrical micelles to lamellar phases and bicontinuous microemulsions, which may coexist with predominantly oil or aqueous phases.



In the so-called reverse micelle method,<sup>17,33</sup> a nonpolar solvent is used to form micelles with a polar core immersed in it (reverse micelle). Into the polar micelle, a small amount of water is present in which precipitation of the nanocrystal of e.g., oxide or other materials can take place.

This method is mostly used to prepare unsupported metal nanoparticles: in this case, a reducing agent is added to the system, which reduces the aqueous salt into the metal. The reverse micelles keep the forming nanoparticles from aggregating into larger structures. After the reaction, the surfactant remains adsorbed to the surface of the nanoparticles stabilizing them against aggregation and oxidation.

This method can be combined with the simultaneous sol–gel synthesis of the support (like silica) to prepare silica-supported metal catalysts.<sup>34</sup> Alternatively, this method can be used to prepare metal or alloy nanoparticles to be supported on presynthesized supports.<sup>35</sup>

#### **2.1.3.6 Hydrothermal and other solvothermal methods**

Solvothermal synthesis is a method for preparing a variety of materials such as metals, semiconductors, ceramics and polymers. The process involves the use of a solvent sometimes under some pressure and at moderate temperature that facilitates the interaction of precursors during synthesis. If water is used as the solvent, the method is called “hydrothermal synthesis”. Upon these treatments, sometimes denoted as aging, a number of phenomena may occur such as crystallization of amorphous matter, particle or crystal growth, change in porosity usually with diminution of pore volume. The process can be used to prepare bulk powders, single crystals, nanocrystals and thin films. Particle morphology may be controlled by manipulating the solvent supersaturation, concentration of chemicals and kinetic control. The method can be used to prepare thermodynamically stable and metastable states including novel materials that cannot be easily formed from other synthetic routes. Over the last decade, a majority (~80%) of the literature concerning solvothermal synthesis has focused on nanocrystals.<sup>36</sup>

A typical example of hydrothermal synthesis in the field of catalysis is the organic-template-free synthesis of aluminosilicate zeolites, developed before the 1960s even at the industrial level to produce A, X and Y zeolites. Such zeolites were and may be synthesized under hydrothermal conditions from reactive gels in alkaline media at temperatures between about 80 and 200 °C.<sup>37</sup> An alternative route is based on fluoride containing compositions as mineralizing media, in which case the pH can be much lower.

#### **2.1.3.7 The “polyol” technique**

The polyol process is a kind of solvothermal method that can also be coupled with an alcohol reduction method for easily reducible metals. In fact in this method, a liquid polyol such as ethylene glycol, 1,2-propandiol, triethylene glycol or diethylene glycol, acts as the solvent and may also act as a mild reducing agent. The catalyst precursor salt is suspended or dissolved in polyols and the resultant suspension or

solution is heated with reflux. The obtained precipitate can be treated thermally. A number of bulk simple and complex metal oxides can be prepared by this way, such as e.g.,  $V_2O_5$ <sup>38</sup> and  $Co_{1-x}Zn_xFe_2O_4$  complex oxides.<sup>39</sup>

With a similar technique, supported oxide on oxide catalysts can be prepared such as  $V_2O_5-ZrO_2$ , showing an improved dispersion of the active species.<sup>40</sup>

According to the reducing behavior of the polyols, this process has allowed the synthesis of monodisperse non-agglomerated unsupported metal particles of cobalt, nickel, copper and precious metals, in the micrometer and submicrometer range. Metal nanoparticles supported on carbonaceous materials<sup>41</sup> as well as on alumina<sup>42</sup> or other supports have been prepared by this method.

#### **2.1.3.8 Template-driven hydrothermal preparation procedures of porous materials**

The use of organic molecules such as alkylammonium cations as “templates” or Structure Directing Agents (SDA) to produce zeolite materials dates to the early 1960s.<sup>37,43,44</sup> The zeolite structure appears to form around them, in some cases encapsulating them with a very close fit between the organic groups and the pore walls. Clearly, this steric requirement will limit the number of organic units that can be accommodated. Thus, for templates such as quaternary salts that also act as charge-balancing cations, the organic guest species impose a restriction on the zeolite framework charge density, resulting in products of increased Si/Al ratio (since only the Al-sites carry Brønsted sites). Today, most zeolites are synthesized using organic templates, which have to be removed from the structure (usually by calcination) to produce the open-pore materials for use in sorption and catalysis. This obviously represents a limit, due to the cost of the organic SDA, which cannot be recovered. Attempts to recover SDA molecules and development of new efficient template-free preparation procedures are undertaken.<sup>43</sup>

#### **2.1.3.9 Solution combustion synthesis**

The solution combustion synthesis approach is based on the use of saturated aqueous solution of the required metal nitrate as oxidizing agent and a suitable organic fuel employed as reducing agent. Among useful fuels, such as, urea, hydrazine, carbohydrazide, maleic hydrazide, etc., this redox mixture ignites upon heating at a determined temperature, usually below 500 °C, to initiate a self-propagating exothermic reaction that sustains high temperatures for a sufficient period of time to decompose all the organic material and metal salts. The final product is usually a crystallized material with nanometric size clusters and has a large specific surface area as a consequence of the large amount of gases produced during the synthesis process.<sup>45</sup> A number of catalysts can be prepared by this way.

#### **2.1.3.10 The citrate autocombustion method**

The citrate autocombustion method was proposed years ago to produce mixed oxide catalysts. Citric acid allows the complexation of almost any metal cation, thus citrate solutions allow a good dispersion and mixing of cations in a single phase. The

solution is then dried upon evaporation and the resulting solid powder heated in air allowing citrate ions to burn leaving a high surface area mixed oxide. Similar procedures apply cellulose, examethylenetetramine, tartaric acid, glycine and urea as complexing agents/fuels.<sup>46</sup>

#### **2.1.3.11 Impregnation methods**

The impregnation method is the most common and simplest way to obtain supported catalyst precursors. The support is contacted with a solution containing the precursor of the supported phase, and then it is aged, dried and calcined. Sometimes, organics may be added to the impregnating water solution. Depending on the volume of solution with respect to that of the support, two types of impregnation can be distinguished: the so-called “incipient wetness” impregnation if the solution volume does not exceed the pore volume of the support; and the “wet” impregnation when an excess of solution is used. The characteristics of the catalyst strictly depend on the posttreatment conditions (rate of heating, time, final temperature, atmosphere) and, obviously, on the type of supporting materials. In fact, during the calcination step, sintering of the precursor and reaction between the metal precursor and the support might occur. Moreover, the use of different conditions can lead to different metal-support interaction, of fundamental importance for the catalytic applications.

#### **2.1.3.12 Deposition/precipitation**

Deposition/precipitation is performed when an insoluble form of the “supported” active phase is generated in solution, and deposited onto the support, which has a contact with the solution. This method appears to be the best suited for preparing precursors of very active supported gold catalysts,<sup>47</sup> where the hydroxide or carbonate are produced and deposited on the support.<sup>48</sup>

#### **2.1.3.13 Ion exchange and adsorption**

Ion exchange consists in the contact of a precursor from aqueous solution onto the support. Ionic species, such as metal cations or oxoanions from salts, dissolved in the aqueous solution, are attracted electrostatically by charged sites on the support surface. After a quite prolonged contact, the solid is separated from the solution, e.g., by filtration. This process is used frequently to produce cationic zeolites from protonic zeolites. Although the real process may be by far more complex, it is supposed that cations exchange the equivalent number of protons in terms of total charge. In a very similar way, ions can adsorb on a surface, such as that of an oxide carrier. Adsorption of cations is supposed to occur mainly  $\text{pH} > \text{PZC}$  (point of zero charge) of the carrier (see Table 2.1<sup>49,50</sup>), while adsorption of anions is supposed to occur at  $\text{pH} < \text{PZC}$ . The same element can be deposited by anion adsorption and by cation adsorption, using different salts (such as  $\text{Au}(\text{OH})_4^-$  or  $\text{Au}(\text{en})_3^{3+}$ , where en = ethylenediamine, for gold,  $\text{PtCl}_6^{2-}$  or  $[(\text{NH}_3)_4\text{Pt}]^{2+}$  for platinum).

#### **2.1.3.14 Grafting**

Grafting is supposed to occur when a chemical species dissolved in a solution or from the gas phase is put into contact with a solid surface and is supposed to react

**Table 2.1** Point of Zero Charge of Metal Oxides

MgO	10.8
ZnO	8.6–10.3
Al <sub>2</sub> O <sub>3</sub>	8.5–9.0
NiO	7.5–10.5
Fe <sub>2</sub> O <sub>3</sub>	7.5–9.3
La <sub>2</sub> O <sub>3</sub>	6.7–9.6
ZrO <sub>2</sub>	6.3–7.1
CeO <sub>2</sub>	6.5
TiO <sub>2</sub>	5.1–6.4
SnO <sub>2</sub>	3.9–4.9
Nb <sub>2</sub> O <sub>5</sub>	3.5–4.0
SiO <sub>2</sub>	2.0–3.8
WO <sub>3</sub>	2.0–2.8

specifically with some surface sites. A typical example is the reaction of some volatile metal chlorides or of alkoxysilanes from organic solutions, supposed to react specifically with the surface hydroxyl groups of silica or of other oxides. This is a procedure allowing, for example, the hydrophobization of silica surfaces<sup>51</sup> (due to the partial disappearance of the silanol groups after their reaction with alkoxysilane groups) and the preparation of supported vanadium oxide catalysts.<sup>52</sup>

#### 2.1.3.15 Plasma—chemical syntheses

A number of inorganic materials such as nitrides, carbides, oxides can be prepared starting mainly from liquid precursors using plasma techniques.<sup>53</sup> Several different plasma techniques have been developed and found to be useful in particular for the production of TiO<sub>2</sub> photocatalysts.<sup>54</sup>

### 2.1.4 Intermediate and final treatments in preparation chemistry

Most of the above techniques can be coupled with the use of additional equipment to improve the quality of the products and sometimes to make simpler and faster the procedure. Among such further or additional procedures, microwave oven heating<sup>55</sup> not only may significantly reduce the preparation time from days to minutes but also may allow screening of a wide range of experimental conditions in order to optimize and scale-up syntheses with low energy consumption.

Sonochemical treatment<sup>56</sup> takes advantage from acoustic cavitation: the formation, growth, and implosive collapse of bubbles in a liquid irradiated with high-intensity ultrasound. This procedure creates local hot spots with controllable very high temperatures, which provides an unusual method, e.g., for the decomposition of volatile organometallic precursors.

In several steps of the chemical preparation methods, procedures such as decantation, filtration, centrifugation and washing must be necessary and the exact procedure adopted can have some effect on the resulting catalyst properties.

However, it is quite evident that the last procedures, very frequently needed to obtain the final fresh catalyst, may have a determinant role on the catalyst properties. Calcination is frequently performed in air or in dry oxygen at a prefixed temperature. Alternatively, or subsequently, heat-treatment could be performed in reducing atmosphere (such as, but not exclusively, hydrogen or hydrogen/nitrogen mixtures) are usually performed to produce metal catalysts. To produce sulfides, heating in  $H_2/H_2S$  flow is most commonly performed. The effects of details, such as the exact temperature adopted, the amount of moisture, flowing or static atmospheres, etc. should not be neglected, because they may influence the properties of the fresh catalyst. It must however be mentioned that catalysts certainly undergo modifications under working conditions, and thus the properties of the “fresh” catalyst charged to the reactor are frequently well different from those of the real catalyst in “operando” conditions.

---

## References

1. *Catalyst preparation: Science and Engineering* by John R. Regalbuto: CRC Press, Taylor & Francis Group; 2007.
2. de Jong KP, editor. *Synthesis of solid catalysts*. Wiley; 2009.
3. Mäki-Arvela P, Murzin DY. *Appl Catal A Gen* 2013;**451**:251–81.
4. Zhong CJ, Regalbuto JR. *Reference module in chemistry, molecular sciences and chemical engineering*. In *Comprehensive inorganic chemistry II*. 2nd ed., vol. 7; 2013. p. 75–102.
5. Gaigneaux EM, Devillers M, Hermans S, Jacobs PA, Martens JA, Ruiz P, editors. *Scientific bases for the preparation of heterogeneous catalysts proceedings of the 10th international symposium. Surface science and catalysis*, vol. 175. Belgium: Louvain-la-Neuve; July 11–15, 2010.
6. Camenzind A, Caseri WR, Pratsinis SE. *Nano Today* 2010;**5**(1):48–65.
7. <http://www.aerosil.com/product/aerosil/en/industries/catalyst-carrier/pages/default.aspx>. [accessed 21.03.14].
8. Haber J, Machej T, Serwicka EM, Wachs IE. *Catal Lett* 1995;**32**(1–2):101–14.
9. Bulushev DA, Kiwi-Minsker L, Zaikovskii VI, Renken A. *J Catal* 2000;**193**(1):145–53.
10. Vanelderden P, Vancauwenbergh J, Sels BF, Schoonheydt RA. *Coord Chem Rev* 2013;**257**(2):483–94.
11. Liu G, Li J, Chen K. *Int J Refract Metals Hard Mater* 2013;**39**:90–102.
12. Martirosyan KS. Dan Luss US7897135 B2 to Houston University; 2011.
13. Aruna ST, Mukasyan AS. *Curr Opin Solid State Mater Sci* 2008;**12**:44–50.
14. Wijngaarden RI, Westerterp KR, Kronberg A. *Industrial catalysis*. Wiley; 2008. p. 33.
15. Maitlis PM, de Klerk A. *Greener Fischer–Tropsch processes for fuels and feedstocks*. Wiley; 2013. p. 174–5.
16. Cushing BL, Kolesnichenko VL, O’Connor CJ. *Chem Rev* 2004;**104**:3893–946.
17. Zaera F. *Chem Soc Rev* 2013;**42**(7):2746–62.

18. Nishimura S, Takagaki A, Ebitani K. *Green Chem* 2013;**15**(8):2026–42.
19. Ciriminna R, Fidalgo A, Pandarus V, Béland F, Ilharco LM, Pagliaro M. *Chem Rev* 2013;**113**(8):6592–620.
20. Fujita K. *Bull Chem Soc Jpn* 2012;**85**(4):415–32.
21. Serrano E, Linares N, Garcia-Martinez J, Berenguer JR. *ChemCatChem* 2013;**5**(4):844–60.
22. Debecker DP, Mutin PH. *Chem Soc Rev* 2012;**41**(9):3624–50.
23. Debecker DP, Vasile Hulea P, Mutin H. *Appl Catal A Gen* 2013;**451**:192–206.
24. Sui R, Charpentier P. *Chem Rev* 2012;**112**(6):3057–82.
25. Omranpour H, Motahari S. *J Non Cryst Solids* 2013;**379**:7–11.
26. Soleimani Dorcheh A, Abbasi MH. *J Mater Process Technol* 2008;**199**(1):10–26.
27. Koebel M, Rigacci A, Achard P. *J Solgel Sci Technol* 2012;**63**(3):315–39.
28. Fröschl T, Hörmann U, Kubiak P, Kučerová G, Pfanzelt M, Weiss CK, et al. *Chem Soc Rev* 2012;**41**:5313–60.
29. Signoretto M, Ghedini E, Menegazzo F, Cerrato G, Crocellà V, Bianchi CL. *Microporous Mesoporous Mater* 2013;**165**:134–41.
30. Gannoun C, Delaigle R, Eloy P, Debecker DP, Ghorbel A, Gaigneaux EM. *Catal Commun* November 15, 2011;**15**(1):1–5.
31. Ganguli AK, Ganguly A, Vaidya S. *Chem Soc Rev* 2010;**39**:474–85.
32. Muñoz-Espí R, Weiss CK, Landfester K. *Curr Opin Colloid Interface Sci* 2012;**17**(4):212–24.
33. Uskoković V, Drogenik M. *Surf Rev Lett* 2005;**12**(2):239–77.
34. Kim M, Heo E, Kim A, Park JC, Song H, Park KH. *Catal Lett* 2012;**142**(5):588–93.
35. Cheney BA, Lauterbach JA, Chen JG. *Appl Catal A Gen* 2011;**394**(1–2):41–7.
36. *Solvothermal synthesis of nanoparticles*. Gersten B, editor. *Chemfiles*, vol. 5. Article 13. <http://www.sigmaaldrich.com/technical-documents/articles/chemfiles/solvothermal-synthesis.html>. [accessed 21.03.14].
37. Cundy CS, Cox PA. *Chem Rev* 2003;**103**:663–701.
38. Uchaker E, Zhou N, Li Y, Cao G. *J Phys Chem C* 2013;**117**(4):1621–6.
39. Tahar LB, Basti H, Herbst F, Smiri LS, Quisefit JP, Yaacoub N, et al. *Mater Res Bull* 2012;**47**(9):2590–8.
40. Sasikala R, Sudarsan V, Sakuntala T, Jagannath, Sudakar C, Naik R, Bharadwaj SR. *Appl Catal A Gen* 2008;**350**(2):252–8.
41. Favilla PC, Acosta JJ, Schvezov CE, Sercovich DJ, Collet-Lacoste JR. *Chem Eng Sci* 2013;**101**:27–34.
42. Bayrakdar E, Gürkaynak Altınçekiç T, Ali Faruk Öksüzömer M. *Fuel Process Technol* 2013;**110**:167–75.
43. Martínez C, Corma A. *Coord Chem Rev* 2011;**255**:1558–80.
44. Valtchev V, Tosheva L. *Chem Rev* 2013;**113**:6734–60.
45. González-Cortés SL, Imbert FE. *Appl Catal A Gen* 2013;**452**:117–31.
46. Dumitrescu AM, Samoila PM, Nica V, Doroftei F, Iordan AR, Palamaru MN. *Powder Technol* 2013;**243**:9–17.
47. Harita M. *Cattech* 2002;**6**:102.
48. Prati L, Villa A. *Catalysts* 2012;**2**:24–37.
49. Kosmulski M. *J Colloid Interface Sci* 2004;**275**:214–24.
50. Kosmulski M. *Adv Colloid Interface Sci* 2009;**152**:14–25.
51. Gokulakrishnan N, Karbowski T, Pierre Bellat J, Vonna L, Saada MA, Louis Paillaud J, et al. *Colloids Surf A Physicochem Eng Asp* March 20, 2013;**421**:34–43.
52. Wegener SL, Kim H, Marks TJ, Stair PC. *J Phys Chem Lett* 2011;**2**(3):170–5.

53. Zaharieva K, Vissokov G, Grabis J, Rakovsky S. *Plasma Sci Technol* 2012;**14**:11.
54. Macwan DP, Dave PN, Chaturvedi S. *J Mater Sci* 2011;**46**:3669–86.
55. Horikoshi S, Serpon N, editors. *Microwaves in nanoparticle synthesis: fundamentals and applications*. Wiley, 2013.
56. Xu H, Zeiger BW, Suslick KS. *Chem Soc Rev* 2013;**42**(7):2555–67.

# Characterization of Real Catalytic Materials: An Overview

## CHAPTER OUTLINE

<b>3.1 Elemental composition of heterogeneous catalysts</b> .....	<b>24</b>
3.1.1 Atomic absorption and emission spectroscopies .....	24
3.1.2 Inductively coupled plasma–mass spectrometry .....	24
3.1.3 X-ray fluorescence .....	25
3.1.4 Energy-dispersive X-ray analysis.....	25
<b>3.2 Structural properties of inorganic materials and its characterization</b> .....	<b>25</b>
3.2.1 XR diffraction .....	26
3.2.2 Electron diffraction.....	26
3.2.3 Neutron diffraction .....	27
3.2.4 Vibrational spectroscopies.....	27
3.2.5 X-ray absorption spectroscopy.....	28
3.2.6 UV–vis spectroscopic data.....	29
3.2.7 Magic angle spinning Nuclear Magnetic Resonance (NMR) techniques .	29
<b>3.3 Morphology characterization</b> .....	<b>30</b>
3.3.1 Measurement of the surface area and analysis of porosity .....	30
3.3.2 Crystal size measurement.....	31
3.3.3 Electron microscopies.....	31
3.3.3.1 <i>Scanning electron microscopy</i> .....	31
3.3.3.2 <i>Field-emission scanning electron microscopy</i> .....	31
3.3.3.3 <i>Transmission electron microscopy</i> .....	31
3.3.3.4 <i>Scanning transmission electron microscopy</i> .....	32
<b>3.4 Analysis of the surface structure and composition</b> .....	<b>32</b>
3.4.1 X-ray photoelectron spectroscopy .....	32
3.4.2 Direct surface analysis by conventional spectroscopies .....	33
3.4.3 Surface acidity and basicity characterization using probe molecules .....	33
3.4.4 Studies of the surface redox behavior .....	34
<b>References</b> .....	<b>34</b>

The optimal use of heterogeneous catalysts implies a deep knowledge of their properties. Only in this case, the mechanism of their activity can be understood to some extent, as the possibility of their improvements is open and the understanding of



their deactivation phenomena is possible. In this chapter, we will give an overview of the most common techniques allowing the characterization of a real catalyst.<sup>1</sup>

A number of other, sometimes very sophisticated, techniques have been largely used to investigate the nature of catalytic surfaces and of the phenomena involved in adsorption and catalysis. They need, however, the preparation of particular forms of materials such as in the case of the several surface science techniques, using e.g., monocrystal surfaces. Although the relevance of these studies is very high, these techniques cannot be applied to real catalyst powders, and thus a “material gap” and sometimes also a “conditions gap” exist between these studies and real catalyst application. We will summarize in this chapter the more common and available techniques that can be applied to real catalytic powders.

---

### 3.1 Elemental composition of heterogeneous catalysts

The most basic information on the solid materials concerns their element composition. We may note here that many catalytic materials are very complex. In particular, real commercial catalysts can contain together few predominant element components, a long list of elements, most of which at trace levels are added as promoters or stabilizers. On the other hand, care must be devoted to the presence of impurities, e.g. the residuals of precipitating agents such as alkali, or the counter-ions in ions deposition and impregnation (e.g. chloride ions from metal chlorides).

#### 3.1.1 Atomic absorption and emission spectroscopies

The main techniques for elemental analysis of solids are atomic absorption and atomic emission spectroscopy and X-ray fluorescence (XRF). In both atomic absorption and emission spectroscopies, the matter is vaporized and atomized or ionized by heating in furnaces or using inductively coupled plasma (ICP) technique. Thus, solid materials must usually first be dissolved to be analyzed. In the case of atomic absorption spectroscopy, the analysis of an element at a time is performed, with lamps that emit characteristic radiation of that element or, rarely, a few elements. In the case of atomic emission spectroscopy, mostly coupled with ICP and denoted as ICP–OES (optical emission spectroscopy<sup>2</sup>), the radiation emitted by the vaporized and excited atoms or ions is analyzed. The elements are identified by their typical electronic transitions and their abundance quantified by the Lambert Beer law and/or using calibration data.

#### 3.1.2 Inductively coupled plasma–mass spectrometry

Also in inductively coupled plasma–mass spectrometry (ICP–MS) technique liquid samples must be introduced. The plasma dries the aerosol, dissociates the molecules, and then removes an electron from the components, thereby forming singly-charged ions, which are directed into a quadrupole mass spectrometer that rapidly scans the

mass range. The ICP–MS instrument measures most of the elements in the periodic table with detection limits at or below the ppt range and also allows isotopic analysis.<sup>3</sup>

### 3.1.3 X-ray fluorescence

The X-rays (XR) are those emitted during the decay of an electron from an outer to an inner level. It applies only to atoms heavier than the Neon. The emission of primary XR is obtained by bombarding a metal (Ag, Mo, W...) with electrons accelerated by a potential of 30,000–50,000 V.

In the XR fluorescence technique, the primary XR are absorbed by the material and cause the expulsion of an electron inside, and the subsequent decay of an electron from one level to a more internal one, with XR emission for secondary fluorescence. The analysis of secondary XR allows the chemical analysis of the sample as the atoms heavier than Ne are concerned. X-ray fluorescence identifies also spent catalyst poisoning by elements such as sulfur, chlorine or unwanted heavy metals that may have caused catalyst failure in service. XR fluorescence does not need any sample preparation.<sup>4</sup>

### 3.1.4 Energy-dispersive X-ray analysis

Energy-dispersive X-ray analysis (EDX) analysis also analyses the emission of XR from atoms. It is usually performed together with scanning electron microscopy analyses (see below), thus being possibly applied to the surface of single particles in the case of complex materials. The electron beam stimulates the atoms in the sample with uniform energy, and they instantaneously send out XR of specific energies for each element, the so-called characteristic XR. EDX mapping provides in addition to the conventional SEM image a meaningful picture of the element distribution of a surface. The acquisition times for a satisfactory resolution and noise performance can take from 30 min to 12 h, because a complete EDX spectrum is made from each image point. EDX can also be coupled with transmission electron microscopy analysis, allowing a bulk chemical analysis too.

---

## 3.2 Structural properties of inorganic materials and its characterization

As for any kind of solids, the bulk structure of catalyst may be, in principle, defined as “ordered” or crystalline or “disordered” or amorphous. Amorphous solids differ from crystalline solids because no long-range order occurs. However, real catalysts are frequently very complex multiphase and metastable solids, and thus ordered and disordered structures may coexist. Additionally, order and disorder may be associated not only with structure but also with porosity and particle morphology.

### 3.2.1 XR diffraction

XRD allows to identify the crystal structure of a material or to highlight its amorphous state.<sup>5</sup> The common instrument consists essentially of three parts: an XR beam source; a goniometer the center of which is mounted and rotates the sample, placed on a flat plate, with a speed of the order of half a degree per minute; a detector, connected to a system of signal recording, which rotates with angular speed twice that of the sample. The phenomenon of coherent diffusion or diffraction implies a change of direction to the propagation of the beam that does not involve a change of the wavelength mode  $\lambda$  (no loss of energy). This behavior is explained in terms of reflection and subsequent interference between the electromagnetic radiation giving rise to positive or negative interference, depending on whether they are in phase or not due to their path difference. The path difference will depend according to the angle at which the rays are made to affect (angle of incidence,  $\theta$ ) and collected (diffraction angle  $2\theta$ ) and by the pitch of the grating,  $d$ , which in this case corresponds to the distances between atom layers in the crystal (crystal planes). The conditions of positive interference are dictated by Bragg's Law,  $n\lambda = 2d \sin \theta$ . The output beams are collected onto a screen located at a distance practically infinite compared to their wavelengths.

In practice, the detection of diffraction peaks reveals the presence of ordered structures, while their absence is due to lack of significant order. The  $2\theta$  position of the peak according to the Bragg's law allows to measure the distance  $d$  between the family of crystal planes.

Thus, the analysis of the overall pattern allows the determination of the crystal structure. Routine analysis is based on comparison of the observed pattern with those collected in the International Centre for Diffraction Data (ICDD) database.<sup>6</sup> Mathematical modeling such as the so-called Rietveld analysis allows a precise determination of atom positions in complex structures. Quantification of phases in multiphasic crystalline mixtures can be based on traditional methods with calibration mixtures, or using the Rietveld analysis. XRD analyses can also be performed in situ, i.e. under controlled conditions, at high temperature and under reaction conditions.<sup>7</sup> Small angle XRD ( $2\theta < 5^\circ$ ) allows to reveal the ordered porosity of some mesoporous materials, including the distance between pores and the size of the pores.<sup>8</sup>

### 3.2.2 Electron diffraction

Diffraction patterns of electrons can give, like for XR diffraction, structural informations. Low-energy electron diffraction is a surface technique applied to monocrystals, giving information on the surface geometry. Diffraction of part of the incident electrons may occur upon transmission electron microscopy (TEM) experiments.<sup>9,10</sup> Analogously as for XRD, the diffraction pattern of electrons depends on the crystal structure of the material and can be interpreted to produce information on it. The so-called selected area electron diffraction technique (SAD or SAED)

performed on TEM experiments allows analysis of particular areas of the material under study to confirm the crystal structure and reveal lattice matching, interfaces, twinning and certain crystalline defects. SAD of nanocrystals gives ring patterns analogous to those from XR powder diffraction, and can be used to identify texture and discriminate nanocrystalline from amorphous phases.

### 3.2.3 Neutron diffraction

XRD is not able to determine the position of hydrogens. The same structure analysis technique may be performed using neutrons.<sup>11</sup> In this case, the position of protons may also be detected. Recent applications of neutron diffraction techniques with Rietveld analyses have been reported concerning the determination of the structure of gallium oxides and hydroxides<sup>12</sup> and the evolution of hydrotalcite structure (Mg–Al layered hydroxyl-carbonate) upon calcination.<sup>13</sup> Neutron diffractions allows the determination of the position of protons in zeolites and their interaction with water.<sup>14</sup>

### 3.2.4 Vibrational spectroscopies

Vibrational spectroscopies (in particular Infrared (IR) spectroscopy<sup>15</sup> and Raman spectroscopy<sup>16</sup>) allow to have information on the structure of both amorphous and crystalline catalytic materials.

In the case of crystalline inorganic materials, the number of vibrational modes may be counted from the number of atoms in the smallest (primitive) Bravais cell, their activity in IR and Raman and their position can be forecasted assuming an hypothetical or known crystal structure.

The analysis of the symmetry of the crystal (i.e., the space and factor groups), according to the site symmetry of every atom, allows the determination of the irreducible representation of the total modes and, after the subtraction of the acoustic modes, the irreducible representation of the vibrational (or “optical”) modes can be obtained. This means that the number of vibrational modes belonging to the symmetry species associated with the molecular or crystal symmetry can be counted. Consequently, the number of active modes can be counted, according to the symmetry selection rules of the different techniques (in particular IR and Raman).

Every vibrational mode is in principle due to motions of the entire primitive unit cell as a whole. In principle, crystal dynamics calculations could define rigorously the motions of every atom of the chemical species upon a vibrational mode. This approach gives rise to a very complex picture (at least for large and complex unit cells), so that the results are sometimes not easily interpreted and comparison between the vibrational behavior of similar species is difficult.

However, a group approximation can be used. In fact, the vibrational modes can often be approximatively attributed to the movements of small groups of atoms or bonds. This is possible in particular if very different bonds are present in the molecule, so that the coupling of their movements is negligible. In this way, it is possible

to “dissect” the chemical species under study into “pieces” and to consider separately the vibrations of groups of few atoms. As for example, in the case of salt-like oxides (e.g., iron molybdate) the vibration of the covalently bonded anion (tetrahedral molybdate) can be quite easily distinguished from those involving the cations and its coordination sphere.

In the case of crystalline solids, more than one equivalent structural unit may be present in the primitive cell. This results in splittings of the fundamental vibrational modes of these units. In the case of many crystalline solid materials, “covalent” units (e.g., oxo-anions for oxo-salts) are present, together with other groups bonded by ionic bonds (e.g., the cations in the oxo-salts). According to the above group approximation, the internal vibrations of the covalent units can be considered separately from their external vibrations (hindered rotations and translations of the group that finally contribute to the lattice vibrations and to the acoustic modes of the unit cell) and those of the other units. If a number of covalent structural units are present in the primitive cell, their internal modes split in consequence. The Raman and IR activity of the different vibrational modes can be considered and forecasted. When the unit cell is centrosymmetric the mutual exclusion rule is valid, so that Raman-active modes are IR-inactive and vice versa. For noncentrosymmetric unit cells, modes that are both Raman and IR active can occur. IR-active modes additionally undergo the translational optical mode/longitudinal optical mode (TO/LO) splitting that may make more complex the identification of the vibrational modes of crystalline solids, but may give some particle morphology information. In practice, for well-crystallized material, the joint use of IR and Raman skeletal spectroscopies can give a very precise structural picture.

Additionally, vibrational spectroscopies are applicable to amorphous materials and are particularly helpful in this field. In fact, IR and Raman spectra reveal the vibrations also for disordered species, including liquid molecular species, glasses and amorphous solids.

### 3.2.5 X-ray absorption spectroscopy

X-ray absorption spectroscopy (XAS) is another typical spectroscopy where absorption of a radiation is monitored as a function of photon energy.<sup>17,18</sup> The most used kind of XAS is recorded in the K-edge region, i.e., the region of the energy of the s electron levels, which is further divided in three sections. The so-called X-ray absorption near-edge structure (XANES) region may be further subdivided in the preedge region, which is, for transition metals, associated with  $1s \rightarrow 3d$  electron transitions, and the edge region where  $1s \rightarrow 4s, 4p$  electron transitions occur. At higher energy, the extended X-ray absorption fine structures (EXAFS) occur. The position of the edge primarily depends on the absorbing element. XANES has a very high level of complex multiple scattering paths, which included electronic and structural components. Thus, the shape of the absorption is informative on

the environment of the atom. The preedge region is informative on the coordination, being forbidden in the octahedral coordination. Also, the shape of the EXAFS is informative on the neighborings of the atom.

The experimental data for a compound with unknown structure are compared with those of known compounds of the same element. On the other hand, the spectra may also be calculated and fitting different models analyzed. Amorphous materials can be studied just as crystalline ones.

### 3.2.6 UV–vis spectroscopic data

UV–vis spectroscopy reveals the electronic absorptions by a powder in the Ultra-violet and visible region.<sup>19,20</sup> While electronic conductors absorb in the entire near-UV–vis region, semiconductors can give rise to absorption edges in the visible region or in the UV region, due to valence-to-conduction band electron transitions. Isolated bands in these regions can also come from anion-to-cation charge transfer transitions as well as d–d transitions of isolated transition metal cations. Insulators are mostly transparent in the overall near-UV and visible region. In practice, UV–vis spectroscopy generally performed on solid powders using the diffused reflectance technique gives information on the electronic properties of a solid and in the presence, coordination state and oxidation state of transition metal cations.

### 3.2.7 Magic angle spinning Nuclear Magnetic Resonance (NMR) techniques

Nuclear Magnetic Resonance (NMR)<sup>21</sup> reveals the excitation of the spin state of some nuclei in the presence of a magnetic field. NMR techniques may be applied to any nucleus having nuclear spin  $>0$ . Thus, this technique may be applied not only to  $^1\text{H}$  ( $S = 1/2$ ), but also to  $^2\text{H}$  ( $S = 1$ ),  $^{11}\text{B}$  ( $S = 3/2$ ),  $^{13}\text{C}$  ( $S = 1/2$ ),  $^{14}\text{N}$  ( $S = 1$ ),  $^{15}\text{N}$  ( $S = 1/2$ ),  $^{17}\text{O}$  ( $S = 3/2$ ),  $^{19}\text{F}$  ( $S = 1/2$ ),  $^{23}\text{Na}$  ( $S = 3/2$ ),  $^{27}\text{Al}$  ( $S = 5/2$ ),  $^{29}\text{Si}$  ( $S = 1/2$ ),  $^{31}\text{P}$  ( $S = 1/2$ ),  $^{51}\text{V}$  ( $S = 7/2$ ).

To avoid line broadening in the solid state, the samples must spin about an axis inclined at  $54^\circ 44'$  (“magic angle”) which is the  $\theta$  value at which  $3 \cos^2 \theta - 1 = 0$ . Magic Angle Spinning (MAS) NMR studies of  $^{27}\text{Al}$  (which is largely the most abundant Al isotope, 99.9%) and  $^{29}\text{Si}$  (which is only 4.67% of natural silicon) that can be applied are very important for the characterization of aluminas, silicas, silica-aluminas, silicates and aluminosilicates including zeolites. Similarly, MAS NMR studies of  $^{51}\text{V}$ ,  $^{31}\text{P}$ ,  $^{11}\text{B}$  are very useful to characterize vanadates, phosphates, borates, etc. Thus, solid-state NMR techniques are very useful in the field of characterization of heterogeneous catalysts.<sup>22–24</sup> Proton NMR<sup>25</sup> is informative in the observation of protons in zeolites and at the surface of any other materials.  $^1\text{H}$ ,  $^{13}\text{C}$ ,  $^{14}\text{N}$  and  $^{31}\text{P}$  MAS NMR studies are also used when organic molecules such as hydrocarbons, amines and phosphines are used as adsorbed probe molecules, in the case of surface acidity and basicity characterization (see chapter 5.3.6).

### 3.3 Morphology characterization

#### 3.3.1 Measurement of the surface area and analysis of porosity

The measurement of the surface area of a solid, usually expressed as square meters of surface area per gram of solid,  $\text{m}^2/\text{g}$ , is one of the main parameters that characterize a powder, particularly catalysts and adsorbents. This fundamental parameter is measured by means of the measure of the physical adsorption of inert gas,<sup>26</sup> most commonly by measuring the physical adsorption and desorption of nitrogen at liquid nitrogen temperature (77 K). The specific volume of nitrogen adsorbed allows the determination of the specific surface area (Brunauer, Emmet and Teller method, BET), the specific volume of mesopores (most commonly with the Barrett–Joyner–Halenda method, BJH) and the specific volume of micropores ( $t$ -Plot method).

By the volumetric measurements of nitrogen adsorption/desorption at 77 K, the adsorption/desorption isotherms are obtained, i.e., the curves  $V_{\text{ads}}$  versus  $P/P_0$  ( $0 < P/P_0 < 1$ ), while, if also desorption is measured, hysteresis loops may be observed, which give information on the nature of porosity. Different isotherms shapes inform on the adsorption strength and porosity too. The BET equation is

$$P/[V_{\text{ads}}(P_0 - P)] = 1/V_m C + (C - 1)P/V_m C P_0$$

where  $P$  is the actual nitrogen pressure lower than the saturation pressure  $P_0$ , and the constant  $C$  is obtainable from the rate constants of adsorption and desorption. From this equation, the theoretical volume of an adsorbed monomolecular layer ( $V_m$ ) can be calculated.

Assuming the area of the nitrogen molecule  $\sigma = 16.2 \text{ \AA}^2$ , the surface area of the solid, usually normalized to unit mass of adsorbent that is in  $\text{m}^2/\text{g}$ , is obtained from the adsorbed nitrogen amount.

A faster surface area measurement, usually not affected by relevant error, consists in the single-point measurement. In this case, the adsorbed amount at  $P/P_0 = 0.3$  is taken, because in these conditions the adsorbed amount is approximately that of the adsorbed monolayer.

The total pore volume is calculated from the total amount of nitrogen adsorbed at  $P/P_0 \sim 1$ ,  $n_{\text{ad}}$ , with the formula  $V_p = n_{\text{ad}} \cdot V_{\text{mol}}$ , i.e., is the volume of adsorbed liquid nitrogen at saturation. The average pore size can be estimated from the pore volume  $V_p$  and the surface area  $S_{\text{BET}}$ . Assuming cylindrical pore geometry (type A hysteresis), average pore radius ( $r_p$ ) can be expressed as:  $r_p = 2V_p/S_{\text{BET}}$ . These simple equations allow a rough evaluation of the pore properties of powders.

A number of different mathematical approaches and gas adsorption models can be applied to a full characterization of the pore structure of powders. According to International Union of Pure and Applied Chemistry (IUPAC), the pores are characterized by their size into three categories:

micropores  $< 2 \text{ nm} = 20 \text{ \AA}$  < mesopores  $< 50 \text{ nm} = 500 \text{ \AA}$  < macropores.

Adsorbates other than nitrogen, such as e.g., Ar and  $\text{CO}_2$ , can also give more information on the porous structure of a catalyst.

### 3.3.2 Crystal size measurement

The crystal size for crystalline materials can be calculated from the breadth of the XRD peaks. The Scherrer formula,<sup>27,28</sup> proposed in 1918,  $B(2\theta) = K\lambda/L \cos \theta$ , where  $B(2\theta)$  is the full width at half maximum (FWHM) measured in  $2\theta$  units,  $\lambda$  is the XR used wavelength, and the K constant (Scherrer constant) is 0.94 for FWHM of spherical crystals with cubic symmetry, allows a rough but easy evaluation of  $L$ , the crystal size. The application of the Scherrer formula is a very easy and rapid procedure. Profile fitting analyses can give more accurate results. Actually, it has been shown that many factors may contribute to the observed XRD peak profile. On the other hand, interesting data can be sometimes obtained by comparing crystal size analysis by XRD with those arising from electron microscopies (SEM and/or TEM) as well as particle size that can be measured from surface area measurements.

### 3.3.3 Electron microscopies

#### 3.3.3.1 Scanning electron microscopy

The scanning electron microscope (SEM) uses a focused beam of high-energy electrons (30–50 kV) to generate a variety of signals at the surface of solid sample. When the incident electrons are decelerated on the solid sample, signals are generated including secondary electrons (that produce SEM images), backscattered electrons (BSE), diffracted backscattered electrons (EBSD that are used to determine crystal structures and orientations of minerals), photons (characteristic XR that are used for elemental analysis EDX and continuum XR), visible light and heat. Secondary electrons and backscattered electrons are commonly used for imaging samples: secondary electrons are most valuable for showing morphology and topography on samples and backscattered electrons are most valuable for illustrating contrasts in composition in multiphase samples (i.e., for rapid phase discrimination). Areas ranging from approximately 1 cm–5  $\mu\text{m}$  in width can be imaged in a scanning mode using conventional SEM techniques (magnification ranging from 20 $\times$  to approximately 30,000 $\times$ , spatial resolution of 50–100 nm).

#### 3.3.3.2 Field-emission scanning electron microscopy

A field-emission cathode in the electron gun of a scanning electron microscope provides narrower probing beams at low as well as high electron energy, resulting in both improved spatial resolution and minimized sample charging and damage. Field-emission scanning electron microscopy (FESEM) produces clearer, less electrostatically distorted images with spatial resolution down to 1.5 nm. That's three to six times better than conventional SEM. Smaller-area contamination spots can be examined at electron accelerating voltages compatible with energy dispersive XR spectroscopy. Reduced penetration of low kinetic energy electrons probes closer to the immediate material surface.

#### 3.3.3.3 Transmission electron microscopy

In the transmission electron microscope,<sup>9,29</sup> a scheme completely analogous to that of the ordinary optical microscope is used, except that highly accelerated electron



beams are used (200–300 kV) instead of light. The incident beam is generated from a tungsten filament and accelerated by a potential difference (electron gun). The focusing of the beam is entrusted to a complex series of electromagnetic lenses, generally six to eight, consisting of electromagnetic windings arranged symmetrically with respect to the incident beam. All must operate in ultra high vacuum, prepared by a series of pumps. The beam goes through the sample. The image is formed by the interference of the diffracted beams with the direct beam (phase contrast). If the point resolution of the microscope is sufficiently high and a suitable crystalline sample oriented along a zone axis, then high-resolution TEM (HRTEM) images are obtained. In many cases, the atomic structure of a specimen can directly be investigated by HRTEM.

HRTEM allows a precise image of the solid particles to be formed, showing also the packing of atoms in the interior. The distance between crystal planes can be precisely measured and the rough geometry of the structure can be evidenced. Upon the measurement, a parallel electron diffraction image can be produced (see chapter 3.2.2). Thus, HRTEM gives information of both structure and morphology of single particles. An obvious limit of this analysis, due to its very high resolution, is that the singly analyzed particle or detail can be not representative of the overall material.

#### **3.3.3.4 Scanning transmission electron microscopy**

A scanning transmission electron microscope (STEM)<sup>30</sup> is a transmission electron microscope (TEM) allowing focusing the electron beam into a narrow spot that is scanned over the sample. This allows mapping by energy dispersive X-ray (EDX) spectroscopy, electron energy loss spectroscopy and annular dark-field imaging. These signals can be obtained simultaneously, allowing direct correlation of image and quantitative data. By using an STEM and a high-angle detector (high-angle angular dark field STEM, HAAD-STEM), it is possible to form atomic resolution images where the contrast is directly related to the atomic number (*z*-contrast image). HAAD-STEM allows the observation of heavy metal species such as gold small clusters in supported catalysts<sup>31</sup> and also supported tungstate species on WO<sub>3</sub>/ZrO<sub>2</sub> catalysts.<sup>32</sup>

---

### **3.4 Analysis of the surface structure and composition**

#### **3.4.1 X-ray photoelectron spectroscopy**

X-ray photoelectron spectroscopy (XPS) is an application of the photoelectric effect, allowing the elemental analysis on the surface of a solid.<sup>33,34</sup> The sample is illuminated by an XR source and, as a result of this, an electron belonging to the element is excited and escapes into the vacuum. From the energy of the photoelectrons, their binding energies are calculated by subtracting the work function constant. Thus, the nature of the element is revealed. The binding energy for a family of electrons of an element significantly depends on the environment and, in particular, from the oxidation state of the element. Thus, the oxidation state is also revealed.<sup>35</sup>

A quantitative analysis of the different elements exposed at the surface of the solid can also be calculated. Thus, a detailed qualitative and quantitative surface elemental analysis is obtained. The normal technique implies ultra-high vacuum, and this limits the reliability of the results for easily reducible or instable elements. Recently, in situ XPS allows the analysis to be performed under small gas pressure.<sup>36</sup>

### 3.4.2 Direct surface analysis by conventional spectroscopies

Several spectroscopies may distinguish surface from bulk species due to the modification of spectroscopic features by adsorption/desorption of molecules from gas phase such as water adsorption/drying and by reduction/oxidation treatments.

IR spectroscopy performed on neat powders without any binder allow some catalytic materials to reveal directly the presence at the surface of some active bonds. Among the active species, this technique allows the detection of surface hydroxyl groups usually present on oxide surfaces, from OH stretching modes, and of oxo-anions such as carbonates, sulphates, vanadates, molybdates, wolframates, chromates, perhenates, etc. from their M–O multiple bond stretchings.<sup>15</sup> The presence at the surface of covalent oxide species vanadates, molybdates, wolframates, chromates, perhenates is also detected efficiently by Raman spectroscopy,<sup>37,38</sup> because of their strong Raman scattering effect. UV–vis spectroscopy can also give information on the location at the surface of metal cations. Their typical absorption in the UV–vis region, due to charge transfer or d–d transitions,<sup>20</sup> is in fact dependent on the hydration state (thus depending from outgassing conditions) or the adsorption of molecules if they are located at the surface. Similarly, <sup>51</sup>V and <sup>93</sup>Nb MAS NMR allows the investigation of surface vanadate and niobate species,<sup>39</sup> while <sup>1</sup>H MAS NMR allows the detection of surface hydroxide species.<sup>23</sup>

Another technique that is mostly used as a surface sensitive technique in the catalysis field is electron spin resonance, also called electron paramagnetic resonance (EPR),<sup>40–42</sup> which can be successfully applied to paramagnetic species such as V<sup>4+</sup> and Co<sup>2+</sup> species due to their hyperfine interaction with nuclear spin. This technique is analogous to NMR but involves the spin-state excitation of the electron of a paramagnetic species.

### 3.4.3 Surface acidity and basicity characterization using probe molecules

As it will be detailed in Chapter 5, several techniques allow to reveal the presence of acidic sites (of the Lewis and of the Brønsted type) and of basic sites at the surface on a solid material. Most of these techniques are “indirect”, i.e., based on the use of probe molecules and the observation of their adsorption and desorption. Different spectroscopies (IR, Raman, NMR, EPR) can be applied to adsorbed probe molecules. Additionally, calorimetric and volumetric adsorption and temperature programmed desorption techniques allow the characterization of the surface properties, thus giving information on the surface composition.

### 3.4.4 Studies of the surface redox behavior

Molecular probes can also give information on the oxidation state of surface metallic species. IR studies of adsorbed carbon monoxide reveal the location on the surface, oxidation state, coordination state and sometimes also agglomeration state of metal species (cationic or neutral) at the surface of solids.<sup>43</sup> Temperature-programmed reduction (TPR) and temperature-programmed oxidation also reveal the surface redox properties of a solid.<sup>44</sup> TPR is mostly performed flowing hydrogen or H<sub>2</sub>/N<sub>2</sub> mixtures during programmed heating and detecting at what temperature H<sub>2</sub> is consumed and to what extent. This allows to calculate how many surface species are reduced and to evaluate how easy is their reduction. Similarly, by flowing oxygen and looking at its consumption, the oxidation of reduced sites will be monitored (Temperature Programmed Oxidation, TPO).

---

## References

1. Che M, Vedrine JC, editors. *Characterization of solid materials and heterogeneous catalysts from structure to surface reactivity*. Wiley; 2012.
2. Rüdell H, Kösters J, Schörmann J. [http://www.ime.fraunhofer.de/content/dam/ime/en/documents/AE/SOP\\_ICP-OES\\_en.pdf](http://www.ime.fraunhofer.de/content/dam/ime/en/documents/AE/SOP_ICP-OES_en.pdf); [accessed 24.03.14].
3. Perkin Elmer. [http://www.perkinelmer.com/CMSResources/Images/44-74849tch\\_icpmsthirtyminuteguide.pdf](http://www.perkinelmer.com/CMSResources/Images/44-74849tch_icpmsthirtyminuteguide.pdf); [accessed 24.03.14].
4. Oxford Instruments. <http://www.oxford-instruments.com/businesses/industrial-products/industrial-analysis/xrf>; [accessed 24.03.14].
5. Perego G. *Catal Today* 1998;**41**:251–9.
6. <http://www.icdd.com/products/index.htm>; [accessed 24.03.14].
7. Schlögl R. In: Gates BC, Knozinger H, Jentoft F, editors. *Advances in catalysis*, vol. 52. Elsevier; 2009. pp. 273–338.
8. Ishii Y, Nishiwaki Y, Al-Zubaidi A, Kawasaki S. *J Phys Chem C* 2013;**117**(35): 18120–30.
9. Zhou W. In: Jackson SD, Hargreaves JSJ, editors. *Metal oxide catalysis*, vol. 1. Wiley-VCH; 2009. pp. 443–83.
10. Viladot D, Véron M, Gemmi M, Peiró F, Portillo J, Estradé S, et al. *J Microsc* 2013; **252**(1):23–34.
11. Wenk H-R. *JOM* 2012;**64**(1):127–37.
12. Playford HY, Hannon AC, Barney ER, Walton RI. *Chemistry* 2013;**19**(8):2803–13.
13. Mourad MCD, Mokhtar M, Tucker MG, Barney ER, Smith RI, Alyoubi AO, et al. *J Mater Chem* 2011;**21**(39):15479–85.
14. Alberti A, Martucci A. *J Phys Chem C* 2010;**114**(17):7767–73.
15. Busca G. Use of infrared spectroscopy methods in the field of heterogeneous catalysis by metal oxides. In: Jackson SD, Hargreaves JSJ, editors. *Metal oxide catalysis*, vol. 1. Wiley-VCH; 2009. pp. 95–175.
16. Fan F, Feng Z, Li C. In: Che M, Vedrine JC, editors. *Characterization of solid materials and heterogeneous catalysts from structure to surface reactivity*. Wiley; 2012. p. 49.
17. Stokenhuber M. In: Jackson SD, Hargreaves JSJ, editors. *Metal oxide catalysis*, vol. 1. Wiley-VCH; 2009. pp. 299–321.

18. Van Bokhoven JA, editor. *Recent developments in X-ray absorption spectroscopy*. *Phys Chem Chem Phys*, vol. 12; 2010. pp. 5502–716 [special issue].
19. Martra G, Gianotti E, Coluccia S. In: Jackson SD, Hargreaves JSJ, editors. *Metal oxide catalysis*, vol. 1. Wiley-VCH; 2009. pp. 51–94.
20. Schoonheydt RA. *Chem Soc Rev* 2010;**39**(12):5051–66.
21. Hanna JV, Smith ME. *Solid State Nucl Magn Reson* 2010;**38**:1–18.
22. Hunger M, Wang W. *Adv Catal* 2006;**50**:149–225.
23. Jiang Y, Huang J, Dai W, Hunger M. *Solid State Nucl Magn Reson* 2011;**39**(3–4): 116–41.
24. Gladden LF, Lutecki M, McGregor J. In: Che M, Vedrine JC, editors. *Characterization of solid materials and heterogeneous catalysts from structure to surface reactivity*. Wiley; 2012. p. 289.
25. Brown SP. *Solid State Nucl Magn Reson* 2012;**41**:1–27.
- 26a. Llewellyn PL, Bloch E, Bourrelli S. In: Che M, Vedrine JC, editors. *Characterization of solid materials and heterogeneous catalysts from structure to surface reactivity*. Wiley; 2012. p. 853.
- 26b. Hammond KD, Conner WC. *Advan. Catal. Relat. Subj.* 2013;**56**:1–101.
27. Langford JJ, Wilson AJC. Scherrer after sixty years: a survey and some new results in the determination of crystallite size. *J Appl Cryst* 1978;**11**:p102–113.
28. Smilgies DM. *J Appl Crystallogr* December 1, 2009;**42**(Pt 6):1030–4.
29. Thomas JM, Ducati C. In: Che M, Vedrine JC, editors. *Characterization of solid materials and heterogeneous catalysts from structure to surface reactivity*. Wiley; 2012. p. 655.
30. Pennycook SJ, Nellist PD, editors. *Scanning transmission electron microscopy imaging and analysis*. Springer; 2011.
31. Akita T, Kohyama M, Haruta M. *Acc Chem Res* 2013;**46**(8):1773–82.
32. Zhou W, Wachs IE, Kiely CJ. *Curr Opin Solid State Mater Sci* 2012;**16**:10–22.
33. Teschner D, Vass EM, Schlogl R. In: Jackson SD, Hargreaves JSJ, editors. *Metal oxide catalysis*, vol. 1. Wiley-VCH; 2009. pp. 243–97.
34. Grünert W. In: Che M, Vedrine JC, editors. *Characterization of solid materials and heterogeneous catalysts from structure to surface reactivity*. Wiley; 2012. p. 537.
35. Riviere JC, Myhr S, editors. *Handbook of surface and interface analysis: methods for problem-solving*. Taylor and Francis; 2009. pp. 504–6.
36. Virnovskaia A, Jørgensen S, Hafizovic J, Prytz Ø, Kleimenov E, Hävecker M, et al. *Surf Sci* January 1, 2007;**601**(1):30–43.
37. Wachs IE, Roberts CA. *Chem Soc Rev* 2010;**39**(12):5002–17.
38. Wu Z, Kim HS, Stair PC. In: Jackson SD, Hargreaves JSJ, editors. *Metal oxide catalysis*, vol. 1. Wiley-VCH; 2009. pp. 177–94.
39. Lapina OB, Khabibulin DF, Shubin AA, Terskikh VV. *Prog Nucl Magn Reson Spectrosc* 2008;**53**(3):128–91.
40. Brückner A. *Adv Catal* 2007;**51**:265–308.
41. Murphy DM. In: Jackson SD, Hargreaves JSJ, editors. *Metal oxide catalysis*, vol. 1. Wiley-VCH; 2009. pp. 1–94.
42. Pietrzyk P, Sojka Z, Giamello E, Che M, Vedrine JC, editors. *Characterization of solid materials and heterogeneous catalysts from structure to surface reactivity*. Wiley; 2012. p. 343.
43. Hadjiivanov K, Vayssilov G. CO as a probe molecule in the characterization of oxide surfaces and zeolites. *Adv Catal* 2002;**47**:307–511.
44. Niemantsverdriet JW. *Spectroscopy in catalysis*. 3rd ed. Wiley; 2011. p. 11.

# Practical Application and Testing of Catalytic Materials: A Synthesis

## CHAPTER OUTLINE

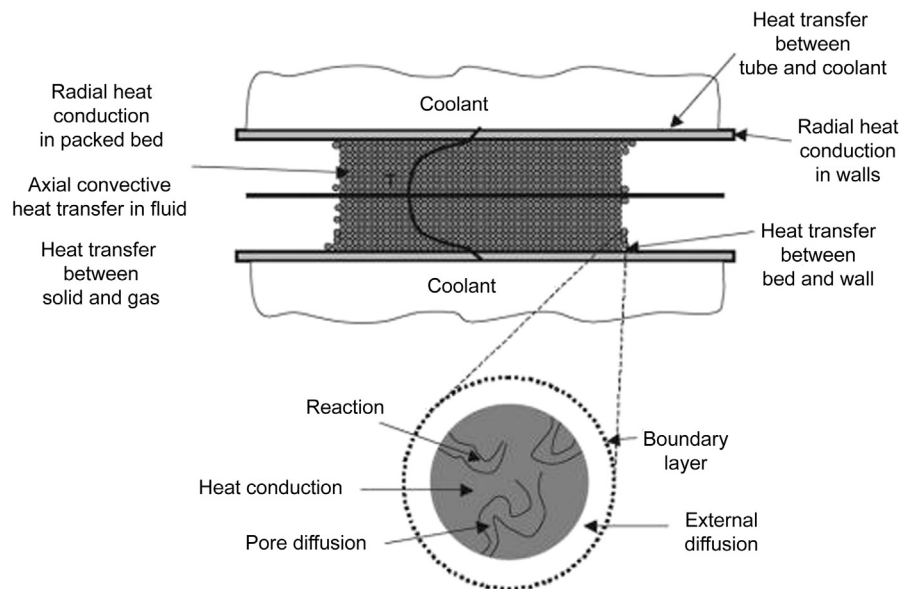
<b>4.1 Shaping of catalysts for industrial catalytic reactions .....</b>	<b>38</b>
<b>4.2 Industrial heterogeneous catalytic reactors .....</b>	<b>41</b>
4.2.1 Temperature control in catalytic reactors .....	41
4.2.2 Gas/solid and liquid/solid fixed-bed reactors .....	41
4.2.2.1 <i>Adiabatic fixed-bed catalytic reactors</i> .....	41
4.2.2.2 <i>Heated fixed-bed reactors for gas/solid endothermic reactions</i> .....	42
4.2.2.3 <i>Cooled fixed-bed reactors for gas/solid exothermic reactions</i> .....	42
4.2.2.4 <i>Cooled fixed-bed reactors for liquid/solid exothermic reactions</i> .....	45
4.2.2.5 <i>Catalytic distillation reactors</i> .....	45
4.2.3 Monolithic reactors.....	45
4.2.4 Catalytic membrane reactors .....	46
4.2.5 Gas/solid fluidized and transported bed reactors.....	46
4.2.6 Raiser reactors and circulating fluidized bed reactors .....	46
4.2.7 Slurry liquid/solid and gas/liquid/solid reactors .....	48
<b>4.3 Deactivation of solid catalysts .....</b>	<b>48</b>
4.3.1 Poisoning .....	50
4.3.2 Coking.....	50
4.3.3 Sintering .....	50
4.3.4 Phase transitions and solid-state reactions .....	51
4.3.5 Breaking of extrudates .....	51
4.3.6 Erosion or breaking of monoliths.....	51
<b>4.4 Regeneration of reversibly deactivated catalysts.....</b>	<b>51</b>
4.4.1 Techniques for regeneration .....	51
4.4.1.1 <i>Burning of coke</i> .....	51
4.4.1.2 <i>Hydrogenation</i> .....	52
4.4.1.3 <i>Washing or rejuvenation</i> .....	52
4.4.1.4 <i>Steaming</i> .....	52
4.4.2 Regeneration of catalysts and the reactors.....	52
<b>4.5 Laboratory evaluation of the catalytic activity .....</b>	<b>53</b>
<b>4.6 Operando methodologies.....</b>	<b>53</b>
<b>References .....</b>	<b>55</b>

### 4.1 Shaping of catalysts for industrial catalytic reactions

Solid catalysts mostly consist of fine powders. Industrial catalytic reactors are either fixed bed or fluid/slurry bed. In all cases, the fine powder used as such would produce important drawbacks.

If packed in fixed-bed reactors, powders tend to form high-density layers opposing the reactants flow, causing high pressure drops. Also, fine particles could be transported out of the reactor by the effluent flow. On the other hand, a number of transport phenomena occur in fixed catalytic beds (Figure 4.1<sup>1</sup>) that can limit and, in any case, may influence the reaction rate. These phenomena that can be taken into account in modeling of fixed-bed reactors<sup>2</sup> are actually influenced by particle or agglomerate size and shapes.

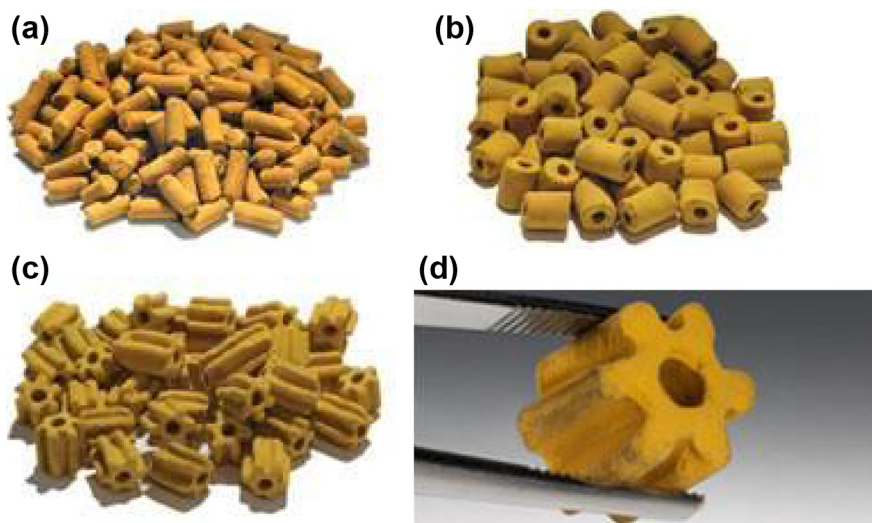
Thus, to optimize flow and transport conditions, solid catalysts are shaped in pellets by extrusion procedures, producing “extrudates”, which resist the reactant pressure and leave sufficient void fraction to limit pressure drops. Such extrudates and “miniliths” are formed by pushing a paste containing the catalyst through a die, followed by cutting, drying and calcining. In Figure 4.2, the different shapes of commercial catalyst extrudates for SO<sub>2</sub> to SO<sub>3</sub> oxidation reactions are shown (MECS<sup>®</sup> Sulfuric Acid Catalyst Products).<sup>3</sup>



**FIGURE 4.1**

Illustration of different transport phenomena on different scales in a packed-bed reactor.

*Reprinted with permission from Ref. 1.*

**FIGURE 4.2**

Sulphur dioxide oxidation catalysts: (a) high pressure drop for low gas-velocity converters; (b) medium pressure drop; (c and d) low pressure drop, MECS<sup>®</sup> Sulfuric Acid Catalyst Products.

*Reprinted with permission from the MECS-Dupont website.*

Another important factor, occurring in particular when multitubular reactors/exchangers are used, is to favor the heat transfer between the gas phase and the tube surface.<sup>4</sup> In fact, in heat exchange (either heating of the reactant mixture in the case of endothermic reactions, or cooling for exothermic reactions) occurs through the tube wall. The formation of a stationary gas film inside the tube wall that reduces the rate of heat transfer must be avoided. Using smaller catalyst particles reduces the thickness of the stationary gas film but increases pressure drops. Optimal behavior is obtained designing an optimal extrudate shape and size. In [Figure 4.3](#) commercial extrudates of methane steam-reforming catalysts and their disposition in the tubular reactor are shown (Johnson Matthey).

Catalysts for moving or fluid bed reactors should resist the attrition due to the catalyst movement.<sup>5</sup> To this purpose, particular agglomeration and extrusion procedures must be applied to form mechanically resistant microspheres.

Extrudates may actually be formed using mixtures of the real catalyst powder with additive powders such as binders (frequently alumina or silica-based inorganics), lubricants, plasticizers, and compaction agents. Among the latter, organics such as stearic acid, oleic acid, naphthenic acid, oils, paraffins, stearates, polymers may be used. Additional inorganic components may also be present, as poison traps as well as graphite as a shaping agent.<sup>6</sup> This is the case, e.g., of Fluid Catalytic-Cracking catalysts where alumina powders are added to trap Ni arising from the feed impurities. These materials protect the catalyst from the formation of Ni metal that would cause unwanted dehydrogenations. Binders may have a relevant role in

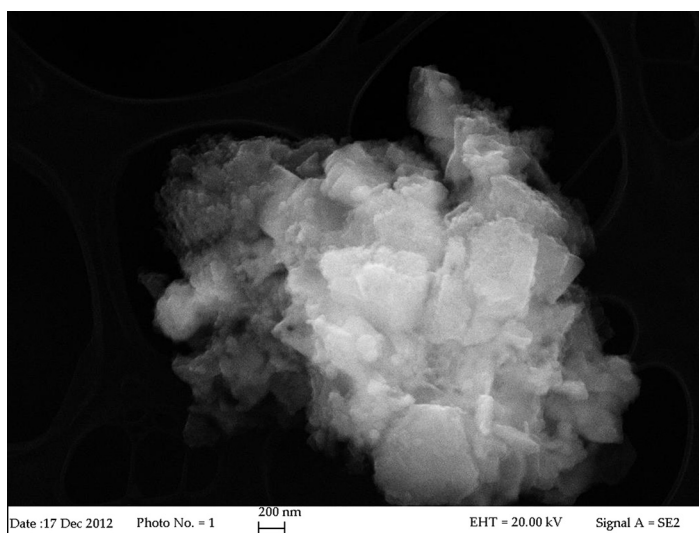
**FIGURE 4.3**

Shape of extrudate catalysts for methane steam reforming and their accommodation in the reactor tube (Johnson Matthey).

*Reprinted with permission from the Johnson Matthey website.*

the catalytic phenomena and, in particular, in the diffusion of reactants and products in the bed.<sup>7</sup> Interparticle mesoporosity may form between catalyst and binder particles, and sums to catalyst and binder intraparticle micro- or mesoporosity.

In [Figure 4.4](#), a Field Emission Scanning Electron Micrograph (FESEM) of a particle aggregate of a fluid catalytic cracking (FCC) catalyst is shown, where the

**FIGURE 4.4**

FESEM micrograph of an agglomerate particle of a fluid catalytic cracking catalyst.



presence of different powders is quite evident. Energy Dispersive X Ray analysis (EDX) allows to reveal the presence of Si, Al and La in some point, providing evidence of Rare Earth X zeolite, Si:Al 1:1 in other, providing evidence of kaolin, and of Al only and Si only spots, showing that alumina and silica particles are also present in the mix. Alumina can work as a binder as well as a Ni trap.<sup>8,9</sup>

---

## 4.2 Industrial heterogeneous catalytic reactors

Industrial catalytic reactors differ for several reasons: the catalyst bed may be fixed, stirred, ebullated, fluidized, transported and circulated. The reactor may be adiabatic, cooled or heated. The shape can be tubular, multitubular, tank, etc.<sup>10–12</sup> In the following, a small summary of industrial reactor configurations is reported.

### 4.2.1 Temperature control in catalytic reactors

In the most common case, the chemical reactor is fed with the reactant mixture previously preheated to allow the reaction rate be sufficiently high in all points of the reactor. The temperature limits (lower and higher) forecasted to be obtained in a working catalyst bed are determined either from the behavior of the catalytic material itself, or by thermodynamics. The lowest temperature to which the bed is designed to work is that at which the minimum useful reaction rate is obtained. The highest temperature forecasted for the bed is frequently determined, to care for the thermal stability of the catalyst in the entire bed; in fact catalytic materials tend to lose progressively catalytic activity above a high temperature limit, due to starting of solid-state phenomena, such as surface area loss by sintering, phase transitions, volatilization of some constituent, etc. For exothermic reactions, the high-temperature limit may also be determined by thermodynamics that can become too unfavored above a temperature limit.

### 4.2.2 Gas/solid and liquid/solid fixed-bed reactors

In the perhaps most simple case, heterogeneous catalysts are stored in one or more fixed beds in a tubular or multitubular reactor, the fluid reactant mixture being fed either axial downflow, axial upflow, radial or radial/axial.<sup>13</sup> Normally, the axial flow causes more pressure losses while the radial flow can give rise to preferential paths and may not allow the appropriate use of the first part of the catalytic bed. The reactor configuration strongly depends on the type of the reaction, with particular relation to the thermal and equilibrium behavior and the optimal time of contact with the catalyst bed.

#### 4.2.2.1 Adiabatic fixed-bed catalytic reactors

Adiabatic reactors, i.e., fixed-bed tubular reactors without any heating or cooling, are used for reactions having a small  $\Delta H$ ; in this case the actual temperatures in the bed do not bypass the lower or the higher acceptable temperatures, for

endothermic and exothermic reactions, respectively, even without heat exchange. Heating and cooling can be performed before or after the adiabatic reactor. Several adiabatic reactors can be used in series with heating or cooling steps in between, to perform endothermic and exothermic reactions, respectively, and fulfilling both temperature limits in the beds and contact time requirements.

#### 4.2.2.2 Heated fixed-bed reactors for gas/solid endothermic reactions

For typical endothermic reactions, tubular reactors filled with the catalyst may be heated from outside in the radiant section of a combustion oven. In Figure 4.5<sup>14</sup> a schematic of the Haldor Topsøe reformer furnace is shown, where the tubes are located in a furnace with wall burners, in the right side of the structure. Alternatively, the tubes may be heated by hot fluids, such as combustion gases in the convective section of a combustion oven. The tube diameter is thin, to limit temperature gradients, and thus several tubes (sometimes hundreds) are needed for high productivity reactors.

#### 4.2.2.3 Cooled fixed-bed reactors for gas/solid exothermic reactions

Exothermic equilibrium reactions must be carried out at the lowest temperature made possible by the activity of the catalyst, because these are the conditions in

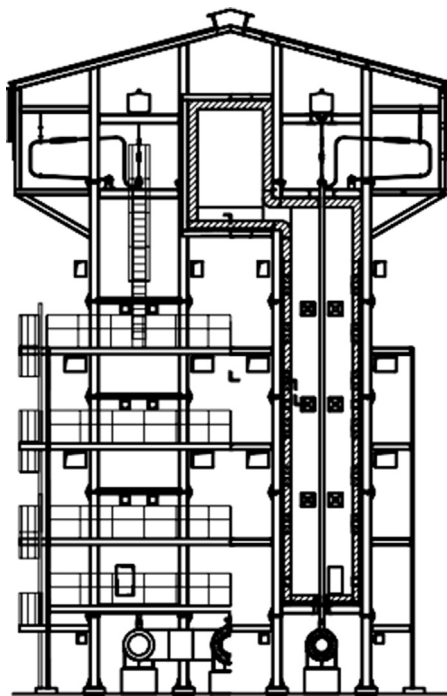


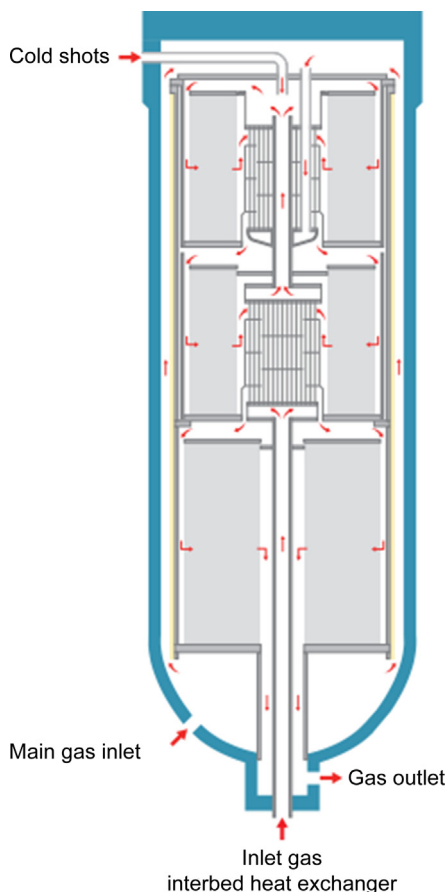
FIGURE 4.5

Schematic drawing of Haldor Topsoe high-flux steam reformer furnace.

Reprinted with permission from Ref. 14.

which the equilibrium is more favorable. On the other hand, the occurrence of the reaction causes the heating of the bed, and thus heat must be subtracted to limit temperature raise. Also for exothermic nonequilibrium reactions, sometimes cooling is needed to protect the catalyst from deactivation phenomena. Cooling may be performed within the reactor with several different configurations.

Heat exchangers can be placed between the beds, using cooling fluids such as water or using the cooler reactants allowing their needed preheating. In the case of radial flow reactors, interbed heat exchangers can be coaxial within the beds. In Figure 4.6<sup>15</sup> the Topsøe S3 ammonia synthesis converter is reported. It is a three fixed beds reactor with radial flow, two interbed heat exchangers and an external



**FIGURE 4.6**

S-300 Topsøe ammonia converter: three radial-flow fixed beds with interbed heat exchanger and external jacket.

*Reprinted with permission from Ref. 15.*

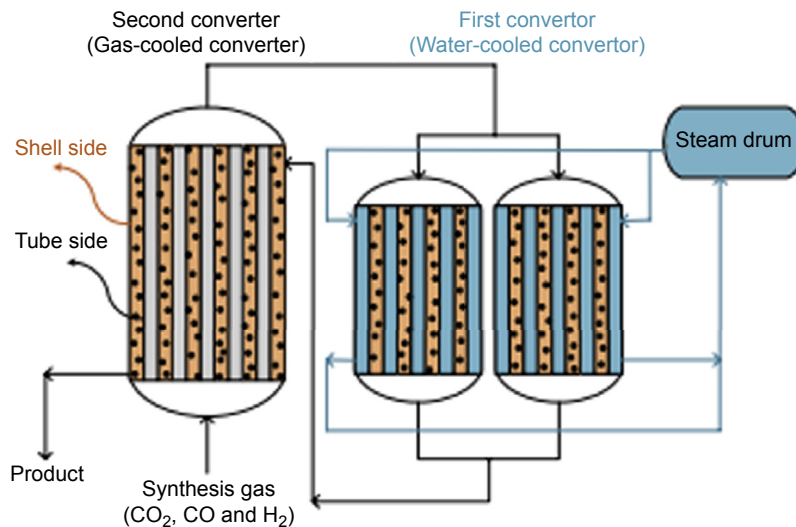
jacket. Sometimes, the heat exchangers are placed outside of the structure of the reactor, with the reactant mixture coming in and out the reactor, each bed.

Alternatively, direct cooling between the beds can be performed, by quenching with cooler reactant flows.

Another configuration is that of exchanger reactors. Gas-cooled reactors (GCRs) are denoted as those reactor/heat exchangers where a coolant gas flows in tubes internal into the catalyst bed.

Water-cooled reactors (WCRs), also denoted as boiling water reactors, are those where the tubes containing the catalyst are in a bath containing flowing water converting into steam. In Figure 4.7<sup>16</sup> a reactor configuration used in methanol synthesis is shown: the GCR allows preheating of the reactant gas, while reaction occurs in the tubes of two parallel WCRs and in the shell side of the GCR. The so-called “isothermal” reactors have been recently developed by Linde, with the heat exchanger inside the bed made by helical coils,<sup>17</sup> and by Casale with cooling elements in perforated vertical plates.<sup>18</sup>

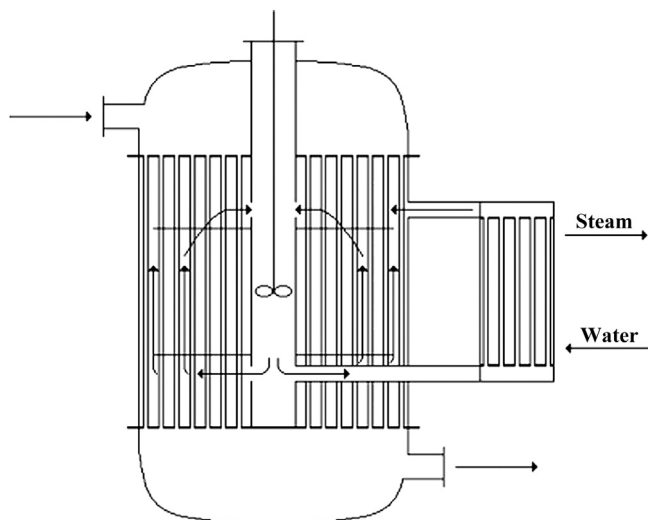
Exchangers/reactors usually denoted as “multitubular” reactors are used for highly exothermic partial oxidation reactions where an impressively high number of very thin tubes (up to 30,000 tubes, 1 in diameter, tubes) are in contact with a bath where gas oils or inorganic liquid eutectics cool them,<sup>19</sup> see Figure 4.8.<sup>20</sup>



**FIGURE 4.7**

Schematic flow diagram of conventional dual-type methanol synthesis reactor.

*Reprinted with permission from Ref. 16.*

**FIGURE 4.8**

Multitubular reaction for phthalic anhydride synthesis from *o*-xylene selective oxidation.

*Reprinted with permission from Ref. 20.*

#### 4.2.2.4 Cooled fixed-bed reactors for liquid/solid exothermic reactions

Exothermic equilibrium reactions can also be performed in the liquid phase. To perform liquid-phase exothermic reactions, fixed-bed reactors can be used. Also in this case, cooling can be performed by interbed heat exchange with cooling fluids such as water, or by interbed quenching with cool reactants. Alternatively, multitubular exchanger–reactors can be applied.

#### 4.2.2.5 Catalytic distillation reactors

Catalytic distillation reactors are distillation towers with sections packed with the catalyst.<sup>21</sup> Reactants are fed to the tower and products formed in the catalytic section are separated simultaneously from each other or from reactants by distillation. Among other advantages, this may allow to remove thermodynamic limitations in several equilibrium reactions.

### 4.2.3 Monolithic reactors

Monolithic reactors are used when minimum pressure drops and high reactant flow rates are needed.<sup>22,23</sup> The catalyst is deposited as a thin layer on the surface of solid structures such as ceramic filters made of cordierite (this is a common case for catalytic converters for cars and diesel oxidation catalysts), honeycomb monoliths made of  $\text{TiO}_2$ , metal plates over which an oxide layer is deposited or formed chemically or electrochemically. Over these systems, both exothermal and endothermal reactions can be performed, with the reaction temperature being controlled by

controlling the feed flow rate. Catalytic burners are usually monolytic, and in this case strongly exothermic reaction occurs. Similarly, metal monoliths such as metal gauze pads are used as the catalyst bed for some highly exothermic reactions such as in the Andrussov process for methane ammoxidation to hydrogen cyanide.

#### 4.2.4 Catalytic membrane reactors

As for catalytic distillation, also catalytic membrane reactors combine a catalytic reaction with separation, thus allowing to remove thermodynamic constraints in equilibrium reactions.<sup>24</sup> In fact, selective membranes allow one of the products to come out from the reactor and thus subtracting itself from equilibrium. A typical application is for dehydrogenation reactions, using membranes allowing the separation of hydrogen. Otherwise, the evolution of oxygen, when it is a reaction product, allows improvements e.g., in  $N_2O$  decomposition reaction.

Another interesting application is the use of “dense oxygen permeable membrane reactor” where an oxygen permeable membrane allows to feed a tuned amount of oxygen, coming from air, in the reaction chamber to feed partial oxidation reaction.<sup>25</sup>

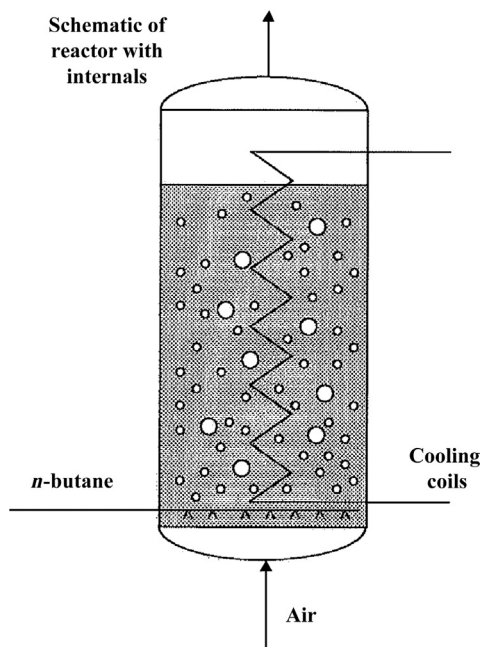
#### 4.2.5 Gas/solid fluidized and transported bed reactors

Powder beds can become “fluidized” when a fluid flow passes through it with a sufficiently high flow rate to expand it and powder grains move in a dynamic fluid-like state.<sup>26</sup>

Fluid bed reactors are applied to some exothermal selective oxidation reactions, such as the maleic anhydride synthesis from *n*-butane air oxidation (Figure 4.9<sup>27</sup>), where air or oxygen is fed from below to a large reservoir containing the catalyst powder. These reactors are cooled internally by serpentines. The resulting temperature gradients are small and there are basically no hot spots, thus allowing an excellent temperature control. Additionally, charge of the catalysts to the reactor is easy, and thus time for catalyst change is fast. However, there is a great remixing and back-diffusion of reaction products that largely cancel the advantage of the better temperature control. On the other hand, since the fluid bed provides a barrier to the flame, it is possible to operate with higher concentrations of the substrate, thus entering safely in the region of explosiveness addressing faster reaction rate conditions. Gas-phase low-pressure bulk polymerization of ethylene and propylene is commonly performed in gas-phase reactors, but in this case the polymer grows on the catalyst particles and the catalyst is consumed with the product thus being continuously fed.<sup>29</sup>

#### 4.2.6 Raiser reactors and circulating fluidized bed reactors

Fluidized catalyst beds can be transported along cyclic reactor systems, usually called circulating fluidized bed (CFB) reactors. In most cases, the reaction occurs in columns, said “raisers”, which are “transport bed” reactors, i.e., tubes where

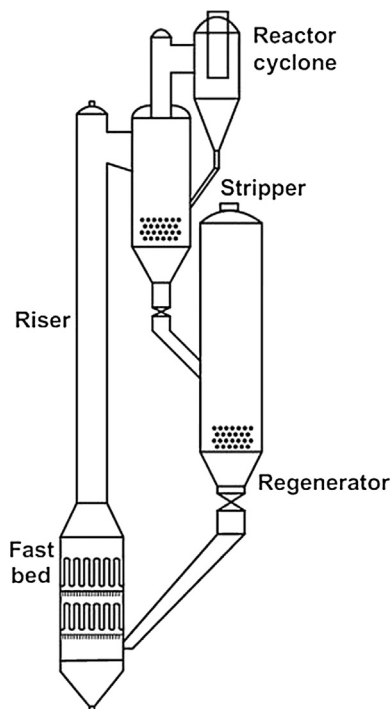
**FIGURE 4.9**

Schematics of the fluidized bed reactor for maleic anhydride synthesis from oxidation of *n*-butane.

*Reprinted with permission from Ref. 27.*

the catalyst moves up-flow pushed by and together with the fluid feed. In the upper part of the riser, there is a cyclone which allows the separation of the catalyst from the fluid products. The catalyst, usually deactivated, moves then in a regenerator reactor to be later fed again to the riser. This continuous circulating system is used for FCC as well as for paraffin's dehydrogenation: in this case, the catalyst is deactivated by coking in the riser and is regenerated by coke combustion in a fluid-bed regenerator. From the regenerator, the cleaned catalyst moves back to the base of the riser. A similar system has been developed for partial oxidation: the catalyst reacts in the riser with the substrate, and oxidizes it becoming reduced. The catalyst is reoxidized by oxygen in the regenerator and comes back to the riser. In Figure 4.10, the CFB system used for some times in a transport bed process for maleic anhydride synthesis is shown.<sup>28</sup>

Similar systems can also be applied in solid–liquid slurry conditions. This is the case of slurry loop polymerization reactors, using Ziegler–Natta or Phillips-type solid catalysts, where reaction occurs, in different conditions, in the riser but also in the downer, such as in the case of the Multizone propene polymerization reactor (Figure 4.11).<sup>30</sup>



**FIGURE 4.10**

Circulating fluidized bed configuration for a commercial process for maleic anhyde from *n*-butane oxidation.

*Reprinted with permission from Ref. 28.*

### 4.2.7 Slurry liquid/solid and gas/liquid/solid reactors

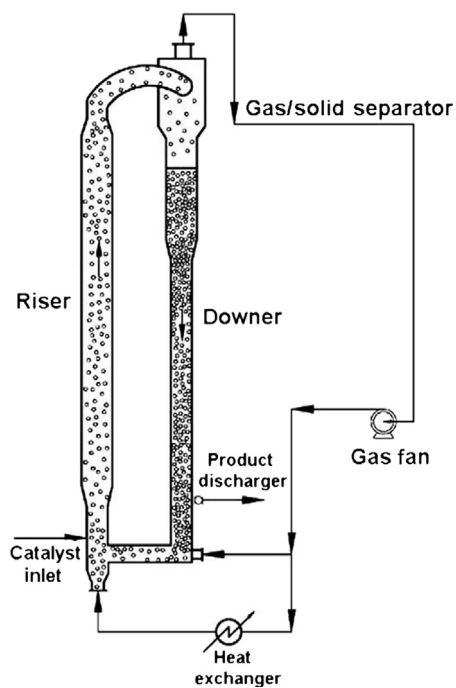
Besides the cited loop reactors, a number of different reactors can be applied to liquid/solid and gas/liquid/solid slurries such as e.g., those that can be applied to the Fischer Tropsch synthesis.<sup>31</sup> The most common reactors for slurry reaction conditions are the continuously stirred tank reactors see Figure 4.12<sup>32</sup> for a scheme, whose temperature may be controlled by external jackets or internal coils, or even by evaporation or boiling/recondensation of the most volatile components or finally with external cycling to heat exchangers. Analogous batch tank reactors may be used.

Fluid bed or ebullating bed reactors can also be used, where fluidization or ebullition is provided by the liquid feed entering the reaction from the bottom.

## 4.3 Deactivation of solid catalysts

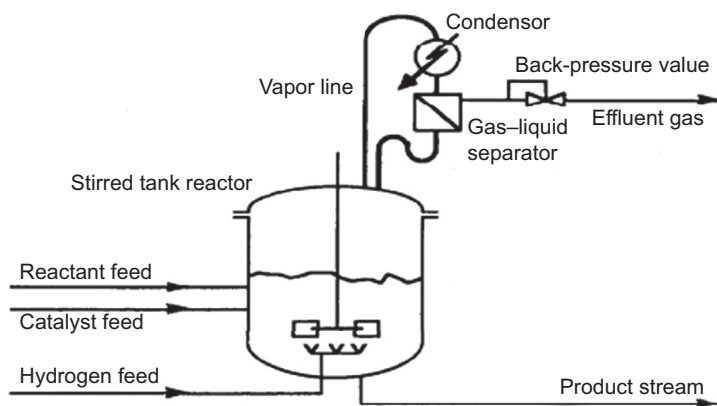
In few cases, catalysts may increase their activity at the beginning of their use. This is sometimes called “conditioning”. More frequently, instead, catalysts tend to lose



**FIGURE 4.11**

Multizone circulating polymerization reactor.

*Reprinted with permission from Ref. 30.*

**FIGURE 4.12**

Flow sheet of the reactor sections with a slurry reactor and applying an evaporating solvent.

*Reprinted with permission from Ref. 32.*

activity with time on stream,<sup>33,34</sup> down to a limit where their prolonged use is uneconomical.

There are several reasons for deactivation. In some cases, the catalyst can be regenerated (reversible deactivation), and in other cases deactivation is irreversible.

### 4.3.1 Poisoning

Deactivation is sometimes due to the deposition (usually from the feed) of contaminants that modify the structure of the catalyst converting the active phase in an inactive form. Sulphur poisoning is a typical deactivation phenomenon for metal hydrogenation catalysts such as those based on Ni and noble metals. Metal catalysts are also poisoned by chlorine compounds, nitrogen compounds or oxygen compounds including water. Similarly, acid catalysts (e.g., zeolites) are deactivated by adsorption of basic compounds (amines, nitriles), but can be regenerated by desorption or washing.

Irreversible poisoning occurs when the contaminant cannot be practically removed. This is the case, e.g., for lead coming from gasoline poisoning platinum present in catalytic converters, because of the formation of inert Pt–Pb alloy.

### 4.3.2 Coking

The thermodynamic instability of hydrocarbons in reducing environment is the cause of one of the most common deactivation phenomena occurring with solid catalysts: coking. Due to the negative  $\Delta S_{\text{form}}$ , the hydrocarbons (except acetylene) become less stable, with respect to the elements, i.e., hydrogen and carbon, above a certain temperature limit. Coking may be considered as the reverse reaction of the formation of hydrocarbons, and is consequently thermodynamically favored at  $T > 200\text{ }^{\circ}\text{C}$  for all hydrocarbons except methane that becomes unstable above ca  $530\text{ }^{\circ}\text{C}$ . Thus, carbonaceous materials, denoted sometimes roughly as “coke”, may form on the surface of catalysts upon high-temperature contact with hydrocarbons. This phenomenon results in catalyst deactivation. Most of solid acid-catalyzed processes for hydrocarbon conversion are influenced by the occurrence of catalyst coking and the need for frequent catalyst regeneration.

In some cases, particular forms of carbon are produced, such as carbon nanotubes (whiskers) produced on Ni catalysts. In this case, before real deactivation phenomena, filling of void volume by carbon whiskers results in enhancement of pressure drop.

### 4.3.3 Sintering

Deactivation may come from the loss of the active surface area resulting from sintering of the active phase. Typically, supported metal nanoparticles can coalesce, thus producing larger particles with smaller surface areas as well as smaller density of defects (corners edges) that can act as active sites.

### 4.3.4 Phase transitions and solid-state reactions

Phase transitions of the components may also be the cause of deactivation. Typically, the phase transitions of anatase to rutile is a main cause of deactivation of  $V_2O_5$ - $TiO_2$  oxidation catalysts, while the volatilization of  $MoO_3$  is a main cause of deactivation of metal molybdates or  $MoO_3$ -containing catalysts. The formation of the  $CuAl_2O_4$  spinel is a main deactivation cause of  $Cu/Al_2O_3$  hydrogenation and dehydrogenation catalysts.

### 4.3.5 Breaking of extrudates

As said, catalysts are shaped in the form of extrudates to limit pressure drop and to improve heat transfer. Catalysts for use in fluidized beds are also formed to produce fluidizable powders. In the case of fixed bed, under use (sometimes under pressure and high temperature), the extrudates can progressively crunch, thus reproducing fine powders. This matter tends to cause an obstacle to the reactants' flow, plugging it, thus resulting in increased pressure drop. This phenomenon can progressively grow finally coming to unacceptable pressure drops.

Fluidized bed matter can also undergo erosion, also producing fine powders that will finally be transported out from the reactor to an excessive extent.

### 4.3.6 Erosion or breaking of monoliths

Monolithic catalysts can be submitted to flows containing powder matter, such as soot from diesel engines and ash from coal combustion or gasification. The catalyst layer can be damaged, the active phase being lost.

---

## 4.4 Regeneration of reversibly deactivated catalysts

Deactivation by solid-state reaction, phase transition, volatilization, breaking and pulverization of the extrudates, erosion, cannot generally be contrasted. After the catalyst activity slowed down to a given extent, the catalyst must be replaced. In contrast, coking and poisoning can usually be contrasted, submitting the deactivated catalyst to some regeneration procedure.

### 4.4.1 Techniques for regeneration

#### 4.4.1.1 *Burning of coke*

Coked catalysts can be usually regenerated by burning coke. Sometimes, trace amount of noble metals are introduced into the catalyst just to favor coke burning. Sometimes, burning of coke can also be used to provide reaction heat just by heating the catalyst, like it occurs in the FCC process, thus converting the process from endothermic to autothermic. In this case, however, a non-negligible fraction of organic reactants is lost, being converted into coke first and carbon oxides later.

#### **4.4.1.2 Hydrogenation**

Hydrogenation of carbonaceous materials is sometimes used to regenerate catalyst. However, most frequently hydrogenation is used to limit coking. For this reason, some acid-catalyzed reactions are performed under hydrogen in the presence of trace amounts of noble metals. In these conditions, coke precursors are hydrogenated.

#### **4.4.1.3 Washing or rejuvenation**

Some catalysts can be regenerated or rejuvenated by washing. This is the case, e.g., of solid catalysts for isobutane/isobutene alkylation, which are washed by liquid isobutane/hydrogen to remove carbonaceous matter. Similarly, polymeric catalysts such as sulfonic acid resins, used mostly in liquid phase reactions, are frequently poisoned by basic organic molecules as well as by metal cationic species coming with the feed. Rejuvenation can be obtained by washing with opportune solvents.

#### **4.4.1.4 Steaming**

Steaming is a possible regeneration procedure, used e.g., to reduce sulfur poisoning of nickel steam-reforming catalysts. This treatment also possibly allows restructuring of nickel with recovery of activity also reduced by sintering.

### **4.4.2 Regeneration of catalysts and the reactors**

Different reactivation procedures are possible, depending on the rate of catalyst deactivation.<sup>35</sup> When deactivation occurs in years, reactivation might not be necessary at all. The catalyst might be substituted after its cycle life or regenerated in situ, during a normal switch-off of the plant for maintenance, can be performed. Alternatively, during maintenance times, the catalyst may be removed, reactivated ex situ elsewhere and reloaded in the reactor.

When deactivation occurs in months or weeks, swing-type regeneration may be performed. An additional reactor may be used (two instead of one or five instead of four) and the reactor beds may be regenerated alternatively, allowing a continuous operation of the plant. This is applied, e.g., in the cyclic catalytic reforming process, as well as in several gas-phase acid-catalyzed processes. When deactivation is even fast, moving-bed reactors with intermittent or continuous addition of active catalyst and withdrawal of deactivated catalyst may be applied. This is applied in the moving-bed continuous regeneration catalytic reforming processes as well as in hydrocracking in slurry-ebullated beds.

In the case of very fast deactivation by coking, occurring in minutes, continuously circulating fluid beds are used. The fluid bed catalyst may recycle from the reactor to the regeneration vessel where coke burning occurs heating strongly the catalyst itself, and in this way it may provide the heat of reaction. This system has been developed for FCC processes and has also been used in the paraffin dehydrogenation.<sup>36</sup>

---

## 4.5 Laboratory evaluation of the catalytic activity<sup>37,38</sup>

Testing of catalytic activity in laboratory reactors represents the first step in the development of new catalysts. The goal is to determine activity/selectivity and life at given temperature, pressure and feed composition conditions. Some commonly applied lab-scale reactors are summarized in Figure 4.13.<sup>38</sup> The most common (and easier to be applied) test reactors used in the experimental laboratory tests for gas-phase reactions are continuous fixed-bed tubular reactors. Gas-flown catalyst beds are often diluted with inert particles such as quartz or silicon carbide in order to improve the isothermicity of the bed and to suppress other potentially disturbing effects such as axial dispersion and bypassing. For heterogeneous catalysts to be used in liquid/solid conditions, stirred tank reactors are most commonly used in the laboratory. A number of liquid phase microreactors can also be applied to test heterogeneous liquid–solid reactions.<sup>39</sup>


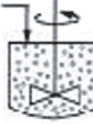
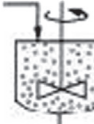






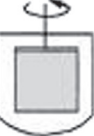
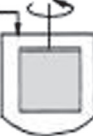
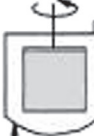
To perform reliable experiments, the reactor should operate in a well-defined operating regime, avoiding relevant temperature gradients and interphase (fluid–catalyst) and interparticle (catalyst–catalyst) transport resistances, as it can be obtained only by accurately designing the experiences and by properly choosing the experimental setup.<sup>40</sup> This evaluation can be made by calculating a number of functions proposed as mathematical criteria for checking diffusive intrusions (e.g., the Thiele modulus for pore diffusion resistance). Evaluation of the apparent activation energy using differential reactor approximation at low conversion can also be indicative on the presence/absence of relevant diffusion limitations. Tests at varying catalyst particle should also be conducted, to assess effectiveness factors or intraparticle transport resistances.

A number of gradientless laboratory testing reactors are also available to measure kinetics in the absence of diffusional limitations in heterogeneously catalyzed gas-phase reactions.<sup>37</sup> Another phenomenon to be accurately taken into account is catalyst deactivation, to reveal whether it is affecting the results obtained.

---

## 4.6 Operando methodologies

Since the beginning of the spectroscopic catalysis research, attempts have been devoted to study the catalysts in real conditions, i.e., during the catalytic act. These experiments were denoted, in those times, as *in situ* studies. More recently, this approach evolved in the concept of *Operando Spectroscopy*<sup>41</sup> applied to different spectroscopic techniques, with the possibility to apply several spectroscopic techniques simultaneously to the same catalyst sample in working conditions.<sup>42</sup> According to the most recent definition, the term *in situ* study should be essentially reserved to studies performed under controlled atmosphere but without measurement of gas-phase concentration.<sup>43</sup> Many catalysis laboratories have today available Operando apparanta.

	Batch	Semibatch	Continuous	Phases
Slurry				L-S G-L-S
Fixed-bed				G-S G-L G-L-S
Fluidized bed				G-S
External recycled				L-S G-S
Internal recycled				L-S G-S
Spinning or Stationary basket				L-S G-S G-L-S

**FIGURE 4.13**

Common laboratory reactors: operation modes and reacting system (L: liquid, G: gas, S: solid).

*Reprinted with permission from Ref. 38.*

Indeed, it seems obvious that under reaction conditions, when the reactants adsorb on the surface, and they transform to intermediates and to the products, that finally desorb rapidly, the concentration at the surface of most or all these species is expected to be very low. In particular, this is expected to be true for species involved in steps successive to the slowest one. Indeed, the detectability of the active adsorbed species (the surface intermediates) is rare, if even possible, in *operando* conditions (i.e., at relatively high temperatures) with usual spectroscopic measurements such as with infrared. These labile-adsorbed species may be detected using unusual measurements such as femtosecond laser excitation followed by nanosecond-time resolved Fourier transform Infrared measurements.<sup>44</sup> On the contrary, heavy adsorbed species that are not involved in the main reaction concentrate at the catalyst surface and can be easily detected. It is possible to forecast that, if a species is detected to be highly concentrated and stable in reaction conditions, it either is the true catalyst (like sometimes surface carbonaceous materials deposited at the surface during the induction period), or a poison (like coke that is a main cause of deactivation of acidic catalysts) or finally, is a spectator species.

Thus, techniques of catalyst characterization performed in *operando* conditions can give important information on the state of the working catalyst more than on the reaction mechanism. In any case, the information obtained in *operando* conditions is always interesting and sometimes also useful for revealing aspects of the reaction mechanisms.<sup>45,46</sup>

---

## References

1. Schuurman Y. *Catal Today* 2008;**138**:15–20.
2. Martin Rodrigues H, Cano A, Matzopoulos M. *Hydrocarbon Process*; December 2010: 43–9.
3. [http://www.mecsglobal.com/Sulfuric%20Acid%20Today%20-%20MECS\\_GEAR-reprint.pdf](http://www.mecsglobal.com/Sulfuric%20Acid%20Today%20-%20MECS_GEAR-reprint.pdf); [accessed 24.03.14].
4. Hartmann VL, Obysova AV, Dulneva AV, Afanas'ev SV. *Chem Eng J* 2011;**176–177**: 102–5.
5. Werther J, Hartge E-U. *Ind Eng Chem Res* 2004;**43**:5593–604.
6. Baldovino-Medrano VG, Le MT, Van Driessche I, Bruneel E, Gaigneaux EM. *Ind Eng Chem Res* 2011;**50**(9):5467–77.
7. [http://www.eni.com/it\\_IT/attachments/azienda/attivita-strategie/petrolchimica/licensing/PBE-1-flyer-lug09.pdf](http://www.eni.com/it_IT/attachments/azienda/attivita-strategie/petrolchimica/licensing/PBE-1-flyer-lug09.pdf); [accessed 24.03.14].
8. Madon R, Harris DH, Xu M, Stockwell D, Lerner B, Dodwell GW. *FCC catalysts for feeds containing nickel and vanadium*, US patent 6716338 to Engelhard Corporation.
9. Harris DH, Xu M, Stockwell D, Madon RJ. *FCC catalysts for feeds containing nickel and vanadium*, US patent 6673235, to Engelhard Corporation.
10. Schmidt L. *The engineering of the chemical reactions*. Oxford University Press; 1998.
11. Fogler HS. *Elements of chemical reaction engineering*. 4rd ed. Upper Saddle River, NJ: Prentice-Hall; 2005.
12. Jayaraman VK, Kulkarni BD. In: *Chemical engineering and chemical process technology. Encyclopedia of Life Support Systems*, vol. III. Unesco; 2012. pp. 122–42.

13. Eigenberger G. Fixed-bed reactors. In: *Ullmann's encyclopedia of industrial chemistry*. Wiley-VCH Verlag GmbH & Co.; 2002.
14. [http://www.topsoe.com/business\\_areas/ammonia/~ /media/PDF%20files/Steam\\_reforming/Topsoe\\_steam\\_reform\\_solutions.ashx](http://www.topsoe.com/business_areas/ammonia/~ /media/PDF%20files/Steam_reforming/Topsoe_steam_reform_solutions.ashx) reformer; [accessed 24.03.14].
15. [http://www.topsoe.com/business\\_areas/ammonia/~ /media/PDF%20files/Ammonia/topsoe\\_ammonia\\_technology.ashx](http://www.topsoe.com/business_areas/ammonia/~ /media/PDF%20files/Ammonia/topsoe_ammonia_technology.ashx); [accessed 24.03.14].
16. Rahimpour MR, Alizadehhesari K. *Int J Hydrogen Energy* 2009;**34**:1349–62.
17. <http://www.linde-india.com/userfiles/image/File/Linde%20Isothermal%20Reactor.pdf>; [accessed 24.03.14].
18. Ostuni R. *Chim. Ind. (Milan)* 2011;(7–8):124–9. [http://www.soc.chim.it/sites/default/files/chimind/pdf/2011\\_6\\_124.pdf](http://www.soc.chim.it/sites/default/files/chimind/pdf/2011_6_124.pdf); 2011.
19. Shin SB, Han SP, Lee WJ, Im YH, Chae JH, Lee DI, et al. *Hydrocarbon Process*; April 2007:83–90.
20. Anastasov AI. *Chem Eng Process* 2003;**42**:449–60.
21. Harmsen GJ. *Chem Eng Process* 2007;**46**:774–80.
22. Boger T, Heibel AK, Sorensen CM. *Ind Eng Chem Res* 2004;**43**:4602–11.
23. Pangarkar K, Schildhauer TJ, van Ommen JR, Nijenhuis J, Kapteijn F, Moulijn JA. *Ind Eng Chem Res* 2008;**47**:3720–51.
24. Czuprat O, Jiang H. *Chem Ing Tech* 2011;**83**(12):2219–28.
25. Wei Y, Yang W, Caro J, Wang H. *Chem Eng J* 2013;**220**:185–203.
26. Werther J. Fluidized-bed reactors. In: *Ullmann's encyclopedia of industrial chemistry*. Wiley-VCH Verlag GmbH & Co.; 2002.
27. Dente M, Pierucci S, Tronconi E, Cecchini M, Ghelfi F. *Chem Eng Sci* 2003;**58**:643–8.
28. Hutchenson KW, La Marca C, Patience GS, Laviolette J-P. *Appl Catal A Gen* 2010;**376**:91–103.
29. Ho YK, Shamiri A, Mjalli FS, Hussain MA. *J Process Control* 2012;**22**:947–58.
30. Yan W-C, Li J, Luo Z-H. *Powder Technol* 2012;**231**:77–87.
31. Davis BH. *Catal Today* 2002;**71**:249–300.
32. Janssen HJ, Vost HJ, Westeterp KR. *Chem Eng Sci* 1992;**47**:4191–208.
33. Forzatti P, Lietti L. *Catal Today* 1999;**52**:165–81.
34. Bartholomew CH. *Appl Catal A Gen* 2001;**212**:17–60.
35. Sie ST. *Appl Catal A Gen* 2001;**212**:129.
36. Sanfilippo D, Miracca I. *Catal Today* 2006;**111**:133.
37. Fomi L. *Catal Today* 1997;**34**:353–67.
38. Perego C, Peratello S. *Catal Today* 1999;**52**:133–45.
39. Protasova LN, Bulut M, Ormerod D, Buekenhoudt A, Berton J, Stevens CV. *Org Process Res Dev* 2013;**17**:760–91.
40. Berger RJ, Pérez-Ramírez J, Kapteijn F, Moulijn JA. *Appl Catal A Gen* 2002;**227**:321–33.
41. Bañares MA. *Catal Today* 2005;**100**:71–7.
42. Tinnemans SJ, Mesu JG, Kervinen K, Visser T, Nijhuis TA, Beale AM, et al. *Catal Today* 2006;**113**:3–15.
43. Meunier FC. *Catal Today* 2010;**155**:164–71.
44. Thibault-Starzyk F, Seguin E, Thomas S, Daturi M, Arnolds H, King DA. *Science* 2009;**324**:1048–51.
45. Operando surface spectroscopy—placing catalytic solids at work under the spotlight. In: Arean CO, Weckhuysen BM, Zecchina A, editors. *Phys Chem Chem Phys*, vol. 14; 2012. p. 2125 [special issue].
46. Operando IV. *Catal Today* 2013;**205**:1–168 [special issue]. Sievers C, Bare SR, Stavitski E, editors.



# Acid and Basic Catalysts: Fundamentals

## CHAPTER OUTLINE

<b>5.1 Acido-basicity in liquid phases. Fundamentals and historical perspective</b> .....	<b>58</b>
5.1.1 Acido-basicity in diluted water solutions.....	58
5.1.2 Protonic acidity in highly concentrated water solutions and in dry conditions.....	62
5.1.3 Brønsted basicity in nonprotic solvents.....	66
5.1.4 Lewis acidity and basicity .....	69
5.1.5 Hard and soft acidity and basicity (HSAB) and nucleophilicity.....	71
5.1.6 Gas phase acidity and basicity.....	72
<b>5.2 Reactant activation and acid–base catalysis in liquid phases</b> .....	<b>73</b>
5.2.1 Reactant activation and acid–base catalysis in diluted water solutions.....	73
5.2.2 Activation of weak basic molecules by acids .....	74
5.2.3 Catalysis in liquid superbasic conditions .....	78
<b>5.3 The surface acidity and basicity of solids</b> .....	<b>79</b>
5.3.1 Structural chemistry versus surface chemistry of solids: a fundamental approach .....	79
5.3.2 Characterization techniques of surface acidity and basicity of solids .....	80
5.3.2.1 <i>Techniques for the characterization of surface acidity and basicity</i> .....	80
5.3.2.2 <i>Molecular probes for surface acidity and basicity characterization</i> .....	80
5.3.2.3 <i>Direct detection of surface hydroxy-groups</i> .....	84
5.3.2.4 <i>Direct evidence of the surface basic sites: UV and XPS spectroscopies and the concept of optical basicity</i> .....	86
5.3.2.5 <i>Quantitative adsorption of probe molecules from gas and liquid phases</i> .....	88
5.3.3 Methods measuring adsorption/desorption energies .....	88
5.3.3.1 <i>Calorimetric methods</i> .....	88
5.3.3.2 <i>Temperature programmed desorption methods</i> .....	89
5.3.4 IR spectroscopic methods .....	91
5.3.5 NMR spectroscopic methods .....	92
5.3.5.1 <i>Theoretical methods</i> .....	93
5.3.6 Catalytic probe reactions.....	93

5.3.7 Strength, amount, and distribution of surface acid and basic sites on the ideal surface of a solid .....	95
<b>5.4 Heterogeneous versus homogeneous acid–base catalysis.....</b>	<b>96</b>
<b>References .....</b>	<b>96</b>

## 5.1 Acido-basicity in liquid phases. Fundamentals and historical perspective

### 5.1.1 Acido-basicity in diluted water solutions

As it is well known, pure water is very weakly dissociated. The water autoprotolysis equilibrium is generally denoted as follows:



and the autoprotolysis constant (or ionic product) of water is defined and measured as:

$$K_w = [\text{H}^+][^-\text{OH}] = 1.008 \cdot 10^{-14} \quad \text{at } 25^\circ\text{C} \quad (5.2)$$

where the molar concentration of the species is used as an approximation of their activity. From this arises that both molar concentrations  $[\text{H}^+]$  and  $[^-\text{OH}]$  are nearly  $10^{-7}$  at  $25^\circ\text{C}$ . When  $[^-\text{OH}] > 10^{-7}$  (thus  $\text{pH} = -\log_{10} [\text{H}^+] > 7$ ) the water solution is denoted as “basic”, while when  $[\text{H}^+] > 10^{-7}$  (thus  $\text{pH} = -\log_{10} [\text{H}^+] < 7$ ) the water solution is called “acidic”.

S.A. Arrhenius,<sup>1</sup> Nobel prize winner for Chemistry in 1903 and a precursor of physical chemistry, defined an acid as any hydrogen-containing species able to release protons,



and a base as any species able to release hydroxide ions. This approach implies metal hydroxides as typical basic compounds, as follows:



where complete dissociation in water solution is supposed.

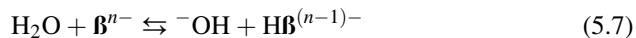
J.M. Brønsted<sup>2</sup> and, simultaneously and independently but less precisely, T.M. Lowry<sup>3</sup> in 1923, modified the definition of the bases: a base is any species capable of combining with protons. In this view, acid–base interactions consist in the equilibrium exchange of a proton from an acid HA to a base B (which may be the solvent, e.g., water) generating the conjugated base of HA,  $\text{A}^-$ , plus the conjugated acid of B,  $\text{HB}^+$  (e.g., the hydroxonium ion  $\text{H}_3\text{O}^+$ ):



Thus, acidic species are either neutral acids ( $\text{H}_n\text{A}$ ) or even the cationic protonated bases  $\text{HB}^+$ . Similarly, basic species in water are either neutral compounds (“molecular bases”) that are able to abstract a proton from water:



or anionic species (like anions  $\mathbf{B}^{n-}$ , arising from the dissociation of salts  $M_n\mathbf{B}_m$ ) that act in the same way, neutralizing themselves or reducing their charge:



In the Brønsted definition, a broader spectrum for the bases is considered than in the Arrhenius definition. The hydroxide anion itself is the basic species, rather than the metal hydroxide.

The acid strengths in diluted water solutions may be described by the dissociation equilibrium:



$$K_a = [\text{H}_3\text{O}^+][\text{A}^-]/[\text{HA}] \quad \text{p}K_a = -\log K_a$$

where the molar concentration of the species is used as approximation of their activity, the activity of water being approximated to 1.

The acid strength in water solution is determined by the dissociation of the acid, which is promoted by the solvation of both protons and anions by water molecules.

Actually, the position of equilibria, like Eqn (5.1), is strongly affected by the neighboring of both reactant and product species. Water (seen as the reactant) is solvated by itself, being involved in a network of hydrogen bondings, where every hydrogen atom bridges two oxygen atoms and each oxygen atom bonds two protons and H-bonds other two. Protons and hydroxide anions are also both solvated by water, which also acts as the solvent.

Although the proton is mostly formally assumed to associate with one water molecule to form the hydronium ion  $\text{H}_3\text{O}^+$ , the real state of proton in water is still matter of discussion. Historically, two main structures have been proposed: according to Eigen<sup>4</sup> a covalently bonded hydronium ion should strongly H-bond the oxygen of three water molecules, thus giving rise to a  $[\text{H}(\text{H}_2\text{O})_4]^+$  ion, while, following Zundel,<sup>5</sup> the proton should symmetrically bond two water molecules forming a  $[\text{H}(\text{H}_2\text{O})_2]^+$  complex. As remarked by Kazansky,<sup>6</sup> the energy of proton hydration by liquid water, 1091 kJ/mol, is so high to suggest that the real state of solvated proton in water is  $[\text{H}(\text{H}_2\text{O})_6]^+$  or even more hydrated species. In fact, recent theoretical studies<sup>7</sup> suggested that the hydronium ion give rises to three very strong bonds (one each proton) with three water molecules, as proposed by Eigen, which are definitely stronger than those among water molecules (18.3 kJ/mol with respect to 7.9 kJ/mol), but that also a second shell of water molecules can be bonded with significantly stronger H-bonds (9.1 kJ/mol) while the third shell is bonded with only slightly strengthened H-bonds (8.1 kJ/mol). This implies that the real state of hydrated proton can be depicted as a  $[\text{H}(\text{H}_2\text{O})_{10}]^+$  or even more hydrated complex. However, IR studies published by Stoyanov et al.<sup>8</sup> support a Zundel-type species, bonded strongly to four additional water molecules, thus supporting a  $[\text{H}(\text{H}_2\text{O})_6]^+$  complex ion. Himmel et al.<sup>9</sup> performed recently calculations on several  $[\text{H}(\text{H}_2\text{O})_n]^+$  complex species, both with Zundel-type and Eigen-type structures, obtaining a similar, and

substantially correct standard chemical potential for the proton with  $n = 4$  to 7, thus suggesting that different species may have similar stabilities and should coexist.

Interestingly, the formation of such  $[\text{H}(\text{H}_2\text{O})_n]^+$  complexes with  $n \sim 6$  is possible only when the amount of available water is sufficient, i.e., only for sufficiently diluted acid solutions with an acid concentration not higher than 5–10 mol/l.

The solvation of the anion  $\text{A}^-$  by water also plays a relevant effect in the stabilization of the anion and in determining, as a consequence, the scale of the acid strengths. As for example, the chloride anion in neutral water solution is surrounded by a number of water molecules H-bonded to it through their own hydrogen atoms. The most probable number is around 6, even if it can vary broadly.<sup>10</sup> Obviously, the solvation state of more complex anions is much more complicated. On the other hand, when acid solutions are concentrated, a direct interaction of the cation and the anion will appear, producing ionic pairs. X-ray absorption fine structure supports the idea that in 16.1 molal concentration of HCl water solutions, all chloride ions interact directly with 1.6 hydronium ions and 4.2 water molecules.<sup>11</sup>

The acid strength for oxoacids is correlated also to the charge delocalization of the anions that stabilize them.<sup>12</sup> For simple inorganic acids, it depends from the number of oxygen atoms where the negative charge of the anion resulting by dissociation may be delocalized. For this reason, the anions  $\text{SO}_4^{2-}$  and  $\text{ClO}_4^-$  are the (very weak) conjugated bases of very strong acids, sulfuric and perchloric acids, while  $\text{SO}_3^{2-}$  and  $\text{ClO}_3^-$  are the conjugated bases of less strong acids, sulfurous and chloric acids. Actually, the four oxygen atoms of  $\text{SO}_4^{2-}$  and  $\text{ClO}_4^-$  anions also allow more extensive H-bonding solvation by water molecules than  $\text{SO}_3^{2-}$  and  $\text{ClO}_3^-$  anions.

According to Eqn (5.4), the basic strength of metal hydroxides, which are considered to be fully dissociated in water, depends consequently from their solubility. The basicity of their solutions depends from the amount dissolved. According to the Brønsted–Lowry approach, the basic strength of molecular bases is related to the acidity of their conjugated acid. Thus, the strengths of basic compounds in diluted water solutions are currently described in terms of Brønsted basicity by the shift of the dissociation equilibrium:



$$K_{\text{HB}} = \frac{[\text{H}_{\text{aq}}^+][\text{B}_{\text{aq}}]}{[\text{HB}_{\text{aq}}^+]} \quad (5.10)$$

$$\text{p}K_{\text{HB}} = -\log K_{\text{HB}} \quad (5.11)$$

where B may be neutral or anionic and  $\text{HB}^+$  may be positively charged or neutral (or even negatively charged) and the molar concentration of the species is used as approximation of their activity.  $K_{\text{HB}}$  is the acidity constant ( $K_{\text{a}}$ ) of  $\text{HB}^+$ , the conjugated acid of the base B.

Several theoretical and experimental studies have been reported in very recent years concerning the interaction of the hydroxide anion with water molecules. The experimental and theoretical study of Cwiklik et al.,<sup>13</sup> concerning  $^-\text{OH}$

impurities in and on ice, concluded that the tetrahedral complex where  $\text{OH}^-$  accepts three H-bonds and donates one, is not stable, resulting in  $\text{OH}^-$  ejection to the surface via a sequence of (barrierless) proton jumps. Instead, complex where  $\text{OH}^-$  accepts four H-bonds donating none, is stable. These data could agree with those that arise from IR and Raman spectroscopy that show an OH-stretching band for hydroxy-groups in water at 3610/cm,<sup>14</sup> which is typical of “free” hydroxy-groups, which are not involved in H-bonding. Studies of the interfacial structures suggest that such  $\text{OH}^-$  species, whose proton is not involved in H-bondings, may be located at the water–air surface,<sup>15</sup> like also it occurs at the ice crystal surface.<sup>13</sup> Neutron diffraction experiments with isotopic H/D substitution suggest that the solvation shell of the  $\text{OH}^-$  ions in water has an almost concentration-independent structure, although with concentration-dependent coordination numbers. The hydrogen site would coordinate a water molecule through a weak bond, while the oxygen site would form strong hydrogen bond with a number of water molecules. On the average, this number would be very close to four at the higher water concentrations, and would decrease to about three at the lowest one.

The state of the hydroxide ion in basic solutions may be alternatively extrapolated by the solid state structures of hydrated metal hydroxides, such as soda hydrates.<sup>16</sup> In the case of  $\text{NaOH} \cdot 7\text{H}_2\text{O}$ , the most hydrated solid soda phase, the hydroxide anions constitute distorted dimeric octahedral complex anions  $[(\text{OH})_2(\text{H}_2\text{O})_{10}]^{2-}$ . The oxygen atoms of the two OHs are H-bonded to five protons of five different water molecules while their own proton interacts with the oxygen of a bridging water molecule. This heptahydrated compound corresponds to 24.1% soda by weight, i.e., 7.57 M caustic solution, i.e., a very strong basic solution.

It seems consequently very reasonable to suppose that the hydroxide anion tends to build-up isolated octahedra  $[(\text{H}_2\text{O})_6\text{OH}]^-$ , when in sufficiently diluted water solution, dissociated from the balancing cation. It seems relevant to remark that the oxygen atom of the hydroxyl ion may be involved not only in three but also in five hydrogen bonds.

The structure of concentrated caustic soda solution (c. 10–50% wt/wt) has been the object of X-ray diffraction and simulation studies.<sup>17</sup> The concentration effect of decreasing coordination numbers around sodium ions by increasing concentration has been proven, and a building up of sodium hydroxide ion pairs has been demonstrated. According to this study, the coordination of sodium ions varies from four to eight, with five and six the most probable, direct coordination of the OH-group to sodium and bridging water molecules coordinated to two sodium ions being present.

From the value of the autoprotolysis constant (or ionic product) of water Eqn (5.2) and the molar concentration of water,  $pK_{\text{BH}}$  for the hydroxide anion (i.e.,  $pK_{\text{a}}$  of water, Eqn (5.11)) can be calculated to be 15.74. Bases definitely stronger than  $\text{OH}^-$  do not exist in water: in fact they abstract protons from water, thus completely neutralizing themselves and producing the hydroxide anions. Those having a basic strength moderately higher than the hydroxide anion ( $pK_{\text{BH}} \sim 18\text{--}20$ ) may exist with small or very small concentration as such in water solution, in equilibrium with the corresponding conjugated acids.

In analogy, the strongest acid existing in water solution is the proton solvated by water,  $[\text{H}(\text{H}_2\text{O})_n]^+$ . In fact, the  $\text{p}K_a$  of hydronium ion can be calculated to be  $-1.74$ , thus any acid having stronger acidity fully dissociates thus disappearing, leaving hydrated proton as the real acid.

In Table 5.1 a list of various basic and acid species is reported with their respective  $\text{p}K_{\text{HB}}$  values.

### 5.1.2 Protonic acidity in highly concentrated water solutions and in dry conditions

As said, the solvation of the proton in water gives rise to hydrated hydronium ion or something similar to the  $[\text{H}(\text{H}_2\text{O})_{10}]^+$  complex cation. However, the formation of such a complex (or of even more hydrated species) is only possible when the amount of available water is sufficient, i.e., only for sufficiently diluted acid solution with an acid concentration not higher than 5–10 mol/l.<sup>8</sup> Thus, this cannot occur on more concentrated solutions. In any case, it is evident that the acidity of acids in water solutions is buffered by the basicity of water itself. Bases which are definitely weaker than water are not largely protonated in water solutions. To protonate very weak bases, very highly concentrated or anhydrous acids are required.

The extent of dissociation of pure anhydrous acids is by far lower than for the corresponding water solutions, just because the ability of the acid molecule to solvate the proton is far lower than that of water. The  $K_a$  values of sulfuric and hydrofluoric acids in water are  $>10^2$  and  $\sim 10^{-3}$  respectively, but they decrease to  $\sim 10^{-4}$  and  $\sim 10^{-10}$ , respectively, in absence of water (100% acids).<sup>8</sup> Obviously, an intermediate case occurs when the concentration of the acid in water solution is very high, not allowing the stoichiometric formation of the highly solvated proton species  $[\text{H}(\text{H}_2\text{O})_6]^+$ .

The acid strength of anhydrous or highly concentrated acids is mostly described in terms of the so-called Hammett acidity function, proposed by L.P. Hammett in the 1930s<sup>18</sup>:

$$\mathbf{H}_0 = \text{p}K_{\text{BH}^+} + \log [\text{B}]/[\text{BH}^+] \quad (5.12)$$

where B is a basic indicator and  $\text{p}K_{\text{BH}^+}$  is the  $\text{p}K_a$  of its conjugated acid. The obtained value of  $\mathbf{H}_0$  is almost independent on the indicator base B. The  $\mathbf{H}_0$  values become identical with pH for diluted acidic solutions. For fully anhydrous  $\text{H}_2\text{SO}_4$  and HF  $\mathbf{H}_0$  values are near  $-12$  and  $-15$  respectively, the strongest liquid acid known being the  $\text{SbF}_5/\text{HSO}_3\text{F}$  solution, called “magic acid”, characterized by  $\mathbf{H}_0 = -23/-26.5$  and the 1:1 complex  $\text{HF}/\text{SbF}_5$  with  $\mathbf{H}_0 = -28$ . As we will discuss later on, both are combinations of a Brønsted acid with a Lewis acid. Acidity strength scales for very strongly acidic liquids may also be derived from spectroscopic measurements, such as the  $^{13}\text{C}$  NMR  $\Delta\delta$  scale proposed by Fărcasiu and Ghenciu<sup>19</sup> (where  $\Delta\delta$  is the difference between the chemical shifts of the  $\alpha$  and  $\beta$  carbons of mesityl oxide upon O-protonation), and the IR  $\Delta\nu\text{NH}$  scale proposed

**Table 5.1**  $pK_a$  Values of Selected Acids

Conjugated Acid	Base		$pK_a$ Water	$pK_a$ Acetonitrile	PA kJ/ mol
	Name	Formula			
Triflic acid	Triflate anion	$F_3C-SO_3^-$	-12	0.7/2.6	
Acetonitrilium cation	Acetonitrile	$H_3CCN$	-10.4		783
Perchloric acid	Perchlorate anion	$ClO_4^-$	-10		
Hydroiodic acid	Iodide anion	$I^-$	-9.5	2.8	1315
Hydrobromic acid	Bromide anion	$Br^-$	-9	5.5	1354
Protonated ketone	Ketone	$(CH_3)_2C=O$	-7.3		823
Hydrochloric acid	Chloride anion	$Cl^-$	-7	10.3/8.9	1395
Protonated ether	Ether	$(C_2H_5)_2O$	-3.6		
Sulfuric acid	Hydrogensulfate anion	$HSO_4^-$	-3	7.9	
Protonated alcohol	Alcohol	$CH_3CH_2OH$	-2.4		788
Triflimide	Triflimidate anion	$(F_3C-SO_2)_2N^-$	<-2	-0.1	
Hydroxonium cation	Water	$H_2O$	-1.74		691
Nitric acid	Nitrate anion	$NO_3^-$	-1.3	8.9	1358
Picric acid	Picrate anion	$(NO_2)_3C_6H_2OH$	0.40	11.0	
Oxalic acid	Hydrogenoxalate anion	$HOCCOO^-$	1.23	14.5	
Hydrogensulfate anion	Sulfate anion	$SO_4^{2-}$	1.92		
Hydrofluoric acid (polymeric)	HF (polymer)-fluoride anion	$[(HF)_nF]^-$	3.45		
Hydrogenoxalate anion	Oxalate anion	$(COO)_2^{2-}$	4.19		
Anilinium cation	Aniline	$C_6H_5NH_2$	4.63	10.6	882.5
Acetic acid	Acetate anion	$H_3CCOO^-$	4.8	21.2	1458
Malonic aldehyde (MA)	MA anion	$^-H_2C(CHO)_2$	5.0		
Pyridinium cation	Pyridine	$H_5C_5N$	5.2	12.5	928

Continued

**Table 5.1** pKa Values of Selected Acids—cont'd

Conjugated Acid	Base		pK <sub>a</sub> Water	pK <sub>a</sub> Acetonitrile	PA kJ/ mol
	Name	Formula			
Carbonic acid	Hydrogencarbonate anion	HCO <sub>3</sub> <sup>-</sup>	6.37		
Lutidinium cation	2,6-Lutidine	(H <sub>3</sub> C) <sub>2</sub> H <sub>3</sub> C <sub>5</sub> N	6.75	14.1	963
Aziridinium cation	Aziridine	C <sub>2</sub> H <sub>4</sub> NH	8.04		905.5
Hydrazinium cation	Hydrazine	H <sub>2</sub> N-NH <sub>2</sub>	8.23		853.2
Phthalimide	Phthalimide anion	C <sub>6</sub> H <sub>4</sub> (CO) <sub>2</sub> N <sup>-</sup>	8.3		
Trimethylphosphonium cation	Trimethylphosphine	(H <sub>3</sub> C) <sub>3</sub> P	8.65	16.6	957
DABCOH <sup>+</sup>	DABCO <sup>a</sup>	N(C <sub>2</sub> H <sub>4</sub> ) <sub>3</sub> N	8.8	18.3	963.4
Acetylacetone	Acetylacetonate anion	(CH <sub>3</sub> CO) <sub>2</sub> CH <sup>-</sup>	8.9		
Ammonium cation	Ammonia	NH <sub>3</sub>	9.24	16.5	853
Hydrogen cyanide	Cyanide anion	<sup>-</sup> CN	9.31		
Phenol	Phenate anion	H <sub>5</sub> C <sub>6</sub> O <sup>-</sup>	10.00	26.6/29	
Hydrogencarbonate ion	Carbonate ion	CO <sub>3</sub> <sup>2-</sup>	10.25		
<i>n</i> -Butylammonium cation	<i>n</i> -Butylamine	<i>n</i> -C <sub>4</sub> H <sub>11</sub> -NH <sub>2</sub>	10.64	18.3	920.4
Ethylammonium cation	Ethylamine	C <sub>2</sub> H <sub>5</sub> NH <sub>2</sub>	10.65	18.4	912
Methylammonium cation	Methylamine	CH <sub>3</sub> NH <sub>2</sub>	10.66	18.4	899
Triethylammonium cation	Triethylamine	(C <sub>2</sub> H <sub>5</sub> ) <sub>3</sub> N	10.75	18.5	981.8
Piperidinium cation	Piperidine	(H <sub>2</sub> C) <sub>5</sub> NH	11.12		933
Ethyl-diisopropyl ammonium cation	Ethyl-diisopropyl amine	C <sub>2</sub> H <sub>5</sub> [(CH <sub>3</sub> ) <sub>2</sub> CH] <sub>2</sub> N	11.40		994.3
Malononitrile (MN)	MN anion	<sup>-</sup> [HC(CN) <sub>2</sub> ]	11.2	22.2	
DBUH <sup>+</sup>	DBU <sup>b</sup>	C <sub>9</sub> H <sub>16</sub> N <sub>2</sub>	12	24.3	1048
Diethylmalonate (DEM)	DEM anion	<sup>-</sup> [HC(CO <sub>2</sub> C <sub>2</sub> H <sub>5</sub> ) <sub>2</sub> ]	13.5	27.8	



Guanidinium cation	Guanidine	$(\text{H}_2\text{N})_2\text{C}=\text{NH}$	13.6	23	986
tBuP1H <sup>+</sup>	tBuP1 <sup>c</sup>	$(\text{tC}_4\text{H}_9\text{N})_3\text{P}=\text{N}(\text{tC}_4\text{H}_9)$	14.9	26.9	997
Cyclopentadiene	Cyclopentadienyl anion	$(\text{C}_5\text{H}_5)^-$	15.5		
Methanol	Methoxide anion	$\text{CH}_3\text{O}^-$	15.5		1587
Water	Hydroxide anion	$\text{HO}^-$	15.74		1635
Ethanol	Ethoxide anion	$\text{CH}_3\text{CH}_2\text{O}^-$	16.0	42	1574
Acetamide	Acetamide anion	$(\text{CH}_3\text{CONH})^-$	17.0		
Isopropanol	Isopropoxide anion	$(\text{CH}_3)_2\text{CHO}^-$	17.1		
Terbutanol	Terbutoxide anion	$(\text{CH}_3)_3\text{CO}^-$	19.2		
$\text{N}[\text{C}_2\text{H}_4(\text{CH}_3)\text{N}]_3\text{PH}^+$	Proazaphosphatrane <sup>d</sup>	$\text{N}[\text{C}_2\text{H}_4(\text{CH}_3)\text{N}]_3\text{P}$		29.6	1025
Acetone	Acetone anion	$(\text{CH}_3\text{COCH}_2)^-$	20		
Acetonitrile	Acetonitrile anion	$(\text{CH}_2\text{CN})^-$	25		
Acetylene	Acetylide anion	$\text{HC}\equiv\text{C}^-$	25		
tBuP4H <sup>+</sup>	tBuP4 <sup>c</sup>	$[(\text{tC}_4\text{H}_9\text{N})_3\text{P}=\text{N}]_3\text{P}=\text{N}(\text{tC}_4\text{H}_9)$	30.6	42.6	1186
Ammonia	Amide ion	$\text{H}_2\text{N}^-$	33		
Ethylene	Vinyl anion	$\text{H}_2\text{C}=\text{CH}^-$	44		
Benzene	Phenyl anion	$\text{C}_6\text{H}_5^-$	48		
Methane	Methyl anion	$\text{CH}_3^-$	50		
<i>n</i> -Butane	Butyl anion	$\text{CH}_3\text{CH}_2(\text{CH}_3)\text{CH}^-$	>50		
Isobutane	<i>tert</i> -Butyl anion	$(\text{CH}_3)_3\text{C}^-$	>50		

<sup>a</sup> DABCO = 1,4-diazabicyclo[2.2.2]octane.

<sup>b</sup> DBU = 1,8-diazabicyclo[5.4.0]undec-7-ene.

<sup>c</sup> Phosphazene bases.

<sup>d</sup> Verkade base.

**Table 5.2** List of Some Relevant Liquid Superacids

HF/SbF <sub>5</sub>	H <sub>0</sub> = -28
SbF <sub>5</sub> /HSO <sub>3</sub> F "magic acid"	H <sub>0</sub> = -23/-26.5
HF (fully anhydrous)	H <sub>0</sub> = -15
HSO <sub>3</sub> F	H <sub>0</sub> = -15
H <sub>2</sub> S <sub>2</sub> O <sub>7</sub>	H <sub>0</sub> = -15
HCl/AlCl <sub>3</sub>	H <sub>0</sub> = -15/-14
HF/BF <sub>3</sub>	H <sub>0</sub> = -15/-14
H <sub>2</sub> O/BF <sub>3</sub>	H <sub>0</sub> = -15/-14
CF <sub>3</sub> SO <sub>3</sub> H "triflic acid"	H <sub>0</sub> = -14.1
100% H <sub>2</sub> SO <sub>4</sub>	H <sub>0</sub> = -11.9

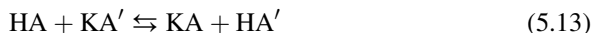
by Stoyanov et al.<sup>20</sup> (where  $\Delta\nu\text{NH}$  is the shift of  $\nu\text{NH}$  of protonated tri-octylamine, measuring the very weak basicity of the anion).

The term "superacidity", first used in 1927 by Conant<sup>21</sup> to describe very strong acids, has been resumed by Gillespie in the 1960s to indicate acids stronger than 100% H<sub>2</sub>SO<sub>4</sub>.<sup>22</sup> This field has been mostly investigated by Olah, the Nobel prize winner in Chemistry in 1994, and his coworkers.<sup>23</sup> A list of liquid superacids is reported in Table 5.2.

Reed and coworkers recently developed carborane superacids,<sup>24,25</sup> (HCB<sub>11</sub>H<sub>11-x</sub>X<sub>x</sub> where X may be Cl, Br, I) which are solid materials able to protonate extensively weakly basic molecules such as, e.g., olefins, aromatics, fullerenes, etc., without the addition of Lewis acids. The application of above cited <sup>13</sup>C NMR  $\Delta\delta$  and IR  $\Delta\nu\text{NH}$  scales, in SO<sub>2</sub> solution, shows that carborane acids are even stronger than "traditional" neat superacids, as HSO<sub>3</sub>F.

### 5.1.3 Brønsted basicity in nonprotic solvents

Nonprotic solvents allow the existence, as stable species, of bases stronger than the hydroxide anion, including "superbases". Based on experiments concerning dissociation or exchange reactions in the presence of strong bases, and correlation between data, the water pK<sub>a</sub> scale can be enlarged to values that are not really measurable in water. The pioneering work of Conant and Wheland<sup>26</sup> was the first attempt to assign pK<sub>a</sub> values to a number of extremely weak organic acids, including hydrocarbons. The position of equilibria like



where KA' is the potassium salt of a very weak acid (e.g., an alkyl-potassium organometallic compound) and HA is another very weak acid (e.g., a hydrocarbon), has been determined in a nonprotic solvent, such as diethylether. McEwen<sup>27</sup> extended the study to include a greater number of acids and improved the method

quantitatively by using colorimetric, spectroscopic or polarimetric methods to determine the position of the equilibria, using benzene as the solvent. The equilibrium constant is the ratio between the direct and inverse kinetic constants; thus kinetic studies of proton or deuterium exchange reactions can also be useful to evaluate the acidity of weak acids. Mainly using spectrophotometric experiments, today many data are available concerning acidity in nonprotic solvents having different dielectric constants, such as dimethyl-sulfoxide ( $\epsilon = 47.2$ ), acetonitrile ( $\epsilon = 36.6$ ), tetrahydrofuran ( $\epsilon = 7.58$ ), dimethoxy-methane ( $\epsilon = 7.20$ ), cyclohexylamine ( $\epsilon = 4.73$ ), diethylether ( $\epsilon = 4.20$ ), benzene ( $\epsilon = 2.27$ ), heptane ( $\epsilon = 1.92$ ), to be compared with those in water and the data arising from calculation.<sup>28,29</sup> Leito summarized many recent data in Ref. 30 and references therein.

With a slightly different but complementary approach, Hammett<sup>31</sup> first suggested suitable acidity functions applicable to the characterization of superbases. Strongly basic solutions can be arbitrarily defined as those solutions that ionize acids with an ability equal to or greater than that of aqueous alkali metal hydroxide 0.1 M solutions.<sup>18</sup> To measure their relative ability to ionize weak indicator acids HA the  $\mathbf{H}_-$  acidity function was defined as

$$\mathbf{H}_- = \text{p}K_a - \log \left( \frac{[\text{HA}]}{[\text{A}^-]} \right) \quad (5.14)$$

where  $\text{p}K_a$  is the negative logarithm of the thermodynamic ionization constant of the indicator acid in water and  $[\text{HA}]/[\text{A}^-]$  is the measured ionization ratio of the indicator. The acidity function of the solution is thus equivalent to

$$\mathbf{H}_- = -\log (a_{\text{H}^+} \cdot f_{\text{A}^-} / f_{\text{HA}}) \quad (5.15)$$

where  $a_{\text{H}^+}$  is the hydrogen ion activity in the solution and  $f$  denotes the activity coefficients of the indicator. The function  $\mathbf{H}_-$  becomes identical with pH in dilute aqueous solution where the activity of hydrogen ion becomes equal to its concentration and the activity coefficients of the indicator approach unity.<sup>32</sup> The function  $\mathbf{H}_-$  measures the ability of the solution to remove a proton from the acid and enables the strength of weak acids to be measured, kinetic mechanistic studies to be interpreted, and the physicochemical composition of solutions to be investigated.

Concentrated water solutions of metal hydroxides such as 10 M alkali hydroxides (corresponding to  $\sim 30\%$  NaOH,  $\sim 40\%$  KOH) have been measured to have  $\mathbf{H}_-$  values of 16–18.<sup>18</sup> Similar values for  $\mathbf{H}_-$  have been found for alcoholic solutions of alkali metal alcoholates. Definitely higher  $\mathbf{H}_-$  value should be measured with very basic species in less acidic solvents than water.

In Table 5.1, data about the basicity of several compounds are compared. The effects of destabilization/stabilization of the anionic charge of the base and of the cationic charge of the acid on the basicity/acidity are evident. Strong bases have very stable acid forms and unstable basic forms. The reverse is true for acids.

Several organic molecules have been synthesized recently and characterized as “superbases”.<sup>33</sup> A definition of the term “superbasicity” is due to Tanabe,<sup>34</sup> in parallel to the definition of the term “superacid”, given by Gillespie. Superacids are the acids stronger than 100%  $\text{H}_2\text{SO}_4$ ,<sup>22</sup> i.e., those characterized by  $\mathbf{H}_0 < -12$ , 19 pH units

lower than neutrality. Thus, superbases are defined as the species whose base strength expressed by the acidity function,  $H_-$ , is higher than 26, i.e., 19 pH units higher than neutrality. Very weak acid indicators such as cumene ( $pK_a \sim 37$ ), diphenylmethane ( $pK_a \sim 35$ ) and 4-chloroaniline ( $pK_a \sim 26.5$ ) can be used to determine superbasicity.

Over the past 30 years, research has been undertaken in order to increase the inherent strength of organic bases, with structures allowing large delocalization of the cationic charge in the protonated form thus allowing a very strong stabilization of the  $HB^+$  conjugated acid, which displaces equilibrium Eqn (5.7) to the left. The field was transformed in the early 1990s by Schwesinger and coworkers<sup>35–37</sup> with the synthesis of a series of strong, uncharged bases, termed peralkylated polyaminophosphazenes. Compared to traditional organic bases, the peralkylated phosphazene bases demonstrate a dramatic increase in basic strength, up to above 30  $pK_{HB}$  units, giving rise to base strengths comparable to that of organometallic bases. Other extremely strong bases are guanidines,<sup>38</sup> vinamidine,<sup>39</sup> the so-called Verkade bases, i.e., proazaphosphatranes,<sup>40</sup> as well as the corresponding imides and ylides.<sup>37</sup> It seems that the strongest molecular bases prepared up to now belong to the peralkylated polyaminophosphazene family, with  $pK_a$  values of above a little above 30.

Superbasicity also occurs with a number of organometallic compounds that are formally the alkali or alkali earth salts of extremely weak acids. They are alkali alcoholates and amides, alkali hydrides and alkali silanes. The most basic species, with  $pK_a$  values up to above 50, arise essentially from alkyl alkali, such as e.g., the *n*-butyl anion, which is formally the result of dissociation of *n*-butyl lithium,



Similar lithium alkyls, sodium alkyls, potassium alkyls as well as alkyl-magnesium-halides (i.e., Grignard reagents) are largely used in organic chemistry for nucleophilic alkylations.<sup>41</sup> They may be assumed to be the salts of hydrocarbons, which are in fact the weakest protonic acids. They must be used as reagents in the dry solvents and have to be handled in perfectly dry atmospheres, to avoid exchange reaction with water or moisture. Organometallics are the more stable, the less basic is the organic anionic species and the less ionic is the C-metal bond. For this reason, organolithium compounds and organomagnesium halides, whose bond is quite covalent, are those produced industrially and available in the market. They may be converted into even more reactive compounds by transmetallation reactions. The most basic (and the less stable) carbanions are branched, such as the *tert*-butyl anion, due to the electron-donating behavior of methyl groups. In several cases, organometallic compounds tend to aggregate with increasing their superbasicity. According to this behavior, Caubère<sup>42</sup> proposed a definition of superbases as the “bases resulting from a mixing of two (or more) bases leading to new basic species possessing inherent new properties”.

A number of solids have also been characterized as “superbasic”. It is worth to know, however, that the characterization of superbasicity on solids is mostly done on the base of titration experiments, whose validity is doubtful for some authors. A review of the literature<sup>34,43</sup> indicates that metal oxides containing alkali-, alkali-earth

and rare-earth cations may give rise to very strong basicity just at the limit of superbasicity. True superbasic solids are alkali metals supported on basic carriers. The strongest superbasic solid appears to be constituted by Na/NaOH/Al<sub>2</sub>O<sub>3</sub><sup>44</sup> whose basicity has been evaluated to correspond to  $H_- = 37$ .

Superbases are relevant reactants in organic chemistry and may be very significant catalysts. In fact, superbases are needed to abstract protons from most hydrocarbons, which are in fact very weak acids, including from allylic and benzylic positions.<sup>43</sup> The most used superbases applied in industrial chemistry are apparently alkali metals, which are most frequently supported on basic carriers.

### 5.1.4 Lewis acidity and basicity

In the same year of the Brønsted and Lowry definitions, 1923, G.N. Lewis<sup>45</sup> proposed a different approach to acidity and basicity. In his view, an acid is any species that, because of the presence of an incomplete electronic grouping, can accept an electron pair thus forming a dative or coordination bond. Conversely, a base is any species possessing an electron pair which can be donated to form a dative or coordination bond. The Lewis-type acid–base interaction can be consequently denoted as follows:



The Lewis classification of acids is broader than that of Brønsted, while Lewis basic species are also Brønsted bases. The Lewis definition is independent from water as the reaction medium. Lewis acid–base interactions are predominant in many practical phenomena, such as in complexation and extraction of metal ions, in adsorption on and dissolution of ionic solids, in solid state and melt reactions, etc.

Although metal-free Lewis acid catalysts also exist (like silyl cation-based catalysts, hypervalent silicon-based catalysts, phosphonium cation-based catalysts, carbocation-based catalysts<sup>46</sup>) most used and typical strong Lewis acids are metal compounds or complexes with very weakly basic ligands. Among the simplest and cheaper Lewis acids, we can mention Al and B trihalides, as well as the halides of other cations such as FeCl<sub>3</sub>, ZnCl<sub>2</sub>, TiCl<sub>4</sub>, SnCl<sub>4</sub>, SbF<sub>5</sub>, BiCl<sub>3</sub>, etc.

The Lewis acidity of several of these compounds is decreased by their tendency to aggregate that produce an increase in cation coordination and a concomitant decrease in Lewis acid strength.

To produce Lewis superacids, the elements must be bonded to very poor electron-donating substituents, such as triflate ions (F<sub>3</sub>C–SO<sub>2</sub>OH is triflic acid) like for Bi(OTf)<sub>3</sub> and Ag(OTf) and triflimidates ((F<sub>3</sub>C–SO<sub>2</sub>)<sub>2</sub>NH is triflimide) of Al<sup>3+</sup>, In<sup>3+</sup>, Ce<sup>3+</sup>, Sm<sup>3+</sup>, Fe<sup>3+</sup>, Sn<sup>4+</sup>, Mg<sup>2+</sup>, Zn<sup>2+</sup> etc. which find catalytic activity for a number of reactions (including Friedel–Crafts alkylations and acylations) some of which with an effect of asymmetric catalysis.<sup>47,48</sup> Aluminum has been combined with bulky perfluorinated alkoxy-ligands such as (CF<sub>3</sub>)<sub>3</sub>CO<sup>−</sup> in order to increase the electron-withdrawing activity of the metal and reduce aggregation, producing very strong Lewis superacids.<sup>49</sup>

Quantification of the Lewis acid strength has been attempted using several techniques like chloride ion affinity, lowest unoccupied molecular orbital (LUMO) energy, methyl ion affinity, hydride ion affinity, and fluoride ion affinity (FIA) whose values are mostly obtained by calculation but can also be determined experimentally. Nuclear magnetic resonance (NMR) spectroscopy of protons or other nuclei of interacting basic probe molecules has also been used. In a recent paper, Hilt et al.<sup>50</sup> measured Lewis acidity of most common Lewis bases using <sup>2</sup>H NMR spectroscopy of deuterated quinolizidine. They also compared the results with those arising from the measured catalytic effect on two Lewis acid-catalyzed test reactions, i.e., (1) the Diels–Alder reaction of naphthoquinone with an excess amount of isoprene; (2) the Povarov reaction of a complex imine with allyl-trimethylsilane. A good correlation exists suggesting the following Lewis strength scale reported in Table 5.3.

According to Kraft et al.<sup>49</sup> Lewis superacids can be defined as molecular compounds that are stronger than the strongest conventional Lewis acid, i.e., monomeric SbF<sub>5</sub> in terms of FIA, i.e., an FIA higher than 489 kJ/mol in the gas phase. A list of Lewis superacids is reported in Table 5.4.

A very important activity of Lewis acids is their ability to activate Brønsted acids, by coordinating the lone pairs of the anionic species, thus stabilizing the conjugated base of the acid. In fact, as shown above, systems like HCl–AlCl<sub>3</sub>, HSO<sub>3</sub>F–SbF<sub>5</sub>

Lewis Acid	$\delta(^2\text{H})$ of 2	$(k_{\text{DA}}/10^{-3})/\text{s}$	$(k_{\text{POV}}/10^{-4})/\text{s}$
None	1.56	–	–
Ti(O <i>i</i> Pr) <sub>4</sub>	1.58	No reaction	No reaction
ZnCl <sub>2</sub>	1.70	–	–
ZnI <sub>2</sub> ·OEt <sub>2</sub>	1.85	$\approx 6.0 \times 10^{-3}$	No reaction
ZnBr <sub>2</sub>	1.94	–	–
BH <sub>3</sub> ·SMe <sub>2</sub>	2.27	–	–
TiCl <sub>2</sub> (O <i>i</i> Pr) <sub>2</sub>	2.36	$\approx 6.0 \times 10^{-2}$	–
AlEt <sub>2</sub> Cl	2.51	1.9 ± 0.3	1.5 ± 0.5
BF <sub>3</sub> ·OEt <sub>2</sub>	2.76	4.6 ± 1.0	2.2 ± 0.4
TiF <sub>4</sub>	2.78	–	–
TiCl <sub>4</sub>	2.93	1.6 ± 0.1	3.0 ± 0.4
TiBr <sub>4</sub>	3.00	–	–
AlCl <sub>3</sub> ·OEt <sub>2</sub>	3.54	6.7 ± 0.4	4.8 ± 0.7
AlEtCl <sub>2</sub>	3.59	22 ± 5	5.3 ± 1.0
BCl <sub>3</sub>	4.08	$\approx 28$	5.6 ± 0.4
BBr <sub>3</sub> ( <i>trans</i> )	3.04		
BBr <sub>3</sub> ( <i>cis</i> )	4.33		13.6 ± 4.0

[a] All NMR spectra were measured in dichloromethane, which was also the solvent for both reactions. From Ref. 50.

**Table 5.4** Overview of the Calculated FIA Values of Some Classical Gaseous Lewis (Super)acids and  $\text{Al}(\text{OR}^{\text{F}})_3$ . All Values Were Assessed at the BP86/SV(P) Level and are Given in kJ/mol

Lewis Acid/Anion	FIA	Lewis Acid/Anion	FIA
$\text{BF}_3/[\text{FBF}_3]^-$	338	$\text{SbF}_5/[\text{FSbF}_5]^-$	489
$\text{PF}_5/[\text{FPF}_5]^-$	394	$\text{AlBr}_3/[\text{FAlBr}_3]^-$	494
$\text{BCl}_3/[\text{FBCl}_3]^-$	405	$\text{AlI}_3/[\text{FAlI}_3]^-$	499
$\text{BBr}_3/[\text{FBBr}_3]^-$	433	$\text{PhF-Al}(\text{OC}(\text{CF}_3)_3)_3$ (6)/ $[\text{FAl}(\text{OR}^{\text{F}})_3]^-$ + PhF	505
$\text{GaBr}_3/[\text{FGaBr}_3]^-$	436	$\text{F}_2\text{C}_6\text{H}_4\text{-Al}(\text{OC}(\text{CF}_3)_3)_3$ (7)/ $[\text{FAl}(\text{OR}^{\text{F}})_3]^-$ + $\text{F}_2\text{C}_6\text{H}_4$	514
$\text{B}(\text{C}_6\text{F}_5)_3/[\text{FB}(\text{C}_6\text{F}_5)_3]^-$	444	$\text{Al}(\text{OC}(\text{C}_5\text{F}_{10})\text{C}_6\text{F}_5)_3$ (2)/ $[\text{FAl}(\text{OR}^{\text{F}})_3]^-$	530
$\text{BI}_3/[\text{FBI}_3]^-$	448	$\text{Al}(\text{OC}(\text{CF}_3)_3)_3$ (1)/ $[\text{FAl}(\text{OR}^{\text{F}})_3]^-$	537
$\text{GaI}_3/[\text{FGaI}_3]^-$	454	$\text{B}(\text{CN})_3/[\text{FB}(\text{CN})_3]^-$	548
$\text{AlCl}_3/[\text{FAlCl}_3]^-$	457	$\text{B}(\text{CF}_3)_3/[\text{FB}(\text{CF}_3)_3]^-$	552
$\text{AlF}_3/[\text{FAlF}_3]^-$	467	$\text{AuF}_5/[\text{FAuF}_5]^-$	556
$\text{OSO-Al}(\text{OC}(\text{CF}_3)_3)_3$ (8)/ $[\text{FAl}(\text{OR}^{\text{F}})_3]^-$ + $\text{SO}_2$	486 <sup>a</sup>	$2\text{Al}(\text{OC}(\text{CF}_3)_3)_3/[(^{\text{F}}\text{RO})_3\text{AlFAl}(\text{OR}^{\text{F}})_3]^-$	685

Abbreviation: FIA, fluoride ion affinity.  
From Ref. 49.

and  $\text{HF-SbF}_5$  are definitely more acidic than  $\text{HCl}$ ,  $\text{HSO}_3\text{F}$  and  $\text{HF}$  attaining superacidity (Table 5.2). The presence of Lewis acids can also activate water as a Brønsted acid. Thus the presence of water allows in some way the conversion of a Lewis acid into a Brønsted acid.

### 5.1.5 Hard and soft acidity and basicity (HSAB) and nucleophilicity

In 1963, Pearson<sup>51,52</sup> introduced the concept of hard and soft acids and bases (HSAB), which may be taken as an evolution of the Lewis acid and base definition. Hard acids are defined as small-sized, highly positively charged, and not easily polarizable electron acceptors. Hard bases are substances that hold their electrons tightly as a consequence of large electronegativities, low polarizabilities, and difficulty of oxidation of their donor atoms. Hard acids prefer to associate with hard bases while soft acids prefer to associate with soft bases. These complexes are thermodynamically more stable than mixed complexes; and also form faster. According to this theory, protons and hydroxide and oxide ions are both hard, such as most O- and N-terminated anions. C- and S-terminated anions, sulphides, phosphines and aromatic hydrocarbons, are soft bases.

A theoretical assessment of the HSAB theory, which is actually an empirical one, has been given by Klopman.<sup>53</sup> According to this approach, the acid–base interactions depend predominantly on two effects: electrostatic interaction and orbital interaction. Electrostatic interactions predominate for hard–hard or “charge-

controlled” acid–base interactions. Orbital interactions occur between the highest occupied molecular orbital of the base and the LUMO of the acid. The closer in energy these orbitals, the stronger the interaction. This factor is predominant for soft–soft or “frontier-orbital-controlled” acid–base interactions. While the application of the HSAB theory proved to be useful for rationalizing stability constants of metal complexes, its application to heterogeneous catalysis is very limited if at all, while that to organic chemistry is controversial.<sup>54</sup>

Similar interactions occur also with molecules (such as, e.g., CO<sub>2</sub>, SO<sub>2</sub>, SO<sub>3</sub>, carbonyl and carboxyl organic compounds) that do not actually have nonbonding empty orbitals (as required by the Lewis definition of an acid) but can give rise to empty orbitals during reaction and/or upon rehybridization. The interactions of basic species with electron-poor carbon-containing species belong to this type of interactions, but are commonly described by organic chemists in terms of nucleophile–electrophile interactions.<sup>55</sup> Nucleophiles are electron rich chemical species, having a full n-type orbital, that can react with an electron-poor carbon atom allowing the formation of a new bond. This occurs in different ways, such as by reacting with: (1) a sp<sup>2</sup> hybridized carbenium ion, such as in the SN<sub>1</sub> nucleophilic substitution and in the electrophilic additions to olefins; (2) a sp<sup>3</sup>-hybridized carbon atom, such as in the SN<sub>2</sub> nucleophilic substitution; (3) a sp<sup>2</sup>-hybridized carbonylic or carboxylic carbon atoms, such as upon the nucleophilic attack to carbonyls and in the acyclic nucleophilic substitution reactions. Actually, the nucleophile–electrophile interactions are mostly evaluated in kinetic more than in thermodynamic terms.<sup>56</sup> A measure of the nucleophilicity of a reactant is in fact usually given as the rate of reaction in a given reaction such as, e.g., a SN<sub>2</sub> nucleophilic substitution. However, the rankings of the nucleophiles in different nucleophile–electrophile interactions are generally quite consistent when the attacking atom is the same, except when very important steric effects are present. This means that the dominating effect also in the nucleophilicity scale is the thermodynamic instability of the nucleophile/base, which also is the dominant effect governing basicity.

This is not always true for nucleophiles having different attacking atoms, such as O- and S-compounds. S-compounds are generally less basic but more nucleophilic than the corresponding O-compounds. In fact, the proton being a hard acid, the Brønsted basicity is stronger for hard than for soft species. Being, in contrast, any electrophilic carbon quite a soft acid (and, in any case, a softer acid than the proton), nucleophilicity is stronger for softer bases, such as sulfur compounds with respect to oxygen compounds.

### 5.1.6 Gas phase acidity and basicity

As already remarked, liquid-phase basicity and acidity are strongly dependent on solvation effects (thus strongly depending from the solvent) and may also be affected by steric hindrance.

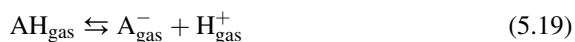
Brønsted basicity and acidity in the gas phase should, instead, be “pure” properties, only depending on the availability of electron pairs on the basic site. The



comparison of liquid-phase basicities/acidities and gas-phase basicities/acidities can consequently give information just on the steric and solvation effects occurring in the liquid phases. Experimentally evaluated gas-phase parameters allowing the determination of basicity and acidity in the gas-phase are proton affinity (PA), deprotonation energies (DPE) and gas-phase basicities (GB) and acidities (GA).<sup>57</sup> PA and GB values correspond to the changes in enthalpies ( $\Delta H$ ) and Gibbs free energies ( $\Delta G$ ), respectively, for the reaction in equation



defined at a finite temperature, usually 298 K. For the acid AH, the deprotonation reaction



is considered. The changes in enthalpies ( $\Delta H$ ) and Gibbs free energies ( $\Delta G$ ), respectively, are called deprotonation enthalpy (DPE) and GA, respectively. For conjugated acid and base  $\text{DPE} = \text{PA}$  and  $\text{GA} = \text{GB}$ . A stronger acid has smaller GA and DPE value, and a stronger base has a larger GB and PA value. In Table 5.1 PA = DPE values are reported for a number of compounds.

Most available data on GA/GB and DPE/EA have been obtained from experiments in which the equilibrium constants of proton transfer reactions are determined. Calculation of gas-phase basicity allows ranking of molecular superbases<sup>28,37</sup> and is perhaps easier today than experiments in this respect. Other parameters concerning gas-phase basicity can also be found in the literature, being more related to Lewis basicity as well as to HSAB behavior. These are cation affinities and cation basicities, such as lithium,<sup>58</sup> sodium,<sup>59</sup> cesium<sup>60</sup> affinities and basicities. However, availability of these data is far lower than for PA.

As evident for the data reported in Table 5.1  $\text{p}K_{\text{a}}$  and PA/DPE scales differ considerably, showing the effect of solvation. It is also relevant to note that PA values of neutral bases are definitely smaller than DPE of neutral acids (corresponding to a reaction that produces two ions from a neutral molecule), even when  $\text{p}K_{\text{a}}$  are similar, thus showing again the role of solvation by water in stabilizing ions more than neutral molecules. Himmel et al. are developing a Unified Brønsted acidity scale based on the calculation of standard Gibbs free energy of proton solvation.<sup>9,61</sup>

---

## 5.2 Reactant activation and acid–base catalysis in liquid phases

### 5.2.1 Reactant activation and acid–base catalysis in diluted water solutions

Acid and bases may act as catalysts when they perturb reactant molecules thus offering to a reactant species a different way to evolve toward products associated to a

lower activation energy. In this case, the reaction may occur faster. Many reactions involving polar molecules may be performed in water solutions and may be catalyzed by acids or by bases or by both. It is well known that, in several cases, polar molecules (which present both a negatively charged and a positively charged pole) can be activated both by bases (by interaction with the positively charged pole) and by acids (by interaction with the negatively charged pole). A typical practical example is the transesterification of triglycerides to fatty acids methyl esters, thus producing biodiesel, which can be catalyzed by bases such as caustic soda or by acids such as sulfuric acid.<sup>62</sup> In fact, in the industry, the cheaper acids and bases are obviously preferred as catalysts, sulfuric acid and caustic soda being the most commonly used. In Table 5.5 some applications of sulfuric acid are reported. In Table 5.6 some base catalyzed industrial reactions are reported. In Table 5.7 some of the many industrial reactions using liquid Lewis acids as catalysts are summarized.

### 5.2.2 Activation of weak basic molecules by acids

Typical basic species have electron pairs in nonbonding ( $n$ -) orbitals. These “doublets” can be used to produce a dative bond with species having empty orbitals, such as protons or coordinatively unsaturated cations. They are consequently denoted as  $n$ -bases. Such an  $n$ -type basic molecule can be activated by protic acids, mostly used in water solution, or by Lewis acids, which can be used in both water solutions and in nonprotic solvents. The protonation of the coordination of lone pairs perturbs the nearest bonds inducing, e.g., nucleophilic attacks by other reactant species. This is, e.g., the case of reactions such as etherifications and esterifications, where both Brønsted and Lewis acid catalysts can be used to attack the most basic oxygen atoms of the reactants.<sup>63</sup>

However, Brønsted and Lewis acid catalysis also occurs with molecules not containing nonbonding orbitals such as hydrocarbons. The ability of hydrocarbons (which do not have  $n$ -orbitals) to interact with protic acids has been recognized long ago. In fact, paraffins give rise to weak hydrogen-bonding interactions with hydroxyls having some acidity, such as those of alcohols, carboxylic acids and also surface hydroxy-groups of silica and protonic zeolites. At higher temperature or in the presence of very strong acidity, these interactions can produce a true proton transfer, thus hydrocarbons acting as Brønsted bases. In Table 5.8 the PA scale of some hydrocarbons is reported.<sup>64</sup> The PA data follow again the trend:  $\pi$ -orbital containing compounds (olefins and aromatics) > isoalkanes >  $n$ -alkanes > methane.

Olefins can react with protic acids and can produce the so-called trivalent “classical” carbocations (carbenium ions) as intermediates of electrophilic addition reactions. The history of carbocations, which are intermediates also in nucleophilic substitution reactions ( $S_N1$ ) and in elimination reactions ( $E_1$ ), begins at the end of the nineteenth century,<sup>16</sup> and involves very distinguished organic chemists such as Meerwein, Ingold, Whitmore, and many others. The reactivity of olefins, through their  $\pi$ -type orbitals, toward protons is evidence of the so-called  $\pi$ -basicity of these

**Table 5.5** Characteristics of Some Industrial Conversion Processes Involving Sulfuric Acid Catalysts

Products/Process	Protonated Species	H <sub>2</sub> SO <sub>4</sub> Concentration	<i>T</i>	<i>P</i>	Reactor Type
Cellulose hydrolysis to glucose “diluted acid process”	Cellulose	0.5%	150–250 °C	1 MPa	Continuous reactors
Ethylene glycol synthesis	Ethylene oxide	1%	50–70 °C	0.1 MPa	Tank reactor
Phenol and acetone synthesis	Cumene hydroperoxide	Few%			Backmixed reactor
<i>i</i> -Butylene hydration to <i>tert</i> -Butanol	<i>i</i> -Butylene	50%	50 °C	0.4–0.5 MPa	Wash towers
Propylene indirect hydration to 2-propanol	Propylene	60%	75–85 °C	0.6–1 MPa	Wash towers
<i>i</i> -Butylene oligomerization	<i>i</i> -Butylene	60–65%	20–25 °C		
Cellulose hydrolysis to glucose “concentrated acid process”	Cellulose	72%	30–55 °C		Batch reactors
Benzene alkylation to cumene	Propylene	90%	35–40 °C	1.15 MPa	Stirred tank
Methyl acetate synthesis	Acetic acid	>90%	55–100 °C	0.1 MPa	Reactive distillation tower
Ethylene indirect hydration to ethanol	Ethylene	94–98%	65–85 °C	1–3.5 MPa	Wash towers
<i>i</i> -Butane/butylene alkylation	<i>i</i> -Butylene	90–98%	20–40 °C	0.3–0.5 MPa	Horizontal stirred tank contactor or cascade reactor
Linear alkylbenzenes	Linear higher olefins	96–98%	10–30 °C		Stirred tank-type

Reaction Name	Reactants (Example)	Products (Example)	Typical Homogeneous Catalyst
Aldol condensation	Heptanal with benzaldehyde	Jasminaldehyde	NaOH or KOH
Claisen–Schmidt	2'-Hydroxycetophenone and benzaldehyde	2'-Hydroxy chalcones	NaOH, CH <sub>3</sub> CH <sub>2</sub> ONa
Henry	Nitroalkanes with aldehydes.	2-Nitroalkanols	Amine
Knoevenagel condensation	Benzyl acetone and ethyl cyanoacetate	2-Cyano-3-methyl-5-phenylpent-2-en-oate	Amine
Wittig	Phosphonium ylide and an aldehyde	Internal olefin	NaH, <i>t</i> -BuOK, or NaOH
Michael addition	Methyl crotonate	3-Methyl-2-vinylglutarate	Alkoxides
Baillis–Hillman	Aldehyde + $\alpha,\beta$ -unsaturated carbonyl	Allyl alcohol	DABCO
Guerbet reaction	Alcohol + alcohol	Higher alcohol	<i>t</i> -BuOK + metal complex
Tishchenko	Acetaldehyde	Ethylacetate	(CH <sub>3</sub> CH <sub>2</sub> O) <sub>3</sub> Al
Cannizzaro	Formaldehyde + trimethylolacetaldehyde	Pentaerythrol (+ formic acid)	NaOH, Ca(OH) <sub>2</sub>
Meerwein–Ponndorf	Aldehyde + alcohol	Alcohol + aldehyde	Al isopropylate
Oppenauer	Alcohol + aldehyde	Aldehyde + alcohol	Al-alkoxides
Cyanoethylation	Acetone + acrylonitrile	5-Oxo-hexanenitrile	Isopropylamine
Addition of alcohols to $\alpha,\beta$ -unsaturated carbonyls	Methanol + crotonaldehyde	3-Methoxy-butanal	NaOH

**Table 5.7** Catalysts of Some Industrial Processes Involving Lewis Acid Catalysts

Product	Process	Reactants	Catalyst
Ethylene dichloride	Ethylene direct chlorination	Ethylene, Cl <sub>2</sub>	FeCl <sub>3</sub>
Chlorobenzenes	Benzene chlorination	Benzene, Cl <sub>2</sub>	FeCl <sub>3</sub>
Ethylchloride		Ethylene, HCl	AlCl <sub>3</sub> , ZnCl <sub>2</sub>
<i>para</i> -Tolualdehyde	Gattermann–Koch carbonylation of toluene (Mitsubishi process)	Toluene CO	HF/BF <sub>3</sub>
Ethylbenzene	Benzene alkylation	Ethylene, benzene	CH <sub>3</sub> CH <sub>2</sub> Cl (HCl)/AlCl <sub>3</sub>
Polyisobutene	Cationic polymerization	Isobutene	HCl/AlCl <sub>3</sub> or BF <sub>3</sub>
<i>o</i> -Benzoyl-benzoic acid (precursor of anthraquinone)	Friedel–Crafts acylation	Phthalic anhydride, benzene	AlCl <sub>3</sub>
Anthraquinone	Diels–Alder cyclization	Naphthoquinone, butadiene	AlCl <sub>3</sub> , ZnCl <sub>2</sub> , FeCl <sub>3</sub>
<i>p</i> -Acetyl-isobutylbenzene (precursor of ibuprofen)	Friedel–Crafts acylation	Isobutylbenzene, acetic anhydride	AlCl <sub>3</sub>
2-Acetyl-6-methoxy-naphthalene (precursor of naproxen)	Friedel–Crafts acylation	2-Methoxy-naphthalene, acetyl chloride	AlCl <sub>3</sub>

**Table 5.8** Proton Affinities (kJ/mol) of Hydrocarbons and of Ammonia for Comparison

Ammonia	846.0	n-Bases
Isobutylene	802.1	$\pi$ -Bases
Toluene	784.0	
1,3-Butadiene	783.4	
Propylene	751.6	
Benzene	750.4	
Ethylene	680.5	
Isobutane	677.8	$\sigma$ -bases
Propane	625.7	
Ethane	596.3	
Methane	543.5	

*From NIST database, Ref. 22.*

compounds, probably first proposed by M.J. Dewar.<sup>65</sup> The result of this interaction, with the intermediacy of protonated  $\pi$ -bonded transition state, is the formation of carbenium ions,<sup>66</sup> where the  $\pi$ -type orbitals disappear and one of carbon atoms rehybridizes from  $sp^2$  to  $sp^3$ , the hydrogen becoming covalently bonded to the carbon atom via a  $\sigma$ -bond. The carbenium ions are more stable and more easily formed on tertiary carbon atoms, while their formation on primary carbon atoms is very difficult. This is associated with the electron-donating properties of alkyl groups that allow the cationic charge to be delocalized, thus stabilizing the cation. Olah and coworkers<sup>67</sup> isolated several carbenium ions as stable species by using very weak nucleophiles as balancing anions.

The  $\pi$ -basicity of aromatic hydrocarbons was also observed long ago<sup>65</sup> and the existence of quite stable protonated forms of benzenes and the methyl substituent effects on them was determined.<sup>68</sup> Protonation of aromatic rings generates arenium ions whose cationic charge is delocalized on the ring and in particular in the *ortho*- and *para*-position with respect to the position where the attack of the electrophile (the proton in this case) occurred.

More recently, Olah and Schlosberg<sup>69</sup> and Hogeveen et al.<sup>70</sup> observed the protonation of alkanes by superacids, thus suggesting that alkanes may behave as  $\sigma$ -bases. The basicity scale for  $\sigma$ -bonds of hydrocarbons is reported to be *tert*-C–H > C–C > *sec*-C–H > *prim*-C–H > CH<sub>4</sub>, although this depends also on the protonating agent and the steric hindrance of the hydrocarbons.<sup>71</sup> In fact, protonation at C–C bond may be significantly affected by steric hindrance.<sup>72</sup> Protonation of alkanes generates the so-called “nonclassical” pentacoordinated carbonium ions, which contain five-coordinated (or higher) carbon atoms.

The carbocations, which may be stabilized by solvation, are more or less stable species and may act as intermediate species or as transition states in the conversion of hydrocarbons.<sup>73</sup> In this case, the acid is regenerated after the completion of the reaction and acts consequently as a catalyst. Many of the hydrocarbon conversion industrial processes are acid catalyzed and the formation of carbenium and carbonium ions is one of the steps in the reaction mechanism, both over liquid- and solid-acid catalysts.<sup>74,75</sup>

### 5.2.3 Catalysis in liquid superbasic conditions

Typical extremely basic species, used mostly as nucleophilic reactants in organic chemistry, are alkali alkoxides, alkali amides and organometallics such as alkyllithium compounds. In recent years, several “superbasic” molecules have been synthesized, characterized by very extensive delocalization of the cationic charge of their protonated conjugated forms. Polyphosphazenes, proazaphosphatranes and polyguanidines are “superbasic” molecules. In Table 5.1 these species are summarized. These molecules may be so basic to extract protons from hydrocarbons molecules, thus generating alkylanions (carbanions). This strongly enhances the reactivity of the corresponding hydrocarbon. In some cases, however, such superbases act more than as catalysts, as initiators of chain reactions.

---

## 5.3 The surface acidity and basicity of solids

### 5.3.1 Structural chemistry versus surface chemistry of solids: a fundamental approach

Solid materials may essentially belong to the following different types:

1. metallic materials, such as metals and alloys;
2. ionic network materials, such as most metal oxides and sulphides;
3. covalent network materials, such as diamond, silicon, some nonmetal oxide (typically silica, see Chapter 6 for a deep discussion), several carbides and nitrides, network polymers;
4. layered structures such as graphite, hexagonal boron nitride, layered sulphides ( $\text{MoS}_2$ ,  $\text{WS}_2$ ), and some layered oxides (molybdena);
5. polymeric molecular solids, among which many polymers, but also boron trioxide and chromic anhydride  $\text{CrO}_3$ ;
6. molecular solids including some oxides like phosphoric and phosphorous anhydrides and sulfur trioxide.

In the case of ionic or covalent network materials, the surface is a defect situation where oxide species and metal or nonmetal centers remain exposed and coordinatively unsaturated at the surface. These sites should be associated to very high free energy and, consequently, should be very unstable. To stabilize the surface, reconstruction phenomena as well as reaction with molecules from the environment (e.g., water and  $\text{CO}_2$ ) occur. This would limit the number of coordinatively unsaturated centers and cause the formation of new surface species such as hydroxy-groups and surface carbonates. However, unsaturated centers at the surface can remain or be generated by desorption of adsorbed water (and  $\text{CO}_2$ ) under heating. As a consequence of these phenomena, the surface of solid oxides can be constituted by surface oxide species, acting as basic sites, and coordinatively unsaturated cations (mostly on ionic surfaces) or surface hydroxy-groups (on both covalent and ionic surfaces) acting as Lewis and Brønsted acid sites, respectively.

It is evident that the surface of an ionic crystal particle is likely predominantly composed by planes which should mainly correspond to the most stable faces. However, to allow the exposition of these most stable faces, other less stable faces must also be exposed, and corners and edges should exist at the surface. These should be the most reactive sites, where most coordinatively unsaturated cations and anions should really exist. On the other hand, these defect sites should also be those first “neutralized” by adsorption of gas phase species and by growing of poisonous species. In any case, it seems really very likely that catalysis occurs mostly on such defect sites more than over plain faces.

Similar considerations can be made for covalent network solids. In this case, at the surface, covalent bonds are broken, thus generating (in theory) an extremely reactive situation. Just because its extreme reactivity, the surface is “saturated” by forming new covalent bonds with species from the gas (water, oxygen). The resulting

surface may be consequently not really or not completely unsaturated in normal conditions. However, the surface is modified by layers (e.g., oxide layers) or sites (e.g., silanol groups of silica) which have a peculiar behavior and may be also decomposed in very hard conditions reproducing an extremely reactive surface.

Computational studies are today powerful techniques in the field of heterogeneous catalysis research. Accordingly, the surfaces of many acid–basic solids have been modeled. However, the deep limit of such theoretical studies is that some of these calculations need periodical structures, and thus defects such as edges and corners are not considered. A similar limit concerns monocrystal studies where, however, the use of stepped surfaces allow to forecast the behavior of edge and corner sites.

### 5.3.2 Characterization techniques of surface acidity and basicity of solids

#### 5.3.2.1 Techniques for the characterization of surface acidity and basicity

Different techniques can be used to study the surface acidity and basicity of solids, either at the gas–solid interface or at the solid–water solution interface. Details concerning the characterization techniques can be found in several books and reviews, some of which are very recent and concern materials and catalysts<sup>76–78</sup> or particular families of catalysts such as oxides,<sup>79,80</sup> zeolites,<sup>81,82</sup> sulfide<sup>83</sup> and metal catalysts.<sup>84,85</sup> We will comment briefly here only on few most widely used and available methods for surface acid–base characterization.

#### 5.3.2.2 Molecular probes for surface acidity and basicity characterization

Most surface characterization techniques are “indirect”: they investigate the strength of adsorption or desorption of bases on acid sites and of acids on basic sites. In [Table 5.9](#) some data on the basic probe molecules typically applied in acidity surface characterization are summarized. Similarly, in [Table 5.10](#), some data on the “acidic” (or electrophilic) probe molecules typically applied in basicity surface characterization are summarized. A careful analysis of the available data and of the conditions in which they have been obtained shows that the data arising from the different techniques and from the use of different probes generally agree quite satisfactorily.<sup>86</sup> In general, the use of several techniques and of different probes is useful to have a deep picture. Most of basic probes allow to obtain a good picture for surface acidity characterization, because they behave (at least for classes of catalysts and in the most typical conditions) quite specifically interacting with acid sites, although most of them interact with both Brønsted and Lewis acid sites. 2,6-diterbutyl pyridine is considered to act as a specific probe for Brønsted sites, due to the steric hindrance of the alkyl groups, which should not allow coordination on Lewis sites.

The variable size of families of basic probe molecules can also be used to test the position of acid sites in zeolites and other microporous materials. In fact, larger molecules cannot penetrate in small pores, while chemically similar small molecules can enter and be adsorbed there. Molecules allowing this kind of analysis are summarized in [Scheme 5.1](#).



**Table 5.9** Molecular Probes Applied for Surface Acidity Characterization

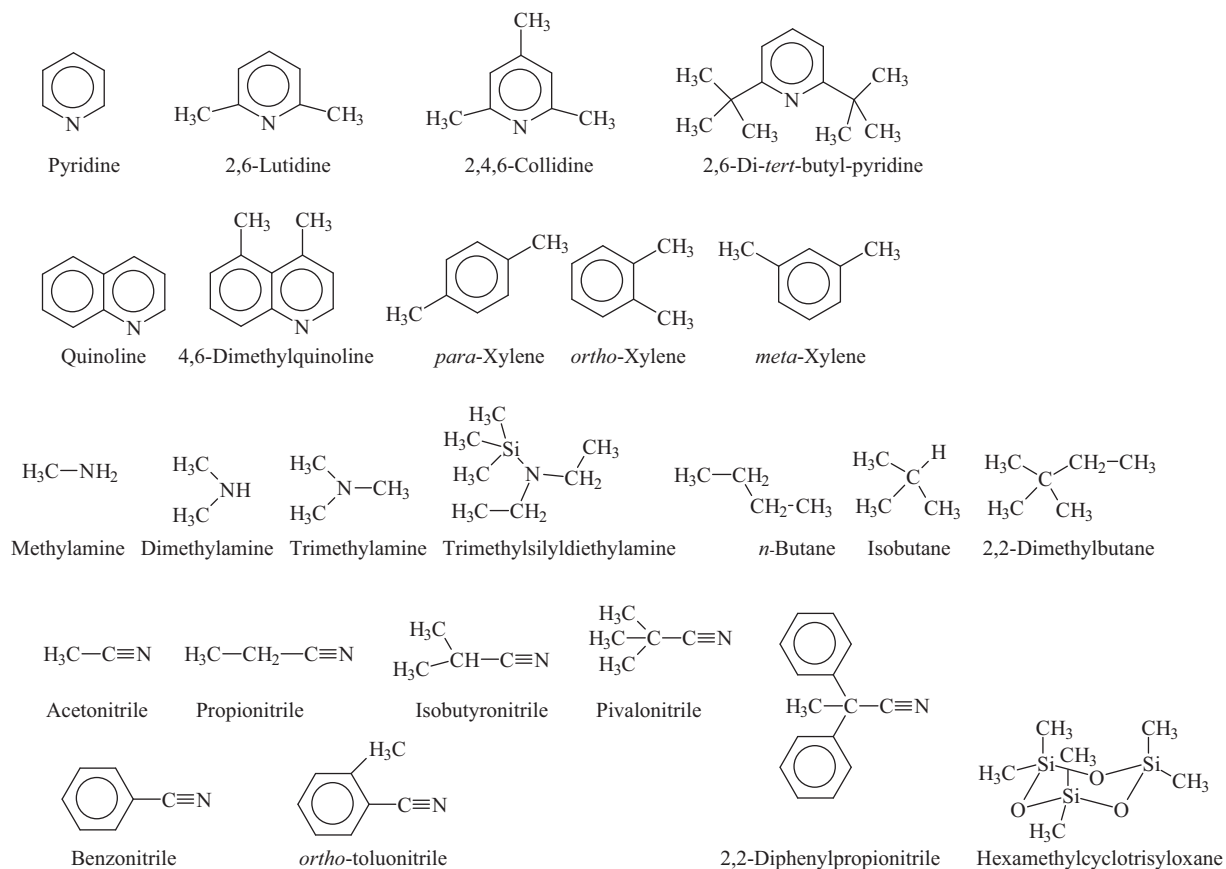
Base		Conjugated Acid	Basic Strength		Mostly Applied Techniques	
Family	Example		pK <sub>a</sub>	PA		
Cyclic amines	Piperidine	C <sub>5</sub> H <sub>10</sub> NH	C <sub>5</sub> H <sub>10</sub> NH <sub>2</sub> <sup>+</sup>	11.1	933	IR, <sup>15</sup> N NMR, calorimetry, TPD
Alkyl amines	<i>n</i> -Butylamine	<i>n</i> -C <sub>4</sub> H <sub>9</sub> -NH <sub>2</sub>	<i>n</i> -C <sub>4</sub> H <sub>9</sub> -NH <sub>3</sub> <sup>+</sup>	10.9	916	Calorimetry, TPD, <sup>15</sup> N NMR, IR
Ammonia		NH <sub>3</sub>	NH <sub>4</sub> <sup>+</sup>	9.2	857	Calorimetry, TPD, <sup>15</sup> N NMR, IR
Phosphines	Trimethyl-phosphine	(CH <sub>3</sub> ) <sub>3</sub> P	(CH <sub>3</sub> ) <sub>3</sub> PH <sup>+</sup>	8.65	957	<sup>31</sup> P NMR, IR
Phosphine oxides	Trimethyl-phosphine oxide	(CH <sub>3</sub> ) <sub>3</sub> P=O	(CH <sub>3</sub> ) <sub>3</sub> P=OH <sup>+</sup>		907	<sup>31</sup> P NMR
Heterocyclic amines	Pyridine	C <sub>5</sub> H <sub>5</sub> N	C <sub>5</sub> H <sub>5</sub> NH <sup>+</sup>	5.2	928	IR, <sup>15</sup> N NMR, calorimetry, TPD
Ketones	Acetone	(CH <sub>3</sub> ) <sub>2</sub> C=O	(CH <sub>3</sub> ) <sub>2</sub> C=OH <sup>+</sup>	-7.2	824	<sup>13</sup> C NMR, IR
Alcohols	Ethanol	CH <sub>3</sub> CH <sub>2</sub> OH	CH <sub>3</sub> CH <sub>2</sub> OH <sub>2</sub> <sup>+</sup>	-2.4	788	<sup>13</sup> C NMR, IR, calorimetry
Nitriles	Acetonitrile	CH <sub>3</sub> -C≡N	CH <sub>3</sub> -C≡NH <sup>+</sup>	-10.4	783	IR, <sup>15</sup> N NMR
Hydrocarbons	Ethylene	H <sub>2</sub> C=CH <sub>2</sub>	CH <sub>3</sub> -CH <sub>2</sub> <sup>+</sup>		680	IR
Carbon monoxide		CO	[HCO] <sup>+</sup>		598	IR, calorimetry
Nitrogen monoxide		NO			531	IR, calorimetry
Nitrogen		N <sub>2</sub>			477	IR
Argon		Ar			371	TPD

Abbreviations: NMR, nuclear magnetic resonance; TPD, temperature-programmed desorption.

**Table 5.10** Molecular Probes Applied for Surface Basicity Characterization

Compound	Formula	Reactivity	Technique
Carbon dioxide	CO <sub>2</sub>	Carbonates, bicarbonates, linear coordination on Lewis sites	IR, TPD, XPS, microcalorimetry
Carbon monoxide	CO	Formates, carbonite, polymeric anionic species, dioxycarbene	IR, ESR
Carbon disulfide	CS <sub>2</sub>	S <sub>2</sub> CO <sup>-</sup> , CO <sub>3</sub> <sup>2-</sup> , other species	IR
Sulfur dioxide	SO <sub>2</sub>	Sulfites, disulfites, hydrogensulfite, sulfates	IR, microcalorimetry
Pyrrole	H <sub>4</sub> C <sub>4</sub> NH	H-bonding, pyrrolate anions, polymers	IR, <sup>1</sup> H NMR, calorimetry
Carboxylic acids	RCOOH	Dissociation, dimers formation	IR, NMR, calorimetry
Carbonyl compounds	R-CO-H R-CO-R	Coordination on Lewis acid sites, enolization, enol condensation	IR, <sup>1</sup> H NMR
Chloroform	H-CCl <sub>3</sub>	H-bonding, coordination by chlorine on Lewis acid sites, hydrolysis	IR, <sup>13</sup> C NMR
Acetonitrile	CH <sub>3</sub> -CN	<sup>-</sup> CH <sub>2</sub> -CN anions, previous coordination by nitrogen on Lewis acid sites	IR
Alcohols	R-OH	R-O <sup>-</sup> anions, undissociative coordination, different H-bondings	IR
Hexafluoroisopropanol	(F <sub>3</sub> C) <sub>2</sub> CHOH	Dissociative adsorption, H-bonding	Calorimetry, IR
Thiols	R-SH	R-S <sup>-</sup> anions, undissociative coordination, different H-bondings	IR
Trimethylborate	(CH <sub>3</sub> O) <sub>3</sub> B	Tetrahedral borate, dissociation	<sup>11</sup> B NMR
Borontrifluoride	BF <sub>3</sub>	F <sub>3</sub> B ← O <sup>2-</sup> , dissociation	TPD
Propyne	H <sub>3</sub> C-C≡CH	H-bonding, π-bonding, dissociation	IR
Ammonia	NH <sub>3</sub>	H-bonding, dissociation to <sup>-</sup> NH <sub>2</sub> anions, coordination by nitrogen on Lewis acid sites	IR
Pyridine	H <sub>5</sub> C <sub>5</sub> N	H <sub>5</sub> C <sub>4</sub> N <sup>-</sup> anions, coordination by nitrogen on Lewis acid sites, dimerization	IR
Nitromethane	CH <sub>3</sub> NO <sub>2</sub>	H <sub>2</sub> CNO <sub>2</sub> <sup>-</sup> , CNO <sup>-</sup> formed by decomposition	IR, <sup>13</sup> C NMR

*Abbreviations: TPD, temperature-programmed desorption; XPS, X ray photoelectron spectroscopy; ESR, electron spin resonance NMR, nuclear magnetic resonance.*



SCHEME 5.1

Molecular probes for determination of the location of acid sites on and in microporous materials.

In contrast to the acidity characterization with basic probes, the use of “acidic” molecules to probe surface basicity is far less satisfactory.<sup>87</sup> In fact, all “acidic” (or electrophilic) molecules (Table 5.9) contain also well-available nucleophilic (basic) atoms than can interact with surface acid sites. It is almost impossible to find simple molecules that actually only interact specifically with basic sites. Metal oxides that display significant surface basicity always are very ionic and also carry Lewis acidity, although weak. On the other hand, this may be not a limit: also in their practical applications, in fact, acido-basicity rather than pure basicity is frequently the relevant property of these metal oxides. The characterization of well-defined very weak Lewis acidity is, in our opinion, a good technique for basic surface characterization. For this reason, probes typically used for acidity characterization (such as carbon monoxide and pyridine) may be used for characterizing basic solids. Carbon monoxide is an excellent probe for weak Lewis acid sites.

To reveal the basicity of oxide catalysts, the reactivity toward the reactant molecules can also be studied. As for example, the detection of aldol condensation products using carbonylic compounds as probe molecules provides evidence of the presence of basic sites.

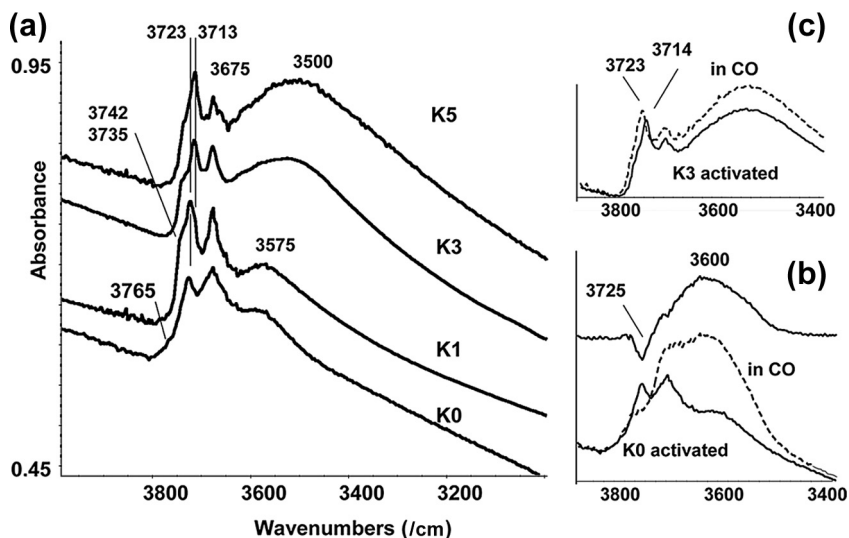
### 5.3.2.3 Direct detection of surface hydroxy-groups

The fragments arising from the dissociative adsorption of water on the surface of solids give rise to hydroxy-groups that are potentially more or less active Brønsted acid sites or basic sites. Such surface hydroxy-groups can be detected, directly, recording the IR spectra of the catalyst powders<sup>86,88</sup> after treatments that allow the desorption of molecularly adsorbed water, in the region  $3800\text{--}3000\text{ cm}^{-1}$ , where the O—H stretching modes ( $\nu\text{OH}$ 's) fall. The position and shape of the  $\nu\text{OH}$  bands of the surface hydroxy-groups is informative on their typical bond (covalent versus ionic) and their coordination.

Brønsted acidity characterization<sup>88</sup> can be performed by looking at what bases (among strong bases like ammonia, pyridine and other amines, including diazines) are protonated by the site (the protonation method), or by investigating the interaction of weak bases via H-bondings with the sites. In this case, the extent of shift of the  $\nu\text{OH}$  can be used to measure the acid strength of the sites (the H-bonding method, according to the Bellamy—Hallam—Williams relation). A third method (the olefin oligomerization method) consists in detecting the proton initiated oligomerization of olefins, following the rate (or extent) trend: 1,3-butadiene > isobutene > propene > ethylene.

In Figure 5.1 the response of typical IR experiments are reported.<sup>89</sup> The spectra of the surface OH groups of alumina (K0) and of K-containing aluminas K1, K2 and K3, with 1, 3, and 5% potassium respectively, are reported after outgassing at  $350\text{ }^\circ\text{C}$ . In the case of K0 (pure alumina support) we find maxima at 3725, 3675 and  $3575\text{ cm}^{-1}$ , with additional shoulders at  $3765\text{ cm}^{-1}$  and near  $3500\text{ cm}^{-1}$ . This spectrum is quite typical for  $\gamma\text{-Al}_2\text{O}_3$  samples outgassed at medium temperature.

In the spectrum of the K-containing aluminas, a new band at  $3713\text{ cm}^{-1}$  progressively increases in intensity with respect to that at  $3723\text{ cm}^{-1}$  that progressively



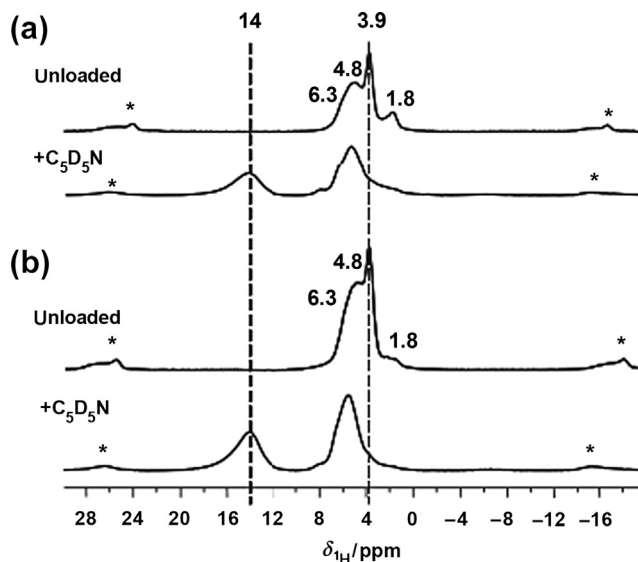
**FIGURE 5.1**

(a) FT-IR spectra of pure powder pressed disks of  $\gamma$ - $\text{Al}_2\text{O}_3$  (K0), 1%  $\text{K}/\text{Al}_2\text{O}_3$  (K1), 3%  $\text{K}/\text{Al}_2\text{O}_3$  (K3), and 5%  $\text{K}/\text{Al}_2\text{O}_3$  (K5) after activation by outgassing at 350 °C in the OH-stretching region. (b) OH-stretching region of  $\text{Al}_2\text{O}_3$  (K0), and (c) OH-stretching region of 3%  $\text{K}/\text{Al}_2\text{O}_3$  (K3) at  $-140$  °C before and after saturation with CO, and the corresponding subtraction (after saturation—before saturation).

*Reprinted with permission from Ref. 89.*

vanishes. All other sharp features tend to weaken while the lowest frequency feature broadens and shifts down to near  $3500\text{ cm}^{-1}$ . The position of the band at  $3713\text{ cm}^{-1}$  is similar to that previously reported for different K-containing catalysts and is attributed to the OH-stretching of KOH species. Upon low-temperature adsorption of CO the band at  $3723\text{--}3725\text{ cm}^{-1}$  due to OH's of alumina is significantly shifted down, showing a significant acidity of the corresponding AlOH groups. In contrast, the band at  $3713\text{ cm}^{-1}$  of K-containing samples does not shift down at all, being instead shifted up a little bit. This shows no acidity of these KOH groups.

Similarly, the  $^1\text{H}$  MAS NMR technique performed on the solid catalyst after activation and upon adsorption allows the detection of the signals due to the magnetic resonance of the protons of the surface hydroxy-groups, whose position is indicative of their environment.<sup>90,91</sup> The perturbation of protonic centers upon adsorption of probes may also be investigated, both looking at the  $^1\text{H}$  NMR signal of the perturbed hydroxy-groups, and looking at the perturbation of NMR spectra of adsorbed probes. The results of a typical  $^1\text{H}$  MAS NMR experiment is shown in Figure 5.2.<sup>92</sup> Two differently loaded La,Na-Y faujasite zeolites with 42% and 72% exchange degree have been studied. The activated samples show peaks at  $\delta_{\text{H}} = 1.8, 3.9$  and  $4.8$  ppm. The first peak is due to external silanol groups, the intermediate one to the active OH's



**FIGURE 5.2**

$^1\text{H}$  MAS NMR spectra of dehydrated (473 K) zeolites La,Na-Y/42 (a) and La,Na-Y/74 (b), recorded before (top) and after (bottom) loading with deuterated pyridine ( $\text{C}_5\text{D}_5\text{N}$ ). Asterisks denote spinning sidebands. (MAS, magic angle spinning; NMR, nuclear magnetic resonance).

*Reprinted with permission from Ref. 92.*

located in the supercage and the last one to OH's located in the sodalite cage, inaccessible to most molecules. In agreement with this assignment, only the peaks at  $\delta_{\text{H}} = 1.8$  and  $3.9$  ppm are perturbed by adsorption of deuterated pyridine. In particular, the peak at  $\delta_{\text{H}} = 3.9$  ppm fully disappears, while a new peak is observed at  $\delta_{\text{H}} = 14$  ppm, which is due to the proton of  $[\text{HNC}_5\text{D}_5]^+$ , the protonated deuterated pyridine, showing the Brønsted acidity of these sites.

As summarized by Jiang et al.,<sup>91</sup>  $^1\text{H}$  NMR of ammonia and ammonium ions,  $^{13}\text{C}$  NMR of adsorbed  $^{13}\text{C}$ -2-acetone,  $^{15}\text{N}$  NMR of adsorbed  $^{15}\text{N}$ -pyridine, and  $^{31}\text{P}$  NMR of adsorbed phosphine and phosphine oxides as molecular probes are sensitive to the strength of interaction with surface OH's.  $^{29}\text{Si}$  and  $^{27}\text{Al}$  MAS NMR techniques are also very relevant in the characterization of aluminas, silicas, zeolites and different silicoaluminates, while advanced magic angle spinning (MAS) NMR techniques such as CRAMPR, TRAPDOR and spin echo experiments allow to study the environment, and hence the structure, of OH's acting as Brønsted acid sites.<sup>90,91,93</sup>

#### 5.3.2.4 Direct evidence of the surface basic sites: UV and XPS spectroscopies and the concept of optical basicity

Techniques allowing the detection of surface anionic centers can give “directly” the information about surface basic sites of solids. Among these techniques,

UV-absorption and luminescence spectroscopies have been largely utilized in the field of oxide catalysts characterization.<sup>94–97</sup> Typical surface  $O^{2-} \rightarrow M^{2+}$  ( $M = Mg, Ca, Sr, Ba$ ) charge transfer (CT) transitions on evacuated alkaline earth oxides occur in the near UV range, i.e., at much lower energy than the corresponding bulk CT transitions, which correspond to valence band  $\rightarrow$  conduction band transitions. They are due to low coordination oxide and  $M^{2+}$  ions differently exposed at the surface. Coordinatively unsaturated (cus) atoms, denoted as  $O_{5C}$  (coordination five, on faces),  $O_{4C}$  (on edges), and  $O_{3C}$  (on corners) were found to exist at the surface of cubic alkaline earth oxides, where full coordination of bulk oxide ions is six. For MgO, several surface CT transitions were found in the range 7–3 eV, i.e., well at lower energy with respect to the bulk absorption found near 7.8 eV. However, their position is also somehow dependent on particle size.<sup>98</sup> Photoluminescence spectra of vacuum-treated MgO show an intense peak, due to emission from surface sites, at 3.18 eV, i.e., at definitely lower energy than the bulk gap, with further components at even lower energy. In terms of energy, the position of the corresponding peaks decreases following the trend  $MgO > CaO > SrO > BaO$ . From this work, a very popular model for the surface of alkaline earth oxides has been proposed, from which the most modern one, proposed by Chizallet et al.,<sup>99</sup> has been derived. Density functional theory (DFT) cluster calculations allowed recently a more detailed assignment of these transitions.<sup>100</sup> The application of these optical techniques to other families of metal oxides is more difficult. In particular, in the case of transition metal oxides other kinds of transitions, such as  $d \rightarrow d$  and intermetallic CT transitions may occur, together with bulk CT transitions, making the picture sometimes very complicated.

Optical spectroscopic measurements have also been at the origin of the concept of Optical Basicity, generally denoted with the symbol  $\Lambda$ , mostly due to Duffy.<sup>101</sup> This model has its origin in the nephelauxetic parametrization proposed by Jørgensen with the application of the ligand field theory. According to Duffy, the basicity of an oxide material can be measured using red shifts in ultraviolet frequencies with respect to the value measured for cations in a very basic environment, taking crystalline calcium oxide as a reference. Simple molecular orbital theory shows that the ratio of the red shifts can be taken as a sensible expression of basicity, especially in terms of the Lewis concept. This ratio (which, in effect, is the ratio of the orbital expansion “nephelauxetic” parameter,  $h$ , for the glass or the oxide to  $h$  for CaO) has been termed the “optical basicity”. The orbital expansion parameter,  $h$ , to a ligand is related to its electron-donating ability. Some limits of the  $\Lambda$  theory have been discussed and bypassed by Leboutteiller and Courtine.<sup>102</sup> The data reported by these authors for binary oxides are in partial agreement with those reported later by Duffy,<sup>103</sup> but are in better agreement with data arising from surface studies. Optical basicity is correlated to electronegativity, cation polarizability and bond strength for simple and complex metal oxides<sup>104</sup> and is very relevant in the production and properties of glasses. An interesting feature of  $\Lambda$  is that it can be calculated for mixed and multi-component oxides as the weighted average of the  $\Lambda$ s of the component oxides.

$\Lambda$  is actually a bulk property, but is quite directly correlated to surface basicity. In fact,  $\Lambda$  values are quite well inversely correlated with the O1s Binding Energy as

measured by XPS. In fact, the position of the O1s Binding Energy XPS peak is correlated to the ionicity<sup>105</sup> (which is again a bulk property) but is also correlated to surface basicity of metal oxides.<sup>106</sup> Actually, the separation of the surface components, due to surface oxide, hydroxide and carbonate ions, from the bulk component of the O1s XPS signal of metal oxides may be not easy.<sup>107,108</sup> On the other hand, both the Optical Basicity scale and the O1s Binding Energy XPS Scale have rough agreement with the scale arise from surface characterization experiments (see below), with some exceptions. Bordes and Courtine<sup>106</sup> calculated  $\Lambda$  for several simple and mixed oxides and correlated successfully  $\Lambda$  values to the catalytic activity of many catalysts in several reactions, mostly of the redox type.

### 5.3.2.5 Quantitative adsorption of probe molecules from gas and liquid phases

Titration method, i.e., the study of the interaction of indicator dyes with the solids from solutions, has been proposed as a technique for both qualitative and quantitative characterization of solid surfaces. If a basic indicator B is used, the proton acidity of the surface is expressed by the Hammett acidity function (Equation 5.12), originally proposed for solution chemistry.

Similarly, the basicity can be defined when an acid is converted by its conjugated base. This allows to define acidity and basicity in the same scale. A similar expression can be proposed for interaction of bases with Lewis sites. Procedures for titrating solid acids and bases have been described by Tanabe et al.<sup>34</sup> The amine titration method consists of titrating a solid acid suspended in benzene with *n*-butylamine using an indicator. The benzoic acid surface titration method consists of titrating a solid acid suspended in benzene with benzoic acid using an indicator. This technique has many limitations to deduce gas–solid phenomena, the surface Hammett acidity and basicity functions, as defined by Tanabe, having doubtful physical meaning and being, according to Corma,<sup>109</sup> intrinsically inappropriate and misleading. In spite of this, titration techniques are still widely applied to characterize very strong acidity<sup>110</sup> and basicity,<sup>111</sup> like those of catalysts applied to biodiesel production, and in the field of colloids and soil sciences.<sup>112</sup>

The quantitative measure of the adsorption of acidic or basic probes on the surfaces from the vapor by adsorption volumetry and gravimetry measured at different temperature and in contact with different vapor pressures is a quite easy technique that gives useful although rough information on global basic or acid properties of the catalyst surfaces.

## 5.3.3 Methods measuring adsorption/desorption energies

### 5.3.3.1 Calorimetric methods

Adsorption microcalorimetry consists in the measure of the heat of adsorption evolved when dosing measured small amounts of a vapor probe on a surface. As done by Auroux and Gervasini<sup>113</sup> for a number of binary metal oxides, calorimetric studies of the acidity and basicity are mostly performed using ammonia as an acidity probe and carbon dioxide as a basicity probe.<sup>114</sup> In his recent reviews on the use of



calorimetry for the characterization of acidity and basicity of metal oxides<sup>115</sup> and of zeolites,<sup>116</sup> Auroux cites ammonia and amines, including pyridine, nitriles, alcohols, NO, CO and N<sub>2</sub> as probes for acidity, CO<sub>2</sub>, SO<sub>2</sub>, carboxylic acids and pyrrole as probes for basicity.

Calorimetric techniques allow to obtain an interesting quantification and evaluation of the gas–solid interactions. However, they give useful information on the strength of different sites without giving information on their quality. Consequently, interactions of amphoteric compounds with acid or basic sites or interaction of bases with Lewis and Brønsted acid sites cannot be distinguished. In particular, the use of ammonia as a probe for acid sites is dangerous, because ammonia adsorbs on both Brønsted and Lewis acid sites but can also react as an acid on basic sites and can be oxidized too. Similarly, the use of CO<sub>2</sub> as a probe for basic sites is not easy, because CO<sub>2</sub> also interacts with Lewis acid sites as such or upon forming carbonate and bicarbonates. On the other hand, by coupling calorimetric data with spectroscopic and theoretical data, a complete information on the actually occurring phenomena can be reached. Other amines (such as pyridine, butylamine, etc.) have been used as probes for acidity. However, also amines are not always specific probes, in particular concerning Brønsted/Lewis sites.

### 5.3.3.2 Temperature programmed desorption methods

The gas-chromatographic, infrared spectroscopic or mass spectrometric analysis of the gases evolved from a surface upon a temperature-programmed heating ramp after adsorption of probes gives also indication on energetics of adsorption/desorption and, consequently, on the strength of acid–base adsorption sites. This technique allows to have an integral quantitative evaluation of the number of adsorption sites as well as allow to distinguish and calculate distribution of more sites having significantly different strength. A typical response of an ammonia-TPD experiment on an acid zeolite is reported in Figure 5.3. The desorption peak centered at 360 °C is evidence of the strong acidity of zeolite.

On the other hand, temperature-programmed desorption (TPD) techniques suffer from limits similar to those of adsorption microcalorimetry: both techniques do not give qualitative information on the nature of the phenomena detected. As for example, they do not give direct evidence on the nature of acid sites (Brønsted versus Lewis) when basic probes are adsorbed and desorbed. Coming back to Figure 5.3, parallel IR experiment (Figure 5.4) shows that ammonia on this zeolite is indeed adsorbed mainly as ammonium ions over Brønsted sites but that also small amounts of Lewis bonded ammonia are detectable.

TPD of ammonia is very largely applied for the study of the catalysts acidity.<sup>117</sup> Niwa and coworkers developed excellent ammonia-TPD systems, performing in parallel IR studies coupled with Mass Spectrometric detection of desorbed species (IRMS) and theoretical calculations.<sup>82,118</sup> TPD curves for ammonia were predicted successfully using Monte Carlo simulation methods.<sup>119</sup>

TPD curves can show features that are artifacts depending on experimental conditions. Recent analysis of the predicted NH<sub>3</sub>-TPD curves reveals that zeolite pore

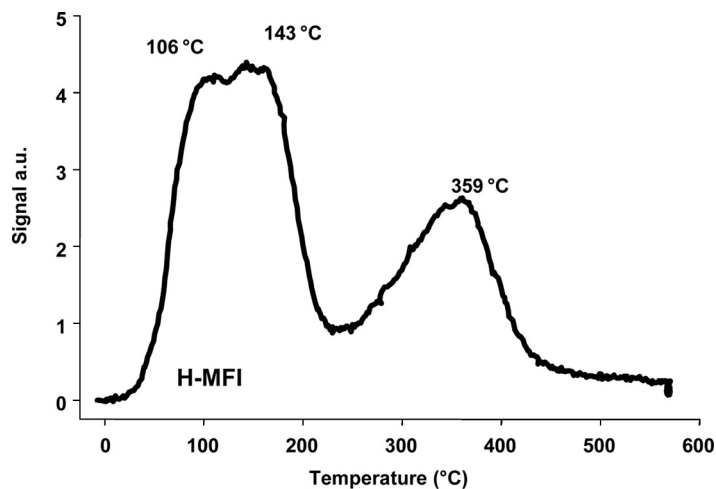


FIGURE 5.3

Ammonia temperature-programmed desorption spectrum of H-ZSM5 zeolite.

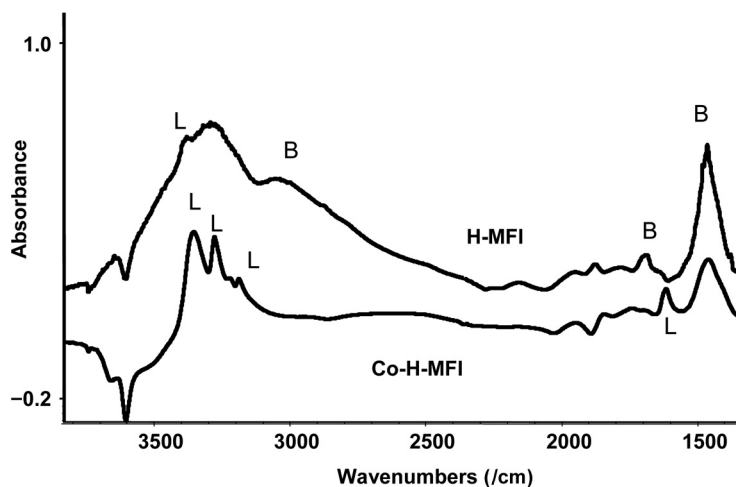


FIGURE 5.4

FT-IR subtraction spectra of ammonia adsorbed on H-ZSM5 zeolite and on partially exchanged Co-H-ZSM-5.

size is a critical factor influencing the curve shape. The so-called weak and strong acid sites of zeolites, which give rise to two peaks in the TPD curve, are roughly related to the interactions among ammonia molecules in the pores and to the interactions between ammonia molecules and the zeolite pore walls, respectively. However, the  $\text{NH}_3$ -TPD curves may still show a double peak feature without any strong

acid centers if the pore is such a size that additional strain is put on the  $\text{NH}_3$ -hydrogen bond network.

Izadbakhsh et al.<sup>120</sup> proposed recently stepwise heating ammonia TPD carried out by keeping the temperature constant as soon as ammonia desorption signal rises until the signal returns to the baseline. These authors report that more ammonia desorption peaks on an SAPO-34 catalyst were identified using TPD with stepwise heating.

Pyridine-TPD has also been used to characterize acidity of catalysts such as mesoporous silica–aluminas.<sup>121</sup>

Ammonia TPD is dangerous for investigating the surfaces of solids that can give redox reactions, because of the possible formation of species like molecular nitrogen and nitrogen oxides. A similar problem can occur with pyridine that can decompose more than desorb like observed on sulfated zirconia.<sup>122</sup> On the other hand, the reactivity of probes during desorption can be used for more information, as proposed by Gorte<sup>123</sup> that applied successfully the TPD of reactive amines, which give rise to the Hoffmann elimination to olefins + ammonia when “desorbing” from protonic zeolites. TPD of Ar has been proposed for characterization of solid acids<sup>124</sup> although according to the theoretical calculations of Bolis et al. it is only sensitive to confinement’s effects, but almost insensitive to specific interaction with acid sites.

TPD of adsorbed carbon dioxide, compared with other techniques, is widely applied for basicity characterization.<sup>89,125–127</sup>  $\text{BF}_3$  has been also proposed as a probe for basicity by TPD.<sup>128</sup>

### 5.3.4 IR spectroscopic methods

Infrared spectroscopy is largely used for surface acidity and basicity characterization.<sup>88,129,130</sup> By using appropriated bases as probes (see Table 5.8), this technique allows the separated characterization of Lewis and Brønsted acid sites and (with more difficulty) of basic sites.

The use of IR spectroscopy for Brønsted acidity characterization has been cited above. Lewis acidity can be tested by using bases whose spectrum presents bands whose position (or sometimes intensity) is highly sensitive to the strength of the Lewis acid–base interaction and whose spectrum is different from that of the corresponding protonated form. Typically quite strong bases such as ammonia and pyridine are largely used. As an example, in Figure 5.1, the spectra of ammonia adsorbed on H-ZSM5 zeolite and on a partially  $\text{Co}^{2+}$  exchanged sample are reported. The bands indicated with B are due to ammonium ions, i.e., ammonia adsorbed on Brønsted acid sites, while those denoted with L are due to molecular ammonia coordinated on Lewis acid sites. It is evident that on H-ZSM5 Brønsted acidity largely predominates while exchange with  $\text{Co}^{2+}$  introduces a huge amount of Lewis sites ( $\text{Co}^{2+}$  cations).

The low-temperature adsorption of CO is today perhaps the most popular technique for Lewis acidity characterization but is also used for characterizing Brønsted sites (i.e., of zeolites) by applying the H-bonding method. It actually allows a very detailed analysis of the surface sites as they appear at low temperature without strong

perturbations of the surface, having also free access to any cavity and avoiding steric hindrances.<sup>131</sup> This is a good opportunity to evaluate “pure acidity” but, together, is a drawback, because additional interactions do occur with most other molecules including the reactants of catalytic reactions.

Data similar to those arise from CO adsorption can be obtained with small and very weak bases like hydrogen, nitrogen or ethylene, and with more hindered and heavy (but still weak) bases like nitriles. The adsorption of strong bases like pyridine is widely used for quantitative analyses and for the determination of the Lewis/Brønsted sites ratios.<sup>132</sup>

The adsorption of strong and heavy bases (like ammonia, amines, pyridines) certainly perturbs to a relevant extent the surface, more than do weak and light bases. As for example, it has been shown that pyridine and ammonia detect strong Lewis sites associated to pentavalent vanadium and hexavalent tungsten when CO does not show them.

In fact, the use of strong bases and of room or higher temperature adsorption experiments is more “perturbing”, likely producing a slight modification of the coordination state of some cations, but gives frequently a more exact view of the surface chemistry of oxides than low-temperature CO adsorption. This is particularly true if related to adsorption and catalysis phenomena that involve high temperatures and more polar reactants.

In recent years, the tentative to go deeper in the analysis of surfaces (in particular, but not exclusively, of zeolites) suggested the use of sets of molecular probes with similar functionality but different steric hindrance. As for example, different nitriles like those reported in [Scheme 5.1](#) allow to explore the position of the sites in porous materials such as zeolites.<sup>86,133</sup>

As said, the choice of a suitable base for basicity characterization is more complex. As said, all of them have strongly limited selectivity for basic sites. The most used probe is again CO<sub>2</sub> showing the formation and stability of surface carbonates and bicarbonates<sup>89</sup> while also methanol is suitable as a probe.<sup>134</sup>

### 5.3.5 NMR spectroscopic methods

The use of MAS NMR spectroscopy for the characterization of Brønsted acidity has been already cited above. As also said, advanced <sup>27</sup>Al MAS NMR spectra are very helpful for probing the quantity, coordination, and location of aluminum atoms in Al-containing materials such as aluminas and aluminosilicate catalysts (see below) and minerals, thus giving information of the state of Al also at the surface. Based on <sup>27</sup>Al MAS NMR spectra Peden and coworkers proposed a determinant role of pentacoordinated Al ions in anchoring of supported phases,<sup>135</sup> their stabilization<sup>136</sup> and alumina phase transitions.<sup>137</sup> The adsorption of basic probes<sup>91</sup> such as <sup>15</sup>N-pyridine<sup>138</sup> and phosphorus-containing probe molecules (phosphine and phosphine oxides)<sup>139</sup> can be followed by <sup>15</sup>N and <sup>31</sup>P NMR while the <sup>13</sup>C NMR of adsorbed <sup>13</sup>C-2-acetone is also sensitive to the strength of interaction with Lewis acid sites.

### 5.3.5.1 Theoretical methods

Theoretical methods applied to heterogeneous catalysis have undergone an impressive development in the last few years and have been largely applied to catalytic materials. Until the end of the 1990s, most studies of zeolite acidity and spectroscopic properties used finite cluster models. They provided valuable data on the average position of zeolitic Brønsted sites on a general acidity scale and helped to assign vibrational spectra and NMR spectra. However, cluster models have two limitations: (1) They allow for a relaxation of the atoms on deprotonation, which is not as constrained as would be the case if the modeled site were part of the periodic solid. (2) They neglect the long-range potential of the periodic solid. In practice, they do not allow detailed studies of sites in different crystallographic positions or in different frameworks; e.g., they did not allow to distinguish the sites of protonic zeolites from those of silica–alumina. The periodic approaches can include all these effects and are increasingly applied in spite of the enormous computational effort needed. A very large number of papers appeared recently reporting applications of DFT and of alternative techniques to catalysts. DFT calculations are increasingly applied to metal oxide systems and allowed to investigate the bulk structure of many catalytic systems. Among the most investigated structures transitional aluminas such as  $\gamma$ -Al<sub>2</sub>O<sub>3</sub> have been object of different DFT calculations.<sup>140,141</sup> Interestingly, theoretical studies suggested doubts on the traditionally accepted structure of Al as a defective spinel, with a still open debate.<sup>142</sup> Cluster DFT calculations have also been devoted to the surfaces of many catalytic systems,<sup>141,143</sup> such as simple oxides but also supported oxides. Among these studies, the surfaces of alumina,<sup>144</sup> chlorided alumina,<sup>145</sup> Ni-oxide supported on alumina,<sup>143</sup> etc. have been studied. As an example, in [Figure 5.5](#) models of the spinel-type alumina and of Ni clusters on its (100) surface are shown.<sup>146</sup>

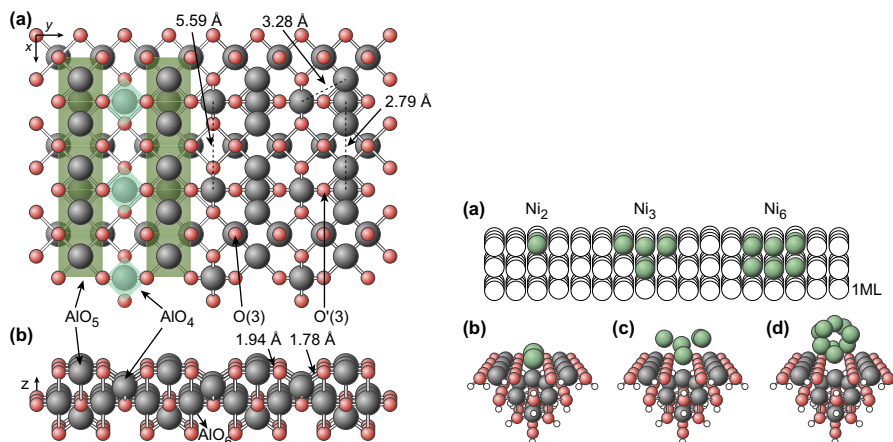
The nature and structure of surface hydroxy-groups on different oxides, both having acidic and basic dominant character, such as alumina, titania and magnesia has been investigated.<sup>147</sup> Similarly, the nature of hydroxy-groups in acidic zeolites, and their reactivity, has been the object of theoretical studies performed in parallel with experiments.<sup>82,148</sup> Also the Lewis acid character of exchanged zeolites has been investigated.<sup>148,149</sup>

The adsorption of probe molecules, reaction steps and entire reaction mechanisms have also been the object of theoretical calculations such as the adsorption of CO<sub>2</sub> on MgO,<sup>150</sup> the formation and stability of carbenium ions in protonic zeolites<sup>151</sup> and the alkylation of benzene on ZSM5 zeolite.<sup>152</sup>

In practice, theoretical calculation can be applied to any acidity and basicity phenomena at catalyst surfaces, although still some limitation exists, such as the difficulty in modeling nonperiodic situations, such as defects, corner sites, edge sites that should be active at the surface of several solid catalysts.

### 5.3.6 Catalytic probe reactions

Catalytic test reactions represent a very important tool for acid–base characterization. Conversion of secondary alcohols like isopropanol, 2-butanol and cyclohexanol,

**FIGURE 5.5**

Left: crystal structure of the  $\gamma$ - $\text{Al}_2\text{O}_3$  (100) spinel surface: (a) top view and (b) side view. Right: models of Ni clusters: (a) cut from Ni(100) surface; as well as deposited + relaxed on the  $\gamma$ - $\text{Al}_2\text{O}_3$  (100) surface represented by  $\text{Al}_{15}\text{O}_{40}\text{H}_{35}$  cluster: (b)  $\text{Ni}_2$  cluster, (c)  $\text{Ni}_7$  cluster, and (d)  $\text{Ni}_9$  cluster.

Reprinted with permission from Ref. 146.

either to olefins or to ketones, is considered to be evidence of acidic and basic behavior, respectively. Similarly, the isomerization of 1-butene to *cis/trans* 2-butene mixtures gives information on acidity (if *cis/trans* ratio is near 1) or basicity (if this ratio much higher). Also toluene alkylation by methanol proceeds differently on basic and on acid catalysts giving rise to xylenes in the first case, and to ethylbenzene in the second. The decomposition of the complex alcohol 2-methyl-3-butyn-2-ol (MBOH)<sup>153</sup> is very popular today. In fact, while on acidic catalysts it produces 2-methyl-but-1-en-3-yne by water elimination, together with 3-methyl-but-2-enale by transposition, on basic catalysts it gives a mixture of acetone and acetylene. On amphoteric catalysts, 3-methyl-3-hydroxy-2-butanone and 3-methyl-but-3-en-2-one are produced.

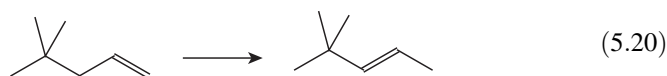
Lercher et al.<sup>154</sup> reported recently a review on the use of test reactions to determine the acid strength of zeolites. They mentioned skeletal (hydro)isomerization of C5–C10 *n*-alkanes and cracking of C4–C8 and C16 *n*-alkanes, disproportionation of xylene and ethylbenzene, cracking of cumene, dehydration of alcohols as test reactions for the acid strength of zeolites. Cyclohexene conversion and hydride transfer reaction are cited as tests for acid site density.

Ethylbenzene disproportionation has been proposed as a standard reaction for acidity evaluation of zeolites by the International Zeolite Association.<sup>155</sup> Liquid-phase reactions like benzylation of toluene, rearrangement of  $\alpha$ -pinene and

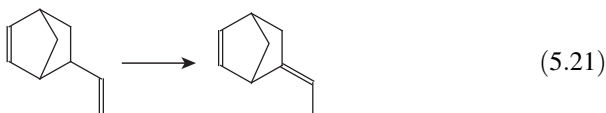
dihydropyran methoxylation can be applied to characterize the acidity, e.g., of acid-treated clays.<sup>156</sup>

For medium-strong basicity characterization,<sup>157</sup> including that of zeolites,<sup>154</sup> reactions involving formation of enolate species are mainly applied, such as retroaldolization of diacetone alcohol, the Knoevenagel condensation between benzaldehyde and carbonyl compounds with hydrogens in  $\alpha$  position, acetyl acetone cyclization and isophorone isomerization.

Selective position double-bond isomerization of complex olefins occurring in very mild conditions has been considered by different authors as an indication of superbasicity, such as the conversion of 4,4-dimethyl-1-pentene to 4,4-dimethyl-2-pentene<sup>158</sup>



and of 5-vinylbicyclo[2.2.1]hept-2-ene to 5-ethylidenebicyclo[2.2.1]hept-2-ene<sup>44</sup>



Moreau et al.<sup>159</sup> used the kinetic analysis of the isomerization of glucose into fructose to determine the basic strength of solid catalysts in water.

### 5.3.7 Strength, amount, and distribution of surface acid and basic sites on the ideal surface of a solid

Acid and basic sites, of the Brønsted as well as of the Lewis type, may exist at the surface of a solid particle. These sites may act as active sites for acid or base catalysis. In heterogeneous catalysis, the catalytic activity (reaction rate) depends on the amount of active sites (e.g., of acid sites having the appropriate strength) present on the catalyst as a whole. This means that the “density” of active sites (amount of sites per gram of the solid or per unit surface area) is an important parameter. On solids, amount and strength of acid or basic sites are quite independent parameters, so both of them must be analyzed independently for a complete characterization. Additionally, several different families of acid sites may occur in the same solid surface, so their “distribution” (density of sites of any site family) must be characterized.

Additionally, both acidic and basic sites can be simultaneously present on the same solid surface in different positions (but frequently near each other), and can work synergistically. This supports the idea of acido-basicity of solids and of acido-basic catalysis on solids, and provides evidence for the significant complexity of acid–base characterization of solids.

---

## 5.4 Heterogeneous versus homogeneous acid–base catalysis

The development and the use of solid acids and bases may, in several cases, improve the chemical and environmental processes, from different points of view. In fact, while the use of liquid acids and bases may result in significant corrosion and safety problems (related to volatility, toxicity of the vapors and causticity and acidity of liquid drops with respect to skin), with the use of solid acids and bases these problems are almost nonexistent. The use of solid acids and bases may also improve chemical processes in terms of performances. In fact, solid catalysts do not mix with liquid products, thus avoiding the need for demanding separation and purification steps. In some cases (like e.g., in the case of biodiesel production), the quality of the product or of byproducts may be also increased by solid catalysts. Finally, the use of solids may result in a reduction of corrosive and toxic wastes.

The use of solid acid and base catalysts in liquid phase reactions may give rise to some problem, in particular when multipurpose plants (where it is possible to perform different reactions in the same reactor and plant) are used. However, it seems not impossible to design multipurpose plants with solid catalysts too.

Acidity and basicity of solids may be tuned, both in terms of strength (from very weak to very strong) and of abundance or density of sites. Solid catalysts may be applied to solid–gas systems as well as to solid–liquid systems, although in this case with some solids-leaching problems may occur. In practice, it seems that solid catalysts give rise to excellent flexibility. This is the reason why the field of heterogeneous catalysis is a greatly developed and developing field.

All these developments have a significant good impact in improving the industrial processes in terms of the green chemistry approach.

---

## References

1. Arrhenius SA. *Recherches sur la conductibilité galvanique des électrolytes* [Ph. D. thesis]. University of Uppsala; 1884; Arrhenius SA. *Z Phys Chem* 1887;**1**:631.
2. Brønsted JN. *Recl Trav Chim Pays Bas* 1923;**42**:718.
3. Lowry TM. *Chim Ind Lond* 1923;**42**:43. *Trans Faraday Soc* 1924;**20**:13.
4. Eigen M. *Angew Chem Int Ed Engl* 1964;**3**:1.
5. Zundel G. *Angew Chem Int Ed* 1969;**8**:499–509.
6. Kazansky VB. *Top Catal* 2000;**11/12**:55.
7. Markovitch O, Agmon N. *J Phys Chem A* 2007;**111**:2253–6.
8. Stoyanov ES, Stoyanova IV, Reed CA. *J Am Chem Soc* 2010;**132**(5):1484–5.
9. Himmel D, Goll SK, Leito I, Krossing I. *Chem Eur J* 2011;**17**:5808–26.
10. Zhao Z, Rogers DM, Beck TL. *J Chem Phys* 2010;**132**:014502.
11. Fulton JL, Balasubramanian M. *J Am Chem Soc* 2010;**132**:12597–604.
12. Raamata E, Kaupmeesa K, Ovsjannikova G, Trummalb A, Kütta A, Saamea J, et al. *J Phys Org Chem* 2013;**26**:162–70.
13. Cwiklik L, Devlin JP, Buch V. *J Phys Chem A* 2009;**113**:7482.



14. Smiechowski M, Stangret J. *J Phys Chem A* 2007;**111**:2889–97.
15. Tian C, Ji N, Waychunas GA, Shen YR. *J Am Chem Soc* 2008;**130**:13033.
16. Rustad JR, Felmy AR, Rosso KM, Bylaska EJ. Ab initio investigation of the structures of NaOH hydrates and their Na<sup>+</sup> and OH<sup>-</sup> coordination polyhedra. *Am Mineral* 2003;**88**:436.
17. Megyes T, Bálint S, Grósz T, Radnai T, Bakó I, Sipos P. *J Chem Phys* 2008;**128**:044501.
18. Bowden K. *Chem Rev* 1966;**66**:119.
19. Fărcasiu D, Ghenciu A. *J Am Chem Soc* 1993;**115**:10901.
20. Stoyanov ES, Kim KC, Reed CA. *J Am Chem Soc* 2006;**128**:8500.
21. Hall NF, Conant JB. *J Am Chem Soc* 1927;**49**:3047.
22. Gillespie RJ. *Acc Chem Res* 1968;**1**:202.
23. Olah GA, Prakash GK, Molnar A, Sommer J. *Superacid chemistry*. New York: Wiley; 2009.
24. Reed CA, Kim KC, Bolskar RD, Mueller L. *Science* 2000;**289**:101.
25. Reed CA. *Chem Commun*; 2005:1669.
26. Conant JB, Wheland GW. *J Am Chem Soc* 1932;**54**:1212.
27. McEwen WK. *J Am Chem Soc* 1936;**58**:1124.
28. Kaljurand I, Koppel IA, Kütt A, Rööm EI, Rodima T, Koppel IA, et al. *J Phys Chem A* 2007;**111**:1245.
29. Alder RW. *J Am Chem Soc* 2005;**127**:7924–31.
30. Leito I. *Acidity – basicity data (pK<sub>a</sub> values) in nonaqueous solvents*. [http://tera.chem.ut.ee/~ivo/HA\\_UT/](http://tera.chem.ut.ee/~ivo/HA_UT/) [accessed 26.03.14].
31. Hammett LP. *Physical organic chemistry*. New York, NY: McGraw-Hill Book Co., Inc.; 1940 [chapter IX].
32. Paul MA, Long FA. *Chem Rev* 1957;**57**:1.
33. Ishikawa T, editor. *Superbases for organic synthesis: guanidines, amidines, phosphazenes and related organocatalysts*. John Wiley & Sons, Ltd; 2009. ISBN: 978-0-470-51800-7.
34. Tanabe K, Misono M, Ono Y, Hattori H. *New solid acid and bases*. Kondasha-Elsevier; 1989. p. 211.
35. Schwesinger R, Willaredt J, Schlemper H, Keller M, Schmidt D, Fritz H. *Chem Ber* 1994;**127**:2435.
36. Schwesinger R, Schlemper H, Hasenfratz C, Willaredt J, Dambacher T, Breuer T, et al. *Liebigs Ann Chem*; 1996:1055–81.
37. Koppel IA, Schwesinger R, Breuer T, Burk P, Herodes K, Koppel I, et al. *J Phys Chem A* 2001;**105**:9575.
38. Bolm C, Hahn FE, Sundermeyer J, Raab V, Gaoutchenova E, Garrelts U, et al. Chapter 2. The chemistry of superbasic guanidines. In: Bolm C, Hahn FE, editors. *Activating unreactive substrates: the role of secondary interactions*. Wiley-VCH Verlag GmbH & Co. KGaA; 2009.
39. Schwesinger R. *Angew Chem Int Ed Engl* 1987;**26**:1164–5.
40. Tang J, Dopke J, Verkade JG. *J Am Chem Soc* 1993;**115**:5015.
41. Clayden J, Greeves N, Warren S, Wothers P. *Organic chemistry*. Oxford: Oxford University Press; 2001. p. 209.
42. Caubère P. *Chem Rev* 1993;**93**:2317–34.
- 42b. Ono Y, Hattori H. *Solid base catalysts*, Tokyo Inst Technol Press; 2011.
- 42c. Chen L, Zhao J, Yin SF, Au CT. *RSC Advances* 2013;**3**:3799–814.
43. Kelly GJ, King F, Kett M. *Green Chem* 2002;**4**:392.

44. Tanaka K, Yanashima H, Minobe M, Suzukamo G. *Appl Surf Sci* 1997;**121/122**:461.
45. Lewis GN. *Valency and structure of atoms and molecules*. New York: Wiley; 1923.
46. Sereda O, Tabassum S, Wilhelm R. *Top Curr Chem* 2010;**291**:349–93.
47. Rueping M, Nachtsheim BJ. *Beilstein J Org Chem* 2010;**6**(6). <http://dx.doi.org/10.3762/bjoc.6.6>.
48. Gal J-F, Iacobucci C, Monfardini I, Massi L, Duñach E, Olivero S. *J Phys Org Chem* 2013;**26**:87–97.
49. Kraft A, Trapp N, Himmel D, Böhler H, Schlüter P, Scherer H, et al. *Chem Eur J* 2012;**18**:9371–80.
50. Hilt G, Pünner F, Möbus J, Naseri V, Bohn MA. *Eur J Org Chem*; 2011:5962–6.
51. Pearson RG. *J Am Chem Soc* 1963;**85**:3533.
52. Pearson RG. *Acc Chem Res* 1993;**26**:250.
53. Klopman J. *Am Chem Soc* 1968;**90**:223.
54. Mayr H, Breugst M, Ofial AR. *Angew Chem Int Ed Engl* 2011;**50**(29):6470–505.
55. Clayden J, Greeves N, Warren S, Wothers P. *Organic chemistry*. Oxford: Oxford University Press; 2001. p. 440.
56. Mayr H, Lakhdar S, Maji B, Ofial AR. *Beilstein J Org Chem* 2012;**8**:1458–78.
57. Raczynska EW, Gal JF, Mariua P-C, Szelag M. *Croat Chem Acta* 2009;**82**:87–103.
58. Burk P, Koppel IA, Koppel I, Kurg R, Gal J-F, Maria P-C, et al. *J Phys Chem A* 2000;**104**:2824.
59. Petrie S. *J Phys Chem* 2001;**105**:9931.
60. Gala J-F, Maria PC, Massi L, Mayeux C, Burk P, Tammiku-Taul J. *J Mass Spectr* 2007;**267**:7.
61. Himmel D, Goll SK, Leito I, Krossing I. *Angew Chem Int Ed Engl* 2010;**49**:6885–8.
62. Shahid EM, Jamal Y. *Renew Sustain Energy Rev* 2011;**15**:4732–45.
63. Azizov AH, Amanullayeva GI, Aliyeva RV, Aliyev BM, Bektashi NR. *Appl Catal A Gen* 2011;**396**:20–33.
64. [www.nist.org](http://www.nist.org).
65. Dewar MJ. *J Chem Soc*; 1946:406.
66. Vogel P. *Carbocation chemistry*. New York: Elsevier; 1985.
67. Olah GA. *J Org Chem* 2001;**66**:5943.
68. Kilpatrick M, Luborsky FE. *J Am Chem Soc* 1953;**75**:577.
69. Olah GA, Schlosberg RH. *J Am Chem Soc* 1968;**90**:2726.
70. Hogeveen H, Bickel A. *Recl Trav Chim Pays Bas* 1967;**86**:1313.
71. Olah GA, Prakash GK, Sommer J. *Science* 1979;**206**:13.
72. Esteves PM, Ramirez-Solis A, Mota CJA. *J Phys Chem B* 2001;**105**:4331.
73. Sommer J, Jost R. *Pure Appl Chem* 2000;**72**:2309.
74. Boronat M, Corma A. *Appl Catal A Gen* 2008;**336**(1–2):2–10.
75. Sani Souna Sido A, Barbiche J, Sommer J. *Chem Commun* 2010;**46**:2913–4.
76. Gates BC, Knozinger H, editors. *Advances in catalysis*, vol. 52. 2009. vol. 51, 2007 and vol. 50, 2006.
77. Wachs IE. Characterization of catalytic materials. In: Che M, Viedrine JC, editors. *Characterization of solid materials and heterogeneous catalysts from structure to surface reactivity*. Momentum Press; March 1, 2010. Wiley, 2012.
78. Che M, Viedrine JC, editors. *Characterization of solid materials and heterogeneous catalysts from structure to surface reactivity*. Wiley; 2012.
79. Fierro JLG, editor. *Metal oxides: chemistry and applications*. Boca Raton, FL, USA: CRC Press; 2005.

80. Jackson SD, Hargreaves JSJ, editors. *Metal oxide catalysis*, vol. 1. Wiley-VCH; 2009.
81. Chester AW, Derouane EG, editors. *Zeolite characterization and catalysis: a tutorial*. Springer; 2009.
82. Niwa M, Katada N, Okumura K. *Solid acidity, characterization and design of zeolite catalysts shape selectivity and loading properties*In *Series in materials science*, vol. 141. Springer; 2010.
83. Breyse M, Geantet C, Afanasiev P, Blanchard J, Vrinat M. *Catal Today* 2008;**130**(1): 3–13.
84. Bond Geoffrey C. *Metal-catalysed reactions of hydrocarbons*. Springer; 2005.
85. Anderson JA, Fernández García M, editors. *Supported metals in catalysis*. 2nd ed. Imperial College Press; 2011.
86. Busca G. *Chem Rev* 2007;**107**:5366–410.
87. Busca G. *Chem Rev* 2010;**110**:2217–49.
88. Busca G. Use of infrared spectroscopy methods in the field of heterogeneous catalysis by metal oxides. In: Jackson SD, Hargreaves JSJ, editors. *Metal oxide catalysis*, vol. 1. Wiley-VCH; 2009. pp. 95–175.
89. Montanari T, Castoldi L, Lietti L, Busca G. *Appl Catal A Gen* 2011;**400**(1–2):61–9.
90. Hunger M. Solid state NMR spectroscopy. In: Chester AW, Derouane EG, editors. *Zeolite characterization and catalysis: a tutorial*. Springer; 2009.
91. Jiang Y, Huang J, Dai W, Hunger M. *Solid State Nucl Magn Reson* 2011;**39**(3–4): 116–41.
92. Huang J, Jiang Y, Reddy Marthala VR, Ooi YS, Weitkamp J, Hunger M. *Microporous Mesoporous Mater* 2007;**104**:129.
93. McGregor J. Solid state NMR of oxidation catalysts. In: Jackson SD, Hargreaves JSJ, editors. *Metal oxide catalysis*, vol. 1. Wiley-VCH; 2009. pp. 195–242.
94. Martra G, Gianotti E, Coluccia S. In: Jackson SD, Hargreaves JSJ, editors. *Metal oxide catalysis*, vol. 1. Weinheim: Wiley-VCH; 2009. pp. 51–94.
95. Anpo M, Dzwigaj S, Che M. *Applications of photoluminescence spectroscopy to the investigation of oxide-containing catalysts in the working state advances in catalysis*, vol. 52; 2009. p. 1–42.
96. Jentoft FC. Electronic spectroscopy: ultra violet-visible and near IR spectroscopies. In: Che M, Vedrine JC, editors. *Characterization of solid materials and heterogeneous catalysts from structure to surface reactivity*. Wiley; 2012. pp. 89–148.
97. Matsuoka M, Saito M, Anpo M. Photoluminescence spectroscopy. In: Che M, Vedrine JC, editors. *Characterization of solid materials and heterogeneous catalysts from structure to surface reactivity*. Wiley; 2012. pp. 149–84.
98. Stankic S, Bernardi J, Diwald O, Knözinger E. *J Phys Chem B* 2006;**110**:13866.
99. Chizallet C, Costentin G, Che M, Delbecq F, Sautet P. *J Phys Chem B* 2006;**110**: 15878.
100. Chizallet C, Costentin G, Lauron-Pernot H, Krafft JM, Che M, Delbecq F, et al. *J Phys Chem C* 2008;**112**:16629–37.
101. Duffy JA, Ingram MD. *J Am Chem Soc* 1971;**93**:6448.
102. Leboutteiller A, Courtine P. *J Solid State Chem* 1998;**137**:94.
103. Duffy JA. *J Phys Chem A* 2006;**110**:13245.
104. Dimitrov V, Komatsu T. *J Solid State Chem* 2012;**196**:574–8.
105. Dimitrov V, Komatsu T. *J Solid State Chem* 2002;**163**:100.
106. Bordes-Richard E, Courtine P. In: Fierro JLG, editor. *Metal Oxides: Chemistry and Applications*. Boca Raton, FL: CRC Press; 2006. p. 319.

107. Pawelec B. In: Fierro JLG, editor. *Metal Oxides: Chemistry and Applications*. Boca Raton, FL: CRC Press; 2006. p. 111.
108. Teschner D, Vass EM, Schlögl R. In: Jackson SD, Hargreaves JSJ, editors. *Metal Oxide Catalysis*. Weinheim, Germany: Wiley-VCH; 2009. p. 243.
109. Corma A. *Chem Rev* 1995;**95**:559.
110. Morena JI, Jaimesa R, Gómezb R, Niño-Gómez ME. *Catal Today* 2011;**172**: 34–40.
111. Xie W, Liu Y, Chun H. *Catal Lett* 2012;**142**:352–9.
112. Sun C, Berg JC. *Adv Colloid Interface Sci* 2003;**105**:151.
113. Auroux A, Gervasini A. *J Phys Chem* 1990;**94**(16):6371–9.
114. Cutrufello MG, Ferino I, Monaci R, Rombi E, Solinas V. *Top Catal* 2002;**19**(3–4): 225–40.
115. Bennici S, Auroux A. In: Jackson SD, Hargreaves JSJ, editors. *Metal oxide catalysis*, vol. 1. Wiley-VCH; 2009. pp. 391–441.
116. Auroux A. *Mol Sieves* 2008;**6**:45–152.
117. Costa C, Lopes JM, Lemos F, Ramoa Ribeiro F. *J Mol Catal A Chem* 1999;**144**: 221–31.
118. Niwa M, Katada N. *J Jpn Pet Inst* 2009;**52**(4):172–9.
119. Liu L, Zhao L, Sun H. *J Phys Chem C* 2009;**113**:16051–7.
120. Izadbakhsh A, Farhadi F, Khorasheh F, Yan Z-F. *J Porous Mater* 2009;**16**:599–603.
121. Souza MJB, Lima SH, Araujo AS, Garrido Pedrosa AM, Coutinho ACSLS. *Adsorpt Sci Technol* 2007;**25**(10):751–6.
122. Stevens RW, Chuang SSC, Davis BH. *Thermochim Acta* 2003;**407**(1–2):61–71.
123. Gorte RJ. *Catal Today* 1996;**28**:405–14.
124. Matsushashi H, Arata K. *Chem Commun*; 2000:387–8.
125. Delgado JA, Sotelo JL, Gómez JM, Gómez P. *Adsorpt Sci Technol* 2007;**25**(3–4): 113–27.
126. Yan A, Liu B, Dong Y, Tian Z, Wang D, Cheng M. *Appl Catal B Environ* 2008;**80**(1–2): 24–31.
127. Peña MA, Fierro JLG. *Chem Rev* 2001;**101**:1981–2017.
128. Abee MW, Cox DF. *J Phys Chem B* 2001;**105**:8375–80.
129. Knözinger H. Infrared spectroscopy for the characterization of surface acidity and basicity. In: Ertl G, Knözinger H, Schüth F, Weitkamp J, editors. *Handbook of heterogeneous catalysis*; 2008. pp. 1135–63.
130. Thibault-Starzyk F, Maugé F. Infrared spectroscopy. In: Che M, Vedrine JC, editors. *Characterization of solid materials and heterogeneous catalysts from structure to surface reactivity*. Wiley; 2012. pp. 3–48.
131. Hadjiivanov KI, Vayssilov GN. *Adv Catal* 2002;**47**:307–511.
132. Platon A, Thomson WJ. *Ind Eng Chem Res* 2003;**42**:5988–92.
133. Busca G. *Curr Phys Chem* 2012;**2**:136–50.
134. Moulin B, Oliviero L, Bazin P, Daturi M, Costentin G, Maugé F. *Phys Chem Chem Phys* 2011;**13**(22):10797–807.
135. Kwak JH, Hu JZ, Kim DH, Szanyi J, Peden CHF. *J Catal* 2007;**251**(1):189–94.
136. Kwak JH, Hu J, Lukaski A, Kim DH, Szanyi J, Peden CHF. *J Phys Chem C* 2008;**112**(25):9486–92.
137. Mei D, Kwak JH, Hu JZ, Cho SJ, Szanyi J, Allard LF, Peden CHF. *J Phys Chem Lett* 2010;**1**:2688–91.

138. Hemmann F, Scholz G, Scheurell K, Kemnitz E, Jaeger C. *J Phys Chem C* 2012;**116**(19):10580–5.
139. Zheng A, Huang S-J, Liu S-B, Deng F. *Phys Chem Chem Phys* 2011;**13**(33): 14889–901.
140. Digne M, Sautet P, Raybaud P, Euzen P, Toulhoat H. *J Catal* 2002;**211**:1–5.
141. Coquet R, Howard KL, Willock DJ. Theory: periodic electronic structure calculations. In: Jackson SD, Hargreaves JSJ, editors. *Metal oxide catalysis*, vol. 1. Wiley-VCH; 2009. pp. 323–90.
142. Ferreira AR, Martins MJF, Konstantinova E, Capaz RB, Souza WF, Chiaro SSX, et al. *J Solid State Chem* 2011;**184**:1105–11.
143. Czekaj I, Wambach J, Kröcher O. *Int J Mol Sci* 2009;**10**:4310–29.
144. Wischert R, Laurent P, Copéret C, Delbecq FR, Sautert P. *J Am Chem Soc* 2012;**134**: 14430–49.
145. Digne M, Raybaud P, Sautet P, Guillaume D, Toulhoat H. Atomic scale insights on chlorinated alumina surfaces. *J Am Chem Soc* 2008;**130**:11030–9.
146. Loviat F, Czekaj I, Warnbach J, Wokaun A. *Surf Sci* 2009;**603**:2210–7.
147. Chizallet C, Digne M, Arrouvel C, Raybaud P, Delbecq F, Costantin G, et al. *Top Catal* 2009;**52**:1005–16.
148. Niwa M, Noda T, Suzuki K, Morishita N, Katada N. *Microporous Mesoporous Mater* 2011;**146**:208–15.
149. Nachtigall P, Delgado MR, Nachtigallova D, Arean CO. *Phys Chem Chem Phys* 2012;**14**:1552–69.
150. Cornu D, Guesmi H, Krafft J-M, Lauron-Pernot H. *J Phys Chem C* 2012;**116**(11): 6645–54.
151. Tuma C, Kerber T, Sauer J. *Angew Chem Int Ed Engl* 2010;**49**:4678–80.
152. Hensen N, Kerber T, Sauer J, Bell AT, Keil FJ. *J Am Chem Soc* 2010;**132**:11525–38.
153. Lauron-Pernot H. *Catal Rev* 2006;**48**:315.
154. Lercher JA, Jentys A, Brait A. *Mol Sieves* 2008;**6**:153–212. 3829\_2007\_017 Springer-Verlag Berlin Heidelberg. Published online.
155. De Vos DE, Ernst S, Perego C, O'Connor CT, Stocker M. *Microporous Mesoporous Mater* 2002;**56**(2):185–92.
156. Hart MP, Brown DR. *J Mol Catal A Chem* 2004;**212**:315–21.
157. Corma A, Iborra S. *Adv Catal* 2006;**49**:239.
158. Matsuhashi H, Oikawa M, Arata K. *Langmuir* 2000;**16**:8201.
159. Moreau C, Lecomte J, Roux A. *Catal Commun* 2006;**7**:941.

# Metal Oxides as Acid-Base Catalytic Materials

## CHAPTER OUTLINE

<b>6.1 Chemistry of metal oxides</b> .....	<b>104</b>
6.1.1 “Bulk” acidity and basicity.....	104
6.1.2 Structural chemistry of metal oxides .....	109
6.1.3 Covalent versus ionic oxides .....	121
6.1.4 Amorphous versus crystalline metal oxides .....	122
6.1.5 Redox behavior, thermal stability, magnetism and electronic conduction .....	122
6.1.6 Effect of particle size in the solid-state chemistry of oxides.....	124
<b>6.2 Composition effect on the surface acido-basicity of metal oxides: an overview</b> ....	<b>125</b>
<b>6.3 Acido-basicity of supports for catalysts</b> .....	<b>128</b>
<b>6.4 Metal oxides as acid and basic catalytic materials</b> .....	<b>129</b>
6.4.1 Supported alkali oxides.....	129
6.4.2 Magnesia and other alkali-earth oxides .....	131
6.4.2.1 Alkali-earth oxides as catalysts.....	133
6.4.2.2 Alkali-earth oxides as supports for catalysts .....	135
6.4.2.3 Alkali-earth oxides as adsorbents or absorbents .....	136
6.4.3 Aluminas .....	136
6.4.3.1 Preparation and solid-state chemistry of aluminas.....	136
6.4.3.2 Surface chemistry of aluminas.....	143
6.4.3.3 Aluminas as catalysts .....	148
6.4.4 Lanthana and rare-earth oxides.....	150
6.4.5 Silicas.....	151
6.4.5.1 Preparation and solid-state chemistry of silicas .....	151
6.4.5.2 Surface chemistry of silicas .....	156
6.4.5.3 Silicas as catalysts.....	159
6.4.5.4 Silicas as support of catalysts .....	160
6.4.6 Titanias .....	161
6.4.6.1 Surface chemistry of titanias.....	163
6.4.6.2 Titania as a catalyst.....	164
6.4.6.3 Titania as support for catalysts .....	164
6.4.7 Zirconias .....	166
6.4.7.1 Zirconia as a catalyst.....	168
6.4.7.2 Sulfated zirconia as a catalyst.....	169

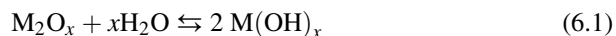
6.4.7.3 Zirconia as a support for catalysts.....	171
6.4.8 Ceria .....	171
6.4.9 Niobia .....	172
6.4.9.1 Niobia as a catalyst .....	173
6.4.9.2 Niobia as a support for catalysts .....	173
6.4.10 Tungsten trioxide (tungsta).....	173
6.4.10.1 Tungsta as a catalyst.....	174
6.4.10.2 Tungsta-zirconia as a catalyst.....	174
<b>6.5 Mixed metal oxides and their acido-basicity .....</b>	<b>174</b>
6.5.1 Silica–aluminas.....	174
6.5.1.1 Silica–aluminas as catalysts .....	178
6.5.2 Alumina-rich silica–aluminas and silicated aluminas .....	178
6.5.3 Aluminated silicas.....	179
6.5.4 Combinations of silica, titania, alumina, ceria and zirconia .....	179
6.5.5 Calcined hydrotalcites and spinels .....	180
<b>References .....</b>	<b>182</b>

## 6.1 Chemistry of metal oxides

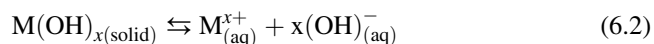
### 6.1.1 “Bulk” acidity and basicity

Oxides are the binary compounds of elements combined with oxygen. A summary of oxides’ properties is given in Table 6.1. According to basic inorganic chemistry, metal oxides can be classified as acidic, basic or amphoteric.

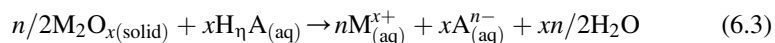
Basic oxides are those of metals, particularly in their low-valence states. The typical behavior a basic oxide implies that, by reacting with water, it gives rise to a hydroxide:



Metal oxides and hydroxides may be soluble in water where they are supposed to fully dissociate, thus giving rise to basic solutions ( $pH > 7$ ):



This is the case, in particular, of alkali hydroxides. Actually, most metal hydroxides are poorly soluble in water but may be dissolved in acidic solutions, producing solutions of their own cation, paired by the anion of the acid used.



Conversely, basic metal oxides or, more frequently, the corresponding hydroxides (or even the oxyhydroxides  $MO_j(OH)_y$ ) may be produced by precipitation from water solutions of salts of their cation in basic or neutral conditions (reverse of reaction (6.2)) or even still at acid pH. Mixed hydroxides and hydroxysalts can be precipitated by solutions containing more cations.

**Table 6.1** Metal Oxides and Their Properties

Ion Configuration	Oxide Formula	Mineralogical Name	Structure	$\Delta H_f^\circ/n_o$ kJ/mol	$T_{\text{melt}}$ C	Optical $E_g$ eV	
2s <sup>0</sup> 2p <sup>0</sup>	BeO	bromellite	Wurtzite (ZnS)	599	2565	>7.0	
	B <sub>2</sub> O <sub>3</sub>		Ribbons structure	424	480	>10	
3s <sup>0</sup> 3p <sup>0</sup>	MgO	periclase	rocksalt	601.7	2800	7.3	
	$\alpha$ -Al <sub>2</sub> O <sub>3</sub>	curundum	corundum	558.4	2045	8.3	
	SiO <sub>2</sub>	$\alpha$ -quartz				phase trans 573	
		$\beta$ -quartz				phase trans 870	
		$\beta$ -tridimite				phase trans 1470	
		cristobalite	cristobalite	429.1	1723	9.1	
4s <sup>0</sup> 4p <sup>0</sup> 3d <sup>0</sup>	P <sub>2</sub> O <sub>5</sub>		molecular	298.1	340		
	CaO	lime	rocksalt	635.1	2600	6.5	
	Sc <sub>2</sub> O <sub>3</sub>		C	635	2485	5.4	
	TiO <sub>2</sub>	rutile	rutile	470.8	1840	3.0	
	V <sub>2</sub> O <sub>5</sub>	shcherbinaite	layered	311.9	690	2.8	
	CrO <sub>3</sub>		chain orthorhombic	193	decomp. 197		
4s <sup>0</sup> 4p <sup>0</sup> 3d <sup>1</sup>	Ti <sub>2</sub> O <sub>3</sub>		corundum	505.7	1880	0.05 → 0 (450 K)	
	VO <sub>2</sub>		monoclinic → rutile 340K		1967	0.6 → 0	
4s <sup>0</sup> 4p <sup>0</sup> 3d <sup>2</sup>	V <sub>2</sub> O <sub>3</sub>	karelianite	corundum		1970	0 (0.2)	
	CrO <sub>2</sub>		rutile		decomp. 375	0	
4s <sup>0</sup> 4p <sup>0</sup> 3d <sup>3</sup>	Cr <sub>2</sub> O <sub>3</sub>	eskolaite	corundum	380.0	2265	3.4	
	MnO <sub>2</sub>	pyrolusite	rutile	260	decomp 535	3.0	
4s <sup>0</sup> 4p <sup>0</sup> 3d <sup>4</sup>	$\alpha$ -Mn <sub>2</sub> O <sub>3</sub>	bixbyite	"C"	323.9	880		
4s <sup>0</sup> 4p <sup>0</sup> 3d <sup>5</sup> /3d <sup>4</sup>	Mn <sub>3</sub> O <sub>4</sub>	hausmannite	Tetragonal spinel	347	1565		
4s <sup>0</sup> 4p <sup>0</sup> 3d <sup>5</sup>	MnO	manganosite	rock salt	385	1945	3.8	
	$\alpha$ -Fe <sub>2</sub> O <sub>3</sub>	haematite	corundum	247.7	1566	2.0	
4s <sup>0</sup> 4p <sup>0</sup> 3d <sup>6</sup> /3d <sup>5</sup>	Fe <sub>3</sub> O <sub>4</sub>	magnetite	Random spinel		1594	0.07	
4s <sup>0</sup> 4p <sup>0</sup> 3d <sup>6</sup>	FeO	wüstite	rock salt		1377	2.4	
4s <sup>0</sup> 4p <sup>0</sup> 3d <sup>7</sup> /3d <sup>6</sup>	Co <sub>3</sub> O <sub>4</sub>		spinel	202.3	decomp to CoO 900		

Continued

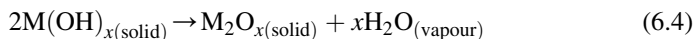


**Table 6.1** Metal Oxides and Their Properties—cont'd

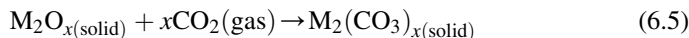
Ion Configuration	Oxide Formula	Mineralogical Name	Structure	$\Delta H_f^\circ/n_O$ kJ/mol	$T_{\text{melt}}$ C	Optical $E_g$ eV
$4s^0 4p^0 3d^7$	CoO		rock salt		1933	2.7
$4s^0 4p^0 3d^8$	NiO	bunsenite	rock salt	245.2	1957	3.8
$4s^0 4p^0 3d^9$	CuO	tenorite	tenorite	157.0	decomp to Cu <sub>2</sub> O 900	2.0
$4s^0 4p^0 3d^{10}$	Cu <sub>2</sub> O	cuprite	Cubic Pn-3m	170	1326	2.2
	ZnO	zincite	Wurtzite (ZnS)	348	1969	3.4
	$\beta$ -Ga <sub>2</sub> O <sub>3</sub>		$\beta$ -gallia	360	1740	4.4
	GeO <sub>2</sub>		$\beta$ -quartz		1115	5.4
			argutite	rutile		
$4s^2 4p^0 3d^{10}$	As <sub>2</sub> O <sub>5</sub>					
	As <sub>2</sub> O <sub>3</sub>					3.3
$5s^0 5p^0 4d^0$	SrO		rock salt	590.7	2430–2650	5.3
	Y <sub>2</sub> O <sub>3</sub>		C	586.2	2680	5.5
	ZrO <sub>2</sub>	baddeleyite	baddeleyite		phase trans 1170	
					tetragonal phase trans 2370	
			fluorite	547.4	2663	5.0
	Nb <sub>2</sub> O <sub>5</sub>			381.1	1512	3.4
	MoO <sub>3</sub>			251.7	795	3.8
$5s^0 5p^0 4d^1$	NbO <sub>2</sub>		dist rutile		1915	
$5s^0 5p^0 4d^2$	MoO <sub>2</sub>		dist rutile		decomp 1100	
$5s^0 5p^0 4d^4$	RuO <sub>2</sub>		rutile		sublimation 1200	0
$5s^0 5p^0 4d^6$	Rh <sub>2</sub> O <sub>3</sub>		corundum	95.3	1100	
$5s^0 5p^0 4d^8$	PdO		cooperite (PtS)		decomp 750	1.0
$5s^0 5p^0 4d^9$	AgO				decomp 100	
$5s^0 5p^0 4d^{10}$	Ag <sub>2</sub> O		cuprite	30	decomp 200	
	CdO		rock salt	258	decomp 900	2.2
	In <sub>2</sub> O <sub>3</sub>		C	308.6	1910	2.8
	SnO <sub>2</sub>	cassiterite	rutile	290.5	1900	3.7
	Sb <sub>2</sub> O <sub>5</sub>					1.4

5s <sup>2</sup> 5p <sup>0</sup> 4d <sup>10</sup>	SnO		litharge	285	1080	
	$\alpha$ -Sb <sub>2</sub> O <sub>3</sub>	senarmontite		233.2	656	3.3
	TeO <sub>2</sub>	tellurite		162.6	732	3.79
4f <sup>0</sup> 6s <sup>0</sup> 6p <sup>0</sup> 5d <sup>0</sup>	BaO		rock salt	553	1923–2015	6.0
	La <sub>2</sub> O <sub>3</sub>		A	699.7	2400	5.0
	CeO <sub>2</sub>		fluorite	544.6	2727	3.2
4f <sup>1</sup> 6s <sup>0</sup> 6p <sup>0</sup> 5d <sup>0</sup>	Ce <sub>2</sub> O <sub>3</sub>		hexagonal		2177	
4f <sup>14</sup> 6s <sup>0</sup> 6p <sup>0</sup> 5d <sup>0</sup>	HfO <sub>2</sub>		fluorite	556.8	2790	5.7
	Ta <sub>2</sub> O <sub>5</sub>			409.9	1879	4.2
	WO <sub>3</sub>		distorted ReO <sub>3</sub>	280.3	1473	2.7
4f <sup>14</sup> 6s <sup>0</sup> 6p <sup>0</sup> 5d <sup>1</sup>	TaO <sub>2</sub>		rutile			
4f <sup>14</sup> 6s <sup>0</sup> 6p <sup>0</sup> 5d <sup>2</sup>	WO <sub>2</sub>		dist. rutile		decomp. 1700	
4f <sup>14</sup> 6s <sup>0</sup> 6p <sup>0</sup> 5d <sup>5</sup>	IrO <sub>2</sub>		rutile		decomp. 1100	
4f <sup>14</sup> 6s <sup>0</sup> 6p <sup>0</sup> 5d <sup>6</sup>	PtO <sub>2</sub>		CdI <sub>2</sub> structure	80	decomp. 450	
4f <sup>14</sup> 6s <sup>0</sup> 6p <sup>0</sup> 5d <sup>8</sup>	PtO		cooperite (PtS)		decomp 325	
	Au <sub>2</sub> O <sub>3</sub>		orthorombic	17	decomp 150	0.85
	Au <sub>2</sub> O		cuprite	22		0.83–1.3
4f <sup>14</sup> 6s <sup>0</sup> 6p <sup>0</sup> 5d <sup>10</sup>	Hg <sub>2</sub> O <sub>2</sub>	montroydite	montroydite	90	decomp 500	2.2 / 1.0
			cinnabar (HgS)			
	Tl <sub>2</sub> O <sub>3</sub>		C			2.2
	PbO <sub>2</sub>	plattnerite	rutile		decomp. 290	2.95
	Bi <sub>2</sub> O <sub>5</sub>					
4f <sup>14</sup> 6s <sup>1</sup> 6p <sup>0</sup> 5d <sup>10</sup>	Hg <sub>2</sub> O					
4f <sup>14</sup> 6s <sup>2</sup> 6p <sup>0</sup> 5d <sup>10</sup>	Tl <sub>2</sub> O		anti-CdI <sub>2</sub>		596	
	PbO	litharge	Litharge		888	2.8
		massicot	Massicot			
	Bi <sub>2</sub> O <sub>3</sub>	bismite	Several phases	192.6	820	2.7
7s <sup>0</sup> 6d <sup>0</sup> 5f <sup>0</sup>	UO <sub>3</sub>			400	decomp 400	
7s <sup>2</sup> 6d <sup>0</sup> 5f <sup>0</sup>	UO <sub>2</sub>	uraninite	fluorite	540	2865	

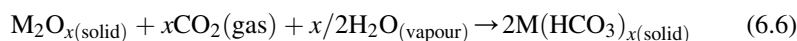
The hydroxide or the oxyhydroxide can be converted into the oxide by decomposition at relatively high temperature:



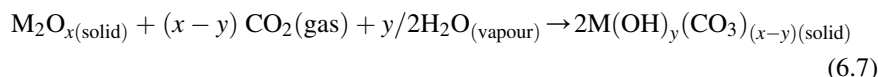
The reactivity of basic oxides depends on the ionicity of the metal–oxygen bond. Alkali and alkali-earth oxides are the most ionic and, thus, the most reactive, and easily convert (even in ambient conditions) into the hydroxide by reacting with water vapor (reaction (6.1)), or, by reacting with gas-phase  $\text{CO}_2$ , to the carbonate



or the bicarbonate.



or even the hydroxycarbonates.



For this reason, very reactive basic oxides, such as alkali-earth oxides and at least some rare-earth oxides, are usually contaminated by hydroxide and carbonates, while alkali oxides are almost nonexistent in normal conditions.

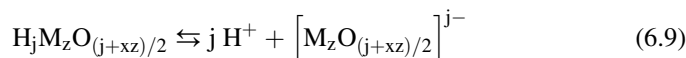
Typical basic oxides usually correspond to well-defined solid hydroxides and are those of monovalent, divalent and trivalent cations. Actually, also for some of these cations amphoteric more than basic hydroxides form, that dissolve both in highly acidic and in highly basic solutions. In the case of poorly soluble amphoteric hydroxides, such as  $\text{AgOH}$ ,  $\text{Be}(\text{OH})_2$ ,  $\text{Zn}(\text{OH})_2$ ,  $\text{Pb}(\text{OH})_2$ ,  $\text{Al}(\text{OH})_3$ , dissociation of the hydroxide in water solution is incomplete, which means that hydroxide anions participate, even in solution, to the coordination sphere of the cation. It is evident that the metal-to-oxygen bond and the solid-state structure stability strongly affect the solubility of metal hydroxides too.

The hydroxides of tetravalent cations are frequently not well characterized and are denoted more as “amorphous hydrates” or “hydrated oxides”. This seems the case, e.g., of hydrated zirconia and tin oxide. In some cases, like for  $\text{Ti}^{4+}$  hydroxides, compounds with more defined structures exist having a weak acidic character, more than the amphoteric one, thus being classified as polyacids (titanic acids) more than hydroxides. Thus, we are here borderline from the chemistry of the low-valence elements with full metallic character and high-valence cations that behave as those of nonmetallic elements.

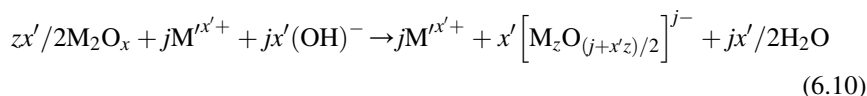
The typical acid oxides are those of nonmetal elements that, reacting with water, give rise to oxoacids:



that dissociate in water giving rise to acidic solutions:



Acidic oxides, also called anhydrides, are typically formed by nonmetal elements or even by metallic elements in very high oxidation states, like  $V^{5+}$ ,  $Nb^{5+}$ ,  $Cr^{6+}$ ,  $Mo^{6+}$ ,  $W^{6+}$ , etc., whose oxides ( $V_2O_5$ ,  $Nb_2O_5$ ,  $CrO_3$ ,  $MoO_3$ ,  $WO_3$ ) are also called vanadic, niobic, chromic, molybdic and wolframic anhydrides. Anhydrides tend to be dissolved in basic solution giving rise to their salts, where the element participate to the oxoanion,



The corresponding oxoacids may be formed by precipitation/condensation from water solutions of the oxosalts in acidic conditions [reverses of reactions (6.9) and (6.8)]. They are denoted as polyoxoacids when their structural formula implies several atoms ( $x > 1$  in the above formula). When more than one nonmetallic element is involved in a polyoxoacid, this is denoted as heteropolyoxoacid or heteropolyacid.

### 6.1.2 Structural chemistry of metal oxides<sup>1,2</sup>

All metal oxides form crystalline phases as their most thermodynamically stable form. In many cases, additional polymorphs, e.g., crystalline phases that have limited stability or no stability at all, i.e., that are metastable at any temperature and pressure, also exist, being their transformation to more stable polymorphs slow, if at all. In Table 6.2 the characteristics of some of the most common crystal phases of metal oxides are summarized.

The size and the charge of the cations are the main but not the only factors determining the crystal structure of metal oxides. Most cations are definitely smaller than the oxide anion, whose crystal radius is estimated to be around 1.40 Å. Thus, the structure of ionic oxides of small cations are mostly generated by the array of the oxide anions, which can be cubic close packed (ccp) or hexagonal close packed (hcp). These close packings allow insertion of small cations either in octahedral or in tetrahedral interstices. Thus, many oxide structures are actually constituted by ccp or hcp oxygen arrays with cations in symmetric octahedral and/or tetrahedral coordination in the interstices. On the other hand, when cation size is comparable or even higher than that of the oxide anions, less compact structures are produced, where less compact arrays for oxygen can occur (such as simple cubic).

Several electronic reasons can appear for distortion of the coordination sphere of cations and, consequently, of the overall structure. The so-called second-order Jahn–Teller effect (SOJT)<sup>3,4</sup> involves structural changes attributable to a nondegenerate groundstate interacting with a low-lying excited state. The distortion occurs if the energy gap between the Higher Occupied Molecular Orbitals (HOMO) and Lower Unoccupied Molecular Orbitals (LUMO) orbitals is small and if there is a symmetry-allowed distortion permitting mixing of these two orbitals. The distortion can occur with  $d^0$  transition metals resulting in asymmetric coordination

environments. This is particularly evident for the oxides of  $V^{5+}$ ,  $Nb^{5+}$ ,  $Mo^{6+}$  and  $W^{6+}$  that present very distorted octahedral coordination spheres for cations (see below for  $V^{5+}$ ). For these high-valence oxides, however, the appearance of a covalent-like structure, with a decrease of the coordination at oxygen, is another factor for modifying the overall structure with respect to those of typically ionic oxides.

For transition metal cations that contain varying numbers of d electrons in orbitals that are not spherically symmetric, the situation is quite different. First, a definite preference for occupation of octahedral versus tetrahedral coordination appears, except for high spin  $d^5$  cations. The shape and occupation of the d-orbitals also becomes a factor introducing distortion of the geometry of the coordination sphere. The so-called first-order Jahn–Teller effect (FOJT) occurs when cations have (when free) uncompletely filled degenerate orbitals, resulting in the loss of their degeneracy. This may cause significant distortions of the coordination spheres, up to the appearance of severe loss of symmetry. This is the case, e.g., for  $d^8$  cations,  $(t_{2g})^6(e_g)^2$ , such as  $Pd^{2+}$  and  $Pt^{2+}$ , where this effect causes an elongation of the axial bonds in the octahedral coordination, with respect to the equatorial ones, thus producing the square planar coordination. A similar situation occurs for  $Au^{3+}$  and also for  $Cu^{2+}$  ( $d^9$ ).

Another very relevant factor producing distortion of the coordination sphere and of the overall crystal structure is the presence of electron pairs at the highest occupied level, such as for  $Tl^+$ ,  $Sn^{2+}$ ,  $Pb^{2+}$ ,  $Bi^{3+}$ ,  $Te^{4+}$ .

Most of monovalent alkali oxides, which, as said, are unstable with respect to hydration and carbonation in normal conditions to being almost not existent, take the antifluorite structure, where oxygen ions are in a perfect ccp array coordinated to eight cations and alkali ions have a tetrahedral coordination. Different structures are taken when monovalent cations are larger:  $Cs_2O$  and  $Tl_2O$  have the layered “antibrucite”-like (anti- $CdI_2$ ) structure with cations in hcp array, bonded to four oxide ions, and oxygen atoms bonded to eight cations.

$Cu_2O$ ,  $Ag_2O$  and  $Au_2O$ , whose cations have a strong preference for linear coordination, have the cuprite structure, where oxygen atoms form a body centered lattice, while metal atoms are located on the vertices of a tetrahedron around each oxygen atom, forming a fcc lattice. Metal–oxygen–metal bonds are in fact linear.

The stable phase of most bivalent metal oxides is the rock-salt (NaCl) or periclase (MgO) structure, with cubic close-packed array of oxide anions and octahedrally coordinated cations and oxide anions. For BeO, where  $Be^{2+}$  cationic radius is very small, but also for ZnO (whose  $Zn^{2+}$  cationic radius is not smaller than that of  $Mg^{2+}$ ) the wurtzite structure with tetrahedral coordinations for both cations and anions is stable in ambient conditions. An alternative metastable phase of ZnO is with the zincblende structure<sup>5</sup> where coordination for both cations and anions is tetrahedral too. Bivalent cations having a defined preference for square planar coordination take, in their oxides, structures preserving it, such as the cooperite (PtS) structure for PdO and PtO and its tetragonally distorted form, tenorite structure, for CuO. In both, oxygen is tetrahedrally coordinated. In the HgO structure, instead, zigzag Hg–O–Hg chains exist with coordination two for both Hg and O atoms.

**Table 6.2** Crystal Structures and Ion Coordinations in Stable Solid Simple Oxides

Cation Valence	Type of Structure	Structure Name	Space Group	Z	Coordination		Examples
					Cation	Oxide	
1	(Layered)	Antifluorite	Fm-3m	4	4 (tetr)	8 (Cub)	Li <sub>2</sub> O, Na <sub>2</sub> O, K <sub>2</sub> O, Rb <sub>2</sub> O
		Cuprite	Pn $\bar{3}m$	2	2 (lin)	4 (tetr)	Cu <sub>2</sub> O, Ag <sub>2</sub> O, Au <sub>2</sub> O, Pb <sub>2</sub> O
2	Network	Anti -CdCl <sub>2</sub>	R $\bar{3}m$	3	3 (pyr)	6 (Oct)	Cs <sub>2</sub> O
		Rock salt	Fm-3m	4	6 (Oct)	6 (Oct)	MgO, CaO, SrO, BaO, MnO, FeO, CoO, NiO, CdO
	Layered	Zinc blende	F $\bar{4}3m$	4	4 (tetr)	4 (tetr)	BeO (H)
		Wurtzite	P6 <sub>3</sub> mc	2	4 (tetr)	4 (tetr)	BeO (L), ZnO
		Tenorite	C2/c	4	4 (sq.pl.)	4 (tetr)	CuO
		Cooperite	P4 <sub>2</sub> /mmc	2	4 (sq.pl.)	4 (tetr)	PdO, PtO
		Litharge	P4/nmm	2	4 (pyr)	4 (dist tetr)	SnO, $\alpha$ -PbO
		Massicot	Pbcm	4	4 (pyr)	4 (dist tetr)	$\beta$ -PbO
	Chain	Montroydite	Pnma	4	2 (lin)	2(bent)	HgO
	Chain	Cinnabar	P3 <sub>1</sub> 21	3	2(lin)	2(bent)	HgO
1,3	Network		P2 <sub>1</sub> /c	4	2 (lin) 4 (sq.pl.)	3 (trig)	AgO
	Molecular/ polymeric Network		P3 <sub>1</sub>	3	3 (trig.)	1,2	B <sub>2</sub> O <sub>3</sub>
Corundum		R $\bar{3}c$	6	6 (Oct)	4	$\alpha$ -Al <sub>2</sub> O <sub>3</sub> , $\alpha$ -Cr <sub>2</sub> O <sub>3</sub> , $\alpha$ -Fe <sub>2</sub> O <sub>3</sub> , $\alpha$ -Ga <sub>2</sub> O <sub>3</sub>	
Tetragonal spinel		I4 <sub>1</sub> /amd	4	4 (tetr), 6 (oct)	3,4	$\gamma$ -Mn <sub>2</sub> O <sub>3</sub>	
Beta-gallia		C2/m	4	4 (tetr), 6 (oct)	3,4	$\theta$ -Al <sub>2</sub> O <sub>3</sub> , $\beta$ -Ga <sub>2</sub> O <sub>3</sub>	
maghemite		P4 <sub>1</sub> 32	8	4 (tetr), 6 (oct)	3,4	$\gamma$ -Fe <sub>2</sub> O <sub>3</sub>	
"A"		P $\bar{3}m1$	1	7	6,4	La <sub>2</sub> O <sub>3</sub> , Ce <sub>2</sub> O <sub>3</sub> , Pr <sub>2</sub> O <sub>3</sub> (H), Nd <sub>2</sub> O <sub>3</sub> (H)	
"B"	C2/m	6	7	4,5,6	Pm <sub>2</sub> O <sub>3</sub> , Sm <sub>2</sub> O <sub>3</sub> , Eu <sub>2</sub> O <sub>3</sub> , Gd <sub>2</sub> O <sub>3</sub> (H), Tb <sub>2</sub> O <sub>3</sub> , Dy <sub>2</sub> O <sub>3</sub> , Ho <sub>2</sub> O <sub>3</sub> , Er <sub>2</sub> O <sub>3</sub> , Tm <sub>2</sub> O <sub>3</sub> , Yb <sub>2</sub> O <sub>3</sub> , Lu <sub>2</sub> O <sub>3</sub> ,		

Continued

**Table 6.2** Crystal Structures and Ion Coordinations in Stable Solid Simple Oxides—cont'd

Cation Valence	Type of Structure	Structure Name	Space Group	Z	Coordination		Examples
					Cation	Oxide	
3		"C" bixbyite	la $\bar{3}$	16	6 (Oct)	4	Gd <sub>2</sub> O <sub>3</sub> (L), Pr <sub>2</sub> O <sub>3</sub> (L), Nd <sub>2</sub> O <sub>3</sub> (L), Yb <sub>2</sub> O <sub>3</sub> , $\alpha$ -Mn <sub>2</sub> O <sub>3</sub> , In <sub>2</sub> O <sub>3</sub> , Tl <sub>2</sub> O <sub>3</sub>
			Fdd2		4(tetr)	3	Au <sub>2</sub> O <sub>3</sub>
2,3		Detective cubic spinel	Fd3m	8	4,6	4	$\gamma$ -Al <sub>2</sub> O <sub>3</sub> , $\eta$ -Al <sub>2</sub> O <sub>3</sub> , $\gamma$ -Ga <sub>2</sub> O <sub>3</sub>
4		(Deformed) spinel			4,6	4	Fe <sub>3</sub> O <sub>4</sub> , Mn <sub>3</sub> O <sub>4</sub> , Co <sub>3</sub> O <sub>4</sub>
4		$\alpha$ -quartz	P3 <sub>2</sub> 21	3	4 (tetr)	2 (Bent)	SiO <sub>2</sub> , GeO <sub>2</sub>
			rutile	P4 <sub>2</sub> /mnm	2	6 (Oct)	3
5		Anatase	I41/amd	4	6 (Oct)	3	TiO <sub>2</sub>
		Baddeleyite	P2 <sub>1</sub> /c	4	7	3, 4	ZrO <sub>2</sub> (L)
		Tetragonal zirconia	P4 <sub>2</sub> /nmc	2	8	4	ZrO <sub>2</sub> (M)
		Fluorite	Fm-3m	4	8 (Cub.)	4	ThO <sub>2</sub> , CeO <sub>2</sub> , HfO <sub>2</sub> , ZrO <sub>2</sub> (H)
5	Molecular		R3c	2	4	2,2	Rhombohedral P <sub>4</sub> O <sub>10</sub>
	Layered	V <sub>2</sub> O <sub>5</sub>	Pmmn	2	5 (6)	1, 2, 3	V <sub>2</sub> O <sub>5</sub> , R-Nb <sub>2</sub> O <sub>5</sub>
6	Network		P2	14	6,4	2,3	H-Nb <sub>2</sub> O <sub>5</sub>
	Molecular				4	1,2	$\gamma$ -SO <sub>3</sub> (S <sub>3</sub> O <sub>9</sub> )
	Chain		C2cm	4	4		CrO <sub>3</sub>
	Layered		Pbnm	4	4 to 6	1,2,3	MoO <sub>3</sub>
	Network	ReO <sub>3</sub>	Pm-3m	4	6	2	ReO <sub>3</sub> , WO <sub>3</sub> (distorted)

L,M,H = low, medium, high temperature form.

Thus, the three oxides of group 12 elements have different structures with tetrahedral (ZnO, wurtzite-type), octahedral (CdO, rock salt-type) and linear (HgO) coordinations, respectively.

A particular situation occurs with the monoxides of group 14 elements that in their bivalent state retain an electron doublet in the external level. This is the case of the two PbO polymorphs (litharge  $\alpha$ -PbO, whose structure is taken also by SnO, and massicot  $\beta$ -PbO): they form layered structures with a square pyramid with a lead atom at the apex and four oxygen atoms at the base, and distorted tetrahedral coordination of the oxide ion.<sup>6</sup> This gives rise to some cation–cation semi-metallic bonding.

A further interesting situation is that of AgO, which is actually a mixed oxide of Ag(I) and Ag(III). Accordingly, monovalent silver is bonded linearly to two oxide ions, while trivalent silver is bonded to four anions in a square pyramidal coordination.

Several elements, in particular Mn, Co and Fe give rise to mixed oxides with bivalent and trivalent cations. The three compounds  $\text{Mn}_3\text{O}_4$ ,  $\text{Fe}_3\text{O}_4$ ,  $\text{Co}_3\text{O}_4$  take structures that are closely related to that of the mineral spinel ( $\text{MgAl}_2\text{O}_4$ ). This structure, very common for mixed oxides, has ccp oxygen array with  $\text{Mg}^{2+}$  ions in tetrahedral coordination and  $\text{Al}^{3+}$  cations in octahedral sites. The structure of  $\text{Co}_3\text{O}_4$  is the same, cubic with the bivalent ion in tetrahedral site and the trivalent one in octahedral site. The structure of hausmannite,  $\text{Mn}_3\text{O}_4$ , is also the same, but tetragonally distorted. This is due to the FOJT effect causing the octahedral site where  $\text{Mn}^{3+}$  ions are located tetragonally distorted.  $\text{Fe}_3\text{O}_4$ , the mineral magnetite, is also a similar structure. However, in this case  $\text{Fe}^{2+}$  are located in octahedral sites, while  $\text{Fe}^{3+}$  distribute among tetrahedral and octahedral sites. For this reason, magnetite is referred to as a cubic “inverse spinel”.

In the case of the oxides of trivalent elements with small cationic size, the corundum ( $\alpha$ - $\text{Al}_2\text{O}_3$ ) or hematite ( $\alpha$ - $\text{Fe}_2\text{O}_3$ ) structure (taken also by chromia, eskolaite,  $\alpha$ - $\text{Cr}_2\text{O}_3$ , and a polymorph of gallia,  $\alpha$ - $\text{Ga}_2\text{O}_3$ , as well as many other compounds such as  $\text{Ti}_2\text{O}_3$ ,  $\text{V}_2\text{O}_3$ ,  $\text{Rh}_2\text{O}_3$  etc.) predominates. This phase has hcp oxide array and octahedral coordination for the cations.

Most of these oxides, however, also have alternative structures that have traditionally been considered to be derived from the structure of spinel,  $\text{MgAl}_2\text{O}_4$ . Being the sesquioxide  $\text{M}_2\text{O}_3$  stoichiometry different from that of spinel, such phases are “nonstoichiometric” or cation-deficient spinels. Well-defined deformed spinel-type structures exist such as the “beta gallia structure” taken by both  $\theta$ - $\text{Al}_2\text{O}_3$  and  $\beta$ - $\text{Ga}_2\text{O}_3$ , which is a monoclinic spinel superstructure where cations are half in octahedral coordination, half in tetrahedral coordination. Interestingly, in the case of Gallia, the spinel-derived phase,  $\beta$ - $\text{Ga}_2\text{O}_3$ , is the most stable, with the corundum structure,  $\alpha$ - $\text{Ga}_2\text{O}_3$ , being metastable. The situation is inverted with respect to alumina where  $\theta$ - $\text{Al}_2\text{O}_3$  is metastable and corundum always the stable phase. Also the structure of  $\gamma$ - $\text{Fe}_2\text{O}_3$  (maghemite), a metastable phase of ferric oxide, can be derived by that of spinel: actually two phases are observed, a cubic disordered spinel and a tetragonal superstructure, where ferric ions are in



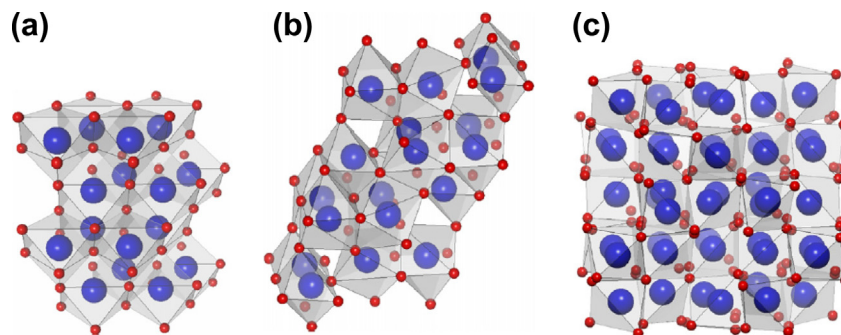
tetrahedral and octahedral coordination in a ratio 1:1.66.<sup>7</sup> Both are unstable with respect to hematite  $\alpha$ -Fe<sub>2</sub>O<sub>3</sub>.

Several other structures, which have still not been completely defined, have assumed to be cation-deficient spinel with partially disorder cation distribution between tetrahedral and octahedral coordination sites. These are the structures denoted as  $\gamma$ -Al<sub>2</sub>O<sub>3</sub>,  $\eta$ -Al<sub>2</sub>O<sub>3</sub>,  $\delta$ -Al<sub>2</sub>O<sub>3</sub>,  $\gamma$ -Ga<sub>2</sub>O<sub>3</sub>,  $\gamma$ -Cr<sub>2</sub>O<sub>3</sub> and  $\gamma$ -Mn<sub>2</sub>O<sub>3</sub>. All these structures are metastable. As it will be discussed below (Chapter 6.4.3), recently, a nonspinel model for  $\gamma$ -Al<sub>2</sub>O<sub>3</sub> has been proposed.  $\kappa$ -Al<sub>2</sub>O<sub>3</sub> is a unic orthorhombic structure with a pseudo-close-packed stacking ABAC of oxygen atoms, with aluminum in octahedral and tetrahedral environments in a 3:1 ratio<sup>8</sup> while the structure of  $\chi$ -Al<sub>2</sub>O<sub>3</sub> has still not been defined.

According to our data, sesquioxides with purely tetrahedral coordination for the cation do not exist. The only sesquioxide with cation coordination four is Au<sub>2</sub>O<sub>3</sub><sup>9</sup> (orthorhombic, SG Fdd2, Z = 8) where Au<sup>3+</sup> ions are in square planar coordination, and two oxygen positions exist, one with nearly trigonal and the other with bent coordination two.

Another structure with trivalent cations in coordination six, alternative to corundum, is that of  $\alpha$ -Mn<sub>2</sub>O<sub>3</sub>, bixbyite, cubic, also called “rare-earth oxide type C” structure (Figure 6.1), being taken by most rare-earth sesquioxides (from Pm to Lu) in normal conditions, as well as by In<sub>2</sub>O<sub>3</sub>, Tl<sub>2</sub>O<sub>3</sub>, Sc<sub>2</sub>O<sub>3</sub> and Y<sub>2</sub>O<sub>3</sub>.<sup>10</sup> The reason for choosing the bixbyite structure with respect to the corundum structure are not only due to cationic size. In fact, even if most cations using this structure have size in the 0.98–0.85 Å range, Mn<sup>3+</sup> is smaller (0.57 Å) than several trivalent cations preferring the corundum structure (usually <0.7 Å).

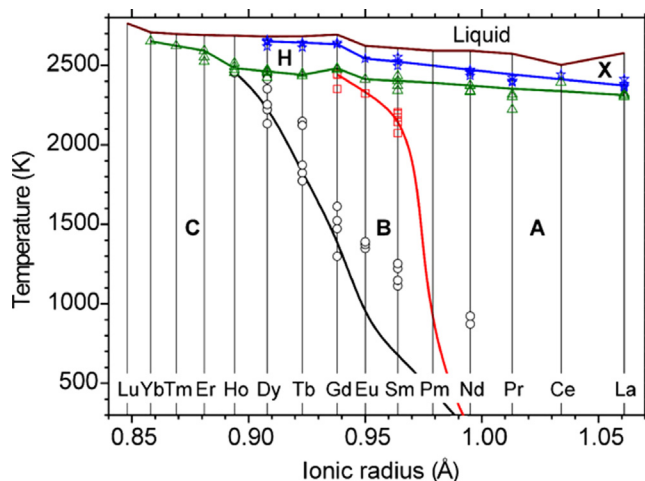
Other trivalent rare-earth oxides, having quite big cations, take alternative structures called A and B phases (Figure 6.1). In the hexagonal A phase, taken at ambient pressure and temperatures by La<sub>2</sub>O<sub>3</sub>, Ce<sub>2</sub>O<sub>3</sub>, Pr<sub>2</sub>O<sub>3</sub> and Nd<sub>2</sub>O<sub>3</sub>, cation



**FIGURE 6.1**

Structures of the rare-earth sesquioxides (a), (b) and (c).

*Reprinted with permission from Ref. 10.*



**FIGURE 6.2**

The scheme of polymorphic transformations in lanthanide sesquioxides. Lines connect the assessed temperatures, various symbols represent the experimental values, as reported in the literature.

*Reprinted with permission from Ref. 10.*

coordination is seven while in the monoclinic B phase (taken at ambient pressure and temperatures by  $\text{Sm}_2\text{O}_3$ ,  $\text{Eu}_2\text{O}_3$  and  $\text{Gd}_2\text{O}_3$ ) two different cation positions exist with coordination six and seven.  $\text{RE}_2\text{O}_3$  systems adopt the structural sequence A-B-C with the increasing atomic number or decreasing ionic radii (Figure 6.2). On the other hand, A-type RE sesquioxide tends to convert into B-type phases by increasing the temperature. All of them at very high temperature can convert into another hexagonal phase or to a cubic one, while corundum structures may be formed at high pressure.

Deformed coordination structures appear with the elements of group 15 that, in their trivalent state, retain an electron doublet at the higher energy level. This is the case of bismuth sesquioxide where  $\text{Bi}^{3+}$  oxidation state results in an electronic configuration  $5d^{10} 6s^2 6p^0$ , with the doublet occupying an inert sp hybrid orbital, which is projected out one side of the Bi atom and distorts the crystal structure.  $\text{Bi}_2\text{O}_3$  has four polymorphic forms. Under ambient condition, the monoclinic  $\alpha\text{-Bi}_2\text{O}_3$  ( $P2_1/c$ ,  $Z=4$ ) is stable. It contains five coordinate Bi atoms with the five oxygens present on one side of the atom.  $\alpha\text{-Bi}_2\text{O}_3$  transforms at  $729^\circ\text{C}$  to the cubic  $\delta\text{-Bi}_2\text{O}_3$ , that is stable up to the melting point of  $824^\circ\text{C}$ . This phase is assumed to be a defective fluorite phase (fluorite is  $\text{CaF}_2$ , whose structure is taken also by several oxides with formulas  $\text{MO}_2$  and  $\text{MO}_{2-\delta}$ , see below) with  $1/4$  of oxygen atoms randomly vacant. In fact, this phase is an excellent oxide ionic conductor. On cooling, two other metastable phases exist. At  $650^\circ\text{C}$ , the tetragonal  $\beta\text{-Bi}_2\text{O}_3$ , which is

considered to be an oxygen vacancy-ordered  $\delta$ - $\text{Bi}_2\text{O}_3$ , can be obtained. The cubic  $\gamma$ - $\text{Bi}_2\text{O}_3$  with body-centered symmetry appears at 639 °C.

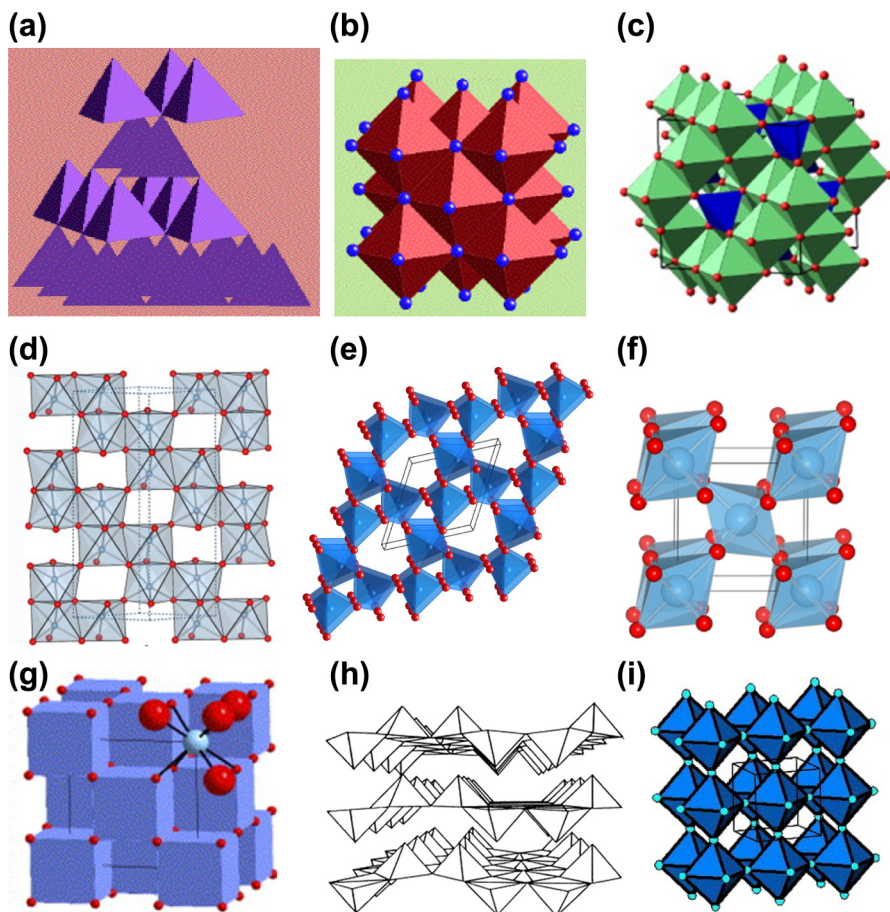
Trivalent nonmetallic or semimetallic elements such as P(III), As(III) and Sb(III) form molecular oxides with the formula  $\text{M}_4\text{O}_6$  and a similar bicyclic cage structure, persisting also at the solid, crystalline state (like for the mineral, senarmonite,  $\alpha$ - $\text{Sb}_2\text{O}_3$ ). However, trivalent arsenic and antimony also present additional polymer-structured oxides. Two slightly different polymeric  $\text{As}_2\text{O}_3$  phases exist, which both crystallize as monoclinic crystals, with sheets of pyramidal  $\text{AsO}_3$  units that share O atoms. Pairs of  $-\text{Sb}-\text{O}-\text{Sb}-\text{O}-$  chains that are linked by oxide bridges between the Sb centers constitute the polymeric form of orthorhombic  $\beta$ - $\text{Sb}_2\text{O}_3$ , which exists in nature as the mineral valentinite. In all these cases, P(III), As(III) and Sb(III) retain an electron pair in a nearly  $\text{sp}_3$ -hybrid orbital, thus having a pyramidal coordination, oxygen being bonded bent to two atoms.

Boron is considered to be a nonmetal. Its high electronegativity is associated to the formation of quite a covalent bond with oxygen. Thus, boria has also a polymeric structure, with oxygen bonded to two boron atoms with bent bridges and boron forming a three-dimensional network of corner-linked planar  $\text{BO}_3$  triangles.<sup>11</sup> According to its  $\text{sp}_2$ -like hybridization, boron is in planar trigonal coordination.

Depending on their size and on the character of the element, tetravalent element oxides take very different crystal structures. Very small tetravalent species like  $\text{Si}^{4+}$  and  $\text{Ge}^{4+}$  tend to stay in tetrahedral coordination, according to the covalent character of their bond with oxygen. They give rise to several different structures with covalently bonded tetrahedra shared through a bicoordinated (usually bent) oxygen atom: the major forms are called  $\alpha$ - and  $\beta$ -quartz,  $\alpha$ - and  $\beta$ -tridymite,  $\alpha$ - and  $\beta$ -cristobalite. Silica also forms stabilized amorphous states.

When the cations have intermediate sizes, such as for  $\text{Ti}^{4+}$ , the most stable structure is rutile (Figures 6.3 and 6.4), with octahedrally coordinated cations and trigonal anions. Actually, the tetragonal structure of rutile, taken by a number of  $\text{MO}_2$  phases ( $\text{M} = \text{Ti}, \text{Cr}, \text{Mn}, \text{V}, \text{Nb}, \text{Ru}, \text{Rh}, \text{Pd}, \text{Ta}, \text{Re}, \text{Os}, \text{Ir}, \text{Ge}, \text{Sn}, \text{Pb}$ ), is sometimes deformed,<sup>12</sup> coming to monoclinic (for  $\text{VO}_2$  (M),  $\text{MoO}_2$ ,  $\text{WO}_2$ ,  $\text{ReO}_2$ ) or orthorhombic ( $\text{PtO}_2$ ) or a different tetragonal phase ( $\text{NbO}_2$ ,  $\text{TaO}_2$ ). Interestingly, a rutile-type silica phase (stishovite) can form at high pressures, while germania can have both rutile structure (with octahedral coordination) and tetrahedral silica-like structures such as coesite,  $\alpha$ -quartz and  $\alpha$ -cristobalite. Rutile-type  $\text{GeO}_2$  (argutite) is the stable phase at low temperature while quartz  $\text{GeO}_2$  may become stable at higher temperature.<sup>13</sup>

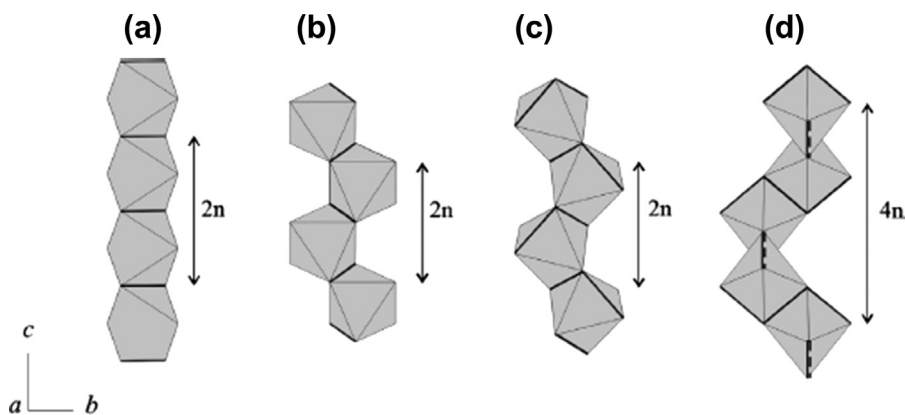
Also for lead dioxide, the most common polymorph is rutile-type structure ( $\beta$ - $\text{PbO}_2$ , plattnerite). A second, more dense polymorph ( $\alpha$ - $\text{PbO}_2$ , scrutinyite) takes a different structure, monoclinic,  $\text{Pbcn}$ ,  $Z = 4$ , where, like in rutile, one half of the octahedral interstice of the hcp oxygen array is occupied. However, while in rutile straight lines of edge-shared  $\text{PbO}_6$  octahedra are formed, in the  $\alpha$ - $\text{PbO}_2$  structure zigzag chains of skew-edge linked  $\text{PbO}_6$  octahedra occur (Figure 6.4). Interestingly, the two  $\text{PbO}_2$  structures differ for their electrical conductivity,  $\alpha$ - $\text{PbO}_2$  being a semiconductor with  $E_g$  (energy gap) ca. 1.5 eV and  $\beta$ - $\text{PbO}_2$  being known to be nearly a

**FIGURE 6.3**

Representation of the crystal structures of several oxides structures using coordination polyhedra: (a): periclase ( $\text{MgO}$ ); (b) wurtzite ( $\text{ZnS}$ ,  $\text{ZnO}$ ); (c): spinel ( $\text{MgAl}_2\text{O}_4$ ,  $\text{Co}_3\text{O}_4$ ); (d) corundum ( $\alpha\text{-Al}_2\text{O}_3$ ); (e): quartz ( $\text{SiO}_2$ ); (f) rutile ( $\text{TiO}_2$ ); (g) fluorite ( $\text{CaF}_2$ ,  $\text{CeO}_2$ ) or antifluorite ( $\text{Na}_2\text{O}$ ); (h)  $\text{V}_2\text{O}_5$ ; (i)  $\text{ReO}_3$ .

metallic conductor due to overlap between the Pb-6s conduction band and the top of the O 2p valence band.<sup>14</sup> As said, the  $\alpha\text{-PbO}_2$  structure is more dense than the corresponding rutile structure. According to this, several rutile-type dioxides convert into  $\alpha\text{-PbO}_2$  structure phase at high pressures.

On the other hand, also  $\text{TiO}_2$  presents alternative structures having similar although less symmetric octahedral cation coordination at ambient pressure (anatase, brookite, Figure 6.4, and  $\text{TiO}_2$  (b)). Also  $\text{MnO}_2$  is a polymorphic material,



**FIGURE 6.4**

Chains of the edge-shared  $\text{MO}_6$  octahedra in rutile  $\text{TiO}_2$  (a),  $\alpha\text{-PbO}_2$  (b), brookite  $\text{TiO}_2$  (c), and anatase  $\text{TiO}_2$  (d) structures. Shared edges are marked by bold lines: visible edges are shown as solid lines, invisible edges as dashed lines.

Reprinted with permission from Filatov S, Bendeliani N, Albert B, Kopf J, Dyuzeva T, Lityagina L. *Solid State Sci* 2005;7:1363–68.

being several structures known. The stable form is  $\beta\text{-MnO}_2$ , pyrolusite, having the rutile structure. Other structures are  $\alpha\text{-MnO}_2$ , hollandite, tetragonal,  $\text{R-MnO}_2$ , ramsdellite, orthorhombic,  $\gamma\text{-MnO}_2$ , nsutite, hexagonal,  $\delta\text{-MnO}_2$ , vernadite, hexagonal, and  $\lambda\text{-MnO}_2$ , cubic. These different structures are all constituted by octahedral manganese and can be conveniently described by filled  $[\text{MnO}_6]$  octahedra sharing opposite octahedral edges to form endless chains, which can in turn be linked to neighboring octahedral chains by sharing corners or edges.<sup>15</sup>

The most typical structure of large tetravalent metal oxides is the cubic fluorite structure. In this case, the coordination at cation is eight, oxide ions being tetrahedrally coordinated by cations. This structure is taken by  $\text{CeO}_2$ ,  $\text{ThO}_2$ ,  $\text{HfO}_2$ ,  $\text{PrO}_2$ ,  $\text{TbO}_2$ , uraninite  $\text{UO}_2$  and  $\text{PuO}_2$ . Some rare-earth elements (Ce, Pr and Tb) also produce oxide-deficient structures (such as e.g.,  $\text{Ce}_7\text{O}_{11}$ ,  $\text{Ce}_{11}\text{O}_{20}$  and  $\text{Ce}_{19}\text{O}_{34}$  for ceria) that have the same fluorite structure, defective, or deformed versions of it. The fluorite structure is also taken by pure zirconia but only at high temperature ( $>2370^\circ\text{C}$ ). At lower temperature, in fact, the fluorite-type structure of zirconia deforms. The tetragonal structure, stable at intermediate temperatures ( $1170\text{--}2370^\circ\text{C}$ ) is tetragonally distorted fluorite, while in the case of monoclinic  $\text{ZrO}_2$ , baddeleyite, the coordination of Zr ions is lowered to seven, and, consequently, half oxygen ions become nearly planar trigonal. The high-temperature forms of zirconia may be stabilized at ambient temperature by doping with other cations such as Y, Mg and Ca cations.

Again, particular coordination states are taken by tetravalent cations retaining electron doublets in their higher occupied level. This is the case of  $\text{Te}^{4+}$  in telluric oxide, which forms three well-recognized modifications.<sup>16</sup> Paratellurite, tetragonal

$\alpha$ -TeO<sub>2</sub>, space group P4<sub>1</sub>2<sub>1</sub>2,  $Z = 4$ , has a three-dimensional fully connected structure. The structure of the crystal may be regarded as a distorted rutile structure with a doubling of the unit cell along the [001] direction where the positions of the tellurium atoms are slightly shifted from the regular rutile positions. Tellurium ion is fourfold coordinated by oxygen, the coordination polyhedron being a distorted trigonal bipyramid with a Te lone pair pointing toward one of the vertices. Each oxygen atom is bonded to two tellurium atoms with an angle of 140° between long and short bonds; other tellurium neighbors are at larger distances. Paratellurite,  $\alpha$ -TeO<sub>2</sub>, converts at high pressure into the orthorhombic  $\beta$ -TeO<sub>2</sub>, tellurite, space group Pbca,  $Z = 8$ , which has a layered structure with similar coordination for Te, but even more asymmetric.

The structure of  $\gamma$ -TeO<sub>2</sub>, which is metastable, can still be seen as formed by corner-sharing TeO<sub>4</sub> units with twofold-coordinated oxygen atoms and fourfold-coordinated Te atoms. However, being one Te–O bond definitely shorter, and one definitely larger than the others, would appear as a network of TeO<sub>3</sub> units with Te atoms threefold coordinated, two oxygen atoms twofold coordinated, and one non-bridging onefold-coordinated oxygen atom, i.e., with a Te=O double bond.

Concerning the other elements of group 16 in the tetravalent state, also SeO<sub>2</sub> gives rise to a polymeric structure in the solid state, with O–(Se=O)–O chains and pyramidal Se atom. SO<sub>2</sub>, instead, retains the monomolecular SO<sub>2</sub> structure also in the solid state.

When oxidation state increases to five and six, the covalence of the bond increases and nonnetwork structures can appear also for the oxides of typical metallic elements. The stable polymorph of vanadium pentoxide ( $\alpha$ -V<sub>2</sub>O<sub>5</sub>) consists in an orthorhombic layered structure (Figure 6.5). The coordination at vanadium is highly asymmetric, according to second order Jahn–Teller effect, and this allows you to consider it either a distorted tetrahedron, or a square pyramid or even an octahedron. In fact, vanadium atoms are bonded with a very short bond (1.576 Å) to a “terminal” or “axial” (vanadyl) oxygen standing up the 001 basal plane, as well as with a very long bond (2.793 Å) to the corresponding oxygen atom in the lower layer. The “on-plane” or “equatorial” V–O bonds have intermediate length (between 1.778 and 2.017 Å). Actually, three different oxygen positions exist: O(1), the “terminal one”, strongly bonded to one vanadium ion forming a “vanadyl” V=O species, and weakly interacting with the corresponding vanadium of the upper layer, O(2), bridging between two V atoms in an “equatorial” position; and O(3) coordinated to three vanadium centers again in an “equatorial” position. In effect, the interaction between layers is very weak, being associated to a large van der Waals component.<sup>17</sup>

The crystal chemistry of the other vanadia polymorphs and of the several polymorphs of niobia and tantalum have coordination complexes that may be taken as ranging from the very deformed ones of vanadia and the highly symmetric octahedra typical of the ReO<sub>3</sub> structure, a tridimensional network with all-corner sharing RbO<sub>6</sub> octahedra.

The crystal chemistry of niobia is indeed very complicated, at least 15 different structures being reported. It seems that the thermodynamically stable form of niobia

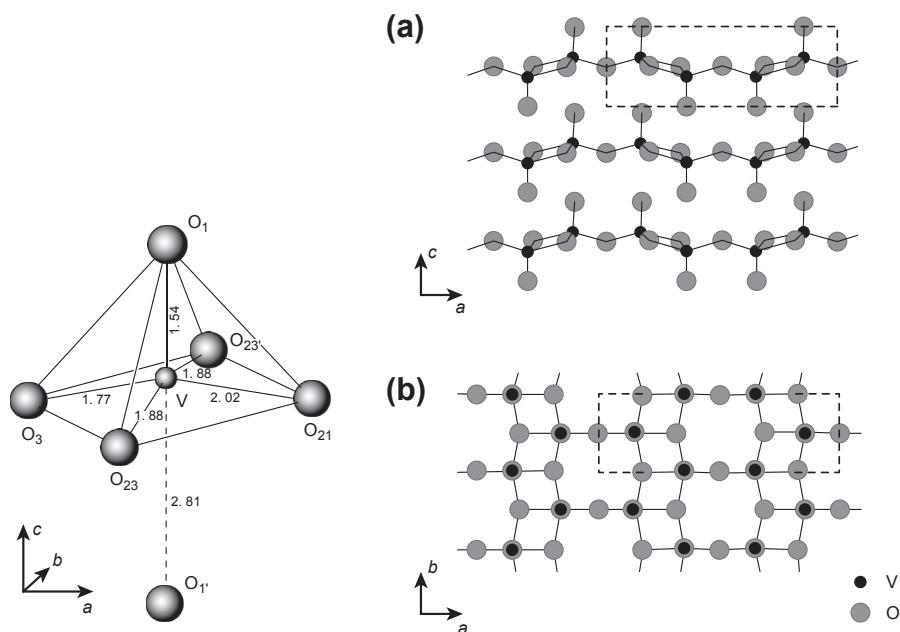
**FIGURE 6.5**

Illustration of the coordination sphere of vanadium in  $V_2O_5$  (left) and of the  $V_2O_5$  bulk structure (right): (a) Projection of the  $V_2O_5$  crystal structure on the  $b$ -plane. Small and large circles are V and O atoms, respectively; (b) projection of  $V_2O_5$  on the  $c$ -plane. The rectangles defined by the broken lines in (a) and (b) represent the unit cell for the  $V_2O_5$  crystal. The cleavages in  $c$ -plane and the holes in the  $c$ -direction are easily found.

*Reprinted with permission from Chiba H, Nishidate K, Baba M, Kumagai N, Sato T, Nishikawa K. Solid State Commun 1999;110:497–502.*

is the so-called H-phase, monoclinic, in whose unit cell, 27 Nb ions are octahedrally coordinated in  $ReO_3$ -type blocks, one only being in a tetrahedral coordination in a position joining such blocks. Most other niobia polymorphs have also structures related to that of  $ReO_3$ . The structures of the two main polymorphs of tantalum, the low-temperature form known as  $\beta$ - $Ta_2O_5$ , and the high-temperature form ( $>1360^\circ C$ ) known as  $\alpha$ - $Ta_2O_5$ , consist of chains built from octahedral  $TaO_6$  and pentagonal bipyramidal  $TaO_7$  polyhedra sharing opposite vertices. These chains are further joined by sharing edges to yield the tridimensional structure.

As for the oxides of group 15 in their pentavalent state, while the structure of  $Bi_2O_5$  has still not been determined,  $Sb_2O_5$  takes the same structure as the B- $Nb_2O_5$  polymorph, with all Sb atoms distorted octahedrally coordinated. In the two polymorphs of  $As_2O_5$ ,  $AsO_4$  tetrahedral and  $AsO_6$  octahedral units link together only by oxygen corners.  $P_4O_{10}$  retains its monomolecular structure also in the solid state.

Important differences exist between the structures of the trioxides of six groups. While the structure of  $\text{CrO}_3$  (chromic anhydride) is a linear polymer with  $\text{Cr}-\text{O}-\text{Cr}$  chains, and two additional terminal oxygens bonded with short bonds to chromium, producing a slightly distorted tetrahedron, molybdena has a (bi)layered structure with a distorted octahedral coordination at molybdenum approaching a square pyramid (the coordination is similar to that of V in  $\text{V}_2\text{O}_5$ ), and, finally, tungsta has several network structures (all distorted  $\text{ReO}_3$ -type) with  $\text{WO}_6$  octahedral coordination where, although distorted, the length of axial and equatorial  $\text{W}-\text{O}$  bonds is quite similar.

Other polymorphs of molybdena are also distorted versions of the  $\text{ReO}_3$  structure, except the hexagonal phase  $\text{h-MoO}_3$  which is actually an impure oxide.<sup>18</sup> As for the trioxides of the group 16,  $\text{SO}_3$  can form both polymeric solids (whose structure is similar to that of  $\text{CrO}_3$ ) or a molecular solid with the cyclic  $\text{S}_3\text{O}_9$  trimer, while  $\text{SeO}_3$  crystallizes as the cyclic tetramer  $\text{Se}_4\text{O}_{12}$ .

### 6.1.3 Covalent versus ionic oxides

In Table 6.2, details on the crystal structures of most metal oxides are reported. Among the most relevant features of such structures, the coordination states of both cations and anions. A typical characteristic of the oxides of most typically metallic elements is that coordination of the metal ion and of the oxide anion is much larger than their oxidation state. This is typical of the ionic bond where the ion tends to bond to the largest number of the opposite ions, allowed by the geometrical size of both ions. On the contrary, a characteristic of oxides of semimetal elements is that coordination state and oxidation state are the same. This is typical of covalent bond. For oxides of nonmetals the coordination state of ions may be even lower than oxidation state, showing that metal–oxygen “double bonds” may form on covalently bonded structures. In the case of covalently bonded oxides, nonnetwork structures, i.e., planar, linear polymeric and monomolecular structures, appear.

In practice, the structures of  $\text{B}_2\text{O}_3$ ,  $\text{As}_2\text{O}_3$ ,  $\text{Sb}_2\text{O}_3$ ,  $\text{SiO}_2$ ,  $\text{SeO}_2$ ,  $\text{TeO}_2$ ,  $\text{P}_2\text{O}_5$ ,  $\text{As}_2\text{O}_5$ ,  $\text{Sb}_2\text{O}_5$ ,  $\text{CrO}_3$ ,  $\text{WO}_3$ ,  $\text{ReO}_3$ ,  $\text{SO}_3$  and  $\text{SeO}_3$  have oxygen atoms in coordination 2, and, correspondingly, the element in the coordination corresponding to its cationic charge or valency. They are thus largely covalent. Structures like those of  $\text{V}_2\text{O}_5$ ,  $\text{Nb}_2\text{O}_5$ ,  $\text{Ta}_2\text{O}_5$ ,  $\text{MoO}_3$  have also most oxygens in coordination two, and are consequently also largely covalent. Thus, predominantly covalent oxides may be molecular ( $\text{P}_4\text{O}_{10}$ ), chain polymeric ( $\text{CrO}_3$ ,  $\text{B}_2\text{O}_3$ ), layered ( $\text{V}_2\text{O}_5$ ,  $\text{MoO}_3$ ) or typically network ( $\text{SiO}_2$ ,  $\text{WO}_3$ ).

In contrast, the oxides of low-valence metal cations present coordination of oxygen higher than 2, up to eight for antiferroite-type alkali oxides. This provides evidence of ionic bonds. Actually, ionicity can be empirically also evaluated by the Pauling’ electronegativity of the element and oxygen ( $\chi_{\text{M}}$  and  $\chi_{\text{O}}$  respectively) with the formula:

$$I = 1 - \exp\left(-(\chi_{\text{M}} - \chi_{\text{O}})^2/4\right) \quad (6.11)$$



as done by Chisallet et al.<sup>19</sup> Using this simple equation, coupled with bond-energy calculations, these authors underlined the ionicity trend is SrO ( $I = 0.79$ ) > CaO (0.77) > MgO (0.68) > TiO<sub>2</sub> > 0.59) > Al<sub>2</sub>O<sub>3</sub> (0.57) > SiO<sub>2</sub> (0.45). Although this approach becomes difficult for transition metal elements presenting several oxidation states, taking into account that boron, phosphorus, antimony and bismuth are all more electronegative than silicon, we can conclude that the structure of ionic oxides is evident in the structure when Pauling's ionicity is higher than  $\sim 0.5$ .

#### 6.1.4 Amorphous versus crystalline metal oxides

Some metal oxides present amorphous or vitreous states very resistant to crystallization. Among binary oxides, this situation is typical of covalent oxides and, in particular, of silica. Many other oxides, even those that are typically ionic, may be prepared in "amorphous" states. These states are however due to large amount of impurities (both from organic precursors or of inorganic nature) or for the presence of water or hydroxyl groups in the case of hydrous oxides (e.g., "niobic acid" or hydrous zirconia). In the latter case, calcination and drying at moderate temperatures give rise to crystallization.

#### 6.1.5 Redox behavior, thermal stability, magnetism and electronic conduction

To act as real heterogeneous catalysts, materials must be stable in reaction conditions, to be (at least formally) recovered as such. For acid and base catalysis, which frequently occurs in reducing conditions (moderate to high temperature in the presence of hydrocarbons or other organic molecules), this means that the catalyst must be essentially stable from the point of view of reduction and decomposition, as well as structurally and morphologically. Conversely, to be used as a redox catalyst, the ability of the material to perform reversible redox cycles during the reaction is normally useful (see Chapter 11).

The most relevant metal oxides from the points of view of practical applications in acid and basic catalysis contain elements with the  $s^0p^0$  electronic state (i.e., cations of base or nontransition metals), such as those based on alumina, silica and their combinations (as most acid catalysts) and those based on alkali-earth oxides and/or containing alkali cations (most basic oxides). According to electrochemistry, in fact, the elements of group 1,2 and some of group 13 (Al, Ga) are among the most stable in the oxidized state and, consequently, least stable in the metallic state in the presence of oxygen. This corresponds to a very negative enthalpy of formation,  $\Delta H_f^\circ < -400$  kJ/at<sub>O</sub>.

In parallel to this, the oxides of these elements are also typical insulators. In fact, in the case of the ionic oxides, the HOMO are the full  $s$ - and  $p$  orbitals of oxide anions, giving rise to the valence band, while the LUMO are the empty orbitals of the metals cations, giving rise to the conduction band. As for network, essentially

covalent oxides such as silica, the valence band can be assumed to be formed by the full, bonding  $\sigma$  element-oxygen orbitals while the conduction band is formed by the corresponding empty, antibonding  $\sigma^*$  element-oxygen orbitals. In both cases, the valence band is very high in energy, just in agreement to the lower tendency of the cations to be reduced. Thus, excitation of electrons from the valence to the conduction band must overcome a very high energy gap ( $E_g$ ) and can occur only by irradiation with high energy far-UV radiation or by heating at high temperatures. This also implies that they are white in color, visible light being not absorbed by these solids. These oxides are also typically diamagnetic, according to the absence of unpaired electrons in normal conditions.

Also for the elements of groups 3 and 4 (thus belonging to the transition metals series), the most stable or applied metal oxide is associated to  $d^0s^0p^0$  configuration. However, in this case, the availability of d orbitals makes these oxides semiconducting, because of the lower energy of the valence band. Thus  $E_g$  lowers to less than 4 eV, typical of Scandia, Lanthana, Titania, Zirconia and Hafnia. The optical gap, however, is still above the limit of the visible region, and no unpaired electrons are present. Thus, these materials are still white and diamagnetic.

On the other hand, some reducibility may appear and quite stable lower oxides may also exist. This is in particular the case of titanium, which presents a large number of suboxide structures. Some of them have “canonic” oxidation numbers and stoichiometries, such as  $Ti_2O_3$  and  $TiO$ . However, a number of other phases exist with complex stoichiometries corresponding to average oxidation numbers for Ti intermediate between +4 and +3. Most of these phases are denoted as “Magnéli phases”, i.e., phases that may be described as “recombination phases based on rebuilding after shear”, corresponding to sequences of chemical formulas  $Ti_nO_{2n-1}$ . In this case, the vertex sharing of  $TiO_6$  octahedra, occurring in the normal rutile structure, is partially substituted (as a result of shearing) by edge-sharing. Formally, parts of titanium ions are reduced to the trivalent state (with one electron in the higher energy level) and some oxygen atoms are lost. The  $Ti^{3+}$  unpaired electrons actually come easily to the conduction band, thus these suboxides have *n*-type semiconductive character or even metallic behavior, are black and paramagnetic. In fact,  $Ti_4O_7$ - and  $Ti_5O_9$ -based solids are commercially available as conducting ceramic materials.<sup>20</sup>

A more complex situation occurs for the elements of the groups 5–6. They present higher oxides still having  $d^0s^0p^0$  cation electron configuration, thus being semiconducting and diamagnetic. These “anhydrides” indeed have already quite a covalent bond and are characterized by red ( $V_2O_5$ ) or very pale colors, due to charge transfer transitions falling at the limit of the visible region. However, these elements have several lower oxides, including some “Magnéli phases”, with similar stability, where cations have electrons in the higher energy level, thus having magnetic behavior. As a result, these oxides undergo easy redox cycles. In fact, the differences in the thermodynamic enthalpies and free energies of formation between  $V_2O_5$  and  $MoO_3$ , and their suboxides are quite small,<sup>21</sup> smaller than those found for  $TiO_2$  and its suboxides.<sup>22</sup>

The light elements of group 7–10 (Mn, Fe, Co, Ni) but also the heavy elements of groups 13 and 14 have intermediate free energies and enthalpies of formation  $-350 < \Delta H_f^\circ < -150$  kJ/at<sub>O</sub>, thus being reducible until the metal in mild conditions. Also, they present several different oxide phases with different oxidation states. Thus, they are active in oxidation catalysis but unstable in the oxide state and thus usually not utilizable in acid-base catalysis. The partial occupancy of d orbitals is frequently associated to the presence of unpaired electrons, thus magnetic properties appear. At high temperature all materials are paramagnetic, but below the Curie and Néel temperature ferromagnetism (e.g. CrO<sub>2</sub>), ferrimagnetism ( $\gamma$ -Fe<sub>2</sub>O<sub>3</sub> and Fe<sub>3</sub>O<sub>4</sub>) and antiferromagnetism (e.g.  $\alpha$ -Fe<sub>2</sub>O<sub>3</sub> and NiO) appear. Most of these oxides are semiconductors but metal-like conductivity occurs e.g. for magnetite Fe<sub>3</sub>O<sub>4</sub>.

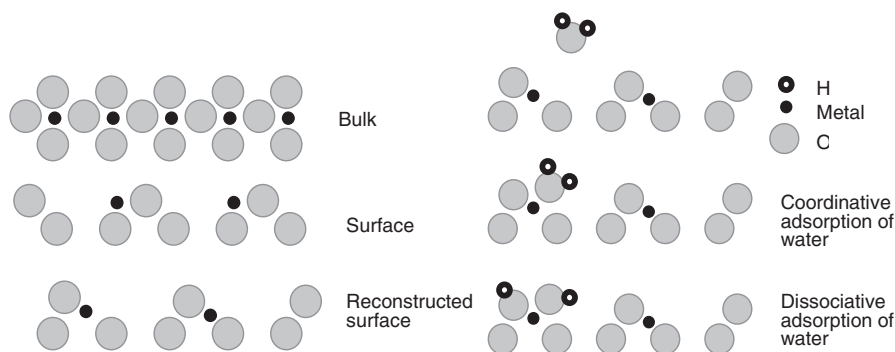
For the heavier elements of groups 8–10 (i.e., the so-called “platinum group metals”, i.e., Ru, Rh, Pd, Os, Ir and Pt), as well as for those of group 11 (Cu, Ag, Au), to which Re and Hg could be added, the stability of the oxides is very low, the free energies and enthalpies of formation being small in absolute value,  $\Delta H_f^\circ > -150$  kJ/at<sub>O</sub>. These are more or less corresponding to the so-called “noble metals” (perhaps with the exception of copper) that may be found in the metallic state also in moderately oxidizing conditions. They are components of metallic catalysts, as it will be shown later on (Chapters 9 and 11).

It is quite obvious that even reducible oxides have acido-basicity. However, they cannot be used as acidobasic catalysts because of their instability in reaction conditions.

### 6.1.6 Effect of particle size in the solid-state chemistry of oxides

In the era of nanotechnology, the effect of crystal or particle size on the solid-state chemistry of materials, including oxides, has been discovered. In practice, for nanopowders the effect of surface free energy may be even more relevant than that of bulk free energy. For this reason, structures that are less stable, with respect to alternative structures, when in large crystal size (where the bulk free energy predominates), may become more stable for nanoparticles if their surface free energy is definitely lower. This has been first reported for  $\gamma$ -Al<sub>2</sub>O<sub>3</sub> with respect to corundum  $\alpha$ -Al<sub>2</sub>O<sub>3</sub>,<sup>23</sup> and has been reported for other polymorphic systems such as anatase TiO<sub>2</sub><sup>24</sup> with respect to the stable phase rutile, as well as for tetragonal ZrO<sub>2</sub> with respect to monoclinic zirconia.<sup>25</sup> Thus, this is a likely reason for the easy formation and stability at room temperature of  $\gamma$ -Al<sub>2</sub>O<sub>3</sub>, anatase TiO<sub>2</sub> and tetragonal ZrO<sub>2</sub> in the form of nanoparticles, in spite of being their bulk metastable in these conditions.

The surface free energy should also have an effect on redox properties of metal oxides, in particular on the different stabilities of two different oxides of the same elements. According to Navrotsky et al. spinels M<sub>3</sub>O<sub>4</sub> (M = Mn, Fe, Co) have lower surface energies than rock-salt monoxides and the corresponding sesquioxides, thus enlarging their stability field for nanoparticles.<sup>26</sup>

**FIGURE 6.6**

Schematics of reconstruction and hydration of the surface of an ionic oxide.

## 6.2 Composition effect on the surface acido-basicity of metal oxides: an overview

The surface of crystalline solids, supposed to be perfectly clean, must be constituted by planes produced by cutting their bulk crystal structures, as well as by corners and edges formed by the intersection of the exposed planes. Surface reconstruction will certainly occur to reduce the surface free energy.

As discussed in [Section 6.1.3](#), most metal oxides are definitely ionic. By cutting the crystal, ionic “coordination” metal-oxygen bonds are broken, thus leaving coordinatively unsaturated cations and oxide anions ([Figure 6.6](#)). Coordinatively unsaturated cations are Lewis acidic, coordinatively unsaturated oxide anions are basic. Surface reconstruction will reduce the exposition of some ions to reduce surface free energy, but coordination of surface ions will remain lower with respect to that of the bulk. When exposed at the atmosphere, the surface can adsorb molecules to reduce its surface free energy. Thus, dissociative adsorption of water on cation-oxide anion couples will produce surface hydroxyl groups, which can act either as Brønsted acids or as bases, depending on the strength of the metal oxygen bond. Desorption of water will occur at high temperatures and in dry atmosphere, thus regenerating Lewis acid and basic sites. Thus, surface Lewis acidity and basicity will strongly depend, at least in some cases, from “activation” procedures.

As for network covalent oxides, such as silica, the surface must be formed by breaking extremely strong covalent bonds. Thus, the surface of such solids should have, as such, extremely high free energy. The reaction with the ambient water vapor will be, consequently, essentially irreversible. The surface will be, then, constituted by surface hydroxyl groups saturating silicon atoms. At the surface of silica, in fact, silanol groups are the only active sites really present in normal conditions, Lewis

acidity being fully absent while the basicity of covalently bonded oxygen atoms being negligible.

Thus, the surface of solid oxides can be constituted by surface coordinatively unsaturated cations (only on ionic surfaces) acting as Lewis acid sites, and by surface oxide and hydroxy species. Depending on the ionicity of the structure, oxide species can have from zero to very high basicity, while hydroxide species may be either acidic or basic.

Basic sites at the surface of ionic oxides (well exposed oxide or hydroxide anions) can work as Brønsted basic sites by abstracting a proton from a Brønsted acidic molecule. However, if this reaction occurs at the solid/vapor interface, it generates an anion that should be adsorbed too. In some way, consequently, Brønsted basicity needs the presence of Lewis acid sites to adsorb the conjugated base of the adsorbed acid molecule. Similarly, when the basic center adsorbs a Lewis acid (thus acting as a Lewis basic site), near-Lewis acid sites may be useful to stabilize the resulting anionic species (e.g., carbonates from  $\text{CO}_2$ ). Thus acid-base couples may exist and can be needed to adsorb molecules and catalyze reactions.

Dominant factors in governing the acidobasicity of metal oxides are the charge ( $C$ ) and the size (i.e., the ionic radius,  $r$ ) of the cations, which may be combined in what can be called “polarizing power”, calculated either as  $C/r$  or as  $C/r^2$ . The larger the cation and the lower its charge, the less Lewis acidic is and, in parallel, the stronger is the basicity of oxide anions. This is true for the bulk but is also reflected at the surface. This is also true for surfaces of complex oxides, where e.g., an oxide is deposited over another material working as a carrier (such as another oxide, active carbon or a polymer) or a mixed oxide phase.

In Table 6.3 the conclusions arising from our studies<sup>27</sup> are compared with data arising from other techniques such as O1s XPS X Ray Photoelectron Spectra binding energy (using the data collected by Dimitrov and Komatsu<sup>28</sup>), optical basicity values (from Leboutellier and Courtine<sup>29</sup>), data on the ionicity of the metal-oxygen bond and  $\text{CO}_2$  thermal desorption studies. Although the agreement is not perfect, the trends are quite parallel.

Studies on several oxides, such as those concerning  $\text{MgO}$ ,<sup>30</sup> demonstrated significant effect of particle morphology on the surface chemistry. It is well evident that the population of the most exposed, less coordinated sites, depending in some way from surface roughness as well as by the crystal shape, occurring at surface corners, edges and kinks, is a key factor governing the number of surface Lewis acid and basic sites on ionic solids, i.e., the density of sites per exposed surface area. On the other hand, particle size and porosity affect the extent of surface area per weight of the solids. Morphology, in terms of surface area, particle size and shape, porosity, is mostly an effect of preparation and pretreatment procedures.

Another factor greatly affecting the surface properties is the presence of impurities. The voluntary doping or the unwanted contamination of oxides with alkali ions (sometimes arising from the precipitation step in the preparation procedure, or residual of the precursor salts) produce neutralization of acid sites on solid acids and/or the formation of basic sites. Conversely, the contamination with acidic

**Table 6.3** Summary of the Acid-Base Properties of Binary Metal Oxides

Element	Oxidation State	Cation Size (Radius, Å)	Polarizing Power Range		M–O Bond Nature	% Ionicity Ref.	Acidity Type	Acidity Strength	Basicity, Nucleophilicity	Examples	XPS O1s BE (eV)	Optical Basicity $\Delta$	$T_{\text{des CO}_2}$ (Carbonates)
			C/r	C/r <sup>2</sup>									
Semi-metal	$\geq +5$	Very small $\leq 0.2$	$>25$	$>60$	Covalent molecular	$<30$	Brønsted	Medium-strong	None	P <sub>2</sub> O <sub>5</sub> (SO <sub>3</sub> )	$>533$	0.33	No adsorption
	+3, +4	Small $\leq 0.4$	$>10$	25–60	Covalent network			Medium-weak		SiO <sub>2</sub> , GeO <sub>2</sub> (B <sub>2</sub> O <sub>3</sub> )	531–533	0.48–0.54	
Metal	High +5 to +7	Small to medium 0.3–0.7	$>8$	12–35	Largely covalent network → layered → polymeric		Brønsted Lewis	Medium to strong		WO <sub>3</sub> , MoO <sub>3</sub> , CrO <sub>3</sub> , Ta <sub>2</sub> O <sub>5</sub> , Nb <sub>2</sub> O <sub>5</sub> , V <sub>2</sub> O <sub>5</sub>	529–531	0.50–0.64	
		Small 0.35–0.5	6–8	12–20	Ionic network	$>30$	Lewis	Strong	Weak	$\gamma$ -Al <sub>2</sub> O <sub>3</sub> , $\beta$ -Ga <sub>2</sub> O <sub>3</sub>		0.65–0.77	$<100^\circ\text{C}$
	Medium +3 to +4	Medium 0.5–0.6	5–6	7–12				Medium	Medium-weak	TiO <sub>2</sub> , Fe <sub>2</sub> O <sub>3</sub> , Cr <sub>2</sub> O <sub>3</sub>			100–200 °C
		Large 0.7–1.2	3.5–5	2–7				Medium-weak	Medium-strong	La <sub>2</sub> O <sub>3</sub> , SnO <sub>2</sub> , ZrO <sub>2</sub> , CeO <sub>2</sub> , ThO <sub>2</sub>			200–400 °C
	Low +1 to +2	Large 0.7–1.0	2–3.5					Medium to	Strong	MgO, CoO, NiO, CuO, ZnO, (Cu <sub>2</sub> O)	527–530	0.78–12	400–500 °C
Very large $>1.0$		$<2$	$<2$				Very weak	Very strong	CaO, SrO, BaO, Na <sub>2</sub> O, K <sub>2</sub> O, Cs <sub>2</sub> O		$>1$	$>500^\circ\text{C}$	

components decreases surface basicity and/or produces additional acidic sites on basic surfaces. Again these contaminants, such as e.g., chloride ions and sulfate species, may be residuals from the starting materials.

A further very determinant factor in the generation of surface basicity is the activation procedure. Extremely strong basic sites may only be generated by desorbing any adsorbed water and carbon dioxide by high-temperature treatment under vacuum or very inert atmosphere.

---

### 6.3 Acido-basicity of supports for catalysts

A number of metal oxides are largely used as support of metal, sulfide or oxide catalysts. In the most common procedures, supporting catalysts are produced by dispersion, such as using impregnation techniques, of a precursor salt over the support surface. After, calcination is performed to destroy the counter-ion of the salt (frequently a nitrate, or an organic anion for low-valence metal cations, ammonium ions for polyoxoanions containing high-valence metals). This results in an oxide supported on the carrier in most cases. To produce a supported metal, a reduction step is generally needed, e.g., with hydrogen or syngas. However, if the metal involved is noble, calcination can directly produce it in the metallic state. For supported metal sulfides, sulfidation is performed e.g., in  $H_2/H_2S$  flows usually producing sulfides with lower-valence ions (e.g., supported NiS-MoS<sub>2</sub> by sulfiding supported NiO—MoO<sub>3</sub>). In any case, both for metal and sulfide catalysts, the nature of the oxide precursor is relevant to determine the properties of the final catalyst.

The deposition steps of the active ions in the impregnation procedures, as well as the chemistry during the calcination step are largely governed by acid-base interactions, where the acid-base nature of both the support surface and the supported species (salt or oxide) are very relevant.

Studies suggest that metallic species such as both reduced metal cations and high-valence metal polyoxoanions have a significant acidic nature. They consequently tend to interact with the basic sites of the support surface. It is quite reasonable to suppose that both most acidic and basic sites are located on the corners, edges and other defects of the microcrystal surfaces. This is quite well established for MgO, but is still not being considered well for other oxides. It is quite reasonable, and also supported by experiments, to suppose that the supported cation/anion couples go first to titrate surface anion—cation couples, which are on the edges, corners and other defects of the crystal surface. Thus, the additional ions will go to deposit on weaker sites that are those located on the main faces. On the other hand, if more cations or anions are deposited together, they will compete to interact with the stronger support sites. The stronger acid cation will tend to displace the weaker ones from the stronger basic sites of the support. Thus, the addition of a more acidic cation will change the position, and the properties, of the supported weaker acidic cation.

This is the reason why ionic oxide carriers such as alumina, titania and zirconia are highly dispersing, allowing metal cations to disperse on the most active sites

before, and in the less active later. Amorphous silica is a much less-dispersing support, because its only highly reactive center is the silanol group. Silanol groups are certainly anchoring sites in supporting ions,<sup>31</sup> but they are relatively few (depending on the silica type) and quite “isolated”. The large majority of the silica surface is inert because covalent, nonionic, neutral, being surface Si—O—Si bridges quite inert at moderate temperature.

Experiments support the idea that similar considerations are valid at the solid solid interface, allowing spreading of low melting oxides on ionic supports in the solid state.<sup>32</sup> Similar considerations are used to explain reactivities of ceramic oxides and glasses at high temperature. This is also valid during the calcination step of the supported salt, where cationic species will tend to react with support anions and vice versa.

By using deposition/calcination techniques, quite stable surface oxide-supported on oxide materials can be prepared. If, however, the acido-base natures of the support and of the supported species are too different, a bulk chemical reactivity would occur producing a bulk mixed oxide. This occurs when a very basic support such as magnesia is heated in contact of an acidic oxide such as silica, vanadia and tungsta, and thus producing bulk magnesium silicate, vanadate and tungstate more than supported oxides. Another effect to be considered is the size of cations. As for example the reactivity of alumina with supported bivalent oxides strongly depends on the size of the bivalent cation. Small bivalent cations such as  $\text{Mg}^{2+}$ ,  $\text{Ni}^{2+}$ ,  $\text{Co}^{2+}$  and  $\text{Cu}^{2+}$  are able to enter the alumina structure producing subsurface or bulk spinel aluminates. Bigger cations such as  $\text{K}^+$ ,  $\text{Ca}^{2+}$ ,  $\text{Ba}^{2+}$ ,  $\text{La}^{3+}$  cannot enter the alumina structure thus being stabilized at the surface and also acting as stabilizers for the alumina morphology.

---

## 6.4 Metal oxides as acid and basic catalytic materials

### 6.4.1 Supported alkali oxides

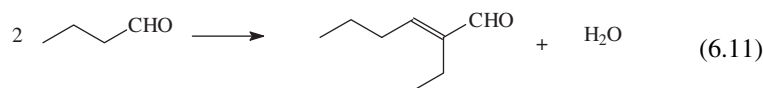
The basic reactivity of oxides of alkali metals is so high that they are essentially unstable in usual conditions. In fact, the presence of water vapor is sufficient to convert them into the corresponding hydroxides, and ambient air  $\text{CO}_2$  converts them into (bi)carbonates. Thus, bulk alkali metal oxides cannot normally be used as basic materials. However, alkali metal oxides can be supported or deposited over carriers, such as high surface-area oxides (silica, alumina, titania, zirconia, magnesia and zeolites) or activated carbons, by impregnation/calcinations or vapor deposition procedures. They are also frequently introduced as dopants at the surface of transition metal oxides and also of metal catalysts, to reduce acidity, to introduce basicity or to modify the activity of other supported species. Potassium is frequently preferred to sodium possibly because of its definitely larger ionic size that limits reactions with supports and the formation of bulk salts. The basicity also tends to increase with cationic size, thus Cs cation giving rise to extremely high basicity.



Alkali metal ions supported or deposited over carriers find much industrial interest as basic catalysts<sup>33–35</sup> and are the object of much academic investigation.<sup>27</sup> As for example, potassium salts deposited on alumina give rise to very active basic catalysts, such as for the industrial synthesis of methyl and ethyl mercaptans from alcohols and H<sub>2</sub>S<sup>36</sup> and for the isomerization of allene to propyne.<sup>37</sup> In the academic research, K/Al<sub>2</sub>O<sub>3</sub> were successfully tested for the aldol condensation,<sup>38</sup> Knoevenagel condensation,<sup>39</sup> the dimerization of ethanol,<sup>40</sup> the cyanoethylation of methanol<sup>41</sup> and for the bioDiesel synthesis by transesterification of vegetable oils,<sup>42</sup> although in this case the reactivity has been associated to potassium leaching.<sup>43</sup> The amount of *K* in these catalysts may typically be of the order of 10% wt or even more; the counterions deposited with potassium also have a significant effect on the catalytic behavior of K/Al<sub>2</sub>O<sub>3</sub> solids.<sup>44</sup>

Indeed, supported alkali oxides are among the most used solid catalysts in basic catalysis. Early examples<sup>45</sup> are the Degussa process for the production of acrolein through condensation of acetaldehyde and formaldehyde, carried out at 300–320 °C over a Na silicate/silica catalyst, and the conversion of (bio)ethanol to 1,3-butadiene (which is a sequence of dehydrogenation, aldol condensation, hydrogenation and dehydration) carried out over silica–magnesia catalysts at 370–390 °C.

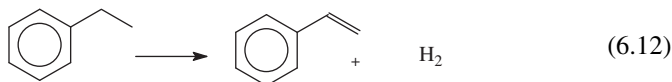
Na-SiO<sub>2</sub> is used for aldol-type condensations. According to Kelly et al.,<sup>46,47</sup> 98% selectivity to 2-ethylhexenal can be obtained by condensation of n-butanal over Na/SiO<sub>2</sub> at 400 °C, as a step in the synthesis of 2-ethylhexanol, an important intermediate in the synthesis of lubricants and plasticizers;



4% Na/SiO<sub>2</sub> catalysts prepared by impregnation with nitrate, allow >>90% selectivity at 40–60% conversion in the production of the unsaturated aldehyde 2-ethyl-hexenal by self-condensation of n-butanal at 350–400 °C in the presence of hydrogen. By adding 0.1% wt Pd to the catalyst, the saturated aldehyde 2-ethyl-hexanal is obtained with 85–95% selectivity without any hydrogenation of the reactant. 2-ethyl-hexanal is selectively converted into 2-ethyl-hexanol by hydrogenation over Cu–ZnO–Al<sub>2</sub>O<sub>3</sub> catalyst at 130 °C. 4% Na/SiO<sub>2</sub> and 4% Cs/SiO<sub>2</sub> catalysts allow the conversion of 2-butanone (Methyl–Ethyl ketone, MEK) into its various crotonic condensation products at 325–400 °C and, after hydrogenation, the production of 5-methyl-heptan-3-ol with 80% selectivity. Cs/SiO<sub>2</sub> catalysts for aldol condensation are reported to be promoted by bismuth.<sup>47</sup> Supported Cs catalysts are used industrially for the production of methylmethacrylate by condensation of methylpropionate and formaldehyde.<sup>33</sup> Other examples are the ketonization of carboxylic acids to produce symmetric ketones, carried out industrially at  $T > 350$  °C over alkali-doped titania and zirconia,<sup>48</sup> the dehydration of ethanolamine to ethyleneimine obtained carried out over Cs-phosphate on silica,<sup>33</sup> the dehydration of 1-cyclohexylethanol to vinylcyclohexene performed over Na/ZrO<sub>2</sub>,<sup>49</sup> the methylation of 2-pyrrolidone with methanol to *N*-methyl-pyrrolidone on Cs/SiO<sub>2</sub> or

Na/Al<sub>2</sub>O<sub>3</sub> catalysts.<sup>48</sup> An interesting point is that alkali can be lost as volatile species if the reaction temperature is too high, leading to catalyst deactivation.<sup>33</sup>

On the other hand, many industrial catalysts are doped, sometimes heavily, by alkali to reduce acidity or to produce basic functions. Among these, we can cite the iron oxide-based catalysts applied to ethylbenzene dehydrogenation to styrene that may contain up to 13% of K<sub>2</sub>O by weight with additional small amounts of MgO and CaO.<sup>50,51</sup>



The active phases for this reaction are potassium ferrite species.

K/Al<sub>2</sub>O<sub>3</sub> solids are also adsorbents to remove CO<sub>2</sub><sup>52</sup> and NO<sub>x</sub><sup>53</sup>; notably, Pt-K/Al<sub>2</sub>O<sub>3</sub> sorbents-catalysts are also used for NO<sub>x</sub> removal under lean conditions, according to the “NO<sub>x</sub> storage-reduction” (NSR) concept developed by Toyota in the early 1990s.<sup>54</sup> While K/Al<sub>2</sub>O<sub>3</sub> is the real adsorbent for NO<sub>x</sub>, Pt particles catalyze the NO to NO<sub>2</sub> conversion favoring the adsorption of NO<sub>x</sub> in the form of nitrites/nitrates, and also catalyze the final nitrite/nitrate reduction to N<sub>2</sub> during the reduction step. A following evolution of this technology is the newer DPNR (Diesel Particulate-NO<sub>x</sub> Reduction) process, also developed by Toyota<sup>55,56</sup> for diesel applications. It allows the simultaneous abatement of both particulate and NO<sub>x</sub> due to the development of a new catalytic filter and a new diesel combustion technology. In this respect, the peculiar reactivity of alkaline ions (and particularly of K ions) in the soot oxidation has also been pointed out.<sup>57</sup>

The presence of potassium on metal oxide surfaces, such as alumina and titania, gives rise to the formation of basic sites that are involved in stronger adsorption of CO<sub>2</sub> in the form of carbonates, but also of new evident hydroxyl groups characterized by an OH-stretching band at 3712 cm<sup>-1</sup>, that to appear to be not able to produce hydrogen bonding through their hydrogen atom. On the other hand, K<sup>+</sup> ions display weak but evident Lewis acidity, revealed by the formation of well-characterized surface complexes with weak bases such as CO<sup>58</sup> and stronger bases such as pyridine.<sup>59</sup> On the other hand, two different levels of potassium doping are found, the lower level allowing to poison the alumina’s acidity, only the higher level allowing to form surface basic sites.

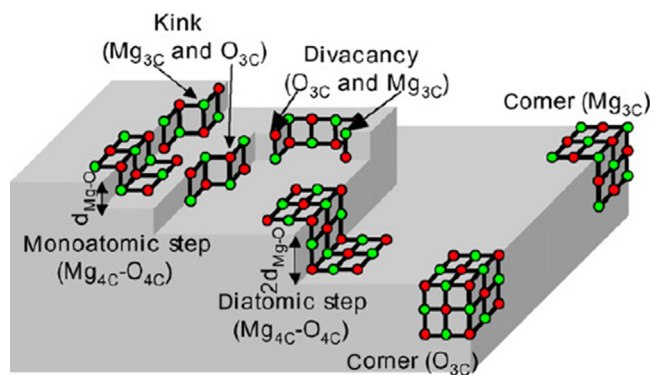
### 6.4.2 Magnesia and other alkali-earth oxides

Alkaline-earth oxides, except BeO, are among the strongest solid bases that may be stable as such in practical conditions. While BeO crystallizes into the wurtzite structure, with tetrahedral coordination for both Be<sup>2+</sup> and O<sup>2-</sup>, all other alkali-earth oxides crystallize in the rock salt-type “periclase” structure, with octahedral coordination of both cations and anions.

The basicity of alkaline-earth oxides increases with the cation atomic number: in fact increasing size and decreasing polarizing power of the cation results in an increased rock-salt-type unit cell size as well as in decreasing Madelung potential,

thus destabilizing the oxide anions. This is reflected, e.g., on the increased temperature for carbon dioxide desorption, taken as a measure of surface basicity. On BaO full desorption of carbonates is only obtained at 900 °C. Actually, like for alkali oxides, also alkaline-earth oxides are so reactive that, when prepared as fine powders, they are generally largely converted into hydroxides and carbonates, or covered by carbonates upon exposure to ambient air.

UV-absorption and luminescence spectroscopies have been largely utilized to investigate the basicity of alkali-earth oxides. In fact, typical surface  $O^{2-} \rightarrow M^{2+}$  ( $M = \text{Mg}, \text{Ca}, \text{Sr}, \text{Ba}$ ) charge transfer (CT) transitions are observed in the near-UV range, i.e., at much lower energy than the corresponding bulk CT transitions that correspond to valence band  $\rightarrow$  conduction band transitions. They are due to low coordination oxide and  $M^{2+}$  ions differently exposed at the surface. These spectroscopic features allow to provide evidence of the role of surface defect sites in determining the surface properties of metal oxides. Coordinatively unsaturated atoms, denoted as  $O_{5C}$  (coordination five, on faces),  $O_{4C}$  (on edges), and  $O_{3C}$  (on corners) were found to exist at the surface of cubic alkaline-earth oxides where full coordination of bulk oxide ions is six (Figure 6.7). For MgO, several surface CT transitions were found in the range 3–7 eV, i.e., well at lower energy with respect to the bulk absorption found near 7.8 eV. However, their position is also somehow dependent on particle size.<sup>60</sup> Photoluminescence spectra of vacuum-treated MgO show an intense peak, due to emission from surface sites, at 3.18 eV, with further components at even lower energy. In terms of energy, the position of the corresponding peaks decreases following the trend  $\text{MgO} > \text{CaO} > \text{SrO} > \text{BaO}$ . Density Functional Theory (DFT) cluster calculations allowed recently a more detailed assignment of these transitions.<sup>61</sup> This work has also been based on the preparation of different MgO powders, having very different



**FIGURE 6.7**

Schematic representation of irregularities on the MgO surface.

Reprinted with permission from Higashimoto S, Costentin G, Morin B, Che M. An EPR study of physico- and chemisorption of NO on MgO: effect of outgassing temperature and nature of surface sites. *Appl Catal B Environ* October 25, 2008;84(1–2):58–64.

morphologies. In fact, magnesium oxide is usually either produced by calcination of natural magnesite ( $\text{MgCO}_3$ ) or produced, also in fine powder form, from calcination of  $\text{Mg}(\text{OH})_2$  obtained by precipitation of  $\text{MgCl}_2$  solutions derived from seawater or brines. Lime or dolomite may be used as precipitating agents. Magnesium hydroxide can be prepared by alternative methods, such as precipitation from nitrate solution, rehydration of  $\text{MgO}$ , sol–gel hydrolysis of Mg alkoxides.  $\text{MgO}$  powders can also be prepared by oxidation of Mg metal in different ways. These different preparation procedures give rise to very different particle morphologies.<sup>30,33</sup> In particular,  $\text{MgO}$  smoke produced by burning Mg has low surface-area nonporous particles with cubic habit and (100) terminations, while much smaller but still cubic particles can be obtained by decomposing  $\text{Mg}(\text{OH})_2$  produced by  $\text{MgO}$  rehydration as well as by Chemical Vapor Deposition, CVD, of  $\text{MgO}$  from Mg vapor. When produced by thermal decomposition of the hydroxycarbonate, the crystal habit is different but apparently still (100) terminations predominate. Instead,  $\text{MgO}$  arising from precipitated  $\text{Mg}(\text{OH})_2$  (brucite) tends to retain the lamellar structure of the hydroxide and may expose (111) terminations. By producing  $\text{Mg}(\text{OH})_2$  as an aerogel, the surface area of the resulting  $\text{MgO}$  may be as high as  $250 \text{ m}^2/\text{g}$ .<sup>62</sup>

According to Bailly et al.,<sup>30</sup> surface hydroxy groups more than surface oxide anions may act as basic sites, e.g., in the conversion of MBOH, the test reaction used. These hydroxyl groups, whose complexity is made evident by the broad tail in the OH-stretching band centered near  $3750 \text{ cm}^{-1}$ , as well as by the complex  $^1\text{H}$  MAS NMR signals on hydrated powders,<sup>63</sup> are supposed to be mainly located on surface defects sites of  $\text{MgO}$ .<sup>19</sup> According to Vidruk et al.,<sup>62</sup> chemical (multiple aerogel condensation) and physical (pressing) densification methods give rise to the formation of distorted zones at the grain boundaries areas of  $\text{MgO}$  particles with resulting strong increase of the density of basic sites.

When free from impurities,  $\text{MgO}$  and  $\text{CaO}$  are considered to be even superbasic, following titration measurements in contact with water solution. When fully cleaned by treating in vacuum at very high temperatures, highly exposed cations and anions are freed. This induces very complex chemistry, like that producing  $(\text{CO}_2)^{2-}$  “carbonite” species and  $(\text{C}_3\text{O}_4)^{2-}$  trimeric species from carbon monoxide,<sup>64</sup> as well as are able to abstract protons from hydrocarbons, which results in the formation of paramagnetic superoxide ions occurring via an SIET mechanism (surface intermolecular electron transfer), as detected by ESR spectroscopy.<sup>65</sup>

#### 6.4.2.1 Alkali-earth oxides as catalysts

Magnesium oxide is reported to find several applications as basic catalysts.<sup>66,67</sup> Among the more relevant we can cite the gas-phase process for the synthesis of 2,6-xyleneol (the monomer of polyphenylene oxide) by methylation of phenol with methanol at  $400\text{--}450^\circ\text{C}$  in the presence of  $\text{MgO}$  in the General Electric process. The industrial catalyst is modified e.g., by iron ions to improve the acid-base properties.<sup>68</sup> Another process also catalyzed by  $\text{MgO}$  allows the production of aniline by reaction of ammonia with phenol.<sup>49</sup>

The gasification of biomasses is one of the possible options for producing renewable gaseous and liquid fuels (biooils),<sup>69</sup> as well as synthesis gases. Biomass gasification is mostly catalyzed by basic solids. Natural basic clays are mostly used. Among them is dolomite, which during the process may convert into Mg, Ca mixed oxides, and olivine (Mg silicate). Depending on the reaction temperature (400–800 °C) more gases or oils are produced.

One of the main technical barriers in biomass gasification development is the presence of organic impurities, denoted as tars, in the obtained fuel gas. Tars, which are mixtures of monocyclic and polycyclic aromatic compounds, can be destroyed by using both acidic catalysts of the Fluid Catalytic Cracking type, or with very basic materials based on alkali-earth oxides mostly derived by limestone, dolomite and other rock calcinations, or also with Ni-containing steam-reforming catalysts.<sup>70</sup> The reaction is performed at ca 850 °C.

Alumina-supported barium oxide finds an interesting application in the already cited NSR and DPNR technologies developed by Toyota for the purification of the waste gases of lean-burn engines. Catalytic materials for both NSR<sup>54</sup> and DPNR<sup>55,56</sup> consist in porous ceramic filters coated with a catalytic layer constituted by a high surface-area support (typically  $\gamma$ -alumina), a noble metal (usually Pt) and Ba or K oxide, which presents a high NO<sub>x</sub>-storage capacity. These catalytic systems work under cyclic conditions, alternating long lean phases (during which NO<sub>x</sub> are adsorbed on the catalyst in the form of nitrate/nitrites) with short phases in rich condition (during which the nitrate–nitrite species are reduced to molecular nitrogen). However, adsorption implies the conversion of NO into NO<sub>2</sub> catalyzed by Pt, which also catalyze the reaction to N<sub>2</sub> in the rich step.

Although bulk Ba carbonate is detected in the fresh catalyst, surface Ba sulfate species form in the presence of SO<sub>2</sub> and must be decomposed at higher temperatures (>500 °C) to avoid “poisoning” of the basic adsorbant. Thus, surface basicity of the solid should be tuned to allow sufficiently strong adsorption of nitrogen oxides in the lean phase, but also easy desorption of sulfur oxides in the rich phase to limit deactivation phenomena.

A very important potential application of alkali-earth oxides is as solid catalysts for triglycerides transesterification producing biodiesel,<sup>42</sup> i.e., fatty acids methyl esters or ethyl esters. Materials based on MgO, CaO and SrO have been deeply investigated. Calcium oxide presents high activity for this reaction, but leaching may occur. SrO has also been investigated, seeming to give less leaching problems.

Another potentially interesting field for basic catalysts, deeply investigated in the past, is the oxidative coupling of methane



The catalytic activity of MgO was found to be enhanced by Ca and Na impurities, which also enhance its basicity.<sup>71</sup>

One of the limits of alkali-earth oxides as basic catalysts is usually their low surface area. Frey et al.<sup>72</sup> prepared stable nanoparticles of alkali-earth oxides supported on surface-oxidized carbon nanofibers, and confirmed the highest basicity and catalytic activity of BaO in acetone aldol condensation, over 1000 times more active (in terms of reaction rate) with respect the bulk oxides.

Another way to provide stability for alkali-earth oxides is to mix them with more stable components. This is essentially what occurs using hydrotalcite, a layered double hydroxide of magnesium and aluminum available commercially. The calcination of this compound gives rise to three MgO–Al<sub>2</sub>O<sub>3</sub> mixed oxides, which retain strong basicity from MgO with stability and high surface area favored by alumina. This material, which is already largely used industrially and also as a solid catalyst, will be considered later on.

#### 6.4.2.2 Alkali-earth oxides as supports for catalysts

The size of Mg<sup>2+</sup> is sufficiently small to enter close packing of oxygen ions, ccp and hcp. For this reason, Mg ions can participate to the formation e.g., of mixed oxides such as spinels and ilmenites, whose oxygen packings are ccp and hcp, respectively. In relation with this, the deposition of Mg ions at the surface of normal carriers such as alumina may give rise to poor stability due to the easy reaction producing Mg aluminate, arising from the penetration of Mg ions into the ccp oxygen packing of alumina.

On the contrary, the size of the higher alkali-earth cations is large enough to not allow the penetration into close packing of oxygen ions. According to this, Ca, Sr and Ba ions are involved in the formation of mixed oxides with less compact packing for oxide anions, such as perovskites and beta-aluminas. Additionally, Sr and Ba ions may be supported on typical oxide carriers such as alumina and titania, forming quite stable basic materials, because they cannot penetrate these structures. These alkali metal cations remain exposed at the surface where their weak Lewis acidity (corresponding to strong basicity of the oxide anions) is well detectable by conventional probes, such as e.g., pyridine on SrO–TiO<sub>2</sub><sup>73</sup> and CaO–Al<sub>2</sub>O<sub>3</sub><sup>74</sup> and CO on BaO–Al<sub>2</sub>O<sub>3</sub>.<sup>75</sup> Such surface layers adsorb very strongly carbon dioxide so that carbonate particles can form like in the case of the catalytic materials belonging to the BaO–Al<sub>2</sub>O<sub>3</sub> system,<sup>75,76</sup> which find applications as traps for nitrogen oxides in the NSR (NO<sub>x</sub> Storage and Reduction) technology for purification of waste gases of diesel cars. On the other hands Mg and Ca aluminates are thermally stable supports for metals to be used in high temperature applications such as steam reforming, partial oxidation and autothermal reforming of methane. Beta-alumina type La and Ba aluminates may be used as supports for catalytic combustion catalysts.

Due to their strong basicity, alkali-earth oxides cannot be covered by “monolayers” of other more covalent oxides, in contrast with what happens with ionic but less basic oxides, such as zirconia, titania, alumina, where oxide-supported-on oxides can be prepared. In practice, the deposition of vanadate, tungstate, molybdate, sulfate, silicate and borate species on MgO and other alkali-earth oxides gives rise easily to bulk salts more than supported oxides. Reactivity is strong also with ionic oxides, such as e.g., NiO, FeO, CoO, CuO, that tend to produce solid solutions with MgO and higher alkali-earth oxides. In reducing atmospheres, these solid solutions give rise to “supported” metal catalysts. In fact, catalysts based on NiO–MgO solid solutions have been patented for the methane catalytic partial oxidation (CPO) to syngas.<sup>77</sup>

Noble metals, likely due to their very big atomic size, do not easily penetrate the rock salt structure. This allows the use of MgO as support for metal catalysts. Pt and

Pd supported on MgO—CeO<sub>2</sub> have been patented for the selective catalytic reduction of NO<sub>x</sub> by hydrogen<sup>78</sup> while catalysts based on Rh/MgO are proposed for the CPO reaction<sup>79</sup> as well as for steam reforming of phenols in tars and biooils.<sup>80</sup>

### 6.4.2.3 Alkali-earth oxides as adsorbents or absorbents

One of the possible ways for utilization of fossil fuels such as coal without producing emissions of carbon dioxide in the atmosphere is the CO<sub>2</sub> capture and sequestration technology. In this process, CO<sub>2</sub> is captured either from the combustion gases or from hydrogen/CO<sub>2</sub> mixtures produced by gasification and water gas shift. CO<sub>2</sub> capture can be performed with liquids (such as potassium carbonate and ethanol amines water solutions, see above) at low temperature (<110 °C) or with solids either at low or high temperature (<800 °C). Strongly basic oxides materials adsorb or absorb strongly CO<sub>2</sub> even at very high temperatures and can be regenerated by carbonate decomposition.<sup>81</sup> Alkali-earth metal oxides, in particular solids based on CaO<sup>82,83</sup> are the most promising for this purpose.

The high temperature removal of contaminants from hot gases such as the abatement of HCl<sup>84</sup> from waste combustion, that of As<sub>2</sub>O<sub>3</sub> from coal combustion gases,<sup>85</sup> as well as the destructive adsorption of heavily chlorided organics such as CCl<sub>4</sub><sup>86</sup> may be performed over CaO-based materials at 200–600 °C.

## 6.4.3 Aluminas

### 6.4.3.1 Preparation and solid-state chemistry of aluminas

Bauxite, an aluminum-iron mixed hydroxide mineral, containing also Si and Ti compounds, is mostly at the origin of Al compounds. The Bayer process is universally applied for the production of alumina and aluminum from bauxites. In the current industrial practice, the Bayer process has three main steps: (1) digestion, where bauxite is digested with caustic soda at elevated temperature and pressure to produce aluminate liquor, containing alumina in the form of [Al(OH)<sub>4</sub>]<sup>-</sup>; (2) precipitation, where the aluminate liquor is hydrolyzed at 55–60 °C to produce gibbsite or hydrargillite, γ-Al(OH)<sub>3</sub>, containing relevant amounts of sodium (300–7000 ppm) and iron (200–600 ppm.); and (3) calcination, when gibbsite is calcined at 1000–1200 °C to produce metallurgical grade alumina, still impure of Na and Fe. This is the starting material for the electrolytic Hall–Heroult production of Al metal (with the intermediate synthesis of cryolite, Na<sub>3</sub>AlF<sub>6</sub>), as well as of alumina ceramics and aluminum compounds such as aluminum sulphates, nitrates and chloride.<sup>87</sup> From these compounds, Al hydroxides can be reprecipitated. Pseudoboehmite gel, which is one of the most important precursor for fine alumina powders, may be produced by reacting sodium aluminate solution with a hydrated acid salt of aluminum such as AlCl<sub>3</sub>·6H<sub>2</sub>O, Al<sub>2</sub>(SO<sub>4</sub>)<sub>3</sub>·18H<sub>2</sub>O, or Al(NO<sub>3</sub>)<sub>3</sub>·9H<sub>2</sub>O or with the equivalent acids themselves. However, the use of acid processes, while producing low-soda gels, results in an acid salt by-product that is hard to dispose of according to environmental regulations. Pseudoboehmite can also produced with the so-called Ziegler process (see below) starting from Al metal and Al alkoxides.

#### 6.4.3.1.1 Aluminum hydroxides

At least seven different crystalline phases of alumina hydrates are known. The availability of refined computational and theoretical methods together with diffraction and vibrational spectroscopic data allowed very recently the reconsideration of the structure of all these phases, in particular in relation to the positions of hydrogen atoms and the geometries of the hydrogen bonds.

Four different polymorphs of Al hydroxide  $\text{Al}(\text{OH})_3$  are known: Bayerite, usually denoted as  $\alpha\text{-Al}(\text{OH})_3$ , Gibbsite, usually denoted as  $\gamma\text{-Al}(\text{OH})_3$ ,<sup>88</sup> and the less common  $\text{Al}(\text{OH})_3$  polymorphs Doyleite and Nordstrandite.<sup>89</sup> The four structures are closely related. They are constituted by four different stacking sequences of the same kind of layers, constituted by  $\text{Al}(\text{OH})_6$  edge sharing octahedral forming a planar pseudohexagonal pattern. Thus, all Al ions are octahedrally coordinated while hydroxyl groups are bridging between two Al atoms. At both sides of the layers, hydroxyl groups stand. The different  $\text{Al}(\text{OH})_3$  polymorphs are thus associated with different geometries of the H-bondings between the layers.

Two polymorphs are known for the Al-oxyhydroxide  $\text{AlOOH}$ , diaspore,  $\alpha\text{-AlOOH}$  and boehmite  $\gamma\text{-AlOOH}$ . Boehmite has a layered structure<sup>90,91</sup> with octahedral Al ions, tetracoordinated oxide ions and bridging hydroxyl groups. Zigzag chains of hydrogen bonds, whose exact geometry has not been completely defined, is formed between the layers.

The structure of diaspore,<sup>92</sup> which is the same of goethite  $\alpha\text{-FeOOH}$ , is based on a tridimensional oxygen network: it may be described as formed by double chains of edge-shared octahedra, linked via corner-sharing octahedra. It involves<sup>93</sup> a slightly distorted hexagonal close-packed O-atom arrangement with Al atoms occupying one-half of the octahedral interstices, and with all atoms located on mirror planes. There are two distinct O sites, O1 and O2, each bonded to three Al atoms, with O2 additionally bonded to an H atom. Thus Al is fully octahedral with tricoordinated oxide ions and triply-bridging and H-bonded hydroxyl groups.

A seventh phase, Akdalaite, a synthetic phase, has been found to be the same structure as the natural phase tohdite. Its composition is  $5\text{Al}_2\text{O}_3 \cdot \text{H}_2\text{O}$ . Three different space groups for the unit cell have been considered<sup>94</sup> but were found to be substantially equivalent in terms of both geometry and energy. Of the 10 Al atoms in the unit cell, eight have octahedral coordination and two have tetrahedral coordination.

Gibbsite, bayerite, diaspore and boehmite are largely present in nature. Gibbsite, bayerite and boehmite are synthesized industrially as the main precursors of transitional aluminas to be used in adsorption and catalysis technologies (Figure 6.8).

#### 6.4.3.1.2 Corundum powders

As it is well known, aluminum oxide is a polymorphic material<sup>95,96</sup> (Table 6.4). The thermodynamically stable phase is  $\alpha\text{-Al}_2\text{O}_3$  (corundum) where all Al ions are equivalent in octahedral coordination in an hcp oxide array. All alumina polymorphs convert into  $\alpha\text{-Al}_2\text{O}_3$  (corundum) by calcination at  $T > c. 1200^\circ\text{C}$ . This exothermic phase transition occurs with loss of porosity and surface area as well as increase of



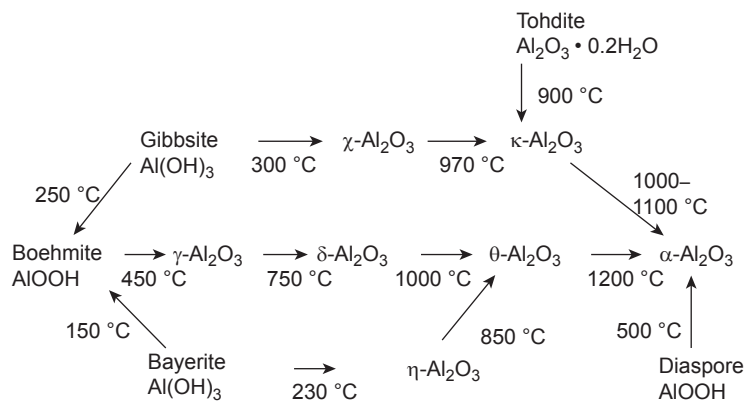


FIGURE 6.8

Schematics of the transformations of aluminum hydroxides into alumina polymorphs.

crystal size.  $\alpha\text{-Al}_2\text{O}_3$  powders produced by high temperature calcination are usually characterized by  $S_{\text{BET}} < 1 \text{ m}^2/\text{g}$ ,  $V_p < 0.5 \text{ cm}^3/\text{g}$ . By controlling reaction temperature and time, higher surface area may be obtained ( $< 50 \text{ m}^2/\text{g}$ ).

$\alpha\text{-Al}_2\text{O}_3$  powders may also be prepared by calcination/decomposition of diaspore ( $\alpha\text{-Al}(\text{OH})_3$ ) at 400–500 °C. In this case, surface area of the order of  $65 \text{ m}^2/\text{g}$  may be obtained.<sup>97</sup> It is commonly stated that the nearly close-packed hexagonal oxygen sublattices in both diaspore and corundum permit a topotactic transformation with little atomic rearrangement. The actual process, however, requires that one quarter of the oxygen atoms be removed and that the hexagonal sublattice then be restored. The powder X-ray diffraction recorded during reaction allowed the detection of an intermediate phase,<sup>98</sup> designated  $\alpha'\text{-Al}_2\text{O}_3$ , indexed to a monoclinic (P2) cell, with  $a = 9.566(5) \text{ \AA}$ ,  $b = 5.124(2) \text{ \AA}$ ,  $c = 9.156(4) \text{ \AA}$ , and  $\beta = 91.76(3)^\circ$ . Nuclear magnetic resonance of the  $\alpha'\text{-Al}_2\text{O}_3$  indicated that 15–20% of the aluminum is on tetrahedral sites, with the remainder in octahedral coordination. More recent study<sup>99</sup> confirmed the existence of an intermediate phase in the diaspore-corundum transformation, and explained the formation of thin dense corundum regions that were separated by nanometer-sized pores forming lamellae with a periodicity of 3.7 nm as due to the misfit of the close-packed oxygen planes of the intermediate and final corundum phase.

#### 6.4.3.1.3 Transitional aluminas (activated aluminas)

All alumina polymorphs other than  $\alpha\text{-Al}_2\text{O}_3$  (corundum) are metastable as bulk compounds, several having structures that have been related to that of spinel, i.e., cubic  $\text{MgAl}_2\text{O}_4$ .  $\gamma\text{-Al}_2\text{O}_3$ , which is the most used form of alumina, is mostly obtained by decomposition of boehmite, the oxyhydroxide denoted as  $\gamma\text{-AlOOH}$ . The morphological properties of the resulting  $\gamma\text{-Al}_2\text{O}_3$  are strictly determined by those of the starting boehmite preparation.<sup>100</sup> Nanocrystalline hydrous oxyhydroxide, once called “pseudoboehmite”, is the best starting material for catalytic  $\gamma\text{-Al}_2\text{O}_3$  aluminas.<sup>101</sup> In fact,

**Table 6.4** Structural Data of Aluminas

	SG	Z Al <sub>2</sub> O <sub>3</sub>	a (Å) b (Å)	c (Å)	Structure Type	Al <sub>IV</sub> %	Al <sub>VI</sub> %	Al <sub>V</sub> %	Ref.
γ-Al <sub>2</sub> O <sub>3</sub>	Fd3m	10.66	7.90	7.90	Cubic disordered nonstoichiometric spinel	30–60	70–40	1–2	Snyder
γ-Al <sub>2</sub> O <sub>3</sub>	I4 <sub>1</sub> /amd	5.33	5.616	7.836	Tetragonal disordered nonstoichiometric spinel	35.6	64.4	0	Paglia
γ-Al <sub>2</sub> O <sub>3</sub>	P2 <sub>1</sub> /m	8	5.587 8.413	8.068 β 90.59°	Orthorhombic nonspinel structure	25	75		Digne
γ'-Al <sub>2</sub> O <sub>3</sub>	P-4m2	16	5.611	24.450	Tetragonal spinel superstructure	34.4	65.6	0	Paglia
δ-Al <sub>2</sub> O <sub>3</sub>	P-4m2	16	7.93	23.50	Tetragonal spinel superstructure	30–45	55–70		Rooksby
δ-Al <sub>2</sub> O <sub>3</sub>	P2 <sub>1</sub> 2 <sub>1</sub> 2 <sub>1</sub>		15.89 7.94	11.75	Orthorhombic spinel superstructure				Levin Wang
θ-Al <sub>2</sub> O <sub>3</sub>	C2/m	4	5.62 2.91	11.79 β 103.8°	Monoclinic β-Ga <sub>2</sub> O <sub>3</sub> structure, ordered spinel-related structure	50	50		
η-Al <sub>2</sub> O <sub>3</sub>	Fd3m	8	7.91	7.91	Cubic disordered nonstoichiometric spinel	20–50	80–50		Snyder
κ-Al <sub>2</sub> O <sub>3</sub>	Pna2 <sub>1</sub>	8	4.844 8.330	c = 8.955	Orthorhombic	25	75		
χ-Al <sub>2</sub> O <sub>3</sub>					Hexagonal or cubic	20	73	7	
ρ-Al <sub>2</sub> O <sub>3</sub>					Amorphous	25	55	20	
α-Al <sub>2</sub> O <sub>3</sub>	R-3c	6	4.76	12.99	Hexagonal-rhombohedral, corundum structure	0	100		

high surface-area nanocrystalline boehmites are even industrially available. They may be prepared by precipitation starting from soluble Al salts, but in this case they usually contain nonnegligible amounts of alkali ions. Another way to obtain microporous boehmite comes from the so-called Ziegler process, industrially denoted as ALFOL process. This process was originally intended to produce linear fatty alcohols starting from trialkyl-aluminum formed by oligomerization reaction of ethylene with Al metal. Oxidation of aluminum trialkyls gives rise to aluminum trialkoxides that can be hydrolyzed to alcohols and boehmite. A modification of this process allows the production of aluminum trialkoxides and hydrogen from alcohols and aluminum metal. Thus, after hydrolysis, boehmite is produced while alcohols may be recycled. This way produces high purity alumina, with less than 20 ppm sodium and potassium, less than 50 ppm calcium and magnesium, less than 100 ppm iron and less than 120 ppm silicon.<sup>102</sup> Calcination at ca 450 °C of nanocrystalline boehmite gives rise to highly microporous high surface area  $\gamma$ -Al<sub>2</sub>O<sub>3</sub> (~500 m<sup>2</sup>/g). If calcination is performed with a low-surface area well-crystallized boehmite medium surface area lamellar powders are obtained, with ~100 m<sup>2</sup>/g.

$\gamma$ -Al<sub>2</sub>O<sub>3</sub> is one of the most used materials in any field of technologies. However, the details of its structure are still matter of controversy. It has a cubic structure described by Lippens and de Boer<sup>103</sup> to be a defective nonstoichiometric spinel.<sup>27</sup>Al NMR spectra show that tetrahedral Al is 25–33% of all Al ions but may also show a small fraction of Al ions in coordination five,<sup>104</sup> or highly distorted tetrahedral. Soled<sup>105</sup> proposed that the cation charge in the defective spinel structure can be balanced, more than by vacancies, by hydroxy ions at the surface. In fact,  $\gamma$ -Al<sub>2</sub>O<sub>3</sub> is always hydroxylated, dehydroxylation occurring only at a temperature where conversion to other alumina forms is obtained. XRD studies, using the Rietveld method,<sup>106</sup> suggested that Al<sup>3+</sup> cations can be in positions different from those of spinels, and also in trigonal coordination. Other possible structures such as that of a “hydrogen-spinel”<sup>107</sup> have also been proposed. DFT calculations have been performed recently, but did not allow to completely solve the problem. The hydrogen spinel structure HAl<sub>5</sub>O<sub>4</sub> was found less stable<sup>108</sup> while the spinel structure with occupation of extra-spinel sites was considered possible.<sup>109,110</sup> On the contrary, Digne et al.<sup>111,112</sup> and Krokidis et al.<sup>113</sup> proposed a structure based on ccp oxide lattice but different from that of a spinel, with 25% of Al ions in tetrahedral interstices and no structural vacancies. According to these authors, this structure, although unstable with respect to corundum, is more stable than the spinel based structures. However, Paglia et al. interpreted again their structural data on  $\gamma$ -Al<sub>2</sub>O<sub>3</sub>, using the tetragonally distorted spinel model,<sup>114</sup> but concluded that there is a substantial occupancy of nonspinel sites.<sup>115</sup> In fact several different models for the bulk structure of  $\gamma$ -Al<sub>2</sub>O<sub>3</sub> have been proposed recently. Menendez Proupin and Gutierrez<sup>116</sup> considered seven different structures, while Ferreira et al.<sup>117</sup> considered by DFT calculations a spinel type model with 37.5% tetrahedrally coordinated Al cations and 62% octahedrally coordinated cations against the nonspinel type model of Kokridis et al., and concluded that the best match with experimental data was obtained for the spinel-type model. In particular, ab initio calculations of the <sup>27</sup>Al MAS NMR spectra for different structural models of  $\gamma$ -Al<sub>2</sub>O<sub>3</sub> allowed to conclude that the best fit is obtained with a model of a spinel-type structure

with space group  $Fd\bar{3}m$  and  $Z = 32$ , where 64% Al ions are octahedral, 34.4% tetrahedral and 1.6% pentacoordinated. The question is actually still open to discussion.

Also, the further sequence of alumina phases obtained upon calcination of  $\gamma$ - $Al_2O_3$  is object of some disagreement, being slightly different in different experiments. While some authors report the direct conversion of  $\gamma$ - $Al_2O_3$  into  $\theta$ - $Al_2O_3$  near 650 °C, most studies find the formation of slightly different intermediate phases, closely related to that of spinel and of  $\gamma$ - $Al_2O_3$ , formed continuously in the range 500–650 °C. Slightly different spinel tetragonal superstructures, such as those denoted as  $\delta$ - $Al_2O_3$ <sup>103,118</sup> and  $\gamma'$ - $Al_2O_3$ <sup>114</sup> have been determined. According to Lippens and de Boer<sup>103</sup> and Wilson et al.,<sup>118</sup>  $\delta$ - $Al_2O_3$  is a tetragonal spinel superstructure whose unit cell is constituted by three spinel unit blocks with tetragonal deformation, likely with a partial ordering of Al ions into octahedral sites. It is formed continuously in the range 800–900 K. This phase transition is associated to partial ordering of Al ions, although data on location of Al ions in the spinel sites are not in full agreement. According to Paglia et al.,<sup>114</sup> a slightly different spinel superstructure is formed, denoted as  $\gamma'$ - $Al_2O_3$ . The surface area of the sample also slightly decreases together with overall porosity.

$\theta$ - $Al_2O_3$  is formed above 650 °C with simultaneous decrease of the surface area to near 120 m<sup>2</sup>/g or less. Its monoclinic structure, which is the same of  $\beta$ -gallia, can be derived from that of a spinel, with deformation and complete ordering of the distribution of Al ions, which are now half tetrahedral and half octahedral.<sup>119</sup>  $\theta$ - $Al_2O_3$  is the main component of most medium-area alumina catalyst supports. Thus, according to <sup>27</sup>Al MAS NMR the ratio between tetrahedrally coordinated and octahedrally coordinated aluminum ions increases upon the sequence  $\gamma$ - $Al_2O_3 \rightarrow \delta$ - or  $\gamma'$ - $Al_2O_3 \rightarrow \theta$ - $Al_2O_3$ . Tetrahedral  $Al^{3+}$  is 25–40% in  $\gamma$ - $Al_2O_3$ , and near 50% in  $\theta$ - $Al_2O_3$ . Data for pure  $\delta$ - $Al_2O_3$  are still incomplete.<sup>120</sup> In the case of the  $\gamma'$ - $Al_2O_3$  phase determined by Paglia,<sup>114</sup> 34% aluminum ions are in tetrahedral coordination.

Further calcination at increasing temperatures converts  $\theta$ - $Al_2O_3$  finally to  $\alpha$ - $Al_2O_3$ , complete above 1200 °C.<sup>118</sup> During the sequence  $\gamma$ - $Al_2O_3 \rightarrow \delta$ - $Al_2O_3$  or  $\gamma'$ - $Al_2O_3 \rightarrow \theta$ - $Al_2O_3 \rightarrow \alpha$ - $Al_2O_3$ , the lamellar morphology of boehmite is mostly retained but with progressive sintering of the lamellae and disappearance of the slit-shaped pores.

A similar sequence of alumina phases is obtained commercially using the flame hydrolysis of  $AlCl_3$ , producing the so-called “fumed aluminas”. The high-temperature reaction gives rise to very small nonporous highly volatile alumina particles. Depending on the reaction conditions, these are constituted by  $\gamma$ - $Al_2O_3$  crystals with approximate size 10 nm and 130 m<sup>2</sup>/g surface area, or mixtures of phases with predominance of  $\delta$ - $Al_2O_3$  or  $\theta$ - $Al_2O_3$  with lower surface areas down to 65 m<sup>2</sup>/g and slightly higher particle size. These materials are very pure from alkali, but may contain chlorine,<sup>121</sup> silicon and titanium. Commercial powders belonging to these families are Aeroxide from Evonik and SpectraAl<sup>®</sup> from Cabot. According to a recent patent,<sup>122</sup> these powders may be further converted by heating at 1350 °C to powders still retaining a surface area of from 3 to 30 m<sup>2</sup>/g, in which the proportion of alpha-aluminum oxide is at least 85% by weight.

By decomposing Bayerite  $\alpha$ - $Al(OH)_3$  at 200–300 °C,  $\eta$ - $Al_2O_3$  is obtained, which is also considered to be a spinel-derived structure very similar to  $\gamma$ - $Al_2O_3$

but with more tetrahedrally coordinated (35%) and less octahedrally coordinated Al ions.<sup>123,124</sup> Calcination at increasing temperatures of  $\eta$ -Al<sub>2</sub>O<sub>3</sub> gives rise directly to  $\theta$ -Al<sub>2</sub>O<sub>3</sub> and finally to  $\alpha$ -Al<sub>2</sub>O<sub>3</sub>.<sup>118</sup>

The decomposition of pure gibbsite hydroxide ( $\gamma$ -Al(OH)<sub>3</sub>) gives rise to different transitional polymorphs,<sup>125</sup>  $\gamma$ -Al(OH)<sub>3</sub>  $\rightarrow$   $\chi$ -Al<sub>2</sub>O<sub>3</sub>  $\rightarrow$   $\kappa$ -Al<sub>2</sub>O<sub>3</sub>  $\rightarrow$   $\alpha$ -Al<sub>2</sub>O<sub>3</sub>. The structure of  $\chi$ -Al<sub>2</sub>O<sub>3</sub> is still not defined. It is either cubic or hexagonal.<sup>126</sup> According to Favaro et al.<sup>127</sup>, it has the same IR skeletal spectrum of  $\gamma$ -Al<sub>2</sub>O<sub>3</sub> (suggesting a similar tetrahedral to octahedral Al distribution) but a different XRD pattern. The structure of  $\kappa$ -Al<sub>2</sub>O<sub>3</sub> is orthorhombic with close-packed planes of oxygen in an ABAC-stacking sequence along the c-axis. 1/4 of the Al ions occupy tetrahedral interstitial positions and 3/4 occupy octahedral positions.<sup>128,129</sup>

The temperature ranges for these transformations have some variability depending on the gibbsite properties. Starting from gibbsite with 25 m<sup>2</sup>/g calcination at 300 °C gives rise to  $\chi$ -Al<sub>2</sub>O<sub>3</sub> with 350–370 m<sup>2</sup>/g and, after further treatment at c. 900 °C to  $\kappa$ -Al<sub>2</sub>O<sub>3</sub> with 100 m<sup>2</sup>/g may be obtained to finally produce  $\alpha$ -Al<sub>2</sub>O<sub>3</sub> above 1100 °C. Other studies<sup>130</sup> report, however, that mild heating at 350 °C of gibbsite gives rise to a largely amorphous solid denoted as  $\rho$ -Al<sub>2</sub>O<sub>3</sub>, containing traces of boehmite  $\gamma$ -AlOOH, which by calcination converts into  $\gamma$ -Al<sub>2</sub>O<sub>3</sub>, and, later, into  $\theta$ -Al<sub>2</sub>O<sub>3</sub>, and, finally, into  $\alpha$ -Al<sub>2</sub>O<sub>3</sub>. However, if previously activated by grinding, thermal treatment of gibbsite gives rise to amorphous  $\rho$ -Al<sub>2</sub>O<sub>3</sub>, containing traces of boehmite  $\gamma$ -AlOOH, which by calcination converts directly into  $\alpha$ -Al<sub>2</sub>O<sub>3</sub>.

#### 6.4.3.1.4 Amorphous aluminas

Amorphous aluminas<sup>131</sup> have also been produced with several methods and investigated. Most of them are possibly impure from organic reagents. They tend to convert into  $\gamma$ -Al<sub>2</sub>O<sub>3</sub><sup>132</sup> or  $\eta$ -Al<sub>2</sub>O<sub>3</sub><sup>133</sup> upon hydrothermal treatment. Amorphous alumina appears to be quite inactive as an acid catalyst and Al ions there appear to be essentially in octahedral coordination or pentacoordinated.

#### 6.4.3.1.5 Mesoporous aluminas

Many attempts have been devoted recently to produce very large surface-area transitional aluminas with mesoporosity. This is done using templating agents. Although many interesting materials have been obtained, several of them appear to be amorphous in their wall structure, thus being also characterized by low acidity and/or catalytic activity. Recently, high surface-area mesoporous crystalline aluminas such as  $\gamma$ -Al<sub>2</sub>O<sub>3</sub> (200–400 m<sup>2</sup>/g),<sup>134</sup>  $\eta$ -Al<sub>2</sub>O<sub>3</sub> (430 m<sup>2</sup>/g) and  $\chi$ -Al<sub>2</sub>O<sub>3</sub> (325 m<sup>2</sup>/g)<sup>135</sup> have been prepared through the assembly of mesostructured surfactant-encapsulated mesophases of boehmite, bayerite and gibbsite, respectively, from amorphous aluminum hydroxide by using an amine surfactant as the structure-templating porogen.

#### 6.4.3.1.6 Stabilized aluminas

As discussed above, high surface-area transitional aluminas are metastable phases tending to transform to higher temperature phases and later to corundum  $\alpha$ -Al<sub>2</sub>O<sub>3</sub>, with resulting loss of surface area. These solid-state reactions, certainly starting by surface diffusion

processes, are inhibited by the presence at the surface of some ionic species. Silica deposited at the surface of alumina (the so-called silicated aluminas) or even coprecipitated with alumina inhibits these phase transformation, thus providing bulk and morphological stability to transition aluminas. This occurs without a relevant change in the surface properties of aluminas if the amount of silica added to alumina is in the range of few % wt. In fact, small amounts of silica do not induce relevant Bronsted acidity, which is typical of silica-rich silica–aluminas (see below). Also, silica does not modify, or even slightly enhance, the Lewis acidity of alumina. However, it may poison some surface basic sites. The addition of silica to alumina is sometimes attempted to modify the state of the supported species in the preparation of supported catalysts.

Another way to induce thermal and morphological stability to aluminas is to deposit at the surface big metal cations, which are not able to enter the close packed array of oxide ions of aluminas. This is the case of big monovalent, bivalent and trivalent cations such as  $\text{Na}^+$ ,  $\text{K}^+$ ,  $\text{Cs}^+$ ,  $\text{Ca}^{2+}$ ,  $\text{Sr}^{2+}$  and  $\text{La}^{3+}$ . In fact, these ions do not enter spinel structures but tend to form, when combined with  $\text{Al}^{3+}$ , beta-alumina-type structures, where in fact spinel-type alumina layers are separated by layers where these big cations are located together with ionically conducting oxide species. When deposited at the surface of transitional aluminas, these cations inhibit surface diffusion thus also inhibiting phase transitions. However, they also induce a significant modification on the surface chemistry of alumina, with a neutralization of acidity and, at increasing coverages, inducing enhanced basicity. On the other hand, in many cases, this chemical effect is beneficial too, i.e., by decreasing the alumina activity to produce coking in reducing conditions in the presence of organic compounds.

#### 6.4.3.2 Surface chemistry of aluminas

The catalytic activity of “transitional” aluminas, in particular those whose structures are related to spinel ( $\gamma$ -,  $\eta$ -,  $\delta$ -,  $\theta$ - $\text{Al}_2\text{O}_3$ ), are undoubtedly mostly related to the Lewis acidity<sup>136</sup> of a small number of low coordination surface aluminum ions, as well as to the high ionicity of the surface Al–O bond.<sup>137–139a</sup> These sites are well characterized by adsorption of probe molecules followed by spectroscopies and calorimetry. The density of the very strong adsorption sites responsible for ammonia adsorption heat of more than 200 kJ/mol is reported to be near 0.1 sites/nm<sup>2</sup>.<sup>131,132</sup> Taking into account the bulk density of  $\gamma$ - $\text{Al}_2\text{O}_3$ , it is easy to calculate that at most one site every 50–100 acts as a strong Lewis site on  $\gamma$ -alumina outgassed at 400–550 °C, the large majority being still hydroxylated or not highly exposed at the surface.

The density of the strongest Lewis acid sites tends to decrease a little by increasing the historical calcination temperature of the alumina (i.e., upon the sequence  $\gamma \rightarrow \delta \rightarrow \theta$ , which is also a sequence of decreasing surface area). As a result of this, the number of strongest acid sites per gram significantly decreases in this sequence, although catalyst stability increases. Surface spectroscopy provides also evidence of a complex pattern of surface hydroxyl groups with medium–high Brønsted acidity, and of its evolution by calcination (Figure 6.9).

Most authors agree that at least three different types of Lewis acid sites (weak, medium and strong) exist on transitional aluminas. Liu and Truitt<sup>140</sup> emphasized

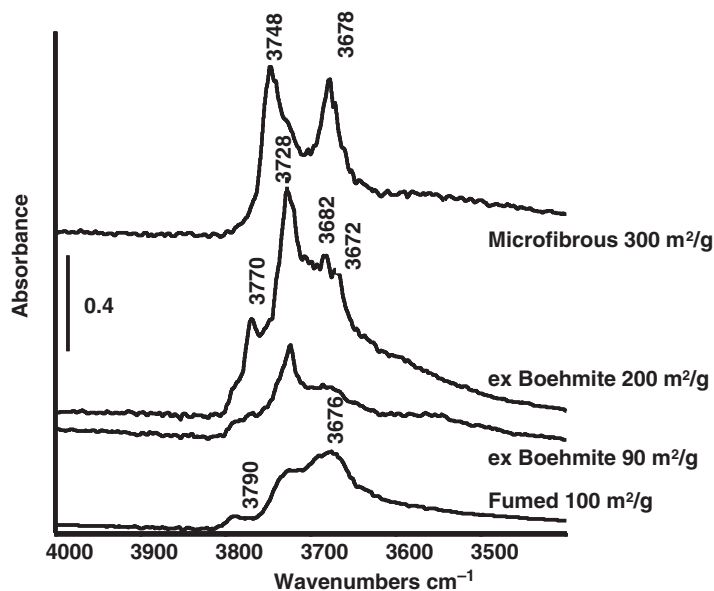


FIGURE 6.9

FT-IR spectra of the surface OH groups of four  $\gamma$ - $\text{Al}_2\text{O}_3$  samples, activated by outgassing at 773 K.

the close proximity of Lewis acid sites with surface OH's, while Lundie et al.<sup>141</sup> identified four different Lewis acid sites arising from coordinatively unsaturated octahedral (the weakest) and tetrahedral sites (the three strongest), three of which are considered to be associated to three different types of hydroxy groups.

Transmission electron microscopy studies of  $\gamma$ - $\text{Al}_2\text{O}_3$  reveal different particle shapes for different preparations. At least three main morphologies can be found, the fibrous type, the lamellar type including rhombic particles, and a "spherical"-like. Fumed alumina presents quite "globular" particles,<sup>142,143</sup> constituted by micro-platelets preferentially exposing the (110) planes as prevailing terminations and, to less extent, the (100) and the (111) ones. Fibrous, lamellar and rhombic  $\gamma$ - $\text{Al}_2\text{O}_3$  particles are formed by fibrous, lamellar and rhombic (pseudo)bohemites

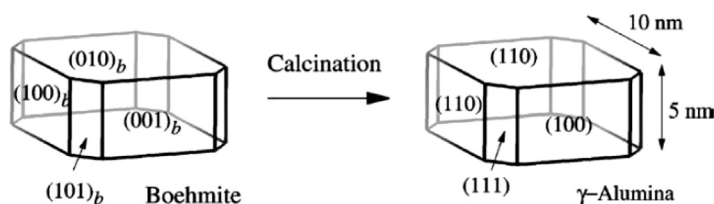


FIGURE 6.10

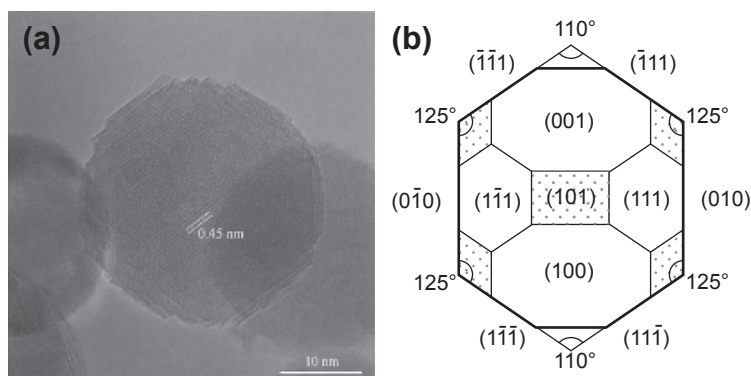
Schematics of the toptactic transformation of boehmite into  $\gamma$ -alumina nanoparticles with the corresponding surface orientations.

Reprinted with permission from Ref. 111.

by topotactic decomposition (Figure 6.10<sup>111</sup>), their surface being supposed to be dominated by (110) spinel-like faces, with a secondary presence of (100) and, almost negligible, (111) faces,<sup>144</sup> or, for other authors, with exposition of significant amount of (111) face.<sup>145</sup> Thus, these two morphologies, although quite well different, should expose the same faces in similar amounts, as supposed by Wischert et al.<sup>146</sup> Spherical particles obtained by evaporation, instead are reported to have a habit where (111) and (100) faces predominate<sup>145,147</sup> (Figure 6.11).  $\eta$ -Al<sub>2</sub>O<sub>3</sub> produced by calcination of bayerite is reported to expose preferentially the (111) crystallographic planes,<sup>148</sup> while, if prepared from Al isopropoxide, it should expose (100), (110) and super-imposed (111)/(211) faces.<sup>142</sup>

Using the nonspinel-type structure they proposed, Digne et al.<sup>112</sup> justified the complexity of the OH-stretching spectrum as well as the existence of different Lewis acid sites on  $\gamma$ -Al<sub>2</sub>O<sub>3</sub> modeling CO and pyridine adsorption on tricoordinated Al<sup>3+</sup> on (110) face, tetracoordinated Al<sup>3+</sup> on (110) face, and pentacoordinated Al<sup>3+</sup> on (110) and (100) faces.

In recent years, the group of Peden and coworkers proposed a determinant role of pentacoordinated Al ions, well detectable in the <sup>27</sup>Al NMR spectra of  $\gamma$ -Al<sub>2</sub>O<sub>3</sub> but also based on calculations considering flat  $\gamma$ -Al<sub>2</sub>O<sub>3</sub> faces, as generating most of the surface and bulk chemistry of this material, i.e., as a structural promoter for phase transition,<sup>149</sup> for anchoring of Pt oxide<sup>150</sup> as well as for the sintering of supported Pt metal particles.<sup>151</sup> Using the nonspinel structural model of Digne et al.,<sup>112</sup> they modeled this adsorption site as located on the (100) face. The same group used the (100) and (110) faces of this nonspinel type structure to model the adsorption of NO<sub>x</sub>.<sup>152</sup> According to Sautet and coworkers, the most abundant surface face on this nonspinel structure is the (110) face<sup>31,146</sup> where (if “dry”) strongest tricoordinated Al sites should exist, in contrast to the pentacoordinated sites on the (100) expected to be less reactive. On the other hand, according to the same authors, tricoordinated Al<sup>3+</sup> is so acidic and the (110) surface so



**FIGURE 6.11**

(a) Magnified TEM image and (b) schematic of a typical spherical alumina particle.

Reprinted with permission from Ref. 145.



reactive to be impossible its dehydroxylation in normal conditions. This should be the reason of the usual abundant hydroxylation of the alumina surface. As said, other authors judge most stable the spinel structure or spinel-like structures, and modeled Lewis acidity as well as cation–anion couples over the exposed faces of these structures, such as on the (100) and (110) faces of the spinel structure<sup>153</sup> or the (001) face of a spinel-like structure.<sup>154</sup> More recently the present author, based also on previous studies,<sup>143</sup> suggested that the most active Lewis acid sites are located on edges and corners of the nanocrystals.<sup>139b,139c</sup> Unfortunately, studies of edges and corners between exposed faces, which are very reasonably the location of the most reactive sites, are not available.

The existence on outgassed transitional alumina surfaces of Lewis sites less coordinated than fivefold is well substantiated by adsorption of probes but certainly depends on activation temperature and can be associated to a small number of defect sites on corners and edges of the crystal surface. On the other hand, it seems very plausible that a bulk technique such as <sup>27</sup>Al NMR spectroscopy would only detect the most abundant species, more than small amounts of defect and surface species. Finally, the existence of more uncoordinated Al ions should be the fundamental reason of the much higher reactivity of transitional aluminas with respect to corundum  $\alpha$ -Al<sub>2</sub>O<sub>3</sub> powders, where indeed weak Lewis acidity is found likely just due to pentacoordinated Al ions.<sup>143</sup>

It must be taken into account that the surface activity of aluminas is also strictly dependent from its purity: in particular, alkali metal impurities arising from the preparation procedure (mostly sodium ions) may decrease significantly surface reactivity.<sup>138</sup> Voluntary doping with alkali is largely used to reduce alumina activity in supported catalysts. It has also been shown that doping with alkali, alkali-earth and rare-earth cations increases stability of alumina against phase transition as well as loss of surface area. In practice to reduce surface activity and to increase stability of alumina when used as the support for metal catalysts, evolved structures ( $\theta$ -Al<sub>2</sub>O<sub>3</sub> or  $\alpha$ -Al<sub>2</sub>O<sub>3</sub>) with moderate to low surface area (100–5 m<sup>2</sup>/g) are needed and doping with alkali, alkali earth or rare earth may also be useful.

Actually, the true particular sites of aluminas for most catalytic reactions are very likely anion–cation couples,<sup>146</sup> which have very high activity and work synergistically. The basic counterpart may be oxide anions or hydroxyl species. Alcohol adsorption experiments<sup>155,156</sup> allow the characterization of such sites where dissociative adsorption occurs. Mechanistic studies suggest that such cation–anion couples are likely those active in alcohol dehydration,<sup>157</sup> in alkylchloride dehydrochlorination,<sup>158,159</sup> and in double-bond isomerization of olefins<sup>160,161</sup> over  $\gamma$ -Al<sub>2</sub>O<sub>3</sub>.

Many studies have been devoted to the multiplicity of the surface hydroxy groups of aluminas. After the work of Peri,<sup>162</sup> and of Tsyganenko and Filimonov,<sup>163</sup> Knözinger and Ratnasamy reported a very popular model of the different exposed planes of spinel type aluminas.<sup>164</sup> This model has been later modified by Busca et al.<sup>165,166</sup> These studies have been reviewed by Morterra and Magnacca.<sup>130</sup> More recently, additional investigations have been published by Tsyganenko and Mardilovich<sup>167</sup> and, on the basis of theoretical calculations by Fripiat et al.<sup>168</sup> and by Digne and Sautet,<sup>121,169</sup>

who also attempted to model the interaction of probe molecules. Lambert and Che<sup>170</sup> reviewed again these models and evidenced that the problem is still not solved. This aspect was also reviewed by Kasprzyk—Hordern<sup>171</sup> and by Busca<sup>139a</sup>. At least five components are usually present in the IR spectrum of the hydroxy groups of aluminas, i.e., at c. 3790, 3770, 3740–3720, 3700–3690 and 3580  $\text{cm}^{-1}$  (Figure 6.9), although in many cases the observed peaks are multiple. Data arising from our laboratory, based on the comparison between the surface hydroxyl-group spectra of other spinel type compounds (e.g., Mg, Zn, Ni and Co aluminate, ferrite and chromite, and  $\gamma\text{-Fe}_2\text{O}_3$ ) compared with corresponding corundum-type oxides ( $\alpha\text{-Al}_2\text{O}_3$ ,  $\alpha\text{-Fe}_2\text{O}_3$  and  $\alpha\text{-Cr}_2\text{O}_3$ )<sup>147</sup> and, more recently, on the comparison with the hydroxyl-group spectra of  $\alpha\text{-Ga}_2\text{O}_3$  and  $\beta\text{-Ga}_2\text{O}_3$ <sup>172</sup> strongly support the assignment of both components near 3790 and 3770  $\text{cm}^{-1}$  to terminal AlOH groups with Al in a tetrahedral-like environment. The splitting, not present in stoichiometric spinels, of these bands is actually in relation to the presence of vacancies with respect to the full stoichiometry of the spinel structure in transitional aluminas. The band located in the range 3740–3720  $\text{cm}^{-1}$  should belong to AlOH groups with Al in an octahedral-like environment, very likely terminal too. Both are active in adsorption and present medium-weak acidity (no protonation of pyridine, protonation of *n*-butylamine and piperidine). The hydroxyl-groups absorbing below 3700  $\text{cm}^{-1}$ , supposed to be more acidic,<sup>145</sup> appear instead to be quite unactive,<sup>152</sup> and could be weakly H-bonded or located into small pores. A complete investigation on the accessibility of these sites has still not been performed, to our knowledge. A definitive picture is still lacking.

Although most authors attribute to transitional aluminas essentially Lewis acidic properties, several studies show that some of their multiple surface hydroxy groups also have medium strong Brønsted acidity.<sup>173</sup> Actually, among the pure ionic oxides, alumina is one of the strongest Brønsted acids. The activity of pure  $\gamma\text{-Al}_2\text{O}_3$  as a good catalyst of skeletal *n*-butylene isomerization to isobutylene has been attributed to its medium-strong Brønsted acidity, sufficient to protonate *n*-butylenes at high temperature, producing carbenium ions, but too low to cause much cracking and coking.<sup>174</sup>

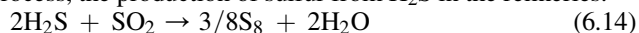
The effect of surface impurities on the acidity of the surface as well as on the corresponding spectroscopic data has been frequently neglected. Sodium content on alumina strongly depends on the preparation method. Aluminas derived from aluminum metal via alkoxide have Na content ( $\leq 40$  ppm as  $\text{Na}_2\text{O}$ ) generally about 10 times lower than those obtained by typical precipitation procedures. Sodium impurities decrease the number of the active sites but also possibly decrease their strength, according to induction effects,<sup>175</sup> so finally decreasing the alumina activity in acid catalyzed reactions. Even when their total concentration is small, sodium cations concentrate at the surface and have a relevant poisoning effect.

Actually, the activity trend, i.e., in *n*-butylene isomerization, correlates well with the total integrated intensity of the  $\nu\text{OH}$ -stretching band of the surface hydroxy groups and, inversely, with the sodium content derived by chemical analysis.<sup>176</sup> This content may be low, but differs significantly among the samples. It seems likely that sodium exchanges the protons of the surface hydroxy groups. It has been concluded that the amount of residual sodium, although always low, is determinant

for decreasing the number of the active sites for n-butylene isomerization on  $\gamma$ - $\text{Al}_2\text{O}_3$ , which is believed to be a proton-catalyzed reaction.

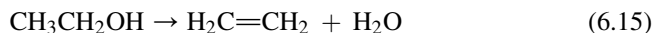
### 6.4.3.3 Aluminas as catalysts

Transition aluminas, mostly denoted as  $\gamma$ - $\text{Al}_2\text{O}_3$ , but actually being sometimes a mixture of  $\gamma$ - $\text{Al}_2\text{O}_3$ ,  $\delta$ - $\text{Al}_2\text{O}_3$  and  $\theta$ - $\text{Al}_2\text{O}_3$ , or of  $\eta$ - $\text{Al}_2\text{O}_3$  and  $\theta$ - $\text{Al}_2\text{O}_3$ , have wide application as catalysts. Among the most prominent ones, they are used in the catalytic steps of the Claus process, the production of sulfur from  $\text{H}_2\text{S}$  in the refineries.<sup>177</sup>

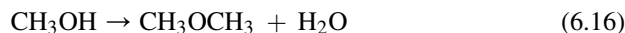


Aluminas for this application have large surface area (300–400  $\text{m}^2/\text{g}$ ), pore volumes 0.5 ml/g of which 0.1 ml/g due to macroporosity  $>750 \text{ \AA}$ , with loss on ignition of 5.5–6.5% wt/wt.<sup>178</sup> They may be promoted by iron to reduce deactivation by sulfation. In the Claus process (Figure 6.12), several reactors in series progressively complete the reaction, with intermediate cooling, condensation of the sulfur product, and reheating. While titania is used for the first reactor (see above), alumina is used in the others, working at c. 200–250 °C. The reactors are horizontal, to limit pressure drop.

Aluminas are very active in the dehydration of alcohols to olefins and to ethers,<sup>179</sup> and have been used in the 1960s for producing ethylene from dehydration of bioethanol at  $>250 \text{ °C}$ .<sup>180</sup>



They are applied to produce dimethylether from methanol



at 250–280 °C and 0.04–0.05 MPa, as a first step in the methanol to olefin process.<sup>181</sup> To increase the rate of this reaction increasing the density of Lewis acid sites is necessary.<sup>182</sup> For this reaction,  $\eta$ - $\text{Al}_2\text{O}_3$  is reported to be more active than  $\gamma$ - $\text{Al}_2\text{O}_3$ .<sup>148</sup>

As reported by deKlerk,<sup>183</sup> aluminas are and have been used largely in the refining of Fischer Tropsch syncrude. In particular, they are used to increase octane number through position isomerization of terminal to internal olefins, for the

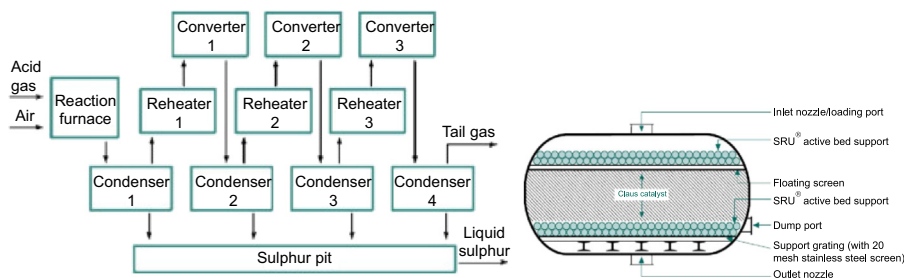


FIGURE 6.12

Flowsheet of the Claus process (left) and schematics of Claus reactors (right).

Reprinted with permission from ZareNezhad B. *J Ind Eng Chem* 2009;15(2):143–47.

iskeletal isomerization of *n*-pentene to isopentene as well as to dehydrate higher alcohols to olefins. They are also used as acid commercial catalysts of the alkylations of phenol with alcohols, such as the synthesis of *o*-cresol and 2,6-xyleneol using methanol at 300–400 °C.<sup>184</sup> Aluminas are reported to be used in the production of chloromethane from methanol and hydrogen chloride.<sup>185</sup>



All these reactions implying alcohols as reactants are mostly activated by chemisorption of the alcohol through one of its oxygen lone pairs to the Lewis sites of alumina.

Aluminas may be used for the dehydrofluorination of alkylfluorides, which are byproducts of the HF-catalyzed isobutane/butylene alkylation process. Fluoroalkanes react at 170–220 °C, being converted to olefins. HF is adsorbed on the alumina to form aluminum fluoride, regeneration being needed every 6 months.<sup>186</sup>

#### 6.4.3.3.1 Aluminas as supports of catalysts

Aluminas find very large application as supports of catalysts. In particular, they are the standard supports for many metal and sulfide catalysts. When applications requiring relatively low reaction temperature (<500 °C) are considered, such as for hydrotreating with supported sulfides (see chapter 10.2.3) or hydrogenation using platinum, palladium or nickel metals (see chapter 9) as the active phases, high surface area  $\gamma$ -,  $\delta$ - or  $\eta$ -Al<sub>2</sub>O<sub>3</sub>, can be used. Transitional aluminas are also used as supports of catalysts for partial oxidation reactions (see chapter 11.3) occurring at quite low temperatures, such as e.g., the oxychlorination of ethylene to ethylene dichloride in the process to produce vinyl chloride monomer, performed over alumina supported copper chloride at 300 °C.

These supports, however, are characterized by high acidity and reactivity, and thus not applicable when very reactive compounds are present in the reactant mixture. For this reason, less reactive and lower surface area  $\theta$ - or  $\alpha$ -Al<sub>2</sub>O<sub>3</sub> are used. This is, e.g., the case of Pd catalysts for 1,3-butadiene hydrogenation, where the oligomerization of the diene on the support has to be avoided.  $\alpha$ -Al<sub>2</sub>O<sub>3</sub> is also used as the support of silver catalysts for ethylene oxidation to ethylene oxide, where also the reactivity of the support must be limited.  $\theta$ -Al<sub>2</sub>O<sub>3</sub> is a common support for total oxidation catalysts, such as those based again on Pt and Pd, where temperatures of the order of 400–800 °C are produced. Similarly,  $\theta$ -Al<sub>2</sub>O<sub>3</sub> seems to be one of the best supports for Rh used in methane Catalytic Partial Oxidation, CPO, to syngas, a promising new process to produce hydrogen. Stabilized aluminas, such as  $\gamma$ -,  $\delta$ -,  $\eta$ - and  $\theta$ -Al<sub>2</sub>O<sub>3</sub> containing either silica or alkali, alkali-earth or rare-earth cations, such as K<sup>+</sup>, Ca<sup>2+</sup>, La<sup>3+</sup>, are largely used also for applications at medium- to high temperature. This is the case for some endothermic reactions such as steam reforming or partial oxidation reactions using nickel–platinum or rhodium catalysts.

#### 6.4.3.3.2 Other applications of aluminas

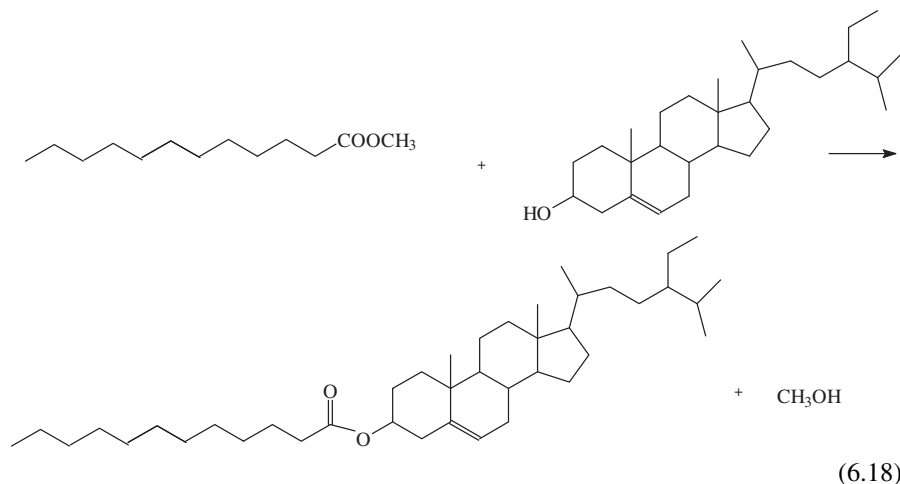
Aluminas find also a number of applications in adsorption,<sup>187</sup> as well as in the field of catalysis, as “binder” or an “active matrix”. This is in particular the case of the use

of alumina as a “separated” component of the mixture used as transport bed catalysts in the Fluid Catalytic Cracking process. In this case, in fact, the real catalyst component is based on Faujasite zeolites, usually Rare-Earth Y (REY) or Mg-HY zeolites (see Chapter 7). However, the mixture of powders used in FCC reactors contains several components, as cocatalysts, binders and active matrices. High surface-area alumina, or their precursors such as boehmites,<sup>188,189</sup> are added to the catalysts to have the role of Nickel scavenger. In fact, the feed to this process usually contain Ni-porphin compounds that deposit somewhere their Ni ions that, reduced to metal, give rise to unwanted dehydrogenating catalytic activity. Ni-porphirins tend to react specifically with alumina, where they are partially stabilized in the bivalent state, thus reducing the amount of Ni metal produced on the catalyst.

Aluminas are also the precursors for fluorided and chlorided aluminas, which may be produced *in situ* upon halogenation, as well as for silicated aluminas (see below), borated aluminas and other “modified aluminas” produced *ex situ* by chemical treatments.

#### 6.4.4 Lanthana and rare-earth oxides

Scandia and, even more, lanthanide sesquioxides like  $\text{La}_2\text{O}_3$ ,  $\text{Nd}_2\text{O}_3$  and  $\text{Eu}_2\text{O}_3$ , in agreement with their large cationic size, are reported to have significant surface basicity, revealed, e.g., by the high temperature of  $\text{CO}_2$  desorption from surface carbonates.<sup>190</sup> The basicity of lanthana allows its use as catalyst of several organic reactions such as dehydration of alcohols,<sup>191</sup> ketonization of acids,<sup>192</sup> dehydrogenation and aldolization including the synthesis of phytosterol esters<sup>193</sup> via transesterification.



$\text{Eu}_2\text{O}_3$  as such and impregnated by KF has been found to be a good catalyst for triglyceride transesterification.<sup>194</sup> Rare-earth sesquioxides, their solid solutions and their combinations with alkali-earth oxides find interesting activity for the direct decomposition of  $\text{NO}_x$ .<sup>195</sup> Similar combinations such as samaria and

neodymia with alkali-earth oxides are among the most promising systems for the oxidative coupling of methane to ethylene and ethane.<sup>196,197</sup> Lanthana and praseodymia can be used as precursors of sulfur-tolerant water-gas shift catalysts, being converted in situ to oxysulfides/oxysulfates.<sup>198</sup> Rare-earth oxides have also been proposed as catalysts for the cleanup of syngases produced by biomass gasification.<sup>199</sup> Lanthana also represents a stable and basic support for catalysts: Ni/La<sub>2</sub>O<sub>3</sub> catalysts have been recently patented for steam reforming of hydrocarbons.<sup>200</sup>

Rare-earth oxides are introduced in the FCC main catalytic component, which are faujasite zeolites of the type Y (see Chapter 7) to increase hydrothermal stability of this catalyst, possibly also with a promotion of its surface acidity. Additionally, rare earths are used as activators of a large number of catalysts as well as a structure stabilizing agent for aluminas<sup>201</sup> and other catalytic systems such as V<sub>2</sub>O<sub>5</sub>–WO<sub>3</sub>–TiO<sub>2</sub>-based catalysts for NO<sub>x</sub> Selective Catalytic Reduction by ammonia.<sup>202</sup>

## 6.4.5 Silicas

### 6.4.5.1 Preparation and solid-state chemistry of silicas

Silica, SiO<sub>2</sub>, forms many different crystalline and amorphous structures. Among them, only in stishovite, a mineral found in some meteoric rocks, Si atom takes an octahedral coordination. Stishovite, characterized by a rutile-type structure, may be prepared only at very high pressure and temperature and is considered to be thermodynamically stable only above 75 kbar. A number of different possible octahedrally coordinated post-stishovite phases may also be formed at even higher pressures, while some data are reported about a silica polymorph with pentacoordinated silicon.<sup>203</sup> All structures having practical interest present tetrahedrally coordinated silicon atom. At ambient pressure, SiO<sub>2</sub> has several major polymorphs. Those having thermodynamic stability ranges are: low-temperature trigonal  $\alpha$ -quartz up to 570 °C, high-temperature hexagonal  $\beta$ -quartz 570–870 °C, hexagonal  $\beta$ -tridymite 870–1470 °C and high-temperature cubic  $\beta$ -cristobalite 1470–1705 °C. On the other hand, forms stable at high temperature or never, may exist, as metastable phases, at room temperature. Crystalline metastable phases with zeolite-like porous structure have also been developed, usually called silicalites. The tetrahedral-based structures of the silica polymorphs are associated to quite a covalent Si–O–Si bond network<sup>204</sup> and differ only for the relative arrangements of the tetrahedra.

The numerous silica forms that are used in the field of adsorption and catalysis are usually metastable materials, most of them being amorphous. In fact, silica is the best-known glass-forming material,<sup>205</sup> i.e., it has very stable amorphous states that also consist of a tetrahedral covalent network structure, although disordered. These amorphous states are actually very stable, their sintering and crystallization, usually to cristobalite,<sup>206</sup> being fast phenomena only at temperatures of the order of >800 °C, giving rise to loss of surface area and porosity.

Amorphous silica materials are available in several different forms, depending on the morphological properties as a result of different preparation processes. One of the most relevant points relative to the preparation of silicas for catalysis is the choice of the starting material. In fact, many academic investigations start their preparations with alkoxy-silanes, which are actually very pure and very expensive, while most industrial preparations start with sodium silicate, which is in fact much less expensive and also, usually, less pure, being mostly contaminated by aluminum and iron, besides sodium. Rice husk ash can also be a cheap raw material for silicas production.<sup>81</sup>

#### 6.4.5.1.1 Precipitated silicas

Although many different recipes have been proposed, precipitated silicas are commonly produced<sup>82</sup> by partial neutralization of sodium- or potassium silicate solutions. Sulfuric acid is mostly used, mixed with sodium silicate in water, still retaining alkaline pH. Reaction is performed under stirring at 50–90 °C. The precipitate is then washed, filtered and dried. During precipitation, progressive particle growth occurs up to 4–5 nm clusters that successively agglomerate to form sponge-like aggregates. Tuning preparation procedure parameters (choice of agitation, duration of precipitation, the addition rate of reactants, their temperature and concentration, and pH of precipitation, as well as drying conditions) allows tuning of final particle size and morphology, thus surface area and porosity. Precipitates typically have a broad meso/macroporous morphology. Very high surface areas may be obtained with these procedures (up to 750 m<sup>2</sup>/g), with pore volume in the 0.4–1.7 cm<sup>3</sup>/g range and average pore diameter in the 4–35 nm range. Typical impurities of these materials are sodium ions (<0.8%) with the likely presence of iron and aluminum ions at the 500–1000 ppm level. Precipitated silica are commercially available such as the Sipernat family from Evonik and the Zeosil–Micropearl materials from Rhodia.

#### 6.4.5.1.2 Silica gels

Silica gels are usually produced<sup>83</sup> by dissolving sodium or potassium silicate (10–20% silica) into an acid, such as sulfuric acid (pH ~0.5–2). If the particles are smaller than 100 nm, they form silica sols, stabile colloidal dispersions of amorphous silicon dioxide particles that can be used e.g., as polishing agent at production of silicon surfaces in the electronic industry. A gel is formed when the molecular weight of the micelles reaches approximately 6 million, thus the hydrosol viscosity reaches the no-pour point. In a second step, the liquid is removed leaving a glass-like gel that is broken down into granules and then washed, aged and dried, with 6% volatiles and 22 Å average pore diameter.

Silica gels have pores with a wide range of diameters, typically between 5 Å and 3000 Å, and broad distributions. Silica gels synthesized with surface area as high as 800–900 m<sup>2</sup>/g, an average pore size of about 20 Å and effective pore volumes of 0.40 cm<sup>3</sup>/g, are known as narrow pore silica gels, while wide-pore silica gels are characterized by surface area ~400 m<sup>2</sup>/g, average pore size of about 110 Å and effective pore volumes of 1.20 cm<sup>3</sup>/g.<sup>207</sup>

#### 6.4.5.1.3 Silica aerogels

Aerogels, first prepared in the late 1920s by Samuel Kistler, are highly transparent materials with very high surface area ( $>1000 \text{ m}^2/\text{g}$ ) and high void volume (85–98%), prepared by supercritical drying of wet silica gels. Supercritical drying process can avoid capillary stress and associated drying shrinkage, which are usually prerequisite of obtaining aerogel structure. The conventional academic method of silica aerogel preparation is sol–gel process using organic silicon compounds, such as tetramethyl-orthosilicate (TMOS), tetraethyl-orthosilicate (TEOS) or poly-ethoxydisiloxane as precursors. Organosilanes are dissolved in a binary solution, typically water–methanol or water–ethanol, and hydrolyzed in the presence of a catalyst, frequently an acid (hydrochloric, hydrofluoric, formic, nitric, sulphuric acid). Additives may be added to modify gel porosity during ageing. Drying is performed after washing the gel with a solvent and then raising temperature and pressure to obtain supercritical conditions for the solvent ( $T > 239.5 \text{ }^\circ\text{C}$ ,  $P > 79.783 \text{ atm}$  for methanol,  $T > 241 \text{ }^\circ\text{C}$ ,  $P > 60,567 \text{ atm}$  for ethanol). In the case of low temperature supercritical drying,  $\text{CO}_2$  is used as the solvent and this allows lower temperature for supercritical drying ( $T > 31.13 \text{ }^\circ\text{C}$ ,  $P > 72.786 \text{ atm}$ ). Industrial preparations likely start from water glass, a much cheaper raw material, and may apply ambient pressure drying by solvent evaporation after previous silylation and hydrophobization of the surface. In fact, commercial aerogels may be hydrophobized, e.g., from aerogels from CABOT, mainly used for insulation and daylighting, as intermetallic dielectric materials and acoustic applications.

#### 6.4.5.1.4 Mesoporous silicas

After the work of Kresge et al.<sup>84</sup> at Mobil, and the even previous work of researchers of Toyota,<sup>85</sup> mesoporous silicas containing somehow ordered structures of well-defined channels or interconnected cavities with size from few to several nm have been developed. The preparation of these materials<sup>86,208</sup> commonly starts from silicon alkoxides hydrolysis performed in the presence of appropriate concentrations of detergent molecules acting as templates or Structure Directing Agents (SDA). With opportune reaction conditions, pores having different geometries can be obtained, see Table 6.5.

Many different materials, with different mostly mesoporous pore structure, but having sometimes also some microporosity, may be obtained by different preparation procedures and SDAs. Surface areas up to  $1500 \text{ m}^2/\text{g}$  are obtained, with well-defined mesoporosity. Such mesopores can be constituted by linear channels or interconnected cages, or even wormhole-like channels with hexagonal symmetry.<sup>209</sup> Although sometimes considered like very large pore zeolites, these materials are essentially amorphous SAs with nonstructural although sometimes ordered mesopores.

#### 6.4.5.1.5 Stöber silica and spherical silica micro/nanomaterials with hierarchical structures

Monodisperse nonporous spherical silica particles were prepared originally by W. Stöber et al., in 1968<sup>210</sup> by hydrolyzing TEOS in a mixed solution of ammonia,



**Table 6.5** A Summary of the Characteristic Properties of Various Silica Mesoporous Materials Employed for Sample Preparation

Mesoporous Materials	Precursors	Template	Space Group	Pore Size (nm)
MCM-41	TEOS, sodium silicate	CTAB, C <sub>a</sub> TMA* ( $n - 12 - 18$ )	p6mm	2–10
SBA-16	TEOS, TMOS	F127, F108, or F98	Im3m	5–30
MCF	TEOS	F127 with TMB	Cellular foam	10–50
MCM-48	TEOS, sodium silicate	CTAB, C <sub>a</sub> TMA <sup>+</sup> ( $n - 14 - 18$ ), C <sub>16</sub> H <sub>33</sub> (CH <sub>3</sub> ) <sub>2</sub> N(CH <sub>2</sub> C <sub>6</sub> H <sub>5</sub> )	la3d	2–4
SBA-15	Sodium silicate	B50-1500 (BO <sub>10</sub> EO <sub>16</sub> ), P123, P85, P65, Brij97(C <sub>18</sub> H <sub>35</sub> EO <sub>10</sub> )	p6mm	5–30
HMS	TEOS	C <sub>17</sub> H <sub>2m+1</sub> NH <sub>2</sub> ( $m - 8 - 22$ )	warm-like	2–10
FDU-12	TEOS	F127 (EO <sub>106</sub> PO <sub>70</sub> EO <sub>106</sub> )	Fm3m	4–27
PMOs	(RO) <sub>3</sub> Si-r'- Si(OR) <sub>3</sub>	CTAB, OTAB, CPB, P123, F127, Brij56, Brij76	Fm3m, Im3m, p6mm	2–15

*Ref. 209.*

alcohol and water followed by condensation of silicic acid in basic conditions and calcination at 600 °C. Depending on reaction conditions, such nonporous spherical particles have diameters mostly between 50 and 600 nm resulting in surface areas between near 100 and few m<sup>2</sup>/g.<sup>211</sup> In more recent years, silica spheres with multi-level pore structure have been obtained. Mesoporous hollow silica spheres may be prepared by different methods such as using hard templates (spherical particles of solids like polymers) and surfactants as pore structure SDAs, or using different fluids (including gas bubbles) as templating molecules.<sup>212</sup> The production of more complex materials such as core-in (hollow porous shell) spheres, multiple shell spheres and hierarchically porous spheres, with several levels of porosity present together, have also been obtained.

#### 6.4.5.1.6 Fumed or pyrogenic silicas

Fumed silicas are produced by flame hydrolysis of silicon tetrachloride, a process invented in 1942 by H. Klöpfer, a chemist at Degussa (now Evonik). This process consists in the reaction of SiCl<sub>4</sub> in a hydrogen–oxygen flame at high temperature, reported to be near 1100 °C (Degussa–Evonik) or 1800 °C (Cabot),<sup>213</sup> producing silica and hydrogen chloride. This procedure produces very small nonporous amorphous primary particles that tend to agglomerate in linear and branched chain-like structures. The surface area of these non porous materials is moderately high (100–400 m<sup>2</sup>/g) essentially depending from the particle size that ranges

5–16 nm. The weight loss by drying is quite low, 1–2.5% depending roughly on the surface area, the morphology being stable nearly up to 800 °C, when sintering starts. From the point of view of the metal content, these materials are very pure. In particular, they do not contain alkali metal impurities. Typical impurity of these materials are residual chlorine, and, to a low extent, aluminum, titanium and iron. A typical practical characteristic of these materials is the very low apparent density (down to 30 g/l) and the volatility of the particles.

#### 6.4.5.1.7 Kieselguhr

Kieselguhr, also called *diatomaceous earth* or *diatomite*,<sup>214</sup> is fossilized diatoms, a type of hard-shelled algae. It is the result of transformation of the siliceous skeleton of living diatom, constituted by microporous silica gel. Porous disk-like skeletons of the original organism, with 50–250  $\mu\text{m}$  diameter, constitute 60–95% of the powder.<sup>215</sup> Actually, the silica content of catalyst-grade kieselguhr does not exceed 83%, with the presence of small amounts of crystalline quartz,<sup>216</sup> together with iron, aluminum, calcium, magnesium and moisture. Kieselguhr is reported to have usually very high macroporosity, with total pore volume of the order of 60–70%,<sup>217</sup> pore volumes in the 0.2–1.5  $\text{cm}^3/\text{g}$  range and surface areas in the range 5–40  $\text{m}^2/\text{g}$ . However, there are several reports concerning catalyst supports constituted by high surface area kieselguhr (150–200  $\text{m}^2/\text{g}$ ),<sup>218</sup> and of industrial catalysts based on these materials, like Ni catalysts for hydrogenation (Harshaw Ni-0104T) whose total surface area is reported to be 150  $\text{m}^2/\text{g}$  with average pore radius of 37 Å.<sup>219</sup>

#### 6.4.5.1.8 Silicalites

Silicalites are fully siliceous zeolites. They are prepared with the typical preparation techniques of zeolites (see Chapter 7), using only a pure silicon source and structure directing agents. Silicalite-1 is largely the better known and most used siliceous zeolite. Its crystalline framework is constituted by Si-oxide tetrahedral structure, with the typical structural microporosity of the MFI structure zeolites. Two types of intersecting channels, both formed by 10-membered silicate rings, characterize this material. One channel type is straight and has a nearly circular opening ( $5.3 \times 5.6$  Å) along [010], while the other one is sinusoidal and has an elliptical opening ( $5.1 \times 5.5$  Å), along [100].

When prepared as a “perfect”, nondefective form, its internal surface has an essentially covalent and hydrophobic character. Only the external surface presents hydrophilicity due to the presence of silanol groups. Alternatively, silicalite may be prepared in defective forms, where silanol nests substitute for vacant silicon atoms in the framework and in the internal cavities, thus generating more hydrophilicity.

Other purely siliceous zeolite-like materials have been prepared. Silicalite-2<sup>220</sup> belongs to the framework denoted MEL, closely related to MFI, containing a two-dimensional 10-ring pore structure. Both sets of pores are straight  $5.3 \times 5.4$  Å wide. Purely siliceous zeolite BEA has also been prepared, both in the defective

and in the nondefective forms.<sup>221</sup> BEA structure has a three-dimensional intersecting channel system, two mutually perpendicular straight channels each with a cross-section of 6.6–6.7 Å, and a sinusoidal channel with a cross-section of 5.6–5.6 Å.

Also other pure silica zeolites, such as ITQ-1, the siliceous form of zeolite MWW (MCM-22),<sup>222</sup> ITQ-3,<sup>223</sup> ITQ-29, the siliceous analog of zeolite A (LTA),<sup>224</sup> and fully siliceous FER<sup>225</sup> have been prepared and characterized.

#### 6.4.5.1.9 Nonporous ceramic crystalline silica powders

Powders constituted by ceramic silica powders such as quartz and cristobalite powders are available commercially. They may be mined natural powders or produced by hydrothermal synthesis, i.e., crystal growth or reaction at high pressure and temperature in aqueous solution in sealed steel autoclaves. The resulting surface area is usually very low, <5 m<sup>2</sup>/g. They are mostly considered to be catalytically inert and thus are frequently used as diluting materials in the catalyst fixed beds. However, the possibility to use a single quartz stereoisomeric form has also been used in the field of asymmetric catalysis. Min-U-Sil<sup>226</sup> is a trade name under which ground quartz dust has been sold by different companies. The number that follows (e.g., Min-U-Sil 5) refers to the particle size of the sample (Min-U-Sil 5 is <5 μm in diameter). The purity is >99% quartz.

#### 6.4.5.2 Surface chemistry of silicas

Silica is a largely covalent oxide<sup>227,228</sup> whose surface is constituted by Si–O–Si “siloxane bridges” and Si–OH “terminal silanol” groups. Indeed the surface chemistry is dominated by the reactivity of terminal silanol groups, Si–OH. As discussed by Zhuravlev and coworkers,<sup>229,230</sup> isolated, geminal and vicinal hydrogen-bonded silanols exist on a porous silica surface. These sites may be exposed at the external surface, or be internal, at least part of them being located in molecular-size micropores of highly porous silicas. The presence of these sites is detected by using IR spectroscopy being these groups responsible for strong OH-stretching bands in the region 3750–3200 cm<sup>-1</sup> (Figure 6.13) as well as by <sup>1</sup>H NMR spectroscopy (signal centered at 1.7–2 ppm,<sup>231</sup> Figure 6.14). Silanol groups are also evident being responsible for <sup>1</sup>H-<sup>29</sup>Si CP/MAS NMR signals Q3 (due to Si atoms bonded through oxygen bridges to three other Si atoms and to an isolated OH group, at 98–102 ppm) and Q2 (due to Si atoms bonded through oxygen bridges to two other Si atoms and to two geminal OH groups, at 90–92.5 ppm), with respect to the bulk Q4 signal, observed at 105–115 ppm.<sup>232</sup>

Isolated silanol groups are responsible for very sharp IR bands (O–H stretching) evident near 3740 cm<sup>-1</sup> already after outgassing in mild conditions. This band sharpens by increasing outgassing temperature, the maximum being at the highest treatment temperature located near 3747 cm<sup>-1</sup>. The band of free silanols is clearly asymmetric, having a pronounced tail toward lower frequency more evident in the cases of highly porous samples. In practice, it seems quite evident that the band of free silanols may actually be composed of different very sharp components, one of them being located more or less at 3744 cm<sup>-1</sup>. This feature, according to

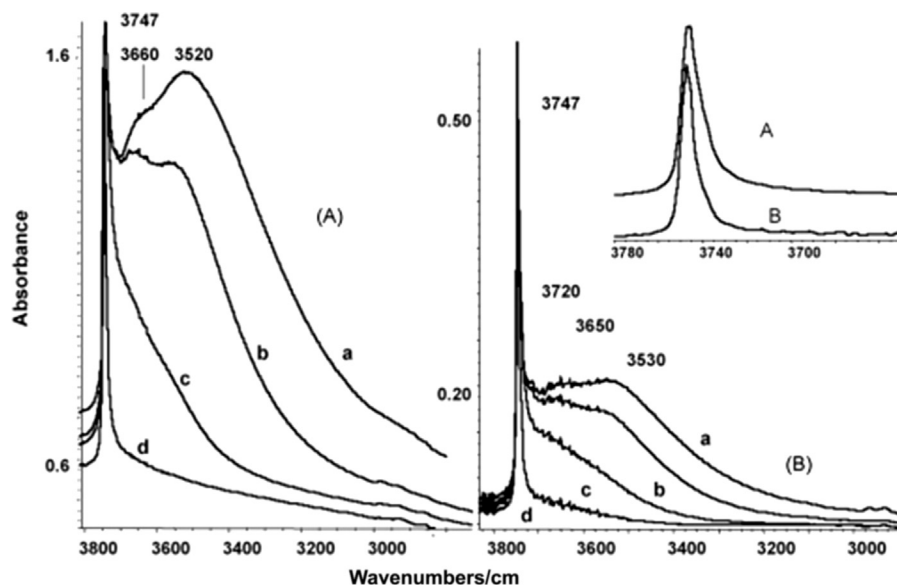


FIGURE 6.13

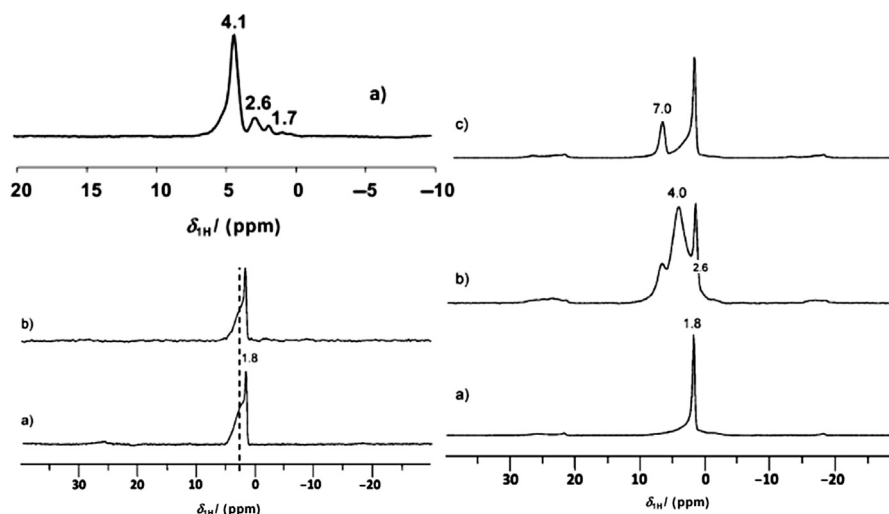
FT-IR spectra of silica gel (A) and fumed silica (B) after outgassing at 300 K (a), 473 K (b), 673 K (c) and 873 K (d). In the inset, the two samples outgassed at 873 K, enlarged.

Reprinted with permission from Bevilacqua M, et al. *Catal Today* 2006;116:132–42.

previous studies,<sup>233,234</sup> could be due to the geminal silanols, which are hardly distinguished from isolated silanols in the IR spectra.

On the other hand, probing the free surface silanols with adsorbed molecules of different sizes<sup>235</sup> indicates that part of the tail is due to silanol groups located in small nanopores having molecular size, thus not accessible to large molecules. The slightly lower OH frequency (c.  $3700\text{ cm}^{-1}$ ) show that these components are associated to free silanol groups very slightly perturbed for some kind of weak interaction. Gallas et al.<sup>236</sup> showed on precipitated silicas OH groups partially inaccessible to D-exchange and to interaction with alcohols, whose accessibility depends inversely on alcohol size.

Two other broad features are usually present in the IR spectra of silicas, recorded after outgassing at mild temperature, at  $3520\text{--}3530\text{ cm}^{-1}$  and at  $3650\text{--}3660\text{ cm}^{-1}$  (Figure 6.13). They correspond to a broader component above 2.2 ppm in the  $^1\text{H}$  MAS NMR spectra (Figure 6.14). They have been assigned to clusters of vicinal H-bonded silanols,<sup>237</sup> which at least in part condense at high temperature, giving rise to siloxane bridges. In fact, their condensations do not contribute significantly to the increase of the band of free silanols.<sup>238</sup> In the case of microporous silica samples, these absorptions are stronger (relative to the band of the free silanols) than in the case of nonporous or less porous powders like fumed silica<sup>239,240</sup> (Figure 6.13).



**FIGURE 6.14**

$^1\text{H}$  MAS NMR spectra of ferrierite zeolite (left up, a), silica (left down activated (a) and after adsorption of ammonia and outgassing, showing complete ammonia desorption (b); and of silica-alumina (right) activated (a), in contact with ammonia (b) and after further outgassing (c).

Reprinted with permission from Marthala VRR, Hunger M, Kettner F, Krautscheid H, Chmelik C, Kärger J, et al. *Chem Mater* 2011;**23**(10):2521–28 and from Refs. 231 and 395.

IR and NMR techniques revealed the presence of silanol groups not only on high surface-area silicas, but also on lower surface area materials such as kieselguhr,<sup>241</sup> quartz, cristobalite and tridimite powders.<sup>232,242–244</sup> The role of nature and structure of surface sites in the biological response to silica particles is still matter of study. The effect of surface hydroxyls and of metal impurities has been proposed.<sup>244</sup> Influence of size, surface area and microporosity have been investigated. It is becoming clear that crystallinity is not a requirement for cytotoxicity, which can be observed also for amorphous silica particles.<sup>245</sup>

Hydrophilic, free silanols are well evident only in the IR spectra of Silicalite-1, characterized by a strong band in the region with the main maximum at  $3730\text{--}3740\text{ cm}^{-1}$ , i.e., at slightly but distinctly lower frequency than for amorphous silica. IR studies of adsorbed probe molecules indicate that the acidity of such hydroxyl groups is comparable with that of silica's silanols,<sup>239,246–248</sup> i.e., weak. A debate was done concerning the location of free silanols on the external surface<sup>249</sup> or in the cavities of silicalite,<sup>250</sup> or both.<sup>246,251,252</sup> Our data<sup>235,248</sup> suggested that, in spite of the anomalously low OH-stretching frequency, almost all silanol groups absorbing at  $3680\text{--}3750\text{ cm}^{-1}$  are indeed exposed at the external surface. Only an extremely small fraction of these groups is not perturbed by large molecular probes, thus being located in some internal structural defect.

Additionally, the spectra of silicalite show a broad absorption at lower frequency (3500–3550  $\text{cm}^{-1}$ ) which is very strong at 3200–3500  $\text{cm}^{-1}$ , for “defective” silicalite samples. The shape and position indicate that it is due to H-bonded silanols. The current opinion is that this absorption is due to silanol nests associated with defects in the crystal lattice<sup>246,252–255</sup> and thus mostly internal to the zeolite cavities. This absorption falls at distinctly lower frequencies and shapes with respect to those of hydrogen-bonded silanols on amorphous silicas showing that such interactions are stronger in the particular structures constituting defects in the internal surface of silicalite.

Silanol groups are very weakly Brønsted acidic as shown by the adsorption of basic molecular probes,<sup>256</sup> but represent the active sites in the adsorption<sup>257</sup> of both polar molecules such as water, giving rise to  $\Delta H_{\text{ads}} \sim -50$  kJ/mol, and of nonpolar molecules such as hydrocarbons, with which hydrogen bonding of moderate strength may occur (<10 kJ/mol). Protonation of strong basic molecules like ammonia can be observed by IR spectroscopy at room temperature but is reversed by simple outgassing. This shows that the Brønsted acidity of silanol groups is definitely weak but nonnegligible. In fact, adsorption energy of ammonia on silicas may give rise to evolution of 150–230 kJ/mol.<sup>258</sup> The reactivity and the toxicity of silica has been associated to the density of surface silanol groups,<sup>259</sup> in particular with the density of geminal silanols, more than that of isolated silanols.<sup>260</sup>

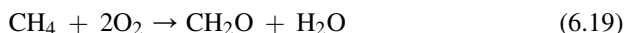
According to the covalency of the Si–O bonds, no coordinately unsaturated silicon and oxide species exist at the surface of silica in usual conditions. In fact, coordinative insaturation is actually saturated by hydroxyl groups producing silanol species. Thus, silicon atoms are not Lewis acidic and, correspondingly, basicity of oxygen species is negligible. Only at high-temperature surface siloxane bonds, Si–O–Si, appear to become reactive.<sup>238</sup>

The inertness of crystalline ceramic silica powders, such as quartz and cristobalite, is mostly associated to their surface area, which is usually not higher than 5  $\text{m}^2/\text{g}$ .

### 6.4.5.3 Silicas as catalysts

Amorphous silica, which has dozens of industrial applications as an adsorbent and a filler, does not seem to have real industrial application as a catalyst, but is very largely used as a support for catalysts and as a binder.

Even if silicas have been usually considered to be quite inert in catalysis, several studies report catalytic activity of silicas in oxidation reactions, in particular in the partial oxidation of methane (MPO) to formaldehyde.

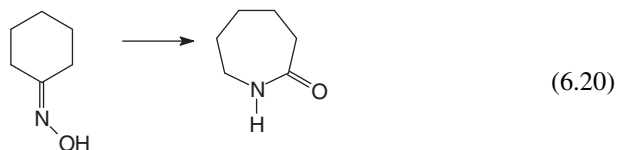


The group of Parmaliana reported data showing that the performance of the silica surface in MPO, performed at 650 °C in the presence of oxygen, is controlled by the preparation method namely for several commercial silica catalysts the following has been disclosed based on the preparation method: precipitation > sol–gel > pyrolysis.

The activity of such silica catalysts has been correlated with both the concentration of strained siloxane bridges and density of surface reduced sites stabilized in steady-state conditions. Actually, small amounts of transition metal ions such as ferric ion on silica<sup>261</sup> seem to increase catalytic activity, and thus this activity could be attributed to impurities of iron on silica. However, the catalytic activity of virtually pure silica was confirmed more recently by Ono et al.,<sup>262</sup> who showed that the addition of another unreducible cation,  $\text{Al}^{3+}$ , can further improve activity in methane partial oxidation. In any case, catalytic performances are too weak for industrial exploitation.

The use of “pure” silica as a catalyst for some “fine chemical” reactions occurring in liquid phase has been recently emphasized.<sup>263</sup>

Defective silicalite-1 has an important industrial application as an acid catalyst in the vapor phase Beckmann rearrangement of cyclohexanone oxime to  $\epsilon$ -caprolactam with the SUMITOMO process,<sup>264,265</sup> occurring near 300 °C.



The active sites for this reaction, which is also catalyzed by siliceous beta zeolite<sup>221</sup> and, less efficiently, by amorphous silica, are thought to be external and/or internal silanol nests.

#### 6.4.5.4 Silicas as support of catalysts

Silicas find a large industrial application as the support of catalysts. This is due, among other reasons, to its good mechanical and thermal stabilities, and ease of scalability. Among the most relevant application, we can mention the catalysts for the oxidation of  $\text{SO}_2$  to  $\text{SO}_3$ , performed at 400–550 °C with air as an oxidizing agent (chapter 11.2.3.4). This is the key step in the production process of sulfuric acid. Industrial catalysts are based on  $\text{V}_2\text{O}_5/\text{SiO}_2$  but also contain an alkali sulfate, i.e.,  $\text{K}_2\text{SO}_4$  or  $\text{Cs}_2\text{SO}_4$ , the latter being the most active.



The catalyst is essentially constituted by a porous silica carrier containing 5–10%  $\text{V}_2\text{O}_5$  and 10–25% of alkali oxide,<sup>266,267</sup> which actually converts into the sulfate in the reaction. During the reaction, the active species are actually in the liquid phase embedded in the silica support. Porous silicas are used as supports, such as silica gels or kieselguhr. Silica gels tend to sinter during reaction.

As said, kieselguhr is the support of solid phosphoric acid, a relevant acid material which will be described in Chapter 8. Kieselguhr-supported Ni catalysts have also been described in the literature for the hydrogenation of acetylenics and of benzene.<sup>219</sup> Although the most common support of metals for hydrogenation of hydrocarbons is alumina, silica is used in several cases. As for example, the hydrogenation of

acetylene to destroy it in C2 cuts is normally performed with Pd/Al<sub>2</sub>O<sub>3</sub> catalysts, but to perform the same reaction to destroy acetylene in the HCl recycle of the vinyl chloride process, Pd/SiO<sub>2</sub> is preferred (Noblyst<sup>®</sup> E 39H from Evonik).<sup>268</sup>

Ni and copper catalysts supported on silica are largely used for hydrogenation. In most cases, indeed, the amount of silica is very small, being thus more a stabilizer than a support. As for example, 3% CuO, 68% NiO/SiO<sub>2</sub> is applied to oxo-aldehydes hydrogenation processes to oxo-alcohols (SC). 60% NiO/SiO<sub>2</sub> (NiSAT<sup>®</sup> 320) are used for slurry application in the hydrogenation of nitro-compounds to anilines,<sup>269</sup> while similar catalysts from the same family (NISAT from Süd Chemie) are applied for benzene hydrogenation to cyclohexane, and nitriles hydrogenation to amines. Cu/SiO<sub>2</sub> and Cu–Cr/SiO<sub>2</sub> are used for both hydrogenation of carbonyls and dehydrogenations of alcohols.<sup>270</sup>

Silica-supported metal catalysts are also used for selective oxidation, such as the Pd/Au/SiO<sub>2</sub> catalyst for the synthesis of vinylacetate monomer from ethylene (Noblyst<sup>®</sup> EJK 3017).<sup>270</sup>



Evonik sells the Aerolyst<sup>®</sup> 3xxx series of materials constituted by formed pyrogenic silica with very high purity to be applied as catalyst supports in fixed bed applications or catalysts. They combine a narrow pore size distribution (with no micropores), a high pore volume and excellent strength and attrition properties.<sup>271</sup>

### 6.4.6 Titanias

Titania, titanium dioxide, exists in nature as four different polymorphs: rutile, anatase, brookite (see Figure 6.11) and TiO<sub>2</sub> (B). They are built by arrangement of the same octahedral structural units [TiO<sub>6</sub>], connected differently by corners and edges. In the case of rutile, anatase and brookite<sup>272</sup> oxygen is coordinated to three titanium atoms. In rutile and anatase, this coordination is such that all atoms lie in a planar unit (oxygen site symmetry), while in brookite possesses two inequivalent oxygen sites that are both slightly distorted from the plane. In TiO<sub>2</sub> (B), four distinct O sites exist that vary in their coordination as follows: (1) atoms with nearly linear 2-fold coordination, (2) atoms with tetrahedral 4-fold coordination, (3) atoms with planar 3-fold coordination parallel to the ac-plane, and (4) atoms with planar 3-fold coordination parallel to the ab-plane.

The different semiconducting behavior is one of the most relevant differences between these solids, caused by the different gap energies, which are 3.0 eV for rutile, 3.2–3.4 eV for anatase due to optical gaps, while for brookite, different data are reported but 3.3 eV seems to be the most reliable. Rutile is always the thermodynamically stable structure, and thus anatase transforms exothermally to rutile at 500–1000 °C, the smaller the crystal size the lower the transition temperature. However, for very small nanoparticles, the surface free energy becomes also a relevant factor and anatase nanoparticles could be more stable than rutile nanoparticles (see chapter 6.1.6).



The anatase-to-rutile phase transition, usually limiting the stability of anatase-based catalysts, is strongly influenced by species deposited on the anatase surface. While vanadia and copper oxide tend to favor the transition, silica, tungsta and molybdena it, allowing the prolonged use of anatase catalyst at quite high temperatures. Brookite too tends to transform into rutile above 500 °C, while it may also transform into anatase.

Titania is produced industrially mostly as a white pigment, starting from the main minerals, which are rutile,  $\text{TiO}_2$  and ilmenite,  $\text{FeTiO}_3$ , the latter being predominant. Three main ways are reported in the literature for the preparation of titania powders: the sulfate process, the chloride process and the flame hydrolysis process. In the sulfate process, ilmenite is digested with sulfuric acid producing a solution of iron and titanyl sulfates.<sup>273</sup> Cooling of the solution allows the precipitation of ferrous sulfate heptahydrate. Careful hydrolysis with anatase seeds gives rise to a Ti rich precipitate that, after calcination at  $<850$  °C, gives rise to  $>98\%$  anatase. From this way high surface-area anatase samples may be obtained ( $<300$   $\text{m}^2/\text{g}$ ) that, however, are highly impure of sulfate species that give rise to high surface acidity. By increasing calcination temperature, sulfate species tend to decompose but the surface area tends to decrease and anatase to rutile transformation may occur. By seeding with rutile and calcination at  $900\text{--}930$  °C, rutile powder with medium-low surface area may be obtained from the same precipitate.

Indeed, the synthesis of anatase and rutile in aqueous medium may be considered to be a two-step process, with the production of amorphous hydrous titania, and, later, crystallization of either rutile or anatase. Formation of rutile is favored in strongly acidic solutions, while anatase is produced in less acidic or even neutral or slightly basic conditions. The crystal shape is also somehow dependent on the pH.<sup>274</sup> From acidic slurries, polytitanic acids,  $\text{H}_2\text{Ti}_n\text{O}_{2n+1}$  ( $n = 2, 3, \text{ and } 4$ ), which are layered isopoly acids, composed of  $[\text{TiO}_6]$  octahedra may also be crystallized.<sup>275</sup> These interesting materials can also be prepared in the form of nanotubes.<sup>276,277</sup> Brookite is more difficult to prepare than anatase and rutile.

The chloride process usually starts from rutile mineral or even from titanium slag ( $72\text{--}87\%$   $\text{TiO}_2$ ) arising from the siderurgic process based on oxidation of ilmenite to pseudoilmenite ( $\text{Fe}_2\text{O}_3\text{--TiO}_2$ ) followed by its reduction to iron. The  $\text{TiO}_2$ -based solid is converted into gaseous  $\text{TiCl}_4$  by reaction with chlorine and carbon at  $900\text{--}940$  °C. After condensation, highly pure  $\text{TiCl}_4$  is obtained, which is also the raw material for Ti metal production.  $\text{TiCl}_4$  is converted back to pure rutile by oxidation at  $>900$  °C. The flame hydrolysis process developed by Degussa (Evonik) implies the flame hydrolysis, i.e., the reaction of the chloride with water in a  $\text{H}_2/\text{O}_2$  flame giving rise to a product that is usually 80% anatase, with medium surface area ( $50$   $\text{m}^2/\text{g}$ ). More recent development allows the production of almost pure anatase with  $90$   $\text{m}^2/\text{g}$  using this route.

As it is well known, titanias are the most active and common photocatalysts.<sup>278</sup> To improve photocatalytic activity, attempts have been recently done to obtain very high surface-area titania samples, in particular of the anatase type. A number of different soft chemistry techniques have been applied to develop high surface-area

mesoporous nanoparticles<sup>279,280</sup> for this purpose, such as sol–gel techniques mostly starting from titanium alkoxides,<sup>281</sup> hydro-thermal, solvo-thermal, sonochemical, microwave and electrodeposition methods. Using sophisticated chemical techniques, a number of very interesting particle morphology have been obtained such as nanosheets, nanowires, nanoribbons and nanotubes.<sup>282,283</sup> Not always, however, these materials are characterized by high surface area and higher photocatalytic activity than conventionally prepared or commercial titanias.

Using tetrabutyl titanate ( $\text{Ti}(\text{OC}_4\text{H}_9)_4$ , TBOT) as precursor by a simple spray-hydrolytic method at 90 °C, Zhu et al.<sup>284</sup> produced mesoporous nanospheres of anatase with  $>600 \text{ m}^2/\text{g}$ . By calcining at 400 °C however, surface area drops to  $88 \text{ m}^2/\text{g}$ .

Using an alkoxide sol–gel method employing a water-immiscible room temperature ionic liquid (1-butyl-3-methylimidazolium hexafluorophosphate, [bmim][PF<sub>6</sub>]) as a new solvent medium and further modified with nonionic surfactant (polyoxyethylenesorbitan monooleate) as a pore templating material<sup>285</sup> Choi et al. prepared nanocrystalline anatase with up to  $573 \text{ m}^2/\text{g}$  which appear to retain up to  $215 \text{ m}^2/\text{g}$  after calcination at 500 °C.

According to the recent data of Ribbens et al.,<sup>286</sup> most titania photocatalysts are constituted by pure  $\text{TiO}_2$  retaining at most  $150 \text{ m}^2/\text{g}$  after calcination at 450 °C, independent from the original surface area. Impurities, such as sodium ions, favor higher surface thermal stability but may affect seriously photocatalytic activity and surface acido-basicity.

In recent years, soft chemistry direct routes to high surface area rutile ( $300 \text{ m}^2/\text{g}$ ) have been developed. Self-hydrolysis of  $\text{TiOCl}_2$  with sodium dodecyl sulfate addition allows to produce rutile powders with  $340 \text{ m}^2/\text{g}$ , surface area, that is reduced to near  $100 \text{ m}^2/\text{g}$  by calcining at 400 °C.<sup>287</sup> Soft chemistry direct routes to high surface-area pure brookite have also been developed<sup>288</sup> and proposed as an efficient photocatalyst.

Rutile is generally assumed to be less useful, both in the catalysis and in the photocatalysis fields, than anatase. However, it is still not fully clear whether this is related to the intrinsic properties of rutile or to the usually low surface area of rutile, which is mainly produced at high temperature.

#### 6.4.6.1 Surface chemistry of titanias

Also titanias are highly ionic oxides with medium–high Lewis acidity, significant basicity and weak Brønsted acidity, if at all. The surface hydroxy groups of  $\text{TiO}_2$  polymorphs anatase and rutile have been the object of several IR studies. Anatase shows a more complex spectrum with a complex OH-stretching band above  $3700 \text{ cm}^{-1}$ , not found for rutile.<sup>289</sup> Characterization data show that on anatase stronger Lewis acid sites are usually detectable than on rutile.<sup>289,290</sup>

Recent data have been related to different morphologies of titania anatase. It has been shown that (100), (001), (101) and (110) cleavage planes predominate, thus justifying morphology-dependent IR features.<sup>291</sup> The most stable, thus expected the less active, face is (101).

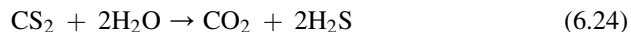
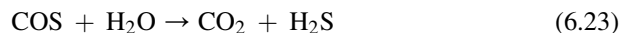
Studies also show that different anatase nanostructured powders (nanotubes, nanofibers and nanoparticles) bring about significant variations in the surface physicochemical properties. According to Toledo–Antonio et al.,<sup>292</sup> nanotubes and nanofibers do not expose coordinatively unsaturated  $\text{Ti}^{4+}$  or basic  $\text{O}^{2-}$  sites, which occur on nanoparticles. On the other hand, lutidine and pyridine adsorption indicate that Ti–OH groups are 2.25 times more populated in nanotubes than in nanoparticles. The greater accessibility to this OH groups is likely derived from the particular topography of the nanotubes, e.g., a greater number of curved surfaces.

Successful attempts to prepare highly photocatalytically active anatase particles with predominant high energy (001) faces have been reported.<sup>293</sup>

Rutile particles are frequently in the form of nanorods with preferential orientation along the [001] direction.<sup>274,294</sup>

#### 6.4.6.2 Titania as a catalyst

As a catalyst, titania finds relevant application in the Claus process for the catalytic steps of the Claus process, the production of sulfur from  $\text{H}_2\text{S}$  in the refineries,<sup>177</sup> as an alternative to alumina (see Figure 6.12 and Chapter 6.4.2.4). In particular, titania is used for the first higher temperature bed where hydrolysis of COS and  $\text{CS}_2$  is also performed at ca 300 °C.<sup>295</sup>



In fact, titania is more active than alumina for both the Claus reaction and the above hydrolysis reactions although alumina is preferred for its robustness in the successive beds. Titanias for the Claus process are anatase 100%, 120  $\text{m}^2/\text{g}$  with loss on ignition of 1.5–2% wt/wt.<sup>178</sup>

As said, titania-anatase is also the basic component of most photocatalysts.

#### 6.4.6.3 Titania as support for catalysts

Medium-to-high surface area anatase is largely used as support of catalysts. The instability of anatase toward phase transformation into rutile does not allow its use for high-temperature reactions. In case of reaction temperatures  $\sim 300$ – $400$  °C normal high-area anatase may be used, in particular when anatase-stabilizing components (such as silicate, molybdate, wolframate species or alkali or rare-earth ions) are also present. Mesoporous very high surface-area anatase may offer good opportunity for relatively low-temperature reactions such as, e.g., low-temperature CO oxidation over titania-supported noble metals.

One of the most important applications of anatase in the field of heterogeneous catalysis is as the support for vanadia-tungsta and vanadia-molybdena catalysts for the Selective Catalytic Reduction of  $\text{NO}_x$ ,<sup>296</sup> using ammonia as the reductant,<sup>297</sup> both in its stationary version and in its automotive version (see Chapter 11).

Another relevant field of application of titania-anatase as a catalyst support is on oxide catalyst, in particular vanadia, for selective partial oxidations of organic, such as the oxidation of *o*-xylene to phthalic anhydride. Similar catalysts are used for other oxidation and ammoxidation reactions to produce aromatic aldehydes, acids and nitriles.

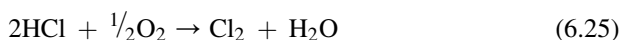
Titania has also been considered, as such or mixed with alumina, as the support of sulphided hydrodesulfurization catalysts, with superior activity, but also in this case the robustness of alumina was finally considered a key factor for its preferred practical utilization.<sup>298</sup>

Titania has also been deeply investigated as the support for metals. In this case, a particular effect has been object of many studies, such as the so-called SMSI effect (Strong Metal Support Interaction), occurring when transition metal oxides are used as supports under reducing conditions and at elevated temperatures. When the platinum metals are supported on titania and reduced in hydrogen at 500 °C, they lose most of their ability to chemisorb hydrogen and carbon monoxide, and for certain reactions they also lose much of their catalytic activity. However, methanation activity is strongly enhanced. Also the activity in a number of other reactions, such as the hydrogenation of several oxygenated organics (acetone, crotonaldehyde, cinnamaldehyde, acetophenone, benzaldehyde, phenyl acetaldehyde, citral and acetic acid) is increased. For molecules where a carbon-carbon double bond is also present in addition to the carbonyl bond (crotonaldehyde, citral, cinnamaldehyde) a higher selectivity toward the hydrogenation of the C=O bond is obtained, enabling the synthesis of industrially important unsaturated alcohols in high yield.

SMSI effect induced over Pt/TiO<sub>2</sub> catalysts is suggested to be originating from (1) the formation of a Pt-Ti alloy; (2), insertion of Pt atoms into oxygen vacancies on the TiO<sub>2</sub> surface; (3) the formation of Pt atoms—Ti<sup>3+</sup> cations bonds; and (4) electron transfer from Ti<sup>3+</sup> to Pt atoms by spontaneous alignment of their Fermi levels.

Titania, in the form of anatase, likely due to its slight reducibility and semiconducting behavior, is one of the best options for activating metal catalysts for low-temperature reactions. In particular, Pt/TiO<sub>2</sub> and Au/TiO<sub>2</sub> have interesting activity for low-temperature water gas shift, Au/TiO<sub>2</sub> catalysts are patented for low-temperature CO oxidation in the purification step of hydrogen and have interesting catalytic activity for low-temperature water-gas shift, while Au-Pd bimetallic catalysts are promising combinations for the direct synthesis of hydrogen peroxide from hydrogen and oxygen, and as the direct synthesis of propene oxide from propene and oxygen.<sup>299</sup>

Rutile titania seems to have less interest as catalyst support. However, it is a stable phase thus allowing higher temperature applications. Sumitomo Chemicals brought a TiO<sub>2</sub> (rutile)-supported RuO<sub>2</sub> catalyst to market for the catalytic oxidation of hydrogen chloride to chlorine,

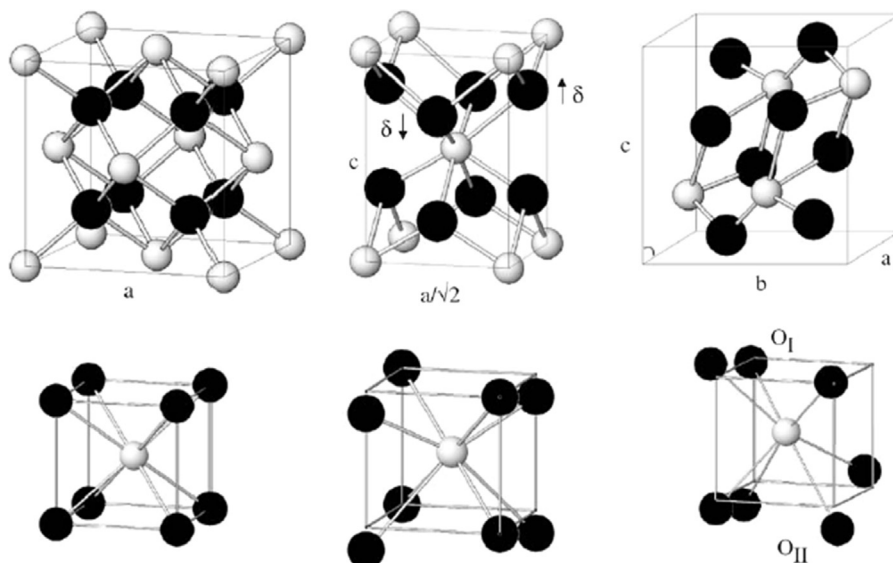


which was optimized for use in a fixed-bed tube bundle reactor.<sup>300</sup>

### 6.4.7 Zirconias

Zirconia presents three structures that are thermodynamically stable in three different temperature ranges (Figure 6.15). Monoclinic zirconia (baddeleyite, space group  $P2_1/c$ ) is the room-temperature form, tetragonal zirconia (space group  $P4_2/nmc$ ) is stable above  $\sim 1170^\circ\text{C}$  while cubic zirconia (space group  $Fm\bar{3}m$ ) is stable above  $\sim 2370^\circ\text{C}$ . Tetragonal and cubic zirconia, however, may exist as metastable forms at room temperature, mostly if stabilized by dopants such as yttrium. Frequently, zirconia powders as prepared are mixed tetragonal and monoclinic.<sup>301</sup>

The orthosilicate mineral called zircon,  $\text{ZrSiO}_4$ , is usually at the origin of all zirconium compounds. In a most used process, zircon is melted with caustic soda at  $650^\circ\text{C}$  to produce sodium zirconate,  $\text{Na}_2\text{ZrO}_3$  and sodium metasilicate. Sodium zirconate is then treated with hydrochloric acid to produce zirconyl chloride,  $\text{ZrOCl}_2$ , from which all other Zr compounds are produced. An alternative treatment with water allows to separate insoluble hydrous zirconia.<sup>34</sup>



**FIGURE 6.15**

Atomic structure (top) and Zr to O coordination units (bottom) for the three low-pressure polymorphs of  $\text{ZrO}_2$ : cubic (fluorite structure, left), tetragonal (middle) and monoclinic (baddeleyite, right). Large dark circles denote O atoms, small light circles, Zr. The depicted cubes are a guide to the eye, and their size corresponds in all cases to the cubic unit cell (top row) or coordination unit (bottom row). The lattice parameters of each structure and the two nonequivalent O sites at m- $\text{ZrO}_2$  are indicated.

*Reprinted with permission from Muñoz MC, Gallego S, Beltrán JI, Cerdá J. Adhesion at metal– $\text{ZrO}_2$  interfaces. Surf Sci Rep September 2006;61(7):303–44.*

To obtain high surface area (70–300 m<sup>2</sup>/g) hydrothermally-stable zirconia supports or catalysts, Zr<sup>4+</sup> or zirconyl ZrO<sup>2+</sup> salts compounds such as ZrCl<sub>4</sub>, ZrOCl<sub>2</sub>, ZrO(NO<sub>3</sub>)<sub>2</sub> or ZrO(CH<sub>3</sub>COO)<sub>2</sub> are dissolved in water and aged either in basic or in acidic conditions. Amorphous hydrous zirconia precipitates at 80–120 °C may have a surface area as high as 400–600 m<sup>2</sup>/g. Depending on the pH of precipitation, the composition of the starting solution and the details of drying and calcination procedure, either monoclinic or tetragonal zirconia, or most frequently a mixture of them is obtained.

Carter et al.<sup>302,303</sup> described an industrial process to produce zirconia from zirconyl chloride: precipitation from ZrOCl<sub>2</sub> water solution was conducted as a continuous double-jet injection that overflowed into an alcohol bath. The overflow product was filtered using a Büchner funnel and subsequently washed using a mixture of methanol, ethanol and water. Washed filtered cake was then dried in an oven at 55 °C for 5 days and subject to different calcination procedures.

According to a recent patent,<sup>304</sup> zirconium hydroxide or hydrated zirconia precipitate can be produced by first aging of zirconium compounds in the presence of a polyacid promoter (sulfuric, phosphoric, silicic, chromic, molybdic and wolframic acids) at pH 0.01–4, then neutralizing or basifying with bases (soda, potash, ammonia, urea, amines) at pH 7.5–9.5. After calcination at 300–1000 °C, zirconia is obtained constituted either of pure tetragonal phase or tetragonal–monoclinic phase mixtures depending on amount of stabilizing agent and calcination temperature.

In another recent patent,<sup>305</sup> details are reported for the preparation of an amorphous zirconia that, after calcination at 500–900 °C or spray drying, gives rise to pure tetragonal zirconia with surface areas ranging from 280 to 70 m<sup>2</sup>/g. Being the tetragonal phase metastable below ~1170 °C, calcination of tetragonal zirconia at 400–1150 °C produces monoclinic zirconia, but this occurs with a drop of surface area. The direct production of high-surface area monoclinic zirconia seems more difficult. A possible reason for this, according to Zhang et al.<sup>25</sup> may be that the lower surface energy of tetragonal phase results in the stability of tetragonal structure at room temperature for small particles, while tetragonal phase is normally stable at high temperature for coarse ceramics. Guo and Chen<sup>306</sup> described a method to produce nearly purely monoclinic zirconia with 75 m<sup>2</sup>/g SA starting from zirconyl chloride precipitation and calcination at 350 °C. In fact, high surface-area commercial preparations (>100 m<sup>2</sup>/g) are mostly mixtures of tetragonal and monoclinic zirconia, while powders purely or predominantly constituted by the monoclinic phase usually do not exceed 85 m<sup>2</sup>/g of surface area.

Recently, attempts have been devoted to the synthesis of mesoporous zirconias, with large surface areas and, together, crystalline pore walls. This has been performed with conventional soft-templating approaches. These materials, however, present low crystallinity and lose mesoporosity by calcination at temperatures higher than 400 °C.

The combination of soft-templating and solid–liquid method reported by Che et al.<sup>307</sup> allowed to prepare zirconia, which after calcination at 600 °C possesses a

wormlike arrangement of mesopores surrounded by tetragonal  $\text{ZrO}_2$ , nanocrystallites of c. 2.3 nm, surface area of  $255 \text{ m}^2/\text{g}$  and pore size c. 4.3 nm.

Zirconia is a largely ionic oxide, characterized by a quite large size of the  $\text{Zr}^{4+}$  cation. Thus, it is characterized by medium Lewis acidity, significant surface basicity and very low Brønsted acidity, if at all. The basicity of zirconia is quite evident due to the difficulty in activating its surfaces, where carbon dioxide is usually strongly adsorbed in the form of surface carbonates. Such carbonates are desorbing only at quite a high temperature ( $500^\circ\text{C}$ ). CO adsorption experiments<sup>308</sup> provide evidence for two slightly different types of Lewis acidic  $\text{Zr}^{4+}$  ions on both monoclinic and tetragonal zirconia. On the other hand, the quality of the sites is very similar in the two phases, but little stronger sites exist on the tetragonal phase. Slightly different concentrations of Lewis sites can be found on the two solids, depending on outgassing temperature.  $\text{CO}_2$  adsorption studies reveal significant basicity. The surface hydroxy groups of  $\text{ZrO}_2$  polymorphs, tetragonal and monoclinic, have also been the object of several studies.<sup>309</sup> A doublet near  $3770$  and  $3670 \text{ cm}^{-1}$  is typically found at the surface of monoclinic zirconia. For tetragonal zirconia a main band is usually found between  $3690$  and  $3660 \text{ cm}^{-1}$ , with additional weaker components.

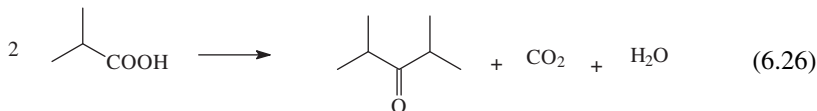
Partially Stabilized Zirconia (PSZ) consists of zirconia mixed with amounts larger than 8 mol% (2.77 wt%) of MgO, 8 mol% (3.81 wt%) of CaO, or 3–4 mol% (5.4–7.1 wt%) of  $\text{Y}_2\text{O}_3$ , or even by  $\text{CeO}_2$  and  $\text{Sc}_2\text{O}_3$ . Y-TZP (Yttria Tetragonal Zirconia Polycrystal) zirconia powder is a specialty material for structural ceramic applications. Y-TZP ceramics are nearly 100% tetragonal, generally produced by alloying zirconia with c. 3% yttria. Similar zirconia compositions based on alloying with ceria have become commercially available and considered superior to  $\text{Y}_2\text{O}_3$ -doped TZP particularly for applications in low-temperature humid environments. Mg partially stabilized zirconia (Mg PSZ), with approximately 10% MgO, have also very high strength, hardness and particularly toughness.

Fully stabilized cubic ceramic powders, mostly yttria-stabilized zirconia (YSZ), with 8%  $\text{Y}_2\text{O}_3$ , are available commercially also with significant surface area ( $50 \text{ m}^2/\text{g}$ ). These materials find relevant industrial application due to their oxide ion-conducting properties. They are in fact the solid electrolytes used in Solid Oxide Fuel Cells as well as in oxygen sensors devices such as the  $\lambda$ -sensor used in the electronic system for the management of catalytic converters of gasoline-fuelled cars.

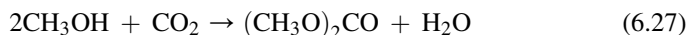
#### 6.4.7.1 Zirconia as a catalyst

Pure zirconia or zirconia doped with alkali or alkali-earth cations is applied industrially for some alcohol dehydration and dehydrogenation reaction in the fine chemicals field,<sup>48</sup> as well as for ketonization of carboxylic acids,<sup>310</sup> an industrial process for the synthesis of several ketones. This reaction is carried out at  $T > 350^\circ\text{C}$  over basic materials such as alkali-doped titania and zirconia as well as thorium oxide.<sup>48</sup> As for example, 3-pentanone can be produced by catalytic ketonization of propionic acid over a solid oxide catalyst at  $350\text{--}380^\circ\text{C}$ .

Production of 2,4-dimethyl-3-pentanone is preferably obtained by ketonization of isobutyric acid over a thorium oxide or zirconium oxide catalyst at 430 °C.



Zirconia-based catalysts are reported to be the most promising for the direct synthesis of dimethylcarbonate from methanol and CO<sub>2</sub>



a novel way to produce this important compound.<sup>311</sup>

The synthesis of light mercaptans such as methyl mercaptan (methanethiol) and ethylmercaptan is obtained by the reaction of the alcohol with H<sub>2</sub>S over alkali/alkaline earth-promoted alumina or zirconia catalysts at 300–400 °C.<sup>312</sup>



Zirconia is also reported to act as a hydrogenation catalyst. Mainly if doped by other components improving basicity, such as lanthana and ceria, it is the best catalyst for the so-called “isosynthesis” process, i.e., the production of small branched hydrocarbons (mainly isobutane) from syngas.<sup>313</sup> This reaction is performed over zirconia or thoria based catalysts at  $T > 400$  °C at 30–60 MPa. Stabilized zirconia is also used industrially as the catalyst for hydrogenation of carboxylic acids to the corresponding aldehydes.<sup>314</sup>

Zirconia-based materials are also considered as high-temperature CO<sub>2</sub> capture sorbents.<sup>315</sup>

#### 6.4.7.2 Sulfated zirconia as a catalyst

Opportunately prepared sulfated oxides display extremely strong Brønsted (super) acidity<sup>316</sup> and, in general, enhanced catalytic activity in several acid-catalyzed reactions. This is reported for alumina, silica, iron oxide, titania, zirconia, hafnia and stannia, but it seems that sulfated zirconia only has been developed commercially<sup>317,318</sup> as catalysts of light skeletal isomerization.

The very high catalytic activity of sulfated zirconia, in particular for C<sub>4</sub>–C<sub>6</sub> paraffin isomerization, appears when a certain number of requirements is satisfied: in particular, it must be prepared by an amorphous sulfated precursor calcined at  $T \geq 550$  °C in order to have tetragonal sulfated phase, and be properly activated.<sup>319</sup> The catalytic activity of these materials may be enhanced by promoters such as Mn and Fe ions, which, however, do not increase the catalyst acidity.

Results of different spectroscopic experiments of the acidity of sulfated zirconia are not really in complete agreement. Spectroscopic studies showed that the sulfate ions on ionic oxides in dry conditions at low coverage are tetraordinated with one



short S=O bond (mono-oxo structure). At higher coverage, disulfate species are assumed to exist,<sup>320,321</sup> although a real proof of this probably does not exist. However, sulfate species are strongly sensitive to hydration. Lewis acidity and basicity of zirconia disappear in part by sulfation, but the residual Lewis sites are a little stronger. However, Brønsted acidity is also formed. IR spectra show a band in the range 3630–3645  $\text{cm}^{-1}$ ,<sup>320,321</sup> which is shifted by 139  $\text{cm}^{-1}$  upon low-temperature CO adsorption,<sup>321</sup> so measuring a medium-weak Brønsted acid strength. More recent IR results<sup>322</sup> do not completely agree with the previous ones, showing that different samples can give not identical spectral features. In any case, it has been concluded that sulfated zirconia has similar, or not stronger, Lewis and Brønsted strength than the less-active sulfated alumina.<sup>322</sup> However, the number of strong Lewis acid sites is, in sulfated zirconia, higher than on sulfated alumina. Characteristic  $^1\text{H}$  MAS NMR are detected for the surface acid sites,<sup>323</sup> whose Brønsted acidity has been determined using  $^1\text{H}$ ,  $^{13}\text{C}$ , and  $^{31}\text{P}$  MAS NMR spectra of adsorbed probe molecules to be stronger than that of zeolites, but lower than that of sulfuric acid. Surface titration experiments indicate that the Brønsted acidity of sulfated stannia, zirconia and hafnia ( $H_0 < -16$ ) should be stronger than that of other sulfated oxides including sulfated alumina, as well as of pure sulfuric acid, allowing the definition of these materials as “superacidic”. In contrast, microcalorimetric ammonia chemisorption studies<sup>324</sup> and ammonia TPD experiments<sup>322,325</sup> suggested that sulfated zirconia surfaces have Brønsted acidity not stronger than protonic zeolites. Water is reported to be needed for high catalytic activity<sup>326</sup> and, according to Katada et al.,<sup>327</sup> should generate “superacidic” Brønsted centers. In contrast, water is cited as a poison during commercial application in paraffin isomerization.<sup>317,318</sup>

Recent studies allowed to obtain a convincing evidence of the existence of an *n*-butane oxidative dehydrogenation step, probably induced by the reduction of sulfate species, during the induction period with the formation of water molecules and butylene.<sup>328</sup> Protonation of butylene gives rise to the sec-butyl cation that leads to a chain mechanism. This chain may involve direct isomerization of the butyl cation and hydride transfer from *n*-butane (monomolecular mechanism), or dimerization of sec-butyl cation, isomerization, cracking and hydrogen transfer (bimolecular mechanism). According to the experimental evidence that the presence of any olefins increases the butane isomerization reaction rate, it has been proposed that the skeletal isomerization reaction could occur on an “olefin-modified site” (i.e., a carbenium ion) more than on the protonic site, giving rise to a bimolecular pathway having the characteristics of a monomolecular one.<sup>329</sup>

Thus, the protonic acidity of these materials, arising from the presence of sulphuric acid species, is certainly strong. The presence of small amounts of water is likely required to retain surface hydroxylation. However, the semiconducting nature of zirconia coupled with the reducibility of sulfate species may play an important role in the behavior of the catalyst, in nonacidic steps.

Sulfated zirconia-based catalysts have already been used in industrial application for C4–C6 paraffin isomerization processes and are commercialized, e.g., by

Clariant-Süd Chemie (HYSOPAR-SA catalysts) constituted by Pt-promoted sulfated zirconia<sup>317,318</sup> and UOP ParIsom catalysts,<sup>330</sup> and are also considered for C7 paraffin isomerization.<sup>331</sup> They work at temperatures (180–210 °C) intermediate between those of the competing chlorided alumina and zeolite catalysts, similar to those of WO<sub>3</sub>–ZrO<sub>2</sub>-based catalysts, with final comparable performances, moderate limits in the allowed feed purity and possible regeneration. They are also active for a number of other acid-catalyzed reactions, many of them of potential industrial interest. We can also cite the isomerization-tracking of long chain paraffins to produce gasoline,<sup>332</sup> alkylations and acylation reactions.

However, recent studies underline how delicate are these materials, being easily converted to inactive materials sometimes even after simple storing or aging in laboratory atmosphere.<sup>333</sup> During reactivity, sulfur loss may also be found to the volatilization of sulfur, as volatile sulfate esters, and reduction to sulfites, with consequent deactivation of the catalyst.<sup>334</sup>

#### 6.4.7.3 Zirconia as a support for catalysts

Zirconia is reported to act as an excellent catalyst support in the open literature, but its use as a carrier for industrial catalysts is hampered by relevant costs, low surface area and instability due to phase transformation. According to its semiconducting character, zirconia is reported to have some activation effect in oxidation catalysis toward noble metals. Several papers report on high activity of zirconia-supported copper, gold, palladium and platinum for water-gas shift<sup>335</sup> even at low temperature, and for low-temperature CO oxidation.<sup>336</sup> On the other hand, zirconia is reported as a promising support for high-temperature catalytic applications such as methane CPO and catalytic combustion.<sup>337</sup>

#### 6.4.8 Ceria

Cerium dioxide, or ceria, becomes quite recently a very important member of the family of catalytic oxides.<sup>337b</sup> It presents, when stoichiometric, the cubic fluorite structure with coordination eight for cerium ions and tetrahedral coordination for oxide anions. According to the big size of the cations, ceria presents a medium Lewis acidity and relevant surface basicity. Actually, its importance is mainly due to its slight easily reversible reducibility that produces the so-called “oxygen storage capacity”. For this reason, it became, as such or mixed with zirconia and alumina, a most important support for metals in oxidation reactions<sup>338</sup> (see Chapter 11).

Among tetravalent metal oxides, CeO<sub>2</sub><sup>339</sup> has attracted much interest for its catalytic functions in the synthesis of organic compounds,<sup>340</sup> which provides evidence of its relevant basicity. In fact, thoria-, zirconia- and ceria-based materials (such as CeO<sub>2</sub>–Al<sub>2</sub>O<sub>3</sub><sup>310,341</sup>) find already practical industrial application in some dehydration and ketonization reactions, such as for the synthesis of diisopropyl ketone from isobutyric acid. CeO<sub>2</sub>–ZrO<sub>2</sub> mixed oxides form a cubic solid solution in the ceria-rich side,<sup>342</sup> which has relevant ability to adsorb NO<sub>x</sub>, further increased by other rare earth doping.

### 6.4.9 Niobia

Niobia, i.e., niobium pentoxide,  $\text{Nb}_2\text{O}_5$ , has a very complex crystal chemistry. Also the terminology to distinguish the many polymorphs is complicated. It seems that the thermodynamically stable form of niobia is the so-called H-phase, monoclinic, which is formed from any other forms on heating in air to about 1100 °C and above. It crystallizes in the P2 space group with  $Z = 14$ . In the unit cell, 27 Nb ions are octahedrally coordinated in  $\text{ReO}_3$ -type blocks (i.e., a tridimensional network with all-corner sharing  $\text{NbO}_6$  octahedra), one only being in a tetrahedral coordination in a position joining such blocks. At least 14 other polymorphs have been reported in the literature. Like H- $\text{Nb}_2\text{O}_5$ , many polymorphs are related to the  $\text{ReO}_3$  structure. Nevertheless, some other polymorphs present entirely different structures like for instance the orthorhombic “low-temperature” T- $\text{Nb}_2\text{O}_5$  phase, whose Nb atoms are mainly surrounded by seven or six O atoms forming pentagonal bipyramids or distorted octahedrons respectively, while the few remaining Nb atoms are coordinated to nine O atoms in interstitial sites.

Niobium suboxides also exist as stable phases in different conditions. Niobium dioxide, with tetravalent Nb ions, exists at room temperature with a distorted rutile structure, but at  $\sim 800\text{--}810$  °C undergoes a reversible second-order phase transition resulting at high temperature in a regular rutile structure.

A number of reduced  $\text{Nb}_2\text{O}_5$  phases, such as  $\text{Nb}_{12}\text{O}_{29}$ ,  $\text{Nb}_{22}\text{O}_{54}$ ,  $\text{Nb}_{47}\text{O}_{116}$ ,  $\text{Nb}_{25}\text{O}_{62}$ ,  $\text{Nb}_{53}\text{O}_{132}$ , also exist. These crystalline oxides are mainly constructed with blocks of  $\text{NbO}_6$  octahedra and, as a minor part, with  $\text{NbO}_4$  tetrahedra, and crystallize in different phases or present extended composition ranges. The possibility of modification of the oxidation state for niobium allows catalytic activity of niobia in oxidation catalysis. However, most interest for it seems to be for acid catalysis.<sup>343,344</sup>

Niobia, according to the high valency and small size of the cations, gives rise to a mostly covalent structure, where most oxygen atoms are bonded to two Nb atoms only. However, its chemistry is influenced by the elasticity of the coordination state of  $\text{Nb}^{5+}$  ions, coming from nearly symmetric hexagonal, to square pyramidal with a short and strong  $\text{Nb}=\text{O}$  bond and, also, to tetrahedral like. At the surface, this behavior gives rise to Lewis acidity, being these ions are able to change their coordination sphere in the presence of adsorbate species.

Indeed, the most commonly used forms of niobia are amorphous. Hydrated niobium oxides (niobic acids) calcined at moderate temperatures of 100–300 °C are reported to show a strong acidic character ( $H_0 -5.6$ )<sup>345,346</sup> with many potential applications in catalysis. This material displays both Lewis and Brønsted acidity, which can be utilized also in the presence of liquid water.<sup>347</sup> Proton NMR data indicate that Brønsted acidity of niobic acid is very high, possibly comparable with that of protonic zeolites.<sup>348</sup> The IR spectrum of niobic acid, after outgassing at 200 °C show a quite sharp peak at  $3708\text{ cm}^{-1}$ , with a shoulder near  $3735\text{ cm}^{-1}$ , assigned to free  $\text{Nb}-\text{OH}$  surface groups. Adsorption of nitriles indicates that  $\text{Nb}-\text{OH}$  groups are less acidic than the bridging hydroxy groups of zeolites.<sup>349</sup> Nb cations also show strong Lewis acidity.<sup>347</sup> Niobic acid is reported to crystallize as niobium oxide at

853 K, so losing all its water and hydroxide species. Slightly distorted  $\text{NbO}_6$ ,  $\text{NbO}_7$  and  $\text{NbO}_8$  sites were reported as structural units in amorphous  $\text{Nb}_2\text{O}_5$ .<sup>346</sup>

In recent years, preparation chemistry of niobia has been investigated to prepare nanostructured solids. A number of different morphologies have been prepared such as nanorods, nanowires, nanobelts, nanotubes and differently porous structures have been prepared.<sup>350</sup>

#### 6.4.9.1 Niobia as a catalyst

Niobic acid finds application as insoluble solid catalysts in water phase<sup>351</sup> and are applied in the industry for some fine chemical acid-catalyzed processes, such as the fructose dehydration reaction.<sup>352,353</sup> Niobic acid is patented as an alternative to solid phosphoric acid for ethylene hydration to ethyl alcohol in the gas phase at 200 °C.<sup>343</sup> Niobia in combination with silica, silica-alumina and other oxides finds also interest as acid catalyst in organic chemistry.<sup>354</sup> Mixed oxides such as  $\text{Nb}_2\text{O}_5\text{--WO}_3$ <sup>355</sup> and  $\text{Nb}_2\text{O}_5\text{--MoO}_3$ <sup>356</sup> have also the object of interest for their acidity. The products of the combination of niobium oxide and phosphoric acid are niobium phosphates<sup>357</sup> reported to be potentially useful in acid catalysis in similar applications.

#### 6.4.9.2 Niobia as a support for catalysts

Interest has been recently devoted to the application of niobia as a support for catalysts to be applied to liquid-phase reactions in the presence of water. This is the case of glycerol oxidation over  $\text{Au/Nb}_2\text{O}_5$ <sup>358</sup> and of  $\text{Pd/Nb}_2\text{O}_5$  for  $\gamma$ -valerolactone to pentanoic acid conversion.<sup>359</sup>

### 6.4.10 Tungsten trioxide (tungsta)

Tungsten oxide  $\text{WO}_3$  exhibits several different crystal structures thermodynamically stable in different temperature ranges (monoclinic *Pc* from  $-140$  to  $-50$  °C, triclinic *P1* from  $-50$  to  $17$  °C, monoclinic *P21-n* from  $17$  to  $330$  °C, orthorhombic *Pmnb* from  $330$  to  $740$  °C, and tetragonal *P4-nmm* above  $740$  °C<sup>360</sup>). All of them are distorted forms of the  $\text{ReO}_3$ -type cubic structure, due to the second-order Jahn Teller effect. These structures, where hexavalent tungsten is in more or less distorted octahedral sixfold coordination, have a highly covalent character, associated to the very high charge and very low size of the  $\text{W}^{6+}$  cation. This material has very strong acidity both of the Lewis and of the Brønsted type.<sup>361</sup> Besides  $\text{WO}_2$ , which crystallizes in a distorted rutile structure, some intermediate oxides also exist, with only some of them belonging to the so-called crystallographic shear structures. The best characterized of these suboxides is a whisker form,  $\text{W}_{18}\text{O}_{49}$ . Another fibrous tungsten oxide is “blue oxide”, with a nominal composition of  $\text{W}_{20}\text{O}_{58}$ .

Recently, mesoporous tungsta has been prepared and tested as a photocatalyst<sup>362</sup> and for applications associated to electrochromic, photochromic and semiconducting properties and possible applications in optical devices, gas sensors and electrochromic windows.<sup>363</sup>

### 6.4.10.1 Tungsta as a catalyst

Pure and silica-supported  $\text{WO}_3$  have had industrial application as acid catalysts, e.g., for commercial direct hydration of ethylene to ethanol in the gas phase.<sup>364</sup> Interest for mixed  $\text{Nb}_2\text{O}_5\text{--WO}_3$  and  $\text{Ta}_2\text{O}_5\text{--WO}_3$ <sup>365</sup> is associated too to their acidity. On the other hand, the partial reducibility of tungsten oxides is associated also to some activity in oxidation catalysis. Silica-supported tungsten oxides are among the most important heterogeneous olefin methathesis catalysts.<sup>366–368</sup>

### 6.4.10.2 Tungsta-zirconia as a catalyst

Much interest has been devoted recently to tungstated oxides<sup>369</sup> as catalysts. Tungstated zirconia is mostly investigated in relation to its activity in the paraffin skeletal isomerization reaction, for which reaction Pt-doped  $\text{WO}_3\text{--ZrO}_2$  catalysts are commercially available.<sup>317,318</sup> This material, if prepared from amorphous state in the form of tetragonal structure, is reported to display superacidity.<sup>316</sup> The hypothesis of the generation, upon reduction in hydrogen, of stronger Brønsted acid sites has been proposed.<sup>370,371</sup>

The strong Brønsted acidity of tungstated oxides is essentially related to the high acidity of tungstic acid species, while the redox properties of tungstic acid species, which may be influenced by the semiconducting/insulating and dispersing/nondispersing behavior of zirconia, may favor the generation of protonic centers by reduction and/or may be related to nonacid catalytic steps. Recently, high-angle annular dark-field imaging of  $\text{WO}_3/\text{ZrO}_2$  catalysts in an aberration-corrected analytical electron microscope allowed to direct imaging of the various species present. With this technique, subnanometer  $\text{Zr--WO}_x$  clusters have been revealed in very active catalysts and supposed to represent the active sites.<sup>372</sup>

Pt- and Mn-promoted  $\text{WO}_3\text{--ZrO}_2$  catalysts are very active, e.g., in the isomerization of n-hexane at 220–250 °C.<sup>373</sup> The so-called EMICT (ExxonMobil Isomerization Catalyst Technology) catalyst, based on promoted  $\text{WO}_3\text{--ZrO}_2$ , is reported to be very effective in C5-C6 paraffin skeletal isomerization at 175–200 °C even in the presence of 20 ppm of water and to be fully regenerable.<sup>374</sup> In this case, the redox properties of the catalyst might also be involved in the oxydehydrogenation of alkane to alkenes that later are protonated and promote a chain skeletal isomerization reaction, like for sulfated zirconia (see below). Reduced tungsten oxides are also mentioned as good catalysts for olefin metathesis.

Sulfated and tungstated hafnia also present high activity in paraffin isomerization.<sup>375</sup>

---

## 6.5 Mixed metal oxides and their acido-basicity

### 6.5.1 Silica–aluminas

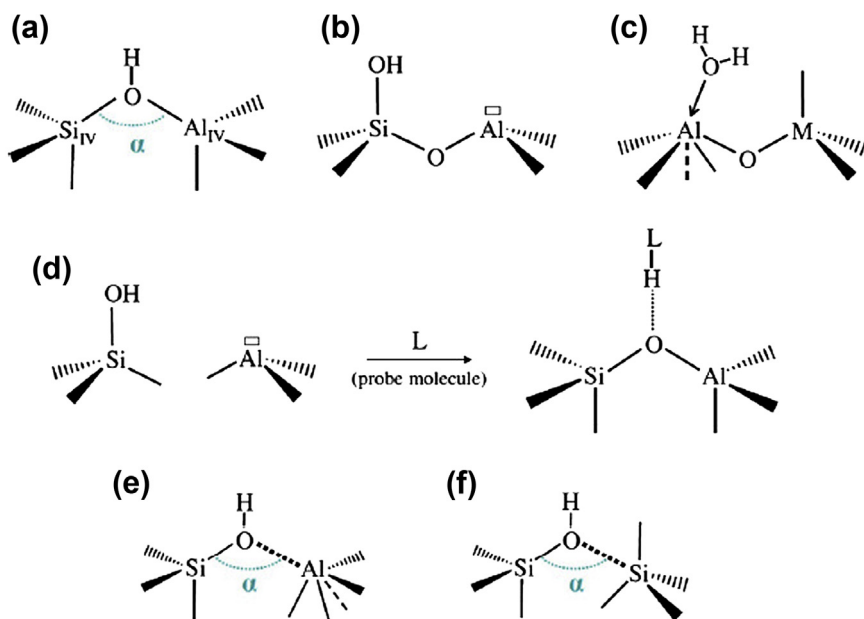
In spite of their large use as catalysts and supports, the structural details of the oxides resulting from coprecipitation or co-gelling of Si and Al compounds are still largely unclear. Amorphous microporous silica–alumina with high surface

area ( $>200 \text{ m}^2/\text{g}$ ) are usually reported to display significant cracking activity in particular when their Si/Al ratio is near 6–7,<sup>376</sup> that means that  $\text{Al}_2\text{O}_3$  represents 11–13% of the total weight. In these materials, Al is found to be exclusively or predominantly in tetrahedral coordination from  $^{27}\text{Al}$  MAS NMR,<sup>377</sup> with small amounts of octahedral and very few pentacoordinated Al ions. Al is supposed to substitute for silicon in the framework of an amorphous silica. It is not clear what is the mechanism for balancing the defect charge in this case, either protons at the surface, protons at the surface and in the bulk, or extraframework Al ions. Recent studies show that amorphous silica–alumina may indeed be constituted by a silica-network with very small amounts of Al in substitutional positions generating Brønsted acidity, and alumina like patches.<sup>378</sup> By decreasing the Si/Al ratio, the amount of octahedrally coordinated Al increases and, at Si to Al ratio well below one  $\gamma\text{-Al}_2\text{O}_3$  features appear in the XRD pattern.

In recent years, a number of differently structured mesoporous SAs containing big pores with size from few to many nm have been developed. Although sometimes considered like very large pore zeolites, these materials are essentially amorphous SA with nonstructural although sometimes ordered mesopores. The surface chemistry of these materials appears to be closely similar to that of amorphous microporous SAs—among the best known, Al-MCM41<sup>379,380</sup> and Al-SBA.<sup>381,382</sup>

The presence of very strong Lewis acid sites as well as of relevant Brønsted acidity at the surface of SAs is well known. However, the structure of the very active Brønsted sites is still matter of debate. In Figure 6.16 some of the proposals given in literature are summarized. The IR spectra of SAs activated in vacuum (Figure 6.17) always present a very sharp IR band near  $3747 \text{ cm}^{-1}$  certainly due to terminal silanols, spectroscopically very similar to those of pure silicas and of any silica-containing material. A tail toward lower frequencies is likely due (as on pure silica too) to H-bonded and geminal silanols. Several papers reported on the characterization of the acidity of terminal silanols and the complete absence of bands assignable to bridging OH's.<sup>239,383</sup> This in spite of the remarkable Brønsted acidity of SAs detected, e.g., by protonation of ammonia, pyridine, amines and also by the strong H-bonding with nitriles and CO detected by IR (see Figure 6.17) and by calorimetric measurements, as well as deduced by its catalytic activity.

Some papers emphasized the additional presence of very small bands near  $3600 \text{ cm}^{-1}$  in the spectra of mesoporous SAs,<sup>384–387</sup> supposed to be due to bridging zeolite-type sites. Also theoretical works at least up to the end of 1990s modeled the active site for zeolites and SA in the same way, as Al-(OH)-Si bridging hydroxy groups. Accordingly, it was previously supposed that the active site for SA and protonic zeolites is the same (i.e., it is constituted by the bridging hydroxy groups bonded to a silicon and an aluminum atom).<sup>388</sup> Very recently, Poduval et al.<sup>389</sup> reported data suggesting that indeed bands typical of bridging OD's are evident in the spectra of deuterated silica alumina, but are masked on those of undeuterated samples. In contrast, Crépeau et al.<sup>390</sup> did not find any other species except terminal silanols on their strongly Brønsted acidic SA samples. The same result has been reported by Luan and Fornier for SBA-15.<sup>381</sup> Garrone et al.<sup>391</sup>

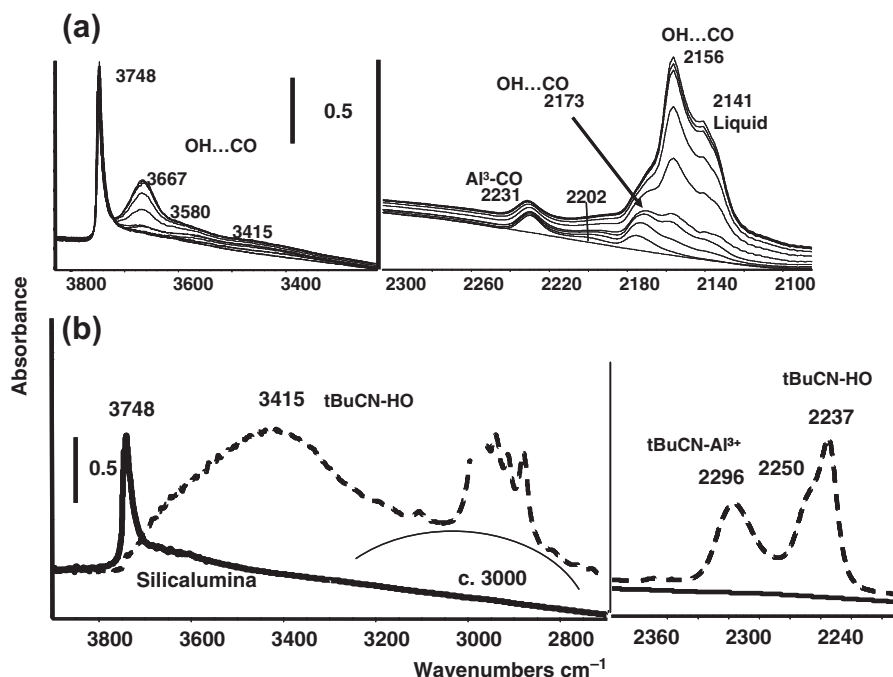
**FIGURE 6.16**

OH-groups invoked at the surface of ASAs, models proposed from experiments (a–d) and DFT calculations (a, c, e, and f): (a) zeolite-like bridging Si–(OH)–Al group, (b) silanol in the vicinity of aluminum atoms [14], called silanol–Al in the following, (c) water molecules on Al atoms, (d) probe molecule induced bridging of specific silanols, (e) alumino pseudo-bridging silanols PBS–Al, (f) silicic pseudo-bridging silanols PBS–Si.

*Reprinted with permission from Ref. 398.*

showed that small amounts of water adsorbed on mesoporous silica–alumina produce a weak band at  $3611\text{ cm}^{-1}$  together with another at  $3697\text{ cm}^{-1}$  (symmetric and asymmetric OH stretchings) and that adsorbed water adsorbs CO showing significant protonic acidity. Cairon<sup>392</sup> confirmed recently the previous data showing very strongly acidic terminal silanols on amorphous SA but emphasized the complexity of the corresponding absorptions.

Bevilacqua et al.<sup>239</sup> reinvestigated the surface hydroxy groups and the surface acidity of silica, silicalite, mesoporous and microporous SAs, silicated aluminas, aluminated silicas and silicalite, and of some zeolites, by IR spectroscopy. CO, pyridine and lutidine have been used as molecular basic probes. The data suggest that bridging hydroxy group Si–OH–Al are fully stable structures only in the cavities of zeolites, where they produce the strong bands at  $3500\text{--}3630\text{ cm}^{-1}$  well correlated with the framework Al content. Extremely small bands near  $3610\text{ cm}^{-1}$  may be found on some SA samples only (mostly prepared in organic media) and on aluminated silicas after activation by outgassing, thus being not due to adsorbed water.



**FIGURE 6.17**

(a) FT-IR spectra of commercial silica–alumina activated at 773 K and after saturation with CO at 130 K and outgassing at increasing temperatures of 130–180 K. (b) FT-IR spectra of the same silica-alumina activated at 673 K (full lines) and in contact with PN vapor 3 Torr (dashed lines, vapor phase spectrum subtracted).

These bands certainly correspond to very few OH groups, and impurities (like bicarbonates) might contribute to their formation. It has been suggested that, in disordered mesoporous or microporous amorphous materials, zeolite-like pores may accidentally form and host zeolite-like bridging hydroxy groups. The conclusion<sup>239</sup> was that terminal silanols whose acidity is enhanced by nearby  $\text{Al}^{3+}$  Lewis acid sites represent the predominant Brønsted acid sites in nonzeolitic materials based on combinations of silica and alumina. Part of these sites may be located in the internal cavity of small pores, even having molecular (or zeolitic) size but, due to the flexibility of the amorphous structure, this does not change significantly their structure and acidity.

Our approach was considered and developed by Chizallet et al.<sup>393,394</sup> on the basis of theory and experiment. These authors confirmed the possible existence and strong acidity of pseudobridging OH's formed by the interaction of silanol groups with the fifth coordinative valency of tetrahedrally coordinated Al or Si atoms. Huang et al.<sup>395</sup> observed the formation of very strong Brønsted sites on flame-derived



silica–alumina and concluded that they may be associated to silanols interacting with one tetracoordinated Al ion and a second pentacoordinated Al ion.  $^1\text{H}$  MAS NMR studies (Figure 6.14) and  $^{27}\text{Al}$  MAS NMR techniques agree with the IR data showing that structurally different active sites are active on SAs with respect to zeolites,<sup>231</sup> while they appear similar to those present on silica. Very recent data from Hensen et al.<sup>396</sup> confirmed the existence of a small number ( $<10\ \mu\text{mol/g}$ ) of very strong Brønsted acid sites on silica–aluminas together with a second family of weaker Brønsted acid sites ( $50\text{--}250\ \mu\text{mol/g}$ ), suggesting that they *might* arise from the interaction of silanol groups with strong Lewis acid sites.

The group at IFP, Lyon, France, based on experiments and calculations, further developed their model suggesting that the driving force for the proton exchange is the stabilization of the deprotonated Brønsted center,<sup>397,398</sup> in agreement with the early hypothesis by Trombetta et al.<sup>379,399</sup>

The lack of substantial formation of well-defined “zeolitic” bridging OH sites by reacting silica surfaces with Al ions or alumina surfaces with silicate ions, and also on mixed oxides like SA, provides evidence for a substantial instability of the Si–OH–Al bridge, which is likely stabilized by the rigidity of the zeolite framework and/or by some interaction of the proton with the opposite wall of the cavity.

### 6.5.1.1 Silica–aluminas as catalysts

Amorphous microporous SA, used in the past for fixed and moving bed catalytic cracking starting from the forties, still finds a number of applications as acid catalysts, e.g., the dehydrochlorination of halided hydrocarbons to linear olefins and the cracking of waste plastics<sup>400</sup> and (waste) vegetable oils<sup>401</sup> into useful products or fuels. Also, SAs are used as supports of sulfide catalysts for hydrotreatings,<sup>402</sup> and of catalysts for ring opening of polycyclic compounds, useful for the improvement of the technical and environmental quality of diesel fuels.<sup>403</sup>

Several recent studies appeared concerning industrial application of mesoporous SAs<sup>403b</sup> and the comparison with microporous SA and zeolite as catalysts for several reactions of industrial interest such as alkylation of aromatics and propene oligomerization. The catalytic activity of mesoporous SAs appear to be sometimes higher than that of microporous SAs, but lower than that of zeolites. SAs may also act as binders in catalysts such as those for the modern FCC process.

### 6.5.2 Alumina-rich silica–aluminas and silicated aluminas

Several commercial aluminas actually contain small amounts of silica mainly for stabilization against the phase transformation to corundum. Alumina-rich silica–aluminas produced by coprecipitation methods have been the object of some interest and of few investigations. They have the structure of  $\gamma$ -Alumina, silica being mostly located at the surface. Similar materials have been investigated more recently by the Topsøe group, and found very active for the dimethylether (DME) synthesis from methanol at  $300\ ^\circ\text{C}$  and atmospheric pressure.<sup>404</sup> The presence of silica would increase acidity and resistance to coking. Similar materials, denoted as “activated alumina”, are

possibly those used in the condensation step of the Topsøe Technology for Large-scale Production of DME, for the coproduction of methanol and DME from syngas.

The so-called “silicated aluminas”, obtained by a “reactive” deposition of silica precursors (like tetraethoxysilane, TEOS) onto the surface of  $\gamma$ -alumina, are a relevant class of materials, reported as excellent catalysts, as such and Pt-doped, for the skeletal isomerization of butylenes to isobutylene at 400–450 °C.<sup>405,406</sup> A similar catalyst composed of silica and alumina is reported to be used in the ARCO tert-butyl alcohol dehydration process to produce pure isobutylene: the reaction occurs in the vapor phase a 260–370 °C at about 14 bar, with a conversion of 98%.

The addition of silicate species to alumina (at the surface or in the bulk) gives rise to terminal silanols but does not produce bands in the region of bridging OHs, nor relevant Brønsted acidity is observed.<sup>407</sup> This is explained supposing that the silicate species tend to maximize the interaction with the bulk of alumina by orienting three oxygen atoms toward the bulk, while the fourth necessarily stands up, with respect to the surface. To limit the free energy, the fourth oxygen standing up bonds with a proton. It seems obvious that it cannot bend to bridge surface aluminum cations. The resulting Brønsted acidity is consequently that of isolated silanols, weak although possibly enhanced by the vicinity of Al ions.

### 6.5.3 Aluminated silicas

The addition of small amounts of aluminum oxide species at the surface of formed silica gives rise to those we called aluminated silicas.<sup>239</sup> These materials appear to be very similar to silica–aluminas, with strong Lewis acidity, due to surface uncoordinated  $\text{Al}^{3+}$  ions, and Brønsted acidity associated to acidity enhanced silanol groups. To these materials belong, likely, the catalysts for the MTBE cracking Snamprogetti process (described as “based on silica”) performed in the gas phase at 140–150 °C, for the production of high-purity isobutylene.

### 6.5.4 Combinations of silica, titania, alumina, ceria and zirconia

Titania and zirconia may be combined with silica<sup>408</sup> and alumina,<sup>409,410</sup> as well as each other,<sup>411</sup> to give interesting and useful high-surface area and high stability materials. These materials still retain high Lewis acidity associated to the  $\text{Al}^{3+}$ ,  $\text{Ti}^{4+}$  and  $\text{Zr}^{4+}$  cations, as well as medium-weak Brønsted acidity, associated to silanols and other hydroxy groups. Titania-aluminas are important materials as catalyst supports, e.g., for hydrodesulfurization catalysts.<sup>412,413</sup>

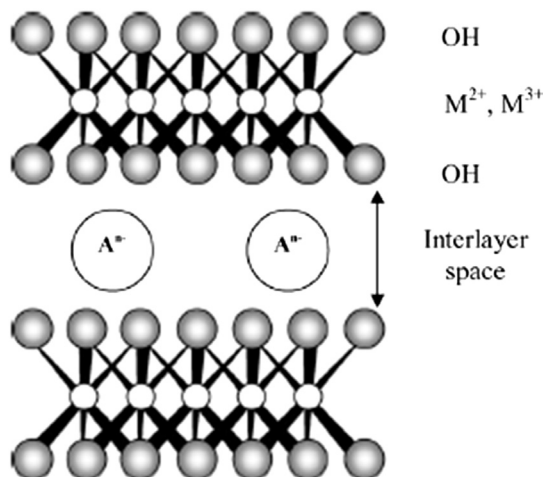
Ceria and zirconia combine together giving rise to crystalline solid solutions. The structure may be a mixture of two, cubic and tetragonal,  $\text{Zr}_{1-x}\text{Ce}_x\text{O}_2$  solid solutions, the cubic fluorite like phase being the more abundant the more the ceria in the composition. By increasing calcination temperature, the stability range of the cubic solid solution even increases. Alumina, depending on amount, preparation procedure and calcination temperature, can enter the  $\text{Zr}_{1-x}\text{Ce}_x\text{O}_2$  cubic solid solution

or segregate as  $\gamma$ - and/or  $\delta$ - $\text{Al}_2\text{O}_3$ , while the compound  $\text{CeAlO}_3$  where trivalent cerium is present can also form.<sup>414</sup> These materials tend to retain the acid-base properties of ceria and zirconia, thus being applicable as acidobasic catalysts<sup>310,340</sup> but also retain part of the Oxygen Storage Capacity typical of Ceria, thus being used as support or washcoat for catalysts such as platinum group metal catalysts used in three way catalysts for gasoline engine waste-gas aftertreatment.<sup>415</sup>

### 6.5.5 Calcined hydrotalcites and spinels

Hydrotalcite (HT, the layered double hydroxide, LDH, with formula  $\text{Mg}_6\text{Al}_2(\text{OH})_{16}\text{CO}_3 \cdot 4\text{H}_2\text{O}$ ) is a natural anionic clay having interesting basic properties. Its structure (Figure 6.18) is formed by brucite-like  $[\text{Mg}_6\text{Al}_2(\text{OH})_{16}]$  layers with carbonate ions and water molecules in the interlayer region. It is also a commercial synthesis product, used in medicine as a stomach antacid, as well as an environmentally friendly, nontoxic and heavy metal-free filler of halogenated polymers (such as PVC) to scavenge acid by-products. Hydrotalcite decomposes, releasing  $\text{CO}_2$  and water, from 260 to 300 °C, thus acting as flame-retardant and smoke-suppressant. The thermal decomposition of HT gives rise to a mixed oxide whose virtual composition is 5 MgO.  $\text{MgAl}_2\text{O}_4$ , although these phases may give rise to mutual solid solubility, depending on decomposition temperature. In fact, calcined HTs are intimate mixtures of rock-salt-type and a spinel-type solid solutions.

Spinel is the mineralogical name of Mg aluminate,  $\text{MgAl}_2\text{O}_4$ , as well as of iso-structural mixed oxides of a trivalent and a bivalent ion. Stoichiometric  $\text{MgAl}_2\text{O}_4$  is essentially a normal spinel phase with tetrahedrally coordinated Mg and



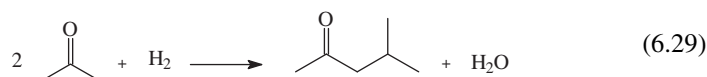
**FIGURE 6.18**

Hydrotalcite structure showing the brucite-like layers and interlayer anions.

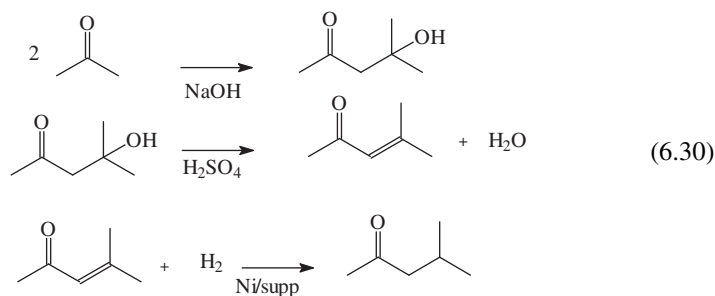
Reprinted with permission from Cantrell DG, Gillie LJ, Lee AF, Wilson K. Structure-reactivity correlations in MgAl hydrotalcite catalysts for biodiesel synthesis. *Appl Catal A Gen* June 22, 2005;**287**(2):183–90.

octahedrally coordinated Al, behaving as an important refractory material. Due to partial inversion of the spinel structure, low-coordination Al cations typical of spinel-type aluminas can be detected at the surface and produce a small density of very strong Lewis acid sites. The surfaces of nearly stoichiometric spinel materials show a compromise between the basic character of rock-salt-type bivalent oxides and the more or less acidic character of the corresponding sesquioxides.<sup>416–418</sup> Excess Mg ions in the case of calcined hydrotalcites cause the predominance of the basic character of MgO. Doping with alkali may further increase the basicity of hydrotalcites.<sup>419</sup>

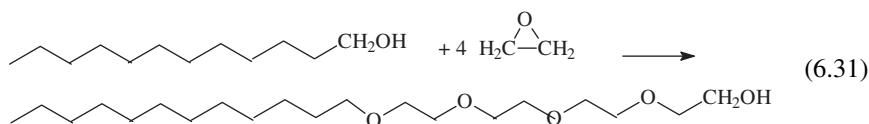
Several reviews have been reported recently concerning the application of Mg-Al HT or calcined HT as basic materials<sup>67,420–422</sup> in particular in the field of fine organic chemistry. These materials, whose basic strength is somehow tunable,<sup>423</sup> are very popular as basic catalysts in academic research. On the other hand, they are also used industrially, for aldol condensations<sup>424</sup> such as the synthesis of, for example, methyl isobutyl ketone, MIBK, by aldol condensation of acetone followed by dehydration and hydrogenation.<sup>425</sup> The full reaction may be performed in a single liquid-phase reactor using Mg–Al hydrotalcite with 0.1% of Pd<sup>426</sup>:



This single-step process substitutes the older three-step one, based on catalysis by caustic, acid catalyzed dehydration and hydrogenation:



as well as for oxyethylation of alcohols with ethylene oxide with the production of nonionic polyethoxylate surfactants.<sup>427</sup>



They have also been used as basic supports for noble metal catalysts,<sup>428</sup> and for the abatement of SO<sub>2</sub> from waste gases. Mg-aluminate spinels find large application as supports or components for Ni-methane steam-reforming catalysts<sup>429</sup> just to limit surface acidity and, consequently, deactivation by coking.

According to the basic properties of both ZnO and ZnAl<sub>2</sub>O<sub>4</sub>, also Zn–Al hydrotalcite present relevant basic properties. In fact Zn–Al hydrotalcites have been patented for industrial oxyethylation.<sup>427</sup> Zn–Al hydrotalcite calcined at moderate temperature form poorly crystalline Zn oxides that adsorb alcohols giving rise to highly ionic alkoxide species.<sup>430</sup> Zinc aluminate has also found interesting recent application as the catalyst for solid-catalyzed biodiesel synthesis by fats transesterification with the IFP process.<sup>431</sup> The use of a solid catalyst allows the distillation of methanol from the reaction medium, the separation of glycerine from biodiesel and fats, and the production of pure water and sodium free glycerine. However, it is needed that no leaching occurs from the solid catalyst.

---

## References

1. Wells AF. *Structural inorganic chemistry*. Oxford University press.
2. Bruce Hyde S. *Inorganic crystal structures*. Andersson Wiley; 1989.
3. Halcrow MA. *Chem Soc Rev* 2013 [Advance Article].
4. Woodward PM, Mizoguchi H, Kim Y-I, Stoltzfus MW. In: Fierro JLG, editor. *Metal oxides chemistry and applications*. CRC Press; 2005. p. 133.
5. Ashrafi A, Jagadish C. *J Appl Phys* 2007;**102**(071101).
6. Canepa P, Ugliengo P, Alfredsson M. *J Phys Chem C* 2012;**116**(40):21514–22.
7. Jørgensen J-E, Mosegaard L, Thomse LE, Jensen TR, Hanson JC. *J Solid State Chem* 2007;**180**:180–5.
8. Ollivier B, Retoux R, Lacorre P, Massiot D, Ferey G. *J of Mater Chem* June 1997;**7**(6).
9. Shi H, Asahi R, Stampfl C. *Phys Rev B* 2007;**75**(205125):9.
10. Zinkevich M. *Prog Mater Sci* 2007;**52**:597–647.
11. Effenberger H, Lengauer CL, Parthé E. *Monatsh für Chem* 2001;**132**(12):1515–7.
12. Romanov DP, Skrobot VN. *Glass Phys Chem* 2009;**35**(5):518–24.
13. Ledyastuti M, Liang Y, Miranda CR, Matsuoka T. *J of Chem Phys* 2012;**137**(034703).
14. Payne DJ, Egdell RG, Law DSL, Glans PA, Learmonth T, Smith KE, Guo J, Walshe A, Watson GW. *J. Mater. Chem* 2007;**17**:267–77.
15. Julien CM, Massot M. *Poinsignon Spectrochim Acta Part A* 2004;**60**:689–700.
16. Ceriotti M, Pietrucci F, Bernasconi M. *Phys Rev B* 2006;**73**(104304):16.
17. Londero E, Schröder E. *Comput Phys Commun* 2011;**182**:1805–9.
18. Lunk HJ, Hartl H, Hartl MA, Fait MJG, Shenderovich IG, Feist M, et al. *Inorg Chem* 2010;**49**:9400–8.
19. Chizallet C, Digne M, Arrouvel C, Raybaud P, delbecq F, Costentin G, et al. *Top Catal* 2009;**52**:1005–16.
20. Siracusano S, Baglio V, D'Urso C, Antonucci V, Aricò AS. *Electrochimica Acta* 2009;**54**:6292–9.
21. Wang L, Maxisch T, ceder G. *Phys Rev B* 2006;**73**(195107).
22. Glasser L. *Inorg Chem* 2009;**48**:10289–94.

23. McHale JM, Auroux A, Perrotta AJ, Navrotsky A. *Science* 1997;**277**(5327):788–9.
24. Zhang H, Chen B, Banfield JF. *Phys Chem Chem Phys* April 14, 2009;**11**(14):2553–8.
25. Zhang YL, Jin XJ, Rong YH, Hsu (Xu Zuyao) TY, Jiang DY, Shi JL. *Mater Sci Eng A* 2006;**438–440**:399–402.
26. Navrotsky A, Ma C, Lilova K, Birkner N. *Science* 2010;**330**:199–201.
27. Busca G. *Chem Rev* 2010;**110**:2217–49.
28. Dimitrov V, Komatsu T. *J Solid State Chem* 2002;**163**:100.
29. Leboutellier A, Courtine P. *J Solid State Chem* 1998;**137**:94.
30. Bailly ML, Costentin G, Lauron-Pernot H, Krafft JM, Che M. *J Phys Chem B* 2005;**109**:2404–13.
31. Rasc\_on F, Wischert R, Copéret C. *Chem Sci* 2011;**2**:1449–56.
32. Debecker DP, Stoyanova M, Rodemerck U, Eloy P, Léonard A, Su B-L, et al. *J Phys Chem C* 2010;**114**(43):18664–73.
33. Al Ghamdi K, Hargreaves SJS, Jackson SD. In: Jackson SD, Hargreaves SJS, editors. *Metal oxide catalysis*. Wiley; 2009. pp. 819–43.
34. Ono Y, Hattori H. *Solid base catalysis*. Springer; 2011.
35. Busca G. *Ind Eng Chem* 2009;**48**:6486–511.
36. Folkins HO, Miller EL. *Ind Eng Chem Proc Res Dev* 1962;**1**:271–6.
37. Tanabe K, Hölderich WF. *Appl Catal A Gen* 1999;**181**:399–434.
38. Sharma SK, Parikh PA, Jasra RV, Mol J. *Catal A Chem* 2007;**278**:135–44.
39. Calvino-Casilda V, Martín-Aranda RM, López-Peinado AJ, Sobczak I, Ziolek M. *Catal Today* 2009;**142**:278–82.
40. Ndou AS, Plint N, Coville NJ. *Appl Catal A Gen* 2003;**251**:337–45.
41. Kobashima H, Hattori H. *Catal Today* 1998;**44**:277–83.
42. Sharma YC, Singh B, Korstad J-. *Fuel* 2011;**90**:1309–24.
43. Martín Alonso D, Mariscal R, Moreno-Tost R, Zafra Poves MD, Lopez Granados M. *Catal Commun* 2007;**8**:2074–80.
44. Blass BE. *Tetrahedron* 2002;**58**:9301–20.
45. Weissermel W, Arpe HJ. *Industrial organic chemistry*. 3rd ed. VCH; 1997.
46. Kelly GJ, King F, Kett M. *Green Chem* 2002;**4**:392–9.
47. King F, Kelly GJ. *Catal Today* 2002;**73**:75–81.
48. Setoyama T. *Catal Today* 2006;**116**:250–62.
49. Tanabe K, Hölderich WF. *Appl Catal A Gen* 1999;**181**:399–434.
50. Rossetti I, Bencini E, Trentini L, Forni L. *Appl Catal A Gen* 2005;**292**:118.
51. Baghalha M, Ebrahimpour O. *Appl Catal A Gen* 2007;**326**:143.
52. Zhao C, Chen X, Zhao C. *Energy Fuels* 2009;**23**:4683–7.
53. Lee MR, Allen ER, Wolan JT, Hoflund GB. *Ind Eng Chem Res* 1998;**37**:3375–81.
54. Epling WS, Campbell LE, Yezerets A, Currier NW, Parks II JE. *Catal Rev* 2004;**46**:163–245.
55. Hirota S. *J Soc Automot Eng Jpn* 2006;**60**(9):112–6.
56. Johnson T. *SAE Int J Fuels Lubr* 2009;**2**(1):1–12.
57. Castoldi L, Matarrese R, Lietti L, Forzatti P. *Appl Catal B Environ* 2009;**90**:278–85.
58. Montanari T, Castoldi L, Lietti L, Busca G. *Appl Catal A General* 2011;**400**:61–9.
59. Resini C, Panizza M, Arrighi L, Sechi S, Busca G, Miglio R, et al. *Chem Eng J* 2002;**89**:75–82.
60. Stankic S, Bernardi J, Diwald O, Knözinger E. *J Phys Chem B* 2006;**110**:13866.

61. Chizallet C, Costentin G, Lauron- Pernot H, Krafft JM, Che M, Delbecq F, Sautet P. *J Phys Chem C* 2008;**112**:16629–37.
62. Vidruk R, Landau MV, Herskowitz M, Talianker M, Frage N, Ezersky V, et al. *J Catal* April 1, 2009;**263**(1):196–204.
63. Chizallet C, Petitjean H, Costentin G, Lauron-Pernot H, Maquet J, Bonhomme C, et al. *J Catal* November 15, 2009;**268**(1):175–9.
64. Spoto G, Gribov EN, Ricchiardi G, Damin A, Scarano D, Bordiga S, Lamberti C, Zecchina A. *Prog Surf Sci* 2004;**76**:71.
65. Paganini MC, Chiesa M, Martino P, Giamello E, Garrone E. *J Phys Chem B* 2003;**107**:2575.
66. Chintareddy VR, Kantam ML. *Catal Surv Asia* 2011;**15**(2):89–110.
67. Corma A, Iborra S. *Adv Catal* 2006;**49**:239–302.
68. Ballarini N, Cavani F, Maselli L, Montaletti A, Passeri S, Scagliarini D, Flego C, Perego C. *J Catal* 2007;**251**:423–36.
69. Kiriubakaran V, Sivaramakrishnan V, Nalini R, Sekar T, Premalatha M, Subramanian P. *Renew Sust Energy Rev* 2009;**13**:179–86.
70. Torres W, Pansare SS, Goodwin Jr JG. *Catal Rev Sci Eng* 2007;**49**:407–56.
71. Kus S, Otremba M, Tórz A, Taniewski M. *Fuel* 2002;**81**:1755.
72. Frey AM, Yang J, Feche C, Essayem N, Figueras F, de Jong KP, et al. *J Catal* 2013;**305**:1–6.
73. Gallardo Amores JM, Sanchez Escribano V, Daturi M, Busca G. *J Mater Chem* 1996;**6**:879.
74. Morterra C, Magnacca G, Cerrato G, Del Favero N, Filippi F, Folonari CV. *J Chem Soc Faraday Trans* 1993;**89**:135.
75. Malpartida I, Larrubia Vargas MA, Alemany LJ, Finocchio E, Busca G. *Appl Catal B Environ* 2008;**80**:214–25.
76. Busca G, Cristiani C, Forzatti P, Groppi G. *Catal Lett* 1995;**31**:65.
77. Ramani S, Allison JD, Minahan DM, Wright HA. *Promoted nickel-magnesium oxide catalysts and process for producing synthesis gas*. ConocoPhillips Company. Patent 7223354, Issued May 29, 2007.
78. Angelos M. Efstathiou (Strovolos, CY) Petros G. Savva (Aglandjia, CY) Costas N. Costa (Limassol, CY) Assignees: Linde Aktiengesellschaft. Catalyst containing platinum and palladium for the selective reduction of NOx with hydrogen (H<sub>2</sub>-SCR)inventors. Patent Application 20100092360.
79. Cimino S, Lisi L. *Ind Eng Chem Res* 2012;**51**(22):7459–66.
80. Polychronopoulou K, Giannakopoulos K, Efstathiou AM. *Appl Catal B Environ* 2012;**111–112**:360–75.
81. Feng Bo, An H, Tan E. Screening of CO<sub>2</sub> adsorbing materials for zero emission power generation systems. *Energy Fuels* 2007;**21**:426–34.
82. Reddy EP, Smirniotis PG. High-Temperature sorbents for CO<sub>2</sub> made of alkali metals doped on CaO supports. *J Phys Chem B* 2004;**108**:7794–800.
83. Grasa GS, Abanades JC. CO<sub>2</sub> Capture capacity of CaO in long series of carbonation / calcination cycles. *Ind Eng Chem Res* 2006;**45**:8846–51.
84. Li Y, Wu Y. Gao, J. *Ind Eng Chem Res* 2004;**43**:1807–11.
85. Li Y, Tong H, Zhuo Y, Li Y, Xu X. *Environ Sci Technol* 2007;**41**:2894–900.
86. Weckhuysen BM, Mestl G, Rosynek MP, Krawietz TR, Haw JF, Lunsford JH. *J Phys Chem B* 1998;**102**:3773–8.
87. Bukel CH, Moretto HH, Werner D, Woditsch P, Buchel KH. *Industrial Inorganic Chemistry*, 2nd Ed., Wiley.

88. Demichelis R, Civalleri B, Noel Y, Meyer A, Dovesi R. *Chem Phys Lett* 2008;**465**: 220–5.
89. Demichelis R, Catti M, Dovesi R. *J Phys Chem C* 2009;**113**:6785–91.
90. Noel Y, Demichelis R, Pascale F, Ugliengo P, Orlando R, Dovesi R. *Phys Chem Miner* 2009;**36**:47–59.
91. Tunega D, Päsalić H, Gerzabek MH, Lischka H. *J Phys Condens Mater* 2011;**23**(404201):1–10.
92. Li M, Snoussi K, Li L, Wang H, Yang W, Gao C. *Appl Phys Lett* 2010;**96**(261902).
93. Yang H, Lu R, Downs RT, Costin G. *Acta Cryst* 2006;**E62**:i250–2.
94. Demichelis R, Noel Y, Zicovich-Wilson CM, Roetti C, Valenzano L, Doves R. *J Phys Conf Ser* 2008;**117**:012013.
95. Wefers K, Misra C. *Oxides and hydroxides of aluminum*. Alcoa; 1987.
96. Oberlander RK. In: Leach BE, editor. *Applied industrial catalysis*, vol. 3. Academic Press; 1984. p. 64.
97. Tsuchida T. *Solid State Ionics* 1993;**63–65**:464–70.
98. Carim AH, Rohrer GS, Dando NR, Tzeng SY, Rohrer CL, Perrotta AJ. *J Am Ceram Soc* 1997;**80**(10):2677–80.
99. Löffler L, Mader W. *J Am Ceram Soc* 2003;**86**:534–40.
100. Paglia G, Buckley CE, Udovic TJ, Rohl AL, Jones F, Maitland CF. *Chem Mater* 2004;**16**:1914–23.
101. Digne M, Revel R, Boualleg M, Chice D, Rebours B, Moreaud M, et al. In: Gaigneaux EM, Devillers M, Hermans S, Jacobs P, Mertnes J, Ruiz P, editors. *10th int. symp. "scientific bases for the preparation of heterogeneous catalysts"*. Elsevier; 2010. pp. 127–34.
102. [http://www.sasoltechdata.com/tds/PURALOX\\_CATALOX.pdf](http://www.sasoltechdata.com/tds/PURALOX_CATALOX.pdf); 2014 [accessed 31.03.14].
103. Lippens BC, deBoer JH. *Acta Crystallogr* 1964;**17**:1312–21.
104. Kim HJ, Lee HC, Lee JS. *J Phys Chem C* 2007;**111**:1579–83.
105. Soled S. *J Catal* 1983;**81**:252–7.
106. Zhou RS, Snyder RL. *Acta Crystallogr B* 1991;**47**:617–30.
107. Tsyganenko AA, Smirnov KS, Rzhhevskij AM, Mardilovich PP. *Mater Chem Phys* 1990;**26**:35–46.
108. Wolverton C, Hass KC. *Phys Rev B* 2001;**63**:24102.
109. Sohlberg K, Pennycook SJ, Pantelides ST. *J Am Chem Soc* 2001;**123**:26–9.
110. Sohlberg K, Pennycook SJ, Pantelides ST. *Chem Eng Commun* 2000;**181**:107–35.
111. Digne M, Sautet P, Raybaud P, Euzen P, Toulhoat H. *J Catal* 2004;**226**:54–68.
112. Digne M, Sautet P, Raybaud P, Euzen P, Toulhoat H. *J Catal* 2002;**211**:1–5.
113. Krokidis X, Raybaud P, Gobichon E, Rebours B, Euzen P, Toulhoat H. *J Phys Chem B* 2001;**105**:5121–30.
114. Paglia G, Buckley CE, Rohl AL, Hart RD, Winter K, Studer AJ, et al. *Chem Mater* 2004;**16**:220–36.
115. Paglia G, Rohl AL, Buckley CE, Gale JD. *Phys Rev B* 2005;**71**:224115.
116. Menendez Proupin E, Gutierrez G. *Phys Rev B* 2005;**72**:035116.
117. Ferreira R, Martins MJF, Konstantinova E, Capaz RB, Souza WF, Chiaro SSX, et al. *J Solid State Chem* 2011;**184**:1105–11.
118. Wilson SJ, Mc Connel JDC. *J Solid State Chem* 1980;**34**:35.
119. Hyde BG, Andersson S. *Inorganic crystal structures*. New York: Wiley; 1989.
120. Ghanti E, Tomar N, Gautam P, Nagarajan R. *J Sol Gel Sci Technol* 2011;**57**: 12–5.



121. Lavalley JC, Benaissa M, Busca G, Lorenzelli V. *Appl Catal* 1986;**24**:249.
122. Schulze-Isfort C, Batz-Sohn C, Habermann H, Hofmann R. *Process for preparing an aluminium oxide powder having a high alpha-Al<sub>2</sub>O<sub>3</sub> content*. Patent Application No. 20110217552, 2011, to Evonik.
123. John CS, Alma NCM, Hays GR. *Appl Catal* 1983;**6**:341–6.
124. Pecharromás C, Sobrados I, Iglesias JE, Gonzalez-Carreño T, Sanz J. *J Phys Chem B* 1999;**103**:6160–70.
125. Coelho ACV, de Souza Santos H, Kiyohara PK, Marcos KNP, de Souza Santos P. *Mat Res* 2007;**10**(2):183–9. ISSN 1516–1439.
126. Tsybulya SV, Galina N. *Kryukov Phys Rev B* 2008;**77**:024112.
127. Favaro L, Boumaza A, Roy P, Lédion J, Sattonnay G, Brubach JB, et al. *J Solid State Chem* 2010;**183**:901–8.
128. Ollivier B, Retoux R, Lacorre P, Massiot D, Ferey G. *J Mater Chem* 1997;**7**:1049–56.
129. a. Yourdshahyan Y, Ruberto C, Bengtsson I, Lundqvist BI. *Phys Rev B* 1997;**56**:8553;  
b. Yourdshahyan Y, Ruberto C, Halvarsson M, Bengtsson L, Langer V, Lundqvist BI, et al. *J Am Ceram Soci* 1999;**82**:1365.
130. MacKenzie KJD, Temuujin J, Okada K. *Thermochim Acta* 1999;**327**:103–8.
131. Cocke DL, Johnson ED, Merrill RP. *Catal Rev Sci Eng* 1984;**26**:163.
132. Abbattista F, Delmastro S, Gozzelino G, Mazza D, Vallino M, Busca G, et al. *J Catal* 1989;**117**:42.
133. Dressler M, Nofz M, Malz F, Pauli J, Jäger C, Reinsch S, et al. *J Solid State Chem* 2007;**180**(9):2409–19.
134. Hicks RW, Pinnavaia TJ. *Chem Mater* 2003;**15**:78.
135. Zhang Z, Pinnavaia TJ. *Angew Chem Int Ed* 2008;**47**:7501–4.
136. Dumesic JA, Fripiat JJ, editors. *Acidity in aluminas, amorphous and crystalline silicoaluminates*, *Topics in Catal* 1997; **4**(1–2):1–171.
137. Busca G. *Phys Chem Chem Phys* 1999;**1**:723.
138. Busca G. In: Fierro JLG, editor. *Metal oxides chemistry and applications*. CRC Press; 2005. p. 247.
- 139a. Busca G. *Chem Rev* 2007;**107**:5366.
- 139b. Busca G. *Catal Today* 2014;**226**:2–13.
- 139c. Busca G. *Advan Catal Relat Subj* 2014;**57**: in press.
140. Liu X, Truitt RE. *J Am Chem Soc* 1997;**119**:9856–60.
141. Lundie DT, McInroy AR, Marshall R, Winfield JM, Jones P, Dudman CC, et al. *J Phys Chem B* 2005;**109**:11592–601.
142. Reller A, Cocke DL. *Catal Lett* 1989;**2**:91–5.
143. Gribov EN, Zavorotynska O, Agostini G, Vitillo JG, Ricchiardi G, Spoto G, Zecchina A. *Phys Chem Chem Phys* 2010;**12**:6474–82.
144. Nortier P, Fourre P, Mohammed Saad AB, Saur O, Lavalley JC. *Appl Catal* May 7, 1990;**61**(1):141–60.
145. Sakashita S, Araki Y, Shiomada H. *Appl Catal A Gen* 2001;**215**:101–10.
146. Wischert R, Laurent P, Copéret C, Delbecq F, Sautet P. *J Am Chem Soc* 2012;**134**:14430–49.
147. Rozita Y, Brydson R, Scott AJ. *J Phys Conf Ser* 2010;**241**:012096.
148. Seo CW, Jung KD, Lee KY, Yoo KS. *Ind Eng Chem Res* 2008;**47**:6573–8.
149. Kwak JH, Hu J, Lukaski A, Kim DH, Szanyi J, Peden CHF. *J Phys Chem C* 2008;**112**:9486–92.

150. Kwak JH, Hu JZ, Mei D, Yi CW, Kim DH, Peden CHF, et al. *Science* 2009;**325**:1670–3.
151. Mei D, Kwak JH, Hu JZ, Cho SJ, Szanyi J, Allard LF, et al. *J Phys Chem Lett* 2010;**1**:2688–91.
152. Mei D, Ge Q, Szanyi J, Peden CHF. *J Phys Chem C* 2009;**113**:7779–89.
153. Dabbagh HA, Taban K, Zamami M, Mol J. *Catal a Chem* 2010;**326**:55–68.
154. Ouyang CY, Sljivancanin Z, Baldereschi A. *Phys Rev B* 2009;**79**:235410.
155. Busca G, Rossi PF, Lorenzelli V, Benaissa M, Travet J, Lavalley JC. *J Phys Chem* 1985;**89**:5433.
156. Knözinger H, Krietenbrink H, Müller HD, Schulz W. *Proceedings of the 6th Int. Congr.* London: Catal; 1976. P. 183.
157. Busca G. *Catal Today* 1996;**27**:457.
158. Pistarino C, Finocchio E, Romezzano G, Bricchese F, DiFelice R, Busca G, et al. *Ind Eng Chem Res* 2000;**39**:2752.
159. Carmello D, Finocchio E, Marsella A, Cremaschi B, Leofanti G, Padovan M, et al. *J Catal* 2000;**191**:354.
160. Busca G, Finocchio E, Lorenzelli V, Trombetta M, Rossini SA. *J Chem Soc Faraday Trans* 1996;**92**:4687.
161. Hong Y, Chen FR, Fripiat JJ. *Catal Lett* 1993;**17**:187.
162. Peri JB. *J Phys Chem* 1965;**69**:211.
163. Tsyganenko A, Filimonov VN. *Spectrosc Lett* 1972;**5**:477.
164. Knözinger H, Ratnasamy P. *Catal Rev Sci Eng* 1978;**17**:31.
165. Busca G, Lorenzelli V, Ramis G, Willey RJ. *Langmuir* 1993;**9**:1492.
166. Busca G, Lorenzelli V, Escribano VS, Guidetti R. *J Catal* 1991;**131**:167.
167. Tsyganenko AA, Mardilovich PP. *J Chem Soc Faraday Trans* 1996;**92**:4843.
168. Fripiat J, Alvarez L, Sanchez Sanchez S, Martinez Morades E, Saniger J, Sanchez N. *Appl Catal A Gen* 2001;**215**:91.
169. Digne M, Sautet P, Raybaud P, Euzen P, Toulhoat H. *J Catal* 2002;**211**:1.
170. Lambert JF, Che M. *J Mol Catal A Chem* 2000;**162**:5.
171. Kasprzyk-Hordern B. *Adv Colloid Interface Sci* 2004;**110**:19–48.
172. Busca G. In: Jackson SD, Hargreaves JSJ, editors. *Metal oxide catalysis*, vol. 1. Wiley-VCH; 2009. p. 140.
173. Tretyakov NE, Filimonov VN. *Kinet Katal* 1972;**13**:815.
174. Trombetta M, Busca G, Rossini S, Piccoli V, Cornaro U. *J Catal* 1997;**168**:334.
175. Mohammed Saad AB, Ivanov VA, Lavalley JC, Nortier P, Luck F. *Appl Catal A Gen* 1993;**94**:71.
176. Busca G. In: Jackson SD, Hargreaves JSJ, editors. *Metal oxide catalysis*, vol. 1. Wiley-VCH; 2009. pp. 95–175.
177. Zagoruiko AN, Shinkarev VV, Vanag SV, Bukhtiyarova GA. *Catal Ind* 2010;**2**(4):343–52.
178. BASF Claus Catalysts, brochure. Available on the web. [www.basf.com](http://www.basf.com).
179. Pines H, Manassen J. *Adv Catal Relat Subj* 1966;**16**:49.
180. Hu YC. In: McKetta JJ, editor. *Chemical processing handbook*. New York: Dekker; 1993. p. 768.
181. Liu Z, Sun C, Wang G, Wang Q, Cai G. *Fuel Proc Technol* 2000;**62**:161.
182. Kim SM, Lee YJ, Bae JW, Potdar HS, Jun KW. *Appl Catal A Gen* September 30, 2008; **348**(1):113–20.
183. de Klerk A. *Catalysis* 2011;**23**:1–49.

184. Frank HG, Stadelhofer JW. *Industrial aromatic chemistry*. Springer Verlag; 1988.
185. Schmidt SA, Kumar N, Zhang B, Eränen K, Murzin DY, Salmi T. *Ind Eng Chem Res* 2012;**51**(12):4545–55.
186. [http://www.basf.com/group/corporate/en/brand/HF\\_200XPHF](http://www.basf.com/group/corporate/en/brand/HF_200XPHF) [accessed 10.12.12].
187. <http://www.catalysts.basf.com/p02/USWeb-Internet/catalysts/en/content/microsites/catalysts/prods-inds/adsorbents/act-alum-adsorb> [accessed 10.12.12].
188. Madon R, Harris DH, Xu M, Stockwell D, Lerner B, Dodwell GW. *FCC catalysts for feeds containing nickel and vanadium*. US Patent 6716338 to Engelhard Corporation.
189. Harris DH, Xu M, Stockwell D, Madon RJ. *FCC catalysts for feeds containing nickel and vanadium*. US Patent 6673235, to Engelhard Corporation.
190. Sato S, Takahashi R, Kobune M, Gotoh H. *Appl Catal A Gen* 2009;**356**(1):57–63.
191. Gotoh H, Yamada Y, Sato S. *Appl Catal A Gen* 2010;**377**(1–2):92–8.
192. Yamada Y, Segawa M, Sato F, Kojima T, Sato S. *J Mol Catal A Chem* 2011;**346**(1–2):79–86.
193. Valange S, Beauchaud A, Barrault J, Gabelica Z, Daturi M, Can F. *J Catal* 2007;**251**:113.
194. Sun H, Hu K, Lou H, Zhen X. *Energy Fuels* 2008;**22**:2756–60.
195. Imanaka N, Masui T. *Appl Catal A Gen* 2012;**431–432**:1–8.
196. Papa F, Luminita P, Osiceanu P, Birjega R, Akane M, Balint I. *J Mol Catal A Chem* July 20, 2011;**346**(1–2):46–54.
197. Papa F, Gingasu D, Patron L, Miyazaki A, Balint I. *Appl Catal A Gen* 2010;**375**(1):172–8.
198. Valsamakis I, Flytzani-Stephanopoulos M. *Appl Catal B Environ* 2011;**106**(1–2):255–63.
199. Dooley KM, Kalakota V, Adusumilli S. *Energy Fuels* 2011;**25**(3):1213–20.
200. Mamedov A. *Nickel/lanthana catalyst for producing syngas, to Sabic*. US Patent Application 20120007025.
201. Rapier CR, Xie S, Hu B, Ortego BC, Simon DE, Minahan DM. *Stabilized alumina supports, catalysts made therefrom, and their use in partial oxidation*. US Patent 7888278. Houston (TX, US): ConocoPhillips Company; 2011.
202. Vargas MAL, Casanova M, Trovarelli A, Busca G. *Appl Catal B Environ* 2007;**75**(3–4):303–11.
203. Tschauner O, Luo SN, Asimow PD, Ahrens TJ. *Am Mineral* 2006;**91**:1857–62.
204. Griffen DT. *Silicate crystal chemistry*. Oxford University Press; 1992.
205. Vogel W. *Chemistry of glass*. Columbus: The American Ceramic Society; 1985.
206. Wang LH, Tsai BJ. *Mater Lett* 2000;**43**:309–14.
207. <http://www.grace.com/Products/Sylobead/>.
208. Zhao L, Qin H, Wu R, Zou H. *J Chromatogr A* 2012;**1228**:193–204.
209. Tanev PT, Pinnavaia TJ. *Science* 1995;**267**:865–7.
210. Stöber W, Fink A, Bohn E. *J Colloid Interface Sci* 1968;**26**:62–9.
211. Plumeré N, Ruff A, Speiser B, Feldmann V, Mayer HA. *J Colloid Interface Sci* 2012;**368**:208–19.
212. Du X, He J. *Nanoscale* 2011;**3**:3984–4002.
213. Katz HS, Milesk JV. *Handbook of fillers for plastics*. Van Nostrand Reinhold; 1987. p.174.
214. Bakr HEGMM. *Asian J Mater Sci* 2010;**2**:121–36.
215. Yuan P, Wu DQ, He HP, Lin ZY. *Appl Surf Sci* April 15, 2004;**227**(1–4):30–9.
216. Prinsloo NM. *Ind Eng Chem Res* 2007;**46**(23):7838–43.

217. Akhtar F, Rehman Y, Bergström L. *Powder Technol* August 12, 2010;**201**(3):253–7.
218. Jibril BY, Al-Kinany MC, Al-Khowaiter SH, Al-Drees SA, Al-Megren HA, Al-Dosari MA, et al. *Catal Commun* February 2006;**7**(2):79–85.
219. Porto LM, Butt JB. *Ind Eng Chem Res* 2002;**41**(22):5420–6.
220. Bibby DM, Milestone NB, Aldridge LP. *Nature* August 23, 1979;**280**:664–5.
221. Fernández A-B, Marinas A, Blasco T, Fornés V, Corma A. *J Catal* 2006;**243**:270.
222. Camblor MA, Corma A, Diaz-Cabanas M-J, Baerlocher C. *J Phys Chem B* 1998;**102**:44.
223. Camblor MA, Corma A, Lightfoot P, Villaescusa LA, Wright PA. *Angew Chem Int Ed Engl* 1997;**36**:2659–61.
224. Corma A, Rey F, Rius J, Sabater MJ, Valencia S. *Nature* 2004;**431**:287.
225. Kuperman A, Nadimi S, Oliver S, Ozin GA, Garces JM, Olken MM. *Nature* 1993;**365**:239.
226. <http://www.ussilica.com/uploads/files/product-data-sheets/industry/building-products/MINUSIL5-MillCreek.pdf>, 10.12.2012.
227. Busca G. *Phys Chem Chem Phys* 1999;**1**:723–36.
228. Gajan D, Copéret C. *New J Chem* 2011;**35**:2403–8.
229. Zhuravlev LT. *Colloids Surf A Physicochem Eng Asp* 2000;**173**:1–38.
230. Potapov VV, Zhuravlev LT. *J Volcanol Seismol* 2007;**5**:310–8.
231. Jiang Y, Huang J, Dai W, Hunger M. *Solid State Nucl Magn Reson* 2011;**39**:116–41.
232. Murray DK. *J Colloid Interface Sci* 2011;**352**:163–70.
233. Hoffmann P, Knözinger E. *Surf Sci* 1987;**188**:181–98.
234. Morrow BA, Mc Farlan AJ. *J Phys Chem* 1992;**92**:1395–400.
235. Busca G. *Curr Phys Chem* 2012;**2**:136–50.
236. Gallas JP, Goupil JM, Vimont A, Lavalley JC, Gil B, Gilson JP, et al. *Langmuir* 2009;**25**:5825–34.
237. Ghiotti G, Garrone E, Morterra C, Boccuzzi F. *J Phys Chem* 1979;**83**:2863–9.
238. Marrone M, Montanari T, Busca G, Conzatti L, Costa G, Castellano M, et al. *J Phys Chem B* 2004;**108**:3563–72.
239. Bevilacqua M, Montanari T, Finocchio E, Busca G. *Catal Today* 2006;**116**:132–42.
240. Burneau A, Barres O, Gallas JP, Lavalley JC. *Langmuir* 1990;**6**:1364–72.
241. Yuana P, Wua DQ, Hea HP, Lin ZY. *Appl Surf Sci* 2004;**227**:30–9.
242. Ghiazza M, Gazzano E, Bonelli B, Fenoglio I, Polimeni M, Ghigo D, et al. *Chem Res Toxicol* 2009;**22**:136–45.
243. Francis SM, Stephens WE, Richardson NV. *Environ Health* 2009;**8**(Suppl. 1):S4. <http://dx.doi.org/10.1186/1476-069X-8-S1-S4>.
244. Fenoglio I, Ghiazza M, Ceschino R, Gillio F, Martra G, Fubini B. *Surf Chem Biomed Environ Sci* 2006;**2**:287–98.
245. Napierska D, Thomassen LCJ, Lison D, Martens JA, Hoet PH. The nanosilica hazard: another variable entity. PMID: PMC3014868 *Part Fibre Toxicol* 2010;**7**:39. <http://dx.doi.org/10.1186/1743-8977-7-39>. Published online December 3, 2010.
246. Zecchina A, Bordiga S, Spoto G, Marchese L, Petrini G, Leofanti G, et al. *J Phys Chem* 1992;**96**:4991–7.
247. Astorino E, Peri J, Willey RJ, Busca G. *J Catal* 1995;**157**:482–500.
248. Armaroli T, Bevilacqua M, Trombetta M, Milella F, Gutiérrez Alejandro A, Ramirez Solis J, et al. *Appl Catal A Gen* 2001;**216**:59–71.
249. Qin G, Zheng L, Xie Y, Wu C. *J Catal* 1985;**95**:609–12.
250. Datka J, Tuznik E. *Zeolites* 1985;**5**:230–2.

251. Yamagishi K, Namba S, Yashima T. *J Phys Chem* 1991;**95**:872–7.
252. Flego C, Dalloro L. *Microporous Mesoporous Mater* 2003;**60**:263–71.
253. Woolery GL, Alemany LB, Dessau RM, Chester AW. *Zeolites* 1986;**6**:14–6.
254. Dessau RM, Schmitt KD, Kerr GT, Woolery GL, Alemany LB. *J Catal* 1987;**104**:484–9.
255. Heitman G-P, Dahlhoff G, Hölderich WF. *J Catal* 1999;**186**:12–9.
256. Busca G. *Catal Today* 1998;**41**:191–206.
257. Parida SK, Dash S, Patel S, Mishra BK. *Adv Colloid Interface Sci* 2006;**121**:77–110.
258. Bennici S, Aroux A. In: Jackson SD, Hargreaves JSJ, editors. *Thermal analysis and calorimetric methods, in metal oxide catalysis*. Wiley; 2009. pp. 391–442.
259. Rosenholm JM, Mamaeva V, Sahlgren C, Lindén M. *Nanomedicine* 2012;**7**(1):111–20.
260. Murashov V, Harper M, Demchuk E. *J Occup Environ Hyg* December 2006;**3**(12):718–23.
261. Parmaliana A, Arena F, Frusteri F, Martínez-Arias A, López Granados M, Fierro JLG. *Appl Catal A Gen* 2002;**226**:163–74.
262. Ono T, Nakamura M, Unno K, Oyun A, Ohnishi J, Kataoka M, Fujio K. *J Mol Catal A Chem* 2008;**285**:169–75.
263. Minakata S, Komatsu M. *Chem Rev* 2009;**109**:711–24.
264. Flego C, Dalloro L. *Microporous Mesoporous Mater* 2003;**60**:263.
265. Heitmann GP, Dahlhoff G, Hölderich WF. *J Catal* 1999;**186**:12.
266. Louie DK. *Handbook of sulphuric acid manufacturing*. 2nd ed. DKL engineering; August 2008.
267. <http://www.sulphuric-acid.com/>.
268. Precious metal powder catalysts, Evonik, brochure. Available on the web. [www.evonik.com](http://www.evonik.com)
269. *General catalyst catalogue, Sud Chemie*; 2012. Available on the web.
270. Continuous process catalysts, Evonik, brochure. Available on the web. [www.evonik.com](http://www.evonik.com)
271. <http://catalysts.evonik.com/product/catalysts/en/products/catalyst-guide/brands/pages/default.aspx>.
272. Landmann M, Rauls E, Schmidt WG. *J Phys Condens Mater* 2012;**24**. 195503, 6 pp.
273. Zhang W, Zhu Z, Cheng CY. *Hydrometallurgy* 2011;**108**:177–88.
274. Chang JA, Vithal M, Baek IC, Seok SI. *J Solid State Chem* 2009;**182**:749–56.
275. Bavykin DV, Friedrich JM, Walsh FC. *Adv Mater* 2006;**18**:2807–24.
276. Ou HH, Lo SL. *Sep Purif Technol* 2007;**58**:179–91.
277. Enyashin AN, Ivanovskii AL. *J Phys Chem C* 2009;**113**:20837–40.
278. Henderson MA. *Surf Sci Rep* 2011;**66**:185–297.
279. Patzke GR, Zhou Y, Kontic R, Conrad F. *Angew Chem Int Ed* 2011;**50**:826–59.
280. Ismail AA, Bahnemann DW. *J Mater Chem* 2011;**21**:11686–707.
281. Macwan DP, Dave PN, Chaturvedi S. *J Mater Sci* 2011;**46**:3669–86.
282. Berger S, Schmuki P, Poulomi Roy. *Angew Chem Int Ed* 2011;**50**:2904–39.
283. Wong CL, Tan YN, Mohamed AR. *J Environ Manage* 2011;**92**:1669–80.
284. Zhou M, Yu J, Liu S, Zhai P, Huang B. *Appl Catal B Environ* 2009;**89**:160–6.
285. Choi H, Kim YJ, Varma RS, Dionysios DD. *Chem Mater* 2006;**18**:5377–84.
286. Ribbens S, Beyers E, Schellens K, Mertens M, Ked X, Bals S, et al. *Microporous Mesoporous Mater* 2012;**156**:62–72.

287. Inada M, Mizue K, Enomoto N, Hojo J. *Sci Adv Mater* 2010;**2**:102–6.
288. Ismaila AA, Kandiel TA, Bahnemann DW. *J Photochem Photobiol A Chem* 2010;**216**: 183–93.
289. Busca G, Saussey H, Saur O, Lavalley JC, Lorenzelli V. *Appl Catal* 1985;**14**: 245–60.
290. Ferretto L, Glisenti A. *Chem Mater* 2003;**15**:1181.
291. Dzwigaj S, Arrouvel C, Breyse M, Geantet C, Inoue S, Toulhoat H, et al. *J Catal* 2005;**236**:245.
292. Toledo-Antonio JA, Cortés-Jácome MA, Navarrete J, Angeles-Chavez C, López-Salinas E, Rendon-Rivera A. *Catal Today* 2010;**155**(3–4):247–54.
293. Liu S, Yu J, Jaroniec M. *Chem Mater* 2011;**23**:4085–93.
294. Reyes-Coronado D, Rodríguez-Gattorno G, Espinosa-Pesqueira ME, Cab C, de Coss R, Oskam G. *Nanotechnology* 2008;**19**. 145605, 10 pp.
295. Svoronos PDN, Bruno TJ. *Ind Eng Chem Res* 2002;**41**:5321.
296. Busca G, Lietti L, Ramis G, Berti F. *Appl Catal B Envir* 1998;**18**:1.
297. Forzatti P, Lietti L, Tronconi E. In: Barbaro P, Bianchini C, editors. *Catalysis for sustainable energy production*. Weinheim: J. Wiley-VCH; 2009. pp. 393–438.
298. Breyse M, Geantet C, Afanasiev P, Blanchard J, Vrinat M. *Catal Today* January 15, 2008;**130**(1):3–13.
299. Corti CW, Holliday RJ, Thompson DT. *Top Catal* June 2007;**44**(1–2):331–43.
300. Seki K. *Catal Surv Asia* 2010;**14**:168.
301. Fernández López E, Sanchez Escribano V, Panizza M, Carnasciali MM, Busca G. *J Mater Chem* 2001;**11**:1891.
302. Carter GA, Ogden MI, Buckley CE, Maitland C, Paskevicius M. *Powder Technol* 2009;**188**:222.
303. Carter GA, Rowles M, Ogden MI, Hart RD, Buckley CE. *Mater Chem Phys* 2009;**116**: 607–14.
304. Liu A, Cole TJ, Turbeville W. *Promoted zirconium oxide catalyst support*. US Patent Application US 2011/0301021 A1, to Sud Chemie; 2011.
305. Shen JP, Fu K, Zheng J, Atanassova P, Hampden-Smith MJ. *High surface area tetragonal zirconia and processes for synthesizing them*. US Patent 7704483 B2, to Cabot Corporation; 2010.
306. Guo GY, Chen YL. *J Solid State Chem* 2005;**178**:1675–82.
307. Che H, Han S, Hou W, Liu A, Wang S, Sun Y, Cui X. *J Porous Mater* 2011;**18**:57–67.
308. Pokrovskii K, Jung KT, Bell AT. *Langmuir* 2001;**17**:4297.
309. Davies LE, Bonini NA, Locatelli S, Gonzo EE. *Lat Am Appl Res* 2005;**35**:23–8.
310. Renz M. *Eur J Org Chem*; 2005:979–88.
311. Leino E, Mäki-Arvela P, Eta V, Murzin DY, Salmi T, Mikkola J-P. *Appl Catal A Gen* 2010;**383**(1–2):1–13.
312. Ziolk M, Kujawa J, Czyniewska J, Nowak I, Aboulayt A, Saur O, et al. *Appl Catal A Gen* 1998;**171**:109–15.
313. McGuire NE, Kondamudi N, Petkovic LM, Ginosar DM. *Appl Catal A Gen* 2011; **429–430**:59–66.
314. Yokoyama T, Yamagata N. *Appl Catal A Gen* 2001;**221**:227–39.
315. Fauth D, Frommell EA, Hoffmann JS, Reasbeck RP, Penline HW. *Fuel Process Technol* 2005;**86**:1503–21.
316. Arata K. In: Jackson SD, Hargreaves SJS, editors. *Metal oxide catalysis*. Wiley; 2009. pp. 665–704.

317. Schmidt F, Köhler E. In: Guisnet M, Gilson JP, editors. *Zeolites for cleaner technologies*. Imperial College Press; 2002. pp. 153–66.
318. Weyda H, Köhler E. *Catal Today* 2003;**81**:51.
319. Bolis V, Magnacca G, Cerrato G, Morterra C. *Top Catal* 2002;**19**:259.
320. Klose BS, Jentoft FC, Joshi P, Trunschke A, Schlögl R, Subbotina IR, et al. *Catal Today* 2006;**116**:121.
321. Manoilova O, Olindo R, Otero Areán C, Lercher JA. *Catal Commun* 2007;**8**:865.
322. Smirnova MY, Toktarev AV, Ayupov AB, Echevsky GV. *Catal Today* 2010;**152**:17–23.
323. Yu H, Fang H, Zhang H, Li B, Deng F. *Catal Commun* 2009;**10**:920–4.
324. Quaschnig V, Auroux A, Deutsch J, Lieske H, Kemnitz E. *J Catal* 2001;**203**(2):426–33.
325. Barthos R, Onyestyak Gy, Valyon J. *J Phys Chem B* 2000;**104**:7311.
326. Dijks IJ, Geus JW, Jenneskens LW. *J Phys Chem B* 2003;**107**:13403.
327. Katada N, Endo J, Notsu K, Yasunobu N, Naito N, Niwa M. *J Phys Chem B* 2000;**104**:10321.
328. Hammache S, Goodwin JG. *J Catal* 2003;**218**:258.
329. Lohitarn N, Lotero E, Goodwin JG. *J Catal* 2000;**241**:328.
330. <http://www.uop.com/products/catalysts/isomerization/>.
331. Alemán-Vázquez LO, Cano-Domínguez JL, Torres-García E, Villagómez-Ibarra JR. *Molecules* 2011;**16**:5916–27.
332. Busto M, Vera CR, Grau JM. *Fuel Process Technol* 2011;**92**(9):1675–84.
333. Klose-Schubert BS, Jentoft RE, Jentoft F. *Top Catal* 2011;**54**:398–414.
334. Cavani F, guidetti S, Trevisanut C, Ghedini E, Signoretto M. *Appl Catal A* 2011;**409–410**:267–78.
335. Ratnasamy C, Wagner J. Water gas shift catalysis. *Catal Rev Sci Eng* 2009;**51**(3):325–440.
336. Liu K, Wang A, Zhang T. *ACS Catal* 2012;**2**(6):1165–78.
337. Domingos D, Rodrigues LMTS, Brandão ST, Da Rocha MDGC, Frety R. *Quimica Nova* 2012;**35**(6):1118–22.
- 337b. Trovarelli A, Fornasiero P, editors. *Catalysis by ceria and related materials*. 2nd ed. London: Imperial College Press; 2013.
338. Polychronopoulou K, Kalamaras CM, Efstathiou AM. *Recent Pat Mater Sci* 2011;**4**(2):122–45.
339. Nagashima O, Sato S, Takahashi R, Sodesawa T, Akashi T. *Appl Catal A Gen* 2006;**312**:175.
340. Vivier L, Duprez D. *ChemSusChem* 2010;**3**(6):654–78.
341. Nagashima O, Sato S, Takahashi R, Sodesawa T. *J Mol Catal A Chem* 2005;**227**:231.
342. Fernández López E, Sánchez Escribano V, Panizza M, Resini C, Gallardo-Amores JM, Busca G. *Solid State Sci* 2003;**5**:1369.
343. Tanabe K. *Catal Today* 2003;**78**:65.
344. Ziolk M. *Catal Today* 2003;**78**:47.
345. Chernyshkova FA. *Russ Chem Rev* 1993;**62**:743.
346. Nowak I, Ziolk M. *Chem Rev* 1999;**99**:3603.
347. Nakajima K, Baba Y, Noma R, Kitano M, N. Kondo J, Hayashi S, et al. *J Am Chem Soc* 2011;**133**(12):4224–7.
348. Martins RTL, Schitine WJ, Castro FR. *Catal Today* 1989;**5**:483.

349. Armaroli T, Busca G, Carlini C, Giuttari M, Raspolli Galletti A, Sbrana G. *J Mol Catal* 2000;**151**:233.
350. Review Article Zhao Y, Zhou X, Ye L, Tsang SCE. *Nano Rev* 2012;**3**:17631.
351. Okuhara T. *Chem Rev* 2002;**102**:3641.
352. Carlini C, Giuttari M, Raspolli Galletti AM, Sbrana G, Armaroli T, Busca G. *Appl Catal A Gen* 1999;**183**:295.
353. Carniti P, Gervasini A, Biella S, Auroux A. *Catal Today* 2006;**118**:373.
354. Lacerda Jr V, dos Santos DA, da Silva-Filho LC, Greco SJ, dos Santos RB. *Aldrichimica Acta* 2012;**45**(1):19–27.
355. Takagaki A, Tagusagawa C, Takanabe K, Kondo JN, Tatsumi T, Domen K. *Catal Today* 2012;**192**(1):144–8.
356. Tagusagawa C, Takagaki A, Iguchi A, Takanabe K, Kondo JN, Ebitani K, et al. *Catal Today* 2011;**164**(1):358–63.
357. Zhang Y, Wang J, Ren J, Liu X, Li X, Xia Y, et al. *Catal Sci Technol* 2012;**2**(12):2485–91.
358. Musialaska K, Finocchio E, Sobczak I, Busca G, Wojcieszak R, Gaigneaux E, et al. *Appl Catal A Gen* 2010;**384**(1–2):70–7.
359. Pham HN, Pagan-Torres YJ, Serrano-Ruiz JC, Wang D, Dumesic JA, Datye AK. *Appl Catal A Gen* 2011;**397**(1–2):153–62.
360. Chatten R, Chadwick AV, Rougier A, Lindan PJD. *J Phys Chem B* 2005;**109**:3146.
361. Ramis G, Cristiani C, Elmi AS, Villa PL, Busca G. *J Mol Catal* 1990;**61**:319.
362. Li L, Krissanasaerane M, Pattinson SW, Stefik M, Wiesner U, Steiner U, et al. *Chem Commun* 2010;**46**(40):7620–2.
363. Nguyen T-A, Jun T-S, Rashid M, Kim YS. *Mater Lett* 2011;**65**(17–18):2823–5.
364. Chu W, Echizen T, Kamiya Y, Okuhara T. *Appl Catal A Gen* 2004;**259**:199.
365. Tagusagawa C, Takagaki A, Iguchi A, Takanabe K, Kondo JN, Ebitani K, et al. *Chem Mater* 2010;**22**(10):3072–8.
366. J.C. Mol *J Mol Catal A Chem* 2004;**213**:39–45.
367. Fierro JLG, Mol JC. In: Fierro JLG, editor. *Metal oxides: chemistry and applications*. Boca Raton (FL, USA): CRC Press; 2005. p. 517.
368. Spamer A, Dube TI, Moodley DJ, van Schalkwyk C, Botha JM. *Appl Catal A Gen* 2003;**255**:133–42.
369. Wachs IE, Kim T, Ross EI. *Catal Today* 2006;**116**:162.
370. Baertsch CD, Komala KT, Chua Y-H, Iglesia E. *J Catal* 2002;**205**:44.
371. Kuba S, Che M, Grasselli RK, Knözinger H. *J Phys Chem B* 2003;**107**:3459.
372. Zhou W, Ross-Medgaarden EI, Knowles WV, Wong MS, Wachs IE, Kiely CJ. *Nat Chem* December 2009;**1**(9):722–8.
373. Hernández ML, Montoya JA, Del Angel P, Hernandez I, Espinosa G, Llanos ME. *Catal Today* 2006;**116**:169.
374. [http://www.exxonmobil.com/Refiningtechnologies/pdf/refin\\_EMICT\\_japan\\_beck110100.pdf](http://www.exxonmobil.com/Refiningtechnologies/pdf/refin_EMICT_japan_beck110100.pdf).
375. Gnanamani MK, Linganiso LZ, Jacobs G, Keogh RA, Shafer WD, Davis BH. *Catal Lett* 2012;**142**(10):1180–9.
376. Van Bokhoven JA. In: Valtchev V, Mintova S, Tsapatsis M, editors. *Ordered porous solids, recent advances and prospects*. Elsevier; 2009. pp. 651–68.
377. Chen T-H, Houthoofd K, Grobet PJ. *Microporous Mesoporous Mater* 2005;**86**(1–3):31–7.



378. Hensen EJM, Poduval DG, Magusin PCMM, Coumans AE, Veen JARV. *J Catal* 2010; **269**(1):201–18.
379. Trombetta M, Busca G, Lenarda M, Storaro L, Pavan M. *Appl Catal A Gen* 1999; **182**(2):225–35.
380. Suzuki K, Aoyagi Y, Katada N, Choi M, Ryoo R, Niwa M. *Catal Today* 2008; **132**(1–4):38–45.
381. Luan Z, Fournier JA. *Microporous Mesoporous Mater* 2005;**79**:235–40.
382. Koekkoek AJJ, Van Veen JAR, Gerrtisen PB, Giltay P, Magusin PCMM, Hensen EJM. *Microporous Mesoporous Mater* 2012;**151**:34–43.
383. Bonelli B, Onida B, Chen JD, Galarneau A, Di Renzo F, Fajula F, et al. *Microporous Mesoporous Mater* 2004;**67**:95–106.
384. Morin S, Ayrault P, El Mouahid S, Gnep NS, Guisnet M. *Appl Catal A Gen* 1997;**159**:317–31.
385. Corma A, Grande MS, Gonzalez-Alfonso V, Orchilles AV. *J Catal* 1996;**159**:375–82.
386. Di Renzo F, Chiche B, Fajula F, Viale S, Garrone E. *Stud Surf Sci Catal* 1996;**101**:851–60.
387. Góra-Marek K, Datka J. *Appl Catal A Gen* 2006;**302**:104–9.
388. Zamaraev KI, Thomas JM. *Adv Catal* 1996;**41**:335–58.
389. Poduval DG, van Veen JAR, Rigutto MS, Hensen EJM. *Chem Commun* 2010;**46**:3466–8.
390. Crépeau G, Montouillout V, Vimont A, Mariey L, Cseri T, Maugé F. *J Phys Chem B* 2006;**110**:15172–85.
391. Garrone E, Onida B, Bonelli B, Busco C, Ugliengo P. *J Phys Chem B* 2006;**110**:19087–92.
392. Cairon O. *Phys Chem Chem Phys* 2010;**12**:6333–6.
393. Chizallet C, Raybaud P. *Angew Chem Int Ed* 2009;**48**:2891–3.
394. Chizallet C, Raybaud P. *Chemphyschem* 2010;**11**:105–8.
395. Huang J, van Vegten N, Jiang Y, Hunger M, Baiker A. *Angew Chem Int Ed* 2010;**49**:7776–81.
396. Hensen EJM, Poduval DG, Degirmenci V, Ligthart DAJM, Chen W, Maugé F, et al. *J Phys Chem C* 2012;**116**(40):21416–29.
397. Chizallet C, Raybaud P. *ChemPhysChem* 2010;**11**(1):105–8.
398. Leydier F, Chizallet C, Chaumonnot A, Digne M, Soyer E, Quoineaud A-A, et al. *J Catal* 2011;**284**(2):215–29.
399. Trombetta M, Busca G, Rossini S, Piccoli V, Cornaro U, Guercio A, et al. *J Catal* 1998;**179**(2):581–96.
400. Serrano DP, Aguado J, Escola JM. *ACS Catal* 2012;**2**(9):1924–41.
401. Sannita E, Aliakbarian B, Casazza AA, Perego P, Busca G. *Renew Sustain Energy Rev* 2012;**16**(8):6455–75.
402. Yu Y, Fonfó B, Jentys A, Haller GL, Van Veen JAR, Gutiérrez OY, et al. *J Catal* 2012; **292**:1–12.
403. Piccolo L, Nassreddine S, Toussaint G, Geantet C. *ChemSusChem* 2012;**5**(9):1717–23.
- 403b. Perego P, Millini R. *Chem Soc Rev* 2013;**42**:3956–76.
404. Yaripour F, Baghaei F, Schmidt I, Perregaard J. *Catal Commun* 2005;**6**:147.
405. Butler AC, Nicolaidis CP. *Catal Today* 1993;**18**:443.
406. Seo G. *Catal Surv Asia* 2005;**9**(3):139–46.

407. Finocchio E, Busca G, Rossini S, Cornaro U, Piccoli V, Miglio R. *Catal Today* 1997;**33**:335.
408. Notari B, Willey RJ, Panizza M, Busca G. *Catal Today* 2006;**116**:99.
409. Gutierrez A, Trombetta M, Busca G, Ramirez J. *Microporous Mesoporous Mater* 1997;**12**:79.
410. Gutierrez A, Gonzalez M, Trombetta M, Busca G, Ramirez J. *Microporous Mesoporous Mater* 1998;**23**:265.
411. Daturi M, Cremona A, Milella F, Busca G, Vogna EJ. *Eur Ceram Soc* 1998;**18**:1079.
412. Ramirez J, Cedeño L, Busca GJ. *Catal* 1999;**184**:59.
413. Maity SK, Ancheyta J, Rana MS, Rayo P. *Energy Fuels* 2006;**20**:427.
414. Wang J, Wen J, Shen M. *J Phys Chem C* 2008;**112**(13):5113–22.
415. Twigg MV. *Catal Today* 2011;**163**(1):33–41.
416. Busca G, Lorenzelli V, Sanchez Escribano V, Guidetti RJ. *Catal* 1991;**131**:167.
417. Busca G, Lorenzelli V, Sanchez Escribano V. *Chem Mater* 1992;**4**:595.
418. Busca G, Lorenzelli V, Ramis G, Willey R. *Langmuir* 1993;**9**:1492.
419. Wang Y, Wei Han X, Ji A, Shi LY, Hayashi S. *Microporous Mesoporous Mater* 2005;**77**:139.
420. Vaccari A. *Appl Clay Sci* 1999;**14**:161.
421. Tichit D, Coq B. *Cattech* 2003;**7**:206–17.
422. Centi G, Perathoner S. *Microporous Mesoporous Mater* 2008;**107**:3.
423. Debecker DP, Gaigneaux EM, Busca G. *Chem Eur J* 2009;**15**:3920.
424. Ueda H, Takamoto T, Okuda K (Sumitomo chemical Co.). US Patent 5,334,770; 1994.
425. [www.chemistryinnovation.co.uk/roadmap/sustainable/files/39021\\_1216793/TechnologyAreaSolidCats.pdf](http://www.chemistryinnovation.co.uk/roadmap/sustainable/files/39021_1216793/TechnologyAreaSolidCats.pdf).
426. Nikolopoulos AA, Jang BW-L, Spivey JJ. *Appl Catal A Gen* 2005;**296**:128.
427. Bialowas E, Szymanowski J. *Ind Eng Chem Res* 2004;**43**:6267.
428. Albertazzi S, Busca G, Finocchio E, Glöckler R, Vaccari A. *J Catal* 2004;**223**:372.
429. Røstrup-Nielsen R, Sehested J, Nørskov JK. *Adv Catal* 2002;**47**:66.
430. Montanari T, Sisani M, Nocchetti M, Vivani R, Herrera Delgado MC, Ramis G, et al. *Catal Today* 2010;**152**:104–9.
431. Bournay L, Casanave D, Delfort B, Hillion G, Chodorge JA. *Catal Today* 2005;**106**:190.

# Zeolites and Other Structurally Microporous Solids as Acid–Base Materials

## CHAPTER OUTLINE

<b>7.1 Zeolites</b> .....	<b>198</b>
7.1.1 Structural chemistry of zeolites .....	198
7.1.2 Preparation chemistry of synthetic zeolites .....	201
7.1.3 Natural zeolites and their surface-related applications .....	201
7.1.4 Alkali and alkali earth cationic zeolites and their industrial applications .....	204
7.1.4.1 LTA zeolites as adsorbents .....	206
7.1.4.2 Alkali and alkali earth exchanged faujasites as adsorbents .....	207
7.1.4.3 Silver zeolites as regenerable mercury removal adsorbents .....	208
7.1.4.4 Alkali and alkaline earth zeolites as catalysts .....	210
7.1.4.5 Alkali zeolites as catalyst supports .....	210
7.1.5 Protonic zeolites: acidity and shape selectivity .....	212
7.1.5.1 The bridging hydroxyl groups .....	212
7.1.5.2 Extraframework material .....	214
7.1.5.3 Molecular sieving and shape selectivity .....	215
7.1.5.4 The external surface of protonic zeolites .....	215
7.1.5.5 Production of hierarchically porous zeolites .....	216
7.1.6 Some particular protonic zeolites applied in the industry .....	216
7.1.6.1 Erionite .....	216
7.1.6.2 Ferrierite (H-FER) .....	217
7.1.6.3 Other medium-pore zeolites of interest in butene skeletal isomerization and <i>n</i> -paraffin hydroisomerization .....	219
7.1.6.4 ZSM5 (H-MFI) .....	220
7.1.6.5 ZSM-12 (H-MTW) .....	224
7.1.6.6 Beta zeolite (H-BEA) .....	224
7.1.6.7 MCM-22 (H-MWW) .....	226
7.1.6.8 Mordenite (H-MOR) .....	229
7.1.6.9 Zeolite omega (H-MAZ) .....	230
7.1.6.10 EU-1 (H-EUO) .....	231
7.1.6.11 Faujasite (H-FAU: H-Y, H-USY, RE-Y) .....	231

7.2 Aluminophosphates (AIPs) .....	234
7.3 Silicoaluminophosphates (SAPs) .....	234
7.4 Metal heteroatom containing aluminophosphates (MAPs) .....	237
7.5 Very large-pore zeolitic inorganic materials .....	237
7.6 Zeolite-like titanosilicates .....	237
7.7 Metal Organic Frameworks (MOFs) and similar materials.....	239
References .....	241

## 7.1 Zeolites

The history of zeolites<sup>1</sup> began in 1756, when Axel Cronstedt, a Swedish mineralogist, reported his observations on “an unknown species of rock” and coined the name zeolite by combining the Greek words ζειν (“zein” = to boil) and λιθος (“lithos” = rock). Milestones in the application of zeolites have been the first assessment of their adsorption properties and the first synthetic preparation of mordenite by Barrer in the forties and the industrial preparation of zeolites A, X, Y in the Linde Air Products division of Union Carbide by Milton and Breck in the fifties.

Zeolites are natural and synthetic silicoaluminates characterized by a microporous crystal structure. The substitution of aluminum for silicon in a silica covalent network leads to a charge unbalance, which must be compensated by “extra-framework” cations, mostly alkaline. This occurs in the cases of the so-called “stuffed silicas”: these alkali aluminosilicate materials have structures strictly related to the crystalline forms of silica, but with cations in the interstices to counterbalance the presence of Al ions substituting for Si. This is the case, for example, of Eucryptite ( $\text{LiAlSiO}_4$ , a stuffed  $\beta$ -quartz) or nepheline ( $\text{NaAlSiO}_4$ , a stuffed tridymite). A similar mechanism also occurs in the amorphous networks of glasses.

In the case of natural zeolites, balancing cations (usually alkali or alkali earth) are located in relatively large cavities formed by the  $[\text{Si}_{1-x}\text{Al}_x\text{O}_2]^{x-}$  negatively charged framework. These cavities are connected by channels that give rise to a variety of microporous structures that can be penetrated only by sufficiently small molecules, thus producing the “molecular sieving” effect, very important in adsorption technologies,<sup>2</sup> as well as the “shape-selectivity” effect, very relevant mostly for the acid catalysis performed by their protonic forms.<sup>3,4</sup> The cations are exchangeable, thus zeolites may also act as cationic exchangers. The exchange can be performed with ammonium ions that can be later decomposed into gaseous ammonia and a proton. This allows to produce protonic zeolites, which are very strong solid Brønsted acids. Today, protonic zeolites are mostly synthesized directly, by using templating agents. In this case, the protons may be residual from the combustion or decomposition of the templating agents.

### 7.1.1 Structural chemistry of zeolites

The framework structure of zeolites<sup>5</sup> is based on the two main structural units (basic building unit, BBU) constituted by silicon or aluminum atoms (sometimes other

elements) bonded to four oxygen atoms forming tetrahedra, and oxygen being bonded to two tetrahedral atoms normally bent (ca  $145^\circ$ ). The zeolite framework is built by combining BBUs into composite building units (CBUs). Tetrahedra are linked together, forming rings: the most common rings contain 4, 5, 6, 8, 10 or 12 tetrahedra, and are denoted as n-rings (e.g. 10-ring for a ring involving 10 tetrahedra) or nMR (10 MR for 10 tetrahedra-Membered Ring). The combination of rings produces more complex CBUs such as “cages”. Other CBUs are “prisms”, “chains”, etc. The periodic arrangement of these complex units produces the framework, with the complex of its cavities, composed of different kinds of channels (e.g. straight, sinusoidal), cages, “pockets”, connected by rings that act as “windows” between the different cavities.

In March 2014, 218 zeolite-type framework structures have been established to exist, which are denoted by a three-capital letter code by the Structure Commission of the International Zeolite Association (IZA). A detailed description of the structure of each zeolite type and their code can be found in the IZA web site as well as in the book by Baerlocher et al. edited by IZA and Elsevier, and available on Internet.<sup>6</sup> The information given here is essentially taken from the website of IZA, which is gratefully acknowledged. In Table 7.1, the pore structure of some of the most common zeolite frameworks that find practical interest are summarized.

Zeolites can be classified according to different criteria.<sup>7</sup> The most commonly used concerns the dimensions of the pore apertures. According to that, zeolites can be divided in the following groups:

1. small-pore zeolites: constituted by channels delimited by 8-ring Member Rings (8 MR) with pore diameters around 4 Å.
2. medium-pore zeolites: constituted by channels delimited by 10 MR and pore apertures around 5–6 Å.
3. large-pore zeolites: constituted by channels delimited by 12 MR with pore diameters around 7 Å.
4. extra-large pore zeolites: constituted by channels delimited by rings of more than 12 MR and pore apertures larger than 7 Å.

This is a rough classification, because the shape of the pores is another important factor, since there are zeolites with pore apertures delimited by the same number of tetrahedra but with different shapes, making them to behave quite differently when adsorbing molecules.

Another criterion for classifying zeolitic materials is the dimensionality of their channels. Thus, zeolite structures comprised of (i) one-dimensional; (ii) two-dimensional; and (iii) three-dimensional pore systems exist, depending on the arrangement of the channels.

Zeolites have also been classified as “hydrophobic” or “hydrophilic”, or as “high silica”, with Si/Al a.r.  $> 10$ , intermediate silica ( $1.5 < \text{Si/Al a.r.} < 10$ ) or “low silica”, with Si/Al ratio  $\sim 1$ . Low-silica zeolites are hydrophilic, due to the presence of highly negatively charged framework and high concentration of either extra-framework cations or protons. High-silica zeolites are hydrophobic, according to the predominance of covalent Si–O–Si bridges at their internal surface.

**Table 7.1** A Summary of Some of the Most Common Zeolite Framework Types Applied in Catalysis and Adsorption

Name	Framework Code	Channel Properties Dimensionality	T Member of Ring	Channels Diameters (Å)	Cage Diameters (Å)
Chabazite	CHA	3D	8	3.8 × 3.8	9.4
Linde A	LTA	3D	8	4.0 × 4.0	13.0
Erionite	ERI	1D	8	3.6 × 5.2	15.1 × 6.3
Clinoptilolite	HEU	2D	8 and 10	3.6 × 4.6, 2.8 × 4.7, 3.1 × 7.5	
Ferrierite	FER	2D	8 and 10	3.5 × 4.8, 0.4 × 4.2	8.3
MCM-22	MWW	2D	10 + large cages	4.0 × 5.5, 4.1 × 5.1	7.0 × 7.0 × 18.7
EU-1	EUO	1D	10 + side pockets	4.1 × 5.4	5.1 × 6.8 × 14.0
ZSM-5	MFI	3D	10	5.1 × 5.5, 5.3 × 5.6	8.6
ZSM-22	TON	1D	10	4.6 × 5.7	
ZSM-48	*MRE	1D	10	5.6 × 5.3	
ZSM-23	MTT	1D	10	4.5 × 5.2	
ZSM-12	MTW	1D	12	5.6 × 6.0	
Linde L	LTL	1D	12	7.1 × 7.1	
Omega	MAZ	1D	12 and 8	3.1 × 31, 7.4 × 7.4	
Beta	*BEA	3D,	12 and 12	5.6 × 5.6, 6.6 × 6.7	13.9
Mordenite	MOR	1D (2D)	12 (12 and 8)	6.5 × 7.0 (2.6 × 5.7)	Side pockets 2.6 × 5.7 Å
Faujasite (Linde X and Y)	FAU	3D	12-rings	7.4 × 7.4	12.0 × 12.0 × 12.0

\* one of the members of the corresponding polytype family.

### 7.1.2 Preparation chemistry of synthetic zeolites

The original method for preparing zeolites was one based on hydrothermal crystallization of reactive alkali metal aluminosilicate gels at high pH and, typically 100 °C and ambient pressure. With this method, where alkali cations play the role of directing the formation of the zeolite structure, materials with low to intermediate Si/Al ratios (1–5) are produced in the cationic form. Exchange with ammonium ions allows the production of the ammonium forms of zeolites that can be converted into protonic forms by calcination with resulting decomposition of ammonium ions.

After the pioneering work of Barrer,<sup>8</sup> new techniques for the preparation of zeolites have been developed, mainly involving the use of “templates” or “organic structure directing agents” (SDAs or OSDAs).<sup>9,10</sup> Protonic zeolites are thus prepared at 100–200 °C, using cationic templates that are later decomposed, burnt off or washed off, leaving protons as the only balancing cationic species. With these techniques, the preparation of a number of new protonic zeolites with many different structures has also been obtained. With this method high-silica zeolites and, in the absence of aluminum species, a number of purely siliceous zeolites have been prepared (Chapter 6.4.5.1.8). From protonic zeolites, cationic zeolites may be produced by cationic exchange.

The addition of fluoride ions to the reactive gel led to more perfect and larger crystals of known molecular sieve structures as well as new structures and compositions. The fluoride ion also is reported to serve as a template (or SDA) in some cases. Fluoride addition extends the synthesis regime into the acidic pH region.

As discussed above for the preparation of silicas, the cheapest source of silicon is waterglass, i.e. an aqueous sodium silicate solution with small contamination of aluminum. Consequently, it cannot be used to prepare pure silica zeolites. To produce purely siliceous zeolites colloidal silica sols, fumed silicas, precipitated silicas as well as alkoxy-silanes can be used as the Si source. They are more expensive, and, at least for alkoxy silanes, toxicity concerns appear. As for the source of aluminum, Al salts or sodium aluminates are used.

### 7.1.3 Natural zeolites and their surface-related applications

A number of zeolites exist in nature as components of igneous rocks. In [Table 7.2](#) a list of properties of the most common natural zeolites can be found. They are mostly present in their alkali and/or alkali earth forms. Among them, clinoptilolite is the most abundant and is widely used, due to its low cost. Clinoptilolite exhibits the same framework topology of heulandite, denoted with the IZA code HEU, but with a higher Si/Al ratio (for clinoptilolites  $\text{Si/Al} > 4$ , while for heulandites  $\text{Si/Al} < 4$ ). The HEU framework ([Figure 7.1](#)) has a two-dimensional channel system consisting of 10-membered-ring ( $7.5 \times 3.1 \text{ \AA}$ ) channels and 8-MR ( $3.6 \times 4.6 \text{ \AA}$ ) intersected by 8-MR ( $4.7 \times 2.8 \text{ \AA}$ ) channels. In the representation of the zeolite framework usually given, as that reported in the left side of [Figure 7.1](#), each segment represent a T–O–T bridge (T = tetrahedral atom), which is almost always bent. A more detailed structure is reported in the right side of [Figure 7.1](#),

**Table 7.2** Some Properties of Natural Zeolites

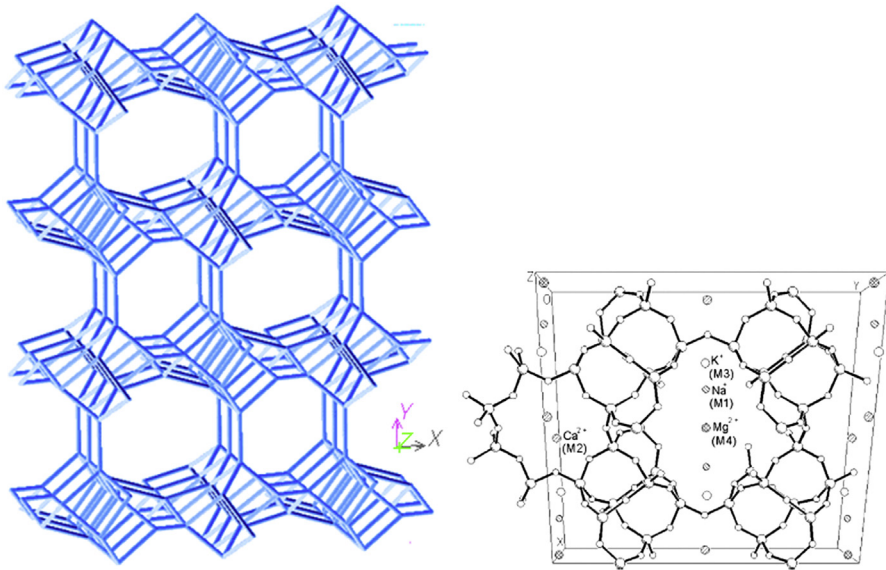
Name	IZA Code	Crystal System	Space Group	Channel Size	Si/Al Ratio	Cations
Analcime	ANA	Cubic	Ia3d	0.16 × 0.42	1.5–2.8	Na
Chabasite	CHA	Rhomohedral or triclinic	P1	0.38	1.4–4.0	Na, K, Ca
Clinoptilolite	HEU	Monoclinic	C2/m	0.31 × 0.75	4.0–5.7	Na, K, Ca
Erionite	ERI	Hexagonal	P6 <sub>3</sub> /mmc	0.36 × 0.51	2.6–3.8	Na, K, Ca
Faujasite	FAU	Cubic	Fd3m	0.74	1.0–2.8	Na, K, Mg
Ferrierite	FER	Orthorhombic	Immm	0.42 × 0.54	4.9–5.7	Ca
Laumontite	LAU	Monoclinic	C2/m	0.40 × 0.53	1.9–2.4	Na, K, Mg
Mordenite	MOR	Orthorhombic	Cmcm	0.65 × 0.70	4.0–5.7	Na, K, Ca
Phillipsite	PHI	Monoclinic	P2 <sub>1</sub> /m	0.38	1.1–3.3	Na, K, Ca

where the oxygen atoms are also shown together with the positions of the most common cations present in the hydrated natural zeolite.<sup>11,12</sup> In fact, in normal conditions cations are largely hydrated. After heating in dry conditions, water is lost and the cations become “naked”. In this case, their positions change significantly, being their interaction with the framework oxygen atoms maximized. Thus metal cations frequently shift near the center of rings constituting the windows of the cage where they are located, taking also into account their mutual repulsions. In [Figure 7.2](#) the most common positions of alkali cations in Faujasite and LTA zeolite are shown. They are in fact close to the centers 6-MR or 4-MR or even in the center of the hexagonal prisms. When cations adsorb molecules different from water, cations may shift to even different sites.

A main application is as adsorbents in the field of wastewater purification, to remove ammonium, heavy metals, inorganic anions, organics, dyes, humic substances etc.<sup>13,14</sup>

Natural zeolites have been tested and proposed for commercial exploitation in several patents for the purification and separation of gases.<sup>15</sup> The abundance and low raw material cost of natural zeolites have rarely offset such disadvantages as variable composition, low purity and often poorer separation performance compared to the more-favored synthetic zeolites. However, they are particularly well suited for trace-gas removal. Clinoptilolite and chabazite were found to outperform commercially available synthetics in N<sub>2</sub>O removal from air.

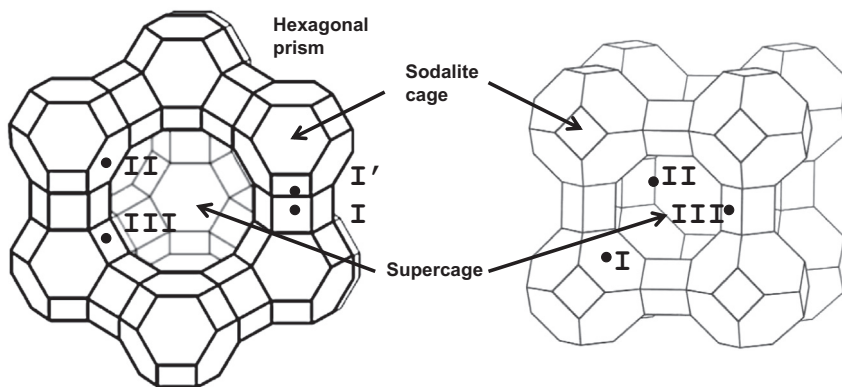




**FIGURE 7.1**

Structure of HEU zeolite (heulandite and clinoptilolite) viewed along [001] (left) and the preferential sites occupied by cations in natural clinoptilolite.

*Reprinted with permission from Refs. 11 and 12.*



**FIGURE 7.2**

Structure and main positions for cationic siting in dry FAU and LTA zeolites.

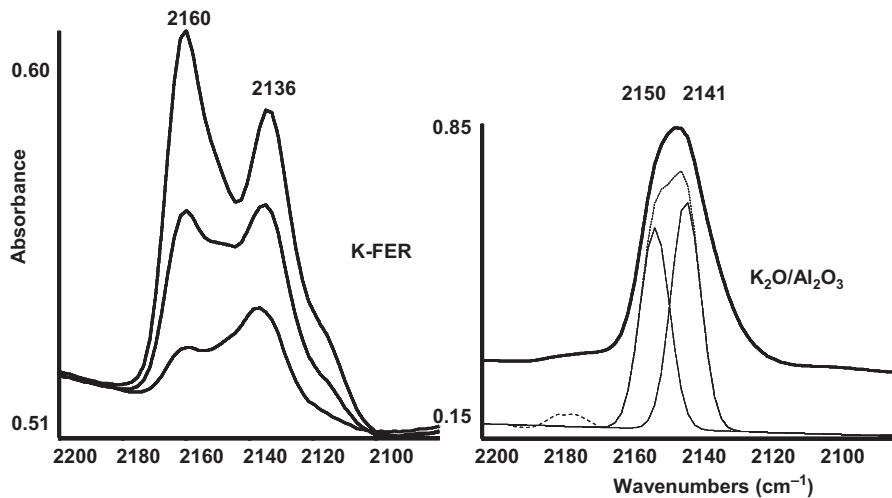
Although several studies demonstrate interesting catalytic activity of natural zeolites in different reactions, it does not seem that the use of natural zeolite is a common practice today, purer synthetic zeolites usually better.

It seems that the only case of commercial utilization of a natural zeolite as a catalyst is the application of proton (ammonium) exchanged natural erionite doped with a hydrogenating function as the catalyst of the Selectoforming process.<sup>2,3</sup> This is probably the first shape selective catalytic process to be introduced, in the sixties. It is a reforming or post-reforming process allowing the conversion of low octane n-paraffins in the presence of hydrogen into propane, thus removing them from naphtha or reformat gasoline. It is based on the “size exclusion” reactant shape selectivity: in fact erionite contains cages  $15.1 \times 6.3 \text{ \AA}$  wide, accessed by 8 MR  $3.6 \times 5.2 \text{ \AA}$  wide. Only linear paraffins access the cavities and can be cracked or hydrogenolyzed. The other molecules are excluded from the catalytic sites. Erionite is a fibrous zeolite, morphologically similar to asbestos and it is assumed to be even more carcinogenic. For this reason its commercialization is now forbidden.

#### 7.1.4 Alkali and alkali earth cationic zeolites and their industrial applications

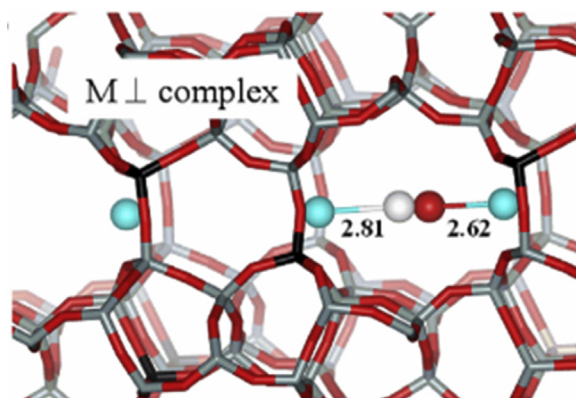
Alkali cation zeolites are formally salts of strong acids, thus being essentially weak bases. Actually, in perfect, extraframework material free, cationic zeolites all oxygen atoms are exposed at the cavity surface and may act as basic sites. The alkali and alkali cations are essentially weak Lewis acids, according to their large size and small charge. However, they are “naked” in ideal dry cationic zeolites, with a relatively weak electrostatic interaction with the negatively charged framework. For this reason they act as stronger Lewis sites with respect to the same cations when at the surface of oxide solids. Evidence for this is provided by the stronger perturbation they produce with respect to basic probes such as e.g. CO. Evidence for this is provided in Figure 7.3, where the spectra of CO adsorbed at low temperature on K-Ferrierite and on 3% K-Al<sub>2</sub>O<sub>3</sub> catalyst are shown. The higher CO stretching frequency observed on K-FER ( $2160 \text{ cm}^{-1}$ ) than on K-Al<sub>2</sub>O<sub>3</sub> for linear on-top CO is evidence of the stronger Lewis acidity of K<sup>+</sup> ions in ferrierite than on alumina.

On the other hand, in the cavities of zeolites, in particular those characterized by a low Si to Al content that, when in cationic form, have a big concentration of cations, multiple interactions can be produced,<sup>16–18</sup> i.e. adsorbed species may interact simultaneously with more sites, what is less common to occur on normal surfaces. The second IR component observed in Figure 7.3, left, for CO adsorbed on K-FER is in fact due to a more strongly adsorbed species (it is more resistant to outgassing) but the  $\nu$ CO frequency is less shifted. This is actually consistent with a double interaction (C– and O– bonding). A model for this double interaction arising from theoretical calculation is shown in Figure 7.4 for CO interacting with two sodium cations in Na-FER.<sup>19</sup> Actually, the excellent adsorption properties and the widespread industrial use<sup>2,7,20</sup> of alkali and alkali earth zeolites as adsorbents are mostly due to



**FIGURE 7.3**

FT-IR spectra of CO adsorbed on K-Ferrierite (adsorption at 140 K, outgassing at 200, 190 and 180 K) and on 3% K-Al<sub>2</sub>O<sub>3</sub> (adsorption at 140 K, outgassing at 140 K).



**FIGURE 7.4**

CO complex with two Na<sup>+</sup> ions across the main channel of ferrierite. Distances between Na<sup>+</sup> ions and atoms of CO molecules shown in Å. Framework atoms depicted in tube mode (O, Si, and Al in red, grey, and black colour, respectively) and extra framework Na, C and O atoms displayed as blue, white, and red balls, respectively.

*Reprinted with permission from Ref. 19.*

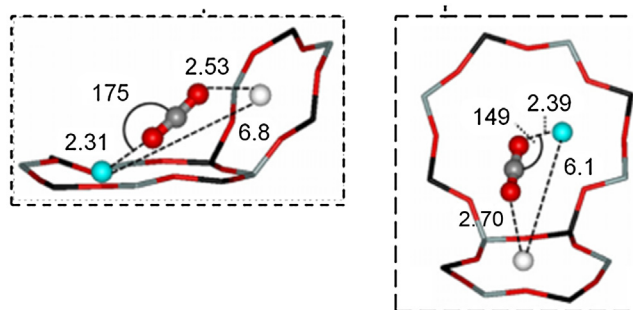


FIGURE 7.5

Models for two possible geometries of CO<sub>2</sub> adsorption complexes in Na-LTA zeolite.

*Reprinted with permission from Ref. 21.*

the weak Lewis acidity of the cations that allow adsorption of several polar molecules but also their quite easy desorption, thus allowing easy regeneration. This is the case, for example, of the very relevant application of Na zeolites such as Na-LTA and Na-X (see below) for the separation of CO<sub>2</sub> from gases: in Figure 7.5<sup>21</sup> two possible models of the adsorption of CO<sub>2</sub> on Na-LTA are shown. It is evident from calculations that, in spite of the “acidic” character of CO<sub>2</sub> (carbon anhydride) and the supposed “basic” nature of cation exchanged zeolites, the adsorption occurs mainly with CO<sub>2</sub> acting as a base donating the oxygen lone pair to the Na<sup>+</sup> ion acting as a Lewis acid. This is confirmed by spectroscopic experiments.<sup>22</sup>

Depending on their size, part of the cavities in some zeolites may be inaccessible to large molecules and also to small ones. On the other hand, cationic zeolites may be “overexchanged”, that means that metal oxide particles may be introduced in the cavities. These particles, which in normal conditions may be carbonated and/or hydrated, may be very strongly basic if they belong e.g. to alkali oxides. This may be the case of commercial 5A zeolite (Ca,Na-LTA) where CaCO<sub>3</sub>-like particles are usually present.<sup>23</sup> This is also the case of Cs oxide impregnated CsX zeolite, reported to be a very basic material.<sup>24</sup>

#### 7.1.4.1 LTA zeolites as adsorbents

Zeolites denoted with the LTA code (Linde Type A, Figure 7.2, right) are small pore zeolites characterized by a cubic structure. The typical Si/Al atomic ratio is near thus the composition of the sodium form is NaSiAlO<sub>4</sub>. Each unit cell consists of 96 AlO<sub>4</sub> and 96 SiO<sub>4</sub> tetrahedra and contains eight  $\alpha$  cages or supercages, and eight  $\beta$  cages (sodalite cages). Supercages are opened each other through eight-membered oxygen rings (8 MR). The  $\beta$  cages connect to the supercages through six-membered rings (6 MR), and each other through four-membered rings (4 MR). Both 6 and 4 MR are assumed to be too small for most molecules to pass through. The pore structure through which molecular diffusion occurs is consequently limited by the size of the

8 MR that are approximately 5 Å across. The presence of charge-balancing cations ( $K^+$ ,  $Na^+$  and  $Ca^{2+}$ ) reduces the effective pore size of the opening to near 3 Å (for K-LTA, also denoted as 3A) and near 4 Å (for Na-LTA, also denoted as 4A). In the case of Ca,Na-LTA (5A) only part of cationic locations is occupied (according to the bi-valence of Ca ions) and the pore size is near 5 Å.

These zeolites gained very large industrial application for their excellent reversible adsorption properties allowing separation of gas mixtures and purification of gases.<sup>25</sup> The potassium exchanged form, K-LTA or Linde 3A, finds relevant application in bioethanol drying processes, for production of fuel grade bioethanol from starch or cellulosic biomasses fermentation, with pressure swing adsorption processes.<sup>26,27</sup> With this material, zeolite membranes can also be applied and this is possibly the only industrial gas separation process performed using zeolite membranes. It is commonly used for drying of gases and other polar liquids (methanol) and easily polymerizable substances, such as unsaturated hydrocarbons (ethylene, propylene, acetylene and butadiene).<sup>28</sup>

The sodium exchanged form, Na-LTA or Linde 4A, can be used to dry several organic compounds as well as gases such as air, hydrogen, natural gas, nitrogen.<sup>29</sup> In the field of petrochemistry, zeolite 4A finds application for the recovery, typically from kerosene or gas oil fractions, of linear paraffins (*n*-paraffins) in the C10 to C14 range, to produce linear paraffins to further allow the synthesis of LABs (linear alkylbenzenes) and LAS detergents (linear alkylbenzene sulphonates),<sup>30</sup> and has also been considered for alkane/alkene separation.<sup>31</sup> This zeolite is also largely used as an ion exchanger in the field of detergency (detergent builder<sup>32</sup>); however, for this application a different preparation procedure is adopted, to produce smoothed cubic nanoparticles to minimise fibre damaging of textiles.

The calcium exchanged form, Ca-LTA (Linde 5A), is commonly used for drying and desulphurization of natural gas,<sup>7</sup> and for the removal of CO<sub>2</sub> from different gases including natural gas, hydrogen, biogas and flue gases<sup>33</sup> and contaminated air,<sup>34</sup> as well for the separation of normal paraffins from branched and cyclic hydrocarbons. Another possible application is for N<sub>2</sub>/O<sub>2</sub> air separation,<sup>35</sup> to adsorb N<sub>2</sub> and produce oxygen enriched air. For hydrogen purification of hydrogen produced by methane steam reforming, adsorbers are packed with a layer of an activated carbon in the feed end and with a layer of 5A zeolite at the product end.<sup>25</sup>

#### 7.1.4.2 Alkali and alkali earth exchanged faujasites as adsorbents

The faujasite (FAU) structure (Figure 7.2, left) is formed by quite wide supercages accessed through 12-member silicate rings with 0.74 nm diameter, much smaller sodalite cages accessed through 6-member silicate rings and hexagonal prisms connecting the sodalite cages. Cations are located in different positions in the cavities depending on hydration/dehydration states or upon adsorption of different molecules.<sup>36</sup>

Depending on the Si to Al ratio faujasite zeolites are denoted either as X or as Y: faujasites X having an Si/Al ratio between 1 and 1.5 and Y having an Si/Al ratio above 1.5. More recently those having an Si/Al ratio of 1.0 have been

denoted as LSX (Low Silica X). Alkali faujasites X, having lower Si to Al ratio, have definitely higher amount of alkali ions than alkali faujasites Y. The medium Lewis acidity of the alkali and alkali earth cations, increased by the loss of ligands in dry zeolites, is the key feature for the use of these materials as regenerable adsorbents. However, the zeolite framework is also reported to display significant basicity that can cooperate in the adsorption of acid molecules. Complex interactions, where more than one cationic site and oxygen atoms cooperate in adsorption have been found.<sup>37</sup>

Mostly in the form of powder packed beds, alkali and alkali earth metal faujasite zeolites are largely used industrially.<sup>25</sup> Na-X faujasite (denoted commercially as 13X molecular sieve, according to the diameter of the supercage, 13 Å) is a highly selective adsorbent designed for the elimination of trace contaminants from air and other gases.<sup>38</sup> It can also be used for the desulfurization (sweetening) of natural gas and other fluids, especially for the removal of mercaptanes, and for drying of gases and liquids. According to its high activity in adsorption of water vapour, 13X molecular sieves are used as regenerative thermo-chemical energy storage for the generation of cold or heat, possibly using renewable or recovered energy sources (sun energy, exhaust heat etc.).<sup>39</sup>

13X molecular sieve is also a very efficient CO<sub>2</sub> adsorbent to remove carbon dioxide from flue gases<sup>33,40</sup> or to upgrade biogas to pure methane,<sup>41</sup> as well as for natural gas<sup>7</sup> and hydrogen purification. It is also used for the purification of C4 cuts from nitriles<sup>42</sup> and for hydrocarbon separations.

The most selective adsorbent for the separation of para-xylene from meta-xylene<sup>43</sup> (ortho-xylene is separated by distillation) is K,Ba exchanged Y, with Si/Al ratio ~ 2.<sup>44</sup> In the UOP Parex process,<sup>45</sup> the zeolite, shaped in extrudates, is put in a single column working in the simulated countercurrent mode, where the xylene mixture and the desorbent (either toluene or paradiethylbenzene) are fed separately. Two streams are withdrawn, one rich in para-xylene, the other rich in meta-xylene. Ca-X has been patented recently for the removal of methane from hydrogen, e.g. to obtain hydrogen from the off-gases of steam cracking.<sup>46</sup>

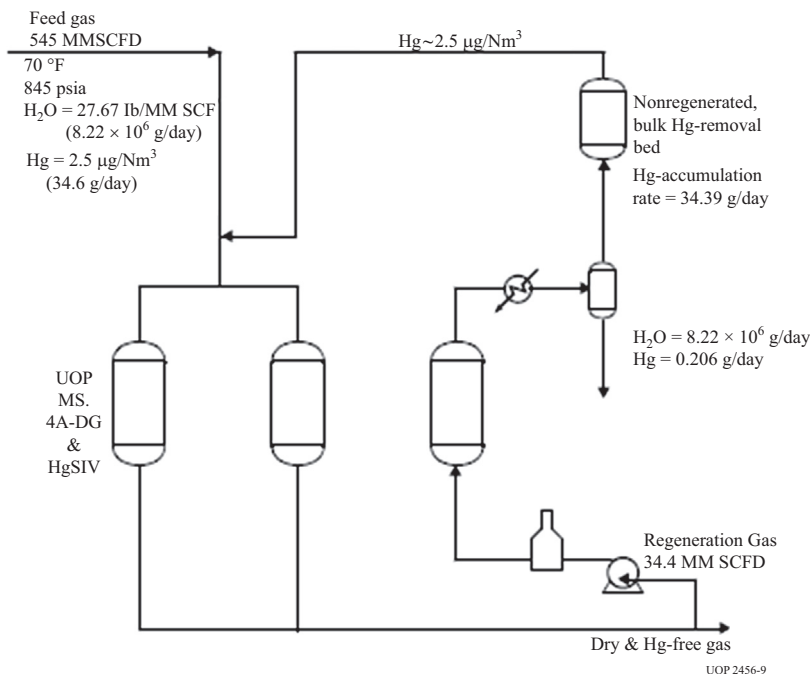
Na, Li, Ca, Sr, Ba exchanged X,<sup>47</sup> and Li and Li-Zn exchanged low silica X (LSX) have been commercially used for air separation for the production of ~90–95% O<sub>2</sub>-enriched air from ambient air. The cations in these adsorbents bind N<sub>2</sub> selectively from air, previously treated with a bed of Na X zeolite to make it dry and CO<sub>2</sub>-free. The currently favored zeolites for air separation are LiX, Li-LSX, and LiZn-X because they provide higher selectivity of adsorption of N<sub>2</sub> over O<sub>2</sub> and Ar, higher PSA cyclic working capacity for N<sub>2</sub>, and moderate heats of adsorption for N<sub>2</sub>, which translate into superior process performance for air separation.<sup>48</sup>

#### **7.1.4.3 Silver zeolites as regenerable mercury removal adsorbents**

The recent development of regenerable zeolitic adsorbents for the removal of mercury from natural gas represents an interesting new application. UOP developed silver-containing zeolites, denoted as HgSIV adsorbents, with mercury removal

properties. These materials perform simultaneously both water and mercury removal. Since nearly all cryogenic plants use molecular sieve dehydrators, such as based on 4A molecular sieves (see above), the mercury removal function can be added to the dehydrator performance by replacing some of the dehydration-grade molecular sieve. Mercury is adsorbed during the dehydration step and, when heated to the normal dehydrator regeneration temperature, releases from the silver and leaves with the spent regeneration gas.<sup>49</sup> In fact, silver, like other noble metals, reacts with mercury at moderate temperatures producing amalgams, while it releases the mercury at temperatures above 227 °C. From the published data, it seems likely that the zeolite used is like 4A or 13X molecular sieve containing significant amounts of silver. In one of the possible process configurations (Figure 7.6)<sup>50</sup> the regeneration gas containing moisture and mercury is first cooled to condense water and then treated with non regenerable adsorbents (such as special activated carbons) to abate and possibly recover mercury.

In recent papers the preparation of a similar silver adsorbent is described.<sup>51</sup> In this case the catalyst is prepared using a magnetic zeolite, i.e. a natural chabazite containing also erionite and clinoptilolite, treated with magnetite to make it



**FIGURE 7.6**

Schematics of the mercury removal and drying section in natural gas plant, with mercury recovery from the regeneration gas.

*Reprinted with permission from Ref. 50.*

magnetic, which can be dispersed in a coal-fired power plant flue gas stream. Ag from 1 to 28% has been loaded producing highly uniform silver nanoparticles on chabazite surfaces with a narrow size distribution (2–4 nm). These particles consist of a mixture of metal and metal oxides. Silver-exchanged molecular sieves have shown great promise also in other applications ranging from antimicrobial materials to the adsorption of xenon and iodide, two key contaminants emitted from nuclear reactors.<sup>52</sup>

#### **7.1.4.4 Alkali and alkaline earth zeolites as catalysts**

Although much work has been done on the catalytic activity of “basic” zeolites, it seems that, up to now, they still have very limited industrial application as catalysts.<sup>53</sup> Alkali-exchanged zeolites, with and without occluded alkali metal compounds, find interesting activity for aldol-type condensation reactions. The effectiveness of these solids for the base catalyzed aldol condensation of propionic acid with formaldehyde to methacrylic acid was directly correlated to the expected basic strength of the alkali-exchanged zeolites ( $\text{NaX} < \text{KX} < \text{CsX}$ ).<sup>54</sup> The impregnated “overexchanged” catalyst 12% Cs/CsX exhibited even higher activity. However, these zeolite materials were found less active than Bi-promoted Cs/SiO<sub>2</sub> catalysts. Side alkylation of toluene with methanol allows the synthesis of ethylbenzene and styrene. Alkali zeolites and alkaline earth oxides were found to act as good catalysts for this reaction. However, according to Serra et al.<sup>55</sup> zeolite-based catalysts are still poor reactive. To give the styrene/ethylbenzene yields required for converting this process in a real alternative to the existing one, based on the alkylation of benzene with ethylene, followed by the dehydrogenation of ethylbenzene to styrene.

Attempts to use basic zeolites in the field of biomass conversion, including for biodiesel synthesis, have been done,<sup>56</sup> still without much success. An interesting new approach is the use of CsNaX zeolite for upgrading of biodiesel by deoxygenation.<sup>57</sup> Other interesting attempts concern the development of new “green” chemical processes, such as the use of Na-ZSM-12 zeolite (Na-MTW) for the green synthesis of diethylcarbonate from CO<sub>2</sub> and ethanol<sup>58</sup> and the further use of dialkylcarbonates as green methylating agents in organic chemistry, using NaX and CsX zeolites as catalysts.<sup>59</sup> Data have also been reported on the possibility of “encapsulating” molecules in cationic zeolites, namely formaldehyde in NaX<sup>60</sup> or acrolein in NaY,<sup>61</sup> thus activating them as electrophilic reactants enough to react with various olefins or aromatics, respectively, in very mild conditions. NaY has also been found to act as a good catalyst for Diels Alder cyclizations.<sup>62</sup> It seems interesting to remark that in most of these applications alkali faujasites appear to act as a mild Lewis acid more than as a basic catalyst.

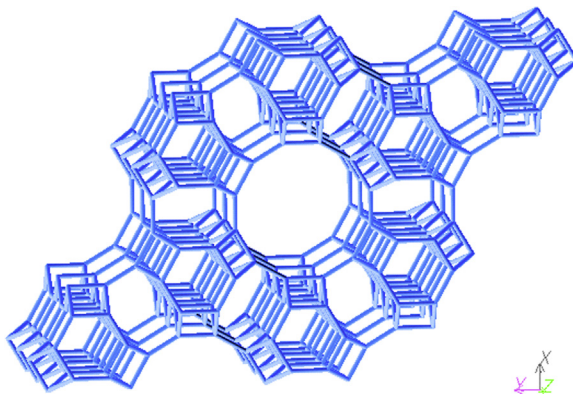
#### **7.1.4.5 Alkali zeolites as catalyst supports**

Widespread application of alkali zeolites in heterogeneous catalysis is the use of Pt/K-LTL (LTL = Linde type L, also denoted as L) catalysts for paraffin aromatization reactions in refinery. A catalyst of this type has been jointly developed by Idemitsu Kosan Co., Ltd. (IKC), and Chevron Phillips Chemical Company LP



(CPCChem) for the Aromax process, used commercially to convert C6–C8 paraffins to benzene.<sup>63</sup> Reaction conditions are 500 °C, 0.6 MPa, weight hourly space velocity (WHSV) of 2/h, and an H<sub>2</sub>/n-C6 molar ratio of 5. An active catalyst similar to commercial one contains 0.5% Pt impregnated on a fluorine and chlorine containing KL zeolite. The LTL zeolite has a one-dimensional (1D) channel with 12-ring undulating channels 7.1 Å in diameter and cavities of about 4.8 (length) × 12.4 (height) × 10.7 Å (width). The structure (Figure 7.7) belongs to the P6/mmm space group and contains two important secondary building, the cancrinite (CAN) cage and a double hexagonal ring (D6R), alternating to form a column. The crystals generally adopt the form of cylinders or hexagonal prisms, for which the {001} surface is at the top and the bottom of the cylinder, and the sidewalls are {100} and {110} planes. The KL zeolite is commercially available (Tosoh)<sup>64,65</sup> in potassium form ion type and has a framework composition with a ratio of [Si]/[Al] ≈ 3. Hence a typical chemical composition of zeolite is K<sub>9</sub>(AlO<sub>2</sub>)<sub>9</sub>(SiO<sub>2</sub>)<sub>27</sub> per unit cell. The cation distribution has been determined, at least for the hydrate zeolite, to be located both in the cage and in the hexagonal rings.<sup>64</sup> IR spectra of KL show, besides the sharp band of external silanols at 3740 cm<sup>-1</sup>, a second band at around 3672 cm<sup>-1</sup>, ascribed to be non-acidic OH's. Thus the catalyst is assumed to be non-Brønsted acidic.<sup>63,65</sup> Halide species are supposed to favor dispersion and small size of Pt particles, without producing acidity, shape selectivity effect occurring possibly in the cancrinite cage, favoring activation of hexane and its cyclization, absence of Brønsted acidity favoring limited or no coking.

Pt-KL zeolite is also the basic formulation of the catalyst of the recent RZ platforming process from UOP.<sup>66</sup> This process is a semiregenerative naphtha reforming process, allowing higher aromatics selectivity than other reforming processes with C6 and C7 paraffins as feed.<sup>67</sup>



**FIGURE 7.7**

Structure of LTL zeolite structure viewed along [001].

## 7.1.5 Protonic zeolites: acidity and shape selectivity

### 7.1.5.1 The bridging hydroxyl groups

Protonic zeolites, i.e. those zeolites where protons act as balancing cations in the cavities, find industrial applications as acid catalysts in a large number of hydrocarbon conversion reactions.<sup>2-4,9,20,53</sup> The excellent activity of these materials is due to two main properties: the strong Brønsted acidity of bridging Si-(OH)-Al sites generated by the presence of aluminum inside the silicate framework; and shape selectivity effects due to the molecular sieving properties associated to the well defined crystal pore sizes, where the catalytic active sites are located.

The strongly acidic hydroxy groups of zeolites are well characterized by the presence, in the IR spectrum, of quite definite and strong bands in the region between 3650 and 3500  $\text{cm}^{-1}$  (Figure 7.8), as well as by evident  $^1\text{H}$  MAS NMR peaks in the region 3.6–8.0 ppm<sup>68</sup> (see Figures 5.2 and 6.14). With both techniques, it is possible to reveal the acidity of these groups. In fact these spectroscopic signals disappear upon contact with bases like ammonia, pyridines, amines and phosphines, in parallel with the appearance of the features of the corresponding protonated bases. In the presence of weak basic probes (CO, nitriles) a strong perturbation of the spectral characteristics of these groups is evident too.

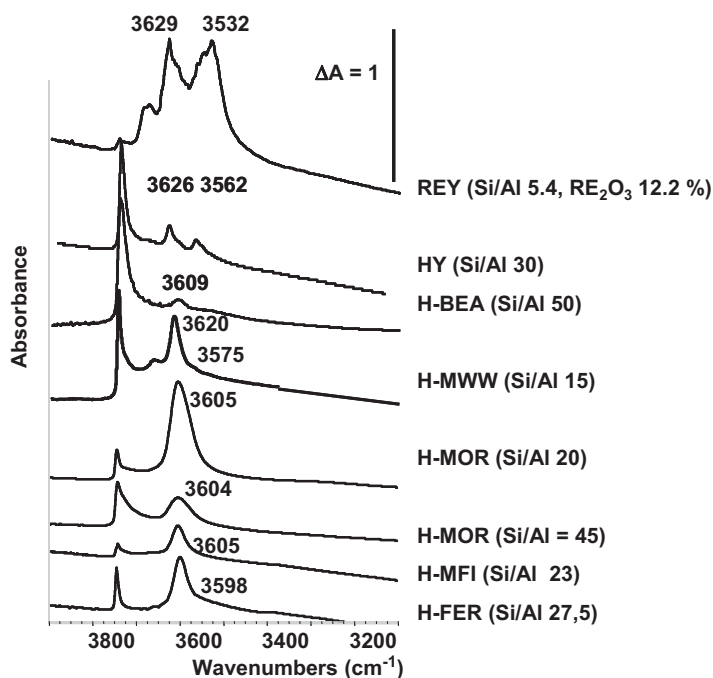
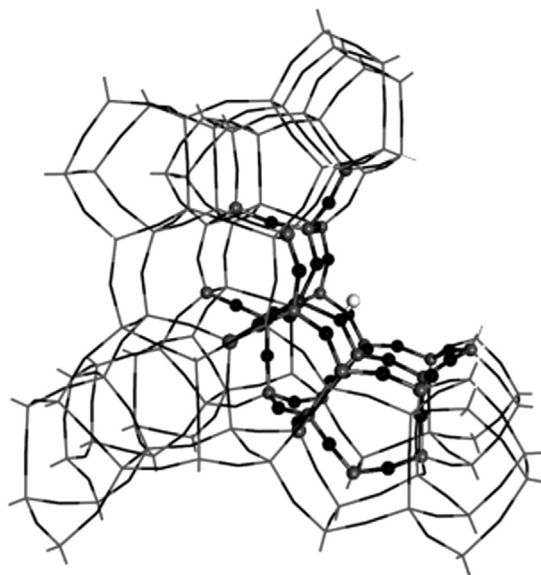


FIGURE 7.8

IR spectra of protonic zeolites in the OH-stretching region.

The position of the IR band due to bridging OH's is somehow dependent on the size of the zeolite cavities,  $\nu$ OH being generally (but not really always) the lower the smaller the cavity. The OH stretching band position and width can be influenced by weak H-bondings through the cavities,<sup>69</sup> which provides evidence of their poor availability for steric hindrance and makes them unreactive toward weak basic molecules. In the case of zeolites with more than one type of quite different cavities, splitting of the band of the bridging hydroxy groups can be observed. Some authors suggested that a correlation exists between OH stretching frequency and the Si–O(H)–Al bond angle.<sup>70</sup> As for <sup>1</sup>H MAS NMR peaks of protonic zeolites, the trend among different studies is for increased chemical shift corresponding to an increase in the intrinsic acid strength (proton affinity),<sup>71</sup> i.e. protons are more deshielded in zeolites perceived to be more acidic. On the other hand, the peak position is also sensitive to location: peaks at 3.6–4.3 ppm are due to bridging OH groups in large cages and channels; peaks at 4.6–5.2 ppm to bridging OH groups in small cages of zeolites, while those at 5.2–8.0 ppm are associated to disturbed bridging OH groups interacting with framework oxygen.<sup>68</sup> Parallel <sup>1</sup>H NMR and IR studies show that the IR extinction coefficient of the zeolite's bridging OH's is far higher than for silanol groups, and this allowed Kazansky et al.<sup>72</sup> to propose to use the intensity of the IR band to determine the surface acid strength.

The data agree suggesting that such acidic protons are actually linked (in the dry zeolite) through a covalent bond to oxygen atoms bridging between a silicon and an aluminum atom, as shown in Figure 7.9 for the proton located on the wall



**FIGURE 7.9**

Model for the acid site of H-MFI (H-ZSM-5) zeolite.

*Reprinted with permission from Ref. 73.*

of a cavity of H-ZSM-5 (H-MFI) zeolite.<sup>73</sup> Interestingly, bridging OH's are only detected in the interior of the zeolitic cavities, being the corresponding spectroscopic features absent in any non zeolitic material based on silica and alumina<sup>74</sup> and also on the external surfaces of different zeolites (see below). Thus, the existence of the bridging hydroxy groups Al—(OH)—Si should imply the existence of the cavity. In other words, the cavities are possibly involved in the generation and/or stabilization of the bridging OH sites, as well as in the strengthening of their acidity.<sup>74</sup> On the other hand, many investigations were carried out, mainly in the eighties and nineties, on the effect of the zeolite structure on the Brønsted acid strength of the bridging OH's. The conclusions of these studies were quite disagreeing. The relations between structural parameters and acid strength of hydroxyl groups of zeolites have been subject of many discussions. Recently this topic was considered by theory by Sastre, Niwa and coworkers. They concluded that a complex mixture of short- and long-range factors is at play.<sup>75</sup> It seems quite established today that protonic zeolites have very similar Brønsted acid strengths, with a relevant role of local geometric factors differentiating their behavior.<sup>76</sup> Experimental as well as theoretical data show that besides the interactions of the functional groups of the reactive molecules with the zeolites Brønsted sites, the van der Waals interactions of other unreactive groups of atoms with the zeolite cavity walls may be very relevant and stabilize the intermediates. These interactions may vary significantly as a function of the type of the zeolite, the dimension and shape of the cavities as well as the Al and proton content and the presence of EF. Also, they depend on the size and shape of the molecule. These “confinement effects” make the cavities of the single zeolite structures unique solvation and reactivity environments and play relevant role in the catalysis by zeolites.<sup>77</sup> Different catalytic activities would predominantly reflect differences in the size and solvating properties (confinement effect) of their cavities, rather than differences in acid strength.<sup>78,79</sup>

#### **7.1.5.2 Extraframework material**

Most data agree suggesting that, when the Al content is relatively low and the zeolite well crystallized, the amount of Brønsted sites in protonic zeolites actually strictly depends on Al concentration, according to the theory. However, at least for quite Al rich zeolites, like faujasites, distorted Al structures that are not associated with acidic protons may also exist, thus the number of active protons may be significantly lower than the number of Al ions.<sup>78</sup> These distorted sites are most frequently associated to the so called “extraframework material” (EF). In fact, zeolite catalysts are actually applied frequently after treatments tending to increase their stability and also, in case, to further enhance surface acidity and shape selectivity effects. These treatments, like steam dealumination, can cause the decrease of the framework Al content and the release from the framework of aluminum-containing species that contribute in stabilizing the framework, but can also contain additional catalytically active acid sites. These particles can also narrow the size of the zeolite channels or of their mouths, thus improving the shape

selectivity effects. Extraframework material is composed of very small particles mostly containing Al cations complexed by OH's but sometimes also involving silicate species, likely interacting with the framework walls, located in the cavities or on the external surface. It can arise from the preparation or the activation procedure or by addition of components by impregnation or ion exchange. The presence of EF gives rise to the presence of strong additional bands in the IR OH stretching, usually above  $3750\text{ cm}^{-1}$  and in the region  $3730\text{--}3650\text{ cm}^{-1}$ . These species are also responsible for  $^1\text{H}$  NMR peaks at  $-0.5 \pm 0.7$  and  $1.7\text{--}2.7\text{ ppm}$ <sup>68</sup> and reveal medium-strong Brønsted acidity. Similarly, the detection of octahedral Al ions in  $^{27}\text{Al}$  NMR techniques is evidence of EF. On the other hand EF species may contain strong Lewis acid sites.

### 7.1.5.3 Molecular sieving and shape selectivity

The main factor allowing molecular sieving and, consequently, shape selectivity is generally considered to be exclusively a steric effect, i.e. only molecules having a critical kinetic diameter lower than the channel diameter are allowed to enter the pores (reactant shape selectivity) and to react on an active site or, in case, to exit them and be recovered as a product of the reaction (product shape selectivity). Alternatively, transition state shape selectivity effects limit the formation of bulky transition state intermediates inside the pores that may be formed and avoid the formation of some reaction products. The molecular sieve effect is actually a dynamic phenomenon which depends on the temperature. In fact, molecules which have moderately larger diameter than the cavities may manage to access them, in particular at high temperature. However, a cut-off size exist. As for example, the access at the supercages of Y-zeolites, limited by  $7.4\text{ \AA}$  rings, can occur with molecules having up to  $10.2\text{ \AA}$  diameter. On the other hand, real zeolite catalysts are frequently pretreated in various ways such as steaming, and are not "perfect" structures: extra-framework species (EF) are frequently present and can also have a role either as active sites or as material hindering the molecular diffusion into the cavities. Additionally, different preparation methods of the same zeolite can give rise to quite different properties, due to several additional effects such as, e.g. different particle sizes<sup>80</sup> and morphologies,<sup>81</sup> different active site densities or different distribution of framework aluminum and, consequently, of protons from surface to bulk.<sup>82</sup>

### 7.1.5.4 The external surface of protonic zeolites

According to studies of the adsorption of hindered probe molecules, which do not enter the cavities, it is well established today that catalytically active sites are also usually present at the external surface of zeolites. In fact, terminal silanols are found at the external surface of zeolites, characterized by OH stretching bands at ca  $3745\text{ cm}^{-1}$  in IR and  $^1\text{H}$  NMR peaks in the  $1.3\text{--}2.2\text{ ppm}$  range. Although the spectral features of these groups are similar to those of silica, the acidity of the external silanol OH's of zeolites can be significantly enhanced with respect to those of silica.<sup>83–85</sup> Lewis acid sites are also found at the external surface of most zeolites.

These external sites are considered to be responsible for unwanted non-selective catalysis. In fact, H-zeolites also catalyze somehow reactions of molecules which do not enter the cavities due to their too large size. Thus, the external surface of “untreated” zeolites is certainly active in acid catalysis. The “selectivation”<sup>86</sup> of the zeolite behavior may be obtained by inertization of the external surface through silanization with alkoxy silanes, which can destroy the external Lewis sites, precoking of the external surface and/or of the most active sites, poisoning of the external acid sites by hindered bases (such as 2,6-di-*tert*-butylpyridine).

#### **7.1.5.5 Production of hierarchically porous zeolites**

While the presence of structural porosity allows probably the real existence of strong Brønsted acid sites (see above) and also molecular sieving and shape selectivity, in some way it is also a limit to reaction kinetics, the catalytic conversion rate being usually strongly limited by the diffusion of reactants or products in or out the channels. Bulk zeolite crystals are frequently unnecessarily large, thus giving rise to unnecessarily long channels to be traveled by molecules. For this reason, too, a small fraction of the zeolite’s active sites are usually used. To reduce mass transport limitations, the access of reactant molecules to active sites and the coming out of products from zeolite channels should be shortened. To do this, two strategies can be attempted: (i) the synthesis of extremely small zeolite nanocrystals; (ii) the generation of intracrystalline mesoporosity (pores with diameters ranging from 2 to 50 nm) which will act as preferential diffusion channels of molecules to and from the active molecular sieving and shape selective channels. In the first case, obviously, the external/internal surface ratio is increased, and this may lead to reduced selectivity. To avoid this, the external surface should be fully passivated. Mesoporosity can be produced during the zeolite crystallization using a hard or soft templating procedure, or through a post-synthetic demetallation treatment, such as alkaline desilication.<sup>87,88</sup> This is quite a recent research field, in large expansion. It is evident that in many cases the presence of hierarchical porosity increases the catalytic performances of zeolites.

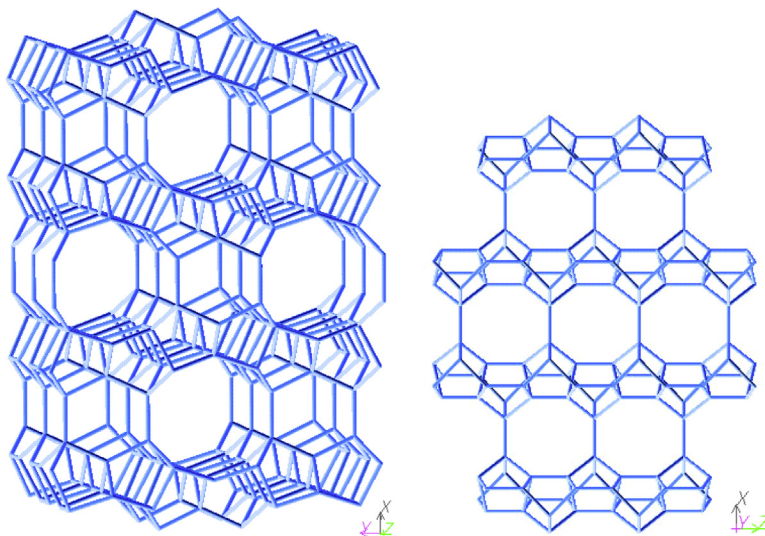
### **7.1.6 Some particular protonic zeolites applied in the industry**

#### **7.1.6.1 Erionite**

As already said, it seems that the first shape selective catalytic process to be introduced, in the sixties, was the Selectoforming process, realized industrially in the sixties. It was based on protonic erionite produced by ammonium exchanged natural potassium erionite. Because of the great similarity structures, offretite and erionite intergrowths are very often observed. The porous structure of the ERI framework consists of columns of erionite cages  $15.1 \times 6.3 \text{ \AA}$  wide, accessed by 8 MR  $3.6 \times 5.2 \text{ \AA}$ . IR spectra of H-ERI shows a split band at 3615, 3565  $\text{cm}^{-1}$  with the additional band of external silanols at 3745  $\text{cm}^{-1}$ .<sup>89</sup> Only linear paraffins access the cavities and can be cracked or hydrogenlyzed. The other molecules are excluded from the catalytic sites. Being Erionite a fibrous zeolite, morphologically similar to asbestos, is carcinogenic: thus its commercialization is now forbidden.

### 7.1.6.2 Ferrierite (H-FER)

The framework of the FER zeolite (Figure 7.10) gives rise to two kinds of intersecting channels, one of which is formed by 10-membered silicate rings along [001] direction, with diameters  $4.2 \times 5.4 \text{ \AA}$ , the other being formed by 8-membered rings along [010] with diameters  $3.5 \times 4.8 \text{ \AA}$ . It is consequently denoted as a medium pore zeolite. It frequently has quite high Al content (Si/Al ratio 8) but may be also prepared in a very highly siliceous form. It presents an unsplit OH stretching band near  $3595 \text{ cm}^{-1}$ , with slight shifts depending on the Al content. According to a spectral deconvolution by Domokos et al.,<sup>90</sup> three components should be present at  $3601$ ,  $3591$  and  $3562 \text{ cm}^{-1}$ . Both Domokos et al.<sup>90</sup> and Bhan et al.<sup>91</sup> supposed that OH's in 8 MR channels absorb near  $3590 \text{ cm}^{-1}$  while OHs in 10 MR channels adsorb near  $3600 \text{ cm}^{-1}$ . The adsorption of hindered nitriles allowed us to investigate independently the OH's located in the two channels of H-FER. In fact, the mono-branched probe isobutironitrile enters only one family of the channels, supposed to be larger channels, where the OH's vibrate at  $3591 \text{ cm}^{-1}$ , leaving free the OH's of the smaller channels whose OH's absorb at  $3598 \text{ cm}^{-1}$ .<sup>92</sup> This result is in good agreement with the neutron diffraction data reported by Martucci et al.<sup>93</sup> who observed two locations for OD groups in D-FER by neutron diffraction. Our IR data contradict the rule: the larger the channels the higher the OH stretching frequency. As already remarked, the state of internal bridging OH's is likely to depend from complex long- and short-range factors together.<sup>75</sup> The  $^1\text{H}$  NMR peak for bridging OH's of H-FER is observed unsplit near  $4.2$ <sup>94</sup> (see Figure 6.15).



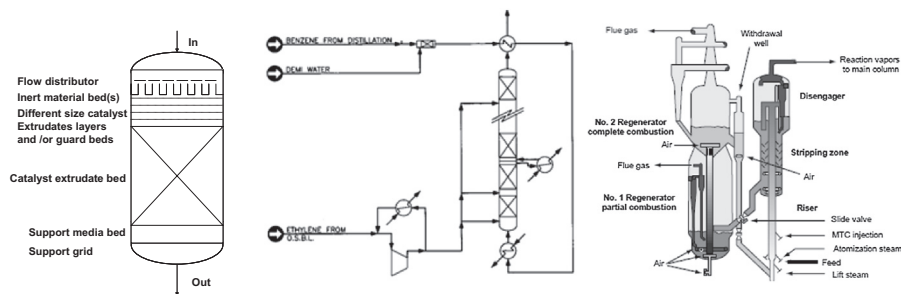
**FIGURE 7.10**

FER structure viewed along [001] 8 left, and [010] right.

H-FER zeolite focused much interest in the nineties for its high catalytic activity and selectivity for the n-butylene skeletal isomerization to isobutylene in view of a potential increase in MTBE production. A commercial process, IsomPlus (Lyon-dell—CDTech) using this catalyst is available commercially.<sup>95</sup> The reaction is performed in a fixed bed reactor (Figure 7.11, left) near 350 °C near ambient pressure and is thermodynamically limited, with conversion >44% of n-butenes with >86% selectivity to isobutene.<sup>96</sup> Today the inverse reaction and process, called the reverse-Isomplus process, may be also of interest. In this case, an isobutylene feed from either a C4-cut raffinate stream or from dehydration of tert-Butyl alcohol (TBA) from the Propylene Oxide process undergoes a “reverse skeletal” isomerization to form n-butenes such as butene-2 (cis and trans) and butene-1. The former can be used with ethylene to produce more valuable propylene via metathesis, and the latter can be used as a comonomer for LLDPE and/or for the production of polybutene.<sup>97</sup> A C5 isomplus process is also available with 66% conversion of n-pentenes and selectivity >95% to isoamylenes.<sup>96</sup>

In the direct process, the selectivity to isobutylene grows with time on stream when coking also proceeds and n-butylene conversion decreases progressively. Quite frequent catalyst regeneration is consequently needed, using swing reactors.

Still controversy exists on the reaction mechanism, with three hypotheses: (i) monomolecular rearrangement; (ii) bimolecular, with cracking of a dimeric octyl cation; (iii) pseudo-monomolecular, where the cracking of the octyl cation regenerates an “active” butyl cation that is the initiator of the reaction chain. It has also been proposed the possible role of carbonaceous materials as “active site” in the reaction.<sup>98</sup> One of the features of the catalyst allowing high selectivity to isobutylene is the impossible (or very highly hindered) diffusion of aromatics in the small pores of ferrierite. Aromatics are among the main products upon olefin conversion over larger pore zeolites like H-ZSM5. Theoretical data<sup>99,100</sup> also suggested that a transition-state shape selectivity effect may occur, just limiting the possibility of formation of C8



**FIGURE 7.11**

Scheme of some typical reactor systems used with zeolite catalysts: typical down-flow fixed bed reactor (left), an up-flow multibed liquid phase alkylation reactor (ENI-PolimeriEuropa, middle) and of a gas/solid fluid/transport bed Resid FCC reactor system (IFP-Axens, right).

Reprinted, in part, with permission from C. Perego, P. Pollesel, *Adv. Nanopor. Mater.* 2010; 1: 97–149. and D. Decroocq, *Oil & Gas Science and Technology—Rev. IFP* 52 5 (1997) 469–489.



adducts that can crack unselectively giving rise to  $C_3 + C_5$  hydrocarbons. This may be even more effective in the case of partially coked materials, so allowing improved shape selectivity. In fact, recent calculations suggested that n-butene isomerization can occur with a monomolecular mechanism through secondary linear butoxide, primary isobutoxide and tert-butyl cation intermediates on the 10 MR channels of ferrierite.<sup>101</sup> Most authors seem to converge today on the monomolecular mechanism.<sup>102,103</sup>

On the other hand, it has been shown that monobranched compounds may diffuse much better in the 10 MR larger channels of FER structure than in the 8 MR smaller ones, where access of branched compounds is strongly hindered.<sup>92</sup> Compounds with the tert-butyl group appear to be unallowed to enter both channels, at least at room temperature. This suggests that the isomerization reaction should not involve as stable intermediates compounds with the tert-butyl group. On the other hand, due to the small size of the pores of H-FER, it seems still difficult to understand how coke and reactants can coexist in the same cavity. It is possible that coking mostly occurs at the external surface and in the larger 10 MR channels, along [001] direction, while the more selective reaction could occur on the smaller (MR channels along [010]). In recent years, however, several studies concern preparation and modification of the structure in particular in relation to Al and proton sitting, to improve catalytic performances. These studies seem to indicate that reaction could occur in the 10 MR channels. According to Márquez-Alvarez et al.,<sup>104</sup> low density of acid sites in 10-membered-ring channels enhances the isobutene selectivity and decreases catalyst deactivation. The presence of high amount of silanol groups and Lewis acid sites increases the yields of by-products and catalyst's decay. Results by Roman-Leshkov et al.<sup>105</sup> indicate that the use of pyrrolidine (Pyr), as an SDA results in the selective population of acid sites in the 8-MR channels, whereas the use of hexamethyleneimine (HMI) generates FER zeolites with an increased concentration of acid sites in the 10-MR channels. A critical point of these studies is, however, the reliability of the method used to evaluate the siting of the acid sites.

According to Kithev et al. composite micro/mesoporous materials with intermediate degree of recrystallization have improved activity,<sup>106</sup> due to proper balance between zeolitic and mesoporous phases.

Catalysts based on Pt-H-ferrierite can also be of interest for the selective cracking of n-alkanes to remove these low octane components from gasolines.<sup>107</sup> An interesting catalytic application of H-FER in the "fine chemicals" field is for the hydration of acrolein.<sup>62</sup>

### **7.1.6.3 Other medium-pore zeolites of interest in butene skeletal isomerization and n-paraffin hydroisomerization**

Other medium-pore zeolites allow easy diffusion of linear hydrocarbons, with hindered diffusion of branched and aromatic molecules. Thus, these zeolites catalyze conversion of linear aliphatic compounds to cracking products. According to a "pore mouth" and/or "key lock" catalysis mechanism, occurring at the mouth of

their monodimensional channels, possibly with a “transition-state shape selectivity” effect, these zeolites when doped by noble metals are active for hydroisomerization reactions of linear paraffins to produce mainly monobranched isomers.<sup>108</sup>

#### 7.1.6.3.1 Clinoptilolite (H-HEU)

Clinoptilolite, which belongs to the Heulandite framework (HEU), is one of the most abundant natural zeolites. The pore structure (Figure 7.1) is similar to that of FER zeolite, but with more elliptical shape. The HEU framework has a two-dimensional channel system consisting of 10-membered-ring ( $7.5 \times 3.1$  Å) channels and 8-membered-ring ( $3.6 \times 4.6$  Å) channels viewed along [001], which are intersected by 8-membered-ring ( $4.7 \times 2.8$  Å) channels viewed along [100]. Data reveal very high selectivity of H-HEU in butene skeletal isomerization to isobutene with low activity.<sup>102</sup>

#### 7.1.6.3.2 ZSM-22 (H-TON)

ZSM-22 zeolites shows comparable performances in butene isomerization with respect to H-FER but only after some time on stream.<sup>103</sup> It has a monodimensional pore structure with 10 MR channels along [001],  $4.6 \times 5.7$  Å. This zeolite is also of interest for n-paraffin hydroisomerization, when doped with Pt.<sup>108</sup>

#### 7.1.6.3.3 ZSM-23 (H-MTT)

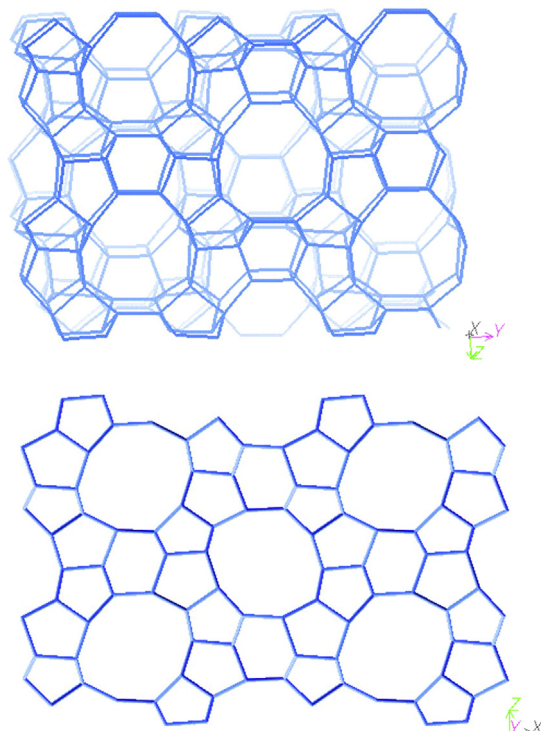
It has a monodimensional pore structure with 10 MR channels along [001],  $4.5 \times 5.2$  Å. This zeolite is also of interest for n-paraffin hydroisomerization, when doped with Pt.<sup>108</sup>

#### 7.1.6.3.4 ZSM-48

ZSM-48 is a family of zeolite polytypes, whose structures are formed by layers built from tubular pores of rolled-up honeycomb-like sheets of fused 6-MR rings with 10-MR ring windows, forming one-directional channels.  $5.3 \times 5.6$  Å. This zeolite is also of interest for n-paraffin hydroisomerization, when doped with Pt.<sup>108</sup>

### 7.1.6.4 ZSM5 (H-MFI)

The structure of MFI zeolite (Figure 7.12) contains two types of intersecting channels, both formed by 10-membered silicate rings, characterizing this material as a medium-pore zeolite. One channel type is straight and has a nearly circular opening ( $5.3 \times 5.6$  Å) along [010], while the other one is sinusoidal and has an elliptical opening ( $5.1 \times 5.5$  Å), along [100]. The Si/Al ratio may vary from infinity (Silicalite-1) to near 10. The bridging hydroxy groups show a single band that shifts from  $3595$  to  $3620$   $\text{cm}^{-1}$  by varying the Si/Al ratio and measurement temperature. Although the channels of H-MFI and framework oxygen positions are very similar to each other, never the  $\nu\text{OH}$  band is found split, although it has been suggested<sup>109</sup> that the OH's in the channels intersection absorb at a slightly higher frequency ( $3610$ – $3620$   $\text{cm}^{-1}$ ) than those located in the channels  $3610$ – $3590$   $\text{cm}^{-1}$ .  $^1\text{H}$  NMR studies allowed to assign peaks, usually in the range near 4 ppm, to the acidic protons of H-MFI. Some studies found the peak split into two<sup>110,111</sup> or even four components with the more intense peak at 3.8 ppm.<sup>112</sup> The Inelastic Neutron Scattering study of



**FIGURE 7.12**

ZSM-5 projection along [010] and [100].

Jobic et al.<sup>113</sup> showed that the deformation mode  $\gamma$ -OH is split for H-MFI, suggesting that at least two well-different OH groups actually exist.

The channels of the MFI structure allow the quite easy diffusion of benzene, monosubstituted benzenes, and para-disubstituted benzenes, as well as of linear and monomethyl-branched aliphatic compounds. Good diffusion, however, requires quite high temperatures ( $>350\text{ }^{\circ}\text{C}$ ) and vapor phase. The diffusion of ortho- and meta-disubstituted benzenes and of dibranched isomers is far more difficult.

Thanks to its porous structure and its stability when with large Si-to-Al ratio, ZSM-5 zeolite finds a number of applications in the chemistry of aromatics. Examples of this are in the application of “selectivated H-ZSM5” in the Selective Toluene Disproportionation (STDP) processes, allowing the highly selective production of benzene and paraxylene from toluene. With a zeolite treated with silicon-containing compounds at the external surface (to limit reaction out of the channels), whose pore mouths may also be narrowed by silication or precoking, working in the vapor phase at  $420\text{--}480\text{ }^{\circ}\text{C}$ ,  $20\text{--}40\text{ bar}$ , WHSV  $3\text{--}5/\text{h}$  small toluene conversion per

pass, the selectivity para-xylenes/total xylenes may be higher than 80%, with cycle lengths of more than 1 year.<sup>114</sup> H-ZSM-5 catalysts are also active in xylene isomerization, ethylbenzene dealkylation, aromatics transalkylations, etc., and are used for these commercial processes in alternative to other zeolite catalysts such as mordenite.<sup>114–116</sup> All these processes are performed in the gas phase at  $T > 350$  °C, usually in the presence of hydrogen and with small amount of a noble metal (Pt) in the catalyst to limit coking.

H-MFI catalysts were also used for the Mobil–Badger process of benzene alkylation by ethylene for the ethylbenzene synthesis, performed in the vapor phase at 390–450 °C.<sup>117,118</sup> Now this process has been substituted by liquid-phase alkylation with larger pore zeolites (BEA, MOR or FAU). Interestingly, H-MFI is not a good catalyst of the gas-phase benzene alkylation by propene for the cumene synthesis, producing an excess of n-propylbenzene. This has been attributed to the high temperature needed to overcome the aromatics diffusion constraints in the 10-membered channels.<sup>119</sup> These constraints limit activity of H-MFI in liquid phase aromatics alkylations. H-MFI are also used to dealkylate ethylbenzene in the xylene isomerization processes.<sup>120</sup>

Due to the product-shape selectivity obtained with H-ZSM-5, catalysts with an additional dehydrogenating component such as Pt-, Zn- and Ga-ZSM-5 are useful catalytic materials for aromatization of paraffins.<sup>121</sup> Different processes have been developed using these catalytic systems. Gallium-loaded and zinc-loaded zeolites are less active compared to Pt/H-ZSM-5, but they combine a high aromatization activity with a moderate hydrogenolysis. These catalysts, however, are more subject to deactivation by coke formation. The Cyclar process (UOP-BP) converts light paraffins directly to a liquid aromatics product in a single operation. The dehydrocyclodimerization reaction is thermodynamically favored at temperatures above 425 °C. The dehydrogenation of light paraffins (propane and butanes) to olefins is the rate-limiting step. Once formed, the highly reactive olefins oligomerize to form larger intermediates, which then rapidly cyclize to naphthenes. These reactions, dehydrogenation, oligomerization and cyclization are all acid catalyzed. The shape selectivity of the zeolite component of the catalyst also promotes the cyclization reaction, and limits the size of the rings formed.<sup>122</sup> For the preparation of Ga/ZSM5 catalysts, extra-framework Ga species are introduced on an H-ZSM-5 (Si/Al a.r.  $\sim 20$ ) with different methods, and substitute part of the protons of H-ZSM-5. According to the literature, the catalysts contain few % Ga wt/wt and should contain, in the active form, monovalent Gallium species, and Lewis and Brønsted acid sites.<sup>123,124</sup> The liquid product contains about 91% BTX and 9% heavier aromatics, with nonaromatic impurities limited to 1500 ppm or less.

As said, the channel size of MFI also does not allow the easy diffusion, if at all, of molecules containing the tert-butyl group. This is a reason for the almost total inactivity of H-MFI in isobutane/butylene alkylation, whose products and intermediate species contain the tert-butyl group. For the same reason, H-ZSM5-based catalysts with SiO<sub>2</sub>/Al<sub>2</sub>O<sub>3</sub> ratio of at least 20, containing c. 40 wt% of a binder (Al<sub>2</sub>O<sub>3</sub>

or  $\text{SiO}_2$ ), have been developed to obtain olefin oligomers with relatively high linearity and low branching that can be applied for use as diesel-blending fuels in the process, denoted as COD, Conversion of Olefins to Diesel, from Lurgi-Süd Chemie.<sup>125,126</sup> Similar processes are MOG, Mobil Olefin to Gasoline and MOGD the Mobil Olefin to Gasoline/Distillate,<sup>3</sup> also with H-ZSM-5 type catalysts.<sup>127</sup> A similar MFI zeolite catalyst with both Al and Ti in the framework has been patented by ENI for a similar application,<sup>128</sup> while other medium-pore zeolites have been patented by Mobil.<sup>129</sup> For this reaction, temperature may be relatively low (100–300 °C).

H-ZSM-5 is also active in converting methanol to hydrocarbons. The Mobil Methanol to Gasoline (MTG) process, performed using a mixture of methanol/dimethylether at  $T > 300$  °C and moderate pressure, operated at New Plymouth in New Zealand from 1985 to 1997 producing a sulfur-free gasoline of approximately 92-RON quality.<sup>3,130</sup> Due to the higher temperature, aromatics are largely present in the liquid product, while light olefins are also produced.

H-ZSM-5 zeolite with high Si/Al ratio is also apparently<sup>131</sup> the basic component of the catalyst, developed by Süd Chemie (now Clariant) for the Lurgi Methanol to Propylene (MTP) process.<sup>132</sup> The reaction is usually realized at nearly normal pressure and reaction temperature of 350–500 °C by using fixed bed reactor. Improvement of performances is attempted by adding promoters, reducing crystal size and inducing additional mesoporosity and defectivity. Gasoline with RON 95 is a byproduct.

A reactant shape selectivity effect allows the use of H-MFI (usually containing also a hydrogenating metal) for the selective cracking of linear paraffins in the catalytic dewaxing of lube oils (such as the Mobil Selective DeWaxing process, MSDW). Linear paraffins enter and diffuse easily in the MFI cavities, while the entrance of branched isomers is hindered. Thus, conversion of linear compounds is favored with respect to those of branched isomers.<sup>133</sup>

An important recent application of H-ZSM-5 is as a component of Fluid Catalytic Cracking (FCC) catalysts based on faujasite Y zeolites. H-ZSM-5 crack selectively the  $\text{C}_{5+}$  olefins, resulting in a reduced gasoline olefinicity and increased gaseous olefins production.<sup>134</sup> On the other hand, the catalytic cracking of various types of hydrocarbons to produce ethylene and propylene is becoming an interesting perspective: the reaction occurs at 550–650 °C, that is about 200 °C lower than the typical temperature of steam cracking, the common process to produce light olefins. Over ZSM-5-type catalysts, the yields of ethylene and propylene are high enough to compete with the steam cracking products. It is noteworthy that the effect of feed type on the light olefins ratio is not as prominent as the steam cracking and the ratios of P/E could be controlled by adjusting catalyst acidity.<sup>135</sup>

There are a large number of other industrial applications of H-MFI-based acid catalysts. In the fine-chemistry field, among many other applications,<sup>62</sup> H-MFI zeolites are applied to produce substituted pyridines.<sup>136</sup> La-H-ZSM-5 is used as a catalyst of a new process allowing the selective synthesis of diethanolamine (DEA) from ethylene oxide and ammonia.<sup>137</sup> H-MFI zeolite can also be applied as heterogeneous

acid catalyst in water phase.<sup>138</sup> A process for cyclohexene hydration to cyclohexyl alcohol in water using highly siliceous H-ZSM-5 zeolite from Asahi Kasei operates successfully at  $\sim 120$  °C.<sup>139</sup>

A number of studies are being undertaken to modify the porous structure of H-ZSM-5 materials with the addition of mesoporosity.

#### 7.1.6.5 ZSM-12 (H-MTW)

ZSM-12 zeolite has a unidimensional 12-membered ring porous structure with pore openings  $5.6 \times 6.0$  Å. The IR band due to bridging OH's is clearly split with two components at c.  $3610$  and  $3580$   $\text{cm}^{-1}$ <sup>140,141</sup> which are strongly acidic and at least partially accessible by so-large molecules as 1,2,4-trimethylbenzene. This zeolite is an excellent catalyst for aromatics alkylation in the liquid phase<sup>119</sup> and is reported<sup>20</sup> to be applied industrially for the synthesis of p-tert-butyl-ethylbenzene. It has also recently been patented for the selective alkylation of naphthalene with methanol to produce 2,6-dimethyl-naphthalene,<sup>142</sup> the precursor for obtaining polyethylenenaphthenate polyesters.

#### 7.1.6.6 Beta zeolite (H-BEA)

The framework of BEA zeolite (Figure 7.13) gives rise to two different channel types, both formed by 12-membered rings, but with definitely different diameters, one ( $0.55 \times 0.55$  nm) in the medium pore range, the other ( $0.76 \times 0.64$  nm) in the large pore range. The Si/Al ratio is typically in the 10–30 range, although particular preparations allow this ratio range to be expanded down to five up to infinity.<sup>143</sup>

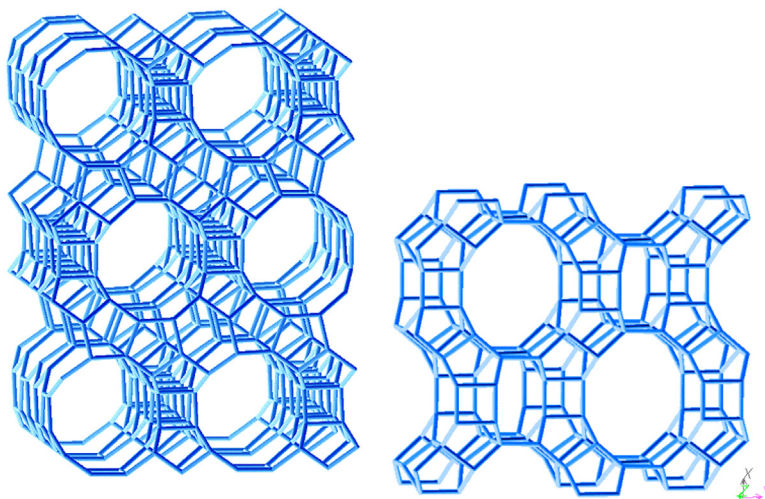


FIGURE 7.13

BEA projection viewed along [100] and MOR viewed along [001].

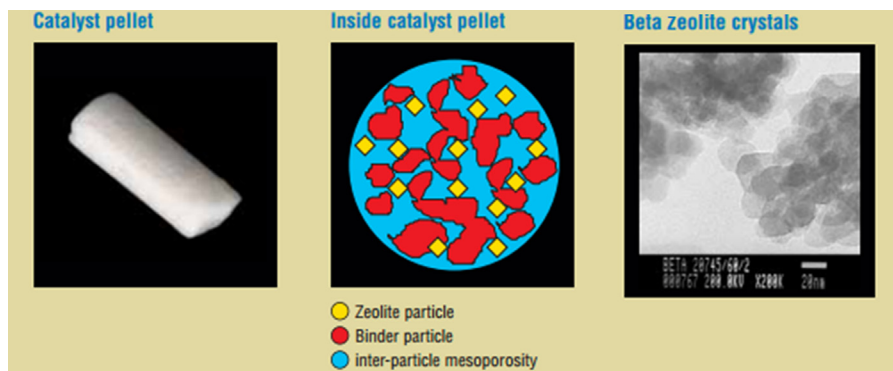
Crystallographic faults are frequently observed in beta-zeolite preparations, as well as in the natural counterpart tschernichite, whose structure is actually an intergrowth of two or three polymorph types. Studies confirm that beta zeolite is normally constituted by an intergrowth of the A polytype, (BEA, tetragonal, with space group symmetry  $P4_122$ ) and polytype B (BEB, monoclinic, with space group symmetry  $C2/c$ ). The latter polytype seems to having been crystallized only together with BEA.

Polytype C (BEC, tetragonal, with space group symmetry  $I4_1/amd$ ) does not generally occur in samples of zeolite beta and tschernichite; sometimes being present but neatly distinguished from the matrix of zeolite beta polytypes.<sup>144</sup> It can be prepared independently from other polymorphs in the presence of fluoride ions.<sup>145</sup>

The structure of beta zeolite is relatively fragile and calcination or steaming above 400 °C causes progressive dealumination with deposition of extra-framework aluminum (EF-Al) inside the channels.<sup>146</sup> The main effects of steaming were the dealumination of some particular sites (T3–T9), the formation and migration of extra-framework Al species, and the healing of defect sites by condensation of silanol groups.<sup>147</sup> At least two different types of extra-framework structures have been identified in unleached beta zeolite,<sup>148</sup> identified as Al hydroxo-ions interacting with the internal wall of the zeolite cavities and bigger oxide particles. Additionally, some big holes may exist which are however in contact with the external atmosphere by very small channels.

The IR band of bridging OH's of beta zeolite is a little split in at least two components ( $\nu\text{OH} \sim 3608 \text{ cm}^{-1}$  and  $\sim 3620\text{--}3612 \text{ cm}^{-1}$ ): OH's located at the smaller channels (unaccessible to t-butyl-containing species at r.t.) are quite homogeneous (sharp band at  $3609 \text{ cm}^{-1}$ ) while those in the larger channels (accessible to t-butyl-containing species at r.t.) are likely much more abundant and are definitely heterogeneous (three components at  $3628, 3608$  and  $3590 \text{ cm}^{-1}$ ).<sup>74</sup> Also  $^1\text{H}$  NMR studies reveal a significant heterogeneity of the bridging OH's of H-BEA with up to four  $\delta_{\text{H}}$  components at 3.28, 3.84, 4.42 and 5.21 ppm.<sup>112</sup> On the other hand, also part of the terminal silanol-groups, absorbing at  $3740 \text{ cm}^{-1}$  (IR) and (2.1 ppm,  $^1\text{H}$  MAS NMR) appear to be very acidic, only those absorbing at  $3745 \text{ cm}^{-1}$  (IR) and (1.8 ppm,  $^1\text{H}$  MAS NMR) behaving as typical silanols with weak acidity.<sup>85</sup>

The size of the larger channels of H-BEA allows quite easily the diffusion of aromatics as well as of molecules containing the tert-butyl group. In fact, beta zeolite finds industrial application in the Polimeri Europa-ENI<sup>149</sup> and in the UOP Q-Max<sup>TM</sup><sup>150,151</sup> processes for the liquid-phase synthesis of cumene by alkylation of benzene with propene. In both cases H-BEA-based catalysts catalyze selectively both the alkylation reaction, in multi-fixed-bed catalytic reactors (Figure 7.11, middle), with a large excess of benzene, and also the transalkylation reaction, where benzene reacts with di-isobutylbenzene producing additional cumene in a separate fixed bed reactor. The ENI catalyst, (Figure 7.14) denoted as PBE-1, is composed of a mixture of very small and uniform beta-zeolite particles with a binder, showing both zeolite microporosity and extrazeolite mesoporosity. Provided by the proprietary-forming procedure, beta zeolite is highly dispersed into the PBE-1 catalyst matrix giving incomparable high strength and negligible loss on attrition to the



**FIGURE 7.14**

Images of the beta-zeolite based ENI-Polimeri Europa PBE catalyst for cumene and ethylbenzene synthesis.

*Reprinted with permission from Ref. 152.*

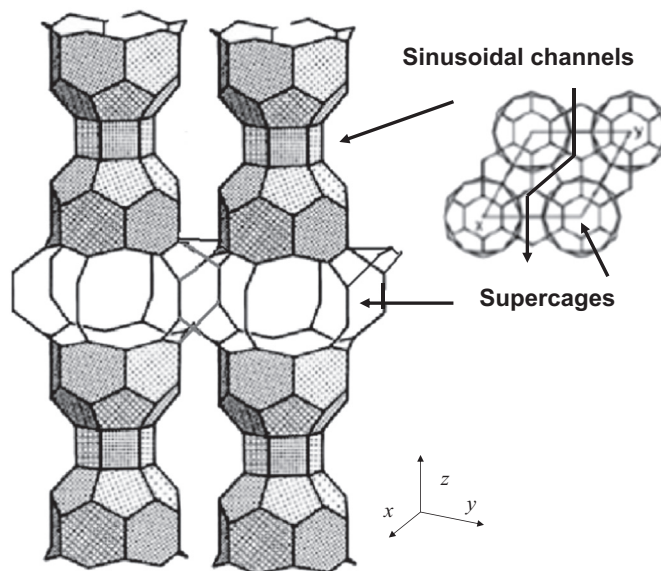
catalyst particle. Mechanical properties of the catalyst ensure very low and constant pressure drop as well as a negligible fine production during loading and unloading operations for several reaction/regeneration cycles in industrial cumene and ethylbenzene synthesis.<sup>152</sup>

Cumene diffusion is much better on large than on medium pore zeolites (where the isopropyl group causes some hindering), while the diffusion of diisopropylbenzenes is more hindered in beta zeolite than in other large pore zeolites, allowing product shape selectivity which limits the production of polyalkylated compounds. Beta-zeolite catalysts can be fully regenerated by coke burning, needed every 2–3 years and should last for at least three cycles with proper care. According to the patent literature, it seems that also the Lummus/UOP EBOne liquid-phase ethylbenzene synthesis process works with an H-BEA-based catalyst,<sup>153</sup> such as also the Polimeri Europa ethylbenzene process.<sup>154</sup> Beta zeolite finds also interesting applications in the field of fine chemistry<sup>62</sup> in liquid phase such as for some acetylation reactions such as that of veratrol, performed by Rhodia in liquid phase with a fixed bed,<sup>155</sup> as well as the shape selective acetylation of 2-methoxy-naphthalene to 2-acetyl-6-methoxynaphthalene, in the way of synthesis of (S)-Naproxen, or (+)-2-(6-methoxynaphthyl)-propionic acid, an important nonsteroidal anti-inflammatory drug.<sup>156</sup>

#### 7.1.6.7 MCM-22 (H-MWW)

MCM-22 zeolite (Figure 7.15, left) possesses a unique crystal structure denoted with the code MWW, containing two independent nonintersecting pore systems. One of the channel systems contains two-dimensional sinusoidal 10-membered silicate ring channels (diameters  $4.1 \times 5.1 \text{ \AA}$ ), while the other system consists of large supercages (12-membered) with dimensions  $7.1 \times 7.1 \times 18.1 \text{ \AA}$ . The supercages stack





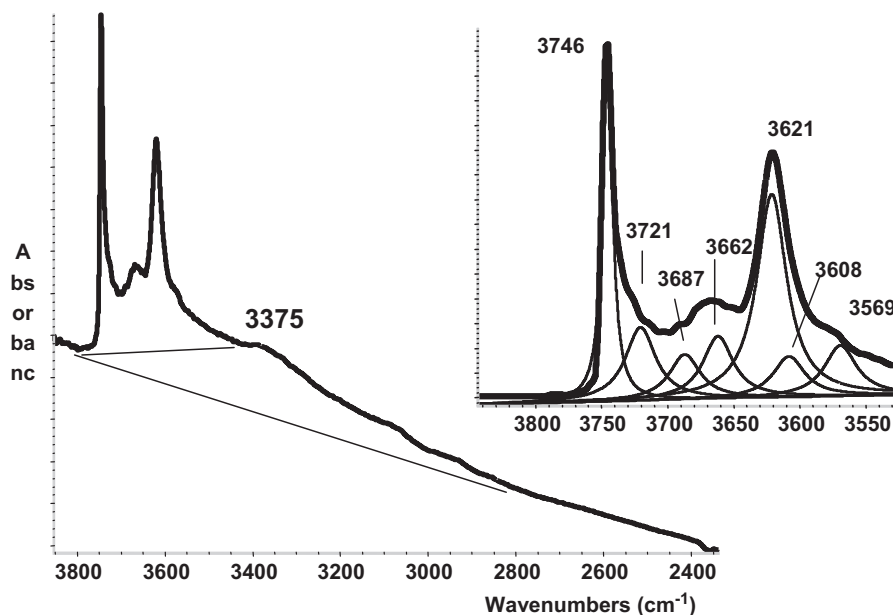
**FIGURE 7.15**

Structural features of MVM-22 (MWW) zeolite.

one above another through double prismatic six-member rings and are accessed by slightly distorted elliptical 10-membered connecting channels ( $4.0 \times 5.5 \text{ \AA}$ ). A buried tetrahedral atom also exists in the structure. In general, the synthesized MCM-22 zeolites crystallized as very thin plates with large external surface area,<sup>157</sup> on which 12-membered hemisupercages pockets ( $7.0 \times 7.1 \times 7.1$ ) should be exposed.

The spectrum of hydroxyl groups of pure MCM-22 sample<sup>158,159</sup> shows sharp OH-stretching bands centered at  $3747$  and  $3620 \text{ cm}^{-1}$ , and broader band at  $3668 \text{ cm}^{-1}$  are evident (Figure 7.16). An additional weak component is also found at  $3575 \text{ cm}^{-1}$ . The peak at  $3747 \text{ cm}^{-1}$  is typical for the OH stretching mode of terminal silanols, observed on all protonic zeolites with variable intensity, as on silica and on any silica-based material. The evident presence of components along the tail toward lower frequencies can be associated, in this case as well as in other cases, to silanols or other hydroxyl groups either in the internal or in the external surface. The broad absorption at  $3668 \text{ cm}^{-1}$  falls in the region typically assigned to OHs on extraframework material.

The peak at  $3620 \text{ cm}^{-1}$  is typical of “zeolitic” bridging Si(OH)Al groups. Two components at  $3621$  and  $3608 \text{ cm}^{-1}$  (the latter being much weaker than the former) are evidenced by deconvolution. The small component observed at  $3575 \text{ cm}^{-1}$  ( $3569 \text{ cm}^{-1}$  in the deconvolution) has been attributed to a third family of “zeolitic” bridging Si(OH)Al groups. Adsorption of hindered probes showed that the more abundant zeolitic OHs are those exposed in the supercage system, absorbing



**FIGURE 7.16**

FT-IR spectrum of MCM-22 pressed disk outgassed at 450 °C. Inset: deconvolution of the OH-stretching band system.

predominantly at c. 3618–3625  $\text{cm}^{-1}$ . Less abundant are those exposed in the sinusoidal channel system, predominantly absorbing in the 3618–3605  $\text{cm}^{-1}$ . The third family, responsible for a weak band at 3575  $\text{cm}^{-1}$  is tentatively assigned to species exposed in the supercages and hemisupercages, too. These assignments found support in a theoretical study of Yan Li.<sup>160</sup>

The spectrum shows an additional broad absorption centered at  $\sim 3375 \text{ cm}^{-1}$ , to which the sharp peaks of zeolitic OHs are superimposed, which has been also observed in the case of other zeolite samples, usually quite Al-rich, centered in the 3400–3300  $\text{cm}^{-1}$  region. This broad and low frequency band may be attributed to H-bonded hydroxyl groups. We can note here that these features may be at even lower frequencies than those characterizing silanol nests in the internal surface of silicalite. This band is assigned to hydroxyl groups located in the nonsurface oxygen positions, bonded to the buried T-atom typical of the H-MWW structure. These positions, if occupied by hydroxyl groups, are not exposed at the zeolite channels and could give rise to hydrogen-bonded hydroxyl groups, again in agreement with the theoretical work of Yan Li et al.<sup>160</sup>

These studies support the conclusion that hemisupercages are exposed at the [001] basal plane of the MCM-22-layered structure, where zeolitic OHs of the same nature of those exposed supercages (bands at 3618–3625  $\text{cm}^{-1}$  and at 3575  $\text{cm}^{-1}$ ) indeed exist.

The Mobil's proprietary MCM-22 zeolite is the catalyst of the EBMax liquid phase ethylbenzene process,<sup>118,161</sup> performed at 160–220 °C. In the EBMax process, benzene is fed to the bottom of the liquid-filled multi-bed reactor. Ethylene is co-fed with benzene and also between the catalyst beds to quench the reaction heat. Typical benzene to ethylene feed ratios are in the range of 3 to 5. H-MWW family materials, including MCM-49, are also the components of the catalyst of the liquid-phase Mobil process for cumene synthesis.<sup>118,162</sup> This catalyst competes with those based on H-BEA (ENI and UOP) and on H-MOR (Dow). The MCM-22 zeolite catalyst may be more monoalkylate-selective than most large pore zeolites, and is very stable. Cycle lengths in excess of 3 years have been achieved. The excellent selectivity to monoalkylated products is attributed to the confinement effect within the 12-membered ring pore system where the reaction occurs, and the easy desorption of alkylbenzenes from the pockets. Mechanistic studies suggest that the reaction should occur in the hemisupercages exposed at the surface. The particular high stability of MCM-22 is attributed to the unique feature of the existence of the buried T (Si or Al) atom not accessible to a channel wall.

#### 7.1.6.8 Mordenite (H-MOR)

The orthorhombic mordenite structure (Figure 7.15, right) is characterized by nearly straight channels running along the [001] crystallographic direction, which are accessible through 12-membered silicon-oxygen rings  $6.5 \times 7.0$  Å wide. Additionally, 8-ring “side pockets” exist in the [010] direction, whose opening is  $3.4 \times 4.8$  Å. The side pockets connect main channels to a distorted eight-ring “compressed” channel also running parallel to the 001 direction, but having an elliptical small opening  $5.7 \times 2.6$  Å wide.

IR spectra show, for typical H-MOR with Si/Al ratio 10, a strong slightly asymmetric band centered at  $3605\text{ cm}^{-1}$ . Several studies have been devoted to the characterization and to the localization of the “framework” protonic sites in H-MOR by IR spectroscopy.<sup>91</sup> Authors agree that the OH's in the so-called side pockets and smaller channels are associated to a band that is located at distinctly lower frequencies (near  $3580\text{ cm}^{-1}$ ) with respect to those located in the main channels.<sup>75</sup>

Studies on the adsorption of hindered nitriles<sup>163–165</sup> allowed to distinguish three families of bridging OH's in H-MOR. The hydroxy groups responsible for the band at  $3588\text{ cm}^{-1}$  are located inside the side-pockets, those absorbing at  $3609\text{ cm}^{-1}$  are likely at the intersection between side pockets and main channels, while those absorbing at  $3605\text{ cm}^{-1}$  are thought to stand near the center of the main channels. Three families of bridging OH's have also been found on H-MOR, later, by Marie et al.<sup>166</sup> A broad OH-stretching band with a maximum near  $3300\text{ cm}^{-1}$  is also observed, not sensitive to adsorption, and is attributed to H-bonded OH's located on oxygen sites (in particular O4 and O8, i.e. pointing toward the chain of four-membered rings) fully hindered to probe molecules. Dealumination mostly occurs in the side pockets and in the compressed channels, leaving the most exposed OH's of the main channels free for catalysis. However, extensive dealumination may make the side pockets accessible to large probes such as alkyipyridines.<sup>167</sup>

$^1\text{H}$  MAS NMR spectroscopy in combination with loading studies involving the basic probe molecule trimethylphosphine showed that about 20–25% acidic hydroxyl groups are located in 8-ring channels, 25–30% are located at the intersections of the side pockets and main channels, and the rest (45–50%) are located in the 12-ring main channels. By carefully examining the structure, it has been concluded that there are four most plausible locations for Brønsted acid sites in zeolite H-MOR: (a) O1/O9, pointing into the center of the 8-ring channel and inaccessible to TMP probe molecules; (b) an adjacent pair of O2 atoms sharing one proton through H-bonding; (c) O5, which points slightly toward the side pocket; and (d) O10, pointing into the center of the 12-ring.<sup>168</sup>

The adsorption of different probes shows that monosubstituted aromatic compounds and compounds having the tert-butyl group diffuse in the main channels, but are not allowed to enter the side pockets. Even the access of n-hexane in the side pockets is hindered. The entrance of ortho-disubstituted benzenes may be hindered also in the main channels. Pyridine is protonated in the main channels. Small amounts of quite strong Lewis sites are mostly if not entirely located at the external surface. These data suggest that acid catalysis would predominantly occur in the main channels, although the location of Na ions and EF material in the side pockets may stabilize the structure and influence in some way the catalytic phenomenon. Recently, Iglesia and coworkers provided evidence that the monomolecular cracking and dehydrogenation of propane and n-butane occur preferentially within constrained 8-MR pockets, where transition states and adsorbed reactants are only partially confined.<sup>77</sup>

Dealuminated mordenite is the basic structure of commercial catalysts for C4–C6 paraffin skeletal isomerization,<sup>169–171</sup> such as Süd Chemie Hysopar, based on alumina-bound Pt-H-MOR with  $\text{SiO}_2/\text{Al}_2\text{O}_3 \sim 15\text{--}17$ , UOP HS-10 and Procatalyse IS-632.<sup>172</sup> Dealumination until a framework/extra-framework Al ratio  $\sim 3$  improves the catalytic activity.<sup>173</sup> The catalyst works near 250 °C, so at a definitely higher temperature than those based on chlorided alumina, when the thermodynamics is less favorable, but are more stable and more environmentally friendly. This catalyst may be applied e.g. with the IPSORB process of IFP.<sup>174</sup> This agrees with the quite easy diffusion of branched molecules in the main channels.

As said, also monosubstituted benzene diffuses easily in the main channels of H-MOR, while o-disubstituted benzenes are hindered to diffuse. In agreement with this, H-MOR also catalyzes selective conversions of aromatics, such as transalkylation and toluene disproportionation.<sup>175</sup> Dealuminated H-MOR is the catalyst of the Dow–Kellogg cumene synthesis process. Noble metal- or nickel-containing H-MOR are applied for the disproportionation of toluene to benzene + an equilibrium mixture of xylenes, generally at 20–40 bar, 380–500 °C, with excess hydrogen ( $\text{H}_2/\text{hydrocarbon}$  1–6).<sup>176</sup>

#### 7.1.6.9 Zeolite omega (H-MAZ)

Zeolite omega, a large pore zeolite with a silica–alumina ratio in the range of 4–10, is the synthetic isotype of the mineral mazzite<sup>177</sup> (topological code MAZ). In its unit

cell, 36 tetrahedral atoms bridged by oxygen atoms form gmelinite-type cages and 12-membered cylindrical channels along [001] direction with 7.4 Å diameters. In addition to its large pore system, secondary mesoporous structure could be created by mild dealumination,<sup>178</sup> which may facilitate the transport of reactant and reduce the deposition of coke. The IR spectra show a complex band due to bridging OH-stretching modes: according to McQueen et al.<sup>179</sup> two components are observed at 3615 and 3600 cm<sup>-1</sup> in the case of a partially dealuminated mazzite sample, while according to Guisnet et al.<sup>180</sup> up to five components can be distinguished in differently dealuminated samples. Shigeishi et al.<sup>181</sup> found two peaks at 3626 and 3606 cm<sup>-1</sup> assigned to structural hydroxy groups. According to these authors, the peak at 3626 cm<sup>-1</sup> would shift down to 3247 cm<sup>-1</sup>, upon low temperature CO adsorption, with a shift of 379 cm<sup>-1</sup>, which would indicate an exceptionally strong acidity of these OH's.

Zeolite omega is apparently the basic structure of modern zeolitic C4–C6 paraffin skeletal isomerization catalysts cited under development by Süd Chemie (Clariant) as HYSOPAR<sup>®</sup> catalysts, reported to be characterized by their outstanding tolerance of feedstock poisons such as sulfur (even more than 100 ppm) and water with very high catalyst lives.<sup>170,171</sup> The catalyst is alumina-bound Pt-H-MAZ with Si/Al ~ 16, working at 250 °C with WHSV 1.5/h and a H<sub>2</sub>/hydrocarbon ratio of 4. Pt and hydrogen have the effect of reducing coking and hydrodesulfurizing S-containing compounds. This catalyst was reported to be more effective than Pt-H-MOR commercial catalysts, and more stable than the catalysts based on chlorided aluminas and sulfated zirconia.

#### 7.1.6.10 EU-1 (H-EUO)

The zeolite denoted as EU-1, whose topology is denoted as EUO, has one-dimensional channel system with 10-MR openings 4.1 × 5.4 Å connected to 12-MR side pockets in the (001) direction. It is reported in the field of catalysis of aromatics reaction, in particular for the isomerization of C8 aromatics<sup>182,183</sup> cracking of naphtha, and methanol to gasoline.<sup>184</sup> This zeolite presents a strong and broad IR band at 3605 cm<sup>-1</sup> due to the acidic hydroxyl groups,<sup>185</sup> corresponding to a <sup>1</sup>H MAS NMR signal at 4.0 ppm.<sup>186</sup>

#### 7.1.6.11 Faujasite (H-FAU: H-Y, H-USY, RE-Y)

As already seen before, the faujasite structure is formed by wide supercages (13 Å diameter) accessed through 12-member silicate rings with 7.4 Å diameter, much smaller sodalite cages accessed through 6-member silicate rings and hexagonal prisms connecting the sodalite cages. All the catalytic chemistry of faujasites is supposed to occur in the supercages. The aluminum content in faujasite is generally very high, the theoretical Si/Al ratio being as low as 1. Faujasites with Si/Al ratio near 1 are usually denoted as X-zeolites. Faujasites with Si/Al ratio higher than 2 are usually denoted as Y-zeolites and are more stable in the protonic form, denoted as H-FAU or H-Y. The resulting materials with Si/Al ratio >30 are hydrothermally more stable (the so-called ultrastable Y zeolite, USY). Their structure and acidic

properties are greatly influenced by the dealumination process. In particular for their application in the FCC process, faujasites are activated by rare earths (RE-Y or RE-USY) to increase stability and, possibly, acidity. The main components of FCC catalysts contain up to 18% wt/wt of the natural mix of rare earth where 80% or more is Lanthanum. Very recently, due to a sharp increase of price of rare earths,<sup>187</sup> “rare earth-free” catalysts have been commercialized based on H-Y, H-USY, Mg-USY, Zn-USY and Mn-USY, or their mixtures.<sup>188</sup>

The multiplicity of the hydroxy groups in H–Y zeolites can be very clearly observed by IR, two well-defined bands appearing for bridging OH's. The high-frequency HF band ( $3626\text{ cm}^{-1}$ ) has been assigned to bridging OH's located in the supercage where are accessible to most molecules. These are the active Brønsted acid sites of protonic Faujasites. The low-frequency LF band ( $3562\text{ cm}^{-1}$ ) has been assigned to OH's located near the middle of the six bond rings connecting the sodalite cages,<sup>189</sup> being possibly weakly H-bonded through the cavity. The LF OH groups do not interact directly even with very small and poorly basic molecules like Ar, H<sub>2</sub>, O<sub>2</sub> and N<sub>2</sub>,<sup>190</sup> but can H-bond with more basic molecules located in the supercages, although being unable, for steric reasons, to protonate them. Romero Sarria et al.<sup>191</sup> observed, by the use of trimethylamine as a probe, a third component in the HY spectrum, which is not perturbed at all by the probe, at  $3501\text{ cm}^{-1}$ , assigned to OH's in the hexagonal prisms. Suzuki et al.<sup>192</sup> reported on the existence of a fourth OH group also located in the supercage, evidenced by a splitting of the HF band.

The strong acidity of HF OH groups of protonic Faujasites is supported by the extent of the shift down of  $\nu\text{OH}$  upon interaction with carbon monoxide ( $\Delta\nu \sim 250\text{--}300\text{ cm}^{-1}$  depending on sample composition). According to Montanari et al.,<sup>193</sup> the shift of part of the HF  $\nu\text{OH}$  band down of  $410$  or  $450\text{ cm}^{-1}$  indicates that stronger Brønsted sites may exist (or stronger OH...CO interactions may be established) in the cavities of USY than on REY and HY. These sites, located in the supercages, may give rise to stronger interactions also than those observed on H-MOR, H-MFI and H-FER zeolites. This is in agreement with the data reported by Navarro et al.<sup>194</sup> In any case, also the predominant normal OH groups on USY appear to establish stronger OH...CO interactions than those of HY and REY ( $\Delta\nu \sim 350\text{ cm}^{-1}$  with respect to  $300\text{--}330\text{ cm}^{-1}$ ). Niwa et al.<sup>195</sup> attributed to a new OH absorbing at  $3595\text{ cm}^{-1}$  the enhanced acidity of USY treated with ethylenediaminetetraacetic acid.

The same Brønsted sites acidity strength scale is obtained using  $\nu\text{CN}$  of H-bonded pivalonitrile (shifted up to  $2277\text{ cm}^{-1}$  on USY), taking into account that such a molecule, much more hindered, appears to not be able to enter all the cavities or to reach all the existing sites in Al-rich HY [196]. USY also displays strongest Lewis acid sites than HY and REY, as deduced by the position of  $\nu\text{CN}$  of pivalonitrile adsorbed on Lewis sites (shifted up to  $2297\text{ cm}^{-1}$  on USY). The strength of Lewis sites of USY resemble those of the strongest sites of silica–alumina and pure alumina. However, REY seems to display the higher density of both Lewis and Brønsted sites among Y-zeolites.

The  $^1\text{H}$  MAS NMR spectra of faujasites show split peaks for protons located in the sodalite cage and in the supercage. As shown in Figure 5.2, a La,Na-Y zeolite shows sharp peak at 3.9 ppm, which disappears upon contact with perdeuteropyridine (thus the OH group being located in the supercage), and another, complex one with maximum at 4.8 and a shoulder at 6.3 ppm, which is not perturbed during this experiment. Indeed La-FAU may present up to six  $^1\text{H}$  MAS NMR peaks assigned to silanol groups (SiOH) at the external surface or at lattice defects (1.7–1.8 ppm), OH groups on extra-framework aluminum species (AlOH, 2.5–2.9 ppm), OH groups associated with  $\text{La}^{3+}$  cations (LaOH, 6.2 and 6.6 ppm), and bridging OH groups (SiOHAl, 3.9–4.0 and 4.5–6.0 ppm).<sup>196</sup>

According to  $^{27}\text{Al}$  3Q NMR and  $^{29}\text{Si}$  MAS NMR studies, van Bokhoven et al.<sup>197</sup> concluded that extra-framework octahedral EF Al species causes a perturbation on framework tetrahedral Al ions. In agreement with this, DFT studies suggest that EF Al species would tend to coordinate to oxygen atoms near the framework Al atoms.<sup>198</sup> In this way, an enhancement of the Brønsted acidity of the regular framework sites discussed above can be obtained. However, it seems that EF species possess their own Brønsted acidity having been identified as silica-alumina debris where part of Al is in a flexible octahedral environment.<sup>199,200</sup> According to Menezes et al.<sup>201</sup>, MQMAS NMR and IR experiments show that tetrahedral Al species are also formed by steaming in USY and give rise to Lewis acidity, which, however, is not completely removed by leaching. Xu et al. showed that the structure of zeolite Y may collapse and be restructured, but this may give rise to quite different materials.<sup>202</sup> Lanthanum is found to be mainly located in the sodalite cage, with small amounts in the supercage.<sup>196</sup>

The FCC is an autothermal process, where the strongly endothermic catalytic cracking step is coupled with the strongly exothermic coke burning catalyst regeneration step. The catalyst continuously moves from the raiser where the cracking reaction occurs at  $\sim 540^\circ\text{C}$ , 2 bar, residence time  $\sim 3\text{--}10$  s, to the regenerator where the burning of coke gives rise to a gas rich in CO (so still useful for further heat generation by burning) and the temperature is enhanced again to  $730^\circ\text{C}$ , 2 bar, residence time  $\sim 15$  min.<sup>203</sup> The catalyst must be very stable to high-temperature hydrothermal treatment to resist such a cyclic process.

Besides RE-Y and RE-USY, the most used FCC catalyst today, several other components are present<sup>204</sup> such as an alumina or silica–alumina matrix or binder, kaolin, and H-ZSM5-containing additives to improve performances and quality of the products. To obtain a deeper cracking of sulfur compounds upon the FCC process, further additives (e.g.  $\text{ZnAl}_2\text{O}_4$ ) may be used.

USY is also a typical component or support of hydrocracking catalysts, to provide acidity. The catalyst contains a sulfur-resistant hydrogenation phase, like Ni–W sulfide. The reaction is performed at  $300\text{--}450^\circ\text{C}$  under 50–200 atm of hydrogen. A heavy low-value feed is transformed into lighter fractions. Hydrodesulfurization, hydrodenitrogenation, hydrodearomatization and hydrodealkylations occur. The wide dimensions of the channels of faujasite allow quite heavy molecules

to be cracked. Deactivation by coking occurs, but USY-based catalysts are less easily coked than those based on silica–alumina.<sup>205</sup>

USY-containing Pt is probably the catalyst of the AlkyClean process proposed by Akzo Nobel/ABB Lummus<sup>206</sup> for solid-catalyzed isobutane/butylene alkylation. The catalyst works at 40–90 °C<sup>207</sup> and is rejuvenated in liquid phase by hydrogen-isobutane mixture, and regenerated at 250 °C by hydrogen in the gas phase. Multiple reactors are used to allow for continuous alkylate production/catalyst rejuvenation cycles. Regeneration is performed intermittently. Also the catalyst proposed by Lurgi and Süd Chemie (LURGI EUROFUEL<sup>®</sup>), where reaction occurs at 50–100 °C, is likely based on acid faujasite. Alternative regeneration procedures of USY-based catalysts are under study, such as supercritical isobutane regeneration at 60 °C and 111 bar.<sup>208</sup>

Acidic faujasites find a number of other applications—among others, as catalysts for the liquid-phase acylation of anisole and veratrol (Rhodia).<sup>155,156</sup>

---

## 7.2 Aluminophosphates (AIPOs)

In the late seventies, after the first development of template-based syntheses of zeolites and silicalites, investigations were undertaken at the Union Carbide Laboratories to develop new molecular sieve materials, starting from tetrahedral framework cations, i.e. aluminum and phosphorus.<sup>209</sup> In fact, aluminum phosphate AIPO<sub>4</sub> is stoichiometrically analogous to silica SiO<sub>2</sub>, gives rise, like silica, to quite stable amorphous forms and crystallizes as well in the same structures as silica: the mineral berlinite is isomorphous to  $\alpha$ -quartz, while other polymorphs exist isostructural with tridymite, cristobalite and  $\beta$ -quartz. A number of microporous AIPO<sub>4</sub> molecular sieves have been then prepared, many of which have direct aluminosilicate zeolite analogues, other being unique framework types. Unlike zeolites, but like nondefective silicalites, AIPOs have a neutral framework with mild hydrophilicity,<sup>210</sup> and moderate to low acidity. In particular, strong zeolite-like Brønsted acidity is essentially absent in stoichiometric AIPO molecular sieves, as expected for the lack of framework charge imbalance. Despite their structural diversity and ease of modification, aluminophosphates do not seem having been so far found used in commercial applications, although a large number of systems have been shown to be catalytically active in potentially important industrial reactions.<sup>211</sup>

---

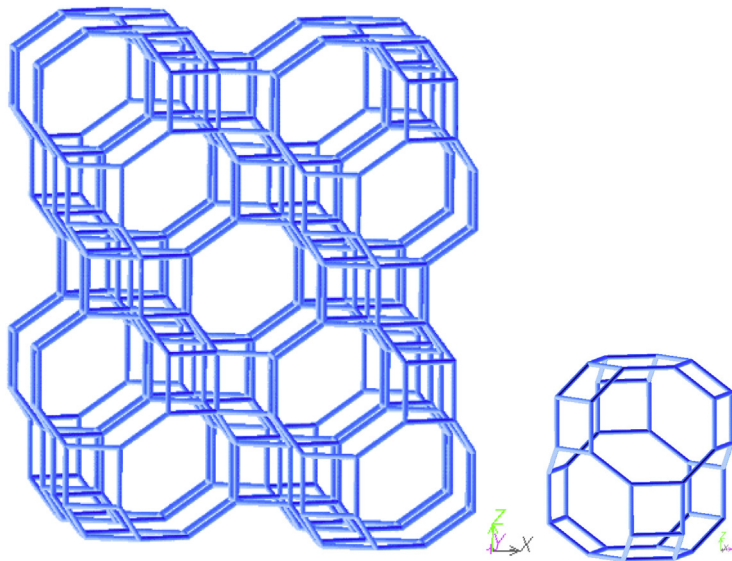
## 7.3 Silicoaluminophosphates (SAPOs)

SAPOs are silicon-containing aluminophosphates. In this case, strong zeolite-like Brønsted acidity is generated mostly by the silicon for phosphorus substitution in AIPO structures. Thus, SAPOs molecular sieves are topologically similar to small or medium pore zeolites, where phosphorus, aluminum and silicon atoms occupy the tetrahedral positions. These materials appear to be characterized a high thermal stability. The acidic properties of SAPO-n depend on the content, location and distribution of Si.



SAPO-34 is likely the most industrially developed SAPO. It is isomorphous to chabazite (CHA) (Figure 7.17) whose topology might be described as layers of double 6-MR that are interconnected by units of 4-MR. The double 6-MR layers stack in an ABC sequence. This leads to a framework with a regular array of barrel-shaped cages with 9.4 Å diameter, interconnected by 8-MR windows ( $3.8 \times 3.8$  Å). The chabazite structure contains only one tetrahedral site but four different oxygen atoms in the asymmetric unit, giving four possible acid-site configurations, depending on to which of the oxygen atoms the proton is attached.<sup>212,213</sup>

After activation, SAPO-34 gives five IR peaks in the range of 3000–4000  $\text{cm}^{-1}$  representing five types of hydroxyl groups. Two peaks at 3625–3628 and 3598–3605  $\text{cm}^{-1}$  can be attributed to two types of Si(OH)Al groups. The bridging group absorbing at  $\sim 3600$   $\text{cm}^{-1}$  is assumed to be localized in the hexagonal prism, forming an H-bond with adjacent oxygen atoms of the framework, whereas the isolated bridging OH groups pointing toward the center of the elliptical cage would give rise to a vibration frequency at  $\sim 3625$   $\text{cm}^{-1}$ . The lower frequency OH groups are considered to be a little less acidic than the high frequency ones. Both have acid strength comparable to those of zeolites, including chabazite, and are the active sites for acid-catalyzed reactions. The other peaks at 3675, 3743 and 3748  $\text{cm}^{-1}$ , with very low intensity, are assigned to P–OH, Si–OH and Al–OH groups, respectively, which are generated by the defect sites of SAPO-34 surface.<sup>213,214</sup>



**FIGURE 7.17**

CHA structure viewed along [010] and the cage viewed normal to [001].

SAPO-34 is an excellent catalyst for the conversion of methanol to ethylene and propylene in the so called Methanol to Olefin (MTO) process. The structures of SAPO-34 along with the small sizes of certain organic molecules are keys to the MTO process, developed by UOP and Norsk Hydro.<sup>215–217</sup> The small pore size of SAPO-34 restricts the diffusion of heavy and/or branched hydrocarbons, and this leads to high selectivity to the desired small linear olefins, with a product shape selectivity effect.

Under reaction conditions, at 400–550 °C, the deactivation by coke of SAPO-34 (containing 10% Si) is very fast<sup>218</sup> although activity is completely recovered after subsequent to combustion of coke with air. The catalyst has demonstrated the degree of attrition resistance and stability required to handle multiple regenerations and fluidized bed conditions over the long term. The better performances of SAPO-34 with respect to H-chabazite as the catalyst have been related to the tunable density of acidity that allow to limit the coking rate.<sup>219</sup> The catalytic performance of SAPO-34 is improved if the surfaces of the crystals are doped with silica by heating with polydimethylsiloxane or an alkyl silicate.<sup>220</sup> Typical compositions for MTO catalyst is Al:P:Si 1:1:0.3–0.1. To reduce coking, low-silica AlPO-34 may be used: the very few Brønsted acid sites on a low-silica AlPO-34 with Al:P:Si 1:1:0.005 produce a much lower total coke content compared with SAPO-34, leading to an extended catalyst lifetime of the former material.<sup>221</sup>

SAPO-18 has a structure and a pore system similar but crystallographically distinct from those of SAPO-34. It displays good activity and selectivity too in the MTO reaction and is reported to have superior lifetime to SAPO-34. It is also known to exist as an intergrowth with SAPO-34.<sup>222</sup>

SAPO-11 catalyst has been developed nearly at the industrial level in particular for the skeletal isomerization of light olefins,<sup>223</sup> constituting apparently the industrial catalyst of the UOP Butesom and Pentosom olefin skeletal isomerization processes,<sup>2,20</sup> and for (hydro)isomerization of *n*-paraffins such as for upgrading of Fischer–Tropsch waxes.<sup>108</sup> This material, characterized by the AEL topology, has channels consisting of elliptical, nonintersecting 10-membered rings with a pore opening of  $3.9 \times 6.3$  Å. Samples with composition  $\text{Al}_2\text{O}_3: y\text{P}_2\text{O}_5: z\text{SiO}_2$ , in which *y* has a value of 0.60–1.20, and *z* has a value of 0.05–1.3, containing also 0.05–1.5% by weight of Pd or Pt and some alumina, have been patented for paraffin hydroisomerization.<sup>224</sup> SAPO-31 (ATO) and SAPO-41 (AFO), also with one-dimensional channels, 12-MR  $5.4 \times 5.4$  Å and 10-MR  $5.7 \times 4.3$  Å, respectively, show even better performance than SAPO-11 in hydroisomerization of lighter *n*-paraffins,<sup>225</sup> with the preferential formation of monobranched isomers.

Also larger pore SAPOs find interesting catalytic activities. As for example, SAPO-5 (AFI), with 12-MR monodimensional channels ( $7.3 \times 7.3$  Å) is reported to be active in several aromatic transformations such as cumene synthesis, xylene isomerization, toluene alkylation by methanol, isopropylation of benzene, transalkylation of toluene with trimethylbenzenes, etc.<sup>226</sup>

---

## 7.4 Metal heteroatom containing aluminophosphates (MAPOs)

A large number of molecular sieve structures constituted by aluminum phosphate-containing metal cations have been developed. The substitution of divalent metal ions such as  $\text{Mg}^{2+}$ ,  $\text{Mn}^{2+}$ ,  $\text{Zn}^{2+}$  and  $\text{Co}^{2+}$ , etc. for  $\text{Al}^{3+}$  in the framework produces Brønsted or Lewis acid sites. On the other hand, the presence of trivalent metal ions, i.e.  $\text{Co}^{3+}$  or  $\text{Mn}^{3+}$ , produces redox sites. Thus the catalytic chemistry of these materials is actually varied. These materials are typically synthesized from an AIPO-based gel medium in the presence of metal heteroatoms and templating agents, like organic amines under hydrothermal, solvothermal or ionothermal conditions.<sup>227</sup> Most MAPOs have substitutionally modified AIPO structures, others are unique zeolotypes.

---

## 7.5 Very large-pore zeolitic inorganic materials

A number of very large pore materials similar to zeolites, with pores larger than 12-MR, i.e. constructed of more than 12 T atoms have been synthesized recently. Some of them are phosphates, such as the aluminophosphate denoted as VPI-5 (VFI framework type) that contains 18-MR 1D channels, with  $12.7 \times 12.7$  Å width, and cloverite, which is a fluorinated gallium phosphate molecular sieve with a complex framework consisting of an 8-MR channel system and a 20-MR channel system, nonintercepting. The 20-membered ring channel has a very large pore opening of about 13.2 Å. At the intersection of the 20-membered ring channels is the center of a very large cavity with a body diagonal of about 30 Å. Recently, the Al analog of cloverite has been prepared and characterized.<sup>228,229</sup>

ECR-34 (ETR framework type) is a galloaluminosilicate, with 18-MR channels  $10.1 \times 10.1$  Å wide. In recent years, a number of very large pore germanosilicates have been prepared denoted as IM-12 and ITQ-15 (both having the UTL type framework with 14-MR,  $9.5 \times 7.1$  Å, and 12-MR,  $8.5 \times 5.5$  Å, intersecting channels), ITQ-33 (with  $18 \times 10 \times 10$  ring windows), ITQ-40 (which can be described as an interrupted, extra-large pore, three-dimensional zeolite framework with intersecting channels of  $16 \times 16 \times 15$ -ring pores) and ITQ-37, which has a three-dimensional 30-ring pore system and is the first chiral zeolite with one single gyroidal channel.<sup>230</sup> Studies on the potential applications of these materials have been undertaken.

---

## 7.6 Zeolite-like titanasilicates

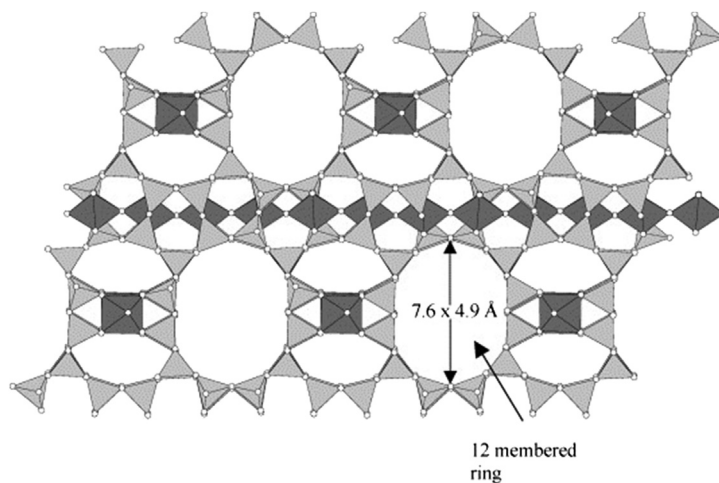
The synthesis of titanium-containing molecular sieves<sup>231</sup> started with the synthesis of Ti-silicalite-1 (TS-1), i.e., Ti-substituted fully siliceous MFI (or ZSM-5) zeolite, prepared by Taramasso and coworkers in the ENI laboratories near Milan (Italy). Shortly after other Ti-substituted siliceous zeolites such as TS-2 (Ti-ZSM-11 or Ti-MEL),

and Ti-BEA were prepared. These materials are very interesting for oxidation catalysis, and will be described later on. They contain very small amounts of tetrahedrally coordinated  $\text{Ti}^{4+}$  substituting for silicon in a tetrahedral silica zeolitic network.

More recently, a number of titanosilicate materials have been prepared with a different coordination for  $\text{Ti}^{4+}$ . The ETS family, produced by Engelhard (ETS = Engelhard Titano-Silicates) consists of several materials among which the most relevant ones are ETS-4 and ETS-10, prepared by Kuznicki in 1989. ETS-4 titanosilicate, whose stoichiometry is  $\text{Na}_9\text{Si}_{12}\text{Ti}_5\text{O}_{38}(\text{OH}) \cdot 12\text{H}_2\text{O}$ , is a small-pore material (pore diameter of 3.7 Å) with an intergrowth structure in two dimensions, whose details are still somehow under debate (probably an intergrowth of zorite and nenadkevichite). ETS-4 has the interesting property of a possible tuning of the pore sizes.<sup>232</sup> ETS-10 (Figure 7.18<sup>233</sup>) whose chemical composition is  $\text{Na}_{1.5}\text{K}_{0.5}\text{TiSi}_5\text{O}_{13} \cdot n\text{H}_2\text{O}$  has a pore system consisting of a three-dimensional network of interconnecting channels defined by rings formed by 12 Si atoms (12-MR) the pore size being about 8 Å. The structure can be described as an intergrowth of two ordered polymorphs (a tetragonal and monoclinic one) with tetravalent Ti atoms in an octahedral coordination.

AM-n series titanosilicates is a family of titanosilicates prepared by researchers from the universities of Aveiro and Manchester. AM-2 ( $\text{K}_2\text{TiSi}_3\text{O}_9 \cdot \text{H}_2\text{O}$ ) has a structure related to the mineral umbite, while AM-3 ( $\text{Na}_2\text{TiSi}_4\text{O}_{11} \cdot 2\text{H}_2\text{O}$ ) is the synthetic analog of the mineral penkvilksite. AM-1 ( $\text{Na}_4\text{Ti}_2\text{Si}_8\text{O}_{22} \cdot 4\text{H}_2\text{O}$ ) and AM-4 ( $\text{Na}_3(\text{Na},\text{H})\text{Ti}_2\text{O}_2[\text{Si}_2\text{O}_6]_2 \cdot 2\text{H}_2\text{O}$ ) are new structures.

Another family are crystalline silicotitanate (CST) produced by researchers at Sandia National Laboratory and Texas A&M University. The best-known component



**FIGURE 7.18**

Crystal structure of ETS-10 molecular sieve.

*Reprinted with permission from Ref. 233.*

is denoted as TAM-5 with formula  $\text{Na}_2(\text{H}_2\text{O})_2\text{Ti}_4\text{O}_5(\text{OH})(\text{SiO}_4)_2\text{Na}(\text{H}_2\text{O})_{1.7}$ , similar to the mineral Sitinakite, which has the pharmacosiderite structure. TAM-5 is characterized by straight uniform channels, 3.5 Å in diameter, which is very close to that of the Cs ion; thus, the ion exchange with Cs is almost irreversible.

In all these cases, alkali cations are exchangeable. Thus, these materials are used as cation exchangers and for the extraction of heavy metals from water.<sup>234</sup> ETS-10 finds also potentiality for separation in the gas phase (ethane/ethylene on Na-ETS-10, Ar/O<sub>2</sub> in Ag/ETS-10).

The applications of these materials in catalysis seem to be still limited. However, according to their composition, they may be of interest for their basicity, such as in the case of ETS-10,<sup>235</sup> which is active, e.g. as a basic catalyst for transesterification of vegetable oils.<sup>236</sup>

---

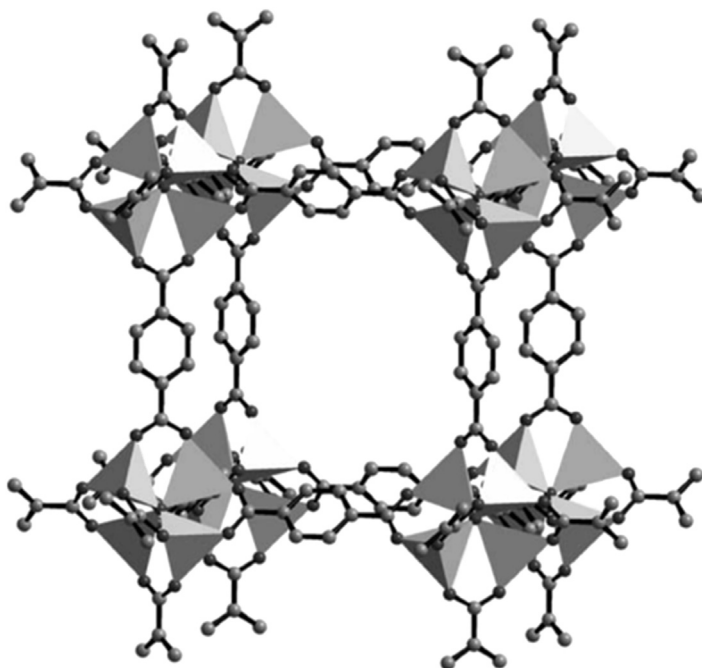
## 7.7 Metal Organic Frameworks (MOFs) and similar materials

Metal Organic Frameworks, developed starting from the nineties, are crystalline network “coordination polymers” constituted by salts or complexes of metal cations with multi-functional organic linkers such as di- or polycarboxylate anions, di- or polysulfonate anions, di- or polyamines. These organic linkers are quite rigid aromatic molecules that act as spacers producing channels and cavities. As a result, molecular size micropores are formed. The linkers may be also variously functionalized providing a wide range of chemical properties. The materials have exceptionally high pore volumes (up to 5 cm<sup>3</sup>/g) and internal surface areas (up to 5000 m<sup>2</sup>/g) resulting in high adsorption capacities, possibly cation exchange properties and catalytic activity.

In [Figure 7.19](#), the structure of one of the most studied materials, denoted as MOF-5, an oxy-terephthalate of zinc of composition  $\text{Zn}_4\text{O}(\text{1,4-benzenedicarboxylate})_3$ , where each carboxylate group bridges two  $\text{Zn}^{2+}$  ions, in such a way that the terephthalate units bridge four  $\text{Zn}^{2+}$  ions.  $\text{Zn}_4\text{O}_{13}$  clusters exist at the corners of cubic units, with an oxygen in the middle, coordinated tetrahedrally to four Zn ions. Zn ions are tetrahedrally coordinated, with three different terephthalate oxygens and the single oxygen.

Zeolitic imidazole frameworks (ZIFs) where imidazolate anions form bridges between, typically,  $\text{Zn}^{2+}$  ions, forming many different microporous structure including several structural analogues of zeolites,<sup>237</sup> belong also to this family.

These relatively new materials have been the object of much interest in particular for their possible use as selective adsorbents to remove CO<sub>2</sub> from gases<sup>33,238,239</sup> as well as to purify hydrogen<sup>240</sup> or natural gas.<sup>7</sup> In contrast with the permanent porosity typical of classical “rigid” adsorbents (carbons, zeolites), according to framework flexibility upon adsorption–desorption cycles, adsorption on MOF may evolve dynamically depending on the nature and quantity of host molecules. In [Figure 7.20](#), the pore size of different MOF’s is compared with that of other microporous

**FIGURE 7.19**

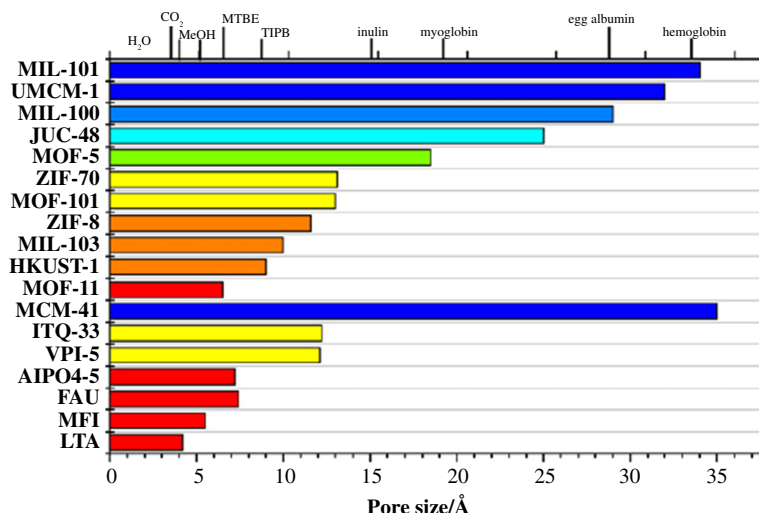
A cubic cage within the MOF-5 structure, bounded by inorganic  $Zn_4O_{13}$  clusters and terephthalate groups.  $ZnO_4$  groups are represented by solid tetrahedra. H atoms omitted for clarity.

*Reprinted with permission from Gonzalez J, Nandini Devi D, Tunstall P, Cox A, Wright A. Microporous and Mesoporous Materials 2005; 84, 97–104.*

materials and zeolites as well as with the critical size of selected molecules. MOF's cover a range of larger sizes, which is unavailable to zeolites and similar molecular sieves.

These materials, and the products of their chemical modification, certainly find enormous interest in the catalysis field.<sup>241</sup> Catalytic activity may be related to the role of the framework cationic center itself, or of the functionalities of the organic linker, or even of other species deposited with various procedures in the cavities, such as e.g. metal clusters or metal oxide particles. Apparently, the only real limit is on thermal stability, thus being interested only for relatively low temperature reactions. A number of interesting investigations are now starting, and we are now only at the beginning of this work. They are also of extremely high interest for asymmetric catalysis.<sup>242,243</sup>

A similar new field involves other structural mesoporous materials, which act as Covalent Organic Frameworks (COFs),<sup>244</sup> where similar structures are built using non-metallic elements, and Porous Organic Polymers (POPs).<sup>245</sup>



**FIGURE 7.20**

Cavity size of porous MOFs as above compared with standard aluminosilicates and aluminophosphates. Porous materials are selected arbitrarily; pore sizes are approximate due to the variety of pore shapes involved.

*Reprinted with permission from Ref. 7.*

## References

1. Breck DW. *Zeolite molecular sieves: structure, chemistry and use*. New York, NY: Wiley; 1974.
2. Sherman JD. *Proc Natl Acad Sci USA* 1999;**96**:3471.
3. Chen NY, Garwood WE, Dwyer FG. *Shape selective catalysis in industrial applications*. 2nd ed. New York: Dekker; 1996.
4. Guisnet M, Gilson JP, editors. *Zeolites for cleaner technologies*. Imperial College Press; 2002.
5. Lobo R. *Handbook of zeolite science and technology*, [chapter 3].
6. Baerlocher Ch, McCusker LB, Olson DH. *Atlas of zeolite framework types*. 6th revised ed. 2007.
7. Tagliabue M, Farrusseng D, Valencia S, Aguado S, Ravon U, Rizzo C, et al. *Chem Eng J* 2009;**155**:553–66.
8. Barrer RM, Denny DI. *J Chem Soc* 1961:971.
9. Martinez C, Corma A. *Coord Chem Rev* 2011;**255**:1558–80.
10. Huo Q. In: *Modern inorganic synthetic chemistry*. Elsevier; 2011. p. 339–73.
11. Koyama K, Takeushi Y. *Zeit Kryst* 1977;**145**:216.
12. Concepcion-Rosabal B, Rodríguez-Fuentes G, Bogdanchikova N, Bosch P, Avalos M, Lara VH. *Microporous Mesoporous Mater* 2005;**86**:249–55.
13. Perego C, Bagatin R, Tagliabue M, Vignola R. *Microporous Mesoporous Mater* January 15, 2013;**166**:37–49.

14. Wang S, Peng Y. *Chem Eng J* 2010;**156**:11–24.
15. Ackley MW, Rege SU, Saxena H. *Microporous Mesoporous Mater* 2003;**61**:25–42.
16. Salla I, Montanari T, Salagre P, Cesteros Y, Busca G. *Phys Chem Chem Phys* 2005;**7**: 2526–33.
17. Nachtigall P, Rodríguez Delgado M, Frolich K, Bulánek R, Turnes Palomino G, López Bauc C, et al. *Microporous Mesoporous Mater* 2007;**106**:162–73.
18. Nachtigall P, Rodríguez Delgado M, Nachtigalloova D, Otero Areán C. *Phys Chem Chem Phys* 2012;**14**:1552–69.
19. Nachtigall P, Rodríguez Delgado M, Frolich K, Bulánek R, Turnes Palomino G, López Bauçà C, et al. *Microporous Mesoporous Mater* November 1, 2007;**106**(1–3):162–73.
20. Vermeiren W, Gilson JP. *Top Catal* 2009;**52**:1131–61.
21. Zukal A, Arean CO, Delgado MR, Nachtigall P, Pulido A, Mayerová J, et al. *Microporous Mesoporous Mater* 2011;**146**:97–105.
22. Montanari T, Busca G. *Vib Spectrosc* January 16, 2008;**46**(1):45–51.
23. Montanari T, Salla I, Busca G. *Microporous Mesoporous Mater* 2008;**109**:216.
24. Li J, Tai J, Davis RJ. *Catal Today* 2006;**116**:226.
25. Sircar S, Myers AL. In: *Handbook of zeolite science and technology*. New York: Dekker; 2003.
26. Lalik E, Mirek R, Rakoczy J, Groszek A. *Catal Today* 2006;**114**:242.
27. Simo M, \*Sivashanmugam S, Brown CJ, Hlavacek V. *Ind Eng Chem Res* 2009;**48**: 9247–60.
28. [http://www.catalysts.pro/downloads/public/pdfs/Adsorbents/82012BF-9394\\_US\\_BASF\\_3A\\_Datasheet.pdf](http://www.catalysts.pro/downloads/public/pdfs/Adsorbents/82012BF-9394_US_BASF_3A_Datasheet.pdf), 21.12.12.
29. [http://www.catalysts.pro/downloads/public/pdfs/Adsorbents/82012BF-9393\\_US\\_BASF\\_4A\\_Datasheet.pdf](http://www.catalysts.pro/downloads/public/pdfs/Adsorbents/82012BF-9393_US_BASF_4A_Datasheet.pdf), 21.12.12.
30. Bozzano A. In: Meyers RA, editor. *Linear alkylbenzene (Lab) manufacture handbook of petroleum refinery processes*. Mc Graw Hill; 2006. p. 1–58.
31. Granato MA, Vlugt TJH, Rodrigues AE. *Ind Eng Chem Res* 2007;**46**:321–8.
32. <http://www.zeolites.eu/downloads/Zeolites.pdf>, 21.12.12.
33. Bae Y-S, Snurr Angew RQ. *Chem Int Ed* 2011;**50**:11586–96.
34. Mulloth LM, Field M, Finn JE. *Carbon dioxide adsorption on a 5A zeolite designed for CO<sub>2</sub> removal in spacecraft cabins* [http://ntrs.nasa.gov/archive/nasa/casi.ntrs.nasa.gov/19980237902\\_1998415422.pdf](http://ntrs.nasa.gov/archive/nasa/casi.ntrs.nasa.gov/19980237902_1998415422.pdf), 21.12.12.
35. Mendes AMM, Costa CAV, Rodrigues AE. *Sep Purif Technol* 2001;**24**:173–80.
36. Beauvais C, Guerrault X, Coudert F-X, Boutin A, Fuchs AH. *J Phys Chem B* 2004;**108**: 399–404.
37. Kozyra P, Salla I, Montanari T, Datka J, Salagre P, Busca G. *Catal Today* 2006;**114**: 188–96.
38. [http://www.catalysts.pro/downloads/public/pdfs/Adsorbents/82012BF-9391\\_US\\_BASF\\_13X\\_Datasheet.pdf](http://www.catalysts.pro/downloads/public/pdfs/Adsorbents/82012BF-9391_US_BASF_13X_Datasheet.pdf), 21.12.12.
39. Ding Yate, Riffat SB. *Int J Low-Carbon Technol* 2012;**0**:1–11.
40. Hedin N, Andersson L, Bergstrom L, Yan J. *Appl Energy* 2013;**104**:n418–433.
41. Montanari T, Finocchio E, Salvatore E, Garuti G, Giordano A, Pistarino C, et al. *Energy* 2011;**36**:314–9.
42. Busca G, Montanari T, Bevilacqua M, Finocchio E. *Colloids Surf A: Physicochem Eng Asp* 2008;**320**:205–12.
43. Finnouche F, Boucheffa Y, Boumaza R, Labeled A, Magnoux P. *Ind Eng Chem Res* 2004; **43**:6708–13.



44. Methivier A. In: Guisnet M, Gilson JP, editors. *Zeolites for cleaner technologies*. Imperial College Press; 2002. pp. 209–21.
45. Commissaris S-E. In: Meyers RA, editor. *Handbook of petrochemicals production processes*. Mc Graw Hill; 2005. p. 513.23–30.
46. Russell BP, Patel KM. *Use of calcium exchanged x-type zeolite for improvement of refinery off-gas pressure swing adsorption, patent Application 20110126709 to UOP LLC*, Read more: <http://www.faqs.org/patents/app/20110126709#b#ixzz2Fhw9Z3x0>.
47. Castle WF. *Int J Refrig* 2002;**25**:158–72.
48. Chai SW, Kothare MV, Sircar S. *Ind Eng Chem Res* 2011;**50**(14):8703–10.
49. <http://www.uop.com/wp-content/uploads/2011/12/UOP-Mercury-Removal-for-Natural-Gas-Production-brochure.pdf>, 21.12.12.
50. <http://www.uop.com/wp-content/uploads/2011/02/UOP-Mercury-Removal-From-Natural-Gas-and-Liquid-Streams-Tech-Paper.pdf>, 21.12.12.
51. Dong J, Xu Z, \*Kuznicki SM. *Environ Sci Technol* 2009;**43**:3266–71.
52. Lin CCH, Dambrowitz KA, Kuznicki SM. *Can J Chem Eng* 2012;**90**:207–16.
53. Cejka J, Centi G, Perez Pariente J, Roth WJ. *Catal Today* 2012;**179**:2–15.
54. Li J, Tai J, Davis RJ. *Catal Today* 2006;**116**:226–33.
55. Serra JM, Corma A, Farrusseng D, Baumes L, Mirodatos C, Flego C, et al. *Catal Today* 2003;**81**:425–36.
56. Perego C, Bosetti A. *Microporous Mesoporous Mater* 2011;**144**:28–39.
57. Danuthai T, Sooknoi T, Jongpatiwut S, Rirksomboon T, Osuwan S, Resasco DE. *Appl Catal A: Gen* December 15, 2011;**409**–410:74–81.
58. Kumar N, Leino E, Mäki-Arvela P, Aho A, Källdström M, Tuominen M, et al. *Microporous Mesoporous Mater* 2012;**152**:71–7.
59. Selva M, Fabris M, Perosa A. *Green Chem* 2011;**13**(4):863–72.
60. Tomita M, Masui Y, Onaka M. *J Phys Chem Lett* 2010;**1**(3):652–6.
61. Imachi S, Onaka M. *Chem Lett* 2005;**34**(5):708–9.
62. De Vos DE, Jacobs PA. *Microporous Mesoporous Mater* 2005;**82**:293–304.
63. Fukunaga T, Katsuno H. *Catal Surv Asia* 2010;**14**:96–102.
64. Ohgushi T, Matsuo T, Satoh H, Matsumoto T. *Microporous Mesoporous Mater* 2009;**117**:472–7.
65. Xing Y, Khare GP, Suib SL. *Appl Catal A Gen* 2011;**399**:179–83.
66. Antos GJ, Moser MD, Lapinski MP. Catalytic naphtha reforming. In: Antos GJ, Aitani AM, editors. *Revised and expanded*. 2nd ed. New York: Dekker; 2004. p. 335–52.
67. Lapinski M, Baird L, James R. UOP platforming process. In: Meyers RA, editor. *Handbook of petroleum refining processes*. 3rd ed. Mc Graw Hill; 2006. p. 4.3–31.
68. Jiang Y, Huang J, Dai W, Hunger M. *Solid State Nucl Magn Reson* May–June 2011;**39**(3–4):116–41.
69. Eichler U, Brändle M, Sauer J. *J Phys Chem B* 1997;**101**:10035.
70. Schroder KP, Sauer J, Leslie M, Catlow CRA, Thomas JM. *Chem Phys Lett* 1992;**188**:320.
71. Simperler A, Bell RG, Anderson MW. *J Phys Chem B* 2004;**108**:7142.
72. Kazansky VB, Seryk AI, Semmer-Herledan V, Fraissard J. *Phys Chem Chem Phys* 2003;**5**:966.
73. Sillar K, Burk P. *Chem Phys Lett* 2004;**393**:285–9.
74. Bevilacqua M, Montanari T, Finocchio E, Busca G. *Catal Today* 2006;**116**:132.
75. Sastre G, Katada N, Niwa M. *J Phys Chem C* 2010;**114**:15424–31.
76. Xu B, Sievers C, Hong SB, Prins R, van Bokhoven JA. *J Catal* 2006;**244**:163.

77. Gounder R, Iglesia E. *Angew Chem Int Ed* 2010;**49**:808–11.
78. Gounder R, Jones AJ, Carr RT, Iglesia E. *J Catal* 2012;**286**:214–23.
79. Simonetti DA, Carr RT, Iglesia E. *J Catal* 2012;**285**(1):19–30.
80. Armaroli T, Simon LJ, Digne M, Montanari T, Bevilacqua M, Valtchev V, Patarin J, Busca G. *Appl Catal A Gen* 2006;**306**:78.
81. Kim J-H, Kunieda T, Niwa M. *J Catal* 1998;**173**:433.
82. Kunieda T, Kim J-H, Niwa M. *J Catal* 1999;**188**:431.
83. Trombetta M, Busca G, Lenarda M, Storaro L, Pavan M. *Appl Catal A Gen* 1999;**182**: 225–35.
84. Trombetta M, Busca G. *J Catal* 1999;**187**:521–3.
85. Gabrienko AA, Danilova IG, Arzumanov SS, Toktarev AV, Freude D, Stepanov AG. *Microporous Mesoporous Mater* 2010;**131**:210–6.
86. Ou, JDY, Hong Z, Tan S, Mcminn, TE. US Patent 7902414 B2 (2011) [to Exxonmobil].
87. Verboekend D, Pérez-Ramírez J. *Catal Sci Technol* 2011;**1**:879–90.
88. Na K, Choi M, Ryoo R. *Microporous Mesoporous Mater* 2013;**166**:3–19.
89. Shannon RD, Staley RH, Vega AJ, Fischer RX, Baur WH, Auroux A. *J Phys Chem* 1989;**93**(5):2019–27.
90. Domokos L, Lefferts L, Seshan K, Lercher JA. *J Mol Catal A Chem* 2000;**162**: 147–57.
91. Bhan A, Allian AD, Sunley GJ, Law DJ, Iglesia E. *J Am Chem Soc* 2007;**129**:4919–24.
92. Montanari T, Bevilacqua M, Busca G. *Appl Catal A Gen* 2006;**307**:21–9.
93. Martucci A, Alberti A, Cruciani G, Radaelli P, Ciambelli P, Rapacciuolo M. *Microporous Mesoporous Mater* 1999;**30**:95.
94. Rachwalik R, Hunger M, Sulikowski B. *Appl Catal A Gen* 2012;**427–428**:98–105.
95. <http://www.cdtech.com/techProfilesPDF/ISOMPLUS%20C4%20Sht%20R-2.pdf>, 26.12.12.
96. [http://www.cbi.com/images/uploads/technical\\_articles/CDTechpdf.pdf](http://www.cbi.com/images/uploads/technical_articles/CDTechpdf.pdf), 26.12.12.
97. T. Zak, A. Behkish, W. Shum, S. Wang, L. Candela, and J. Ruszkay, Isomerization of butenes: LyondellBasell's isomplus, technology developments production and use of light olefins DGMK Conference September 28–30, 2009, [Dresden, Germany]
98. de Ménorval B, Ayrault P, Gnep NS, Guisnet M. *Appl Catal A Gen* 2006;**304**:1.
99. Millini R, Rossini S. In: Chon H, Ihm SK, Uh YS, editors. *Progress in zeolite and microporous materials*. Amsterdam: Elsevier; 1997. p. 1389.
100. Gleeso D. *J Phys Chem A* 2011;**115**(51):14629–36.
101. Wattanakit C, Nokbin S, Boekfa B, Pantu P, Limtrakul J. *J Phys Chem C* 2012;**116**: 5654–63.
102. Seo G. *Catal Surv Asia* 2005;**9**:139–46.
103. Kangas M, Kumar N, Harlin E, Salmi T, Murzin D Yu. *Ind Eng Chem Res* 2008;**47**: 5402–12.
104. Márquez-Alvarez C, Pinar AB, García R, Grande-Casas M, Pérez-Pariente J. *Top Catal* 2009;**52**(9):1281–91.
105. Román-Leshkov Y, Moliner M, Davis ME. *J Phys Chem C* 2011;**115**:1096–102.
106. Khitev YP, Ivanova II, Kolyagin YG, Ponomareva OA. *Appl Catal A Gen* 2012; **441–442**:124–35.
107. Smolikov MD, Goryanskaya NI, Zatolokina EV, Kiryanov DI, Bikmetova LI, Doronin VP, et al. *Catal Industry* 2012;**4**(3):162–7.
108. Bouchy C, Hastoy G, Guillon E, Martens JA. *Oil Gas Sci Technol Rev IFP* 2009;**64**: 91–112.

109. Armaroli T, Trombetta M, Gutiérrez Alejandro A, Ramirez Solis J, Busca G. *Phys Chem Chem Phys* 2000;**2**:3341–8.
110. Baba T, Komatsu N, Ono Y. *J Phys Chem B* 1998;**102**:804.
111. Böhlmann W, Michel D. *Top Catal* 2001;**202**:421.
112. Ramos Pinto R, Borges P, Lemos MANDA, Lemos F, Védrine J, Derouane EG, et al. *Appl Catal A Gen* 2005;**284**:39.
113. Jobic H, Tuel A, Krossner M, Sauer JJ. *Phys Chem* 1996;**100**:19545.
114. Alario F, Guisnet M. In: Guisnet M, Gilson JP, editors. *Zeolites for cleaner technologies*. Imperial College Press; 2002. p. 189.
115. Bradley TW. In: Meyers RA, editor. *Handbook of petrochemicals production processes*. Mc Graw Hill; 2005. p. 13.3–13.14.
116. Bradley TW. In: Meyers RA, editor. *Handbook of petrochemicals production processes*. Mc Graw Hill; 2005. p. 13.15–22.
117. Degnan Jr TF, Morris Smith C, Venkat Chaya R. *Appl Catal A Gen* 2001;**221**:283.
118. Beck JS, Dandekar AB, Degnan TF. In: Guisnet M, Gilson JP, editors. *Zeolites for cleaner technologies*. Imperial College Press; 2002. p. 223–37.
119. Perego C, Ingallina P. *Green Chem* 2004;**6**:274.
120. Tsai T-C, Wang I, Huang C-K, Liu S-D. *Appl Catal A Gen* 2007;**321**:125–34.
121. Pop G. In: Anthos GI, Aitani AM, editors. *Catalytic naphtha refovrming*. 2nd ed. Dekker; 2004. p. 353–89.
122. Zhou L. In: Meyers RA, editor. *Handbook of petroleum refinery processes*. Mc Graw Hill; 2006. p. 2.29–37.
123. Pidko EA, Kazansky VB, Hensen EJM, van Santen RA. *J Catal* 2006;**240**:73.
124. Faro Jr AC, Rodrigues V de O, Eon J-G. *J Phys Chem C* 2011;**115**:4749–56.
125. Liebner W, Wagner M. *Tagungsbericht* 2004;**1**:281–8.
126. de Klerk A. *Energy Fuels* 2006;**20**(5):1799–805.
127. Bellussi Giuseppe, Mizia Franco, Calemma Vincenzo, Pollesel Paolo, Millini Roberto. *Microporous Mesoporous Mater* 2012;**164**:127–34.
128. Flego C, Marchionna M, Perego C. *Stud Surf Sci Catal* 2005;**158 B**:1271–8.
129. Patent application: 20110147263 Process and system to convert olefins to diesel and other distillates, inventors: B. S. Umansky, M. C. Clark, C.N. Lopez, K.L. Weiger, Assignees: Exxonmobil Research and Engineering Company. Read more: <http://www.faqs.org/patents/app/20110147263#b#ixzz2GO4EHJc9>.
130. Keil FJ. *Microporous Mesoporous Mater* 1999;**29**:49.
131. Lønstad Blekena F, Chavana S, Olsbye U, Boltz M, Ocampob F, Louis B. *Appl Catal A Gen* 2012;**447–448**:178–85.
132. Liebner W. In: Meyers RA, editor. *Handbook of petrochemicals production processes*. Mc Graw Hill; 2005. p. 10.3–14.
133. Daage M. In: Guisnet M, Gilson JP, editors. *Zeolites for cleaner technologies*. Imperial College Press; 2002. p. 167–88.
134. Wallenstein D, Harding RH. *Appl Catal A Gen* 2001;**214**:11.
135. Rahimi N, Karimzadeh R. *Appl Catal A Gen* 2011;**398**(1–2):1–17.
136. Kdepi VVKM, Narender N. *Catal Sci Technol* 2012;**2**:471–87.
137. Tsuneki H. *Catal Surv Asia* 2010;**14**:116–23.
138. Okuhara T. *Chem Rev* 2002;**102**:3641.
139. Ishida H. *Catal Surv Jpn* 1997;**1**:241.
140. Wu W, Wu W, Kikhtyanin OV, Li L, Toktarev AV, Ayupov AB, et al. *Appl Catal A Gen* 2010;**375**(2):279–88.

141. Dimitrov L, Mihaylov M, Hadjiivanov K, Mavrodinova V. *Microporous Mesoporous Mater* 2011;**143**:291–301.
142. Girotti G, Terzoni G, Cappellazzo O, Bignazzi R, Pazzuconi G. US Patent 7718836 B2, 2010, to ENI.
143. Mintova S, Valtchev V, Onfroy T, Marichal C, Knözinger H, Bein T. *Microporous Mesoporous Mater* 2006;**90**:237.
144. Merlino S, Zanardi S. *Atti Soc Tosc Sci Nat Mem Ser A* 2006;**111**:31–44.
145. Bushuev YG, Sastre G, Vicente de Julián-Ortiz J. *J Phys Chem C* 2010;**114**:345–56.
146. Marques JP, Gener I, Ayrault P, Bordado JC, Lopes JM, Ramoa Ribeiro F, Guisnet M. *Microporous Mesoporous Mater* 2003;**60**:251.
147. Maier SM, Jentis A, Lercher JA. *J Phys Chem C* 2011;**115**(16):8005–13.
148. Trombetta M, Busca G, Storaro L, Lenarda M, Casagrande M, Zambon A. *Phys Chem Chem Phys* 2000;**2**:3529–37.
149. [www.polimerieuropa.it](http://www.polimerieuropa.it).
150. Schmidt RJ. *Appl Catal A Gen* 2005;**280**:89.
151. Peterson GA, Schmidt RJ. In: Meyers RA, editor. *Handbook of petrochemicals production processes*. Mc Graw Hill; 2005. p. 4.2–19.
152. [http://www.eni.com/en\\_IT/attachments/azienda/attivita-strategie/petrochimica/licensing/PBE-1-flyer-lug09.pdf](http://www.eni.com/en_IT/attachments/azienda/attivita-strategie/petrochimica/licensing/PBE-1-flyer-lug09.pdf), 15.1.13.
153. Perego C, Ingallina P. *Catal Today* 2002;**73**:3.
154. Assandri F, Bencini E. In: Meyers RA, editor. *Handbook of petrochemicals production processes*. Mc Graw Hill; 2005. p. 5.13–21.
155. Jasra V. *Bull Catal Soc India* 2003;**2**:157–83.
156. Guidotti M, Coustard J-M, Magnoux P, Guisnet M. *Pure Appl Chem* 2007;**79**(11):1833–8.
157. Lawton SL, Leonowicz ME, Partridge RD, Chu P, Rubin MK. *Microporous Mesoporous Mater* 1998;**23**:109–17.
158. Ayrault P, Datka J, Laforge S, Martin D, Guisnet M. *J Phys Chem B* 2004;**108**:13755–63.
159. Bevilacqua M, Meloni D, Sini F, Monaci R, Montanari T, Busca G. *J Phys Chem C* 2008;**112**:9023–33.
160. Li Y, Guo W, Fan W, Yuan S, Li J, Wang J, et al. *J Mol Catal A Chem* 2011;**338**:24–32.
161. Maerz B, Smith CM. In: Meyers RA, editor. *Handbook of petrochemicals production processes*. Mc Graw Hill; 2005. p. 5.23–38.
162. Dandekar, Hrynyszak N, Stern DL. US patent 7868215 B2, to Exxonmobil, 2011.
163. Bevilacqua M, Gutiérrez Alejandro A, Resini C, Casagrande M, Ramirez J, Busca G. *Phys Chem Chem Phys* 2002;**4**:4575–83.
164. Bevilacqua M, Busca G. *Catal Commun* 2002;**3**:497–502.
165. Montanari T, Bevilacqua M, Resini C, Busca G. *J Phys Chem B* 2004;**108**:2120–7.
166. Marie O, Massiani P, Thibault-Starzyk F. *J Phys Chem B* 2004;**108**:5073–81.
167. Nesterenko NS, Thibault-Starzyk F, Montouillout V, Yuschenko VV, Fernandez C, Gilson J-P, et al. *Microporous Mesoporous Mater* 2004;**71**:157–66.
168. Huo H, Peng L, Gan Z, Grey CP. *J Am Chem Soc* 2012;**134**:9708–20.
169. van Bokhoven JA, Tromp M, Koningsberger DC, Miller JT, Pieterse JAZ, Lercher JA, et al. *J Catal* 2001;**202**:129.
170. Schmidt F, Köhler E. In: Guisnet M, Gilson JP, editors. *Zeolites for cleaner technologies*. Imperial College Press; 2002. p. 153–66.
171. Weyda H, Köhler E. *Catal Today* 2003;**81**:51.

172. De Klerk A, Furimsk E. *Catalysis in the refinement of Fischer Tropsch syncrude*. London: RSC; 2010. p. 86.
173. Corma A, Martinez A. In: Guisnet M, Gilson JP, editors. *Zeolites for cleaner technologies*. Imperial College Press; 2002. p. 29–56.
174. Decroocq D. *Rev l'Institut Français Pétrole* 1997;**52**:469.
175. Tsai T-C. *Appl Catal A Gen* 2006;**301**:292–8.
176. Butler JR, Hall R, Xiao X. US Patent application number: 20120071317, to Fina, 2012.
177. Martucci A, Alberti A, Guzman-Castillo ML, Di Renzo F, Fajula F. *Microporous Mesoporous Mater* 2003;**63**:33.
178. Chen J, Chen T, Guan N, Wang J. *Catal Today* 2004;**93–95**:627.
179. McQueen D, Chiche BH, Fajula F, Auroux A, Guimon C, Fitoussi F, et al. *J Catal* 1996;**161**:587.
180. Guisnet M, Ayrault P, Datka J. *Microporous Mesoporous Mater* 1998;**20**:283.
181. Shigeishi RA, Chiche BH, Fajula F. *Microporous Mesoporous Mater* 2001;**43**:211.
182. Guillon E, Lacombe S, Sozinho T, Magnoux P, Gnep S, Moreau P, et al. *Oil Gas Sci Technol* 2009;**64**(6):731–44.
183. Guillon E, Sanchez E. US Patent 7838456, 2010, to IFP.
184. Hu S, Gong Y, Xu Q, Liu X, Zhang Q, Zhang L, et al. *Catal Commun* 2012;**28**:95–9.
185. Mihindou-Koumba PC, Comparot J-D, Laforge S, Magnoux P. *J Catal* 2008;**255**:324–34.
186. Arnold A, Hunger M, Weitkamp J. *Microporous Mesoporous Mater* 2004;**67**:205–13.
187. Baillie C, Schiller RK. *Refin Oper* 2, (6); 1–4.
188. Hu R, Zhao X, Wormsbecher RF, Ziebart MS. Gasoline sulphur reduction catalyst for FCC process, US Patent 8,084,383 B2 (2011) [to WR Grace & Co].
189. Sastre G, Katada N, Suzuki K, Niwa M. *J Phys Chem C* 2008;**112**:19293–301.
190. Gribov EN, Cocina D, Spoto G, Bordiga S, Ricchiardi G, Zecchina A. *Phys Chem Chem Phys* 2006;**8**:1186–96.
191. Romero Sarria F, Blasin-Aube V, Saussey J, Marie O, Daturi M. Trimethylamine as a probe molecule to differentiate acid sites in Y–FAU Zeolite: FTIR study. *J Phys Chem B* 2006;**110**:13130–7.
192. Suzuki K, Katada N, Niwa M. *J Phys Chem C* 2007;**111**:894–900.
193. Montanari T, Finocchio E, Busca G. *J Phys Chem C* 2011;**115**:937–43.
194. Navarro U, Trujillo CA, Oviedo A. *J Catal* 2002;**211**:64–74.
195. Niwa M, Suzuki K, Isamoto K, Katada N. *J Phys Chem B* 2006;**110**:264–9.
196. Schußler F, Pidko EA, Kolvenbach R, Sievers C, Hensen EJM, van Santen UA, et al. *J Phys Chem C* 2011;**115**:21763–76.
197. van Bokhoven JA, Roest AL, Koningsberger DC, Miller JT, Nachttegaal GH, Kentgens PM. *J Phys Chem B* 2000;**104**:6743.
198. Behring DL, Ramirez-Solis A, Mota CJA. *J Phys Chem B* 2003;**107**:4342.
199. Omegna A, Van Bekhoven JA, Prins R. *J Phys Chem B* 2003;**107**:8854.
200. Omegna A, Prins R, Van Bokhoven JA. *J Phys Chem B* 2005;**109**:9280.
201. Menezes SMC, Camorim VL, Lam YL, San Gil RAS, Bailly A, Amoureux JP. *Appl Catal A Gen* 2001;**207**:367.
202. Xu B, Rotunno F, Bordiga S, Prins R, van Bokhoven JA. *J Catal* 2006;**241**:66.
203. Habib ET, Zhao X, Yaluris G, Cheng WC, Boock LT, Gilson JP. In: Guisnet M, Gilson JP, editors. *Zeolites for cleaner technologies*. Imperial College Press; 2002. p. 105.

204. Sadeghbeigi R. FCC catalysts. In: *Fluid catalytic cracking handbook*. 3rd ed. Elsevier; 2012. p. 87–116. ISBN: 9780123869654.
205. Van Veen JAR. Hydrocracking. In: Guisnet M, Gilson JP, editors. *Zeolites for cleaner technologies*. Imperial College Press; 2002. p. 131.
206. *AlkyClean; A true solid acid gasoline alkylation process*, [www.abb.com/lummus](http://www.abb.com/lummus).
207. Dautzenberg FM, Van der Pull N. *Advanced reactors and catalyst concepts*, [www.abb.com](http://www.abb.com).
208. Ginosar DM, Thompson DN, Burch KC. *Ind Eng Chem Res* 2006;**45**:567.
209. Flanigen EM, Lok BN, Lyle Patton R, Wilson ST. *Pure Appl Chem* 1986;**58**(10): 1351–8.
210. Pillai RS, Jasra RV. *Langmuir* 2010;**26**(3):1755–64.
211. Pastore HO, Coluccia S, Marchese L. *Annu Rev Mater Res* 2005;**35**:351–95.
212. Regli L, Zecchina A, Vitillo JG, Cocina D, Spoto G, Lamberti C, et al. *Phys Chem Chem Phys* 2005;**7**:3197.
213. Bordiga S, Regli L, Cocina D, Lamberti C, Bjorgen M, Lillerud KP. *J Phys Chem B* 2005;**109**:2779.
214. Wei Y, Zhang D, Liu Z, Su BL. *J Catal* 2006;**238**:46.
215. Chen JQ, Bozzano A, Glover B, Fuglerud T, Kvisle S. *Catal Today* 2005;**106**:103.
216. Pujadó PR, Andersen JM. In: Meyers RA, editor. *Handbook of petroleum refinery processes*. Mc Graw Hill; 2006. p. 15.3–15.14.
217. Andersen JM. In: Meyers RA, editor. *Handbook of petrochemicals production processes*. Mc Graw Hill; 2005. p. 10.15–26.
218. Chen D, Moljord K, Holmen A. *Microporous Mesoporous Mater* 2012;**164**:239–50.
219. Dahl IM, Mostad H, Akporiaye D, Wendelbo R. *Microporous Mesoporous Mater* 1999;**29**:185.
220. US Patent 6,903,240, ExxonMobil Chemical Patents Inc, Houston, TX, USA, 2005, Focus Catal, 2006(10), p. 7.
221. Dai W, Wang X, Wu G, Li L, Guan N, Hunger M. *ChemCatChem* 2012;**4**(9):1428–35.
222. Wragg DS, Akporiaye D, Fjellvåg H. *J Catal* 2011;**279**:397–402.
223. Miller SJ. U.S. Patent 6,281,404 (2001), [to Chevron].
224. Zhang F, Liu Y, Shu X, Wang W, Qin F. US Patent 6596156, 2003 [to Sinopec].
225. Deldari H. *Appl Catal A Gen* 2005;**293**(1–2):1–10.
226. Danilina N, Castelanelli SA, Troussard E, Van Bokhoven JA. *Catal Today* 2011;**168**(1): 80–5.
227. Li J, Yu J, Xu R. *Proc R Soc A* 2012;**468**:1955–67.
228. Wei Y, Tian Z, Gies H, Xu R, Ma H, Pei R, et al. *Angew Chem Int Ed* 2010;**49**: 5367–70.
229. Martineau C, Bouchevreau B, Tian Z, Lohmeier S-J, Behrens P, Taulelle F. *Chem Mater* 2011;**23**(21):4799–809.
230. Sun J, Bonneau C, Cantín Á, Corma A, Díaz-Cabañas MJ, Moliner M. *Nature* April 30, 2009;**458**:1154–7.
231. Popa K, Pavel CC. *Desalination* 2012;**293**:78–86.
232. Kuznicki SM, Bell VA, Nair S, Hillhouse HW, Jacobinas RM, Braunbarth CM, et al. *Nature* 2001;**412**:720.
233. Uma S, Rodrigues S, Martyanov IN, Klabunde KJ. *Microporous Mesoporous Mater* 2004;**67**:181–7.
234. Lopes CB, Lito PF, Otero M, Lin Z, Rocha J, Silva CM, et al. *Microporous Mesoporous Mater* 2008;**115**:98.

235. Guo M, Pidko EA, Fan F, Feng Z, Hofmann JP, Weckhuysen BM, et al. *J Phys Chem C* 2012;**116**(32):17124–33.
236. Suppes GJ, Dasari MA, Doscocil EJ, Mankidy PJ, Goff MJ. *Appl Catal A Gen* 2004;**257**(2):213–23.
237. Lewis DW, Rabdel Ruiz-Salvador A, Gomez A, Marleny Rodriguez-Albelo L, Coudert F-X, Slater B, et al. *CrystEngComm* 2009;**11**:2272–6.
238. Hao GP, Li WC, Lu AH. *J Mater Chem* 2011;**21**:6447.
239. Hedin N, Andersson L, Bergström L, Yan J. *Appl Energy*; 2013:418–33.
240. Fischer M, Hoffmann F, Fröba M. *RSC Adv* 2012;**2**:4382–96.
241. Ranocchiari M, Bokhoven JAV. *Phys Chem Chem Phys* 2011;**13**(14):6388–96.
242. Yoon M, Srirambalaji R, Kim K. *Chem Rev* 2012;**112**(2):1196–231.
243. Wang C, Zheng M, Lin W. *J Phys Chem Lett* 2011;**2**(14):1701–9.
244. Bunk DN, Dichtel WR. *Angew Chem Int Ed* 2012;**51**:1885–9.
245. Zhang Y, Nurhanna Riduan S. *Chem Soc Rev* 2012;**41**:2083–94.

# Other Solid Acid and Basic Catalytic Materials

## CHAPTER OUTLINE

<b>8.1 Acid–base catalytic materials from minerals</b> .....	<b>252</b>
8.1.1 Clays as catalytic materials .....	252
8.1.2 Chemically modified clays .....	255
8.1.3 Pillared clays (PILC) and acidic porous clay heterostructures.....	256
8.1.4 Calcareous minerals.....	258
8.1.5 Basic silicate clays .....	258
<b>8.2 Halide salts and halided oxides</b> .....	<b>259</b>
8.2.1 Solid chlorided catalytic materials .....	259
8.2.1.1 Chlorided alumina .....	259
8.2.1.2 Other metal chlorides .....	261
8.2.1.3 Silica chloride.....	261
8.2.1.4 Supported metal chlorides.....	262
8.2.2 Fluorided inorganic solids .....	262
8.2.2.1 Fluorided chromia .....	262
8.2.2.2 Aluminum fluoride and fluorided alumina.....	262
8.2.2.3 Bivalent fluorides: $\text{CaF}_2$ , $\text{MgF}_2$ and $\text{ZnF}_2$ .....	263
8.2.2.4 Fluorided silica–alumina .....	264
8.2.2.5 Solids containing boron trifluoride .....	264
8.2.2.6 Basic catalysts based on supported alkali fluorides.....	264
<b>8.3 Sulfides, (oxy)nitrides, carbides, phosphides as acid–base materials</b> .....	<b>265</b>
<b>8.4 Heteropolyacids and polyoxometallates</b> .....	<b>267</b>
<b>8.5 Solid carbonates, phosphates, sulfates and other salts</b> .....	<b>270</b>
<b>8.6 Supported inorganic acids</b> .....	<b>272</b>
8.6.1 Solid phosphoric acid .....	272
8.6.2 Silica sulfuric acid.....	273
8.6.3 Supported triflic acid .....	274
8.6.4 Supported ionic liquids.....	274
<b>8.7 Supported alkali and alkali-earth metals or organometallics as “basic catalysts”</b> .....	<b>275</b>
<b>8.8 Organo-inorganic hybrid materials</b> .....	<b>275</b>
<b>8.9 Carbon-based materials</b> .....	<b>276</b>
8.9.1 Carbon materials .....	277
8.9.1.1 Activated carbons and impregnated activated carbons .....	277



8.9.1.2 AC fibers .....	277
8.9.1.3 Carbon blacks .....	278
8.9.1.4 Ordered mesoporous carbons .....	278
8.9.1.5 Carbon gels .....	279
8.9.1.6 High surface-area graphite .....	279
8.9.1.7 Graphene nanosheets .....	279
8.9.1.8 Carbon nanotubes and nanofibers .....	279
8.9.1.9 Fullerenes and fullerene black .....	280
8.9.2 Carbon materials as catalyst supports .....	282
8.9.3 Modified carbons as catalysts .....	283
8.9.3.1 Sulfonated carbon materials as acid catalysts .....	283
8.9.3.2 Nitrided carbon material as basic catalysts .....	284
<b>8.10 Polymeric solid acids and bases (ion exchange resins) .....</b>	<b>284</b>
<b>References .....</b>	<b>287</b>

---

## 8.1 Acid–base catalytic materials from minerals

A number of materials based on natural minerals find application in catalysis technologies. Their low cost, sometimes coupled with interesting useful or even unique properties, represents an obvious main reason for their application. Some authors performed synthesis of mineral-like materials such as clays,<sup>1</sup> obtaining purer and better defined materials. Obviously, the advantage of using cheap natural materials is relaxed in this case.

### 8.1.1 Clays as catalytic materials

Clay minerals are phyllosilicates (layer silicates) that are predominant components of the fine-grained fraction of soils and sediments.<sup>2</sup> The basic structures of clays are phyllosilicate sheets (“tetrahedral sheets”) formed by silicate tetrahedra sharing three corners, and “octahedral sheets”, formed by octahedra containing mostly  $\text{Al}^{3+}$  or  $\text{Mg}^{2+}$  cations, linked by sharing edges. When  $\text{Al}^{3+}$  ion is the cation, only two of every three octahedral sites are occupied in the sheet in order to maintain electrical neutrality. The resultant structure (found also in the mineral hydroxide  $\text{Al}(\text{OH})_3$  gibbsite) is referred to as “dioctahedral”. When  $\text{Mg}^{2+}$  is the central cation, all the three octahedral positions are filled, like in the sheets forming the mineral hydroxide  $\text{Mg}(\text{OH})_2$  brucite: in this case the sheet is denoted as “trioctahedral”.

Condensation of one tetrahedral (T) sheet with one octahedral (O) sheet gives rise to a 1:1 (T–O) layer structure. Thus, one basal plane of the 1:1 layer consists of oxygens (from the tetrahedral sheet), the other is formed by hydroxyls (from the octahedral sheet). Among the most used 1:1 clays kaolin finds applications in catalysis; see below.

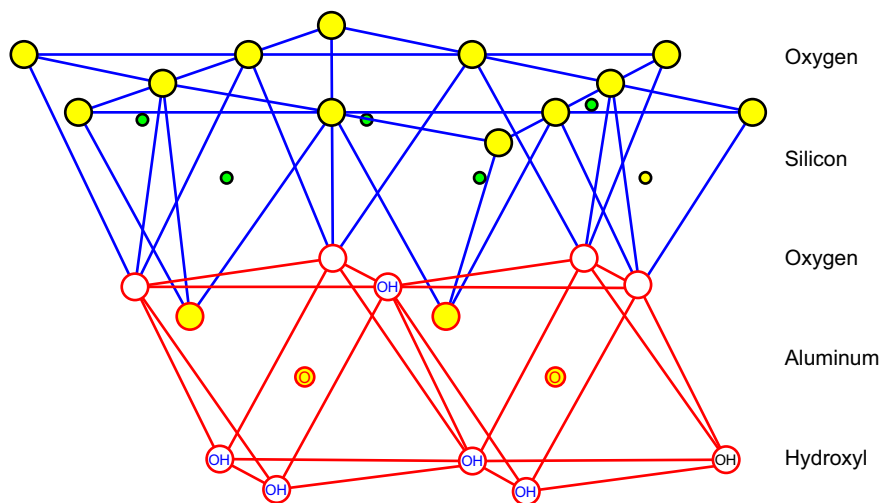
Condensation of two tetrahedral sheets sandwiching one octahedral sheet gives rise to a 2:1 (T–O–T)-type layer structure. In this case, both basal planes of

individual layers are composed of oxygens (belonging to the tetrahedral sheets). Among the 1:2 clay families, smectites are historically applied as catalysts.

Untreated clays may be applied in the field of adsorption and catalysis, as cheap and readily available acido-basic materials. Their catalytic activity, however, is generally weak and activation procedures (e.g., acid treating and delamination) are needed to increase surface area and acidity.

Kaolin is used as a matrix, binder or filler component of fluid catalytic cracking (FCC) catalysts,<sup>3,4</sup> whose main active phase is an acidic faujasite (see Chapter 7.1.6). Kaolin is mainly constituted by kaolinite (triclinic  $\text{Al}_2\text{Si}_2\text{O}_5(\text{OH})_4$ ), the most common 1:1 clay structure (see Figure 8.1<sup>5</sup>), but containing also impurities such as quartz ( $\text{SiO}_2$ ) and traces of anatase ( $\text{TiO}_2$ ), analcime ( $\text{NaAlSi}_2\text{O}_6 \cdot \text{H}_2\text{O}$ ), nefeline ( $\text{NaAlSi}_3\text{O}_8$ ), and illite polymorphs, as well as magnesium, calcium and potassium compounds. The kaolin surface is almost neutral,<sup>6</sup> with a very small amount of medium acidity-active centers. These centers give rise to weak protonic acidity arising from bridging hydroxy-groups on the exposed basal planes (exposed gibbsite-like layers), and silanol groups likely formed on nonbasal planes, as well as medium strength Lewis acid sites likely exposed on nonbasal planes. Lewis and Brønsted sites may also arise from mineral impurities. Kaolinite actually decomposes above  $550^\circ\text{C}$  producing metakaolin, an impure amorphous silica–alumina material, characterized by high surface area and medium-low acido-basicity<sup>7</sup> due to an effect of “neutralization” by impurities such as alkali and alkali-earth components.

These materials represent usually 20–50% of the mass of FCC catalysts. They are believed to react with Ni and V compounds present in the feed (atmospheric



**FIGURE 8.1**

The kaolinite structure.

*Reprinted with permission from Ref. 5.*

gasoil or deasphalted vacuum gasoil),<sup>8</sup> so preserving the active component (acid faujasite zeolite) from contamination. Although it is generally supposed to act as a mesoporous matrix where reactant and product molecules diffuse to reach the active zeolite particles, it has been shown that kaolin, in spite of its poor acidity, participates to reaction, catalyzing the cracking of the largest molecules that do not enter the zeolite cavities,<sup>9</sup> and/or contributing in a synergic way to the total acidity of the catalyst.<sup>10</sup> Acid treatment of kaolin binder is reported to further improve the efficiency of FCC catalysts.<sup>11</sup>

In the scientific literature, many additional applications of kaolin in the catalysis field are reported. In particular, several studies report the use of kaolin or metakaolin as support for acid or of metal catalysts, as well as a starting material in zeolite preparation.

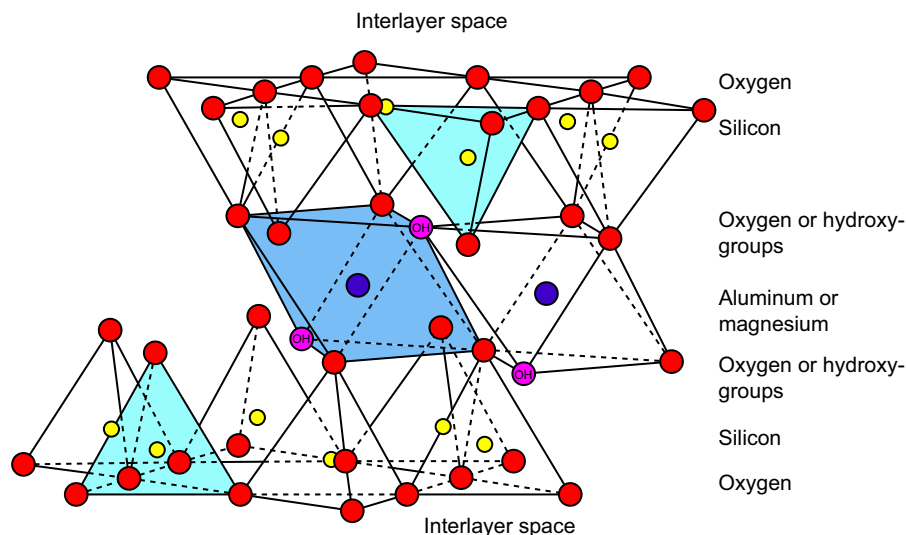
Halloysite ( $\text{Al}_2\text{Si}_2\text{O}_5(\text{OH})_4 \cdot 2\text{H}_2\text{O}$ ) can be regarded as a hydrated kaolinite phase, with interlayer water content depending on various factors, thus often being highly interstratified or completely dehydrated. The morphology of halloysite particles is variable, but the most common shapes are elongated, curled kaolinite-like particles forming nanotube-analogue morphologies similar to polygonal spirals (“nanorolls” or “nanoscrolls”). Raw halloysite has been tested as a catalyst, for example, being found to be active as an esterification catalyst.<sup>12</sup>

Smectite clays are sheet silicates in which a layer of octahedrally coordinated cations is sandwiched between two tetrahedral phyllosilicate layers (2:1 layer type). To complete the coordination of the cations, hydroxy-groups are also present in the layers, the theoretical formula for each layer being  $\text{Al}_2\text{Si}_4\text{O}_{10}(\text{OH})_2$ , which is the formula of pyrophyllite. When ionic substitution occurs, smectites are formed, among which montmorillonites and saponites are the most widely present in nature. In the case of montmorillonites (bentonites) Mg substitutes for Al in the octahedral layers, and hydrated alkali or alkali-earth cations in the interlayer space compensate the charge defect (Figure 8.2<sup>5</sup>). In saponites, additional Al for Si substitution occurs in the tetrahedral sheets.

The acidity of such clays is relatively low and their surface area is also relatively low. IR spectra show a strong OH-stretching band centered at  $3645\text{ cm}^{-1}$ , due to bulk hydroxy-groups, with a weaker one at  $3742\text{ cm}^{-1}$ , due to surface terminal silanols, the acidity of the latter being weak, similar to that found on pure silica. The experiments did not detect any Lewis site.

Smectite clays have a limited thermal stability, losing water from interlayer region at relatively low temperature ( $<200\text{ }^\circ\text{C}$ ) while decomposing to a mixture of crystalline phases at temperature  $>500\text{--}600\text{ }^\circ\text{C}$  with further loss of water.

Attapulgite (Palygorskite) has been considered in early times as a cracking catalyst. It is a 2:1 magnesium aluminosilicate having needle-shaped crystals. Its structure consists of talc-like ribbons parallel to the fiber axis. Differently than for other 2:1 clays, in attapulgite the tetrahedral sheet inverts its apical directions (apices alternately pointing up and down in adjacent sheets) in adjacent ribbons, each ribbon alternating with channels (dimension  $6.4 \times 3.7\text{ \AA}$ ) along the fiber axis. Octahedral sheets are discontinuous at each inversion of the tetrahedra. Its ideal unit cell

**FIGURE 8.2**

Structure of a layer of montmorillonite.

*Reprinted with permission from Ref. 5.*

formula is  $\text{Mg}_5\text{Si}_8\text{O}_{20}(\text{OH})_2(\text{OH}_2)_4 \cdot 4\text{H}_2\text{O}$  in which magnesium is considerably replaced by aluminum and iron. Acid-treated attapulgite was found to act as a performant acid catalyst in several reactions including esterification of alcohols with acetic acid.<sup>13</sup>

### 8.1.2 Chemically modified clays

While the use of pyrophyllite, as such or chemically modified, appears to be scarce, much interest has been focused on the use of smectites due to their various interlamellar chemistry and the increased activity produced by their swelling. In fact, both acidity and surface area of smectite clays, in particular montmorillonite, can be significantly enhanced by acid treatment, as done since very early times. In fact, acid-activated bentonite clays were the earliest cracking catalysts applied in the Houdry fixed-bed catalytic cracking process since 1936, being replaced in the 1940s by synthetic silicaluminas and in the 1960s by faujasite zeolites. Acid-treated montmorillonites are today commercial products and can be purchased from a variety of commercial sources. Different grades of acid-activated montmorillonites are tailored to different applications. Materials denoted as K-10 ( $220\text{--}270\text{ m}^2/\text{g}$ <sup>14,15</sup>), K-30 ( $\sim 330\text{ m}^2/\text{g}$ <sup>15,16</sup>) and KSF (8–12% free sulfuric acid,  $\leq 12\%$  humidity,  $20\text{--}40\text{ m}^2/\text{g}$ ) are among the most used. The process by which natural calcium bentonites are acid-activated involves treatment of the uncalcined clay with mineral acids of variable concentration and for different

duration at  $\sim 100$  °C. Such a treatment leads to leaching of aluminum, magnesium and iron cations from the octahedral layer, to partial removal of aluminum ions from the tetrahedral layer that relocate in the interlayer space, and to the reduction of cation exchange capacity. During acid activation, swelling also occurs at the edges of clay platelets which open up and separate, while still remaining tightly stacked at the center. The surface area increases notably, and pore diameters increase and assume a three-dimensional (3D) form.

IR spectroscopy<sup>15</sup> allowed to reveal that acid treatment results in weakly Brønsted acidic but much more abundant silanol groups, and in the appearance of strong and medium Lewis acid sites. On the other hand, acid-activated clays may be not stable in their acid form, undergoing autotransformation that results in a very sensitive dependence of the acidity on the water content of the clay. The interconversion that may occur among Brønsted and Lewis sites makes difficult the interpretation of the experimental data.<sup>17</sup>

Clays and acid-treated clays, mainly montmorillonites, are today largely used in the petrochemical industry mostly as adsorbents for purification and decoloration of oils. They may be sometimes used as components of FCC catalysts, and are also proposed as catalysts for several acid catalyzed reactions such as cracking of heavy fractions, etherifications, esterifications, alkylation. They have also been considered for industrial applications in the field of hydroprocessing and hydroisomerization,<sup>18</sup> mild hydrocracking<sup>19</sup> and as support for other acid catalysts.<sup>20</sup> Very recently, an acid-treated smectite clay has been patented for the transalkylation process of dialkylated LAB (linear-alkylbenzene) plus benzene to LAB, the precursor of LAS (linear alkylbenzene-sulphonates) detergents.<sup>21</sup> Acid-treated montmorillonite is a versatile catalyst for several fine chemical reactions<sup>22,23</sup> in particular of interest in the pharmaceutical industry.<sup>24</sup> Saponites, both natural<sup>22</sup> and synthetic<sup>18</sup> are also active as acidic catalysts, e.g., for hydroisomerization of *n*-heptane and alkylation of benzene with propylene providing also shape selectivity effect.

Hectorite is another trioctahedral 2:1 mineral clay with formula  $\text{Si}_8[\text{Mg}_{6-x}\text{Li}_x](\text{OH},\text{F})_4\text{O}_{20}\text{M}^{n+}_{x/n}\cdot m\text{H}_2\text{O}$ , where some substitution of Mg(II) by Li(I) in the octahedral (Oh) sheet causes the negative charge of layers, which must be compensated by interlayer exchangeable cations. Hectorite, either natural or synthetic (Laponite), is an important industrial material, with its suspensions having very interesting optical and rheological properties. It has been tested as a catalyst, as such or after acid treatment, as well as to prepare pillared clays and supported catalysts. It seems that its practical interest in catalysis is far lower than that of montmorillonite-derived materials.<sup>25</sup>

When treated with appropriate materials, natural smectites can also become very active basic catalysts such as for cesium- and other alkali-saponites.<sup>22,26</sup>

### 8.1.3 Pillared clays (PILC) and acidic porous clay heterostructures

As said, smectite clays have a lamellar structures constituted by negatively charged aluminosilicate layers, with compensating cations in the interlamellar space.

The modification or substitution of these cations allows functionalization of clays as well as widening of the interlamellar space, producing microporosity, thus allowing to design new advanced porous materials with a wide range of potential applications. A number of different procedures and strategies have been recently investigated, which allowed development of a number of new catalytic materials based on clays.<sup>27</sup>

Exchanging the charge-compensating cations with an oligomeric polyoxometal cation such as the  $[\text{Al}_{13}\text{O}_4(\text{OH})_{24}(\text{H}_2\text{O})_{12}]^{7+}$  Keggin-type homopolyocation, denoted as  $\text{Al}_{13}$ , results in a two-dimensional porous material known as alumina-pillared clay (PILCs).<sup>28,29</sup> Upon heating, the cationic pillars form oxide clusters that permanently open the clay layers, creating an interlayer space of molecular dimensions and a well-defined pore system. Alumina-pillared montmorillonite is a commercial material, but its use as a catalyst at the industrial level is hampered by its complex and not always reproducible preparation procedure,<sup>30</sup> which may be improved by ultrasonic treatments.<sup>31</sup>  $\text{Al}_{13}$  montmorillonites are the most common pillared clays: the Al polyoxocation gives a large expansion of the basal  $d$ -spacing (to near 19 Å from the thickness of the clay layer, which is 9.6 Å and a normal value for Na-montmorillonite, which is near 12.5 Å). These materials are quite stable at high temperatures, up to about 750 °C. Characterization studies<sup>32</sup> show that alumina-pillared montmorillonite shows strong Lewis acidity similar to that of spinel-type aluminas, and medium-low Brønsted acidity. With similar procedures, gallia-, chromia-, titania- and zirconia-pillared montmorillonites (PILM) can be prepared. In many cases, these materials find interesting catalytic activities for a number of organic reactions,<sup>22</sup> alumina-PILM being sold (12–19% loss on ignition, 4–8% loss on drying, surface area 250 m<sup>2</sup>/g<sup>33</sup>) as a Lewis acid catalyst.

Efforts have been made to obtain, by clay pillaring, large pore materials stable to regeneration treatments to perform cracking of very large molecules (>8 Å).<sup>34</sup> In any case, materials based on pillared clays are applied in some catalytic cracking processes<sup>35,36</sup> and as molecular sieves. They may also be useful as medium acidity supports of noble metal catalysts for hydrocarbons fuel hydrotreating.<sup>37,38</sup> Also, the catalytic activity of pillared clays in ethylene glycol synthesis from ethylene oxide hydration, formation of ethylene glycol ethers<sup>39</sup> and of propene oxide from *n*-propanol<sup>40</sup> appear to be of industrial interest. Titania pillared montmorillonite<sup>41</sup> can be prepared with different procedures and can be modified with transition metal cations to produce catalysts, e.g., for the reduction of  $\text{NO}_x$ .<sup>42</sup>

A different family of related materials are the so-called “PCH”<sup>43</sup> prepared by the surfactant-directed assembly of mesostructured silicas<sup>44</sup> and silicaluminas<sup>45</sup> in the two-dimensional galleries of 2:1-layered silicates. These materials are reported to have strong acidity, stability to 750 °C and a particular porous structure. Unlike in the pillaring mechanism, PCHs are formed by the surfactant-directed assembly of mesostructured silica or silica–alumina within the two-dimensional galleries of a 2:1-type clay. PCHs are intrinsically acidic and uniquely combine supermicro- and mesoporosity, making them potential catalysts for size selective conversion of molecules with diameter too large to be processed over conventional zeolite

catalysts. However, in the preparation of PCH materials, a high-temperature calcination (typically 600–650 °C) is necessary to remove the templates and to complete the cross-linking of the gallery silica structure. Such a process causes degradation of some thermally unstable clay minerals and precludes their use in preparation of PCH-type materials containing organic functional groups.

With a similar chemistry, organoclays can be prepared.<sup>46</sup> They are, most usually, obtained from bentonites by intercalating them with surfactant cations, mostly tetralkyl ammonium or tetralkyl phosphonium cations. In this way, the hydrophilic clay is turned into organophilic. In principle, by modifying the organic chains in the interlamellar region, these materials can be modified to prepare acido-basic catalysts or even redox materials and supported catalysts by depositing transition metal ions, to be used for low temperature catalytic applications.

#### 8.1.4 Calcareous minerals

Limestone, one of the largest constituents of the earth's crust, is a readily available and cheap mineral based on calcium carbonate,  $\text{CaCO}_3$ , in the two polymorphic forms calcite and aragonite, very poorly soluble in water. Its thermal decomposition, obtained at 900 °C, produces the corresponding oxide,  $\text{CaO}$ , also called quicklime, as well as gaseous  $\text{CO}_2$ . The hydration of  $\text{CaO}$  gives rise to the hydroxide,  $\text{Ca}(\text{OH})_2$ , also called hydrated or slaked lime, which is slightly soluble in water (0.05 mol  $^-\text{OH}/\text{l}$ ) to give basic solutions.

In the chemical industry, one of the largest applications of limestone is in the so-called Solvay process for the production of soda ash ( $\text{Na}_2\text{CO}_3$ ) and of Na hydrogen-carbonate  $\text{NaHCO}_3$ . Limestone and lime are largely applied in the field of flue gas desulfurization technologies,<sup>47,48</sup> i.e., for the abatement of  $\text{SO}_2$  from coal-fired power plant combustion waste gas.

A closely related material is dolomite, the mixed carbonate of Mg and Ca, decomposing above 700 °C in two steps giving rise to a mixed Mg,Ca oxide.<sup>49</sup>

In recent years, calcite and dolomite found catalytic application in the biomass gasification technologies.<sup>50</sup> They may be added to the biomass reactor to catalyze the biomass gasification reaction, performed in the 400–800 °C temperature range, depending on the process and reactor configurations. Depending on the reaction temperature, more gases or oils are produced. One of the main technical barriers in biomass gasification development is the presence of organic impurities, denoted as tars, in the obtained fuel gas. Tars, which are mixtures of monocyclic and polycyclic aromatic compounds, can be at least partially destroyed (steam reformed) using again basic materials such as limestone, dolomite and other rocks, performed at 850 °C.<sup>51</sup>

#### 8.1.5 Basic silicate clays

Alkali and alkali-earth metal orthosilicates, such as olivine ( $\text{Mg}_2\text{SiO}_4$ ) and lithium silicates ( $\text{Li}_4\text{SiO}_4$ ) and zirconates,<sup>52</sup> besides being important refractories, find

application for high-temperature catalytic processes, as substituents of calcareous materials, in biomass gasification and tar removal catalysis as well as for high-temperature CO<sub>2</sub> adsorption.<sup>53</sup>

Sepiolite is a hydrated magnesium silicate with the ideal formula Si<sub>12</sub>Mg<sub>8</sub>O<sub>30</sub>(OH)<sub>4</sub>(OH<sub>2</sub>)<sub>4</sub>·8H<sub>2</sub>O, characterized by a chain-like structure producing needle-like particles, instead of plate-like particles typical of phyllosilicate clays. Most of the world production of this clay comes from deposits of sedimentary origin located near Madrid, Spain. Sepiolite is an excellent material for cat and pet litters: the popularity of sepiolite pet litters is due to its light weight, high liquid absorption and odor control characteristics. This material is poorly thermally stable, decomposing in several steps with a main water loss in the ranges about 150 and 450 °C.<sup>54</sup> Its possible application as catalyst or catalyst support has been proposed.

Synthetic basic silicates such as lizardite (a 1:1 clay with Mg<sub>3</sub>Si<sub>2</sub>O<sub>5</sub>(OH)<sub>4</sub> stoichiometry) and talc (a 2:1 clay, triclinic Mg<sub>3</sub>Si<sub>4</sub>O<sub>10</sub>(OH)<sub>2</sub>), which are the Mg-corresponding form of the Si:Al clays kaolin and pyrophyllite, respectively, have been prepared and tested as glycerol etherification catalysts, showing interesting properties.<sup>55</sup>

---

## 8.2 Halide salts and halided oxides

As it has been discussed in Chapter 5.1.4, metal halides behave as the most typical and strongest Lewis acids. This behavior is mostly applied in the liquid phase. However, solids based on halide salts can also be prepared and used as heterogeneous catalysts.

### 8.2.1 Solid chlorided catalytic materials

#### 8.2.1.1 Chlorided alumina

Aluminum trichloride, AlCl<sub>3</sub>, has been proposed as a catalyst for aromatic alkylation and acylation reactions by C. Friedel and J.M. Crafts at the end of the nineteenth century. AlCl<sub>3</sub> melts at 193 °C, producing a typical molecular liquid mostly composed by the dimer Al<sub>2</sub>Cl<sub>6</sub> although higher polymers may also exist. It also produces several low temperature eutectics with other metal chlorides and gives rise to liquid complexes with hydrocarbons and ionic liquids<sup>56</sup> with organohalide precursors. When additivated with proton donor species, such as water or HCl, or its precursors such as alkyl halides, alkyl amine salts, imidazolium halides, pyridinium halides, or phosphonium halides, AlCl<sub>3</sub> gives rise to the formation of ionic liquids with very strong Brønsted superacidity, whose strength was evaluated to be similar to that of dry HF (H<sub>0</sub> ~ -15). Classical Friedel–Crafts chemistry implies liquid-phase catalysis mostly performed with metal chloride catalysts activated by proton donor species. Due to the severe drawbacks of these catalytic systems, the substitution of these systems with solid catalysts is under development.<sup>57</sup>

Chlorided aluminas are in some way one of the evolutions of Friedel–Crafts catalysts. They have been used for decades in particular in refinery. In fact,



chloride ions at the surface of alumina, produced by adsorption of HCl or by surface decomposition of alkyl chlorides, or being residual from incomplete decomposition of  $\text{AlCl}_3$  from the preparation method, or finally by deposition of  $\text{AlCl}_3$ , further enhance the acidity of alumina. The IR spectrum of the surface hydroxy-groups of alumina is modified by the presence of chlorine, with the disappearance of the higher frequency alumina's OH's.<sup>58–60</sup> Chlorided aluminas are very acidic materials<sup>61</sup> that show high catalytic activity in demanding reactions, such as, e.g.,<sup>62</sup> isobutane/butylene alkylation. The adsorption of pyridine shows that, in the same conditions, more acidic  $\text{Al}^{3+}$  cations are formed on chlorided alumina (band at  $1625\text{ cm}^{-1}$ ) than on the parent  $\gamma\text{-Al}_2\text{O}_3$ , and that few Brønsted sites able to protonate pyridine are also formed by chlorination. Recent theoretical calculations<sup>60</sup> confirm that terminal OH's of alumina are preferentially exchanged by chlorine, and suggest that the increased Brønsted acidity results from the increased availability of bridging OH's arising from weakening of H-bonds when the nearest OH groups are substituted by chlorine.

Chlorided aluminas have been used for decades as catalyst for C4 and C5–C6 paraffin skeletal isomerization as well as the catalytically active support for Pt-based catalysts for naphtha reforming. In both cases, the chlorided alumina-based catalysts require the continuous addition of small amounts of alkyl chlorides to maintain high catalyst activities. In effect, chlorided hydrocarbons, such as alkyl chlorides, trichloroethylene and  $\text{CCl}_4$ , decompose on alumina at  $150\text{--}400\text{ }^\circ\text{C}$  producing HCl that is adsorbed on alumina. Additionally, hydrogen is fed and Pt metal is present, to slow catalyst coking.

For paraffin isomerization<sup>63,64</sup> to use chlorided alumina catalysts the feed must be free of water and other oxygen sources in order to avoid catalyst deactivation and potential corrosion problems.<sup>65</sup> Pt-doped chlorided alumina catalysts compete, for this application, with more poison-resistant catalysts such as those based on zeolites (MOR and MAZ) and sulfated or tungstated zirconia. However, they may work at definitely lower temperature ( $150\text{--}200\text{ }^\circ\text{C}$ ) and this allows to have more favorable equilibrium conditions, so their performances are better. Thus, in spite of the non-regenerability of chlorided aluminas (life is usually in the range of 2–3 years) and their low environmental friendliness, they are very largely applied. Their chlorine content in reaction may be as high as 10% Cl wt/wt.<sup>60</sup>

In the catalytic reforming process,<sup>66</sup> that works at much higher temperature ( $\sim 500\text{ }^\circ\text{C}$ ) with depentanized naphtha, the chlorided alumina support acts as the catalyst of skeletal isomerization of linear paraffins as well as of alkylicyclopentanes, favoring the formation of high octane-branched isomers and also of cyclohexanes ready to aromatization. Also in this case chlorine compounds are fed to allow a constant chlorine content in the catalyst. A typical catalytic-reforming catalyst<sup>67</sup> is based on a support constituted by gamma alumina with  $160\text{--}250\text{ m}^2/\text{g}$  containing 0.5–2% chlorine and, according to a recent patent application,<sup>68</sup> also 0.07–0.65% phosphorus and 580–1050 ppm of sulfur. Modern catalytic reforming catalysts are “multimetallic”, containing 0.1–0.8% Pt and other Platinum group metals, usually Rhenium,  $\sim 0.3\%$  Tin, and other promoters such as In,<sup>69</sup> W and Mo.

Chlorided alumina is probably the key component of the HAL-100 catalyst applied in the solid-catalyzed UOP ALKYLENE process for isobutane/butylene alkylation to isooctane.<sup>70</sup> The catalyst should contain metals for the hydrogenation function and possibly alkali metal ions to moderate catalyst acidity, preventing excessive cracking and coking.<sup>71</sup> After reaction occurring in a riser, the catalyst is disengaged and moves to the reactivation zone where hydrogen is fed with isobutane, for hydrogenation and washing. Part of the catalyst is transported to a separate reactivation vessel where also regeneration occurs. The reaction temperature is 10–40 °C and the isobutane to olefin ratio in the reactor is 8–15.

Drawbacks common to these processes concern the difficult regenerability of the catalyst, the deliquescent behavior of aluminum chloride with the consequent leaching, corrosion and disposal problems.

### 8.2.1.2 Other metal chlorides

Among solid chlorides,  $\text{MgCl}_2$  finds a very relevant application in the catalysis field: it is the support for the modern  $\text{TiCl}_4/\text{MgCl}_2$  Ziegler–Natta type catalysts for the production of isotactic polypropylene, which is constituted by  $\text{MgCl}_2$  as the support and  $\text{TiCl}_4$  as active component or its precursor.  $\text{MgCl}_2$  plays a crucial role in adsorbing  $\text{TiCl}_4$  and activating it for stereoregular polymerization with the help of a cocatalyst (triethylaluminum) and an electron donor compound (Lewis base, diether) as stereoregulating component.<sup>72</sup> Bulk  $\text{MgCl}_2$  can adopt two ordered crystalline forms:  $\alpha\text{-MgCl}_2$  with the  $\text{CdCl}_2$  crystal structure, and the thermodynamically less stable  $\beta\text{-MgCl}_2$ , which adopts the  $\text{CdI}_2$  structure.  $\alpha\text{-MgCl}_2$  is characterized by a cubic close packed array of chloride ions with bivalent cations sitting in 1/2 of adjacent octahedral sites, forming layers where a Mg cation plane is sandwiched between two chloride anion planes. The  $\beta\text{-MgCl}_2$ -form is based on the hexagonal close packing of the chloride anions with the cations also placed in octahedral interstices. In practice, the two structures differ only for the relative position of the same layers. The basal surface is in both cases only exposing chloride ions, while Mg cations can be exposed only in the lateral cuts. IR studies of adsorbed CO reported the formation of three surface species characterized by  $\nu\text{CO}$  at 2210, 2190 and 2170  $\text{cm}^{-1}$ , attributed to CO interacting with three, four and five coordinated Mg cations.<sup>73</sup>

Theoretical investigations suggest that interaction of  $\text{TiCl}_4$  on  $\text{MgCl}_2$  occurs in these lateral cuts, in particular in the (104) and (110) lateral cuts supposing the  $\alpha\text{-MgCl}_2$  structure. More precisely, it has been proposed a short (110) stretch may be formed joining the (104) edges: the adsorption of  $\text{TiCl}_4$  there would result in the active sites for polymerization.<sup>74</sup>

### 8.2.1.3 Silica chloride

Silica chloride ( $\text{SiO}_2\text{-Cl}$ ) is a solid produced by reaction of silica gel with  $\text{SOCl}_2$  or  $\text{SO}_2\text{Cl}_2$ . A preparation of silica chloride may imply the dispersion of silica gel (20 g) in  $\text{CH}_2\text{Cl}_2$  (50 ml) and the addition, dropwise, of  $\text{SOCl}_2$  (20 g) at room temperature.<sup>75</sup> Evolution of copious amounts of HCl and  $\text{SO}_2$  occurs instantaneously. After stirring for 1 h, the solvent is removed to dryness under reduced pressure (1 Torr).

The  $\text{SiO}_2\text{-Cl}$  can be stored in sealed vessels for 6 months without any critical decline in activity. This catalyst is promising for high acidity, cheapness, easy production, and insolubility in all organic solvents. It has been reported as an efficient catalyst for several organic chemistry reactions such as esterification of carboxylic acids (aliphatic, aromatic and conjugated) with alcohols (primary, secondary and tertiary) as well as for transesterification of esters (by both alcoholysis and acidolysis),<sup>76</sup> highly selective Claisen–Schmidt condensation,<sup>77</sup> conversion of thiols to disulfides.<sup>78</sup>

#### **8.2.1.4 Supported metal chlorides**

As seen in Chapter 5.1.4, many metal chlorides (such as  $\text{ZnCl}_2$ ,  $\text{AlCl}_3$ ,  $\text{GaCl}_3$ ,  $\text{BCl}_3$ ,  $\text{SbCl}_3$ ,  $\text{SnCl}_4$ ,  $\text{TiCl}_4$ ,  $\text{ZrCl}_4$ ,  $\text{SbCl}_5$ , etc.) are strong Lewis acids. Many studies report on the high catalytic activity of solid acids produced by supporting these materials on solid surfaces, such as silica gel, polymeric solids,<sup>79</sup> MOFs.<sup>80</sup> Limits for these materials are poor thermal stability and leaching in liquid phase.

### **8.2.2 Fluorided inorganic solids**

Fluorine is the only element more electronegative than oxygen. In fact, the metal-fluorine bond may be even more ionic than the metal-oxygen bond. Thus, coordinatively unsaturated metal cations (especially those characterized by small size and high charge) may, at the surface of metal fluorides, be even more Lewis acidic than at the surface of metal oxides. Thus, aluminum fluorides are very strong Lewis acid materials, even stronger than aluminas. Otherwise, the fluoride anions are very electron rich and may be even more basic than oxide anions. For this reason, compounds such as alkali fluorides may act as very basic solids.

#### **8.2.2.1 Fluorided chromia**

Fluorided chromia is reported to be the most widely used catalyst precursor for large-scale fluorination processes, producing fluorocarbons.<sup>81</sup> The treatment of chromia with  $\text{CCl}_2\text{F}_2$  gives rise to the formation of chromium oxide chloride fluoride species whose Lewis acidity is increased as shown by IR spectroscopy of pyridine adsorption. No Brønsted acidity is detected. The presence of  $\text{CrF}_3$  and/or  $\text{CrCl}_3$  phases on the activated chromia samples was not found. The partial halogenation of the surface is sufficient to provide catalytic activity.<sup>82</sup>

#### **8.2.2.2 Aluminum fluoride and fluorided alumina**

Aluminum fluoride is a polymorphic,<sup>83,84</sup> high-melting point ( $1260^\circ\text{C}$ ) solid. It is essentially a nontoxic chemical. However, if heated to above  $500^\circ\text{C}$  in the presence of moisture hydrogen fluoride vapor evolution occurs. Its stable form,  $\alpha\text{-AlF}_3$ , crystallizes in a rhombohedral distorted  $\text{ReO}_3$ -like structure, SG R-3c, and transforms reversibly to the cubic  $\text{ReO}_3$ -type polymorph at  $452^\circ\text{C}$ .  $\beta\text{-AlF}_3$  is a metastable form with an orthorhombic “pseudo-hexagonal” structure (S.G: Cmcm) related to hexagonal tungsten bronze, in which six  $[\text{AlF}_6]$  octahedra form hexagonal channels.

This form transforms slowly and irreversibly to the cubic polymorph. As for other polymorphs,  $\eta$ -AlF<sub>3</sub> adopts the cubic (defective) pyrochlore structure,  $\kappa$ -AlF<sub>3</sub> adopts the tetragonal tungsten bronze structure.  $\theta$ -AlF<sub>3</sub> is reported to have a more complex structure based on intrications of tetrahedra of octahedra (as in the pyrochlore structure) and infinite chains. In all cases all Al ions are coordinated to six fluorine atoms in a nearly octahedral coordination.

AlF<sub>3</sub> can be prepared in different ways, among which by fluoridation of alumina with different reactants such as fluorocarbons and SF<sub>4</sub>,<sup>85</sup> and is largely used as catalyst in the industrial chemistry of fluorocarbons and fluorochlorocarbons,<sup>81,86</sup> to catalyze fluorine–chlorine exchange reactions, hydrodehalogenations and dehydroalogenations. The  $\beta$ -AlF<sub>3</sub> polymorph is considered to be the most active, with very high Lewis acidity,<sup>87,88</sup> being perhaps the strongest among common Lewis acidic solids, as deduced by the adsorption of basic probes ( $\nu$ 8a of pyridine at 1627 cm<sup>-1</sup>,  $\nu$ CN of pivalonitrile at 2309 cm<sup>-1</sup>,  $\nu$ CO of carbon monoxide at 2230 cm<sup>-1</sup><sup>89</sup>). Fluorination of alumina with HF causes the progressive formation of AlF<sub>3</sub> polymorphs,  $\alpha$ -AlF<sub>3</sub> more than  $\beta$ -AlF<sub>3</sub>.<sup>90</sup> Fluorided aluminas can also be prepared by impregnation of NH<sub>4</sub>F followed by thermal decomposition. Fluorided aluminas and AlF<sub>3</sub> are reported to present surface OH's which are strong Brønsted acid sites.<sup>91,92</sup> Fluorination of alumina causes the progressive disappearance of the OH's absorbing at 3790, 3770 cm<sup>-1</sup>, with the progressive growth of bands at 3730 and 3655 cm<sup>-1</sup>.<sup>93</sup> According to Corma et al.,<sup>94</sup> the total number of Lewis acid sites decreases when the fluorine content increases, whereas the number of sites with strong acidity exhibits a maximum for samples with 2–4% of fluorine content. Also the number of Brønsted acid sites presents a maximum for the same fluorine content, despite the fact that only a small fraction of the sites created by fluorination exhibit strong acidity.

Besides their activity in fluorocarbons conversions, fluorided alumina and AlF<sub>3</sub> have been proposed for several acid-catalyzed hydrocarbon conversion (such as benzene alkylation, where a very high selectivity to monoalkylated products has been claimed<sup>93</sup>) and as support for hydrodesulfurization catalysts.<sup>95</sup>

High surface-area aluminum fluoride, HS-AlF<sub>3</sub>, has been recently prepared using a nonaqueous sol–gel synthesis followed by a fluoridation step.<sup>96,97</sup> The obtained solid has surface areas between 150 and 350 m<sup>2</sup>/g, and may have crystalline  $\beta$ -AlF<sub>3</sub> structure or be amorphous. These materials have been found to possess an extraordinarily high Lewis acidity:<sup>87</sup> in particular high concentration of sites adsorbing CO with a shift of the CO-stretching frequency up to near 2225 cm<sup>-1</sup>, while no Brønsted acid sites were found on the dry surface.

### 8.2.2.3 Bivalent fluorides: CaF<sub>2</sub>, MgF<sub>2</sub> and ZnF<sub>2</sub>

CaF<sub>2</sub>, fluorite, crystallizes with calcium ions coordinated to eight fluorine atoms, while F<sup>-</sup> ions are tetrahedrally coordinated to Ca<sup>2+</sup> cations. Magnesium and zinc difluorides, instead, crystallize in the rutile structure type, in which Mg<sup>2+</sup> and Zn<sup>2+</sup> ions are surrounded by six F<sup>-</sup> ion and each F<sup>-</sup> ion by three divalent cations. In recent years, the fluorolytic sol–gel route was applied by Kemnitz and coworkers

for the preparation of these materials in a high surface area form (HS). Both HS-MgF<sub>2</sub><sup>98</sup> and HS-ZnF<sub>2</sub><sup>99</sup> were characterized by spectroscopy measurements showing predominantly weak Lewis acid sites, while CaF<sub>2</sub> is reported to be essentially a neutral material with some interest in catalysis.<sup>100</sup>

With the same method, a number of different Mg oxyfluorides and hydroxyfluorides have also been prepared and characterized.<sup>101</sup> The catalytic activity of HS-MgF<sub>2</sub> and of Mg oxy- and hydroxy-flurides, as well as of modified MgF<sub>2</sub> has been subject of a recent review,<sup>102</sup> and found very interesting and “tunable” acido-basic catalytic activity.

In spite of its low acidity, the presence of CaF<sub>2</sub> may improve the catalytic activity of AlF<sub>3</sub>, e.g., in the catalytic pyrolysis of chlorodifluoromethane (CHClF<sub>2</sub>, R22) carried out at 650 °C: the selectivity of tetrafluoroethylene (TFE), the monomer for manufacturing fluorinated compounds, such as polytetrafluoroethylene commercially known as Teflon is improved.<sup>103</sup> The catalytic process may compete with the most widely used process for the commercial production of TFE, which consists in the thermal pyrolysis of R22 in the temperature range of 750–950 °C.

#### **8.2.2.4 Fluorided silica–alumina**

The alkylation of benzene with long chain olefins has been performed since many years using liquid catalysts such as HF, H<sub>2</sub>SO<sub>4</sub> and AlCl<sub>3</sub>-based liquids. In the 1990s, UOP in cooperation with CEPSA developed a new process, Detal™, using a heterogeneous catalyst.<sup>104</sup> According to early UOP patents,<sup>105,106</sup> the catalyst is an amorphous fluorided silica–alumina having a silica:alumina weight ratio of from 65:35 to 85:15 and contains from 1 to 6 weight percent fluoride. The catalyst consists of cogelled silica alumina impregnated by HF or ammonium fluoride and dried at 125–175 °C and later calcined at 350–550 °C. This treatment does not result in fluorine loss. It does not seem that a careful characterization of this catalyst has been published up to now.

#### **8.2.2.5 Solids containing boron trifluoride**

BF<sub>3</sub> is also a very strong Lewis acidic compound, giving rise to Brønsted superacidic behavior with proton-donor species. Attempts to produce stable very acidic solids based on BF<sub>3</sub> have been reported in the literature. Impregnation of BF<sub>3</sub> onto alumina gives rise to solid acids that found interesting activity in isobutane/iso-butylene alkylation.<sup>71</sup> Similar materials have been apparently used in industrial ethylbenzene synthesis catalysis (Alkar UOP process<sup>107</sup>). However, leaching of BF<sub>3</sub> and its reactivity with water to produce volatile compounds are relevant drawbacks. New interest for supported BF<sub>3</sub>, such as on alumina and chromia<sup>107b</sup> arises also from the catalytic chemistry of (chloro)fluorocarbons, while BF<sub>3</sub>/SiO<sub>2</sub> has been proposed as an efficient reactant in the organic chemistry.<sup>107c</sup>

#### **8.2.2.6 Basic catalysts based on supported alkali fluorides**

The strong electronegativity of fluorine is a reason for the application of KF/Al<sub>2</sub>O<sub>3</sub> as a strong basic catalytic material, which is largely used in organic chemistry.<sup>108,109</sup>

Other supported alkali metal fluorides, such as CsF/ $\alpha$ -Al<sub>2</sub>O<sub>3</sub><sup>110,111</sup> and CsF/CaO,<sup>112</sup> have been found to display good basic catalytic activity. RbF, CsF and/or KF impregnated on alumina and zirconium oxide have been patented as catalysts for the synthesis of polyglycerol.<sup>113</sup>

---

### 8.3 Sulfides, (oxy)nitrides, carbides, phosphides as acid–base materials

According to the smaller electrophilicity of sulfur, nitrogen, phosphorus and carbon with respect to oxygen, their bond with metals and semimetal has lower ionic character and, consequently, the corresponding binary compounds (sulfides, nitrides, phosphides, carbides) are expected to show lower basicity than oxides. Transition metal sulfides are largely used in industry as catalysts for hydrodesulfurization (HDS) and hydrotreating of hydrocarbon flows (see Chapter 10). Although traditional catalysts are alumina-supported Co–Mo, Ni–Mo or Ni–W catalysts, the corresponding bulk unsupported sulfides, as well as other transition metal sulfides (such as the pure or mixed sulfides of V, Fe, Rh, Ru, Cr, Cu, ...) have been studied. Some of the new more efficient HDS catalysts allowing to obtain the limit of 10 ppm in Diesel fuel belong to mixed unsupported sulfides.<sup>114</sup> Transition metal sulfide catalysts are thought to have Lewis acid sites able to interact with sulfur atoms of (di)benzothiophenes, coupled with basic sites forming acid–base pairs, and some Brønsted acidity too, such as is the case of unsupported MoS<sub>2</sub>.<sup>115</sup> The acidity of supported sulfide catalysts is influenced by the acidity of the support, which is a key property for hydrocracking catalysts.<sup>116</sup> Studies on basicity of ZnS did not report significant basicity.<sup>117</sup> On the other hand, we can remind that, in general, sulfur compounds are weaker bases than the corresponding oxygen compounds.

Sulfides can be produced by reacting of oxides with hydrogen sulfide or other sulfide compounds. In this way, sulfur compounds may be removed from gases. This is the case of ZnO application to desulfurize natural gas or other gases at near 400 °C.<sup>118</sup> With lanthana and praseodymia, partial sulfidation produce oxysulfides lanthanum oxysulfide (La<sub>2</sub>O<sub>2</sub>S) and praseodymium oxysulfide (Pr<sub>2</sub>O<sub>2</sub>S), which were identified as an excellent sulfur-resistant catalyst for the water–gas shift and the reverse water–gas shift reactions.<sup>119</sup>

Metal nitrides, phosphides and carbides are becoming very interesting catalytic materials, mainly when transition metals are involved, due to their “metal-like” activity e.g., in hydrogenation reactions<sup>120</sup> (Chapter 10). On the other hand, base metal or nonmetal nitrides and carbides are interesting ceramic materials with application as catalyst supports. The weak basicity of silicon nitride<sup>121</sup> and oxynitride,<sup>122,123</sup> as well as of aluminum nitride<sup>124,125</sup> and boron nitride<sup>126,127</sup> was recognized several years ago. These solids were found to expose, at their surface, hydroxy-groups and nitrogen atoms such as NH and/or NH<sub>2</sub> groups. More recently, other nitride, oxynitride and phospho-oxy-nitride materials such as VAIONs, AIPONs, ZrPONs,

AlGaPONs have been developed and proposed as possible basic catalysts.<sup>128</sup> More recent studies allowed to define BN in its hexagonal form, isostructural with graphite, as a very inert material.<sup>129</sup> However, these materials, in particular aluminum nitride, suffer also from easy hydrolysis.<sup>130</sup>

Transition metal nitrides are well known as excellent hydrotreating catalysts.<sup>131</sup> They have also drawn considerable interest in recent years for their potential use as catalysts for other hydrogenation reactions. Using MBOH catalytic conversion as a reaction probe, Keller et al.<sup>132</sup> found a significant surface acidity of  $W_2N$ ,  $Mo_2N$  and  $NbN$  catalysts: dehydration is thought to occur on Brønsted acid sites, whereas isomerization should occur on metal-oxo ones. Conversely, using  $CO_2$ -TPD and MBOH decomposition, McGee et al.<sup>133</sup> found relevant basicity at the surface of  $W_2N$ , and  $Mo_2N$ , with basic site strength and density similar to those of ZnO, but lower than those of MgO. However, Bej and Thompson found higher activity in acetone aldol condensation for  $Mo_2N$  than for MgO.<sup>134</sup>

Transition metal phosphide catalysts such as nickel phosphides, usually supported on oxide carriers, are also active catalysts with respect to hydrotreating: HDS and hydrodenitrogenation of hydrocarbon mixtures, but also hydrodeoxygenation (HDO) of bio-oils<sup>135</sup> and hydrodechlorination of chloroorganics.<sup>136</sup> Ni phosphide catalysts are reported to display Lewis acidity attributed to Ni cations and Brønsted acidity attributed to phosphate species associate to incomplete reduction.<sup>135</sup> Other transition metal phosphides have good catalytic properties: in HDO of bio-oils at 300 °C and 1 atm, the order of activity was  $Ni_2P/SiO_2 > WP/SiO_2 > MoP/SiO_2 > CoP/SiO_2 > FeP/SiO_2 > Pd/Al_2O_3$ .<sup>137</sup>

Carbides are important materials in catalysis. Among others, silicon carbide-based materials represent useful supports for catalysts, due to its interesting properties: a high thermostability, high mechanical strength, high heat conductivity and chemical inertness up to 800 °C. The main drawback of SiC, i.e., the very low surface area of the commercially available material, was overcome by new preparation methods, such as templated synthesis, sol-gel processing, and polycarbosilane pyrolysis, allowing higher surface area (20–200 m<sup>2</sup>/g) carbides with high synthesis yield. Common SiC materials consist of a mixture of the 6H polytype, one of the several hexagonal polytypes that are collectively denoted as  $\alpha$ -SiC and whose structure is related to the wurtzite-type structure, and  $\beta$ -SiC (zinc blende, cubic). High-temperature oxidation treatment eliminates the graphitic region and leads to an enrichment in  $SiO_xC_y$  and especially  $SiO_2$  units, without any important structural changes.<sup>138</sup> Surface studies of high surface-area SiC are really scarce. It has been reported that few surface silanol groups may be the only reactive sites over nonoxidized surface, which by oxidation convert on a silica-like surface.<sup>139</sup> A number of nanostructured forms of silicon carbide may be prepared and are also commercially available, such as foams, nanowires<sup>140</sup> and 6H-type whiskers.<sup>141</sup>

According to its chemical inertness, low surface-area silicon carbide (carborundum) is used in the catalysis field as an inert material to fill empty spaces of catalyst beds. However, it seems that it has also been used as a support for low surface

area catalysts such as oxides for ethane selective oxidative dehydrogenation and ammoxidation.<sup>142</sup> In recent years, high surface-area SiC materials became interesting supports for catalyst. As for example,  $\beta$ -SiC foam with moderate surface areas (15–25 m<sup>2</sup>/g) have been tested as supports for Pd catalysts for methane combustion,<sup>143</sup> as well as supports of complex stable activity.

Transition metal carbides, such as those of molybdenum and tungsten, are also active catalysts in hydrotreating,<sup>144</sup> although it was found that they convert partially into sulfides by reacting with the sulfur feed. On the other hand, several metal catalysts when working in the presence of reactive hydrocarbons or of CO really become, at least in part, carbided. This is, e.g., the case of Pd catalysts for acetylene hydrogenation and of iron catalysts for Fischer–Tropsch synthesis. Interest for these materials is mainly on their metal-like properties.<sup>120</sup>

---

## 8.4 Heteropolyacids and polyoxometallates

As briefly discussed in Chapter 6.1.1, nonmetallic elements as well as metallic elements in very high oxidation states may produce acids whose molecular structure is formed by the condensation of several oxo-units in the form of linear polymeric species or globular units. When more than one different metallic or nonmetallic element is present in globular molecules, the acid is denoted as heteropolyacid (HPA) while their salts are frequently denoted as “polyoxometallates” (POM).

The most common and thermally stable primary structure of HPAs<sup>145,146</sup> is that of the Keggin unit that consists of a central atom (usually P, Si, or Ge) in a tetrahedral arrangement of oxygen atoms, surrounded by twelve octahedra, usually containing tungsten or molybdenum. There are four types of oxygen atoms found in the Keggin unit, the central oxygen atoms, two types of bridging oxygen atoms, and terminal oxygen atoms. Since the Keggin unit possesses a net negative charge, charge-compensating protons or cations must be present for electroneutrality. The acid form of HPAs is generally soluble in water and acts as a Brønsted liquid acid, and as a homogeneous acid catalyst in water solutions, as well as in liquid biphasic systems.<sup>147,148</sup> Evaluation of acid strength in solution has shown that HPA's composed of tungsten are more acidic than those composed of molybdenum, and the effect of the central atom is not as great as that of the addenda atoms. Nevertheless, phosphorus-based HPAs are slightly more acidic than silicon-based HPAs. This gives the general order of acidity as  $\text{H}_3\text{PW}_{12}\text{O}_{40} > \text{H}_4\text{SiW}_{12}\text{O}_{40}$  and  $\text{H}_3\text{PW}_{12}\text{O}_{40} > \text{H}_4\text{PMo}_{12}\text{O}_{40}$ .<sup>149</sup>

HPAs and POMs are also interesting materials as solid heterogeneous catalysts. HPAs are active as solid acid catalysts while, mainly when molybdenum and vanadium are involved, redox properties become relevant. Thus, these materials are also of interest as oxidation catalysts (see Chapter 11).

In the solid state, a secondary structure exists, with the Keggin units located at the lattice positions of the Bravais lattices. Keggin units are bound by hydrogen bondings involving also structural water molecules external to the polyoxometallate



units, or their protonated forms. In HPAs, water may be present in three different forms.<sup>150</sup> HPAs obtained by crystallization from water solution may contain up to above 30 molecules of water per one HPA anion. Most of these water molecules desorb easily by heating just a little above room temperature. The rest of the crystallization water is bonded in the form of  $\text{H}_3\text{O}^+$  or  $\text{H}_5\text{O}_2^{2+}$  ions forming H-bonding network holding together the units, and is given off at 150–200 °C. Anhydrous forms of HPA lose their water of constitution (dehydroxylation) at 350–500 °C, with the decomposition of the structure.

At least two different kinds of catalysis may occur with solid HPAs: besides “normal” surface-type catalysis, another unique “pseudo-liquid” mechanism can occur where polar and small reactant molecules penetrate in between the heteropolyanions and react inside the solid bulk, followed by the release of products outside the solid bulk.<sup>151</sup>

According to the literature, the following property trends have been established for HPAs:

Acid strength:  $\text{PW} > \text{SiW} > \text{PMo} > \text{SiMo}$

Oxidation potential:  $\text{PMo} > \text{SiMo} \gg \text{PW} > \text{SiW}$

Thermal stability:  $\text{PW} > \text{SiW} > \text{PMo} > \text{SiMo}$  (decomposition temperatures are 465, 445, 375, and 350 °C, respectively)

Hydrolytic stability:  $\text{SiW} > \text{PW} > \text{SiMo} > \text{PMo}$ .

The surface area of solid HPAs is generally very low (few square meters per gram), and this makes accessible protons to the reactants very few. The salts of HPA's with large cations such as  $\text{Cs}^+$ ,  $\text{K}^+$ ,  $\text{Rb}^+$  and  $\text{NH}_4^+$ , when obtained by precipitation from aqueous solution of the parent acid  $\text{H}_3\text{PW}_{12}\text{O}_{40}$ , are micro/mesoporous materials with much larger surface areas, up to 200  $\text{m}^2/\text{g}$ . Thus, in the case of partial cation exchange, such as for  $\text{Cs}_x\text{H}_{3-x}\text{PW}_{12}\text{O}_{40}$ , the number of protons accessible to nonpolar reactant molecules is very much enhanced, and in parallel also the catalytic activity is enhanced. However, for practical application such salts have a few problems; that is, Cs and W are rather expensive and their mechanical strength is sometimes insufficient for practical use in commercial chemical processes.<sup>151</sup>

According to several studies,  $\text{H}_3\text{PW}_{12}\text{O}_{40}$ , the most stable and strongest acid in the Keggin series, has acid sites stronger than those of H-ZSM5 zeolite and even has superacidic centers based on adsorption calorimetry experiments.<sup>152</sup> It has also been shown that its acid strength depends strongly on the presence of crystallization water. In agreement with this, it has been found that  $\text{H}_3\text{PW}_{12}\text{O}_{40}$  and  $\text{Cs}_{1.9}\text{H}_{1.1}\text{PW}_{12}\text{O}_{40}$  are very active for very demanding acid-catalyzed reactions such as the isomerization of *n*-butane to isobutane at 473 K, but their catalytic activity decreased when small amounts of water were added.<sup>153</sup>  $\text{Cs}_{2.5}\text{H}_{0.5}\text{PW}_{12}\text{O}_{40}$ , the so-called  $\text{Cs}_{2.5}$ , possesses a maximum acid amount on the surface (surface acidity) in most gas-phase reactions such as dehydration of ethanol in liquid phase, but in the case of transesterification of triglycerides with methanol the  $\text{Cs}_2\text{HPW}_{12}\text{O}_{40}$  salt exhibited the highest catalytic activity.<sup>154</sup> The  $\text{Cs}^+$  forms of HPAs are generally not soluble in water

but can work as heterogeneous catalysts in liquid water or in liquid water/organic biphasic systems.<sup>155</sup>

Dehydrated  $\text{H}_3\text{PW}_{12}\text{O}_{40}$  shows a well-evident  $^1\text{H}$  MAS NMR peak at 9 ppm, assigned to protons bonded to surface bridging oxygens of the anion.<sup>156</sup> The IR spectrum shows a broadband centered at  $3100\text{ cm}^{-1}$ , assigned to two families of H-bonded OH's,<sup>157,158</sup> although both the nuclear magnetic resonance (NMR) peak and the IR band have been more recently reattributed to  $\text{H}_3\text{O}^+$ .<sup>159</sup> All protons are reported to be able to protonate pyridine up to forming  $\text{Py}_2\text{H}^+$  cations.<sup>158</sup> In the hydrated form, the formation of a “pseudoliquid phase” occurs, with the formation of  $\text{H}_5\text{O}_2^+$ , corresponding to the disappearance of the NMR peak.

Solid HPAs and their salts are active as heterogeneous catalysts for several gas-phase and liquid-phase hydrocarbon conversion reactions,<sup>160</sup> and have been the object of several theoretical investigations.<sup>161</sup> However, their use in the industry for gas-phase reactions seems to be still very limited, if at all, possibly due to their rapid deactivation.<sup>162</sup> Supported HPAs apparently may have better properties.<sup>151</sup>

Concerning acid catalysis, liquid-phase hydration of the olefins to the corresponding alcohols is performed industrially with HPA catalysts at  $100\text{--}350\text{ }^\circ\text{C}$  and  $1\text{--}2.5\text{ MPa}$  for some decades: ethanol from ethylene, 2-propanol from propene and *tert*-butanol (TBA) from isobutene are produced using catalysts such as mono- or di-potassium salts of tungstosilicic or tungstophosphoric supported on silica or niobia.<sup>151</sup>

Silica-supported  $\text{H}_4\text{SiW}_{12}\text{O}_{40}$  catalysts have been developed industrially for the production of ethylacetate from acetic acid and ethylene, at  $130\text{--}230\text{ }^\circ\text{C}$ ,  $0.5\text{--}1.5\text{ MPa}$ , and  $\text{C}_2\text{H}_4/\text{acetic acid}$  molar ratio 5:15.<sup>151</sup> The process can be also performed using ethanol or ethanol + ethylene mixtures instead of pure ethylene.

HPA catalysts, namely phosphotungstic acid, have been used for years for the synthesis of poly(tetramethylene ether)glycol from tetrahydrofuran.<sup>163</sup> Later, the catalyst was immobilized on the surface of a silica carrier modified by the amine groups of organosilane  $\gamma$ -aminopropyl triethoxysilane<sup>164</sup> to improve the process.

Among the many other applications of HPAs reported in the literature (production of polyisobutylene, synthesis of MTBE, dehydration of alcohols), it is reported to be active for glycerol dehydration to acrolein.<sup>165</sup>

Other HPA structures exist besides Keggin-type phases. In particular, the so-called Wells–Dawson structures, with the  $\text{H}_6\text{P}_2\text{W}_{18}\text{O}_{62} \cdot n\text{H}_2\text{O}$  stoichiometry, also give rise to strong acid catalysts,<sup>166,167</sup> with many potential applications.<sup>168,169</sup> The structure, known as  $\alpha$  isomer, possesses two identical “half units” of the central atom surrounded by nine octahedral units  $\text{XM}_9\text{O}_{31}$  linked through oxygen atoms. The isomeric  $\beta$  structure originates when a half unit rotates  $\pi/3$  around the  $X\text{--}X$ -axis. Similar to many heteropolyanions, the Wells–Dawson structure can be chemically manipulated to generate “holes” by removing up to six  $\text{WO}_6$  units (from  $\text{X}_2\text{M}_{18}$  to  $\text{X}_2\text{M}_{12}$ ).

A number of other polyacid structures have been prepared,<sup>170</sup> whose catalytic behavior is far less studied, such as the Preyssler structure,  $[\text{NaP}_5\text{W}_{30}\text{O}_{110}]^{14-}$ , the Anderson–Evans–Perloff structure  $[\text{X}^{n+}\text{M}_6\text{O}_{24}]^{(8-n)-}$ , the Lindquist structure

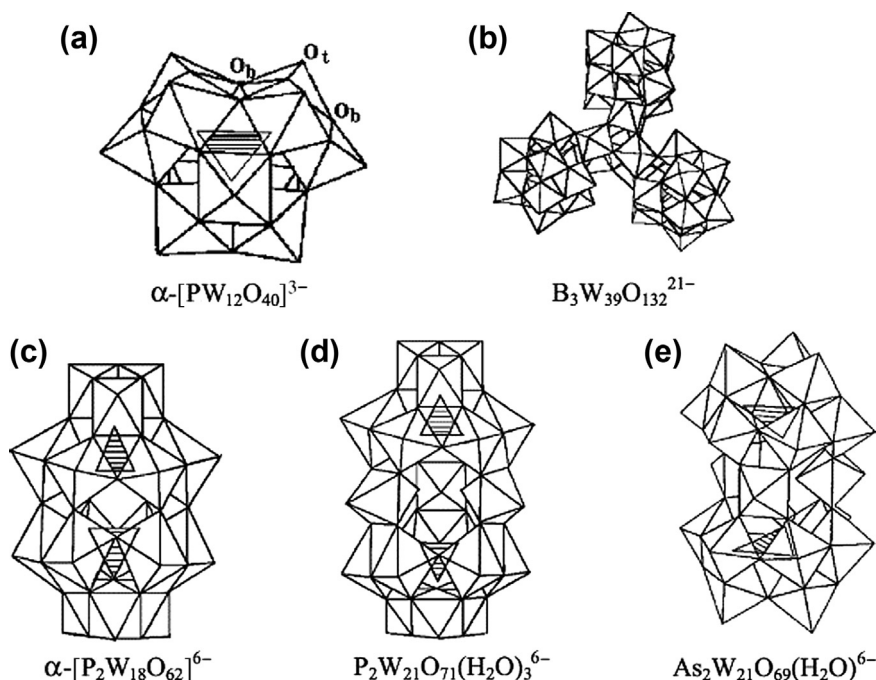


FIGURE 8.3

Ball-and-stick representation of typical polyoxometalates: (a) Dawson structure,  $\alpha\text{-}[\text{P}_2\text{W}_{18}\text{O}_{62}]^{6-}$ . (b) Preyssler structure,  $[\text{NaP}_5\text{W}_{30}\text{O}_{110}]^{14-}$ . (c) Keggin structure,  $\alpha\text{-}[\text{PW}_{12}\text{O}_{40}]^{3-}$ . (d) Heptamolybdate,  $[\text{Mo}_7\text{O}_{24}]^{6-}$ . (e) Lindquist structure,  $[\text{Mo}_6\text{O}_{19}]^{2-}$ .

Reprinted with permission from Ref. 171.

$[\text{M}_6\text{O}_{19}]^{2-}$ , the Waugh structure  $[\text{X}^{n+}\text{M}_9\text{O}_{32}]^{(10-n)-}$  and the Silverton structure  $[\text{X}^{n+}\text{M}_{12}\text{O}_{42}]^{(12-n)-}$ . In Figure 8.3, the structure of five different heteropolyanions are shown.<sup>171</sup>

## 8.5 Solid carbonates, phosphates, sulfates and other salts

A number of thermally and chemically stable salts find real or potential application as acid–base catalytic materials. As already reported, carbonate minerals such as limestone and dolomite find important application as catalysts for biomass gasification as well as biomass tar destruction (steam reforming) catalysts (see above Section 8.1.4). Calcium carbonate, which is stable up to nearly 800 °C, is used also as the support for catalysts, namely palladium, when basic-low surface area material is needed as the support. This is the case of the so-called Lindlar catalyst, an old and

“mythic”<sup>172</sup> but still largely used catalyst based on Pd–Pb/CaCO<sub>3</sub>, applied in organic chemistry for selective hydrogenations of C≡C bonds to C=C bonds.<sup>173,174</sup> Solid alkali carbonates are used as catalysts but actually mostly act as basic homogeneous catalysts.<sup>175</sup> Alkali carbonates are frequently used as supports for alkali metallic catalysts.<sup>176–178</sup>

As seen in Chapter 6.4.7, sulfation of oxides (like for sulfated zirconia) may generate very strong Brønsted acidity.<sup>179</sup> Metal sulfates may also have significant acidity, but usually have low surface area. Alkali and alkali earth sulfates are quite interesting materials according to their mild Lewis acidity. Barium sulfate finds application since decades as the support of palladium in a second version of the Pd-based Lindlar selective hydrogenation catalyst. It is also a component of recent washcoats or thermally stable supports of three-way catalysts.<sup>180</sup>

Alkali and alkali-earth sulfates and phosphates have been reported to act as catalysts for several dehydration reactions. In particular, promoted sodium and calcium sulfate, calcium phosphates and their mixture are reported to act as excellent catalysts for the dehydration of lactic acid and methyl lactate to acrylic acid and methyl acrylate, respectively,<sup>181,182</sup> very interesting reactions in the field of green and renewable chemistry. Calcium phosphates<sup>183</sup> are in fact interesting acid–base catalysts such as for dehydration and dehydrogenation of alcohols, the Knoevenagel condensation and the Friedel–Crafts alkylation.

Phosphates of tetravalent elements such as tin, germanium, titanium, and, in particular, zirconium have been the object of a number of studies.  $\alpha$ -zirconium phosphate  $\alpha$ -Zr(HPO<sub>4</sub>)<sub>2</sub>·H<sub>2</sub>O is one of the most widely investigated layered compounds: it is an acidic inorganic ion exchanger, characterized by highly ordered structure, ease of synthesis and ease of crystallinity and size control. A hydrated form of  $\alpha$ -zirconium phosphate can be the host to intercalate bulky molecules, including ionic liquids,<sup>184</sup> and can be also pillared.<sup>185</sup> Its decomposition produces layered ZrP<sub>2</sub>O<sub>7</sub>. Zirconium phosphates have medium Lewis acidity and Brønsted acidity.<sup>186</sup> Mesoporous zirconium phosphate has also been prepared<sup>187</sup> and found to act as an active catalyst in several organic reactions in solvent-free conditions. Additionally, a number of related organo-inorganic materials based on zirconium phosphates and phosphonates have been prepared.

Zirconium phosphates and phosphonates are useful catalysts for several reactions<sup>188</sup> including the preparation of pyrroles.<sup>189</sup> Zirconium phosphates and other metal (IV) phosphates are active catalysts for the selective dehydration of sorbitol to isosorbide.<sup>190</sup> Microspherical  $\alpha$ -zirconium phosphate catalysts for conversion of fatty acid methyl esters to monoethanolamides.<sup>191</sup> Several bivalent, trivalent and tetravalent metal phosphates, in particular AlPO<sub>4</sub>, CePO<sub>4</sub>, YPO<sub>4</sub> and Zr<sub>3</sub>(PO<sub>4</sub>)<sub>4</sub>, were found to be active for SF<sub>6</sub> decomposition at 530–730 °C.<sup>192</sup> Mesoporous tantalum phosphate has been found active for transesterification.<sup>193</sup>

Alkali phosphates such as Cs and K phosphates are reported to act as basic catalysts.<sup>125</sup> Alkali-promoted rare-earth metal phosphates, in particular Cs–SmPO<sub>4</sub>, are active for vapor phase *O*-alkylation of  $\alpha$ - and  $\beta$ -naphthols with methanol.<sup>194</sup>

## 8.6 Supported inorganic acids

### 8.6.1 Solid phosphoric acid

The so-called “solid phosphoric acid” catalyst (SPA) has been developed at UOP in the 1930’s.<sup>195,196</sup> It is produced by mixing phosphoric acid 85% with Kieselguhr (a natural form of silica, see Chapter 6.4.5) followed by extrusion and calcination. New recipes for “SPA with controlled porosity” have been developed<sup>197</sup> and patented recently.<sup>198,199</sup> The phosphoric acid is retained by the catalyst due to capillary forces, as well as the inherent high viscosity of phosphoric acid at a hydration state exceeding 100%  $\text{H}_3\text{PO}_4$ . The heat treatment causes the partial polymerization of orthophosphoric acid  $\text{H}_3\text{PO}_4$  to pyro-phosphoric acid  $\text{H}_4\text{P}_2\text{O}_7$ , and higher polymers such as triphosphoric acid  $\text{H}_5\text{P}_3\text{O}_{10}$ , as well as the formation of silicon phosphates such as  $\text{Si}_5\text{O}(\text{PO}_4)_6$ , hexagonal  $\text{SiP}_2\text{O}_7$ ,  $\text{Si}(\text{HPO}_4)_2 \cdot \text{H}_2\text{O}$  and  $\text{SiHP}_3\text{O}_{10}$ .<sup>200</sup> However, the real constitution of the acid phase strictly depends on water content in the catalyst, which is also greatly influenced by the amount of water vapor in the feed during the reaction.<sup>201</sup>

According to NMR studies, the acidity of this catalyst is associated to a liquid or glassy solution of phosphoric acid oligomers supported on the silicon phosphate phases.<sup>200</sup> The IR spectrum of the SPA catalyst shows the typical broad features of strong hydrogen-bonds between POH groups and water molecules, while, after outgassing, bands of free (PO)—H groups appear, absorbing at  $3658 \text{ cm}^{-1}$ . These free POH groups appear to be the most available to adsorbates. The position of the band is similar to that observed on low coverage-supported  $\text{H}_3\text{PO}_4$  on silica, as well as on phosphoric acid supported on other oxides<sup>202</sup> as well as on metal phosphates and pyrophosphates<sup>203a,203b</sup> and their Brønsted acidity, as measured by the hydrogen-bonding and by the olefin oligomerization methods via IR, is significant, but definitely lower than that of silica—alumina and zeolites. Interestingly, no bands of free silanol groups are observed in the case of SPA, while they are evident for silica-supported phosphoric acid. Also, the skeletal spectrum of SPA shows that silica, as such, does not exist in the SPA bulk. No Lewis acidity is found. The Hammett acidity function of SPA has been evaluated to be in the range  $-5$  to  $-7$ .<sup>200</sup>

SPA is applied industrially since decades for several processes: it is the catalyst for gas-phase propene and isobutylene oligomerization industrial processes<sup>204,205</sup> producing polymerate gasoline, as well as it has been used for decades for cumene synthesis from propene and benzene and for the hydration of light olefins to the corresponding alcohols. It also finds actual application in the treatment of Fischer—Tropsch syncrude.<sup>206</sup>

The hydration state of the catalyst is reported to affect in opposite ways the activities in olefin oligomerization and cumene synthesis<sup>201</sup> and also affects strongly the catalyst lifetime. However, excessive water in the feed leads to loss of mechanical properties of the catalyst and its destruction, mostly due to the hydrolysis of silicon phosphates. Acid leaching and coking are additional causes of deactivation.

Reaction temperature for industrial propene oligomerization to trimers and tetramers (UOP, IFP processes<sup>206</sup>) is in the range 150–245 °C, but usually below 205 °C to limit deactivation, at 18–80 atm, with relatively high space velocities. In the case of isobutene-rich feed, the upper temperature limit is around 175 °C to promote dimerization and limit further oligomerization. In the feed, 250–300 ppm water are recommended and catalyst life may be more than 1 year.<sup>201</sup> Multiple fixed-bed or multitubular reactors are used.

SPA can also be used to produce diesel-range olefin oligomers.<sup>207</sup> The selectivity to such products has been shown to have a peak when the concentration of pyrophosphoric acid  $H_4P_2O_7$  in the catalyst becomes relatively high, and space velocities are low.<sup>208</sup> Recently, the preparation of the catalyst has been modified to improve the crushing strength, which is controlled by the relative amounts of the silicon ortho- and pyrophosphate phases present. A new commercial catalyst was formulated that requires no binders and showed a 30% increase in catalyst lifetime.<sup>197</sup> Oligomerization of higher olefins such as dimerization of butene<sup>198</sup> and 1-hexene is also possible.<sup>209</sup> On the frame of Fischer–Tropsch plants, solid phosphoric acid finds application for olefin oligomerization-feeding complex mixtures of olefins (C3–C7), other hydrocarbons and oxygenated compounds.<sup>206,210</sup>

For gas-phase UOP cumene synthesis, typical reaction temperatures are 200–260 °C, at pressures 30–45 bar, with a large excess of benzene (5:1 to 10:1 benzene to propene) to limit multiple alkylation. Typical reactors are multiple fixed-bed with quenching to control the exothermic reaction temperature. Water of 100–150 ppm is recommended and the catalyst life may be more than 1 year.<sup>201</sup>

SPA is also used for the direct hydration of ethylene to ethanol in liquid phase at 230–300 °C, 60–80 atm,<sup>206,211</sup> and to produce other alcohols by acid-catalyzed hydration of olefins. The phosphoric acid is continually lost from the carrier, and water must be supplied with the feed. However, the use of other carriers causes a diminution of the catalytic activity.

The catalyst cannot be regenerated,<sup>212</sup> is slightly deliquescent and can give corrosion problems. However, the spent catalyst can be milled, neutralized with lime and ammonium hydroxide, and then calcined to yield a phosphate-rich fertilizer,<sup>213</sup> which improves very much its environmental friendliness.

### 8.6.2 Silica sulfuric acid

Silica sulfuric acid (SSA) is a solid material developed by M.A. Zolfigol by reacting silica with chlorosulfuric acid,<sup>214</sup> in a ratio near 3:1 wt/wt. According to the evolution of hydrochloric acid during the preparation, SSA is supposed to be formed by silica where silanol groups SiOH are converted into Si–O–SO<sub>3</sub>H. This material has been proven to act as an excellent and reusable catalyst for a number of organic reactions, performed in liquid aqueous phase. Recently, it has been found to be an excellent catalyst for model bio-oil upgrading with olefins/alcohols.<sup>215</sup>

More recently, using silica nanospheres, nanosphere silica sulfuric acid has been prepared and tested.<sup>216</sup> The grafting of sulfuric acid results in a strong lowering of the surface area and pore volume. Decomposition of the sulfonic acid groups takes place at about 380 °C.

### 8.6.3 Supported triflic acid

Attempts to produce acid solids based on liquid superacids (see table 6.2) are also in progress. The activity of triflic acid (trifluoromethylsulfonic acid,  $\text{CF}_3\text{SO}_3\text{H}$ ) in isobutane/butylene alkylation has been studied by Olah and coworkers.<sup>217</sup> Triflic acid supported on silica is used in the Haldor Topsøe FBA™ process of isobutane/butylenes alkylation.<sup>218,219</sup> The reaction occurs at 273–293 K in a fixed bed reactor. The catalyst, however, may be withdrawn without stopping the production, and transported in a regeneration unit. Traces of acid are leached in the product, which must be purified. A  $^1\text{H}$  NMR study shows that the peak position of the triflic acid proton at  $\delta = 12$  ppm is substantially unchanged in the case of the silica-supported catalyst until a water-to-acid molar ratio of 1, while it shifts to 10 ppm at higher water content, possibly according to the formation of the  $\text{TFA}\cdot 2\text{H}_2\text{O}$  complex. The IR OH-stretching band is reported to be at  $3397\text{ cm}^{-1}$ .<sup>219</sup> Similar solids are reported to act as efficient and recyclable catalysts for the addition of  $\beta$ -dicarbonyl compounds to alcohols and alkenes.<sup>220</sup> In an interesting paper, Liu et al.<sup>221</sup> described the preparation triflic acid-functionalized silica-coated magnetic nanoparticles  $\gamma\text{-Fe}_2\text{O}_3@\text{SiO}_2\text{-TfOH}$  that can be separated by magnetic decantation from the reaction mixture and reused. Triflic acid supported on titania was also tested as an acidic catalyst and found active. Its acidity decreases by increasing heating temperature.<sup>222</sup>

### 8.6.4 Supported ionic liquids

Ionic liquids are low-melting point salts ( $T_m < 100$  °C) constituted by monovalent organic cations and inorganic anions such as  $\text{Cl}^-$ ,  $\text{CuCl}_2^-$ ,  $\text{ZnCl}_3^-$ ,  $\text{SnCl}_3^-$ ,  $\text{BF}_4^-$ ,  $\text{Al}_2\text{Cl}_7^-$ ,  $\text{PF}_6^-$ ,  $\text{AsF}_6^-$ ,  $\text{SbF}_6^-$ ,  $\text{F}(\text{HF})_n^-$ , etc. When the cation is a protonated base, they are carriers of hydrogen halides (HCl, HF) and may act as Brønsted acid catalysts. These materials<sup>223</sup> are interesting as alternatives to liquid acids because of their lower volatilities and less corrosion problems, as well as the very large variety of applications and conditions they offer. These materials find very interesting catalytic activities in many fields, but with many limitations due to the liquid state of the catalysts. Supported ionic liquid catalysts could guarantee the advantages of heterogeneous catalysts and solid liquids, and thus these systems have been successfully applied in different catalytic processes, such as hydrogenations, alkylations, and carbonylations.

Among recent examples, silica-supported 1-butyl-3-methylimidazolium chloroaluminate ionic liquid<sup>224</sup> and 1-(4-Sulfobutyl)-3-methylimidazolium trifluoromethanesulfonate ionic liquid<sup>225</sup> were found to be highly efficient catalysts for the industrially important trimerization of isobutene.

---

## 8.7 Supported alkali and alkali-earth metals or organometallics as “basic catalysts”

As seen in Chapter 5, alkali and alkali-earth metals, as well as their organometallics, are extremely strong bases and nucleophiles, acting as catalysts or as initiators in anionic chain reactions such as, e.g., anionic polymerizations. This reactivity is performed in dry organic solvents or in liquid ammonia, where alkali metals dissolve and ionize. Alkali metals can be deposited on solid surfaces such as on alkaline earth oxides<sup>226,227</sup> producing solid materials with a strong reactivity that can be considered as superbasic. Electrons released from the alkali metal atoms are assumed to be entrapped in the oxygen vacancies. Very strong reactivity has been reported for alkali metals supported on carbon materials,<sup>228</sup> on alumina<sup>229</sup> and on alkali carbonates,<sup>177</sup> as well as for  $\text{KNH}_2$  and  $\text{RbNH}_2$  species supported on alumina.<sup>108</sup> Alkali metal clusters can also be grown in the cavities of zeolites.<sup>230</sup> These materials are largely used e.g., as initiator/catalysts in hydrocarbon conversions.<sup>231,232</sup> Superbasic catalysts have been developed by Sumitomo, based on  $(\text{NaOH})_x/\text{Na}_y/\gamma\text{-Al}_2\text{O}_3$  with  $x = 5\text{--}15\%$  wt/wt;  $y = 3.8\%$ , allowing alkylation of benzylic positions of alkylaromatics with olefins and olefin double bond isomerization at so low a temperature as  $-30\text{ }^\circ\text{C}$ .<sup>233</sup> An important example of this chemistry is the production of isobutylbenzene, an intermediate for the synthesis of ibuprofen (a relevant anti-inflammatory agent) by side alkylation of toluene with propene<sup>178</sup> at  $200\text{--}250\text{ }^\circ\text{C}$  in the presence of an alkali metal such as the Na–K alloy<sup>234,235</sup> or of an organometallic compound<sup>234</sup> under  $\sim 30$  atm of olefin. Heterogeneous catalysts constituted by potassium on alumina and on magnesia<sup>236</sup> or  $\text{K}_2\text{CO}_3$ <sup>178</sup> or cesium on nanoporous carbon are also active for this reaction.<sup>237</sup> Similar reactions occur with ethylene.<sup>237</sup> In similar industrial processes, ortho-xylene reacts with 1,3-butadiene forming 5-tolyl-2-pentene with fixed bed K/CaO (AMOCO process) or Na/ $\text{Na}_2\text{CO}_3$  catalysts at  $140\text{ }^\circ\text{C}$  (Teijin process).<sup>177</sup>

For selective position isomerization of complex olefins, strong bases are needed working at low temperature. Sumitomo developed Na/ $\text{NaOH}/\text{Al}_2\text{O}_3$  catalysts for the isomerization of 5-vinylbicyclo-[2.2.1]-hept-2-ene into 5-ethylidenebicyclo-[2.2.1]-hept-2-ene, and of 2,3-dimethyl-1-butene into 2,3-dimethyl-2-butene.<sup>177</sup>

---

## 8.8 Organo-inorganic hybrid materials

An extremely large variety of materials<sup>238,239</sup> have been prepared and tested in catalysis, adsorption and other applications, which can be defined as organo-inorganic hybrid materials.

Among them, a first family consists of functionalized microporous and mesoporous solids,<sup>240</sup> mainly based on silica. The surface acido-basicity of silica-based oxides may be modified by grafting functionalized organosilicon compounds.<sup>241</sup> A very simple approach consists in the impregnation of organic molecules or



precursors on the silica surface, a second more selective approach is grafting of organosilanes.<sup>242</sup> Trialkoxy-silyl derivatives carrying organic functions react with surface silanol groups,<sup>243–245</sup> producing materials carrying this function (e.g., amine or thioalcohol groups) at its surface. Mesoporous materials such as aminopropyl-modified HMS<sup>246</sup> and aminopropyl-functionalized SBA-15<sup>247</sup> were prepared and used to anchor organic molecules that can show basicity<sup>248</sup> and activity in basic catalysis as first shown by Macquarrie.<sup>249</sup> These solid materials, carrying basicity similar to that of amines, need to be used in mild conditions to avoid decomposition of the organic moieties. Similar amine-treated solid surfaces, such as aluminas impregnated with amines have been developed, mainly as adsorbents for CO<sub>2</sub>,<sup>250</sup> but could also find application as catalysts or modified catalyst supports.

The oxidation of mercaptopropylsilyl groups grafted on silicas allows the production of sulfonic groups giving rise to acidic micro- and mesoporous solids active in catalysis.<sup>251</sup> Alternatively, grafting of aromatic molecules followed by sulfonation can produce acidic arenesulfonic groups anchored on silica, giving rise to acidic catalysts too.<sup>251</sup> Polymer-oxide hybrid materials based on nonporous silica-supported sulfonic acid-containing polymer brush materials can also be prepared and are proposed as a new class of potentially water-tolerant solid acid catalysts.<sup>252</sup>

Another approach to produce mesoporous organosilicas is cocondensation.<sup>241</sup> During cocondensation synthesis, the kind of organosilanes added to undergo coassembly with the silica precursor (e.g., TEOS) and the kind of templating agents used in the reaction can determine what types of mesophases, template–silicate aggregates, and organic-functionalized mesoporous silica materials form.

These kinds of materials are commercial, such as the SiliaCat products,<sup>253</sup> polymer grafted silicas, etc. All these materials have or may have large surface area and variable functionalities, allowing acid or basic catalytic behavior or grafting or supporting of metal complexes, thus being available to heterogenize homogeneous catalysts.

A second family of hybrid organo-inorganic materials<sup>254</sup> consists in lamellar materials, such as clays<sup>255</sup> and hydrotalcites, zirconium phosphates, etc., whose interlayer structure contains intercalated organic species.<sup>239</sup> These materials are applied to different technologies, and can also find application in heterogeneous catalysis as supports or as catalysts.

---

## 8.9 Carbon-based materials

A number of different materials essentially or entirely constituted by elemental carbon are available commercially or can be prepared in laboratories. They are of interest in the field of catalysis, mainly as catalyst supports<sup>256–261</sup> but also, in some cases, as active catalytic materials.

Most of them (Table 8.1) attract interest due to several specific properties, such as (in many cases) the high surface area, the ability to disperse metal particles, a moderate thermal stability, the resistance to acid/basic media, the possibility to control (up to certain limits) porosity and surface chemistry, and the easy recovery of

**Table 8.1** Adsorption Properties of CNT, GNF, Activated Carbon (AC) and Graphite<sup>256</sup>

Type of Carbon	Porosity (cm <sup>3</sup> /g)	S (m <sup>2</sup> /g)	Thermal Resistance in Air Atmosphere (°C)
SWNT	Microporous, $V_{\text{micro}}$ : 0.15–0.3	400–900	~800
MWNT	Mesoporous, $V_{\text{meso}}$ : 0.5–2	200–400	~650
GNF	Mesoporous, $V_{\text{meso}}$ : 0.5–2	10–200	~600–900
AC	Microporous	700–1200	~500–600
HSAG	Mesoporous	60–300	~800

*Abbreviations: SWNT, single wall carbon nanotubes; MWNT, multiply walled CN; GNF, graphite nanofibers; HSAG, high surface-area graphite.*

supported precious metals by support burning resulting in a low environmental impact. Among these materials, some of them are also cheap and easily available, others are more specialized and expensive.

## 8.9.1 Carbon materials

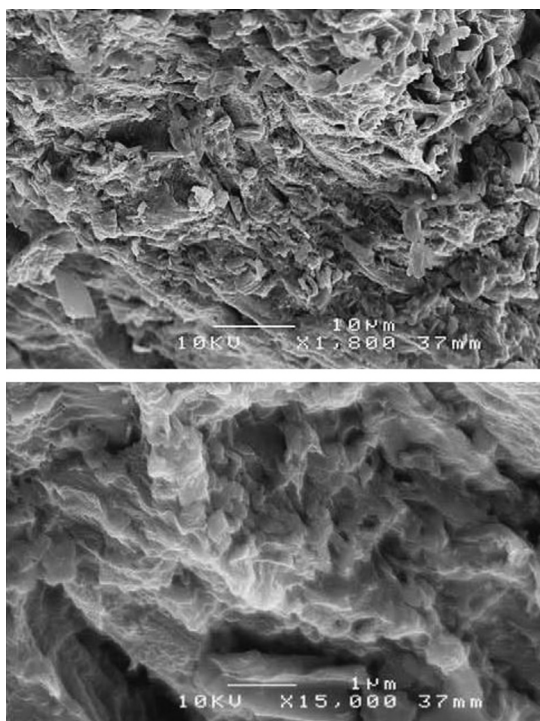
### 8.9.1.1 Activated carbons and impregnated activated carbons

Activated carbons (ACs)<sup>262</sup> are produced by pyrolysis of different carbonaceous materials such as coal, polymers, vegetables, etc. They are very high surface-area materials (>1000 m<sup>2</sup>/g), very active in adsorption, both at the liquid–solid and at the gas–solid interfaces. In Figure 8.4 scanning electron micrographs of a commercial sample are shown.<sup>263</sup> The real nature (weakly acidic or weakly basic) of the AC surfaces in contact with water strongly depends on pH. At low pH, the basic surface sites (ketonic groups, alcoholic groups) are protonated while, at high pH, carboxylic acid groups are dissociated. The presence of carboxylic acid groups gives rise to higher acidity: these groups may be produced by oxidation by chemical oxidants such as HNO<sub>3</sub>, and decompose by heating at c. 240 °C with the evolution of CO<sub>2</sub>. Carbonyl-quinone groups are more thermally stable and decompose with the evolution of CO: they are responsible for slightly basic surface chemistry.

Additionally, the nature of inorganic matter in coal-derived ACs may also play a role in determining surface acid–base behavior. To increase adsorption ACs are frequently impregnated, e.g., by alkali oxides or carbonates, thus becoming strongly basic materials. ACs have large application as adsorbents for both wastewater and waste-gas purification, but find significant industrial application as catalyst supports (see below).

### 8.9.1.2 AC fibers

AC fibers are produced by carbonization of polymeric fabrics, such as e.g., rayon fibers. High surface area (>1000 m<sup>2</sup>/g), the high carbon purity, and the presence of functional groups on the surface are among the most interesting properties of these materials.

**FIGURE 8.4**

Scanning electron micrographs of active carbon NORIT ROW 0.8 SUPRA.

*Reprinted with permission from Ref. 263.*

### **8.9.1.3 Carbon blacks**

The furnace black process represents the most important production method of carbon blacks, in which the starting material (hydrocarbons such as natural gas or oil fractions from petroleum processing) is fed to a furnace and burned with a limited supply of air at about 1400 °C. Carbon blacks have high specific surface area contributed mostly by micropores less than 1 nm. Due to the nature of the starting materials, the ash content of carbon black is very low, frequently well below 1 wt %. Due to its low cost and high availability, oil-furnace carbon black has been used widely as the support for platinum catalyst in low-temperature fuel cells.

### **8.9.1.4 Ordered mesoporous carbons**

Ordered mesoporous carbons, with controllable pore sizes, high surface areas (up to 1800 m<sup>2</sup>/g), and large pore volumes, may be synthesized using ordered mesoporous silica templates. Infiltration of the pores of MCM-48, SBA-1, SBA-15, KIT-6 mesoporous silicas, used as templates, is performed with appropriate carbon precursors (furfuryl alcohol, sucrose, acenaphthene and mesophase pitch, etc.). By

introducing amines, nitride carbon can be produced.<sup>264</sup> Carbonization of the organic matter is followed by template removal. The resultant carbon morphology depends on the structure of the template. The template needs to exhibit 3D pore structure in order to be suitable for the ordered mesoporous carbon synthesis, otherwise disordered microporous carbon is formed. They were successfully used to synthesize carbons with cubic or hexagonal frameworks and narrow mesopore-size distributions.

#### **8.9.1.5 Carbon gels**

Carbon gels are obtained by the carbonization of organic gels, commonly obtained by polycondensation of resorcinol [ $C_6H_4(OH)_2$ ] and formaldehyde (HCHO) (R/F) in a slightly basic aqueous solution, followed by drying and pyrolysis in an inert atmosphere. There are three type of carbon gels, depending on the synthesis method: carbon aerogels, carbon xerogels and carbon cryogels. Their synthesis method only differs in the way of drying. An aerogel is produced when the solvent contained within the voids of a gelatinous structure is exchanged with an alternative solvent, such as liquid  $CO_2$ , that can be removed supercritically in the absence of a vapor–liquid interface and thus without any interfacial tension. A xerogel is produced when the solvent is removed by conventional methods such as evaporation under normal, nonsupercritical conditions. Cryogels are obtained by freeze drying. The surface area, pore volume, and pore-size distribution of carbon gels are tunable surface properties related to the synthesis and processing conditions.

#### **8.9.1.6 High surface-area graphite**

High surface-area graphite (HSAG) is obtained by recrystallization of the spherical carbon black particles at 2500–3000 °C. The partially crystallized material possesses well-ordered domains. The degree of graphitization is determined by process temperature. After a special grinding process, resulting surface areas are of the order of 100 m<sup>2</sup>/g.

#### **8.9.1.7 Graphene nanosheets**

Graphene is a two-dimensional one-atom-thick planar sheet of sp<sup>2</sup>-bonded carbon atoms, having a thickness of 0.34 nm. The most common method to obtain graphene nanosheets (GNS) consists in the oxidation of graphite to graphene oxide (GO), followed by exfoliation and reduction of GO to GNS.

#### **8.9.1.8 Carbon nanotubes and nanofibers**

Carbon nanotubes (CNs) and nanofibers are graphitic filaments, also denoted as whiskers, with diameters ranging from 0.4 to 500 nm and lengths from several micrometers to millimeters.<sup>265</sup> Commonly, staked and herringbone forms are denoted as “carbon nanofibers” or “graphite nanofibers”, while tubular graphene is denoted as “nanotube”. A main difference between nanotubes and nanofibers is the absence of inner hollow space in the latter. CNs can be divided essentially into two

categories: single wall carbon nanotubes (SWNT) and multiply walled CN (MWNT). Ideally, a SWNT is made of a perfect graphene sheet rolled up into a cylinder and closed by two caps (semifullerenes). The internal diameter of these structures can vary between 0.4 and 2.5 nm. MWNT can be considered as concentric SWNT with increasing diameter and coaxially disposed. The number of walls present can vary from two (double-wall nanotubes) to several tens, so that the external diameter can reach 100 nm. The concentric walls are regularly spaced by 0.34–0.39 nm the larger the external diameter, the lower the internal intershell spacing, a little higher than the interlayer distance evidenced in graphite single crystals (0.335 nm). It is worth noting that residual metallic particles coming from the production process can be found in the inner cavity of MWNT. In Figure 8.5, transmission and scanning electron microscopies of CNs are reported.<sup>266</sup> In Figure 8.6 a TEM image of a CNT-supported Pd catalyst is shown.<sup>267</sup>

The current existing methods for CNT production are energy- and resource-intensive, and include (but are not limited to) electric arc discharge method, laser ablation method, catalytic chemical vapor deposition (CVD), flame synthesis and the solar energy route. Among these methods, CVD seems to currently be the most promising and preferred method for large-scale production. In this case, hydrocarbons such as methane, ethylene, acetylene, etc. are converted over metal catalysts such as supported Fe, Co, Ni at 400–1000 °C.

CNs and nanofibers are active as catalysts in some reactions, but, after functionalization, e.g., by oxidation with nitric acid, are supports for excellent metal catalysts mainly for hydrogenations, as well as fuel cell electrocatalysts.<sup>256</sup>

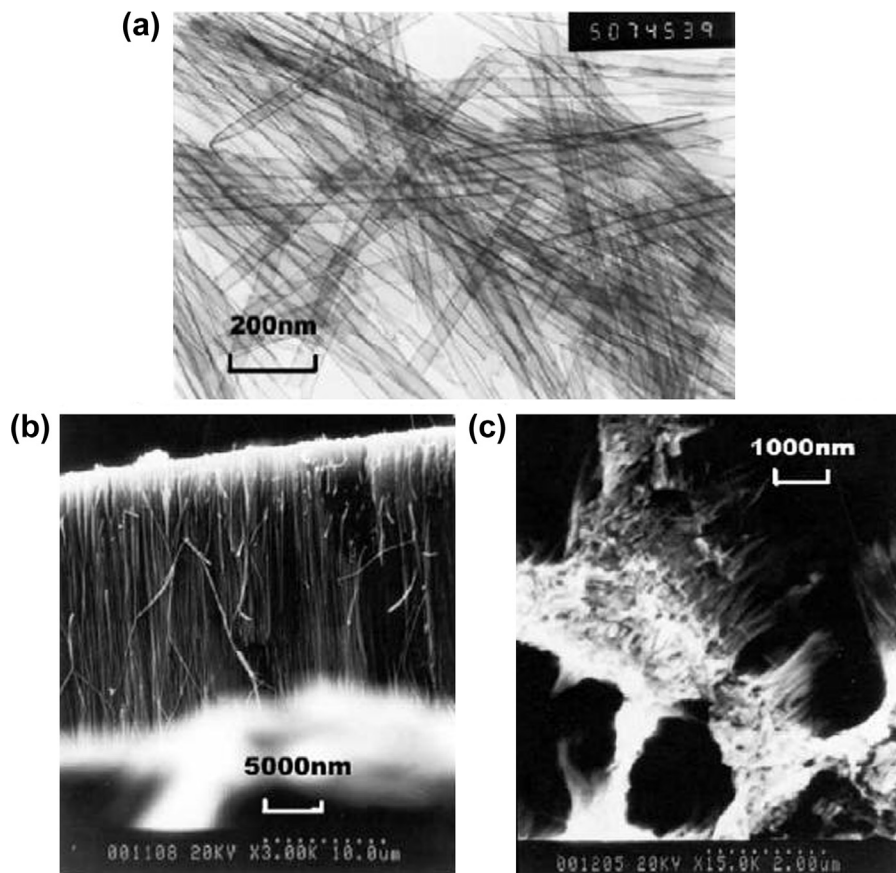
### 8.9.1.9 Fullerenes and fullerene black

The production of higher fullerenes by the classical method of graphite vaporization encounters problems due to the low yield, nonselective carbon cage formation and very demanding associated purification issues. Therefore, synthetic methods are needed that will produce a single isomer of a desired fullerene, free from impurities of other isomers or fullerenes of different sizes.

Fullerene black is the insoluble residue after extraction of fullerenes from the product of electric arc or laser evaporation of carbon materials such as graphite.<sup>268</sup> It is a fine black powder with high surface area (300 m<sup>2</sup>/g) that represents the larger product of the process.

Fullerenes were found to catalyze coupling and transalkylation reactions of mesitylene, engage in transfer hydrogenations with dihydroaromatics, and cleave strong bonds such as those in diarylmethanes. In all of these reactions, fullerenes show a marked ability to accept and to transfer hydrogen atoms.<sup>269</sup>

Fullerenes (C<sub>60</sub> and C<sub>70</sub>) were recently shown to be active in the hydrogenation of nitrobenzene, after activation to form the fullerene anion. However, the catalyst in this reaction is shown to contain residual nickel from the activation of the catalyst, which, as indicated by a series of control experiments, is most likely responsible for the catalytic conversion.<sup>270</sup>



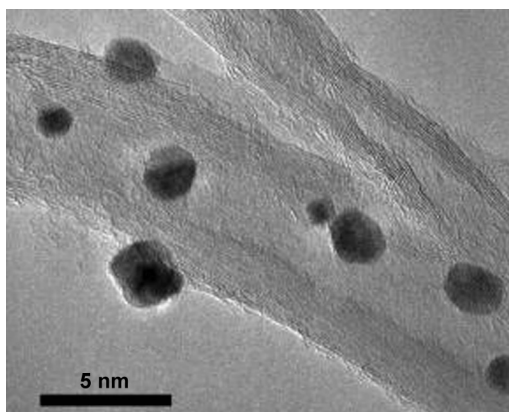
**FIGURE 8.5**

Transmission electron microscopy (TEM) and scanning electron microscope (SEM) images of carbon nanotubes (CNs) and its array electrode membranes prepared by alumina template. (a) TEM image of CNs prepared by alumina template; (b) and (c) are SEM images of CN array electrodes membranes: (b) cross-section, (c) upper surface of the CN array membrane.

*Reprinted with permission from Ref. 266.*

Fullerene-like cages, which can be opened and closed through simple thermal treatments, have been prepared.<sup>271</sup> Catalytic measurements show that the open cages displayed strikingly higher activity for the oxidative dehydrogenation of isobutane in comparison to the closed ones.

Fullerene and fullerene black can be used as support for metal catalysts<sup>268</sup> platinum nanoparticles on fullerene black are effective catalysts of 1-decene and nitrobenzene hydrogenation.<sup>272</sup>

**FIGURE 8.6**

Transmission electron microscopy micrograph of a catalyst composed of Pd-supported on carbon nanotubes.

*Reprinted with permission from Ref. 267.*

### 8.9.2 Carbon materials as catalyst supports

ACs,<sup>257</sup> carbon blacks and graphites find large application as supports for industrial metal catalysts.<sup>273,274</sup> ACs are reported to act as activating supports for noble metals and base metals such as iron, manganese, copper for hydrogenations and hydrotreatings, as well as for oxidations performed in mild conditions, such as low-temperature CO oxidation, catalytic wet air oxidation for the destruction of organic pollutants in water and for liquid-phase oxidations in water with hydrogen peroxide, and for partial oxidations.

In particular, metals supported on carbons are largely applied to liquid-phase hydrogenation reactions. Hydrogenation of nitrobenzene to aniline is performed with different processes and reactor systems, mainly using carbon supported metals as catalysts. The Dupont–KBR process<sup>275</sup> uses a noble-metal-on-carbon catalyst in a plug flow reactor. A similar process is reported to be carried out in liquid phase at 75 °C, 30 bar over carbon supported palladium to produce toluene diamine from dinitrotoluene. Selectivity in hydrogenation of nitro compounds may become an issue if other functional groups like double bonds, triple bonds or halogen substituents, aromatic rings, carbonyls and even oximes are present.<sup>276</sup> Vanadium-promoted Pt catalysts (1–3% Pt, 0.5–2% V) are available from Evonik for this application.<sup>277</sup>

Another reaction performed on carbon-supported platinum group metals is the reductive alkylation of alkyl and aryl amines with ketones or aldehydes. Platinum is more effective than palladium in alkylating amines and carbonyls of higher molecular weight. Typical operating conditions for reductive alkylation include pressure of 5–35 bars and temperature of 50–150 °C.

Carbon-supported noble metals are also applied to hydrogenate acetylenics: hydrogenation of the  $\alpha$ -methyl-styrene is performed in the cumene synthesis processes using Ni- or Pd-based catalysts, on alumina or on carbon supports.<sup>278</sup> Carbon supports can also be used for supporting alkali metal catalysts: cesium on nanoporous carbon is an excellent catalyst for the synthesis of isobutylbenzene from toluene and propylene in this reaction.<sup>237</sup>

More stable supports such as graphites can also be applied to gas-phase reactions: in the 1990s, Kellogg Brown and Root (KBR) developed a new ammonia synthesis process based on Ru/C catalysts denoted as KAAP™ (Kellogg Advanced Ammonia Process), in substitution of the classical iron-based catalysts. The proprietary KAAP™ catalyst, which is manufactured and guaranteed by BASF Catalysts LLC under exclusive license to KBR, consists of ruthenium on a stable, HSAG carbon base.<sup>279</sup> According to the literature, it should contain alkali and alkali earth promoters such as K, Cs and Ba.<sup>280,281</sup>

The direct synthesis of hydrogen peroxide from hydrogen and oxygen,<sup>282</sup> which could substitute the older anthraquinone based process, may be performed over noble metal catalysts. The catalysts described in the literature are based on noble metals or combinations thereof supported on a great variety of substrates such as alumina, silica and carbon. Palladium is the most suitable active metal in most catalyst formulations. Acids are often incorporated into the reaction medium in addition to the heterogeneous. Degussa–Headwaters developed a production plant for the direct synthesis of hydrogen peroxide coupled with propylene oxide production. The patents of these companies reveal that palladium nanoparticles deposited on carbon and an appropriate solvent (in general an alcohol), as well as the use of concentrations of hydrogen outside the flammability limits, are appropriate for industrial H<sub>2</sub>O<sub>2</sub> production.

Carbon-supported metals are also used for oxidation reactions such as gold supported on carbon for glycerol oxidation.<sup>260,283,284</sup>

### 8.9.3 Modified carbons as catalysts

#### 8.9.3.1 Sulfonated carbon materials as acid catalysts

Sulfonic-acid containing carbon materials can be prepared by two different routes, such as incomplete carbonization of sulfonated organic compounds, leading to high concentration of sulfonic acid groups (>4 mmol/g) and sulfonation of partially carbonized materials, producing less densely sulfonated carbons (<2.5 mmol SO<sub>3</sub>H/g).<sup>285,286</sup> The latter is the most common and safe procedure. The starting materials to be carbonized are either synthetic polymers or natural carbon-rich materials such as sugars, starch, celluloses. The carbonization temperature is a key factor in determining the nature of the carbon material and also the amount of sulfonic acid groups that can be introduced: higher carbonization temperature results in more sp<sup>2</sup>-hybridized carbon and lower concentration of sulfonic groups. The acid strength of the resulting materials is similar to that of sulfonic acids. However, the catalytic activity of such materials for some reaction



performed in aqueous phase is far higher (based on catalyst weight) than that of other sulfonated solids (such as nafion and amberlyst resins), and inorganic solids such as niobic acid and zeolites. This is the case, e.g., of the hydrolysis of  $\beta$ -1,4-glucan, i.e., cellulose oligomers. This is an important process of very high potential interest to produce glucose without the use of enzymes, to further convert it into bioethanol of cellulosic origin.

A number of other carbon materials presenting sulfonic<sup>287,288</sup> and carboxylic functionalities are reported to be active acid catalysts.

### **8.9.3.2 Nitrided carbon material as basic catalysts**

3D mesoporous carbon nitride (C/N ratio c. 4.3), produced using mesoporous silica KIT-6 with 3D porous structure and different pore diameters as hard templates, and ethylenediamine and carbon tetrachloride as the sources for N and C, respectively, were recently prepared and tested as basic catalyst. These materials revealed excellent activity in the base-catalyzed Knoevenagel condensation of benzaldehyde and malononitrile, allowing high yield of the  $\alpha,\beta$ -unsaturated nitrile in a short reaction time even at room temperature. These catalysts are highly stable and can be recyclable several times without affecting their activity.<sup>264</sup>

---

## **8.10 Polymeric solid acids and bases (ion exchange resins)**

Ion exchange resins were introduced in the 1960s and find today large application in many fields,<sup>289</sup> in particular in absorption processes including water purification as well as catalysts in the chemical industry.<sup>290–293</sup> The most used materials are macroreticular polystyrene-based ion-exchange resins with 20% divinylbenzene, like the materials of the Amberlyst<sup>®</sup> family produced by Rohm and Haas.<sup>294</sup> A number of similar materials are available from other suppliers.<sup>293</sup> Sulfonated cation exchange resins in the protonic form, whose surface area is near 50 m<sup>2</sup>/g, have a strong acidity associated to the aryl-sulfonic acid groups Ar–SO<sub>3</sub>H. These are actually the active sites in nonpolar conditions, but at high water or alcohol contents in the medium, the less-active solvated protons act as the acids.<sup>295</sup> These materials are prepared as “gel” resins in the form of uniform beads, and as “macroporous” materials. Due to restricted diffusion, the acid sites in the gels are only accessible when the beads are swollen. “Macroporous” resins are prepared with permanent porosity, thus more acid sites are accessible also in nonswelling solvents, although diffusion of the reactant in the polymer matrix is also determinant.<sup>296</sup> The number of acid sites in sulfonated polystyrene is relatively high, 4.7 eq/kg for Amberlyst<sup>®</sup> –15, 5.4 eq/kg for the hypersulfonated resin Amberlyst<sup>®</sup> –36. However, the acid strength is considered to be relatively low, the Hammett acidity function being evaluated to be  $H_0 = -2.2$ . Another limit of these materials consists in the limited stability temperature range, <150–180 °C.

The application of these materials is limited to relatively nondemanding acid-catalyzed reactions in the liquid phase. They are in fact the catalysts for branched

olefin etherification industrial processes such as MTBE,<sup>297</sup> ETBE, TAME and TAEE syntheses. In the Snamprogetti process, MTBE synthesis is performed in the liquid phase at 40–80 °C and 7–15 atm C<sub>4</sub> cut pressure, with a water-cooled multitubular reactor and an adiabatic finishing reactor in series.<sup>298</sup> CD-tech proposes catalytic distillation reactors using cylindrical bales containing the ion exchange resin in the packing of the tower.<sup>299</sup> The MTBE process may be modified to obtain MTBE/isobutylene dimer coproduction.<sup>300</sup> The same catalysts and modified MTBE processes may be applied for isobutylene di- and trimerization.<sup>301</sup> The reaction conditions are similar, but the inactive alcohol TBA is added instead of methanol. TBA does not react with isobutylene, but its presence strongly increases dimer selectivity although decreasing isobutylene conversion. Oligomerization of propene and isoamylene can also be performed. When a real C<sub>4</sub> cut is fed, also linear butylenes react, together with isobutylene, to a small extent.<sup>302</sup> Similar resins are also amply used in phenol alkylation processes.<sup>41</sup> In this case, the reaction temperature is in the range 100–130 °C. Another relevant industrial application is the synthesis of Bisphenol A by condensation of phenol and acetone, performed with fixed bed of sulfonic acid resins at 50–80 °C.<sup>303</sup> In the QBIS process from Dow several fixed bed reactors plus a rearrangement reactor, also with a fixed bed of the “QCAT” catalyst (a sulfonated resin), to convert byproducts into the desired product Bisphenol A, i.e., the para-, para- isomer.<sup>304</sup>

Sulfonated polystyrene polydivinylbenzene (PDVB) resins are deactivated by basic impurities in the feed such as nitriles (typically present in the C<sub>4</sub> cut after FCC),<sup>305</sup> as well as by cations such as Na<sup>+</sup> and Fe<sup>3+</sup>.<sup>306</sup> Washing procedures can be applied to the catalysts to rejuvenate them. By using water-cooled multitubular reactors, the hot spot due to the exothermic reaction is, when the bed is fresh, at the entrance of the tubes, but it tends to move toward the exit by increasing time on stream due to partial deactivation of the bed. This allows to follow the progressive catalyst deactivation. When the hot spot is at the exit of the bed the catalyst must be substituted. In the use of sulfonated resins for olefin oligomerization catalyst, fouling by higher oligomers may occur.

Nafion<sup>®</sup> is a strongly acidic resin produced by Dupont,<sup>307</sup> a copolymer of TFE and perfluoro-3,6-dioxa-4-methyl-7-octenesulfonyl fluoride, converted to the proton (H<sup>+</sup>) form. Nafion is definitely more acidic than polystyrene-based sulfonic resins. This material, largely used in electrochemical processes as membrane for chlor-alkali cells and as electrolyte for proton exchange membrane fuel cells, may also act as a very strong Brønsted-acid solid catalyst. It carries the strongly acidic terminal –CF<sub>2</sub>CF<sub>2</sub>SO<sub>3</sub>H group, which is however converted into solvated protons in the presence of water.<sup>308</sup> This material is both chemically stable (as expected due to the fluorocarbon nature of the backbone) and thermally stable up to 280 °C, at which temperature the sulfonic acid groups begin to decompose. It is commercialized in the form of membranes, of beads and of dispersions in water and aliphatic alcohols solutions.

It is generally accepted that perfluorinated resinsulfonic acids are very strong acids with values of the Hammett acidity function ( $H_0 = -11$  to  $-13$ ), which allow

the application of the term “superacid”. However, the density of the protonic sites in the pure polymer is very small (0.9 eq/kg), the surface area very low (0.02 m<sup>2</sup>/g) and the site availability is very small. Consequently, the activity of this material either in nonswelling solvents or in the gas phase is very low. This limited very much actual application in catalysis.

A different perspective is born with the development of Nafion<sup>®</sup> resin/silica nanocomposites, which may function in nonswelling solvents. A nanometer-sized colloidal dispersion of Nafion in polar solvents is mixed with a soluble silica precursor. Those materials<sup>309</sup> are called SAC (Solid Acid Catalysts) followed by the Nafion loading, e.g., SAC 80 for 80% Nafion in the silica matrix. The BET surfaces of such materials are up to 20,000 times higher than pure Nafion depending on the preparation method. The pore size can be adjusted to values larger than 100 Å. Due to the better accessibility of the catalytically active acid sites, the activity of these composites is much higher than of pure Nafion. Furthermore, the higher thermostability of these new catalysts of up to 320 °C enables the possibility to work in the gas phase. There is no need of polar solvents for swelling the Nafion anymore allowing working in nonpolar solvents. This material has been successfully tested in several reactions such as isobutane/butylene alkylation.<sup>310</sup> Attempts to develop industrial processes are reported, e.g., for the liquid-phase oligomerization of tetrahydrofuran and for the oligomerization of olefins.<sup>163</sup>

The used Nafion-based catalysts can be regenerated by washing with nitric acid. However, a relevant limit of Nafion-based materials is related to this unsafe disposal and to the toxicity of their thermal degradation products in case of heating above 280 °C.<sup>311</sup>

Basic anion exchangers are mostly characterized by the presence of the trimethylammonium functional group bonded to the aromatic rings, counterbalanced by anions such as the hydroxide anion. These materials are active as catalysts e.g., of methanol carbonylation to methyl formate and in the Knoevenagel and aldol condensations.<sup>312</sup>

Anionic exchange resins are alternative to metal oxides for aldol condensation catalysts.<sup>293,313</sup> They are used industrially for acrylate/HCHO-condensation to alpha-hydroxymethylacrylate in liquid-phase (Nippon Shokubai<sup>313</sup>) and methanol-carbonylation with CO to methyl formate in liquid phase for replacing alkali alkoxide (Mitsubishi Gas Chemical<sup>312,313</sup>). Condensation of acetone to diacetone alcohol can be readily catalyzed by various weak base (Amberlyst<sup>™</sup> A21 weak-base macroporous polystyrene-based catalyst) and strong-base (Amberlyst<sup>™</sup> A26) polymeric catalysts. The aldol condensation of citral with acetone at 55 °C under a strong-base gel resin catalyst (Amberlite<sup>™</sup> IRA400) allows 90–95% conversion with 5–10% unreacted citral. The resulting product is pseudoionone, which is a commercial intermediate for the production of flavors like alpha and beta ionones and also for the synthetic production of vitamins.

A very important additional application of ion exchange resins is as supports for homogeneous metal catalysts, allowing heterogenization, easier recovery and recycle (chapter 12.2)<sup>314</sup>. Among the many examples, we can cite the heterogeneous catalysts

based on Rh complex immobilized on polyvinylpyridine resin used in the Chyoda Acetica process for the synthesis of acetic acid via carbonulation of methanol.<sup>315</sup>

High surface-area mesoporous resins<sup>316</sup> can be prepared (>500 m<sup>2</sup>/g) whose functionalization could give rise to active catalysts.

---

## References

- Zhang D, Zhou C-H, Lin C-X, Tong D-S, Yu W-H. *Appl Clay Sci* 2010;**50**(1):1–11.
- Theng BKG. Chapter 1 – The Clay Minerals. *Dev Clay Sci* 2012;**4**:3–45.
- Sadeghbeigi R. FCC catalysts. In: *Fluid catalytic cracking handbook*. 3rd ed. Elsevier; 2012, ISBN 9780123869654; 2012. pp. 87–116.
- Hu R, Zhao X, Wormsbecher RF, Ziebart MS. *Gasoline sulphur reduction catalyst for FCC process*. US Patent 8,084,383 B2 to WR Grace & Co; 2011.
- Bhattacharyya KG, Gupta SS. *Adv Colloid Interface Sci* 2008;**140**:114–31.
- Castellano M, Turturro A, Riani P, Montanari T, Finocchio E, Ramis G, et al. *Appl Clay Sci* 2010;**48**(3):446–54.
- Lenarda M, Storaro L, Talon A, Moretti E, Riello P. *J Colloid Interface Sci* July 15, 2007;**311**(2):537–43.
- Liu C, Denga Y, Pan Y, Zheng S, Gao X. *Appl Catal A Gen* 2004;**257**:145.
- Mahgoub KA, Al-Khattai S. *Energy & Fuels* 2005;**19**:329.
- Ding Y, Liang J, Fan Y, Wang Y, Bao X. *Catal Today* July 30, 2007;**125**(3–4):178–84.
- Gao X, Tang Z, Lu G, Zhang H, Wang B. *J Industrial Eng Chem* 2012;**18**(2):591–3.
- Zatta L, Gardolinski JEFDC, Wypych F. *Appl Clay Sci* 2011;**51**(1–2):165–9.
- Pushpaletta P, Lalithambika M. *Appl Clay Sci* 2011;**51**:424–30.
- <http://www.sigmaaldrich.com/catalog/product/aldrich/69866?lang=it&region=IT>; 21.01.2013.
- Flessner U, Jones DJ, Rozière J, Zajac J, Storaro L, Lenarda M, et al. *J Mol Catal A Chem* 2001;**168**:247.
- <http://www.sigmaaldrich.com/catalog/product/fluka/69904?lang=it&region=IT>; 21.01.2013.
- Hart MP, Brown DR. *J Mol Catal A Chem* 2004;**212**:315.
- Vogels RJMJ, Klopogge JT, Geus JW. *J Catal* 2005;**231**:443.
- Yang H, Wilson M, Fairbridge C, Ring Z. *Energy & Fuels* 2002;**16**:855.
- Yadav GD, Salgaonkar SS. *Ind Eng Chem Res* 2005;**44**:1706.
- Goncalvez De Almeida JL, Berna Tejero JL. US Patent 8148592, to Cepso Quimica, S.A.; 2012.
- Nagendrappa G. *Appl Clay Sci* 2011;**53**:106–39.
- Baghernejad B. *Lett Org Chem* April 2010;**7**(3):255–68.
- Kaur N, Kishore D. *J Chem Pharm Res* 2012;**4**(2):991–1015.
- Zhou CH, Tong D, Li X. In: Gil A, Korili SA, Trujillano R, Vicente MA, editors. *Pillared clays and related catalysts*. Springer; 2010. pp. 67–98.
- Velasco J, Pérez-Mayoral E, Mata G, Rojas-Cervantes ML, Vicente-Rodríguez MA. *Appl Clay Sci* November 2011;**54**(2):125–31.
- Zhou CH. *Appl Clay Sci* 2011;**53**:87–96.
- Gil A, Korili SA, Vicente MA. *Catal Rev Sci Eng* 2008;**50**(2):153–221.
- Gil A, Korili SA, Trujillano R, Vicente MA, editors. *Pillared clays and related catalysts*. Springer; 2010.

30. Aouad A, Mandalia T, Bergaya F. *Appl Clay Sci* 2005;**28**:175–82.
31. Duong LV, Klopogge JT, Frost RL, van Veen JAR. *J Porous Mater* 2007;**14**:71–9.
32. Trombetta M, Busca G, Lenarda M, Storaro L, Ganzerla R, Piovesan L, et al. *Appl Catal A Gen* 2000;**193**:55.
33. <http://www.sigmaaldrich.com/catalog/product/aldrich/69907?lang=it&region=IT>; 21.01.2013.
34. Ocelli ML. *Chemtech* 1994;**24**.
35. Tanabe K, Hölderich WF. *Appl Catal A Gen* 1999;**181**:399.
36. Ding Z, Klopogge JT, Frost RL, Lu GQ, Zhu HY. *J Porous Mater* 2001;**8**:273.
37. Albertazzi S, Baraldini I, Busca G, Finocchio E, Lenarda M, Storaro L, et al. *Appl Clay Sci* 2005;**29**:224.
38. Kanda Y, Iwamoto H, Kobayashi T, Uemichi Y, Sugioka M. *Top Catal* 2009;**52**:765–71.
39. Chauvel A, Delmon B, Holderich W. *Appl Catal A Gen* 1994;**115**:173.
40. De Stefanis A, Tomlinson AAG. *Catal Today* 2006;**114**:126.
41. Binitha NN, Sugunan S. *Microporous Mesoporous Mater* 2006;**93**:82–9.
42. Chmielarz L, Piwowarska Z, Kuśtrowski P, Wegrzyn A, Gil B, Kowalczy A, et al. *Appl Clay Sci* 2011;**53**:164–73.
43. Belver C, Aranda P, Martín-Luengo MA, Ruiz-Hitzky E. *Microporous Mesoporous Mater* 2012;**147**:157–66.
44. Galarneau A, Borodawalla A, Pinnavaia TJ. *Nature* 1995;**374**:529.
45. Polverejan M, Liu Y, Pinnavaia TJ. *Chem Mater* 2002;**14**:2283.
46. de Paiva LB, Morales AR, Valenzuela Díaz FR. *Appl Clay Sci* 2008;**42**(1–2):8–24.
47. Miller BC. *Coal Energy Systems*. Elsevier; 2005. p 292.
48. Srivastava RK, Jozewicz W. *J. Air & Waste Manage. Assoc.* 2001;**51**:1676–88.
49. Gunasekaran S, Anbalagan G. *Bull Mater Sci* 2007;**30**:339–44.
50. Kiriubakaran V, Sivaramakrishnan V, Nalini R, Sekar T, Premalatha M, Subramanian P. *Renew Sust Energy Rev* 2009;**13**:179–86.
51. Torres W, Pansare SS, Goodwin Jr JG. *Catal Rev Sci Eng* 2007;**49**:407–56.
52. Fauth D, Frommell EA, Hoffmann JS, Reasbeck RP, Pennline HW. *Fuel Process Technol* 2005;**86**:1503.
53. Feng B, An H, Tan E. *Energy & Fuels* 2007;**21**:426.
54. Frost RL, Kristof J, Horvath E. *J Therm Anal Calorim* 2009;**98**(3):749–55.
55. Sivaiah MV, Robles-Manuel S, Valange S, Barrault J. *Catal Today* 2012;**198**:305–13.
56. Conrad Zhang Z. *Adv Catal* 2006;**40**:153.
57. Sartori G, Maggi R. Update 1 of: use of solid catalysts in Friedel–Crafts acylation reactions. *Chem Rev* 2011;**111**(5):PR181–214.
58. Baumgarten E, Weinstrauch F. *Spectrochim Acta* 1979;**35A**:1315.
59. Carmello D, Finocchio E, Marsella A, Cremaschi B, Leofanti G, Padovan M, et al. *J Catal* 2000;**191**:354.
60. Digne M, Raybaud P, Sautet P, Guillaume D, Toulhoat H. *J Am Chem Soc* 2008;**130**:11030–9.
61. Davis BH, Antos GJ. In: Antos GJ, Aitani AM, editors. *Catalytic naphta reforming*. CRC Press; 2004. pp. 199–274.
62. Clet G, Goupil J-M, Szabo G, Cornet D, Clet G. *Appl Catal A Gen* 2000;**202**:37.
63. Schmidt F, Köhler E. In: Guisnet M, Gilson JP, editors. *Zeolites for cleaner technologies*. Imperial College Press; 2002. pp. 153–66.

64. Weyda H, Köhler E. *Catal Today* 2003;**81**:51.
65. Cusher NA. In: Meyers RA, editor. *Handbook of petroleum refining processes*. Mc Graw Hill; 2005. p. 9.15–27 and 9.41–46.
66. Lapinski M, Baird L, James R. In: Meyers RA, editor. *Handbook of petroleum refining processes*. Mc Graw Hill; 2005. p. 4.3–31.
67. Regalbuto JR, Antos GJ. In: Antos GJ, Aitani AM, editors. *Catalytic naphtha reforming*. CRC Press; 2004. pp. 141–98.
68. Lacombe S, Boualleg M, Sanchez E. US Patent application 2012/0091038 A1 to IFP; 2012.
69. Jumas JC, Sougrati MT, Olivier-Fourcade J, Jahel A, Avenier P, Lacombe S. *Hyperfine Interact* 2013;**217**:137–44.
70. Roeseler C. In: *Handbook of petroleum refining processes*. Mc Graw Hill; 2005. p. 1.25–32.
71. Feller A, Lercher JA. *Adv Catal* 2004;**48**:229.
72. Rinaldi R, ten Berge G. In: Meyers RA, editor. *Handbook of petrochemical production processes*. Mc Graw Hill; 2005. p. 16.21–39.
73. Trubitsyn DA, Zakharov VA, Zakharov II. *J Mol Catal A Chem* June 1, 2007; **270**(1–2):164–70.
74. Correa A, Credendino R, Pater JTM, Morini G, Cavallo L. *Macromolecules* 2012;**45**:3695–701.
75. Sathe M, Gupta AK, Kaushik MP. *Tetrahedron Lett* 2006;**47**(18):3107–9.
76. Srinivas KVNS, Mahender I, Das B. *Synthesis* 2003;(16):2479–82.
77. Hazarkhani H, Kumar P, Kondiram KS, Shafi Gadwala IM. *Synth Commun* 2010; **40**(19):2887–96.
78. Sathe M, Ghorpade R, Kaushik MP. *Chem Lett* 2006;**35**:1048–9.
79. Borujeni KP, Tamami B. *Catal Commun* 2007;**8**(8):1191–6.
80. Tanabe KK, Cohen SM. *Inorg Chem* July 19, 2010;**49**(14):6766–74.
81. Winfield JM. *J Fluor Chem* 2009;**130**:1069–79.
82. Unveren E, Kemnitz E, Lippitz A, Unger WES. *J Phys Chem B* 2005;**109**:1903–13.
83. Le Bail A, Calvayrac F. *J Solid State Chem* 2006;**179**:3159–66.
84. König R, Scholz G, Scheurell K, Heidemann D, Buchem I, Unger WES, et al. *J Fluor Chem* 2010;**131**:91–7.
85. Barclay CH, Bozorgzadeh H, Kemnitz E, Nickkho-Amiry M, Ross DEM, Skapin T, et al. *J Chem Soc Dalton Trans*; 2002:40–7.
86. Manzer LE, Rao VNM. *Adv Catal* 1993;**39**:329.
87. Morterra C, Cerrato G, Cuzzato P, Masiero A, Padovan MJ. *Chem Soc Faraday Trans* 1992;**88**:2239–350.
88. Krahl T, Vimont A, Eltanany G, Daturi M, Kemnitz E. *J Phys Chem C* 2007;**111**(49):18317–25.
89. Busca G. *Catal Today* 1998;**41**:191–206.
90. Chupas PJ, Corbin DR, Rao VNM, Hanson JC, Grey CP. *J Phys Chem B* 2003;**107**:8327.
91. Scokart O, Selim SA, Damon JP, Rouxhet PG. *J Colloid Interface Sci* 1979;**70**:209.
92. Matulewicz ERA, Kerkhof PJM, Mooulijin JA, Reitsma HJ. *J Colloid Interface Sci* 1980;**77**:161.
93. Rodriguez LM, Alcaraz J, Hernandez M, Dufaux M, Ben Taarit Y, Vrinat M. *Appl Catal A Gen* 1999;**189**:53.
94. Corma A, Fornés V, Ortega E. *J Catal* 1985;**92**:284.

95. Cuevas R, Ramírez J, Busca G. *J Fluor Chem* 2003;**122**:151.
96. Rüdiger S, Eltanany G, Groâ U, Kemnitz EJ. *Sol-Gel Sci Technol* 2007;**41**:299–311.
97. Dambournet D, Eltanamy G, Vimont A, Lavalley J-C, Goupil J-M, Demourgues A, et al. *Chem Eur J* 2008;**14**:6205–12.
98. Wuttke S, Vimont A, Lavalley J-C, Daturi M, Kemnitz E. *J Phys Chem C* 2010;**114**:5113.
99. Guo Y, Wuttke S, Vimont A, Daturi M, Lavalley J-C, Teinz K, et al. *J Mater Chem* 2012;**22**:14587–93.
100. Patil PT, Dimitrov A, Kirmse H, Neumann W, Kemnitz E. *Appl Catal B* 2008;**78**:80–91.
101. Wuttke S, Coman SM, Kröhnert J, Jentoft FC, Kemnitz E. *Catal Today* 2010;**152**:2–10.
102. Kemnitz E, Wuttke S, Coman SM. *Eur J Inorg Chem* 2011:4773–94.
103. Sung DJ, Moon DJ, Moon S, Kim J, Ho SJ. *Appl Catal A General* 2005;**292**:130–7.
104. Bozzano A. In: *Handbook of petroleum refining processes*. Mc Graw Hill; 2005. p. 1.57–68.
105. Kocal JA. US Patent 5196574 to Uop; 1993.
106. Kocal JA. European Patent 0615968 B1 to Uop; 1993.
107. Olson AC. *Ind Eng Chem* 1960;**52**:833.
- 107b. Klapötke TM, McMonagle F, Spence RR, Winfield JM. *J Fluor Chem* 2006;**127**:1446–53.
- 107c. Sadeghi B, Mirjalili BF, Hashemi MM. *Tetrahedron Lett* 2008;**49**:2575.
108. Ono Y. *J Catal* 2003;**216**:406.
109. Blass BE. *Tetrahedron* 2002;**58**:9301–20.
110. Clacens JM, Genuit D, Veldurthy B, Bergeret G, Delmotte L, Garcia-Ruiz A, Figueras F. *Appl Catal B* 2004;**53**:95.
111. Clacens JM, Veldurthy B, Figueras F. *J Catal* 2005;**229**:237.
112. Villemain D, Hachemi M. *React Kinetics Catal Lett* 2001;**72**:3–10.
113. Roberts G, Minihan AR, Laan JAM, Eshuis JJW. United States Patent 5723696, to Unichema; 1998.
114. Eijsbouts S, Mayo SW, Fujita K. *Appl Catal A Gen* 2007;**322**:58.
115. Tsyganenko AA, Can F, Travert A, Maugé F. *Appl Catal A General* August 10, 2004; **268**(1–2):189–97.
116. Leyva C, Ancheyta J, Travert A, Maugé F, Marley L, Ramírez J, et al. *Appl Catal A General* May 28, 2012;**425–426**:1–12.
117. Tanabe K, Misono M, Ono Y, Hattori H. *New solid acid and bases*. Kondasha-Elsevier; 1989. p. 211.
118. Garcés HF, Espinal AE, Suib SL. *J Phys Chem C* 2012;**116**(15):8465–74.
119. Valsamakis I, Flytzani-Stephanopoulos M. *Appl Catal B* July 21, 2011;**106**(1–2):255–63.
120. Alexander A-M, Hargreaves JSJ. *Chem Soc Rev* 2010;**39**:4388–401.
121. Busca G, Porcile G, Lorenzelli V, Baraton MI, Quintard P, Marchand R. *Mater Chem Phys* 1986;**14**:123.
122. Sorlino M, Busca G, Lorenzelli V, Marchand R, Baraton MI, Quintard P. *Ann Chim Sci Mater* 1985;**10**:105.
123. Lednor PW. *Catal Today* 1992;**15**:243.
124. Merle-Méjean T, Baraton MI, Quintard P, Laurent Y, Lorenzelli V. *J Chem Soc Faraday Trans* 1993;**89**:3111.

125. Radhakrishnan R, Do DM, Jaenicke S, Sasson Y, Chuah GK. *ACS Catal* 2011;**1**:1631–6.
126. Baraton MI, Merle T, Quintard P, Lorenzelli V. *Langmuir* 1993;**9**:1486.
127. Baraton MI, Boulanger L, Cauchetier M, Lorenzelli V, Luce M, Merle T, et al. *J Eur Ceram Soc* 1994;**13**:371.
128. Wisme H, Cellier C, Grange P. *J Catal* 2000;**190**:406.
129. Postole G, Gervasini A, Caldararu M, Bonnetot B, Auroux A. *Appl Catal A General* 2007;**325**(2):227–36.
130. Binner J, Zhang Y. *Ceram Int* 2005;**31**(3):469–74.
131. Furimsky E. *Appl Catal A Gen* 2003;**240**:1.
132. Keller V, Laron-Pernot H, Djéga-Mariadassou G. *J Mol Catal A Chem* 2002;**188**:163.
133. McGee RCV, Bej SK, Thompson LT. *Appl Catal A Gen* 2005;**284**:139–46.
134. Bej SK, Thompson LT. *Appl Catal A Gen* 2004;**264**:141.
135. Cecilia JA, Infantes-Molina A, Rodríguez-Castellón E, Jiménez-López A, Oyama ST. *Appl Catal B. Envir* 2013;**136–137**:140–9.
136. Cecilia JA, Jiménez-Morales I, Infantes-Molina A, Rodríguez-Castellón E, Jiménez-López A. *J Mol Catal A Chem* March 2013;**368–369**:78–87.
137. Bui P, Antonio Cecilia J, Oyama ST, Takagaki A, Infantes-Molina A, Zhao H, et al. *J Catal* October 2012;**294**:184–98.
138. Guerfi K, Lagerge S, Meziani MJ, Nedellec Y, Chauveteau G. *Thermochim Acta* August 15, 2005;**434**(1–2):140–9.
139. Ramis G, Cauchetier M, Quintard P, Busca G, Lorenzelli V. *J Am Ceram Soc* 1989;**72**:1692–7.
140. Longkullabutra H, Nhuapeng W, Thamjaree W. *Curr Appl Phys* September 2012; **12**(Suppl. 2):S112–5.
141. Shi Y, Yang J, Liu H, Dai P, Liu B, Jin Z, et al. *J Cryst Growth* June 15, 2012;**349**(1):68–74.
142. Nguyen TT, Burel L, Nguyen DL, Pham-Huu C, Millet JMM. *Appl Catal A Gen* August 8, 2012;**433–434**:41–8.
143. Marín P, Ordóñez S, Díez FV. *J Chem Technol Biotechnol* 2012;**87**:360–7.
144. Furimsky E. *Appl Catal A Gen* February 10, 2003;**240**(1–2):1–28.
145. Okuhara T, Mizuno N, Misono M. *Adv Catal* 1996;**41**:113.
146. Hill CL. *Chem Rev* 1998;**98**(1).
147. Kozhovnikov IV. *Chem Rev* 1998;**98**:171.
148. Timofeeva MN. *Appl Catal A Gen* 2003;**256**:19.
149. Misono M. *Catal Rev Sci Eng* 1987;**30**:269.
150. Micek-Ilnicka A. The role of water in the catalysis on solid heteropolyacids. *J Mol Catal A Chem* 2009;**308**(1–2):1–14. 113.
151. Kamiya Y, Okuhara T, Misono M, Miyaji A, Tsuji K, Nakajo T. Catalytic chemistry of supported heteropolyacids and their applications as solid acids to industrial processes. *Catal Surv Asia* 2008;**12**(2):101.
152. Bennici S, Auroux A. In: Jackson SD, Hearegraves JSJ, editors. *Metal oxide catalysis*. Wiley; 2009. pp. 391–441.
153. Essayem N, Coudurier G, Védrine JC, Habermacher D, Sommer J. *J Catal* 1999;**183**:292.
154. Matachowski L, Zieba A, Zembala M, Drelinkiewicz A. *Catal Lett* 2009;**133**(1–2):49–62.
155. Okuhara T. *Chem Rev* 2002;**102**:3641.



156. Uchida S, Inumaru K, Misono M. *J Phys Chem B* 2000;**104**:8108.
157. Pazé C, Bordiga S, Zecchina A. *Langmuir* 2000;**16**:8139.
158. Vimont A, Travert A, Binet C, Pichon C, Mialane P, Sécheresse F, et al. *J Catal* 2006;**241**:221.
159. Stoyanov ES, Kim KC, Reed CA. *J Am Chem Soc* 2006;**128**:1948.
160. Mizuno N, Misono M. *Chem Rev* 1998;**98**:199.
161. Janik MJ, Davis RJ, Neurock M. *Catal Today* 2006;**116**:90.
162. Kozhovnikov IV, Holmes S, Siddiqui MRH. *Appl Catal A Gen* 2001;**214**:47.
163. Mitsutani A. *Catal Today* 2002;**73**:57.
164. Huang M, Chu W, Liao XM, Dai XY. *Chin Sci Bull* August 2010;**55**(24):2652–6.
165. Martin A, Armbruster U, Atia H. *Eur J Lipid Sci Technol* 2012;**114**(1):10–23.
166. Sambeth JE, Baronetti GT, Thomas HJ. *J Mol Catal A Chem* 2003;**191**:35.
167. Briand LE, Baronetti GT, Thomas HJ. *Appl Catal A Gen* 2003;**256**:37.
168. Sambeth J, Romanelli G, Autino JC, Thomas J, Baronetti G. *Appl Catal A Gen* 2010;**378**:114–8.
169. Pasquale G, Vázquez P, Romanelli G, Baronetti G. *Catal Commun* 2012;**18**:115–20.
170. Prudent R, Moucadet V, Laudet B, Barette C, Lafanechère L, Hasenknopf B, et al. *Chem Biol* July 21, 2008;**15**(7):683–92.
171. Timofeeva MN. *Appl Catal A Gen* December 30, 2003;**256**(1–2):19–35.
172. Díaz J, Novell-Leruth G, Vargas-Fuentes C, Bellarosa L, Bridier B, Pérez-Ramírez J, et al. *Theor Chem Acc* 2011;**128**(4):663–73.
173. Albers PW, Möbus K, Frost CD, Parker SF. *J Phys Chem C* 2011;**115**(50):24485–93.
174. <http://www.sigmaaldrich.com/catalog/product/aldrich/62145?lang=it&region=IT;11.02.2013>.
175. Da Silva E, Dayoub W, Mignani G, Raoul Y, Lemaire M. *Catal Commun* 2012;**29**:58–62.
176. Olah GA, Molnár A, editors. *Hydrocarbon chemistry*. 2nd ed. New York: Wiley; 2003.
177. Hattori H. *Appl Catal A Gen* 2001;**222**:247.
178. Steinbrenner U, Böhlring R, Zehner P. US Patent 6984766 to BASF; 2006.
179. Arata K. In: Jackson SD, Hargreaves SJS, editors. *Metal oxide catalysis*. Wiley; 2009. pp. 665–704.
180. Gramiccioni GA, Brown KR, Deeba M, Kotrel S, Wassermann K. US Patent application 2012/0165185 A1 to BASF.
181. Zhang J, Lin J, Cen P. *Can J Chem Eng* December 2008;**86**(6):1047–53.
182. Zhang J, Lin J, Xu X, Cen P. *Chin J Chem Eng* 2008;**16**(2):263–9.
183. Stošić D, Bennici S, Sirotnin S, Calais C, Couturier J-L, Dubois J-L, et al. *Appl Catal A Gen* 2012;**447–448**:124–34.
184. Hu H, Martin JC, Zhang M, Southworth CS, Xiao M, Meng Y, et al. *RSC Adv* 2012;**2**:3810–5.
185. Alberti G, Costantino U, Dionigi C, Murcia-Mascarós S, Vivani R. *Supramol Chem* 1995;**6**(1–2):29–40.
186. Busca G, Lorenzelli V, Galli P, La Ginestra A, Patrono P. *J Chem Soc Faraday Trans 1* 1987;**83**:853–64.
187. Sinhamahapatra A, Sutradhar N, Roy B, Pal P, Bajaj HC, Panda AB. *Appl Catal B* April 5, 2011;**103**(3–4):378–87.
188. Curini M, Rosati O, Costantino U. *Curr Org Chem* 2004;**8**:591–606.
189. Curini M, Montanari F, Rosati O, Liroy E, Margarita R. *Tetrahedron Lett* 2003;**44**:3923–5.

190. Gu M, Yu D, Zhang H, Sun P, Huang H. *Catal Lett* 2009;**133**(1–2):214–20.
191. Zhang F, Xie Y, Lu W, Wang X, Xu S, Lei X. *J Colloid Interface Sci* September 15, 2010;**349**(2):571–7.
192. Kashiwagi D, Takai A, Takubo T, Nagaoka K, Inoue T, Takita Y. *Ind Eng Chem Res* 2009;**48**(2):632–40.
193. Jiménez-Morales I, Santamaría-González J, Maireles-Torres P, Jiménez-López A. *Appl Catal B* 2012;**123–124**:316–23.
194. Reddy BM, SaralaDevi G, Pavani MS. *Res Chem Intermed* 2002;**28**(6):595–601.
195. Ipatieff VN, Corson BB. *Ind Eng Chem* 1938;**30**:1316.
196. Egloff G. *Ind Eng Chem* 1936;**28**:1461.
197. Coetzee JH, Mashapab TN, Prinsloo NM, Rademan JD. *Appl Catal A Gen* July 10, 2006;**308**:204–9.
198. Hamamatsu T, Kimura N, Takashima I, Morikita T. US Patent 7741527 B2 to Nippon Oil Co; 2010.
199. Xu L, Turbeville W, Korynta GA, Braden JL. US Patent 8063260 B2 to Sud Chemie; 2011.
200. Krawietz TR, Lin P, Lotterhos KE, Torres PD, Barich DW, Clearfield A, et al. *J Am Chem Soc* 1998;**120**:8502.
201. Cavani F, Girotti G, Terzoni G. *Appl Catal A Gen* 1993;**97**:177.
202. Ramis G, Rossi PF, Busca G, Lorenzelli L, La Ginestra A, Patrono P. *Langmuir* 1989;**5**:917.
- 203a. Ramis G, Busca G, Lorenzelli V, La Ginestra A, Galli P, Massucci MA. *J Chem Soc Dalton Trans*; 1988:881.
- 203b. Busca G, Centi G, Trifirò F. *J Am Chem Soc* 1985;**107**:7757.
204. Jones EK. *Adv Catal Relat Subj* 1958;**10**:165.
205. Chauvel A, Lefebvre G. *Petrochemical processes*. Paris: Technip; 1989. p. 185 and p. 215.
206. de Klerk A. *Catalysis* 2011;**23**:1–49.
207. de Klerk A. *Ind Eng Chem Res* 2004;**43**:6325.
208. Prinsloo NM. *Fuel Proc Technol* 2006;**87**:437.
209. Schwarzer RB, Du Toit E, Nicol W. *Appl Catal A Gen* 2009;**369**:83–9.
210. Mashapa TN, de Klerk A. *Appl Catal A Gen* 2007;**332**:200–8.
211. Fougret CM, Atkins MP, Hölderich WF. *Appl Catal A Gen* 1999;**181**:145.
212. Degnan Jr TF, Morris Smith C, Venkat Chaya R. *Appl Catal A Gen* 2001;**221**:283.
213. Merwe W. *Environ Sci Technol* 2010;**44**(5):1806–12.
214. Zolfigol MA. *Tetrahedron* 2001;**57**:9509.
215. Zhang Z, Sui S, Tan S, Wang Q, Pittman Jr CU. *Bioresour Technol* 2013;**130**:789–92.
216. Zolfigol MA, Khazaei A, Mokhlesi M, Derakhshan-Panah F. *J Mol Catal A Chem* 2013;**370**:111–6.
217. Olah GA, Batamack P, Deffieux D, Török B, Wang Q, Molnár Á, et al. *Appl Catal A Gen* 1996;**146**:107–17.
218. Hommeloft SI, Tøpsoe HFA. US Patent 5,245,100; 1993.
219. de Angelis A, Flego C, Ingallina P, Montanari L, Clerici MG, Carati C, et al. *Catal Today* 2001;**65**:363.
220. Liu PN, Xia F, Wang QW, Ren YJ, Chen JQ. *Green Chem* 2010;**12**:1049–55.
221. Liu Y-H, Deng J, Gao J-W, Zhang Z-H. *Adv Synth Catal* February 2012;**354**(2–3):441–7.

222. Bennardi DO, Romanelli GP, Autino JC, Pizzio LR. *Appl Catal A Gen* 2007;**324**:62–8.
223. Selvam T, MacHoke A, Schwieger W. *Appl Catal A Gen* 2012;**445–446**:92–101.
224. Liu S, Shang J, Zhang S, Yang B, Deng Y. *Catal Today* February 1, 2013;**200**:41–8.
225. Fehér C, Kriván E, Kovács J, Hancsó k J, Skoda-Földes R. *J Mol Catal A Chem* 2013;**372**:51–7.
226. Matsuhashi H, Oikawa M, Arata K. *Langmuir* 2000;**16**:8201.
227. Chiesa M, Napoli F, Giamello E. *J Phys Chem* 2007;**111**:5481.
228. Stevens MG, Anderson MR, Foley HC. *Chem Commun* 1999:413.
229. Tanaka K, Yanashima H, Minobe M, Suzukamo G. *Appl Surf Sci* 1997;**121/122**:461.
230. Nakayama H, Klug DD, Ratcliffe CI, Ripmeester JA. *J Am Chem Soc* 1994;**116**:9777.
231. Olah GA, Molnár A. *Hydrocarbon chemistry*. 2nd ed. New York: Wiley; 2003.
232. Ostrowski S, Dobrowolski JC. *J Mol Catal A Chem* 2008;**293**:86–96.
233. Gorzawski H, Hoelderich WF. *J Mol Catal A Chem* 1999;**144**:181.
234. Smith RS. US Patent 4,977,124; 1990; 4,929,783; 1990.
235. Staton JS, Turnblad Jr RA; Agree RB. US Patent 4,950,831; 1990.
236. Kijeński J, Radomski P, Fedoryńska E. Alkylation of alkyl aromatic hydrocarbons over metal oxide–alkali metal superbasic catalysts. *J Catal* 2001;**203**:407–25.
237. Stevens MG, Anderson MR, Foley HC. Side-chain alkylation of toluene with propene on caesium/nanoporous carbon catalysts. *Chem Commun* 1999:413–4.
238. Wight AP, Davis ME. *Chem Rev* 2002;**102**:3589.
239. Mehdi A, Reye C, Corriu R. *Chem Soc Rev* 2011;**40**:563–74.
240. Wang W, Lofgreen JE, Ozin GA. *Small* December 6, 2010;**6**(23):2634–42.
241. Asefa T, Tao Z. *Can J Chem* 2012;**90**(12):1015–31.
242. Walcarius A, Mercier L. *J Mater Chem* 2010;**20**:4478–511.
243. Marrone M, Montanari T, Busca G, Conzatti L, Costa G, Castellano M, et al. *J Phys Chem B* 2005;**108**:3563.
244. Finocchio E, Macis E, Reiteri R, Busca G. *Langmuir* 2007;**23**:2505.
245. Castellano M, Conzatti L, Turturro A, Costa G, Busca G. *J Phys Chem B* 2007;**111**:4495.
246. Macquarrie DJ, Jackson DB, Tailland S, Utting KA. *J Mater Chem* 2001;**11**:1843.
247. Wang X, Lin KSK, Chan JCC, Cheng S. *J Phys Chem B* 2005;**109**:1763.
248. Taguchi A, Schüth F. *Microporous Mesoporous Mater* 2005;**77**:1.
249. Macquarrie DJ. *Chem Commun* 1996:1961.
250. Yu C-H, Huang C-H, Tan C-S. *Aerosol Air Qual Res* 2012;**12**:745–69.
251. Melero JA, van Grieken R, Morales G. *Chem Rev* 2006;**106**(9):3790–812.
252. Long W, Jones CW. *ACS Catal* 2011;**1**:674–81.
253. Michaud A, Gingras G, Morin M, Béland F, Ciriminna R, Avnir D, et al. *Org Process Res Dev* 2007;**11**(4):766–8.
254. Pomogailo AD. *Polym Sci Ser C* 2006;**48**:85–111.
255. Finocchio E, Baccini I, Cristiani C, Dotelli G, Gallo Stampino P, Zampori L. *J Phys Chem A* 2011;**115**(26):7484–93.
256. Serp P, Corrias M, Kalck P. *Appl Catal A Gen* 2003;**253**:337–58.
257. Calvino-Casilda V, López-Peinado AJ, Durán-Valle CJ, Martín-Aranda RM. Last decade of research on activated carbons as catalytic support in chemical processes. *Catal Rev* 2010;**52**(3):325–80.
258. Antolini E. *Appl Catal B* 2009;**88**:1–24.
259. Yang Y, Chiang K, Burke N. *Catal Today* 2011;**178**:197–205.

260. Prati L, Villa A, Lupinib AR, Veithb GM. *Phys Chem Chem Phys* 2012;**14**:2969–78.
261. Antolini E. *Appl Catal B* 2012;**123–124**:52–68.
262. Bandosz TJ, editor. *Activated carbon surfaces in environmental remediation. Interface science and technology*, vol. 7. San Diego: Academic Press; 2006.
263. Putra EK, Pranowo R, Sunarso J, Indraswati N, Ismadji S. *Water Res* 2009;**43**: 2419–30.
264. Talapaneni SN, Anandan S, Mane GP, Anand C, Dhawale DS, Varghese S, et al. *J Mater Chem* 2012;**22**(19):9831–40.
265. Teo KBK, Singh C, Chhowalla M, Milne WI. In: Nawa HS, editor. *Encyclopedia of nanoscience and nanotechnology*, vol. 10. American Scientific Publishers; 2003. pp. 1–22.
266. Zhao J, Gao QY, Gu C, Yang Y. *Chem Phys Lett* 2002;**358**(1–2):77–82.
267. Amadou J, Chizari K, Houllé M, Janowska I, Ersen O, Bégina D, et al. *Catal Today* October 15, 2008;**138**(1–2):62–8.
268. Kuscch SD, Kuyunko NS. *Proc Int Conf Nanomater Appl Prop* 2012;**1**. PROC NAP 1, 01NDLCN05.
269. Malhotra R, Hirschon AS, McMillena DF, Bell WL. *MRS Proc* 1997;**497**.
270. Pacosová L, Kartusch C, Kukula P, van Bokhoven JA. *ChemCatChem* January 10, 2011;**3**(1):154–6.
271. Liang C, Xie H, Schwartz V, Howe J, Dai S, Overbury SH. *J Am Chem Soc* June 10, 2009;**131**(22):7735–41.
272. Kushch SD, Kuyunko NS, Tarasov BP. *Russ J Gen Chem* June 2009;**79**(6):1106.
273. Precious metal powder catalysts, EVONIK. Available on internet 20.02.2013.
274. *The catalyst technical handbook*. Johnson Matthey Catalysts; 2008. Available on internet 20.02.2013.
275. Birkhoff R. In: Meyers RA, editor. *Handbook of petrochemicals production processes*. McGraw-Hill; 2005. p. 2.3–9.
276. Chen B, Dingerdissen U, Krauter JGE, Lansink Rotgerink HGJ, Möbus K, Ostgard DJ, et al. *Appl Catal A Gen* 2005;**280**:17–46.
277. *Evonik. Selective nitro group hydrogenation*. <http://catalysts.evonik.com/product/catalysts/en/products/technology-platforms/selective-nitro-group-hydrogenation/pages/default.aspx>.
278. Moore A, Birkhoff R. In: Meyers RA, editor. *Handbook of petrochemicals production processes*. McGraw-Hill; 2005. p. 9.31–50.
279. <http://www.kbr.com/Technologies/Proprietary-Equipment/KAAP-Ammonia-Synthesis-Converter/>.
280. Foster AI, James PG, McCarroll JJ, Tennison SR. US Patent 4,250,057 to BP Co. Ltd.; 1986.
281. Rossetti I, Pernicone N, Ferrero F, Forni L. *Ind Eng Chem Res* 2006;**45**:4150–5.
282. Campos-Martin JM, Blanco-Brieva G, Fierro JLG. *Angew Chem Int Ed* 2006;**45**: 6962–84.
283. Bianchi CL, Canton P, Dimitratos M, Porta F, Prati L. *Catal Today* 2005;**102–103**: 203–12.
284. Pollington SD, Enache DI, Landon P, Meenakshisundaram S, Dimitratos N, Wagland A, et al. *Catal Today* 2009;**145**:169–75.
285. Nakajima K, Hara M. *ACS Catal* 2012;**2**:1296–304.
286. Sukanuma S, Nakajima K, Kitano M, Hayashi S, Hara M. *ChemSusChem* 2012;**5**(9): 1841–6.

287. Luque R, Budarin V, Clark JH, Macquarrie DJ. *Appl Catal B* 2008;**82**:157.
288. Ji X, Chen Y, Wang X, Liu W. *Kinetics Catal* July 2011;**52**(4):555–8.
289. Alexandratos SD. *Ind Eng Chem Res* 2009;**48**(388–398).
290. Charakrabarty A, Sharma MM. *React Polym* 1993;**20**:1.
291. Harmer MA, Sun Q. *Appl Catal A Gen* 2001;**221**:45.
292. Di Girolamo M, Marchionna M. *J Mol Catal A Chem* 2001;**177**:33.
293. Gelbard G. Organic synthesis by catalysis with ion exchange resins. *Ind Eng Chem Res* 2005;**44**:8468–98.
294. [http://www.amberlyst.com/literature/Amberlyst\\_Catalysts\\_LabProcedures.pdf](http://www.amberlyst.com/literature/Amberlyst_Catalysts_LabProcedures.pdf); 15.02.2013.
295. Thornton R, Gates BC. *J Catal* 1974;**34**:275.
296. Siril PF, Brown DR. *J Mol Catal A Chem* 2006;**252**:125.
297. Hutchings GJ, Nicolaides CP, Scurrrell MS. *Catal Today* 1992;**15**:23.
298. Miracca I, Tagliabue L, Trotta R. *Chem Eng Sci* 1996;**51**:2349.
299. [http://www.cdtech.com/techProfilesPDF/MTBE\\_RefC4Feeds-CDMTBE.pdf](http://www.cdtech.com/techProfilesPDF/MTBE_RefC4Feeds-CDMTBE.pdf).
300. Di Girolamo M, Tagliabue L. *Catal Today* 1999;**52**:307.
301. Marchionna M, Di Girolamo M, Patrini R. *Catal Today* 2001;**65**:397.
302. Honkela ML, Krause AOL. *Ind Eng Chem Res* 2005;**44**:5291.
303. de Angelis A, Ingallina P, Perego C. *Ind Eng Chem Res* 2004;**43**:1169–78.
304. Fraini E, West D, Mignin G. In: Meyers RA, editor. *Handbook of petrochemical production processes*. Mc Graw Hill; 2005. p. 9.51–59.
305. Quiroga M, Capeletti MR, Figoli N, Sedran U. *Appl Catal A Gen* 1999;**177**:37.
306. Honkela ML, Root A, Linblad M, Krause AOI. *Appl Catal A Gen* 2005;**295**:216.
307. <http://www.fuelcells.dupont.com>.
308. Zecchina A, Spoto G, Bordiga S. *Phys Chem Chem Phys* 2005;**7**:1627.
309. Hinze R, Laufer MC, Hölderich WF, Bonrath W, Netscher T. *Catal Today* 2009;**140**(1–2):105–11.
310. Kumar P, Vermeiren W, Dath J-P, Hölderich WA. *Energy & Fuels* 2006;**20**:481.
311. [http://www2.dupont.com/FuelCells/en\\_US/assets/downloads/dfc301.pdf](http://www2.dupont.com/FuelCells/en_US/assets/downloads/dfc301.pdf).
312. Di Girolamo M, Marchionna M. Acidic and basic ion exchange resins for industrial applications. *J Mol Catal A Chem* 2001;**177**:33–40.
313. Tanabe K, Hölderich WF. Industrial application of solid acid–base catalysts. *Appl Catal A Gen* 1999;**181**:399–434.
314. Barbaro P, Iguori F. *Chem Rev* 2009;**109**:515–29.
315. Hosono Y, Tasaki M. In: Meyers RA, editor. *Handbook of petrochemical production processes*. Mc Graw Hill; 2005. p. 1.3–13.
316. Meng Y, Gu D, Zhang F, Shi Y, Cheng L, Feng D. *Chem Mater* 2006;**18**:4447–64.

# Metal Catalysts for Hydrogenations and Dehydrogenations

## CHAPTER OUTLINE

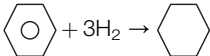
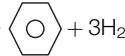
<b>9.1 Bulk metal catalysts</b> .....	<b>302</b>
9.1.1 Surface science studies on metal monocrystal faces and model surfaces .....	302
9.1.2 Unsupported metal nanoparticles .....	304
<b>9.2 Supported metal catalysts</b> .....	<b>304</b>
9.2.1 Supports for metal catalysts .....	304
9.2.2 Supported metal nanoparticles .....	306
9.2.3 Isolated and very highly dispersed metal centers .....	308
<b>9.3 Fundamentals of hydrogenation/dehydrogenation</b> .....	<b>309</b>
9.3.1 Adsorption of hydrogen on metals .....	309
9.3.2 Adsorption of organic substrates on metals .....	310
9.3.3 Hydrogenation of hydrocarbons .....	311
9.3.4 Fundamentals of dehydrogenation.....	312
9.3.5 Steam-reforming and related processes .....	312
<b>9.4 Metal catalysts for hydrogenation and dehydrogenation reactions</b> .....	<b>313</b>
9.4.1 Iron-based metal catalysts.....	313
9.4.1.1 <i>Fe-based ammonia synthesis</i> .....	313
9.4.1.2 <i>Fe-based high-temperature Fischer Tropsch catalysts</i> .....	314
9.4.2 Cobalt-based metal catalysts .....	314
9.4.2.1 <i>Co-based low-temperature Fischer Tropsch catalysts</i> .....	315
9.4.2.2 <i>Co-based catalysts for ethanol steam reforming</i> .....	315
9.4.3 Nickel-based metal catalysts .....	316
9.4.3.1 <i>Nickel Raney and sponge nickel catalysts</i> .....	317
9.4.3.2 <i>Nickel/silica catalysts</i> .....	318
9.4.3.3 <i>Ni-alumina- and Ni-aluminate-based catalysts</i> .....	318
9.4.4 Copper-based catalysts .....	321
9.4.4.1 <i>Cu-based methanol synthesis catalysts</i> .....	322
9.4.4.2 <i>Cu-based water–gas shift and reverse water–gas shift catalysts</i> .....	323
9.4.4.3 <i>Cu-based methanol decomposition and steam-reforming catalysts</i> .....	324

9.4.4.4	<i>Cu-based catalysts for partial hydrogenations of oxygenates at carbonyl and carboxyl groups</i> .....	325
9.4.4.5	<i>Cu-based catalysts for dehydrogenation of alcohols to carbonyl compounds</i> .....	325
9.4.4.6	<i>Cu-based catalysts for hydrogenation of nitrogenated compounds</i> .....	326
9.4.5	Ruthenium-based catalysts .....	326
9.4.6	Rhodium-based catalysts .....	327
9.4.7	Palladium-based catalysts.....	327
9.4.7.1	<i>Pd-based catalysts for hydrogenation of acetylenic compounds, dienes and olefins</i> .....	327
9.4.7.2	<i>Pd-based catalysts for methanol synthesis and steam reforming and for hydrogenation of oxygenated compounds</i> ..	330
9.4.8	Rhenium metal in catalysis .....	331
9.4.9	Iridium-based catalysts .....	331
9.4.10	Platinum-based catalysts .....	331
9.4.10.1	<i>Pt-based catalysts for hydrogenation of olefins</i> .....	332
9.4.10.2	<i>Pt-based catalysts for aromatic saturation</i> .....	332
9.4.10.3	<i>Pt-based catalysts for aromatization and naphtha reforming</i> ..	333
9.4.10.4	<i>Pt-based catalysts for liquid-phase hydrogenation of nitrobenzenes</i> .....	334
9.4.10.5	<i>Pt-based catalysts for dehydrogenation of alkanes to olefins and dienes</i> .....	334
9.4.10.6	<i>Pt-based catalysts for water–gas shift and steam reforming</i> ..	334
9.4.11	Gold-based catalysts for water–gas shift .....	335
<b>References</b>	.....	335

Catalysis by solid metals, in particular noble metals, is very relevant in terms of both technology and business. Enormous number of studies have been published concerning the effects of different catalyst characteristics (support type, dispersion of the metals, size and shape of metal particles and role of additives).<sup>1–4</sup>

In [Table 9.1](#), a summary of some most relevant industrial reactions using metal catalysts are reported. A limited number of elements are or can stay in the metallic state in the conditions of catalytic reactions. The real state of metallic elements composing of a catalyst obviously depends on the reaction conditions (reducing or oxidizing atmosphere, feed composition, temperature and pressure). Hydrogenations are exothermic equilibrium reactions, thus performed usually at moderate or low temperature and high pressure. When the substrate to be hydrogenated is carbon monoxide, a hydrocarbon or another organic compound, the atmosphere is reducing, and thus metallic elements tend to be reduced to the metallic state. However, only part of the transition metals are actually reduced in practical conditions ([Figure 9.1](#)). On the other hand, in the presence of hydrogen and carbon compounds, metal




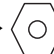
**Table 9.1** Typical Industrial Reactions Performed on Metal Catalysts

Reaction Family and Example	Process	Temperature	Pressure	Typical Catalyst
Methanation $\text{CO} + 3\text{H}_2 \rightarrow \text{CH}_4 + \text{H}_2\text{O}$ ; $\text{CO}_2 + 4\text{H}_2 \rightarrow \text{CH}_4 + 2\text{H}_2\text{O}$	LT	170 °C	30–50 bar	0.3% Ru/Al <sub>2</sub> O <sub>3</sub>
	HT	200–350 °C	30–50 bar	20% Ni/Al <sub>2</sub> O <sub>3</sub>
		300–500 °C	20–50 bar	25% Ni/Al <sub>2</sub> O <sub>3</sub> stab
Steam reforming: e.g., methane steam reforming $\text{CH}_4 + \text{H}_2\text{O} \rightarrow \text{CO} + 3\text{H}_2$	Tubular	750–850 °C	30–50 bar	Ni/CaAl <sub>12</sub> O <sub>19</sub>
Hydrocarbon partial oxidation: e.g., Methane catalytic partial oxidation (CPO) $\text{CH}_4 + \frac{1}{2} \text{O}_2 \rightarrow \text{CO} + 2\text{H}_2$		700–900 °C	2–50 bar	Rh/ $\alpha$ -Al <sub>2</sub> O <sub>3</sub>
Methanol synthesis $\text{CO} + 2\text{H}_2 \rightarrow \text{CH}_3\text{OH}$ ; $\text{CO}_2 + 3\text{H}_2 \rightarrow \text{CH}_3\text{OH} + \text{H}_2\text{O}$	LT	200–300 °C	50–200 bar	Cu/ZnO/Al <sub>2</sub> O <sub>3</sub>
Water-gas shift $\text{CO} + \text{H}_2\text{O} \rightarrow \text{CO}_2 + \text{H}_2$	HTWGS	350–450 °C	30–50 bar	(Cu) Fe <sub>3</sub> O <sub>4</sub> -Cr <sub>2</sub> O <sub>3</sub>
	LTWGS	200–300 °C	30–50 bar	Cu/ZnO/Al <sub>2</sub> O <sub>3</sub>
Fischer Tropsch synthesis $n \text{CO} + 2n \text{H}_2 \rightarrow (\text{CH}_2)_n + n \text{H}_2\text{O}$	LTFTS	200–250 °C	25–40 bar	Co/Al <sub>2</sub> O <sub>3</sub>
	HTFTS	300–350 °C	25–30 bar	Fe (carbide)
Acetylenics partial hydrogenation: e.g., propine hydrogenation $\text{H}_3\text{C}-\text{C}\equiv\text{CH} + \text{H}_2 \rightarrow \text{H}_3\text{C}-\text{HC}=\text{CH}_2$	Liquid phase	15–25 °C	15–25 bar	0.3% Pd/Al <sub>2</sub> O <sub>3</sub>
	Gas phase	50–120 °C	15–25 bar	0.03% Pd/Al <sub>2</sub> O <sub>3</sub>
Olefins saturation: e.g., iso-octene hydrogenation to isooctane $(\text{H}_3\text{C})_2\text{C}=\text{CH}-\text{C}(\text{CH}_3)_3 + \text{H}_2 \rightarrow$ $(\text{H}_3\text{C})_2\text{CH}-\text{CH}_2-\text{C}(\text{CH}_3)_3$	Liquid phase	70–130 °C	10–30 bar	0.3% Pd/Al <sub>2</sub> O <sub>3</sub>
Paraffin dehydrogenation	Gas phase (higher paraff.)	450–475 °C	0.5–3 bar	Pt-Sn/Al <sub>2</sub> O <sub>3</sub>
	Gas phase (isobutane)	500–650 °C	0.5–3 bar	Pt-Sn/Al <sub>2</sub> O <sub>3</sub>
Dearomatization: benzene saturation 	Slurry phase	180–250 °C	20–60 bar	Ni Raney
	Vapor phase	180–400 °C	10–35 bar	Pt/Al <sub>2</sub> O <sub>3</sub>
Paraffin aromatization: naphtha catalytic reforming $\text{H}_3\text{C}-(\text{CH}_2)_4-\text{CH}_3 \rightarrow$  $+ 3\text{H}_2$	Naphtha reforming	480–530 °C	15–35 bar	Pt-Re-Sn/Al <sub>2</sub> O <sub>3</sub> -alCl <sub>3</sub>
	Aromax	500 °C	6–10 bar	Pt/K-L zeolite

Continued



**Table 9.1** Typical Industrial Reactions Performed on Metal Catalysts—cont'd

Reaction Family and Example	Process	Temperature	Pressure	Typical Catalyst
Carbonyl compounds hydrogenation: e.g., hydrogenation of ethylhexanal to ethylhexanol $\text{H}_3\text{C}-(\text{CH}_2)_3-(\text{C}_2\text{H}_5)\text{CH}-\text{CHO} + \text{H}_2 \rightarrow \text{H}_3\text{C}-(\text{CH}_2)_3-(\text{C}_2\text{H}_5)\text{CH}-\text{CHO}$ e.g., hydrogenation of acetophenone		130 °C	3–10 bar	Cu–ZnO–Al <sub>2</sub> O <sub>3</sub>
 CO–CH <sub>3</sub> + H <sub>2</sub> →  CHO–CH <sub>3</sub>	Liquid phase	5–100 °C	1–10 bar	Pd/C
Selective hydrogenation of α,β-unsaturated carbonyl compounds on the C=C double bond: e.g., MIBK synthesis $(\text{H}_3\text{C})_2\text{C}=\text{CH}.\text{CO}-\text{CH}_3 + \text{H}_2 \rightarrow$ $(\text{H}_3\text{C})_2\text{CH}-\text{CH}_2-\text{CO}-\text{CH}_3$		150–200 °C	3–10 bar	Pd/Al <sub>2</sub> O <sub>3</sub>
Alcohol dehydrogenation: e.g., 2-butanol dehydration to methyl-ethyl-ketone (MEK) $\text{H}_3\text{C}-\text{CH}_2-\text{CHOH}-\text{CH}_3 \rightarrow \text{H}_3\text{C}-\text{CH}_2-$ $\text{CO}-\text{CH}_3 + \text{H}_2$		240–260 °C	1 bar	Cu–ZnO–Al <sub>2</sub> O <sub>3</sub>
Hydrogenation of vegetable oil to margarine		180–230 °C	2–6 bar	Ni/SiO <sub>2</sub>
Esters hydrogenations: hydrogenation of vegetable oil to fatty alcohols		200 °C	250 bar	Cu/CuCr <sub>2</sub> O <sub>4</sub>
Ammonia synthesis $\text{N}_2 + 3\text{H}_2 \rightarrow 2\text{NH}_3$	Traditional	300–500 °C	80–300 bar	Fe
	KAAP	300–400 °C	60–100 bar	Ru/graphite
Nitriles hydrogenation: Adiponitrile hydrogenation to hexamethylenediamine $\text{N}\equiv\text{C}-\text{C}_4\text{H}_8-\text{C}\equiv\text{N} + 2\text{H}_2 \rightarrow \text{H}_2\text{N}-$ $\text{C}_6\text{H}_{12}\text{NH}_2$	Slurry	120–150 °C	35 atm	Ni Raney
Nitrobenzene hydrogenation to aniline  NO <sub>2</sub> + 3H <sub>2</sub> →  NH <sub>2</sub> + 2H <sub>2</sub> O	Gas phase	250–350 °C	5–10 bar	Cu–Ba–Mn/CuCr <sub>2</sub> O <sub>4</sub>
	Liquid phase	5–50 °C	1–20 bar	Pd/C, Pt/C

LT, low-temperature; HT, high-temperature; LTWGS, low-temperature water–gas shift; HTWGS, high-temperature water–gas shift; MIBK, methyl-isobutyl ketone.

hydrides and carbides can also be formed. Additionally, in many cases, relevant amounts of sulfur are present in the feed, thus the catalyst may become partially or fully sulfided. Thus, it is not always well established whether real metallic catalysis really occurs in these conditions.

On the other hand, during oxidation reactions (see Chapter 11), the atmosphere is oxidizing, and thus only very few metals [the so-called noble metals, i.e. platinum group and group 1B (or group 11) metals i.e. copper, silver and gold] may stay (but not always are entirely) in the metallic state (Figure 9.1).

Another field where metal catalysts are used is that of hydrogen and syngas production processes, using steam reforming (SR) and water–gas shift (WGS) processes. In these cases, the atmosphere is predominantly reducing but water vapor is present and, at least formally, acts as an oxidant toward reactants. Thus it is not excluded that it also acts as an oxidant toward the metal catalyst. In autothermal processes, also oxygen is present in small amounts together with water, and reducing reactant and products, thus the atmosphere is not fully reducing.

Metal catalysts may also be applied to dehydrogenations. In the cases of these endothermic reactions, the temperature is relatively high and the pressure low, and no oxidizing species are usually present in the reactant mixture, thus the real occurrence of metal catalysis is likely.

In any case, heterogeneous metal catalysis is essentially associated to groups 8–11 metals, i.e. Fe, Co, Ni, the Platinum Group Metals (PGMs, i.e. Ru, Rh, Pd, Os, Ir, Pt), Cu, Ag and Au. For hydrogenation reactions, the interest is essentially limited to Fe, Co, Ni, Cu, Ru, Rh, Pd, Ir and Pt.

1	2	3	4	5	6	7	8	9	10	11	12	13	14	15	16	17	18
IA	IIA	IIIB	IVB	VB	VIB	VII B	VIII B			IB	IIB	IIIA	IVA	VA	VIA	VIIA	
H																	He
Li	Be											B	C	N	O	F	Ne
Na	Mg											Al	Si	P	S	Cl	Ar
K	Ca	Sc	Ti	V	Cr	Mn <sub>c</sub>	Fe <sub>bcc</sub>	Co <sub>hcp</sub>	Ni <sub>fcc</sub>	Cu <sub>fcc</sub>	Zn	Ga	Ge	As	Se	Br	Kr
Rb	Sr	Y	Zr	Nb	Mo		Ru <sub>hcp</sub>	Rh <sub>fcc</sub>	Pd <sub>fcc</sub>	Ag <sub>fcc</sub>	Cd	In	Sn	Sb	Te	I	Xe
Cs	Ba	La*	Hf	Ta	W	Re <sub>hcp</sub>	Os <sub>hcp</sub>	Ir <sub>fcc</sub>	Pt <sub>fcc</sub>	Au <sub>fcc</sub>	Hg	Tl	Pb	Bi	Po	At	Rn
Fr	Ra	Ac**															

Platinum-group metals
  Group 1B metals

FIGURE 9.1

The periodic table of the elements and the elements involved in metal catalysis.

## 9.1 Bulk metal catalysts

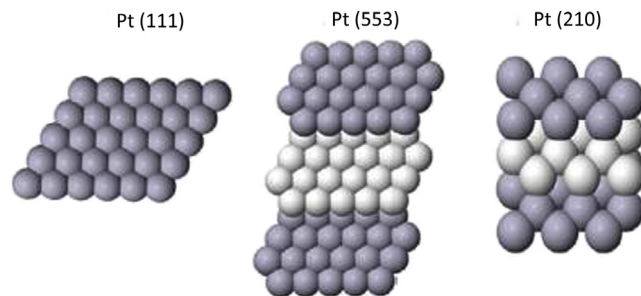
Only in some cases bulk metals are practically applied as catalysts. In fact, bulk metals usually are stable in relatively big particles, thus exposing small surface area per weight and per volume. This situation is, however, used for some important and historical processes such as ammonia synthesis as well as the high-temperature Fischer–Tropsch process (see below), both performed on iron catalysts containing a number of additional promoter and stabilizing components. Another important application of bulk metals is the case of the so-called “Raney metals”, largely used mainly for liquid-phase slurry hydrogenation reactions. In the case of some oxidation reactions metal gauzes are used as catalysts when very low contact times are needed (see Chapter 11).

The use of bulk metals is mostly not practical in particular in the case of noble metals, which are very expensive, when there is no need for very low contact time. Supporting metals on carriers and wash-coats may allow to stabilize nanoparticles, thus allowing the use of much less metal weight for the same surface. In some cases, particular supports also allow a modification of the properties of the metal surface with improving catalytic activity.

### 9.1.1 Surface science studies on metal monocrystal faces and model surfaces

Surface science studies on the metal monocrystal faces helped very much to the understanding of metal catalysis. With these studies, using techniques such as Electron Energy Loss Spectroscopy (EELS), Reflection Absorption Infrared Spectroscopy (RAIRS), Low-Energy Electron Diffraction (LEED), the basic chemistry of metal surfaces has been characterized and the chemistry of reactants at the interface with metal surfaces has been determined. Most of these studies take into account low-index exposed faces of metal monocrystals (such as the 111 face of hexagonal close-packed metals, [Figure 9.2](#)), and their interaction with adsorbates, as well as the evolution of such molecules on the surface. This allowed, in several cases, to propose reliable mechanisms for catalytic reactions, such as, e.g. ammonia synthesis. Recognition of this work is represented by the Nobel Prize 2007 for Chemistry, awarded to Gerhard Ertl, the most eminent surface scientist.

It is however quite clear that most of these studies suffered both a conditions gap (they are mostly realized under high vacuum while catalysis is performed at medium to high pressure<sup>5</sup>) as well as of a materials gap (real catalysts are not monocrystals and, more precisely, not single, low-faces of monocrystals).<sup>6</sup> Experimental methods for these studies underwent further developments in recent years, with the application of stepped surfaces (modeling surface edges, [Figure 9.2](#)) and the developments of surface science techniques that can be applied at atmospheric pressure, such as PMIRAS<sup>7</sup> and the further evolution of techniques such as theoretical calculations.<sup>8</sup> Theoretical studies, indeed, became more and more available and important.<sup>9</sup> However, also these techniques suffer of the material gap. In fact, surface defects, corners, edges, complex centers may be difficult to model, and

**FIGURE 9.2**

Schematic representation of three faces, a low index face (111) and two-stepped faces (553 and 210) of hcp metal (Pt).

*Reprinted with permission from Ref 24.*

thus these studies mainly concern extended faces too. An example of this are the recent studies of hydrogenations of 1,3-butadiene on supported Pd catalysts and the relative modeling studies. It has been found that this reaction is structure-sensitive. Modeling of the adsorption of 1,3-butadiene, 1-butene and hydrogen on the predominant (111) and (100) faces of Pd have been performed. The thermodynamic differences between Pd(111) and Pd(100) for the relative stabilization of butadiene vs but-1-ene reveal that the effect of surface orientation is intimately associated to the effect of hydrogen coverage.<sup>10</sup> According to the authors, further studies are needed to go deeper on the reaction mechanism. However, the possibility of the organic molecules to adsorb on edges, which seems indeed very likely, is neglected, possibly due to the difficulty in modeling.

In fact, complete understanding of catalytic reactivity cannot be achieved by utilizing metal single crystals alone, because the interaction between metal and supports and particle size effects can alter the activity and selectivity of supported catalysts in a remarkable way. This can be due to changes in the average metal atom coordination number, in the morphology, and in the different nature of metal-support interaction as the fraction of metal atoms in direct contact with the substrate varies.

The preparation of model oxide-supported metal catalysts in UHV represents an approach to partially overcome the materials' gap. The approaches developed by Goodman and coworkers<sup>11</sup> and by Freund and coworkers<sup>12</sup> allowed the preparation and the characterization of metal particles or clusters deposited on planar oxide surfaces. These solids allow IR reflection/absorption spectroscopy of probe molecules and reactants, as well as IR–VIS sum frequency generation SFG vibrational spectroscopy.<sup>13</sup> Scanning tunneling microscopy (STM) images allow the observation of the crystal shape and exposed faces.<sup>14</sup> These studies indeed allow to bridge a large part of the material gap, which, however, still exists.

Even for some well-established industrial processes, authors still disagree on the real state of the working catalyst, the nature of the active sites and reaction mechanisms. This is in part due to the reason that metal catalysts may indeed change

significantly their surface and even bulk composition depending on the reactant environment. Additionally, the above cited techniques may fail when very small clusters, very defective species and several additives are present at the surface.

### 9.1.2 Unsupported metal nanoparticles

In recent years, a number of methods have been developed allowing the preparation of well-characterized and shaped metal nanoparticles.<sup>15</sup> This allowed testing the effect of the shape of such particles with respect to catalytic activity. As for example, Alayouglu et al.<sup>16</sup> were able to prepare monodisperse platinum nanoparticles with well-controlled sizes in the 1.5–10.8 nm range, with the shapes of octahedron, cube, truncated octahedron and sphere. The catalytic activity of these materials was tested in methyl-cyclopentane ring opening in the presence of hydrogen. While the octahedra produced mainly hexane, truncated octahedra and spheres produced 2-methylpentane and cubes mainly gave rise to cracking products. These studies could also allow to compare the catalytic data with those arising from monocrystal data, thus attributing the catalysis on nanoparticles to the activity of the exposed faces or, alternatively, of corners and edges. It is evident, however, that this work is still largely to be done. Indeed, bulk metal nanoparticles may act as very good catalysts, as found, for example, for ethanol steam reforming over unsupported vs supported cobalt nanoparticles.<sup>17</sup> In other cases, e.g. Ni, a remarkably different behavior is observed for conversion of ethanol in the presence of steam from unsupported and alumina-supported nanoparticles.<sup>18</sup> Pd metal nanoparticles are indeed very efficient catalysts for a number of organic reactions.<sup>19</sup> However, the thermal stability of unsupported metal nanoparticles is weak, and thus they may be essentially regarded as model catalysts.

---

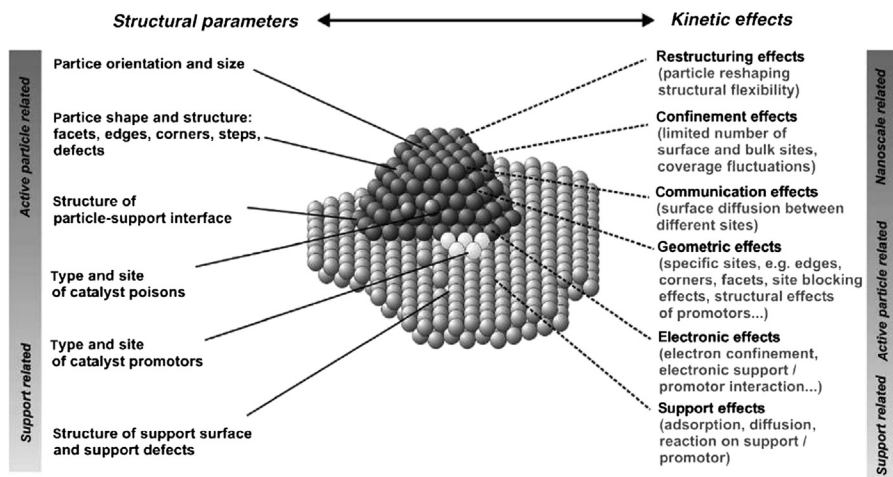
## 9.2 Supported metal catalysts

Actually, most metal catalysts of industrial interest are supported. This makes clearly very complex the nature of these materials (Figure 9.3<sup>20</sup>). Supporting allows to reduce the metal amount and to produce very active metal species. Properties of these catalysts depend from many factors such as the nature and morphology of the support, the preparation procedure, the metal precursor compound, metal loading, calcination and reduction pretreatments, etc.

### 9.2.1 Supports for metal catalysts

The following materials are most commonly used industrially for supporting catalysts:

1. Aluminas. As reported in Chapter 6.4.3, when applications require relatively low reaction temperature (<500 °C), high surface-area  $\gamma$ -,  $\delta$ - or  $\eta$ -Al<sub>2</sub>O<sub>3</sub> are common industrial catalyst supports ( $S_{\text{BET}} > 150 \text{ m}^2/\text{g}$ ). These are typically

**FIGURE 9.3**

Structural parameters and kinetic effects on supported metal catalysts.

*Reprinted with permission from Ref. 20*

highly ionic and highly dispersing catalyst carriers. These supports, however, are characterized by high acidity and reactivity, and thus not applicable when very reactive compounds are present in the reactant mixture. They are also unstable at temperatures  $>500\text{ }^{\circ}\text{C}$ , tending to convert into  $\theta\text{-Al}_2\text{O}_3$  or  $\alpha\text{-Al}_2\text{O}_3$  with a loss in the surface area. For these reasons, less reactive and more stable lower surface-area aluminas are used in several applications, such as  $\theta\text{-Al}_2\text{O}_3$  ( $S_{\text{BET}}\ 50\text{--}100\ \text{m}^2/\text{g}$ ),  $\alpha\text{-Al}_2\text{O}_3$  or  $\alpha\text{-Al}_2\text{O}_3/\theta\text{-Al}_2\text{O}_3$  mixed phases ( $S_{\text{BET}} < 50\ \text{m}^2/\text{g}$ ).

2. Metal aluminates. Mg and Ca aluminates, with spinel and  $\beta$ -alumina structures, are also largely used as refractory, stable and quite unreactive carriers for high-temperature applications such as steam reforming, partial oxidation, autothermal reforming and catalytic total oxidations. The surface area of these materials may be low or very low and dispersion of their surface is frequently not high.
3. Silicas. According to their covalent character, silicas are typically non-dispersing carriers in spite of their high surface areas (Chapter 6.4.5). They usually give rise to medium-size-supported metal particles. These supports have quite high thermal stability and chemical inertness.
4. Titanias and zirconias. These are supports with weak redox properties, medium acido-basicity (Chapter 6.4.6 and 6.4.7), high dispersing ability, and high reactivities toward the metal, giving rise to Strong Metal–Support Interaction effects (SMSI). Titania (anatase) and monoclinic zirconia (baddeleyite) have limited thermal stability tending to convert into more stable phases rutile and tetragonal/cubic zirconia.
5. Ceria. Ceria (Chapter 6.4.8) is a typical support or support component characterized by redox properties and oxygen storage capacity, useful for redox

reactions. This, however, gives also rise to some instability. In any case, ceria has high dispersing ability for metal sites and some surface basicity.

6. Zinc oxide. Zinc oxide (Chapter 10) has some hydrogenation/dehydrogenation activity. It is largely used as an activating support, in particular for copper and palladium hydrogenation catalysts. Reduced Zn is supposed to have a synergy with copper metal for methanol synthesis and water–gas shift, while the formation of Pd–Zn alloy is very likely in the case of the corresponding Pd-based catalysts.
7. Magnesia. Strongly basic support (Chapter 6.4.2), it is quite unstable in the presence of CO<sub>2</sub> and water. As a catalyst support, it suffers from quite a low surface area and poor mechanical strength. In spite of this, it is reported to be an excellent support for some metal catalysts.
8. Zeolites. Zeolites (Chapter 7) have high dispersing ability for cations. After reduction, the size of the metal particles may be limited by the size of the cavity. They may allow to associate metal catalysis with shape selectivity. They also allow to associate metal and strong protonic acid catalysis, or even metal and basic or neutral acid-basic catalysis when alkali-cationic zeolites are used (e.g., Pt–K–zeolite catalysts for aromatization reactions).
9. Carbons. Different forms of carbons such as activated carbons and graphite, are used as supports (see Chapter 8.9) mainly for noble metal catalysts. They are used mainly for low-temperature liquid-phase applications, or gas-phase applications in reducing atmospheres. Their dispersing ability may be tuned, depending on the carbon pretreatment (oxidizing or reducing).
10. Calcium carbonate and barium sulfate are the supports of Pd in the so-called Lindlar catalysts, Pd–Pb/CaCO<sub>3</sub> and Pd–Pb/BaSO<sub>4</sub>, applied in organic chemistry for selective hydrogenations of C≡C bonds to C=C bonds.

### 9.2.2 Supported metal nanoparticles

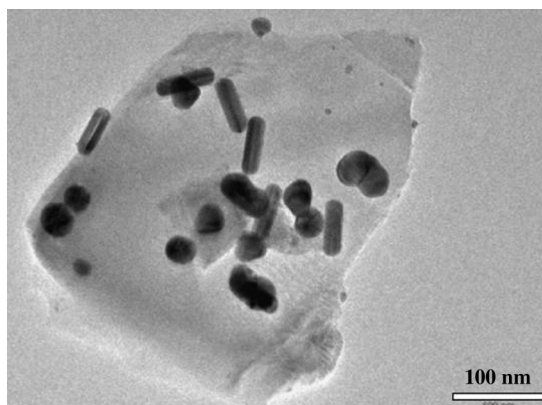
Most of the supported catalysts are prepared by impregnation of the supports with salts or other precursors of the metal, followed by calcination and reduction to metal state. Depending on the nature of the support, either poorly dispersing (such as silica and untreated carbon supports) or highly dispersing (such as alumina, titania, zirconia, ceria), and on the loaded amount, well defined nanocrystalline metal particles can be formed at the surface of the supported metal catalysts. When the metal loading is higher, as for some heavily charged catalysts like usually those based on nickel, techniques like X-ray diffraction and Transmission Electron Microscopy provide evidence of them and can be used to analyze the size and the shape of such particles as well as the nature of the exposed faces. When metal particles are small, other techniques, such as IR spectroscopy of adsorbed carbon monoxide, can be applied to obtain information on particle size.<sup>21</sup>

Actually, in the case of most noble metal-based industrial catalysts, the amount of the metal is small or even very small. In this case, the dispersion of metal may be very high and the size of the metal particles very small. Thus, not always the supported metal particles can be well characterized even by using electron

microscopies, and they are not always evident by using X-ray diffraction. In recent years, alternative colloidal methods have been developed to prepare well shaped metal nanoparticles first and supporting them later.<sup>22,23</sup>

The presence of these particles justifies comparison with data obtained on monocrystal faces as well as theoretical calculations performed with periodic methods on metal crystal faces. The only limit, frequently somehow uncorrectly neglected, is that, although these particles may expose the typical low index faces well known to physicists and theoreticians, they have a very high density of defects, such as edges and corners between faces. It is quite reasonable to suppose that, even if studies mainly deal with interaction of reactants on main low index faces (such as the 111 face of hcp metals, Figure 9.2), the chemistry of edges and corners may be even more relevant. Surface scientists are today able to provide more reliable data by using stepped surfaces (such as the 533 and 210 faces of hexagonal close-packed metals,<sup>24</sup> Figure 9.2) to model surface defects and also using model surfaces. Theoreticians still have difficulty in approaching more complex surface defects of metal particles.

Supported catalysts with relevant metal loadings with respect to the support surface present frequently well-shaped metal nanoparticles. In Figure 9.4 a TEM micrograph of a butadiene hydrogenation catalyst composed of 0.15% Pd/ $\alpha$ -Al<sub>2</sub>O<sub>3</sub> with 8 m<sup>2</sup>/g is shown.<sup>25</sup> It clearly presents two families of particles, rod-like polycrystalline particles together with nanopolyhedra called multiply twinned particles (MTP). The latter are typical morphologies found on supported Pd<sup>25,26</sup> and Au catalysts.<sup>27</sup> They appear to be hexagonal at TEM analysis formed by six icosahedra subunits, covered only by (111) planes. For Pd, cuboctahedra are also sometimes evident by HRTEM.<sup>28</sup> In the case of heavily loaded supported-Ni catalysts, hexagonal, rhombic or more complex shapes of Ni particles are observed, such as “spear-head-like” and “drill-like” particles with the (111) face largely exposed favoring the formation of carbon whiskers or nanotubes.<sup>29</sup> On the other hand, the supported



**FIGURE 9.4**

TEM micrograph of a Pd/Al<sub>2</sub>O<sub>3</sub> butadiene hydrogenation catalyst.

*Reprinted with permission from Ref. 25.*



small crystals may have nonbulk properties, such as negative thermal expansion, as observed for the small supported Pt particles.<sup>30,31</sup> The nature of the support surface influences the shape of the catalyst nanoparticles and clusters, as shown by theoretical calculations for Pt clusters on hydrated or dehydrated alumina surfaces.<sup>32</sup> Also, the supported nanoparticles tend to sinter at high temperature,<sup>33</sup> but this occurs more slowly than for unsupported ones.

### 9.2.3 Isolated and very highly dispersed metal centers

Most literature concerning redox-properties of the supported metal catalysts refer to the presence of metal particles of different sizes and oxide particles and their interconversion. This is in part because these species are those that can be detected with common techniques such as XRD and TEM, thus allowing parallelism with the surface science studies of monocrystals, and can be modeled by theoretical approaches. However, this approach is certainly an oversimplification. As for example, in the TEM micrograph of the Pd/Al<sub>2</sub>O<sub>3</sub> catalyst reported in figure 9.4, together with well shaped and “big” metal particles, a number of much smaller nanocrystals are evident, with quite undefined shape. Additionally, the photograph cannot exclude the existence of even smaller clusters or of isolated Pd atoms. Although not evident to TEM, these additional particles could have a role in catalysis. It is more and more clear today that, together with extended metal particles, dispersed atoms and clusters usually also exist on metal catalysts supported over “dispensing” carriers. High-resolution microscopy studies of Pt on alumina systems provide evidence of the existence of atomically dispersed Pt metal and of Pt<sub>3</sub> clusters under reducing conditions.<sup>34,35</sup> It is quite evident that one cannot exclude the presence of isolated Pd atoms and/or extremely small clusters or even very small metal particles on the support surface in the case of the catalysts represented in Figure 9.3. Even if not very evident in the TEM micrograph, sites of this kind, if they exist, could carry the main catalytic activity of the catalyst.

According to Xiao and Schneider,<sup>36</sup> atomically dispersed Pd and Pt on supports ( $\alpha$ -Al<sub>2</sub>O<sub>3</sub>) can be quite easily oxidized, and oxidation is also favored by support hydroxylation. Isolated zerovalent Pd centers can apparently be easily oxidized by oxygen to Pt<sup>2+</sup>, usually with the intermediacy of species like Cu<sup>+</sup>/Cu<sup>2+</sup> or heteropolyacids, in both homogeneous water solutions or heterogeneous solid/water and solid/vapor states at 300–400 K, as it occurs in the reoxidation step of the Wacker ethylene oxidation process.<sup>37</sup>

Theoretical studies reported on the stabilization of highly uncoordinated Pt and Pd metal centers by alumina, providing a relevant difference of the alumina-supported catalysts with respect to bulk metal surfaces.<sup>32</sup> This work also confirmed on the effect of hydroxylation/dehydroxylation of the support on the state of Pt and Pd, that become positively charged when deposited on hydroxylated alumina faces, while they are neutral or even negatively charged over dry surfaces. Other studies report the existence of Pd particles decorated with a thin layer of an aluminate phase on Pd/Al<sub>2</sub>O<sub>3</sub>-supported catalysts.<sup>38</sup> The existence and the likely catalytic activity of isolated centers has been proposed recently for CO oxidation and water–gas shift on Pt/Al<sub>2</sub>O<sub>3</sub> and different oxide-supported Pd catalysts.<sup>39–41</sup> Appropriate catalyst

preparation procedures allow indeed the preparation of atomically dispersed metal centers that find catalytic activity and are supposed even to represent the real active sites in reactions such as CO oxidation and water–gas shift.<sup>42</sup>

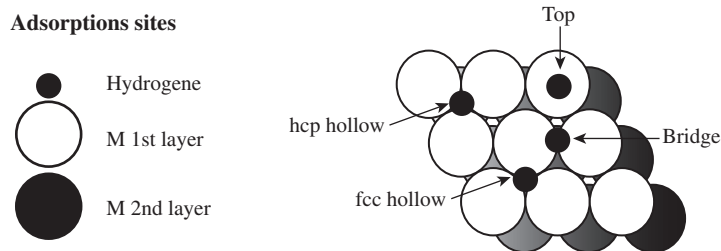
## 9.3 Fundamentals of hydrogenation/dehydrogenation

Hydrogenation reactions are exothermic equilibrium reactions, thus performed at the lowest temperature allowed by the catalyst activity, and at medium to high pressure. Most of them are performed in the presence of solid metal-based catalysts, most frequently in multiple fixed beds with interbed cooling by heat exchange or quenching, in gas/solid or gas/liquid/solid conditions, or in slurry conditions, depending on the volatility of the reactants as well as on the reaction temperature and pressure. In recent years, catalytic distillation processes have been developed, where reaction occurs in a distillation towers partly packed with catalyst bed.

### 9.3.1 Adsorption of hydrogen on metals

There is general agreement that hydrogen adsorbs dissociatively very fast on almost all relevant metal surfaces, being the dissociation of hydrogen only weakly activated or even barrierless. As for example, it has been found that when an  $H_2$  molecule chemisorbs on a Pt surface, the antibonding  $\sigma^*$  orbital of  $H_2$  is completely filled by electrons from platinum. Thus, dissociative adsorption occurs nonactivated, i.e. it is not kinetically hindered.<sup>43</sup> Only on group-11 metals (Cu, Ag, Au), hydrogen dissociation is significantly activated and may be endothermic.<sup>44</sup> On  $Cu/Al_2O_3$  an activation energy of 42 kJ/mol was found<sup>45</sup>. On-top, bridge or hollow sites can be occupied by atomic hydrogen species on metal surfaces (Figure 9.5<sup>46</sup>).

In all cases,<sup>47</sup> hydrogen dissociation gives rise to strongly bonded surface atomic hydrogen, mostly occupying hollow sites. For face-centred cubic metals, (111) surfaces have been mostly investigated, while for hexagonal close-packed metals, (0001) surfaces have been the object of most investigations. For body-centered cubic metals, most studies are on (110) faces. In all three cases, occupancy of 3-fold sites



**FIGURE 9.5**

Representation of the high-symmetry madsorption sites on an fcc metal.

*Reprinted with permission from Ref. 46.*

is essentially favored, although other adsorption sites such as bridge sites (such as found on Pd(100)) and top sites (such as found on Pt(111)) may be competitive with 3-fold sites.<sup>10</sup> Only in the case of Ir(111), top sites appear more favored than hollow sites for surface atomic hydrogen location.

The formation of subsurface atomic hydrogen is also possible, usually with an endothermic process. Tetrahedral and octahedral subsurface sites are occupied in this case. Only in the case of palladium, migration of hydrogen in the interior of the bulk is apparently exothermic too, due to a very large binding energy (−2.5 eV). This agrees with the data that show that only in the case of Pd a significant population of subsurface hydrogen can occur and bulk hydrides also form.<sup>48</sup> At early stages, the alpha phase is formed, where hydrogen atoms randomly populate small interstices in the lattice structure. At a critical point, the lattice expands, allowing hydrogen to cluster at higher density (the beta phase).<sup>49,50</sup>

In the case of Ni surfaces, they also remain unreconstructed under H<sub>2</sub> exposure. At room temperature (or above), H atoms adsorbed on Ni(100) do not show any ordering. According to Density Functional Theory (DFT) studies,<sup>51</sup> the dissociation of the hydrogen molecule is possible only over the topmost Ni atom, and the resulting H atoms may adsorb either on two free hollow sites (but the adjacent bridge sites must be free) or two bridge sites (the adjacent hollow sites must be free).

Most studies are limited by the fact that they only consider mono-crystal faces. As for nickel powder, TPD studies<sup>52</sup> evidenced three distinct forms of hydrogen permanently chemisorbed at 100 K:  $\gamma$ -form, located in the subsurface layer and desorbed at about 186 K,  $\beta$ -form adsorbed in the so-called second layer and evolved at about 327 K, and  $\alpha$ -form, fixed directly on nickel surface and desorbed at 350–670 K range. Different supports modify differently the state of hydrogen adsorbed on nickel.<sup>53</sup> Alumina and silica insignificantly affect hydrogen strongly adsorbed on nickel, but significantly affect weakly adsorbed hydrogen; in particular, the effect of silica depends qualitatively on the way of preparation of the examined sample. Carbon affects significantly both strongly and weakly adsorbed hydrogen. As for small supported Pt particles,<sup>54</sup> it has been reported that, at very low H<sub>2</sub> pressure or high temperature, the strongest bonded H is chemisorbed in an atop position. With decreasing temperature or at higher H<sub>2</sub> pressure, only  $n$ -fold ( $n = 2$  or  $3$ ) sites are occupied. At high hydrogen pressure or low temperature, the weakest bonded H is positioned in an “ontop” site, with the chemisorbing Pt already having a stronger bond to an H atom in an  $n$ -fold site. DFT calculations<sup>54</sup> show that the adsorption energy of hydrogen increases for Pt particles on ionic (basic) supports. Both the H coverage and/or the type of active Pt surface sites, which are present at high-temperature catalytic reaction conditions, strongly depend on the ionicity of the support, with relevant consequences for Pt catalyzed hydrogenolysis and hydrogenation reactions.

### 9.3.2 Adsorption of organic substrates on metals

Surface metal atoms, according to their coordinative unsaturation, present both Lewis acidity toward  $n$ -bases, as well as  $\pi$ -bonding activities toward unsaturated

hydrocarbons. In fact, heteroatom-containing molecules such as saturated oxygenated compounds (including water<sup>55</sup>), amines (including ammonia), sulfur compounds (including hydrogen sulfide) and halogens are supposed to interact by donation of their full n-type orbitals with empty d-type orbitals of transition metal atoms, on-top. On the other hand, olefins, dienes and aromatics are thought to adsorb on metal centers by electron donation from their full  $\pi$ -orbitals to empty d-type orbitals of transition metal and the simultaneous electron back-donation from full d-type orbitals of transition metal to empty  $\pi^*$ -antibonding orbitals.

This interaction with olefinic double bonds can be rapidly converted into di- $\sigma$ -bonding,<sup>10</sup> while in the case of acetylene a tetra- $\sigma$ -bonding likely is formed.<sup>56</sup> In the case of aromatic rings, hexa- $\sigma$ -bonding are thought to form.<sup>57</sup> For heteroaromatic compounds such as thiophene, both  $\sigma$ -bonding and  $\pi$ -backbondings may occur simultaneously.<sup>58</sup> Later sequential addition of single hydrogen atoms to the adsorbed hydrocarbon intermediate are thought to occur.

### 9.3.3 Hydrogenation of hydrocarbons

Many metals, including platinum group metals, nickel, cobalt, iron, copper, etc. are active in hydrocarbon hydrogenation. However, some noble metals are far more active, but quite easily deactivated in particular by sulfur compounds. For these reasons, the catalyst composition for hydrocarbon hydrogenation is strongly dependent on the amount of sulfur impurities in the feed. Palladium, and, to a lesser extent, platinum are the choice catalysts for hydrogenation of clean feeds while nickel is mostly used for hydrogenation of medium sulfur-containing feeds. Bimetallic noble metal catalysts or other modified noble metal catalysts may also have interesting resistance to medium–low concentrations of sulfur. Feeds that are heavily contaminated by sulfur may be hydrogenated over typical hydrotreating sulfide catalysts, such as alumina-, silica–alumina- or zeolite-supported Ni–W, Ni–Mo or Co–Mo catalysts,<sup>59</sup> or bulk transition metal sulfides,<sup>60,61</sup> among which  $\text{RuS}_2$  is reported to be the most active (Chapter 10.2).

The mechanisms of catalytic hydrogenation of unsaturated hydrocarbons have been the object of many experimental and theoretical studies. A typical case concerns the hydrogenation of acetylene, preferentially producing ethylene, over palladium metal as well as over Ni-based alloys. A key point concerns the exothermal adsorption of acetylene. The transition-state energies for the following steps, i.e. the first and second hydrogenation steps finally producing adsorbed ethylene are both below the energy of gas-phase acetylene. A selective catalyst that hydrogenates only acetylene, thus producing ethylene selectively, should have an activation barrier for the hydrogenation of ethylene that is greater than the barrier for ethylene desorption. According to theoretical calculations, this indeed occurs with Pd and, even more, with Pd alloys such as Pd–Ag (in fact industrial catalysts usually contain this alloy) as well as with some Ni alloys.<sup>62</sup> Reactivity of adsorbed unsaturated hydrocarbons with adsorbed atomic hydrogen appears to be indeed easy, although the presence of adsorbed hydrogen may modify the energy of adsorption of unsaturated hydrocarbons on metal surfaces.<sup>10</sup>

### 9.3.4 Fundamentals of dehydrogenation

Dehydrogenation reactions are endothermic equilibrium reactions, thus performed at moderately high temperature and at low pressure. They are performed industrially in the presence of either metal-based catalysts or oxide catalysts (Chapter 10.1), most frequently in single or multiple fixed beds with previous or interbed heating.<sup>63,64</sup> Being reactions occurring at relatively high temperature and in the presence of organics and reducing environment, catalyst coking usually occurs. Reactor configurations must take into account this, allowing frequent or continuous regenerations. For this, several optional configurations have been developed: semiregenerative processes; cyclic regenerative processes; moving bed and continuous regenerative processes. Most of active hydrogenation catalysts act also as active dehydrogenation catalysts, according to a “reversibility” principle. This suggests that the ability to absorb or adsorb hydrogen is a key feature for dehydrogenation catalysis too. It seems likely that the ability of the catalyst to abstract and adsorb the first hydrogen atom from the reacting molecule speeds up the rate determining step of the dehydrogenation reaction.

### 9.3.5 Steam-reforming and related processes

Several important reactions imply the use of water to produce hydrogen. Steam-reforming processes are endothermic equilibrium reactions performed to convert organics and water to syngases, i.e. hydrogen and  $\text{CO}_x$  mixtures. They are typically performed in fixed bed-heated tubular reactors.<sup>65a,b</sup> In these reactions, water formally acts as an oxidant. Nickel and, to a lesser extent, noble metals such as Pt and Rh are applied for these reactions. Metal catalysis is mostly considered to occur, although the existence and role of unreduced centers is likely. This is also object of discussion for steam reforming of oxygenates such as methanol on copper catalysts and ethanol on cobalt catalysts, where a role of unreduced centers is supported by recent results.

Another option to produce hydrogen from organics is partial oxidation. This is the exothermic reaction with stoichiometric amounts of oxygen, also allowing the production of syngases. The advantages of this reaction with respect to steam reforming (exothermicity, no catalyst coking) are balanced by the drawbacks (use of expensive pure oxygen, lower hydrogen yield). This process is usually performed without any catalyst. However, a recent development is Catalytic Partial Oxidation (CPO), where gas-phase reaction is initiated by a catalytic step. Also in this case, the respective roles of metal and oxide catalysis have still not been fully defined.

The two reactions (steam reforming and partial oxidation) can also be performed together, balanced to have an autothermal process. These processes are with two-section reactors, a burner followed by a catalytic fixed bed.

In most cases, these processes are followed by one or more water–gas shift steps, where CO is converted by water to  $\text{CO}_2$ , thus producing more hydrogen and allowing easiest purification by separation of  $\text{CO}_2$ . Mechanisms for this reaction are under discussion.<sup>66</sup> In the case of the so-called redox mechanism, it is suggested that water oxidizes the metal, CO acting as the reductant for the oxidized catalyst.<sup>67</sup>

To further abate the residual CO, which is a poison for metal catalysts and fuel cell electrodes, either methanation or preferential oxidation (PROX) of CO are performed.<sup>67</sup> Also in the case of the PROX reaction, a redox mechanism with the catalyst oscillating between a metal and an oxide state is very likely to occur.

## 9.4 Metal catalysts for hydrogenation and dehydrogenation reactions

### 9.4.1 Iron-based metal catalysts

Iron is a very cheap element, easily reducible, and is active in hydrogen adsorption as well as the catalyst for hydrogenation reactions. However, its use in hydrogenation catalysis is limited to few but very relevant processes. Few applications are documented, in particular, for supported iron. Among them, supported iron has been reported to be active in the steam reforming of biomass tars (phenolic compounds and aromatic hydrocarbons).<sup>68</sup> Iron oxide-based catalysts are used since decades as high-temperature water–gas shift catalysts: although slightly reduced and pyrophoric when reduced, they are reported to be still oxides, mainly constituted by magnetite  $\text{Fe}_3\text{O}_4$ .<sup>65a,b,66</sup> Iron is quite sensitive to poisons, its hydrogenation activity being strongly affected by oxygenates including water, sulfur and chlorine. In the presence of carbon-containing compounds, carbides are quite easily formed.

#### 9.4.1.1 Fe-based ammonia synthesis

Ammonia synthesis from nitrogen and hydrogen (Haber process) is one of the few industrial processes where an unsupported metal catalyst is mostly used.<sup>69</sup> The most-used catalyst is very similar to one of the first tested by Karl Bosh at BASF in 1909. It is based on bulk iron, containing several elements for activation and stabilization. It was originally obtained from a Swedish magnetite mineral. Reaction is mostly performed at 300–500 °C and 80–300 atm using  $\text{N}_2/\text{H}_2$  feed ratio = 3 with some methane and Ar inert impurities. The catalyst may be charged in the oxidized form (either magnetite  $\text{Fe}_3\text{O}_4$  or wüstite  $\text{FeO}$ ) or in the prereduced form, both available commercially from most producers.

Topsøe sells the KM1 unreduced catalyst, 91–95% wt of iron oxides with 5–9% wt  $\text{K}_2\text{O}$ ,  $\text{Al}_2\text{O}_3$ ,  $\text{CaO}$  and  $\text{SiO}_2$ , as well as the prereduced KM1R catalyst (89–93% Fe,  $\text{FeO}$ ). The working temperature range is 340–550 °C, pressure with range 80–600 bar.<sup>70</sup>

The catalysts of the  $\text{KATALCO}_{\text{JM}}$  35 series and  $\text{KATALCO}_{\text{JM}}$  S6-10 series proposed by Johnson Matthey<sup>71</sup> are based on magnetite multipromoted and/or stabilized by  $\text{K}_2\text{O}$ ,  $\text{Al}_2\text{O}_3$  and  $\text{CaO}$ . To achieve higher activity at low pressures in the region of 80–150 bar,  $\text{KATALCO}_{\text{JM}}$  74-1 catalysts containing also  $\text{CoO}$  as a promoter are proposed alternatively.

Süd Chemie (now Clariant) proposes the AmoMax-10 catalyst, which is a wüstite-based ammonia synthesis catalyst (98%  $\text{FeO}$  plus promoters<sup>72</sup>) that, according to the firm, features significantly higher activity than magnetite-based catalysts.

This high activity level is also evident at low operating temperatures, allowing improved conversion at thermodynamically more favorable conditions. AmoMax-10 is available in oxide and pre-reduced, stabilized form.

BASF Ammonia Synthesis Catalyst is a multipromoted iron-based catalyst: in its commercial form, it contains  $\geq 67\%$  of iron in metal form with  $\geq 2.3\%$   $\text{Al}_2\text{O}_3$ ,  $\geq 2.1\%$  of promoter I and small amounts of oxidized iron, and three other promoters.<sup>73</sup>

#### 9.4.1.2 Fe-based high-temperature Fischer Tropsch catalysts

The High-Temperature Fischer Tropsch process (HTFT)<sup>74</sup> consists in the hydrogenation of CO and  $\text{CO}_2$  mixtures at c. 300 °C and 20–40 atm producing paraffins, olefins and oxygenates mainly with straight long-carbon chains. It is performed on iron-based catalysts.<sup>75</sup> Due to their high activity for the water–gas shift reaction, iron catalysts are more indicated for coal-based FT syntheses, i.e. with syngas characterized by a quite low  $\text{H}_2/\text{CO}_x$  ratio. This process produces more oxygenates and a slightly different molecular weight distribution for hydrocarbons with respect to Co-based catalysts applied in the Low-Temperature Fischer Tropsch process (Co-LTFT).<sup>75</sup>

A typical iron FT catalyst contains also a few percent of silica, copper and potassium. Copper is added to aid in the reduction of iron, while silica is a structural promoter added to stabilize the surface area but may also have a chemical effect on the catalyst properties. Potassium is considered to increase the catalytic activity for FT synthesis and water–gas shift reactions, to promote CO dissociation and enhance chain growth, increasing olefin yield and lowering the  $\text{CH}_4$  fraction.<sup>76,77</sup> Under reaction conditions, the catalyst converts into mixtures of carbides, like  $\chi\text{-Fe}_5\text{C}_2$  and  $\epsilon\text{-Fe}_{2.2}\text{C}$ , and magnetite  $\text{Fe}_3\text{O}_4$ , with only small amounts of  $\alpha\text{-Fe}$ . Carbide rather than metallic catalysis should really occur.<sup>76</sup> Recently, the possibility of use of zeolite-containing iron-based “multifunctional” catalysts for HTFT synthesis has been proposed. These catalysts offer opportunities in the modification of desired product distributions and selectivity, to eventually overcome the quality limitations of the fuels prepared under intrinsic FT conditions.<sup>78</sup>

#### 9.4.2 Cobalt-based metal catalysts

Cobalt catalysts are used sometimes commercially for hydrogenation reactions. Cobalt is definitely cheaper than noble metals but is significantly more expensive than Ni and Fe. Some cobalt compounds are classified as carcinogenic and toxic to reproduction, thus some problem exists in preparation and disposal of catalysts. Sponge cobalt (see below for sponge nickel) is commercially available for use in the hydrogenation of nitriles and nitro compounds to amines.<sup>79</sup>  $\text{CoO}/\text{SiO}_2$ ,  $\text{CoO}/\text{SiO}_2\text{--Al}_2\text{O}_3$  and  $\text{CoO}/\text{ZrO}_2\text{--Kieselguhr}$  catalysts ( $\text{CoO} > 39\%$ ) offered by Clariant, previously Sud Chemie, for hydrogenation of oxoaldehydes.<sup>80</sup> The manufacture of ethylamines and propylamines is performed by amination of the corresponding alcohols or reductive amination of aldehydes and ketones over the supported cobalt (or nickel) catalysts.<sup>81–83</sup>

#### 9.4.2.1 Co-based low-temperature Fischer Tropsch catalysts

The low-temperature Fischer Tropsch process, performed at 200–250 °C, 20–30 bar over Co-based catalysts (Co-LTFT), represents today a promising option to convert syngas produced from natural gas into middle distillate and hydrocarbon waxes both applicable to produce high cetane number and sulfur-free diesel fuels.<sup>84</sup> Among the different metals active as FT catalysts, cobalt represents the best choice for this application<sup>85</sup> for its moderate price, high activity with stoichiometric syngases arising from methane steam reforming, good selectivity to high molecular weight paraffins and low selectivity to methane, olefins and oxygenates. Among possible supports, alumina is a good choice because of its availability with texture suitable to Slurry Bed Catalytic Reactors (SBCR-LTFT). The cobalt FT catalysts are usually supported on high surface-area alumina (150–200 m<sup>2</sup>/g) and typically contain 15 ÷ 30% weight of cobalt. To stabilize them and decrease selectivity to methane, these catalysts also contain small amounts of noble metal promoters<sup>86</sup> (typically 0.05–0.1% weight of Ru, Rh, Pt or Pd) and/or an oxide promoter as well (zirconia, lanthana, cerium oxide, 1–10%). The role of noble metal doping has been supposed to be to improve the reducibility of cobalt, while the support and the oxide promoters may have a role in controlling the size of the cobalt metal to an optimal value. Authors agree that cobalt metal should represent the active phase in FT, the formation of cobalt carbide<sup>87</sup> and oxide (which may arise from reaction with water<sup>88</sup>) representing deactivation processes. *Via*-carbide mechanisms, i.e. implying surface carbidic species formed by dissociative adsorption of CO as active intermediates, have been found for Fischer Tropsch reaction over Co monocrystals<sup>89</sup> and seem to be today preferred for FT reaction over Co-based catalysts.<sup>90,91</sup> However, mechanisms through oxygenates are also being proposed for the main reaction to hydrocarbons<sup>92,93</sup> or for ways to oxygenates.<sup>94</sup>

#### 9.4.2.2 Co-based catalysts for ethanol steam reforming

A number of investigations are currently being undertaken to discover effective catalysts, to understand the reaction mechanism and to develop industrial or pilot scale processes for Ethanol Steam Reforming (ESR<sup>95–103</sup>). Yet, consensus has not been reached on the best composition of catalysts for ESR, as well as on the best conditions to perform it.

Co-based catalysts have been found to be active and selective for near-complete ESR at low temperature, when Ni catalysts produce methane reach syngases. Studies using unsupported cobalt oxide as catalyst showed that this oxide is essentially not active in ESR, and low-temperature steam-reforming activity was observed when the oxide is reduced to the metal.<sup>104–106</sup> In parallel, high activity was found for unsupported Co-metal nanoparticles.<sup>17</sup> The situation may be different for supported or coprecipitated cobalt catalysts. Recent studies suggested<sup>107–109</sup> that unreduced cobalt (Co<sup>2+</sup> species) may have an important role in ESR at least in some catalytic systems, where a very limited amount of metallic cobalt was observed, which is supposed to be the reason for limited coking.<sup>110,111</sup> In fact, combining the catalyst with an oxide carrier favors the formation of highly dispersed cationic species

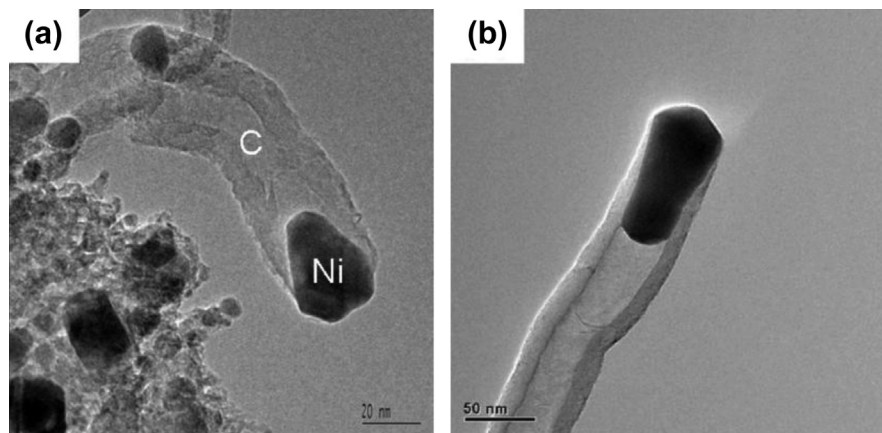


that may be stabilized in high oxidation states.<sup>41</sup> Thus, coalesced metal particles and dispersed cationic species may coexist, and it is not always clear what is active in catalysis or in deactivation phenomena, or whether some synergism occurs. On the other hand, different oxide carriers have a different behavior in dispersing metal species and redox-active carriers, such as ceria, have an effect in determining their oxidation state. Oxide phases can also participate differently in the water activation step. In very recent times, a number of different formulations have been studied and proposed for Co catalysts for ESR such as different supports as well as promotion of cobalt or alloying it with other metals such as Ni, Ru, Ir, Fe, Cu, Cr, Na and K.

### 9.4.3 Nickel-based metal catalysts

Nickel is a very active metal in hydrogenation catalysis. It is also a cheap element thus allowing its use as a bulk metal (e.g. as Raney nickel) as well as in the form of highly loaded supported catalysts. This also gives rise to some sulfur resistance, just because much sulfur is needed to fully poison highly loaded catalysts. On the other hand, the carcinogenic toxicity of nickel compounds is a big concern in the preparation and disposal of catalysts.

Another relevant problem concerning the use of nickel catalysts is the formation of carbon nanotubes in the presence of hydrocarbons or other carbon sources. Nanotubes form specifically on the external surface of “spearhead-like” and “drill-like” Ni particles with the (111) face largely exposed<sup>29</sup> (see Figure 9.6<sup>112</sup>). These materials do not cause directly the deactivation of the catalysts, but increase the density of the bed occupying the empty spaces, thus increasing pressure losses. Real deactivation can occur later on. This is a main problem in several processes, such as methanation, steam-reforming of higher hydrocarbons, and of ethanol.



**FIGURE 9.6**

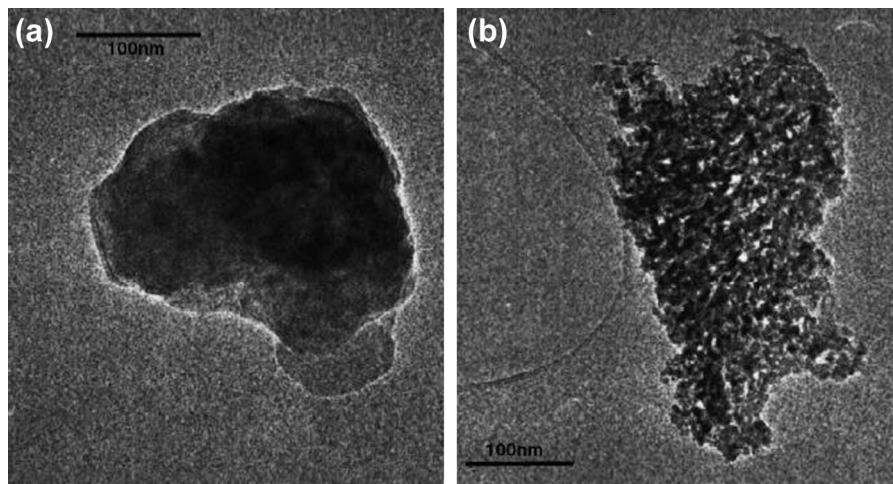
(a and b) HRTEM images of carbon whiskers forming on Ni-based steam reforming catalysts.

*Reprinted with permission from Ref. 112.*

Another relevant aspect of Ni catalysts when working in the presence of CO is the possibility of formation of the very volatile carbonyl  $\text{Ni}(\text{CO})_4$ , with abstraction of Ni from the catalyst. This may occur in the range 120–200 °C causing the loss of nickel from the catalyst and its transport to other sections of the plant.

#### 9.4.3.1 Nickel Raney and sponge nickel catalysts

Raney Nickel and sponge nickel catalyst<sup>79</sup> are prepared starting from a Ni–Al alloy produced by dissolving nickel in molten aluminum followed by cooling (“quenching”). In the activation process, the alloy, usually as a fine powder, is treated with a concentrated solution of sodium hydroxide which dissolves aluminum with the formation of sodium aluminate ( $\text{NaAl}(\text{OH})_4$ ) leaving a porous and quite impure metallic nickel “sponge” (Figure 9.7<sup>113</sup>). Raney Nickel is mostly used in slurry-phase catalytic hydrogenations. As a relevant example, cyclohexane is produced in liquid phase by benzene hydrogenation; the organic liquid and hydrogen-rich gas are fed to a liquid-phase slurry reactor containing Raney nickel catalyst at 200–225 °C and 50 bar. The nickel suspension is circulated to improve heat removal, benzene being completely hydrogenated in a second fixed-bed reactor. In this process, there are several drawbacks with respect to gas-phase hydrogenation processes: a continuous consumption of catalyst leading to the generation of waste-exhausted catalyst to be disposed as dangerous residue, and the limited exploitation of the heat released upon the exothermic reaction due to the low reaction temperature. Nickel Raney, doped by iron and chromium or by molybdenum and alumina, is also used in several other processes such as adiponitrile hydrogenation to



**FIGURE 9.7**

TEM images of Ni Raney. (a) Grain of starting alloy; (b) grain of Raney-type nickel catalyst, clearly illustrating the terminology “sponge nickel”.

*Reprinted with permission from Ref. 113.*

hexamethylenediamine in slurry phase over Ni Raney at 120–150 °C—35 atm<sup>79,114</sup> such as the BASF Actimet 8040P catalyst (92% Ni, 1% Mo, 7% Alumina, Average Particle Size 35 μm). This catalyst is supplied immersed in water to protect it from air oxidation. In a dry state, it is pyrophoric.<sup>115</sup>

#### 9.4.3.2 Nickel/silica catalysts

According to the weak dispersing ability of silicas, Ni on silica gives rise to Ni-metal particles weakly interacting with this quite inert “support”. Catalysts, containing up to 70% NiO with kieselguhr, amorphous silica or silica–alumina in the fresh unreduced state, are largely applied for a number of hydrogenations such as of oxoaldehydes to alcohols, reductive amination of carbonyls, alcohols and nitriles and nitro-compounds hydrogenation to amines. These catalysts are used also for hydrocarbons hydrogenation such as naphtha dearomatization.

Several processes imply the hydrogenation of aromatic or olefinic multiple CC bonds without reducing the copresent oxygenated functions. Among traditional processes, we can mention the hydrogenation of C=C double bonds of unsaturated fatty acid chains in converting vegetable oils into margarine. Small crystal-size nickel on high surface area and pore volume silicas including diatomite, working at 180–230 °C, 2–6 bar, represent the traditional catalysts,<sup>116</sup> like the catalysts of the PRICAT series from Johnson Matthey,<sup>117</sup> and NYSOSEL from BASF.<sup>118</sup> As for example, Pricat 9910 is reported to be constituted by 22% Ni, 4% SiO<sub>2</sub> dispersed in hydrogenated edible fats.<sup>119</sup> Batch processes are most commonly used in the oil industry. The carbon double bonds are partially or fully saturated during the hydrogenation. Concomitantly, the catalytic isomerization of naturally occurring *cis* fatty acids (CFAs) to *trans* fatty acids (TFAs), which have negative health effects, takes place to some extent. The selectivity of the process represents a considerable challenge, aiming to enhance the hydrogenation rate of the double bonds saturation and simultaneously to suppress the isomerization. Doping nickel catalysts with silver seems to reduce *cis-trans* FA isomerization.<sup>120</sup>

Hydrogenation of nitrobenzene to aniline is performed with different processes and reactor systems. Slurry-phase processes apply mostly Ni-based catalysts such as Ni-silica containing small amounts of iron.

#### 9.4.3.3 Ni-alumina- and Ni-aluminate-based catalysts

In contrast with what happens on silica, where nickel and other metals are not really dispersed, on alumina Ni tends to be dispersed atomically to some extent, producing hardly reducible surface cations that can give rise even to isolated metal centers or small clusters.<sup>120a</sup> At intermediate loadings, NiO is observed by XRD on the unreduced catalyst, but other techniques (such as TPR and UV) reveal a behavior different than that of “normal” NiO particles<sup>120b</sup>; small metal particles predominate on the corresponding reduced catalysts. When loading is high, particles similar to unsupported NiO are also present in the unreduced catalyst, quite large Ni crystals being formed upon reduction. Interestingly, in some cases, hexagonal nickel is produced instead of cubic nickel, possibly because a stabilization of hexagonal phase by carbon species.

Ni/Al<sub>2</sub>O<sub>3</sub>-based catalysts may be used, as an alternative to Pd or Pt catalysts (Chapters 9.4.7 and 9.4.10), for hydrogenations of unsaturated hydrocarbons such as to reduce acetylenics and aromatics. Hydrogenation of C2 and C3 acetylenics in steam-cracked cuts may be performed simultaneously in the so-called front-end hydrogenation configuration<sup>121,122</sup>; if the feed contains significant amounts of sulfur compounds, a multipromoted NiO catalyst supported on silica–alumina (0.6–2.6% NiO), as the OleMax 10 (Clariant, previously Süd Chemie) can be used. Hydrogenation of  $\alpha$ -acetylenic compounds (1-butyne and vinylacetylene) may be performed with 100% yield to purify the steam cracking C4 cut in order to simplify the further extraction of 1,3-butadiene (e.g. by *N*-methyl pyrrolidone). This occurs in the UOP KLP process,<sup>123,124</sup> using a single fixed-bed of the KLP-60<sup>TM</sup> catalyst, Cu–Ni/Al<sub>2</sub>O<sub>3</sub>, in the liquid phase. Temperatures are not allowed to exceed 85 °C. The reactor pressure is set to maintain the reaction mixture in the liquid phase. Two or three reactors are used one of which is in regeneration by a solvent wash. The catalyst selectively converts acetylenes, with a significant amount being converted to butadiene. The process produces a high-quality butadiene product, with typically less than 5 ppm acetylenes.

The Hüls Selective Hydrogenation Process (SHP) was developed for hydrogenation of dienes and acetylenes in C3–C5 olefin fractions to their respective mono-olefins. The conversion of dienes and acetylenes is nearly 100%. There is minimal loss of olefins via nonselective saturation reactions. H-15 SHP catalyst from UOP<sup>125</sup> is nickel-based, sulfur-resistant catalyst optimized for use in Hüls Selective Hydrogenation process units. The H-15 catalyst can provide an economical operation at feed sulfur levels up to 300 ppm. Small amounts of straight chain C10 to C13 diolefins are selectively hydrogenated to the mono-olefins in the feed to alkylation reactor in the process of production of Linear Alkyl Benzene (LAB). The reaction is carried out in a liquid phase at 170–230 °C and 10–20 bar on nickel–alumina (Ni/Al<sub>2</sub>O<sub>3</sub>) catalyst.<sup>126,127</sup>

Pyrolysis gasoline is purified from acetylenics and dienes by hydrogenation, before hydrodesulfurization. Johnson Matthey offers the HTC NI 200 (12% Ni on alumina<sup>128</sup>), which is available in three forms—oxidic (OX), prereduced and air passivated (RP) and prereduced, air passivated and presulfided (RPS).<sup>129</sup>

Supported Nickel catalysts may be used for dearomatization of hydrocarbon flows, in competition with Pt catalysts. Due to the wide pore structure and small nickel crystals providing high strength, activity, selectivity and poison resistance, together with lower gum/polymer formation and side reactions, nickel catalysts can offer comparable performance to noble metal catalysts. Nickel catalysts contain 20–50 times more active metal atoms than noble metal catalysts. For this reason, Ni catalysts may be more tolerant to poisons than noble metal catalysts, and therefore they are preferred in case of highly contaminated feedstocks. Süd Chemie (now Clariant) offers Ni-based catalysts (the NiSAT<sup>®</sup> family, with NiO content from 43% to 77%) for naphtha dearomatization.<sup>72</sup> For the same reaction, Axens proposes the Benfree<sup>TM</sup> reactive distillation process, integrating reactive hydrogenation with the reformat splitter column, thus reducing equipment and associated costs. The

catalyst (AX 744) is a nickel catalyst, recommended for its high resistance to poisons when the feed contains a few ppm of sulfur or other contaminants.<sup>130</sup>

Methanation, i.e. the synthesis of methane from hydrogenation of  $\text{CO}_x$  is performed industrially according to two main configurations, both using, usually, Ni/ $\text{Al}_2\text{O}_3$ -based catalysts.<sup>131,132</sup> Low-temperature methanation allows to destroy carbon oxides impurities in hydrogen to avoid the presence of such oxygenated poisons from hydrogenation catalysts such as e.g. ammonia synthesis and adiponitrile hydrogenation catalysts. To do this, Topsøe produces the prereduced PK-7R catalyst, constituted by 23% Ni wt on an alumina carrier, which ensures that CO and  $\text{CO}_2$  are fully converted to methane at an operating temperature of 190 °C.<sup>133</sup> The composition is similar to that of Süd Chemie (now Clariant) METH<sup>132</sup> catalyst. These catalysts cannot be used below 190–200 °C to avoid the formation of  $\text{Ni}(\text{CO})_4$ . Methanation can also be performed using syngases rich in carbon oxides, like those that arise from coal or biomass gasification, to convert them into Substitute or Synthetic Natural Gas (SNG).<sup>134</sup> In this case, the exothermicity of the reaction causes the temperature to increase, interbed cooling being needed to control it into limits to make the reaction thermodynamically favored and the catalyst stable. The high-temperature methanation-catalyst Topsøe MCR is reported to have stable activity up to 700 °C.<sup>135</sup> Publications report about the use of a 22% Ni catalyst on a stabilized support, with a surface area decreasing from 50  $\text{m}^2/\text{g}$  (fresh) to 30  $\text{m}^2/\text{g}$  (used).<sup>136</sup>

Until the 1970s, the mechanism of methanation was supposed to occur through oxygenated intermediates.<sup>137</sup> A *via*-carbide mechanism has been mostly considered recently for methanation over pure Ni catalysts.<sup>138,139</sup> However, infrared spectroscopy methods provide evidence of the easy formation of oxygenate intermediates and, in particular, of the evolution of methoxy groups into methane by hydrogenation over Ni- $\text{Al}_2\text{O}_3$ .<sup>140</sup> Ni/ $\text{Al}_2\text{O}_3$  catalysts are also active for  $\text{CO}_2$  methanation, an interesting option for utilization of carbon dioxide.<sup>140b</sup>

Hydrogen is mostly produced today through steam reforming of hydrocarbons, usually natural gas,<sup>65a,b</sup> performed at 750–900 °C, 30–50 bar. The industrial catalysts are mostly based on Ni supported on an alumina-based carriers, usually stabilized by the presence of alkali and/or alkali-earth cations. Typical methane steam-reforming catalysts contain 10–25% wt Ni, 70–85%  $\text{Al}_2\text{O}_3$  or aluminate supports and up to 5% K, Ba, Ca. These catalysts need an important refractory character. The support phase is in fact a refractory oxide such as alpha-alumina, Mg aluminate spinel  $\text{MgAl}_2\text{O}_4$ , calcium aluminate  $\text{CaAl}_2\text{O}_9$  and calcium–potassium aluminate  $\text{CaK}_2\text{Al}_{22}\text{O}_{34}$ .<sup>72</sup> Modern large hydrogen production plants contain a previous adiabatic fixed-bed-prereforming reactor, where higher molecular weight are reformed. These catalysts, working at lower temperature (500–600 °C), contain much more Ni (NiO 45–60%), with other additional components (some silica and chromia).

Ni-based steam reforming catalysts, however, are reported to be rapidly irreversibly deactivated in case of daily start-up and shut-down operations, typical in case of hydrogen and Fuel Cells' domestic use. In this case, Ni catalysts doped with small amounts of noble metals are reported to display an “intelligent” behavior, with suppression of such deactivation phenomena.<sup>141</sup>

Oxygen-blown autothermal reformers and secondary reformers require a mixed loading of catalysts, comprising an active heat shield (Ni on alfa alumina) and a reforming catalyst of excellent physical stability and thermoshock resistance.

The production of low H<sub>2</sub>/CO ratio syngases through the dry reforming of methane, i.e. the reaction of methane with carbon dioxide, is also a potentially useful process. Coking in this case is a more serious problem, and, for this reason, noble metal catalysts, which suffer coking less than Ni-based ones, have longer life.<sup>142–144</sup> Also in this case, bimetallic catalysts such as Pt-doped Ni catalysts may have optimal behavior.<sup>145</sup>

Different technologies are currently under development to produce biofuels, in order to reduce greenhouse gas emissions and dependence from fossil fuels.<sup>146</sup> Gasification of biomasses represents a promising and already quite established approach to produce syngases,<sup>147</sup> whose combustion or conversion may give rise to renewable energy, biohydrogen and liquid biofuels. However, gasification technologies present a number of drawbacks, among which the production of tar<sup>148</sup> (1–50 g/Nm<sup>3</sup> depending mainly on the reactor type) and the presence of sulfur (20–600 ppmv H<sub>2</sub>S depending on the biomass<sup>149</sup>) and chlorine (up to some hundreds of ppm depending on the biomass<sup>150</sup>) as pollutants of the resulting syngas. Biomass tar is a complex mixture of quite heavy organic molecules produced together with other low-volatility oxygenates.<sup>151</sup> These molecules can condense in the cool sections of the plant (like on heat exchangers) producing fouling, or may cause coking and deactivation of catalysts (such as for water–gas shift) and anodes of fuel cells.<sup>152</sup> Catalytic steam reforming (SR) appears to be one of the most interesting approaches to destroy such molecules. Ni-based SR catalysts similar to those used for methane SR<sup>153</sup> appear to be active to this purpose but sensitive to sulfur-poisoning. Noble metal-based catalysts are active at lower temperature and less prone to coking and more sulfur-resistant.<sup>154,155</sup> In spite of this, catalysts specific for biomass tar SR, apparently based on nickel,<sup>156</sup> are commercialized and are reported to be active in real pilot-plant conditions.<sup>157</sup> Similar nickel catalysts are reported to be useful for steam reforming of bio-oils produced by biomass pyrolysis, as well as for “bio-ethanol” steam reforming, to produce “bio-hydrogen”. In the case of ESR indeed Ni catalysts are effective at quite a high temperature, but produce much methane at lower temperature.<sup>95–103</sup>

#### 9.4.4 Copper-based catalysts

Copper catalysts find large application for hydrogenation and dehydrogenations of oxygenated compounds, with retention of C–O bonds. This contrasts what happens with other metals, including nickel, where C–O bonds are more easily hydrogenolyzed. Thus copper-based catalysts are used for methanol synthesis and decomposition, as well as for hydrogenation of carbonylic or carboxylic compounds and dehydrogenation of alcohols. Bulk copper, such as Raney or sponge copper, is available commercially, being used sometimes for dehydrogenations.<sup>79</sup>

Among the most common combinations, the systems Cu–ZnO, Cu–ZnO–Al<sub>2</sub>O<sub>3</sub> and Cu–ZnO–Cr<sub>2</sub>O<sub>3</sub> find a number of practical applications. These systems have been exploited commercially when sulfur-free feeds became available. In fact, copper metal suffers poisoning by sulfur, as well as by halogens. Zinc oxide, zinc aluminate and zinc chromite are likely not only real supports, because solid-state solubility occurs between copper and zinc oxides and spinels, and activating effects are evident. Although authors in the past suggested that zinc oxides, which have their own activity in hydrogenation and dehydrogenation, could participate in the reactions, most authors agree today that copper metal particles represent the active phase on these catalysts. Other supports used for copper are alumina and silica.

Another largely applied system is “copper–chromite”, or CuO–Cr<sub>2</sub>O<sub>3</sub>.<sup>158</sup> The basic compound is CuCr<sub>2</sub>O<sub>4</sub> with the spinel type structure, although a composition of Cu<sub>2</sub>Cr<sub>2</sub>O<sub>4</sub> has also been reported. Usually, copper amount is in large excess with respect to the spinel stoichiometry, and thus copper oxides are also present in the unreduced catalysts producing copper metal particles in the reduced state. The application of this catalytic system suffers from the presence of highly toxic hexavalent chromium in the fresh catalyst and during preparation, and of problems for the disposal of the spent catalyst.

#### 9.4.4.1 Cu-based methanol synthesis catalysts

Syngases containing carbon monoxide and dioxide and hydrogen may be converted into methanol.<sup>159</sup> Waugh reviewed the main catalytic aspects of the process.<sup>160</sup> Today, the reaction is performed at 200–250 °C, 50–150 bar, in the so-called low-temperature synthesis process. Most commercial catalysts are based on the Cu–Zn–Al system, prepared by coprecipitation, with Cu:Zn atomic ratio in the two to three range, and minor alumina amounts.<sup>161</sup> The better composition in terms of Cu:ZnO:Al<sub>2</sub>O<sub>3</sub> is 60:30:10.<sup>160</sup> Cu–Zn–Cr and Cu–Zn–Cr–Al systems have also been considered and used at the industrial level.<sup>162,163</sup> The MK-121 catalyst from Topsøe contains, in the unreduced form, >55% wt CuO; 21–25% ZnO, 8–10% Al<sub>2</sub>O<sub>3</sub> in the fresh catalyst, graphite, carbonates, moisture balance.<sup>164</sup> Also the BASF Catalysts (such as S3-85, 83 m<sup>2</sup>/g,<sup>165</sup> and S3-86) and Süd Chemie (now Clariant) MegaMax<sup>®</sup> 700 catalysts are reported to be constituted by CuO/ZnO/Al<sub>2</sub>O<sub>3</sub>.<sup>72</sup>

The formulation of KATALCO<sub>JM</sub> methanol synthesis catalysts<sup>166</sup> is based on a copper-containing mineral in which a controlled proportion of the cations have been replaced by zinc ions. The active phase is supported on a specifically designed zinc aluminate compound. The support provides a catalyst that has good mechanical strength throughout operating life, while allowing reactant gases access to the active copper metal surface. Microcrystalline zinc oxide is also present to protect the copper metal surface sites from poisons such as sulfur and chlorine compounds. A further unique aspect of this catalyst, patent protected, is that magnesia is added to modify the catalyst structure during manufacture to maximize activity throughout catalyst life.

Several authors<sup>167,168</sup> agree that the actual reactant for methanol synthesis over Cu–ZnO–Al<sub>2</sub>O<sub>3</sub> is CO<sub>2</sub>, usually present with a concentration near 10% in the reactant syngas, although the reaction can also be performed with CO only. Studies suggested that, for methanol synthesis, the more reducing the gas the more active the catalyst, and the more dispersed the zerovalent copper particles,<sup>169,170</sup> where the reaction should occur. However, CO<sub>2</sub> should oxidize copper<sup>171</sup> so providing the active sites for methanol synthesis.<sup>168</sup> Most authors agree that the reaction should occur through oxygenated intermediates, i.e. by the formation of formates and their hydrogenation to methoxy groups.<sup>168,172,173</sup> This step should be rate-determining. Carbon dioxide actually acts as an oxidation agent for copper metal surfaces, while hydrogen and CO reduce it. On the other hand, oxygen species on the oxidized copper metal surface should react with another CO<sub>2</sub> molecule forming carbonates (in agreement with IR spectroscopy data<sup>174</sup>), which are later hydrogenated to formates and then, slowly, to methoxy groups.<sup>160</sup> According to Zandler et al., the actual active site for methanol synthesis should be a defect on the copper surface coupled to a reduced zinc center.<sup>175</sup> According to these authors, the presence of ZnO is useful for synthesis of methanol from CO<sub>2</sub>-containing gas, but is detrimental when CO<sub>2</sub> is absent: Cu–MgO catalysts are definitely more active than Cu–ZnO catalysts for pure CO hydrogenation.

#### 9.4.4.2 Cu-based water–gas shift and reverse water–gas shift catalysts

Commercial low-temperature water–gas shift (LTWGS) catalysts, allowing the reaction of CO with water-producing CO<sub>2</sub> and hydrogen at so low a temperature as 200 °C, also mostly belong to the Cu–ZnO–Al<sub>2</sub>O<sub>3</sub> family<sup>66</sup>: they are thought to be constituted too by copper metal with ZnO and Al<sub>2</sub>O<sub>3</sub> components, in reaction conditions. Topsøe sells three different catalysts for the SCR process: besides the “classical” Cu–ZnO–Al<sub>2</sub>O<sub>3</sub> (40% Cu) catalyst, Cs-promoted Cu–ZnO–Al<sub>2</sub>O<sub>3</sub> (40% Cu) is produced to limit byproducts formation, thus allowing lower methanol levels in the process condensate and CO<sub>2</sub> stream leaving the plant, and Cu–ZnO–Cr<sub>2</sub>O<sub>3</sub> (14% Cu) as a guard catalyst located on the top of the bed to protect copper/zinc/aluminum against chlorine poisoning. These catalysts work at 185–275 °C.<sup>176</sup> Cu–ZnO–Al<sub>2</sub>O<sub>3</sub> and alkali-promoted Cu–ZnO–Al<sub>2</sub>O<sub>3</sub> are also sold by Johnson Matthey. According to these producers,<sup>177</sup> alkali doping suppresses methanol formation and also boosts poison’s pickup, resulting in the highest poison capacity of any commercially available low-temperature shift catalyst.

Süd Chemie (now Clariant) sells for LTWGS 58% CuO/31% ZnO/11% Al<sub>2</sub>O<sub>3</sub>, as well as a promoted catalyst with 1% promoter.<sup>72</sup> A commercial low-temperature shift catalyst, BASF K3-110 contains nominally 40% CuO, 40% ZnO, 20% Al<sub>2</sub>O<sub>3</sub>, BET area 102 m<sup>2</sup>/g, pore volume 0.35 ml/g, copper area 9.83 m<sup>2</sup>/g, dispersion 4.8%, copper crystallite size 219 Å.<sup>178</sup> BASF patented a new preparation method to produce water–gas shift catalysts that, in the unreduced form, have 50.5–52.3 wt% CuO, 27.1–29.6 wt% ZnO, 18.8–19.7 wt% Al<sub>2</sub>O<sub>3</sub>, 0.08–0.1 wt% Na.<sup>179</sup>

According to the literature, two different mechanisms may justify the WGS reaction over Cu–Zn–Al catalysts: (1) the redox mechanism, where water oxidizes



the catalyst producing hydrogen and CO reduced back it producing CO<sub>2</sub>, (2) the “associative” mechanism through formate species, where water hydrates the surface producing active OH species. In both cases, the active catalyst surface is expected to be somehow oxidized, and thus it is not fully clear whether metal catalysis really occurs,<sup>180,181</sup> According to Waugh,<sup>160</sup> the redox mechanism should predominate over these catalysts. According to Kniep et al.,<sup>182</sup> the activity correlates with the decreasing copper particle size and the increasing microstrain in the copper nanoparticles.

While widely used in large hydrogen and ammonia production plants, such catalysts cannot be applied for small-scale devices like those that are concerned for fuel cell technologies. This is due to the need of an activation step carried out in the reformer by slow addition of H<sub>2</sub> carefully controlling the exotherm to avoid sintering, the problems related to their pyrophoric behavior, and their relatively low catalytic activity implying too big reactor beds. Thus, more active and safe low-temperature WGS catalysts are needed for fuel cell applications, mostly based on Pt.<sup>67</sup> However, Zn-free Cu–Al<sub>2</sub>O<sub>3</sub>–CuAl<sub>2</sub>O<sub>4</sub> water–gas shift seem to have advantages among which they can be activated by simple calcination.<sup>183</sup>

Cu-based catalysts can also be applied to accomplish the reverse water–gas shift reaction (RWGS),<sup>184</sup> which is becoming of interest in the field of CO<sub>2</sub>-utilization processes.

#### **9.4.4.3 Cu-based methanol decomposition and steam-reforming catalysts**

Methanol is a liquid fuel that shows potentiality as a “hydrogen vector” for small-scale stationary production of hydrogen and also for on-board hydrogen production.<sup>185</sup> Several medium-size plants (100–1000 Nm<sup>3</sup>/h) are in operation worldwide for the stationary production of hydrogen from methanol for chemical and electronic industry with the Tøpsoe “package hydrogen plants”.<sup>186,187</sup> Methanol and water vapor are fed into a multitubular reactor heated externally by a hot-oil circulation. Although the Tøpsoe process is reported to be “based on methanol decomposition”, the published data suggest that the reaction mostly occurs through endothermic steam reforming of methanol (MSR). BASF patented for this reaction catalysts with composition CuO 67% wt, ZnO 26.4% wt, Al<sub>2</sub>O<sub>3</sub> 6.6% wt (atomic ratios 65:25:10) with surface areas 80–100 m<sup>2</sup>/g.<sup>188</sup> Catalysts with similar compositions (30–50% wt/wt as CuO) to those of water–gas shift catalysts are tested in the literature for the reaction,<sup>189–192</sup> such as BASF F3-01 and K3-110 (CuO 40 wt%, ZnO 40 wt%, Al<sub>2</sub>O<sub>3</sub> 20 wt%) in several methanol steam-reforming studies.<sup>193</sup> Also in the case of methanol steam reforming, the real oxidation state of the Cu–Zn–Al catalysts is object of discussion.

As already discussed, however, catalysts based on the Cu–ZnO–Al<sub>2</sub>O<sub>3</sub> system, due to their pyrophoric behavior and the need of careful and long start-up and shut-down procedures, cannot find application in fuel cell technologies. Alternative catalysts based on oxide-supported Pd–Zn alloys have been developed for this application.<sup>194</sup>

#### 9.4.4.4 *Cu-based catalysts for partial hydrogenations of oxygenates at carbonyl and carboxyl groups*

Several processes imply the partial hydrogenation of oxygenated compounds (such as carbonyl compounds or esters) to alcohols, thus retaining the C—O single bond. Most of these processes are currently performed over copper-containing catalysts. Three predominant catalytic systems are used for these processes: those based on copper chromite, those based on copper/zinc oxide and those based on Zn-free copper on alumina.<sup>195</sup> Copper/silica, nickel/silica and nickel/alumina catalysts are also offered e.g. by Johnson Matthey.<sup>129</sup>

Copper chromites, mostly with large copper excess with respect to the spinel stoichiometry, are the traditional catalysts for the production of fatty alcohols by hydrogenation either of triglyceride fats or of fatty acid methyl esters (FAMES) at 200 °C, 200–250 bar.<sup>82</sup> Copper chromites are generally promoted by barium and/or manganese. As for example, the fixed bed hydrogenation of furfural to furfuryl alcohol can be performed on the Süd Chemie (now Clariant) G22F catalyst whose composition is CuO 38%, Cr<sub>2</sub>O<sub>3</sub> 37%, BaO 11%, silica-balance. For the slurry phase furfural hydrogenations Süd Chemie (now Clariant) G99D catalyst is proposed whose composition is CuO 46%, Cr<sub>2</sub>O<sub>3</sub> 44%, MnO<sub>2</sub> 4% with a high surface area of 70–80 m<sup>2</sup>/g.<sup>72</sup>

Copper–zinc oxide catalyst 33% CuO, 66% ZnO, entirely Cr-free, is used in the hydrogenation of butyraldehyde and 2-ethyl-hexenal to the corresponding alcohols and for the hydrogenation of maleic acid dimethyl esters to 1,4-butandiol, in substitution of copper chromite.<sup>82,196</sup> A catalyst with different composition, 64% CuO, 24% ZnO, Al<sub>2</sub>O<sub>3</sub> balance, is used for the gas-phase hydrogenation of maleic anhydride to 1,4-butandiol. 2-Ethylhexanale is selectively converted into 2-ethylhexanol by hydrogenation over Cu–ZnO–Al<sub>2</sub>O<sub>3</sub> catalyst at 130 °C.<sup>197,198</sup>

For the hydrogenation of maleic anhydride, a catalyst constituted by CuO 56%, MnO<sub>2</sub> 10%, alumina balance can be used. By variation of the standard catalyst, selectivity can be shifted either in the direction of the diols, or the intermediate  $\gamma$ -butyrolactone, or tetrahydrofuran.<sup>72</sup>

In the case of the oxo-synthesis products, in general two steps are performed, like in the case of the Johnson Matthey Oxo-Alcohols Process<sup>199</sup> a copper–zinc catalyst (PRICAT CZ 29/2) is used to hydrogenate oxo-aldehydes to oxo-alcohols, while a nickel catalyst (HTC-400) is used later to hydrorefine the product with removal of traces of carbonyls. Mn-promoted CuO/Al<sub>2</sub>O<sub>3</sub> catalyst can be used for the gas-phase hydrogenations of oxo-aldehydes. NiO 68%, CuO 3%, silica balance is usually applied in specific trickle-phase oxo-aldehyde hydrogenation processes.<sup>72</sup>

#### 9.4.4.5 *Cu-based catalysts for dehydrogenation of alcohols to carbonyl compounds*

The industrial synthesis of some carbonyl compounds is performed by dehydrogenation of the corresponding alcohols, thus exactly the reverse reactions with respect to those discussed above. Cu-based catalysts such as Cu–ZnO, Cu/SiO<sub>2</sub>, Cu–Al<sub>2</sub>O<sub>3</sub> or copper chromite catalysts at 200–450 °C are employed to this purpose.<sup>200</sup>

The dehydrogenation of 2-butanol to methyl-ethylketone (MEK) represents one of the most important processes of this kind. The Deutsche Texaco process employs a Cu-based catalyst at 240–260 °C under normal pressure.<sup>201</sup> Copper on silica<sup>202,203</sup> or Cu–Zn–Al catalyst<sup>204</sup> are reported for this reaction.

The dehydrogenation of cyclohexanol to cyclohexanone may be performed at 230–300 °C with a CuO(33%)–ZnO catalyst while the dehydrogenation of cyclododecanol to cyclododecanone is performed with a CuO(31%)–ZnO catalyst.<sup>72</sup>

#### 9.4.4.6 Cu-based catalysts for hydrogenation of nitrogenated compounds

Copper catalysts such as copper chromites are used for the synthesis of long chain amines via amination of alcohols.<sup>82</sup> Gas-phase process for hydrogenation of nitrobenzenes to anilines mostly use Mn- and Ba-promoted copper chromite. The process is conducted at temperature values within 250–350 °C, low pressure values (below 10 atm) but with a large excess of hydrogen to make the nitrobenzene conversion practically complete.

### 9.4.5 Ruthenium-based catalysts

Ruthenium is a very active metal in a number of catalytic hydrogenations, such as methanation and Fischer Tropsch catalysis and ammonia synthesis. Its use is hampered by the high costs, the advantages of its use being frequently not so determinant.

Methanation of carbon oxides is an exothermic equilibrium reaction, thus being favorably displaced the more the lower the temperature. While for medium-temperature reaction Ni-based catalysts are mostly used, for very low-temperature methanation Süd Chemie (now Clariant) sells a 0.3% Ru/Al<sub>2</sub>O<sub>3</sub> catalyst (METH 150), active even below 170 °C.<sup>72</sup> Ruthenium is reported indeed to be the most active metal in the CO hydrogenation, allowing CO/H<sub>2</sub> conversions higher than that obtained with Fe or Co, leading to lower Fischer Tropsch synthesis fuel's production costs and producing high molecular-weight paraffinic waxes.<sup>205,206</sup> Furthermore, Ru catalysts can operate in the presence of high partial pressure of water (FTS coproduct), and other oxygenate-containing atmospheres, which is an important property to convert syngas obtained from biomass.<sup>207,208</sup> Ru/Al<sub>2</sub>O<sub>3</sub> catalysts are also of interest for low-temperature methanation of CO<sub>2</sub> a interesting option for carbon dioxide utilization.<sup>208b,208c</sup>

The liquid-phase partial saturation of benzene to cyclohexene is also of industrial interest. For this reaction, ruthenium catalysts offer the best selectivity. In the Asahi Chem. Process, Ru/La<sub>2</sub>O<sub>3</sub>–ZnO catalysts are used.<sup>208d</sup>

In the 1990s, Kellogg Brown and Root (KBR) developed a new ammonia synthesis process based on Ru-based catalysts denoted as KAAP™ (Kellogg Advanced Ammonia Process). The proprietary KAAP™ catalyst, which is manufactured and guaranteed by BASF Catalysts LLC under exclusive license to KBR, consists of ruthenium on a stable, high surface-area graphite carbon base.<sup>209</sup> According to the literature, it should contain alkali and alkali-earth promoters such as K, Cs and Ba.<sup>210,211</sup> The KAAP™ catalyst is reported to have an intrinsic activity 10 to

20 times higher than conventional iron catalysts. This allows operation at 90 bar synthesis loop pressure, which is one-half to two-thirds the operating pressure of a conventional magnetite ammonia synthesis loop. At this low pressure, only a single-casing synthesis gas compressor is needed and pipe wall thicknesses are reduced. This results in savings in plant capital equipment and operating costs.

5% Ru on carbon, pure or mixed with Pd, is also commercially available for hydrogenation of oxygenates (such as aliphatic carbonyls and sugar) and heterocyclic compounds in liquid phase.<sup>79</sup>

#### 9.4.6 Rhodium-based catalysts

Rhodium is very active in hydrogenation catalysis, but quite expensive. In most cases, advantages with respect to other metals are not sufficient to justify the use Rh-metal catalysts. Rhodium/carbon and Rh/Al<sub>2</sub>O<sub>3</sub> catalysts are commercially proposed for some hydrogenations, such as aromatic saturation.<sup>79</sup> Rh-based catalysts are reported to be optimal catalysts for ethanol steam reforming: Duprez and co-workers propose the composition RhNi/Y<sub>2</sub>O<sub>3</sub>-Al<sub>2</sub>O<sub>3</sub> as a promising catalyst to be used with crude bioethanol at 948 K.<sup>102</sup> Rh-based catalysts are also proposed for steam reforming of biomass tar (e.g. Rh/MgO<sup>212</sup>). Supported Rh catalysts are proposed as the best catalysts for the CPO of methane to syngas, the support being a refractory ceramic material such as  $\alpha$ -Al<sub>2</sub>O<sub>3</sub>, zirconia<sup>213,214</sup> or MgO.<sup>215</sup> Solids containing Rh, which work as a nonmetallic monoatomic catalyst, are largely applied as heterogenized homogeneous catalysts (Chapter 12.2).

#### 9.4.7 Palladium-based catalysts

As already remarked, for many hydrocarbon hydrogenation reactions Ni, Pd and Pt catalysts, and even other metals such as Ru and Rh, compete with each other. Relevant difference on the corresponding catalysts however exists, taking into account that Ni is a cheap element and can be used to produce the highly loaded supported catalysts (see above) while Pt and Pd are very expensive and are normally used in very low amounts. Being sulfur frequently present in hydrocarbon flows, a main factor for the choice is the sulfur resistance of the catalyst, which largely depends on the amount of sulfur in the feed.

Palladium is the most active metal in catalyzing hydrogenation of acetylenic carbon-carbon multiple bonds, but also shows high propensity in favoring the migration of the resulting double bond. Pd is also very useful for partial hydrogenation of oxygenates.

##### 9.4.7.1 Pd-based catalysts for hydrogenation of acetylenic compounds, dienes and olefins

As said, the hydrogenation of acetylenic hydrocarbons is performed mostly to destroy these compounds present in small amounts in different flows. This subject has been thoroughly reviewed years ago by Molnár et al.<sup>216</sup> Pd/Al<sub>2</sub>O<sub>3</sub> catalysts and, less

frequently, Pd/SiO<sub>2</sub> perform very well in sulfur-free environment. Hydrogenation of acetylene in the C2 cut from steam cracking is performed to reduce this noxious impurity in polymer-grade ethylene (from near 1% to <5 ppm, frequently <0.5 ppm).<sup>217</sup> The feed is usually previously cleaned by caustic washing, thus allowing the use of noble metal catalysts.<sup>218</sup> The reaction should convert acetylene to ethylene almost completely, with low conversion of it or of ethylene to high molecular weight hydrocarbons (“green oil”), with high stability toward poisoning by traces of CO and sulfur in the feed. Thus the metal should be very active and the support very inactive. For these reasons, Pd is the preferred metal today, the loading is quite small, e.g., 0.04% wt, the support being a low surface-area alumina, e.g.,  $\alpha$ -Al<sub>2</sub>O<sub>3</sub> with c. 20 m<sup>2</sup>/g<sup>219</sup> but silica-supported Pd catalysts are also proposed,<sup>220</sup> that may reduce the oligomerization activity thus leading to a low green oil formation.<sup>221</sup> The reaction is performed in the gas phase at 25–100 °C and 20–35 bar using multiple fixed catalyst beds (from one to four beds, depending on the initial acetylene concentration in the feed) with intermediate cooling.<sup>217</sup> Acetylene is hydrogenated much faster than ethylene when both are present, because acetylene occupies the active adsorption sites preferentially. However, over the same catalyst ethylene or other olefins may be also hydrogenated to alkanes.

It seems that the most usual catalyst composition for this application (tail-end configuration, sulfur free feed) is today Ag-promoted Pd/Al<sub>2</sub>O<sub>3</sub>, although the actual concentration of Ag may be higher than that of Pd (es. Pd 0.03%, Ag 0.18% for the Süd Chemie—Clariant OleMax 201 catalyst). Silver concentration must be optimal to increase selectivity without a relevant decrease in activity. Gold is also reported as a promoter for Pd, while potassium and chromium have been reported as additional or alternative promoters.<sup>220</sup>

Acetylene hydrogenation reaction is performed also to purify HCl flow coming from ethylene dichloride (EDC) cracking, in the process of production of vinyl chloride monomer (VCM), e.g. in the Vinnolit process.<sup>222</sup> In fact, HCl is recycled to ethylene oxychlorination reactor to reproduce EDC. The presence of acetylene due to VCM overcracking here would result in the production of polychlorinated byproducts in the oxychlorination unit. The catalysts Noblyst<sup>®</sup> E 39 H and Noblyst<sup>®</sup> E 39 KHL,<sup>223</sup> produced by Evonik, are specific for this application: they are both reported to be constituted by Pd on silica. The lower reactivity of the support with respect to HCl is a key feature here.

Hydrogenation of methylacetylene and propadiene in the steam cracking C3 cut or after propane dehydrogenation must be performed too to limit their content in polymer-grade propylene. This reaction may either be performed in the gas phase with multiple beds or in the liquid phase in a single bed. In both cases, promoted Pd/Al<sub>2</sub>O<sub>3</sub> is used but the Pd content for liquid phase use must be much higher (0.3%) than for the gas-phase use (0.03%).<sup>72</sup> In gas-phase hydrogenation, the reaction is controlled by means of the operating temperature, which may be between 50 and 120 °C, 15–20 bar, depending on the preparation and aging state of the catalyst. With liquid-phase hydrogenation, the reaction is controlled by the hydrogen partial pressure. The operating temperature of 15–25 °C is considerably lower in this case.<sup>216,217</sup>

Hydrogenation of C2 and C3 acetylenics may also be performed simultaneously in the so called front-end hydrogenation configuration,<sup>121,122</sup> in the gas phase with three fixed beds and intermediate cooling, with promoted Pd/Al<sub>2</sub>O<sub>3</sub>.

Major catalyst producers offer Pd-based catalysts for the hydrogenation of butynes in the C4 steam-cracking cut. Süd Chemie—Clariant offers a 0.2% Pd/Al<sub>2</sub>O<sub>3</sub> catalyst (Ole Max 400 and 353)<sup>72</sup>, while Axens offers a bimetallic Pd-containing catalyst (LD 277).<sup>224</sup> Alves et al.<sup>225</sup> recently described and tested a commercial catalyst for this reaction, 0.21% Pd/Al<sub>2</sub>O<sub>3</sub>, 70 m<sup>2</sup>/g total surface area, 3.6 nm Pd crystal size, 27% Pd dispersion.

Another important reaction is the hydrogenation of phenylacetylene impurities in styrene, just after the ethylbenzene dehydrogenation step. This reaction<sup>226</sup> is carried out in liquid phase at 25–80 °C, 1–4 bar, over eggshell 0.3% Pd/Al<sub>2</sub>O<sub>3</sub> catalyst (Süd Chemie—Clariant DMaxPA catalyst<sup>72</sup>) or 0.5 wt% Pt/γ-Al<sub>2</sub>O<sub>3</sub> (ESCAT-26, Engelhard<sup>227</sup>).

Similarly, several industrial hydrocarbon flows must be purified from dienes and other unsaturated hydrocarbon impurities, to avoid formation of oligomers or unwanted products in further steps.

C4 cuts from the Fluid Catalytic Cracking can be used to produce 1-butene, e.g. as a comonomer of ethylene in the production LLDPE. Hydrogenation is needed to reduce butadiene content to the ppm range, achieving high 1-butene yields, and minimizing 2-butene and butane formation. Conventional Pd-only catalysts have poor butene-1 selectivity because they significantly promote 1-butene isomerization to 2-butene. Thus, either Pt catalysts, or special catalysts based on Pd and appropriate promoters reducing isomerization () are used, such as the Axens LD 271 catalyst<sup>224</sup> and the Süd Chemie – Clariant Olemax 200, catalyst, likely composed of Pd–Ag/Al<sub>2</sub>O<sub>3</sub>.<sup>72</sup>

C4-cuts treatment may alternatively have the objective to produce 2-butene. Appropriately activated palladium catalysts, such as Axens LD 267 R, achieve efficient residual butadiene removal with a high isomerization of 1-butene to 2-butene that approaches the thermodynamic equilibrium. Over-hydrogenation to butanes is held to a minimum.<sup>228</sup> Similar catalysts for either 1-butene or 2-butene production are produced by BASF (Selop C4<sup>221</sup>). The catalyst's selectivity for isomerization and olefin recovery can also be obtained by a specific pre-treatment step that moderates the catalyst hydrogenation activity.

Total saturation of a C4 olefin cut to a stream containing mainly butanes is another option. This stream can then be recycled to the cracking furnaces as its ethylene yield is higher than that of naphtha, or sold as LPG. Pd-based catalysts (e.g. Axens LD 265<sup>224</sup>) are also available for this.

0.2–0.4% Pd/Al<sub>2</sub>O<sub>3</sub><sup>72</sup> are alternative to Ni catalysts for the selective hydrogenation of diolefins and alkenylaromatics in the first step of pyrolysis gasoline upgrading,<sup>216,229</sup> while minimizing olefin hydrogenation and avoiding aromatics hydrogenation. In the Selective Hydrogenation Unit (SHU), operated in the liquid phase and at a low temperature of 40–100 °C, about 90% of diolefins and styrene but only less than 10% of monoolefins are removed. BASF SELOP C5+

hydrogenation process treats gasoline over a commercial catalyst containing 0.25 wt % Pd on high surface-area alumina.<sup>216</sup> Similar hydrogenation processes may also be performed with reformate gasolines to stabilize them.<sup>229</sup>

Hydrogenation of the byproduct  $\alpha$ -methyl-styrene (AMS) is performed in the cumene synthesis processes using Pd-based catalysts, on alumina or on carbon supports<sup>230</sup> where the catalyst can be used in a fixed-bed system in the liquid phase, or in a trickle-bed system with both vapor and liquid phases. The Noblyst<sup>®</sup> H 14108 catalyst from Evonik 225, suggested for this application, is based on Pd/Al<sub>2</sub>O<sub>3</sub>. Palladium catalyst having a metal content of between 1 and 5% is noted as being preferred, for use at temperatures of 24–50 °C and pressures of 1.5–5 bar. A double-bed reactor with a Ni catalyst on the first bed and a noble metal catalyst in the second is a possible option.<sup>231</sup>

#### 9.4.7.2 Pd-based catalysts for methanol synthesis and steam reforming and for hydrogenation of oxygenated compounds

Palladium presents, like copper, a pronounced ability to hydrogenate C=O multiple bonds to C–O single bonds. Thus, it is used for methanol synthesis and carbonyl compound hydrogenations.

The synthesis of methanol can be carried out over Pd catalysts: in particular, Pd-doped Cu-ZnO based catalysts and Pd-Ga/SiO<sub>2</sub> catalysts have been reported to be optimal for CO<sub>2</sub> hydrogenation to methanol.<sup>231b</sup> On the other hand, methanol is also assumed to be a suitable liquid source for on-board production of hydrogen by steam reforming in the case of fuel cell electric engine cars and boats.<sup>185</sup> As already discussed, however, catalysts based on the Cu–ZnO–Al<sub>2</sub>O<sub>3</sub> system, due to their pyrophoric behavior and the need of careful and long start-up and shut-down procedures, cannot find application in fuel cell technologies. Catalysts based on oxide-supported Pd–Zn alloys have been developed for this application.<sup>194</sup>

On the other hand, Pd catalysts are also effective for hydrogenation of carbonyl groups. Actually, they are excellent catalysts for the hydrogenation of aromatic aldehydes and ketones, not for the corresponding aliphatic compounds.<sup>79</sup>

Pd is also able to promote the selective hydrogenation of C=C double bonds in C=O containing oxygenated compounds. Recently, new catalysts containing 0.2% Pd on boron-treated alumina have been proposed for the hydrogenation of triglyceride oils to avoid possible contamination of margarine by nickel.<sup>232</sup>

The selective hydrogenation of  $\alpha,\beta$ -unsaturated carbonyl compounds on the C=C double bond is promoted by Pd catalysts.<sup>233</sup> A typical example is the synthesis of Methyl-Isobutyl Ketone (MIBK) by hydrogenation of Mesityl Oxide (MO) previously produced by acetone condensation. Pd catalysts allow the highly selective hydrogenation of the C=C bond without any reduction of the C=O bond (150–200 °C, 3–10 bar). Nowadays, MIBK is industrially obtained from acetone in one step in trickle-type reactors at low temperatures (120–140 °C) and high pressures (10–100 bar) on multifunctional catalysts such as Pd- or Pt-supported on sulfonated resins, which contain condensation, dehydration and hydrogenation functions.<sup>234</sup> Both the aldol condensation and the dehydration reactions are

reversible under these reaction conditions but the catalyst shifts the equilibrium in favor of MO by hydrogenating it to MIBK. The full reaction may also be performed in a single liquid-phase reactor using Mg–Al hydrotalcite with 0.1% Pd.<sup>235</sup> Similarly, 0.1 wt% Pd added to 4% Na/SiO<sub>2</sub> catalysts allow the one-step synthesis of the saturated aldehyde 2-ethylhexanal with 85–95% selectivity, by self-condensation of *n*-butanal at 350–400 °C in the presence of hydrogen.<sup>197,198</sup>

Many other industrially significant examples may be cited. Among others, the selective hydrogenation of phenol to cyclohexanone/cyclohexanol mixtures (the KA mixture intermediate in the adipic acid and Nylon6 syntheses) is performed industrially over Pd-based catalysts<sup>236,237</sup> such as Pd/Ca–Al<sub>2</sub>O<sub>3</sub><sup>238,239</sup> or Pd/C<sup>79</sup> at 140–170 °C, 1–20 bar. Pd/C catalyst was used to produce cyclohexane carboxylic acid from the hydrogenation of benzoic acid at 170 °C and 10–17 bar.<sup>196</sup>

### 9.4.8 Rhenium metal in catalysis

It seems that the more important application of metallic rhenium in catalysis is as a component of catalytic reforming catalysts, where it is present as an activator for platinum.<sup>240</sup> The most common recent composition of these catalysts is trimetallic Pt–Re–Sn on chloride alumina.<sup>240</sup>

### 9.4.9 Iridium-based catalysts

The selective ring opening (SRO) of cyclic paraffins, in particular tetralins<sup>241</sup> and decalins, is a useful reaction in upgrading cetane qualities of Diesel fuels. This reactivity is usually performed together with aromatic saturation in new refinery processes still under development. It has been shown that the most active catalysts for these reactions contain iridium metal.<sup>242</sup> Typical reaction conditions are 250–350 °C with 30 bar hydrogen. A promising catalyst formulation has been reported to be 1% Ir supported on mesoporous silica–alumina.<sup>243</sup>

### 9.4.10 Platinum-based catalysts

Platinum is also a very effective metal in hydrogenation, but is sensitive to sulfur. Interestingly, Pt–Pd bimetallic catalysts are reported to be less prone to sulfur poisoning than monometallic ones.

Platinum is less active than palladium for hydrogenation of carbon–carbon triple bonds, but it is less active in favoring a double-bond migration, thus being preferred to palladium for some applications.

Besides typical hydrogenation catalysts, Pt is also frequently used as a minority component in several acid hydrocarbon catalysts, which are subject to coke deactivation. Some of these catalysts are used in the presence of hydrogen and contain traces of Pt, in order to limit coking by its hydrogenation. A typical case is that of catalysts for light paraffin skeletal isomerization, performed in refinery. Several catalysts are available for this reaction, such as chloride alumina, sulfated zirconia, tungsta–zirconia and mordenite and omega zeolites,<sup>244,245</sup> all doped with Pt.



Similarly, also catalysts for xylenes isomerization, toluene disproportionation to benzene and xylenes, as well as for transalkylation reactions, based on acid zeolites, are doped with Pt and fed with hydrogen.

#### **9.4.10.1 Pt-based catalysts for hydrogenation of olefins**

Pt catalysts may be used in competition with Ni and Pd catalysts for the hydrogenation of olefins to alkanes. As a relevant example, 0.3% Pt/Al<sub>2</sub>O<sub>3</sub> catalysts are used in the hydrogenation of isooctene to isooctane,<sup>72</sup> obtained by isobutene dimerization, in the “indirect alkylation process”. The reaction can be carried out in the liquid phase at 70–130 °C, 10–30 bar.<sup>246</sup>

#### **9.4.10.2 Pt-based catalysts for aromatic saturation**

The activity of heterogeneous metal catalysts for the hydrogenation of aromatics was reported to be in order Rh > Ru ≫ Pt ≫ Pd ≫ Ni > Co.<sup>247,248</sup> However, the sulfur resistance of pure noble metals is quite limited, but significantly improved using acidic supports like zeolites (e.g. Ultra Stable Y, USY), and appropriate alloying of noble metals such as Pt–Pd alloys. Typical hydrotreating catalysts based on alumina-supported NiMo or NiW sulfides are used with sulfur-rich feeds. Thus, also in this case the choice of the catalyst can depend largely on the sulfur content in the feed.

The conventional benzene reduction process in gasoline employs a hydrogenation unit downstream from the reformat splitter. Pt/Al<sub>2</sub>O<sub>3</sub> catalysts are used in the vapor phase BenSat™ benzene saturation technology from UOP. Recently, the previous UOP H-8™ catalyst has been updated in response to a demand for improved economics. According to UOP patents, its preferred form, the alumina support will comprise spheres having a surface area of from about 160 to 200 m<sup>2</sup>/g with an apparent bulk density of from about 0.45 to 0.6. The platinum metal may be present on the catalyst in a concentration of from 0.375 to 0.75 wt%.<sup>249</sup> The new BenSat process uses a new catalyst, the UOP H-18™ catalyst, resulting in lower catalyst volume, reduced recycle, and lower precious metal requirements.<sup>250</sup> According to people from UOP, unlike Ni-based catalysts, Pt-based saturation catalysts are not permanently poisoned by sulfur or heavies upsets and do not cause cracking to light ends. Competitive processes such as the GT BenZap process, use Ni-based catalysts.<sup>251</sup>

Hydrodearomatization of naphthalenes in gasoils may be needed in the near future to fulfil the more stringent limits of these polyaromatics in commercial diesel fuels.<sup>252</sup> One-step technologies (with dearomatization and desulfurization performed together over sulfide catalysts) or two-stage technologies (that perform deep aromatics reduction with noble metal catalysts after HDS of the feed with sulfide catalysts) may be applied. This is due to the deactivation of noble metal by sulfur compounds. The rate of aromatic saturation is up to about 70–90% for the two-stage processes in contrast with the 40–55% HDA level of one-stage processes using sulfide catalysts. High intrinsic activity and sulfur tolerance may be enhanced by deposition of noble metals on acidic, high surface-area supports, e.g., a large-pore zeolites beta and

HY. It has been established that noble metals deposited on acidic supports show higher turnover frequencies (TOF) than when they are supported on nonacidic carriers.<sup>253,254</sup> Catalytic systems based on zeolite-supported noble metals, such as Pt–Pd/H-USY, are now under development,<sup>255</sup> as the ASAT™ catalysts from Süd Chemie–Clariant.<sup>72</sup>

Saturation of higher polyaromatics can be performed to upgrade lube oils to medicinal grade white oil: the MAXSAT process from ExxonMobil uses a noble metal, likely Pt, containing molecular sieve catalyst.<sup>256</sup>

#### 9.4.10.3 Pt-based catalysts for aromatization and naphtha reforming

Catalytic naphtha reforming is a main industrial process converting aliphatic hydrocarbons into mononuclear aromatics both in refinery (to produce high-octane gasoline) and in petrochemistry, to produce benzene, toluene and xylenes (BTX).

Bifunctional metal-acid catalysts are typically used for naphtha catalytic reforming<sup>240</sup>: the acidic function allows isomerization and cyclization of paraffins while the noble metal function catalyzes dehydrogenation to aromatics. In the typical reforming catalyst formulations, the metal function is provided by Pt, which is supported over the acid function, chlorinated gamma alumina (150–300 m<sup>2</sup>/g). In the more recent multimetallic catalysts, the catalytic properties of Pt is improved by the addition of another metal, such as usually Re, with the further addition of some other element among Sn, Si, Ge, Pb, Ga, In, Ir, Th La, Ce, Co and Ni.<sup>257</sup> Also at least 10 wppm of one or more alkaline-earth metals selected from Ca, Mg, Ba and Sr, wherein the total amount of modifier does not exceed about 5000 wppm can be present.<sup>258</sup> These additives modify the activity, selectivity and stability of the catalyst. The effects of the additives are multiple. (1) They decrease the deep dehydrogenation capacity of Pt and thus decrease the formation of unsaturated coke precursors. (2) They decrease the hydrogenolysis capacity and therefore also decrease the formation of light gases. (3) They modify the concentration of surface hydrogen. This has an effect on the relative production of different reaction intermediates and therefore on the final reaction selectivity. (4) A portion of the additives remains oxidized on the surface and modifies the amount and strength of the acid sites of the support. The typical composition of an industrial catalyst, such as R-98 catalyst from UOP to be used in fixed-bed, semiregenerative reforming units, the claimed composition is 0.25% wt Pt, 0.25% wt Re, proprietary promoters.<sup>259</sup> For application in continuous regenerative reforming R-232 (0.375% Pt) and R-234 (0.290% Pt) catalysts are produced by UOP.<sup>260</sup>

When aromatization is performed in a petrochemistry environment, the additional paraffin skeletal isomerization is not needed. For these applications, Pt on cationic zeolites, such as Pt–K–L zeolite, are such as in the case of the recent RZ platforming process from UOP.<sup>261</sup> This process is a semiregenerative naphtha-reforming process, allowing higher aromatics selectivity than other reforming processes with C6 and C7 paraffins as feed.<sup>262</sup> A catalyst of this type has also been jointly developed by Idemitsu Kosan Co., Ltd. (IKC), and Chevron Phillips Chemical Company LP (CPChem) for the Aromax process, used commercially to convert C6–C8 paraffins to benzene.<sup>263</sup>

#### **9.4.10.4 Pt-based catalysts for liquid-phase hydrogenation of nitrobenzenes**

Hydrogenation in fixed-bed liquid phase in a plug flow reactor (Dupont–KBR process<sup>264</sup>) uses a noble metal on a carbon catalyst. A similar process is reported to be carried out in liquid phase at 75 °C, 500 psig over carbon-supported palladium to produce toluene diamine from dinitrotoluene. Hydrogenation in fixed-bed liquid phase in a plug flow reactor (Dupont–KBR process<sup>264</sup>) uses a noble-metal-on-carbon catalyst. A similar process is reported to be carried out in liquid phase at 75 °C, 500 psig over carbon-supported palladium to produce toluene diamine from dinitrotoluene<sup>196</sup>.

Nitro groups are readily hydrogenated. However, selectivity may become an issue if functional groups like double bonds, triple bonds or halogen substituents, aromatic rings, carbonyls and even oximes are present<sup>79</sup>. Vanadium-promoted Pt-catalysts (1–3% Pt, 0.5–2% V) are available from Evonik for this application.<sup>265</sup>

Nitro groups are readily hydrogenated. However, selectivity may become an issue if functional groups like double bonds, triple bonds or halogen substituents, aromatic rings, carbonyls and even oximes are present<sup>79</sup>. Vanadium-promoted Pt-catalysts (1–3% Pt, 0.5–2% V) are available from Evonik for this application.<sup>265</sup>

#### **9.4.10.5 Pt-based catalysts for dehydrogenation of alkanes to olefins and dienes**

Pt/Al<sub>2</sub>O<sub>3</sub> catalysts are also quite largely used in this field, more stable at higher temperature and in the presence of steam than oxide-based catalysts such as chromia alumina.<sup>63,64</sup> Additional components are used to reduce alumina acidity and improve performances. In fact, alkalinized 0.3–0.5% Pt/Al<sub>2</sub>O<sub>3</sub> (such as the UOP Oleflex™ DeH-14 catalyst) with Sn, Zn and/or Cu as promoters acts as the catalyst in the Oleflex light paraffin dehydrogenation technology and in the Pacol long linear paraffin dehydrogenation technology, both from UOP.<sup>266</sup> Such catalysts may contain less than 1% of both Pt metal and alkali wt/wt, and additionally an activator metal, on a medium surface-area alumina (100–200 m<sup>2</sup>/g).<sup>267</sup> Pt–Sn/Al<sub>2</sub>O<sub>3</sub> catalyst is also used in the IFP process for heavy paraffin dehydrogenation<sup>268</sup> at 450–475 °C, 2.5 atm. It has been established that relative to monometallic Pt/Al<sub>2</sub>O<sub>3</sub> catalyst, bimetallic Pt–Sn/Al<sub>2</sub>O<sub>3</sub> promotes desorption of olefins and hence may follow a different mechanism.

#### **9.4.10.6 Pt-based catalysts for water–gas shift and steam reforming**

The most promising types of water–gas shift catalysts in the frame of small Fuel Cell-based energy production systems,<sup>66,67</sup> and those most extensively studied for these applications, are based on supported noble metals, like Pt/CeO<sub>2</sub>–Al<sub>2</sub>O<sub>3</sub>-based catalysts,<sup>269</sup> in monolytic structures. However, instability of this catalyst under fuel processing conditions has been a recurring problem. There is much debate over what deactivation mechanisms are actually involved, and research on the Pt–CeO<sub>2</sub>-based catalyst continues with a particular emphasis on increasing catalytic activity and stability.

Pt catalysts are active in steam-reforming reactions, but usually their advantages to Ni catalysts are not sufficient to justify their use. However, in micronized plants for fuel cell their application is effective.<sup>67</sup> On the other hand, very small amount of Pt to Ni can improve, in many respects, the application of Ni-based catalysts.<sup>141</sup>

Low-temperature ESR can indeed be performed effectively over noble metal-based catalysts such as supported Pt,<sup>270,271</sup> but methanation is significant.

#### 9.4.11 Gold-based catalysts for water–gas shift

Gold metal catalysts are becoming very important for oxidation reactions (Chapter 11). Catalysts based on gold, such as Au–Fe<sub>2</sub>O<sub>3</sub>, Au–CeO<sub>2</sub> and Au–TiO<sub>2</sub> find high activity and commercial interest for low-temperature water–gas shift LTWGS.<sup>272</sup>

---

### References

1. Bond GC. *Catalysis by metals*. London: Academic Press; 1962.
2. Ponec V, Bond GC. *Catalysis by metals and alloys* (Stud Surf Sci Catal vol. 95). Amsterdam: Elsevier Science BV; 1995.
3. Bond GC. *Metal-catalysed reactions of hydrocarbons*. Springer Science; 2005.
4. Anderson JA, Fernandez Garcia M, editors. *Supported metals in catalysis*. Imperial College Press; 2011.
5. Iyngaran P, Madden DC, Jenkins SJ, King DA. *Proc Nat Acad Sci* 2011;**108**:925–30.
6. Goodman DW. *J Phys Chem* 1996;**100**:13090–102.
7. Gao F, Wang Y, Cai Y, Goodman DW. *J Phys Chem C* 2009;**113**(1):174–81.
8. Nørskov JK, Scheffler M, Toulhoat H. *Mat Res Soc Bull* 2006;**31**:669.
9. Bligaard T, Nørskov JK, Lundqvist BI. *Handbook of surface science*, vol. 3; 2008. p. 269–340.
10. Chizallet C, Bonnard G, Krebs E, Bisson L, Thomazeau C, Raybaud P. *J Phys Chem C* 2011;**115**:12135–49.
11. Gao F, Goodman DW. *Annu Rev Phys Chem* 2012;**63**:265–86.
12. Schauer mann S, Nilius N, Shaikhutdinov S, Freund HJ. *Acc Chem Res* 2013;**46**:1673–81.
13. Dellwig T, Hartmann J, Libuda J, Meusel I, Rupprechter G, Unterhalt H, et al. *J Mol Catal A Chem* 2000;**162**:51.
14. Schauer mann S, Hoffmann J, Johánek V, Hartmann J, Libuda J, Freund H-J. *Angew Chem Int Ed* 2002;**41**:2532.
15. Burda C, Chen X, Narayanan R, El-Sayed ME. *Chem Rev* 2005;**105**:1025–102.
16. Alayoglu S, Aliaga C, Sprung C, Samorjai GA. *Catal Lett* 2011;**141**:914–24.
17. Garbarino G, Riani P, Lucchini MA, Canepa F, Kawale S, Busca G. *Int J Hydrogen Energy* 2013;**38**(1):82–91.
18. Riani P, Garbarino G, Lucchini MA, Canepa F, Busca G. *J Mol Catal A Chem* 2014;**383-384**:10–6.
19. Ranu BC, Chattopadhyay K, Adak L, Saha A, Bhadra S, Dey R, et al. *Pure Appl Chem* 2009;**81**:2337–54.
20. Libuda J, Freund HJ. *Surf Sci Rep* 2005;**57**:157–298.

21. Hadjiivanov K, Vayssilov G. *Adv Catal* 2002;**47**:307–511.
22. Lee I, Morales R, Albiter MA, Zaera F. *Proc Natl Acad Sci* 2008;**105**(40):15241–6.
23. Peng Z, Kisielowski C, Bell AT. *Chem Commun* 2012;**48**:1854–6.
24. Zhu T, van Grootel PW, Filot IAW, Sun SG, van Santen RA, Hensen EJM. *J Catal* 2013;**297**:227–35.
25. Berhault G, Bisson L, Thomazeau C, Verdon C, Uzio D. *Appl Catal A Gen* 2007;**327**:32–43.
26. Xiong Y, McLellan IM, Yin YD, Xia YN. *Angew Chem Int Ed* 2007;**46**:790.
27. Kuo CH, Chiang TF, Chen LJ, Huang MH. *Langmuir* 2004;**20**:7820.
28. Rupprechter G, Weilach C. *Nano Today* 2007;**4**:21–9.
29. Wen JG, Huang ZP, Wang DZ, Chen JH, Yang SX, Rena ZF, et al. *J Mater Res* 2001;**16**:3246–53.
30. Kang JH, Menard LD, Nuzzo RG, Frenkel AI. *J Am Chem Soc* 2006;**128**:12068.
31. Sanchez SI, Menard LD, Bram A, Kang JH, Small MW, Nuzzo RG, et al. *J Am Chem Soc* 2009;**131**:7040.
32. Hu CH, Chizallet C, Mager-Maury C, Corral-Valero M, Sautet P, Toulhoat H, et al. *J Catal* 2010;**274**(1):99–110.
33. Benavidez AD, Kovarik L, Genc A, Agrawa N, Larsson EM, Hansen TW, Karim AM, Datye AK. *ACS Catal* 2012;**2**:2349–56.
34. Nellist PD, Pennycook SJ. *Science* 1996;**274**:413.
35. Sohlberg K, Rashkeev S, Borisevich AY, Pennycook SJ, Pantelides ST. *Chem Phys Chem* 2004;**5**:1893.
36. Xiao Li, Schneider WF. *Chem Phys Lett* 2010;**484**:231–6.
37. Stobbe-Kreemers AW, van der Zon M, Makkee M, Scholten JFF. *J Mol Catal A Chem* 1996;**107**(1–3):247–53.
38. Ivanova AS, Slavinskaya EM, Gulyaev RV, Zaikovskii VI, Stonkus OA, Dsnilova IG, et al. *Appl Catal B Environ* 2010;**97**:57–71.
39. Specchia S, Finocchio E, Busca G, Palmisano P, Specchia V. *J.Catal* 2009;**263**:134–45.
40. Vedyagin AA, Volodin AM, Stoyanovskii VO, Mishakov IV, Medvedev DA, Noskov AS. *Appl Catal B Environ* 2011;**103**:397–403.
41. Busca, Finocchio E, Escibano VS. *Appl Catal B Environ* 2012;**113–114**:281–9.
42. Flytzani-Stephanopoulos M, Gates BC. *Annu Rev Chem Biomol Eng* 2012;**3**:545–74.
43. Huda MN, Kleinman L. *Phys Rev B* 2006;**74**:195407.
44. Kristinsdóttir L, Skúlason E. *Surf Sci* 2012;**606**:1400–4.
45. Tabatabaei J, Sakakini BH, Watson MJ, Waugh KC. *Catal Lett* 1999;**59**:151–5.
46. Paul JF, Sautet P. *Surf Sci* 1996;**356**:L403–9.
47. Greeley J, Marikakis M. *J Phys Chem B* 2005;**109**:3460–n3471.
48. Zaginaichenko SY, Matysina ZA, Schur DV, Teslenko LO, Veziroglu A. *Int J Hydrogen Energy* 2011;**36**:1152–8.
49. Cobden D, Nieuwenhuys BE, Gorodetskii YV, Parmon YN. *Platin Met Rev* 1998;**42**:141–4.
50. Jewell LL, Davis BH. *Appl Catal A Gen* 2006;**310**:1–15.
51. Panczyk T, Szabelski P, Rudzinski W. *J Phys Chem B* 2005;**109**(21):10986–94.
52. Znak L, Zieliński J. *Langmuir* 2006;**22**:8758.
53. Znak L, Zieliński J. *Appl Catal A Gen* 2008;**334**(1–2):268–76.
54. Oudenhuijzen MK, van Bokhoven JA, Miller JT, Ramaker DE, Koningsberger DC. *J Am Chem Soc* 2005;**127**:1530–40.

55. Meng S, Wang EG, Gao S. *Phys Rev B* 2004;**69**:195404.
56. Sheth PA, Neurock M, Smith CM. *J Phys Chem B* 2003;**107**:2009–17.
57. Hafner J. *Monatsh Chem* 2008;**139**:373–87.
58. Orita H, Itoh N. *Surf Sci* 2004;**550**:177–84.
59. Topsøe H, Clausen BS, Massoth FE. In: Anderson JR, Boudart M, editors. *Catalysis, science and technology*, vol. 11. Berlin: Springer; 1996. pp. 1–269.
60. Eijbsbouts S, Mayo SW, Fujita K. *Appl Catal A Gen* 2007;**322**:58–66.
61. Chianelli RR, Berhault G, Torres B. *Catal Today* 2009;**147**:275–86.
62. Studt F, Abild-Pedersen F, Bligaard T, Sørensen RZ, Christensen CH, Nørskov JK. *Science* 2008;**320**(5881):1320–2.
63. Sanfilippo D, Miracca I. *Catal Today* 2006;**111**:133–9.
64. Vora BV. *Top Catal* 2012;**55**:1297–308.
- 65a. Røstrup-Nielsen JR. In: Anderson JR, Boudart M, editors. *Catalysis science and technology*, vol. 5. Berlin: Springer; 1984. pp. 1–118.
- 65b. Aasberg-Petersen K, Dybkjær I, Ovesen CV, Schjødt NC, Sehested J, Thomsen SG. *J Nat Gas Sci Eng* 2011b;**3**(2):423–59.
66. Ratnasamy C, Wagner JP. *Catal Rev* 2009;**51**:325–440.
67. Farrauto R, Liu X, Ruettinger W, Ilinich O, Shore L, Giroux T. *Catal Rev Sci Eng* 2007;**49**:141–96.
68. Polychronopoulou K, Bakandritsos A, Tzitzios V, Fierro JLG, Efstathiou AM. *J Catal* 2006;**241**:132–48.
69. Nielsen SE. Innovations in industrial and engineering chemistry. In: Flank WH, Abraham MA, Mathews MA, editors. *A century of achievements and prospects for the new millennium. ACS symposium series*, vol. 1000. Washington: ACS; 2008. pp. 15–39.
70. Ammonia synthesis catalysts, [www.topsøe.com](http://www.topsøe.com).
71. KATALCO<sub>JM</sub> ammonia synthesis catalysts, [www.jmcatalysts.com](http://www.jmcatalysts.com).
72. [www.catalysts.clariant.com](http://www.catalysts.clariant.com) [accessed 03.07.13].
73. BASF, Ammonia synthesis catalyst, Multi-promoted iron technology, [www.catalysts.basf.com](http://www.catalysts.basf.com).
74. Steynberg AP, Espinoza RL, Jager B, Vosloo AC. *Appl Catal A Gen* 1999;**186**:41–54.
75. de Klerk A. *Energy Fuels* 2009;**23**:4593–604.
76. Luo M, Hamdeh H, Davis BH. *Catal Today* 2009;**140**:127–34.
77. Gaube J, Klein HF. *Appl Catal A Gen* 2008;**350**:126–32.
78. Abelló S, Montané D. *ChemSusChem* 2011;**4**:1538–56.
79. Matthey J. *The catalyst technical handbook*; 2008 [available on internet].
80. Süd Chemie, General catalyst catalogue. [www.sudchemie.com](http://www.sudchemie.com) [accessed 12.12.2011].
81. Renken TL, Forkner MW. US Patent Application 20080227632, to Huntsman petr. Co; 2008.
82. Chen B, Dingerdissen U, Krauter JGE, Lansink Rotgerink HGJ, Möbus K, Ostgard DJ, et al. *Appl Catal A Gen* 2005;**280**:17–46.
83. Likhar PR, Arundhathi R, Kantam ML, Prathima PS. *Eur J Org Chem* 2009;**31**:5383–9.
84. Leckel D. *Energy Fuels* 2009;**23**:2342–58.
85. Khodakov AY, Chu W, Fongarland P. *Chem Rev* 2007;**107**:1692–744.
86. Diehl F, Khodakov AY. *Oil Gas Sci Technol Rev IFP* 2009;**64**:11–24.
87. Cheng J, Hu P, Ellis P, French S, Kelly G, Lok CM. *J Phys Chem C* 2010;**114**:1085–93.

88. Dalai AK, Davis BH. *Appl Catal A Gen* 2008;**348**:1–15.
89. Beitel GA, de Groot CPM, Oosterbeek H, Wilson JH. *J Phys Chem B* 1997;**101**:4035–43.
90. Schulz H. *Appl Catal A Gen* 1999;**186**:3–12.
91. Davis BH. *Fuel Proc Technol* 2001;**71**:157–66.
92. Brady RC, Pettit R. *J Am Chem Soc* 1980;**102**:6181–2.
93. Carter MK. *J Mol Catal* 2001;**172**:193–206.
94. van Dijk HAJ, Hoebink JHBJ, Schouten JC. *Chem Eng Sci* 2001;**56**:1211–425.
95. Haryanto A, Fernando S, Murali N, Adhikari S. *Energy Fuels* 2005;**19**:2098–106.
96. Vaidya PD, Rodrigues AE. *Chem Eng J* 2006;**117**:39–49.
97. Ni M, Leung DYC, Leung MKH. *Int J Hydrog Energy* 2007;**32**:3238–47.
98. Frusteri F, Freni S. *J Power Sources* 2007;**173**:200–9.
99. Ramirez de la Piscina P, Homs N. *Chem Soc Rev* 2008;**37**:2459–67.
100. Bshish A, Yaako Z, Narayanan B, Ramakrishnan R, Ebshish A. *Chem Pap* 2011;**65**:251–66.
101. Nahar G, Dupont V. *Biofuels* 2012;**3**:167–119.
102. Bion N, Duprez D, Epron F. *ChemSusChem* 2012;**5**:76–84.
103. Mattos LV, Jacobs G, Davis BH, Noronha FB. *Prod Hydrogen Ethanol Rev React Mech Catal Deactiv Chem Rev* 2012;**112**:4094–123.
104. de la Peña O'Shea VA, Homs N, Pereira EB, Nafria R, Ramirez de la Piscina P. *Catal Today* 2007;**126**:148–52.
105. Tuti S, Pepe F. *Catal Lett* 2008;**122**:196–203.
106. Gac W, Zawadzki W, Tomaszewska B. *Catal Today* 2011;**176**:97–102.
107. de la Peña O'Shea VA, Nafria R, Ramírez de la Piscina P, Homs N. *Int J Hydrogen Energy* 2008;**33**:3601–6.
108. Busca G, Costantino U, Montanari T, Ramis G, Resini C, Sisani M. *Int J Hydrogen Energy* 2010;**35**:5356–66.
109. Bayram B, Ilgaz Soykal I, von Deak D, Miller JT, Ozkan US. *J Catal* 2011;**284**:77–89.
110. Espinal R, Taboada E, Molins E, Chimentao RJ, Medina F, Llorca J. *RSC Adv* 2012;**2**:2946–56.
111. Espinal R, Taboada E, Molins E, Chimentao RJ, Medina F, Llorca J. *Appl Catal B Environ* 2012;**127**:59–67.
112. Helveg S, Sehested J, Rostrup-Nielsen JR. *Catal Today* 2011;**178**:42–6.
113. Devred F, Hoffer BW, Sloof WG, Kooyman PJ, van Langeveld AD, Zandbergen HW. *Appl Catal A Gen* 2003;**244**(2):291–300.
114. Alini S, Bottino A, Capannelli G, Carbone R, Comite A, Vitulli G. *J Mol Catal A Chem* 2003;**206**:363–70.
115. Actimet™ 8040P, Activated skeletal nickel catalyst. [www.castalysts.basf.com](http://www.castalysts.basf.com).
116. Balakos MW, Hernandez EE. *Catal Today* 1997;**35**:415–25.
117. Catalysts for Edible Oil hydrogenation, brochure. [www.jmcatalysts.com](http://www.jmcatalysts.com).
118. Nysosel® 820 Fats and oils hydrogenation catalyst. [www.catalysts.basf.com](http://www.catalysts.basf.com).
119. Fernández MB, Sánchez M. JF, Tonetto GM, Damiani DE. *Chem Eng J* 2009;**155**:941–9.
120. Stanković M, Gabrovska M, Krstić J, Tzvetkov P, Shopska M, Tsacheva T, et al. *J Mol Catal A Chem* 2009;**297**:54–62.
- 120a. Garbarino G, Campodonico S, Romero Perez S, Carnasciali MM, Riani P, Finocchio E, et al. *Appl Catal A: Gen* 2013;**452**:163–73.

- 120b. Garbarino G, Valsamakis I, Riani P, Busca G. *Catal. Commun* 2014;**51**:37–41.
121. Bowen CP. In: Meyers RA, editor. *Handbook petrochemicals production processes*. McGraw-Hill; 2005. p. 6.21–50.
122. Borsos S, Ronczy S. In: Meyers RA, editor. *Handbook of petrochemicals production processes*. McGraw-Hill; 2005. p. 6.51–63.
123. Krupa S, Foley T, McColl S. In: Meyers RA, editor. *Handbook of petrochemicals production processes*. McGraw-Hill; 2005. p. 3.11–14.
124. [http://www.uop.com/objects/KLP\\_60\\_Catalyst.pdf](http://www.uop.com/objects/KLP_60_Catalyst.pdf).
125. UOP H-15 selective hydrogenation catalyst, <http://www.uop.com/objects/H-15%20catalyst.pdf>.
126. Rajeshwer D, Sreenivasa Rao G, Krishnamurthy KR, Padmavathi G, Subrahmanyam N, Rachh JD. *Int J Chem React Eng* 2006;**4**:A17.
127. Kravtsov AV, Zuev VA, Kozlov IA, Milishnikov AV, Ivanchina ED, Uriev EM, et al. *Petroleum Coal* 2009;**51**:248–54.
128. Hoffer W, Bonn e RLC, van Langeveld AD, Griffiths C, Lok CM, Moulijn JA. *Fuel* 2004;**83**:1–8.
129. <http://www.jmcatalysts.com>.
130. [http://www.axens.net/html-gb/offer/offer\\_processes\\_29.html.php](http://www.axens.net/html-gb/offer/offer_processes_29.html.php).
131. Wender I. *Fuel Proc Technol* 1996;**48**:189–297.
132. Pearce BB, Twigg MV, Woodward C. In: Twigg MV, editor. *Catalyst handbook*. 2nd ed. London: Wolfe Pub; 1989. pp. 340–83.
133. [http://www.topsoe.com/business\\_areas/ammonia/processes/methanation.aspx](http://www.topsoe.com/business_areas/ammonia/processes/methanation.aspx).
134. Kopyscinski J, Schildhauer TJ, Biollaz SMA. *Fuel* 2010;**89**:1763–83.
135. <http://www.topsoe.com/products/CatalystPortfolio.aspx>.
136. R ostrup-Nielsen JR, Pedersen K, Sehested J. *Appl Catal A Gen* 2007;**330**:134–8.
137. Mills GA, Steffgen FW. *Catal Rev Sci Eng* 1974;**8**:159–210.
138. Alstrup I. *J Catal* 1995;**151**:216–25.
139. Sehested J, Dahl S, Jacobsen J, R ostrup-Nielsen JR. *J Phys Chem B* 2005;**109**:2432–8.
140. Sanchez-Escribano V, Larrubia Vargas MA, Finocchio E, Busca G. *Appl Catal A Gen* 2007;**316**:68–74.
- 140b. Riani P, Garbarino G, Lucchini MA, Canepa F, Busca G. *J Mol Catal A: Chem* 2014;**383–384**:10–6.
141. Takehira K. *J Nat Gas Chem* 2009;**18**:237–59.
142. Bradford MCJ, Vannice MA. *J Catal* 1998;**173**:157–71.
143. Wei J, Iglesia E. *J Catal* 2004;**224**:370–83.
144. Garcia-Di eguez M, Pieta IS, Herrera MC, Larrubia MA, Malpartida I, Alemany LJ. *Catal Today* 2010;**149**:380–7.
145. Pawelec B, Demyaniova S, Arishtirova K, Fierro JLG, Petrov L. *Appl Catal A Gen* 2007;**323**:188–201.
146. Huber GW, Iborra S, Corma A. *Chem Rev* 2006;**106**:4044–98.
147. Knoef HAM, editor. *Handbook biomass gasification*. The Netherlands: The Biomass Technology Group (BTG); 2005.
148. Wu W-G, Luo YH, Su Yi, Zhang YL, Zhao SH, Wang Y. *Energy Fuels* 2011;**25**:5394–406.
149. Cheah S, Carpenter DL, Magrini-Bair KA. *Energy Fuels* 2009;**23**:5291–307.
150. Calvo LF, Gil MV, Otero M, Mor n A, Garc a AI. *Bioresour Technol* 2012;**109**:206–14.



151. Milne TA, Evans RJ, Abatzoglou N. *Biomass gasifier "tars": their nature, formation, conversion*, NREL/TP-570-25357, Available on internet; November 1998.
152. Lorente E, Millan M, Brandon NP. *Int J Hydrogen Energy* 2012;**37**:7271–8.
153. Røstrup-Nielsen JR, Bøgild Hansen J. *Fuel Cells*; 2011:49–71 [Chapter 4].
154. Torres W, Pansare SS, Goodwin Jr JG. *Catal Rev Sci Eng* 2007;**49**:407–56.
155. Yung MM, Jablonski WS, Magrini-Bair KA. *Energy Fuels* 2009;**23**:1874–87.
156. <http://www.nextechmaterials.com>.
157. Basile F, Albertazzi S, Barbera D, Benito P, Einvall J, Brandin J, Fornasari G, Trifiro F, Vaccari A. *Biomass Bioenergy* 2011;**35**:S116–22.
158. Prasad R, Singh P. *Bull Chem React Eng Catal* 2011;**6**(2):63–114.
159. Lee S. In: Lee S, Speight JG, Loyalka SK, editors. *Handbook of alternative fuel technologies*. CRC Press; 2007. pp. 297–322.
160. Waugh KC. *Catal Lett* 2012;**142**:1153–66.
161. Behrens M. *J Catal* 2009;**267**:24–9.
162. Weissmehl K, Arpe HJ. *Industrial organic chemistry*. 4th ed. Wiley-VCH; 2003. p. 32.
163. Ma L, Tran T, Wainwright MS. *Top Catal* 2003;**22**:295–304.
164. High activity methanol synthesis catalyst. [http://www.topsoe.com/Business\\_areas/Methanol/Processes/~media/PDF%20files/Methanol/Topsoe\\_methanol\\_mk%20121.ashx](http://www.topsoe.com/Business_areas/Methanol/Processes/~media/PDF%20files/Methanol/Topsoe_methanol_mk%20121.ashx).
165. Jiang CJ, Trimm DL, Wainwright MS, Cant NW. *Appl Catal A Gen* 1993;**93**:245–55.
166. KATALCO<sub>JM</sub> methanol synthesis catalysts. [www.jmcatalysts.com](http://www.jmcatalysts.com).
167. Chinchin GC, Spencer MS. *Catal Today* 1991;**10**:293–301.
168. Waugh KC. *Solid State Ionics* 2004;**168**:327–42.
169. Greeley J, Gokhale AA, Kreuser J, Dumesic JA, Topsøe H, Topsøe N-Y, et al. *J Catal* 2003;**213**:63–72.
170. Topsøe N-Y, Topsøe H. *J Mol Catal A Chem* 1999;**141**:95–105.
171. Spencer MS. *Catal Today* 1992;**12**:453–64.
172. Weigel J, Koepfel RA, Baiker A, Wokaun A. *Langmuir* 1996;**12**:5319–29.
173. Yang R, Zhang Y, Iwama Y, Tsubaki N. *Appl Catal A Gen* 2005;**288**:126–33.
174. Larrubia Vargas MA, Busca G, Costantino U, Marmottini F, Montanari T, Patrono P, et al. *J Mol Catal A Chem* 2007;**266**:188–97.
175. Zander S, Kunkes EL, Schuster ME, Schumann J, Weinberg G, Teschner D, et al. *Angew Chem Int Ed* 2013;**52**:6536–40.
176. Topsøe H. Brochure “Leading edge performance LTS catalysts”. <http://www.topsoe.com>.
177. KATALKO<sub>JM</sub> low temperature shift catalysts. [www.jmcatalysts.com](http://www.jmcatalysts.com).
178. Peppley BA, Amphlett JC, Kearns LM, Mann RF. *Appl Catal A Gen* 1999;**179**:21–9.
179. Madon RJ, Nagel P. US Patent Application 0102278, to BASF; 2010.
180. Fujita S, Usui M, Takezawa N. *J Catal* 1992;**134**:220–5.
181. Callaghan C, Fishtik I, Datta R, Carpenter M, Chmielewski M, Lugo A. *Surf Sci* 2003;**541**:21–30.
182. Kniep BL, Ressler T, Rabis A, Girgsdies F, Baenitz M, Steglich F, et al. *Angew Chem Int Ed* 2004;**43**:112–5.
183. Ilinich O, Ruettinger W, Liu X, Farrauto R. *J Catal* 2007;**247**:112–8.
184. Stone FS, Waller D. *Top Catal* 2003;**22**(3–4):305–18.
185. Palo DR, Dagle RA, Holladay JD. *Chem Rev* 2007;**107**:3992–4021.
186. Topsøe H. Brochure “Package hydrogen plants”. Available in the web: <http://www.topsoe.com>.

187. *Hydrocarbon processing: gas processes*. Gulf Pub. Co.; 2004.
188. Kumberger O, Sprague MJ, Hofstadt O. US Patent 6051163, to BASF; 2000.
189. Won JuY, Jun HK, Jeon MK, Woo SI. *Catal Today* 2006;**111**:158–63.
190. Pfeifer P, Schubert K, Emig G. *Appl Catal A Gen* 2005;**286**:175–85.
191. Lee JK, Ko JB, Kim DH. *Appl Catal A Gen* 2004;**278**:25–35.
192. Löffler DG, McDermott SD, Renn CN. *J Power Sources* 2003;**114**:15–20.
193. Lee M-T, Greif R, Grigoropoulos CP, Park HG, Hsu FK. *J Power Sources* 2007;**166**:194–201.
194. Illinich O, Liu Y, Castellano C, Koerner G, Moini A, Farrauto R. *Plat Met Rev* 2008;**52**:134–43.
195. Twigg MV, Spencer MS. *Appl Catal A Gen* 2001;**212**:161–74.
196. Gunardson H. *Industrial gases in petrochemical processes*. New York: Dekker; 1998.
197. King F, Kelly GJ. *Catal Today* 2002;**73**:75–81.
198. Kelly GJ, King F, Kett M. *Green Chem* 2002;**4**:392–9.
199. Butcher J, Reynolds G. Process. In: Meyers RA, editor. *Handbook of petrochemicals production processes*. McGraw-Hill; 2005. p. 8.3–14.
200. Ertl G, Knözinger H, Weitkamp J. *Handbook of heterogeneous catalysis*, vol. 5. Weinheim (Germany): VCH; 1997. 2140.
201. Neier W, Strehlke G. Copyright ©. In: *Ullmann's encyclopedia of industrial chemistry*. Wiley-VCH Verlag GmbH & Co; 2002.
202. Keshavaraja A, Samuel JV, Ramaswamy AV. US Patent 5723679, to CSIR, India; 1998.
203. Keuler JN, Lorenzen L, Miachon S. *Appl Catal A Gen* 2001;**218**:171–80.
204. Liu Z, Huo W, Ma H, Qiao K. *Chin J Chem Eng* 2006;**14**:676–84.
205. van Der Laan GP, Beenackers AACM. *Catal Rev Sci Eng* 1999;**41**:255–318.
206. Hindermann JP, Hutchings GJ, Kiennemann A. *Catal Rev Sci Eng* 1993;**35**:1–127.
207. Kang J, Zhang S, Zhang Q, Wang Y. *Angew Chem Int Ed* 2009;**48**:2565–8.
208. Claeys M, van Steen E. *Catal Today* 2002;**71**:419–27.
- 208b. Kwak JH, Kovarik L, Szanyi L. *ACS Catal* 2014;**3**:2449–55.
- 208c. Janke C, Duyar MS, Hoskins M, Ferrauto R. *Int J Hydr En* 2014;**152-3**:184–91.
- 208d. Nagahara H, Ono M, Konishi M, Fukuoka Y. *Appl Surf Sci* 1997;**121-122**:448–51.
209. <http://www.kbr.com/Technologies/Proprietary-Equipment/KAAP-Ammonia-Synthesis-Converter/>.
210. Foster AI, James PG, McCarroll JJ, Tennison SR. US Patent 4,250,057, to BP Co. Ltd; 1986.
211. Rossetti I, Pernicone N, Ferrero F, Forni L. *Ind Eng Chem Res* 2006;**45**:4150–5.
212. Polychronopoulou K, Giannakopoulos K, Efstathiou AM. *Appl Catal B Environ* 2012;**111–112**:360–75.
213. Torniaainen PM, Chu X, Schmidt LD. *J Catal* 1994;**146**:1–10.
214. Enger BC, Lodeng R, Holmen A. *Appl Catal A Gen* 2008;**346**:1–27.
215. Naito S, Tanaka H, Kado S, Miyao T, Naito S, Okumura K, et al. *J Catal* 2008;**259**(1):138–46.
216. Molnár A, Sárkányi A, Varga M. *J Mol Catal A Chem* 2001;**173**:185–221.
217. Mohundro EL. Overview on C2 and C3 selective hydrogenation in ethylene plants. <http://kolmertz.com/pdf/edm64a.pdf>.
218. Kapur S. In: Meyers RA, editor. *Handbook of petrochemicals production processes*. McGraw-Hill; 2005. p. 6.3–20.
219. Schbib NS, Garcia MA, Gigola CE, Errazu AF. *Ind Eng Chem Res* 1996;**35**:1496–505.

220. Flik K, Herion C, Allmqann HM, US Patent 5856262, to BASF; 1999.
221. Büchele W, Roos H, Wanjek H, Müller HJ. *Catal Today* 1996;**30**:33–9.
222. Woike U, Kammerhofer P. In: Meyers RA, editor. *Handbook of petrochemicals production processes*. McGraw-Hill; 2005. p. 18.3–36.
223. Evonik. Continuous process catalysts, brochure. <http://catalysts.evonik.com>.
224. Axens' portfolio of selective hydrogenation catalysts. <http://www.axens.net>.
225. Alves JA, Bress SP, Martínez OM, Barreto GF. *Chem Eng J* 2007;**125**:131–8.
226. Vergunst T, Kapteijn F, Moulijn JA. *Ind Eng Chem Res* 2001;**40**:2801–9.
227. Wilhite BA, McCready MJ, Varma A. *Ind Eng Chem Res* 2002;**41**:3345–50.
228. Axens' portfolio of selective hydrogenation catalysts. [www.axens.net](http://www.axens.net).
229. Uhde. Aromatics, brochure. [www.uhde.com](http://www.uhde.com).
230. Moore A, Birkhoff R. In: Meyers RA, editor. *Handbook of petrochemicals production processes*. McGraw-Hill; 2005. p. 9.31–50.
231. Birkhoff R, Griffiths C, Shah K, Subramanian A. US Patent 7381854, to Kellogg Brown & Root LLC Houston (TX, US); 2008.
- 231b. Collins SE, Delgado JJ, Mira C, Calvino JJ, Bernal S, Chiavassa DL, et al. *J Catal* 2012;**292**:90–8.
232. Savchenko VI, Makarian IA. *Platin Met Rev* 1999;**43**:74–82.
233. Nikolopoulos AA, Howe GB, Jang BW-L, Subramanian R, Spivey JJ, Olsen DJ, et al. In: Ford ME, editor. *Catalysis of organic reactions*. New York: Dekker; 2001. p. 533.
234. Gelbard G. *Ind Eng Chem Res* 2005;**44**:8468–98.
235. Nikolopoulos AA, Jang BW-L, Spivey JJ. *Appl Catal A Gen* 2005;**296**:128–36.
236. Chen YZ, Liaw CW, Lee LI. *Appl Catal A Gen* 1999;**177**:1–8.
237. Liu H, Jiang T, Han B, Liang S, Zhou Y. *Science* 2009;**326**:1250–2.
238. Weissmehl K, Arpe HJ. *Industrial organic chemistry*. 4th ed. Wiley-VCH; 2003. p. 363.
239. Scirè S, Minicò S, Crisafulli C. *Appl Catal A Gen* 2002;**235**:21–31.
240. Antos GJ, Aitani AM. In: *Catalytic naphtha reforming, revised and expanded*. CRC Press; 2004.
241. Calemma V, Giardino R, Cornaro U. Patent WO 2007/006473, to ENI; 2007.
242. McVicker GB, Daage M, Touvelle MS, Hudson CW, Klein DP, Baird Jr WC, et al. *J Catal* 2002;**210**:137–48.
243. Calemma V, Giardino R, Ferrari M. *Fuel Proc Technol* 2010;**91**:770–6.
244. Schmidt F, Köhler E. In: Guisnet M, Gilson JP, editors. *Zeolites for cleaner technologies*. Imperial College Press; 2002. pp. 153–66.
245. Weyda H, Köhler E. *Catal Today* 2003;**81**:51–5.
246. Sarkar A, Seth D, Ng FTT, Rempel GL. *AIChE J* 2006;**52**:1143–56.
247. Greenfield H. *Ann NY Acad Sci* 1973;**214**:233–42.
248. Stanislaus A, Cooper BH. *Catal Rev Sci Eng* 1994;**36**:75–123.
249. Haizmann RS, Rice LH, Turowicz MS. US Patent 5453552, to UOP; 1995.
250. Schiavone BJ. *2007 O&A and technology forum*. NIPRA; 2007 [available on the web].
251. <http://www.digitalrefining.com/data/literature/file/671496434.pdf>.
252. Stanislaus A, Marafi A, Rana MS. *Catal Today* 2010;**153**:1–68.
253. Cooper BH, Donniss BBL. *Appl Catal A Gen* 1996;**137**:203–23.
254. Sidhpuria KB, Parikh PA. *Bull Catal Soc India* 2004;**3**:68–71.
255. Nagy G, Hancsó J, Varga Z, Pölczmán G, Kalló D. *Petroleum Coal* 2007;**49**:24–32.
256. [http://www.exxonmobil.com/apps/refiningtechnologies/lubes/mn\\_maxsat.html](http://www.exxonmobil.com/apps/refiningtechnologies/lubes/mn_maxsat.html).
257. Modica FS, McBride TK, Galperin LB. Patent WO/2006/078240, to UOP LLC; 2006.

258. Shoukri EI. Patent 5013704, to Exxon Res. & Eng. Co.; 1991.
259. <http://www.uop.com/pr/releases/Hunt.pdf>.
260. <http://www.uop.com/objects/R%20230%20Series%20Catalyst.pdf>.
261. Antos GJ, Moser MD, Lapinski MP. Catalytic naphtha reforming. In: Antos GJ, Aitani AM, editors. *Revised and expanded*. 2nd ed. New York: Dekker; 2004. pp. 335–52.
262. Lapinski M, Baird L, James R. UOP platforming process. In: Meyers RA, editor. *Handbook of petroleum refining processes*. 3rd ed. Mc Graw Hill; 2006. p. 4.3–31.
263. Fukunaga T, Katsuno H. *Catal Surv Asia* 2010;**14**:96–102.
264. Birkhoff R. In: Meyers RA, editor. *Handbook of petrochemicals production processes*. McGraw-Hill; 2005. p. 2.3–9.
265. Evonik. Selective nitro group hydrogenation. <http://catalysts.evonik.com/product/catalysts/en/products/technology-platforms/selective-nitro-group-hydrogenation/pages/default.aspx>.
266. Bhasin MM, McCain JH, Vora BV, Imai T, Pujadó PR. *Appl Catal A Gen* 2001;**221**: 397–419.
267. Dyroff DR. US Patent No. 6,700,028 B2, to Huntsmann Petrochem. Co.; 2004.
268. Zahedi G, Yaqubi H, Ba-Shammakh M. *Appl Catal A Gen* 2009;**358**:1–6.
269. Phatak AA, Koryabkina N, Rai S, Ruettinger W, Farrauto RJ, Blau GE, et al. *Catal Today* 2007;**123**:224–34.
270. Ciambelli P, Palma V, Ruggiero A. *Appl Catal B* 2010;**96**:18–27.
271. Panagiotopoulou P, Verykios XE. *Appl Catal B* 2012;**37**:16333–45.
272. Corti CW, Hollyday TJ, Thompson DT. *Appl Catal A Gen* 2005;**291**:253–61.

# Catalysts for Hydrogenations, Dehydrogenations and Metathesis: Sulfides and Oxides

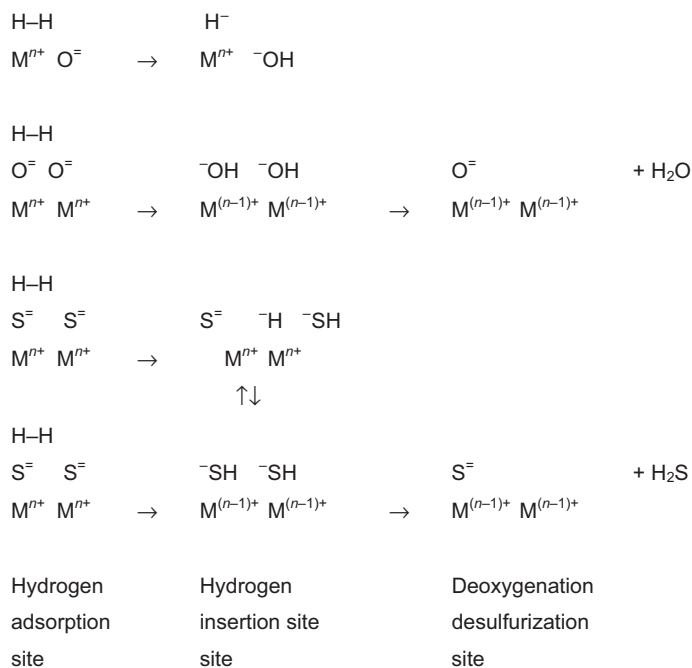
## CHAPTER OUTLINE

<b>10.1 Metal oxides in hydrogenation and dehydrogenation reactions.....</b>	<b>346</b>
10.1.1 Iron oxide-based catalysts for hydrocarbon dehydrogenation and water gas-shift .....	348
10.1.1.1 <i>Fe oxide-based catalysts for high-temperature water-gas       shift (HTWGS)</i> .....	348
10.1.1.2 <i>K-Fe oxides for ethylbenzene dehydrogenation</i> .....	349
10.1.2 Chromia–alumina for alkane dehydrogenation and hydrodealkylation .....	351
10.1.2.1 <i>K-Cr<sub>2</sub>O<sub>3</sub>-Al<sub>2</sub>O<sub>3</sub> catalysts for paraffin dehydrogenation</i> .....	351
10.1.2.2 <i>Cr<sub>2</sub>O<sub>3</sub>-Al<sub>2</sub>O<sub>3</sub> catalysts for toluene hydrodealkylation</i> .....	352
10.1.3 Gallium oxide-based catalysts for dehydrogenations.....	352
10.1.4 Zinc oxide for dehydrogenation reactions .....	353
10.1.5 Oxide-based catalysts for carboxylic acid hydrodeoxygenation.....	353
10.1.6 Oxide catalysts for catalytic transfer hydrogenation.....	354
<b>10.2 Sulfide catalysts.....</b>	<b>354</b>
10.2.1 Adsorption of hydrogen on metal sulfides.....	355
10.2.2 Layered bulk sulfides and their applications.....	356
10.2.3 Supported bimetallic sulfides .....	360
10.2.4 Other sulfide catalysts.....	362
10.2.5 Hydrocracking catalysts .....	364
10.2.6 Other catalytic materials for hydrotreatings.....	365
<b>10.3 Olefin metathesis catalysts .....</b>	<b>366</b>
10.3.1 Heterogeneous tungsten-based metathesis catalysts .....	366
10.3.2 Heterogeneous rhenium-oxide metathesis catalysts .....	367
10.3.3 Molybdenum-based metathesis catalysts .....	368
<b>References .....</b>	<b>368</b>

## 10.1 Metal oxides in hydrogenation and dehydrogenation reactions

A number of oxides adsorb significantly hydrogen and show useful activity as catalysts for hydrogenation and dehydrogenation reactions. Adsorption of hydrogen on metal oxides is mostly reported to be heterolytic, occurring on exposed cation-oxide couples, and being strongly favored by the basicity of the oxide species. Thus hydrogen dissociation produces a metal hydride species on cationic centers and a new hydroxyl group on an oxide site (Scheme 1). The best-known case is that of ZnO, which has been the object of a number of studies.<sup>1–3</sup> This oxide is an active catalyst in hydrogenations such as methanol synthesis<sup>4</sup> as well as in dehydrogenation reactions. Well-evident surface hydride species have been observed by vibrational spectroscopies (IR, HREELS, INS), both of the terminal Zn–H type I (1700–1600 cm<sup>-1</sup>), which is more weakly adsorbed, and of the bridging Zn–H–Zn type II (1450–1200 cm<sup>-1</sup>), which is quite strongly adsorbed, formed together with new OH groups.

Neither of the two species could be observed in well-controlled single crystal ultrahigh vacuum UHV experiments, while are observed on powders and at significant



**SCHEME 10.1**

Mechanisms of hydrogen adsorption on oxides and sulfides.

hydrogen pressure. At higher temperature, these species disappear while a contact with hydrogen can produce reduction of the surface.

Spectroscopic studies confirmed that some of the hydride species are indeed active in hydrogenation, e.g., producing CHO formyl species from CO as an intermediate in methanol synthesis.<sup>5</sup>

Heterolytic dissociation of hydrogen has also been observed on chromia ( $\text{Cr}_2\text{O}_3$ ), where only terminal hydride species were found ( $\nu\text{Cr-H}$  1714, 1697  $\text{cm}^{-16}$ ) and their combination  $\text{ZnO-Cr}_2\text{O}_3$ , as well as other mixed chromites such as  $\text{Co-Cr}$  and  $\text{Mn Cr}$  oxides, where both terminal and bridging species were found.<sup>6</sup>

Two terminal hydride species ( $\nu\text{Ga-H}$  2003 and 1980  $\text{cm}^{-1}$ ) have also been found to be formed by hydrogen adsorption on gallium oxide polymorphs,<sup>7</sup> and assigned to hydride species bonded to tetrahedral and octahedral Ga ions, respectively.

Dissociative adsorption of hydrogen was also observed on zirconia: to terminal hydride species was assigned a sharp  $\nu\text{Zr-H}$  band at 1562  $\text{cm}^{-1}$ , while a band at 1540  $\text{cm}^{-1}$  was assigned to a dihydride  $\text{H-Zr-H}$  species and a broad band at 1371  $\text{cm}^{-1}$  was assigned to bridging species ( $\text{ZrHZr}$ ).<sup>8-10</sup>

Dissociative adsorption of  $\text{H}_2$  was also observed to occur on defect sites of  $\text{MgO}$ . Calculations allowed to assign a band of the reversible species at 1325  $\text{cm}^{-1}$  to the terminal  $\text{Mg-H}$  hydride group on tricoordinated magnesium. The hydrogen atoms bridging two or three neighboring, low-coordinated Mg atoms of the surface are suggested to be responsible for a complex band in the 1130–880  $\text{cm}^{-1}$  region.<sup>11</sup>

The results reported above suggest that the reducing species upon hydrogenation catalysis on oxides are surface hydride species. This mechanism seems mainly to involve quite hardly reducible cations on ionic oxides, i.e., with some surface basicity.

A different approach has been proposed in other cases,<sup>12</sup> and may occur in particular in de-oxygenation reactions such as reduction of carboxylic acids. In this case, an “inverted” version of the so-called Mars-van Krevelen mechanism, or redox mechanism (see Chapter 11), can occur. This mechanism is well evident in the case of oxidation reactions, implying the reduction of the catalyst surface by the substrate and its reoxidation by oxygen. In the case of hydrogenation reactions, the redox mechanism implies that hydrogen may reduce the oxide surface forming water. The surface may be reoxygenated by the substrate, which is consequently de-oxygenated. Thus, this mechanism is possible on the oxides of partially reducible cations, such as e.g.,  $\text{Ce}^{4+}$  and  $\text{Fe}^{3+}$ .

In recent years, interest is growing on the use of ceria as hydrogenation catalyst. In particular, it has been found to be active for the hydrogenation of alkynes to olefins.<sup>13</sup> The adsorption of hydrogen on ceria has been studied by Density Functional Theory (DFT) calculations.<sup>14</sup> These studies have shown that  $\text{H}_2$  may adsorb dissociatively on  $\text{CeO}_2(111)$  with a relatively low activation barrier (0.2 eV) and strong exothermicity. Hydrogen dissociation is supposed to lead to two OH groups. Indeed, during hydrogenation reaction, an increase of absorption in the OH-stretching region of the IR spectra bands was observed.<sup>13</sup> This is a mechanism of oxidative adsorption (Scheme 1) leading to the reduction of cerium ions to the trivalent state. This

mechanism of adsorption may be seen as the precursor of the deoxygenation redox mechanism discussed above, being water easily formed from the hydroxyl groups of the reduced surface, and desorbed.

The two latter mechanisms, both implying the oxidation of hydrogen and the reduction of the metal centers, are parallel to those are supposed to occur in the case of hydrodesulfurization over sulfide catalysts (see below).

It can be supposed that inverse mechanisms with the same intermediate states can be applied in the case of dehydrogenation reactions. In fact, catalysts based on zinc, chromium and gallium oxide are supposed to be able to abstract hydrides from organic molecules, with the intermediate formation of metal-hydride surface species. These species will give rise to gaseous hydrogen after abstraction of a proton. On the other hand, dehydrogenation on more reducible oxides (e.g., ferric oxide) would occur with reduction of the surface and its reoxidation by an evolution of hydrogen.

### 10.1.1 Iron oxide-based catalysts for hydrocarbon dehydrogenation and water gas-shift

#### 10.1.1.1 *Fe oxide-based catalysts for high-temperature water-gas shift (HTWGS)*

For decades, the high-temperatures water-gas shift process using iron oxide-based catalysts is applied to convert CO and water to CO<sub>2</sub> and hydrogen. These catalysts have been developed at the industrial level in spite of the relatively high temperature limit for catalytic activity (350–400 °C), mainly because of their resistance to significant amount of sulfur in the feed. In these temperature conditions, the conversion of CO within this exothermic reaction is still significantly limited by thermodynamics, and thus 1–3% CO still remains in the treated gas, depending on the number of fixed bed used.<sup>15,16</sup>

In more recent years, effective gas desulfurization technologies became available, thus allowing the use of Cu/ZnO–Al<sub>2</sub>O<sub>3</sub> catalysts (Low-Temperature Water-Gas Shift (LTWGS) catalysts, see Chapter 9.4.4.2), which work at significantly lower temperatures (down to 180 °C), thus allowing higher conversion (down to 0.1% CO in the treated gas), but are sensitive even to 0.1 ppm of sulfur.

In the modern practice, a first bed of HTWGS catalysts is mostly used in a first step of treatment of syngases, allowing a large part of CO to be converted, and also working as a guard bed for the more sensitive LTWGS catalysts.

The original composition of HTWGS is based on Cr-stabilized iron oxides. Under reaction conditions, Fe<sub>2</sub>O<sub>3</sub> (hematite) is reduced to Fe<sub>3</sub>O<sub>4</sub> (magnetite), which is stabilized morphologically and structurally by near-10% of chromium, producing a spinel structure with a composition Fe[Fe<sub>2-x</sub>Cr<sub>x</sub>]O<sub>4</sub>, with medium-low surface area (10–50 m<sup>2</sup>/g). In the most recent formulation, 1% copper is added to the catalyst, improving catalytic activity. It has been concluded that copper metal is present in working conditions, mainly acting as an activator for iron oxide. Further additives may also be present.



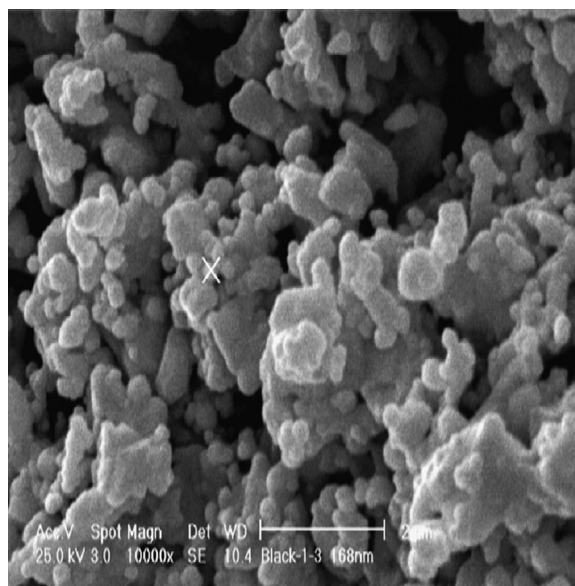
High steam-to-dry gas ratio is needed in the feed to prevent iron carbide formation on these catalysts. One of the limits of this catalytic system is associated to the pyrophoricity of the reduced working catalyst, thus needing a complex procedure for process shutdown. Another drawback is associated to the presence of chromium that, upon the preparation of the catalyst, comes to the hexavalent state, characterized by high toxicity. For this reason, Cr-free catalysts are under development.<sup>17</sup> Substitution of chromium with Al gives rise to lower activity catalysts. Addition of other elements such as Zn, Ce, Mn is under study.

Also in the case of these magnetite-based catalysts, as for the Cu-based LTWGS catalysts (Chapter 9.4.4.2), the reaction mechanism is still under discussion, with the two alternatives (regenerative or redox mechanism, versus associative mechanism via formate species) being, possibly, both active in different conditions. However, most authors are in favor of the redox mechanism that implies that CO reduces two surface ferric ions to the ferrous state and deoxygenates the surface, thus producing CO<sub>2</sub>. Water would reoxygenate the surface, reoxidizing two ferrous ions to the ferric state and producing hydrogen. This is a Mars-van Krevelen type mechanism.

#### 10.1.1.2 K–Fe oxides for ethylbenzene dehydrogenation

Styrene, one of the prominent industrial monomers, is mostly produced by catalytic dehydrogenation of ethylbenzene,<sup>18,18b</sup> previously prepared by alkylation of benzene with ethylene. The reaction is carried out at 590–720 °C, reduced pressure (200–760 Torr) and low space velocities (LHSV < 1 h<sup>-1</sup>) in the presence of steam (steam to oil ratio 1 - 1.5). Steam acts as a heat source and a diluent and also helps to reduce coking. Because of the low pressures required, the pressure drop across the catalyst is critical and adiabatic radial flow reactors are applied after preheating in most industrial processes.<sup>19</sup> The main byproducts are toluene and benzene produced by dealkylation. Selectivity to styrene is higher than 90% with conversions of the order of 70%. In the more recent Smart SM process (UOP-Lummus<sup>20,21</sup>), selective oxidation of hydrogen is performed in between the two adiabatic reactors. This allows to shift the equilibrium to a more favorable position, allowing 80% conversion, also providing reaction heat. Unconverted ethylbenzene, separated by distillation, is recycled back.

Many catalysts have been described for this reaction, but those actually applied in the industry are based on potassium-promoted ferric oxide, with surface area of ~2 m<sup>2</sup>/g. The Shell 105 catalyst dominated the market for many years. This catalyst, whose initial composition was reported to be 93% Fe<sub>2</sub>O<sub>3</sub>, 5% Cr<sub>2</sub>O<sub>3</sub>, 2% KOH<sup>22</sup>, was later enriched in potassium until the composition of 84.3% Fe<sub>2</sub>O<sub>3</sub>, 2.4% Cr<sub>2</sub>O<sub>3</sub>, 13.3% K<sub>2</sub>CO<sub>3</sub>. It has good physical properties and good activity, and it gives good yields. In more recent catalysts, additives are CeO<sub>2</sub>, V<sub>2</sub>O<sub>5</sub> and MoO<sub>3</sub> as structural promoters to stabilize the catalyst morphology and to prevent sintering. The composition of a recent industrial catalyst is ~70% Fe<sub>2</sub>O<sub>3</sub>, ~11% CeO<sub>2</sub>, 11–13% K<sub>2</sub>O, with CaO, MgO and MoO<sub>3</sub> all 1.5–2%.<sup>23,24</sup> The surface area is very low (<2 m<sup>2</sup>/g<sup>23</sup>). In Figure 10.1, an SEM micrograph of a used industrial

**FIGURE 10.1**

SEM micrograph of a used industrial ethylbenzene dehydrogenation catalyst, 10,000 magnification.

*Reprinted with permission from Ref. 23.*

catalyst is reported. According to Muhler et al.,<sup>25</sup> the working catalyst consists of regions of  $K_2Fe_{22}O_{34}$ , surrounded by the catalytically active phase  $KFeO_2$  as a thin surface layer. According to Kotarba et al.,<sup>26</sup> doping with Cr, Mn, Ce, Al and Mg of the  $K_2Fe_{22}O_{34}$  phase exclusively is required to prepare a robust catalyst with suitable activity and enhanced thermal stability of constitutional potassium under the operating conditions. To limit K loss associated to the volatility of some of its compounds, BASF developed a Catalyst Stabilization Technology with continuous K-feeding.<sup>18b</sup> The role of Ce is to favor the formation of the  $K_2Fe_{22}O_{34}$  phase.<sup>27</sup> Cs is reported to further improve the catalyst forming  $\beta''$ -alumina type of  $K_{2-z}Cs_zFe^{2+}Fe^{3+}_{10}O_{17}$  composition.<sup>28</sup> Cr is reported to stabilize the iron oxide against reduction whereas V destabilized the iron oxide, but has a positive effect on selectivity.<sup>29</sup> Industrial catalysts may also contain ppm levels of Pd.<sup>30</sup>

Studies on the industrial catalyst<sup>30</sup> as well as on model or alternative catalysts, such as La–Ba–Fe–Mn perovskites<sup>31</sup> and those based on Fe–Co–Mg–Al oxides<sup>32</sup> showed a redox mechanism occurring in the reaction and underlined the cooperation of the basicity induced by the presence of alkali or alkali earth cations and the redox properties of Fe ions. The basic component would favor the abstraction of a proton from the benzylic position of ethylbenzene, first, while the reduction of iron ions would result in the abstraction of the second hydrogen atom with two electrons

(formally a hydride species). The surface is regenerated by desorption of hydrogen and formal regeneration of ferric ions, as it occurs in the case of water gas shift reaction, with a Mars Van Krevelen-type mechanism.

## 10.1.2 Chromia–alumina for alkane dehydrogenation and hydrodealkylation

### 10.1.2.1 $K\text{-Cr}_2\text{O}_3\text{-Al}_2\text{O}_3$ catalysts for paraffin dehydrogenation

Dehydrogenation of light paraffins such as propane and isobutane to produce propene and isobutene, respectively, may be performed to enhance the availability of such intermediates in refinery (to feed alkylation, polymerization and ether synthesis units) or in petrochemistry, starting from Natural Gas Liquids or refinery gases.<sup>33</sup> Also these endothermic reactions need more than 550 °C and low pressure to allow sufficient thermodynamically limited conversion.

As mentioned previously (Chapter 9), two main catalytic systems are used industrially for alkane dehydrogenation: metal catalysts based on Pt/Al<sub>2</sub>O<sub>3</sub> (Chapter 9.4.10.5) and oxide catalysts based on chromia–alumina. Chromium-oxide (typically 10–20% by weight) deposited on alumina or on silica-stabilized transition ( $\gamma$ -/ $\delta$ -/ $\theta$ -) aluminas is the basic component of catalysts for these processes.<sup>34</sup> Chromia may give rise to different structures when combined with alumina,<sup>34</sup> as schematized in Figure 10.2. Isolated and clustered species together with supported chromia particles represent likely active phases. Additionally, Cr<sub>2</sub>O<sub>3</sub> and Al<sub>2</sub>O<sub>3</sub> may give rise to defective spinel-type solid solutions, which are also active catalysts,<sup>35</sup> as well as to corundum-type solid solutions,<sup>36</sup> which are inactive catalysts. The surface areas of the catalysts are few tens of square meters per gram. However, the catalyst formulation includes promotion with alkali metals (e.g., 1% K<sub>2</sub>O wt<sup>37</sup>), which is fundamental for increasing the amount of chromium-active sites and decreasing the surface acidity of both Cr and Al oxides. K has the best effect, if provided in the right amount. Typically, a volcano shape curve of activity and selectivity is obtained by increasing the potassium content.<sup>38</sup> However, not all alkali metals are effective promoters, only Cs, K, and Rb. This has been attributed to an increasing stabilization effect over the structure of alumina induced by the alkali cations that are larger in size. The increase in selectivity by destruction of the acid sites is a minor effect. Potassium, like rubidium and cesium, should increase the intrinsic activity by

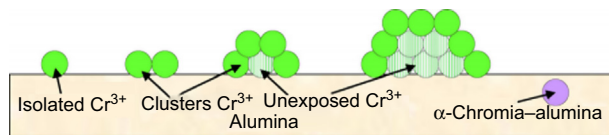


FIGURE 10.2

Model for the chromia–alumina interaction.

Reprinted with permission from Ref. 34.

increasing the number of active  $\text{Cr}^{3+}$  sites and inhibiting recrystallization of alumina to the  $\alpha$ -phase.

The catalyst deactivates rapidly by coking (timescale: minutes/hours) and does not allow the use of steam in the feed. A periodical regeneration with air is mandatory to burn off the coke. In the Catofin process (Houdry technology) commercialized by ABB Lummus,<sup>39</sup> as well as in the previous Houdry Catadiene process for the synthesis of 1,3-butadiene by dehydrogenation of *n*-butane, adiabatic fixed-bed reactors are used. In the fluidized bed dehydrogenation (FBD) technology by Snamprogetti–Yarsintez, the reaction system includes a fluidized bed reactor and a regenerator.<sup>40</sup> The reaction heat is supplied by the heat capacity of the “hot” ( $>650\text{ }^\circ\text{C}$ ) circulating catalyst, continuously moving to the reactor top from the bottom of the regenerator. The catalyst cools down again ( $<560\text{ }^\circ\text{C}$ ) from the bottom of the reactor to the top of the regenerator through a transfer line system.<sup>40</sup>

### 10.1.2.2 $\text{Cr}_2\text{O}_3$ – $\text{Al}_2\text{O}_3$ catalysts for toluene hydrodealkylation

Hydrodealkylation of toluene to benzene and methane may be performed industrially to increase benzene production in the “aromatics loop”. The reaction is exothermic and the typical operating conditions (Houdry DETOL process) are  $550\text{ }^\circ\text{C}$ – $660\text{ }^\circ\text{C}$ , and 20–70 bar. The typical catalysts are based on 10–15% chromia on alumina.<sup>41–43</sup>

### 10.1.3 Gallium oxide-based catalysts for dehydrogenations

Gallium oxides have been reported to have interesting dehydrogenation activity. For many years Ga-zeolites, in particular Ga-ZSM5 zeolite, have been found to act as active catalysts for propane aromatization.<sup>44</sup> Materials based on this catalytic system are applied in particular in the UOP Cyclar process,<sup>45</sup> which converts liquefied petroleum gas (LPG) at c.  $500\text{ }^\circ\text{C}$  directly into a liquid, aromatic product in a single processing step. The reaction is best described as dehydrocyclodimerization, and is thermodynamically favored at temperatures higher than  $425\text{ }^\circ\text{C}$ . The dehydrogenation of light paraffins (propane and butanes) to olefins is the rate-limiting step. Once formed, the highly reactive olefins oligomerize to form larger intermediates, which then rapidly cyclize to naphthenes. This process (developed jointly by BP and UOP) provides a route to upgrade low value propane and butane, recovered from gas fields or petroleum refining operations, into a high value, BTEX-rich liquid aromatic concentrate.

Gallium oxide-containing catalysts have been reported to be active also in the dehydrogenation of paraffins to olefins.<sup>46</sup> The occurrence of a heterolytic cleavage of the C–H bonds producing gallium hydride and alkoxy species was proposed. More recently, the formation of surface metal-alkyl groups by breaking paraffin C–H bonds have been reported.<sup>47,48</sup> In particular, catalysts compositions comprising gallium, one or more alkaline or alkaline-earth metals with small platinum addition, supported on an alumina are reported to allow good yields in light olefins, such as propylene from propane in a fluidized transport bed process.<sup>49</sup>

A similar catalytic system based on alkaliized  $\text{Ga}_2\text{O}_3\text{--Al}_2\text{O}_3$  with manganese and silica has been later developed in a new industrial process for styrene synthesis by ethylbenzene dehydrogenation.<sup>50</sup> Also in this case the process, denoted as SNOW being developed jointly by SNamprogetti and DOW, is based on a “fast raiser” reactor, where the catalyst moves entrained by the cocurrent hydrocarbon stream at a gas velocity of 4–20 m/s. The reaction occurs with space time 1–5 s at 590–700 °C.<sup>34</sup> In this case, the abstraction of a hydride species from the benzylic position of ethylbenzene is supposed to occur in the key step.

#### 10.1.4 Zinc oxide for dehydrogenation reactions

As said, zinc oxide powders are active in hydrogen adsorption as well as in catalysis of both hydrogenation and dehydrogenation reactions. The older literature reports on industrial use of zinc oxide in some relevant reactions, in particular in the dehydrogenation of alcohols. Apparently, the syntheses of acetone from isopropanol dehydrogenation,<sup>51</sup> of methyl–ethyl-ketone (MEK) by 2-propanol dehydrogenation, and of butyraldehyde from 1-butanol dehydrogenation<sup>52,53</sup> have been performed even at the industrial level over bare ZnO catalysts or on Zn chromites, silicates and titanates. It seems that today these catalysts have been substituted by the more active Cu–ZnO or Cu–ZnO– $\text{Al}_2\text{O}_3$  catalysts (Chapter 9.4.4.5).

A recent paper reports on zinc-based oxide catalysts for the direct conversion of bioethanol to isobutene, a promising reaction in the frame of green chemistry based on renewables.<sup>54</sup>

According to the literature, ZnO/ $\gamma\text{-Al}_2\text{O}_3$ /H-ZSM-5 catalysts are applied in the Alpha process developed by Sanyo Petrochemical Co. Ltd, a subsidiary of Asahi Chemical, the only process tailored for the production of BTX aromatics from olefin-rich feeds.<sup>55</sup>

#### 10.1.5 Oxide-based catalysts for carboxylic acid hydrodeoxygenation

As said, a number of other oxides such as zirconia and chromia have been reported in the scientific literature to have some activities in hydrogenation and dehydrogenation reactions. Zirconia as such or in combination with titania<sup>56</sup> is active in several hydrogenation/dehydrogenation processes. A commercial process for the production of benzaldehyde from benzoic acid hydrogenation has been developed using zirconia-based catalysts by Mitsubishi Chemicals Co. (MCC), Japan, in 1988.<sup>57</sup> The catalyst is modified or stabilized by the addition of chromium oxide.<sup>58</sup> MCC later developed the industrial production of aliphatic aldehydes using highly pure  $\text{Cr}_2\text{O}_3$  catalysts and started the commercial production of undecanal and 10-undecylenic aldehyde.<sup>58</sup> The same groups also developed  $\text{Cr}_2\text{O}_3/\alpha\text{-Al}_2\text{O}_3$  for hydrogenation of other carboxylic acids, such as stearic acid, pivalic acid, cyclohexancarboxylic acid and methylnicotinate, in vapor phase to the corresponding aldehydes.<sup>59</sup> More recently, the benzoic acid hydrogenation

reaction is under investigation also on ZnO,<sup>60</sup> CeO<sub>2</sub><sup>61</sup> and Mn oxide-based catalysts.<sup>62</sup>

The hydrogenation of carboxylic acids to produce aldehydes is supposed to occur, over oxide catalysts such as zirconia and ceria, through a Mars-Van Krevel mechanism, with reduction of the catalyst by hydrogen and its reoxygenation by the carboxylic acid.<sup>12</sup>

### 10.1.6 Oxide catalysts for catalytic transfer hydrogenation

Some metal oxide catalysts can be used as heterogeneous catalysts for the so-called catalytic transfer hydrogenation (CTH) also known as catalytic hydrogen transfer reaction (CHTR) or catalytic transfer reduction (CTR). This reaction implies the hydrogenation of an oxygenated species such as ketones, aldehydes..., using the hydrogen released by a donor, such as an alcohol (producing a ketone) or formic acid (producing CO<sub>2</sub>). This family of reaction is of great interest for converting biomass-derived intermediates to most useful products.<sup>63</sup> An interesting application of this reaction can be the hydrogenation of glycerol by formic acid<sup>64</sup> that has been studied mostly using metal catalysts.

The CTH reaction may include the so-called Meerwein–Ponndorf–Verley reaction in which a direct and concerted hydride transfer occurs between an alcohol and a carbonyl compound. Magnesium oxide is among the most active heterogeneous catalysts for this reaction,<sup>65</sup> but much interest is devoted to zirconia<sup>66,67</sup> and ceria zirconia,<sup>63</sup> with all solids able to activate hydrogen. It seems likely that some basicity is a relevant requirement for the catalyst.

---

## 10.2 Sulfide catalysts

As reported before (Chapter 9), most metal-based hydrogenation catalysts suffer sulfur deactivation. Thus problems arise for their use to perform hydrogenations in heavily sulfided environment and hydrodesulfurizations.<sup>68</sup> On the other hand, metal sulfides (Table 10.2) are active in hydrogenations and are usually stable in sulfur containing environments, needing sulfur in the feed to stay stable in a sulfided state. They are, consequently, the choice catalysts for hydrodesulfurization and hydrocracking, and can be used for hydrogenation in sulfide-containing atmospheres.

The field of refinery hydrotreatments developed continuously in the last years, due to the legislation for sulfur in commercial fuels becoming more and more stringent until the 10 ppm maximum level due today by law in most developed countries. This led to the progressive development of new continuously improved catalytic materials. Indeed, a number of different hydrotreatments are realized in refineries, including hydrodesulfurization and hydrocracking, but also pretreatments involving mainly hydrodemetallization (with the decomposition of Ni-, V- and Fe-porphyrins) and hydrodenitrogenation. On the other hand, sulfide catalysts are also reported to be

**Table 10.1** Industrial Processes Using Sulfide Catalysts

Feedstock	Naphtha	Kerosene	Diesel	VGO	Resid
Application/ condition	Naphtha HT (pretreat)	Jet HT/ULSK KHT	ULSD DHT	FCC-PT/MHC/ HC-PT	E-bed, fixed bed
LHSV (1/h)	2–10	2–5	0.5–4	0.5–2	0.2–0.6
ppH <sub>2</sub> (bar)	6–20	12–30	15–70	40–100 (FCC-PT/MHC) 100–160 (HC-PT)	100–170
WABT (°C)	275–290	275–290	325–350	335–360	350–380
H <sub>2</sub> /oil (Nm <sup>3</sup> /m <sup>3</sup> )	35–100	100–200	90–300	200–450	500–1100
Cycle length (years)	4–6	3–5	1–5	1–3	1–2

*Typical range of hydroprocessing unit operating conditions for a variety of feeds. HT = hydrotreating, ULSK KH = ultra low sulfur kerosene, kerosene HT, ULSD DHT = ultra low sulfur diesel, diesel HT, FCC-PT = fluid catalytic cracking pretreatment, MHC = mild hydrocracking, HC-PT = hydrocracking pretreatment, WABT = weighted average bed temperature  
From Ref. 71.*

used for hydrotreatments of vegetable oils and bio-oils, producing mainly hydrodeoxygenations. Some data on refinery and petrochemistry processes using sulfide catalysts are reported in Table 10.1. Among recent developments, the desulfurization processes of Fluid Catalytic Cracking gasoline<sup>69</sup> and for the production of Ultra Low Sulfur Diesel fuel,<sup>70</sup> have been introduced to fulfill the 10 ppm sulfur limit in commercial fuels.

Most of the catalysts used in the last decades are bimetallic sulfides supported on alumina, mainly of the Co–Mo, Ni–Mo and Ni–W couples. In recent years, however, bulk sulfide catalysts have also been (re)introduced.

The presence of toxic metals, such as nickel and cobalt, creates some concern with the use of these catalysts<sup>71</sup> as well as with their disposal, thus contributing to the development of metal recovery processes from spent catalysts.<sup>72</sup>

### 10.2.1 Adsorption of hydrogen on metal sulfides

As we will see, the largely most-studied sulfide catalytic systems are based on MoS<sub>2</sub>, which has been the object of many studies dealing with the adsorption and activation of hydrogen. According to Bryesse et al.,<sup>73</sup> who reviewed this subject in 2002, heterolytic dissociation, involving both metal and sulfur ions, is the predominant mode of hydrogen activation. It leads to the formation of metal–H and S–H moieties. The homolytic dissociation, occurring on the sulfur ion pairs, is much less evident.

Based on the radioisotopic data of measuring <sup>1</sup>H/<sup>3</sup>H kinetic isotopic effect in the course of thiophene hydrodesulfurization (HDS) in the (<sup>3</sup>H)-labelled molecular hydrogen atmosphere, Kogan et al.<sup>74</sup> also proposed a heterolytic dissociation of

hydrogen to occur on MoS<sub>2</sub>, with the formation of hydride species on Mo. To our knowledge, however, while the formation of SH groups has been directly detected by spectroscopic methods (e.g., bands at 2500 cm<sup>-1</sup>, νSH, and 650 cm<sup>-1</sup>, δSH, in inelastic neutron scattering spectra<sup>75,76</sup>), no experimental evidence for molybdenum hydride species has been provided on MoS<sub>2</sub> catalysts, so far.

More recently, most authors suppose that the main activation mechanism for hydrogen, which occurs also on MoS<sub>2</sub> without any coordinative unsaturation,<sup>77</sup> is dissociative adsorption occurring through an oxidative mechanism, on sulfur pairs, producing two sulfidryl groups.<sup>78</sup> This implies the reduction of two Mo ions (see Scheme 1). This result is mainly based on theoretical calculations.<sup>79</sup>

Interestingly, hydride species have been observed by Inelastic Neutron Scattering on another catalytically active sulfide phase, RuS<sub>2</sub>,<sup>80,81</sup> thus providing evidence of a heterolytic dissociative adsorption mechanism there.

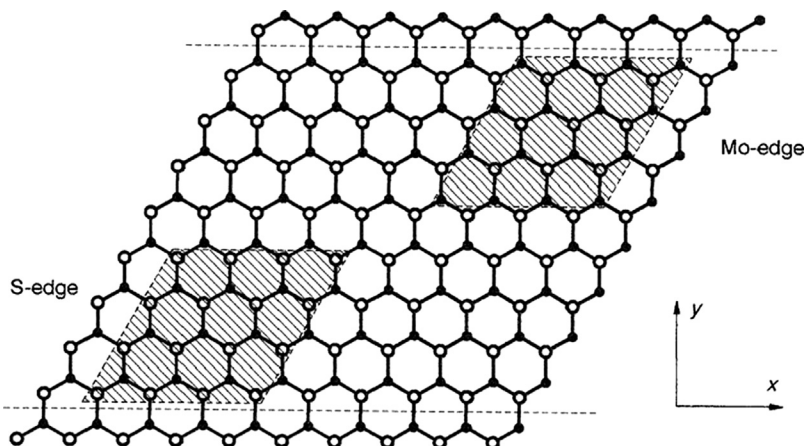
On the other hand, hydrogen surface species are supposed to be highly mobile and can recombine to form molecular hydrogen. Indeed, the activation energies for the surface migration processes are smaller than those for the dissociative adsorption process, supporting a highly dynamic nature and mobility of surface hydrogen species. In particular, the migration of a hydrogen from Mo–H to a sulfur atom to produce SH has a low energy barrier. This is supported by the chemistry of several ruthenium, titanium, rhodium and iridium hydrido–hydrosulfido complexes. The dynamic behavior of the hydrido–sulfide clusters [Rh<sub>3</sub>(μ-H)(μ<sub>3</sub>-S)<sub>2</sub>], which involves hydrogen migration from rhodium to sulfur with a switch from hydride to proton character, models the hydrogen mobility on metal sulfide hydrotreating (HT) catalyst by interconversion between surface metal hydrides and SH.<sup>82</sup>

### 10.2.2 Layered bulk sulfides and their applications

The use of unsupported metal sulfides in hydrotreatment processes may originate from the coal liquefaction process developed starting from 1920 by Bergius and co-workers. In the original Bergius process, finely grounded coal is mixed with the heavy oil and fed with the H<sub>2</sub> to a reactor at 673–773 K and 20–70 MPa, producing gases, light, middle and heavy oil fractions. The catalyst was constituted of bulk tungsten, molybdenum or iron sulfide.<sup>83</sup>

A similar system has been recently developed by the ENI group in the so-called Eni Slurry Technology (EST).<sup>84</sup> This technology is a slurry hydrogenation/hydrocracking process for converting oil residues (the bottom of the barrel) to lighter fractions. A catalyst precursor, consisting of an oleo-soluble molybdenum carboxylate (i.e., naphthenate or octoate), is dissolved in the feedstock and the mixture is fed to the reactor, which operates in the temperatures range 673–723 K under a total pressure of 15 MPa. H<sub>2</sub> is fed through a distributor located at the reactor bottom. Under these conditions, the catalyst precursor is converted to molybdenite (Figure 10.3), which is crystalline layered MoS<sub>2</sub>, with an average particle size of a few nanometers. It is possible to improve the catalytic performances by combining the hydrogenation, hydrodesulfurization and hydrodemetallation





**FIGURE 10.3**

Infinite hexagonal array of Mo and S atoms.

*Reprinted with permission from Ref. 88.*

properties of dispersed  $\text{MoS}_2$  with those of a conventional cracking catalyst. Dispersed  $\text{MoS}_2$  particles protect the cracking catalyst against rapid decay due to coke accumulation and metal poisoning.

Among the many bulk sulfides that are active in hydrodesulfurization and hydrogenation catalysis,<sup>85,86</sup> those that are largely applied commercially seem to be essentially constituted by mixed molybdenum and tungsten sulfides, promoted by Ni or cobalt, i.e., the same components of the common alumina-supported HDS catalysts but apparently in a different formulation.

Molybdenum and tungsten sulfides,  $\text{MoS}_2$  and  $\text{WS}_2$ , are isostructural layered phases. The tetravalent element forms a layer sandwiched between two two-dimensional hexagonal sulfide layers stacked over each other in an eclipsed fashion<sup>87</sup> (Figure 10.3<sup>88</sup>). Thus, the coordination around the metal is trigonal prismatic. Each sulfur center is pyramidal, being connected to three Mo centers. Because of the weak van der Waals interactions between the sheets of sulfide atoms,  $\text{MoS}_2$  has a low coefficient of friction, resulting in its useful lubricating properties.

Two main polymorphs of  $\text{MoS}_2$  are reported to exist, due to the different relative position of the slabs.  $\alpha$ - $\text{MoS}_2$  (molybdenite) hexagonal (space group  $P6_3/mmc$ ), most stable, is the most common and studied polymorph and the natural form.  $\beta$ - $\text{MoS}_2$  is the rhombohedral modification (space group  $R3m$ ).

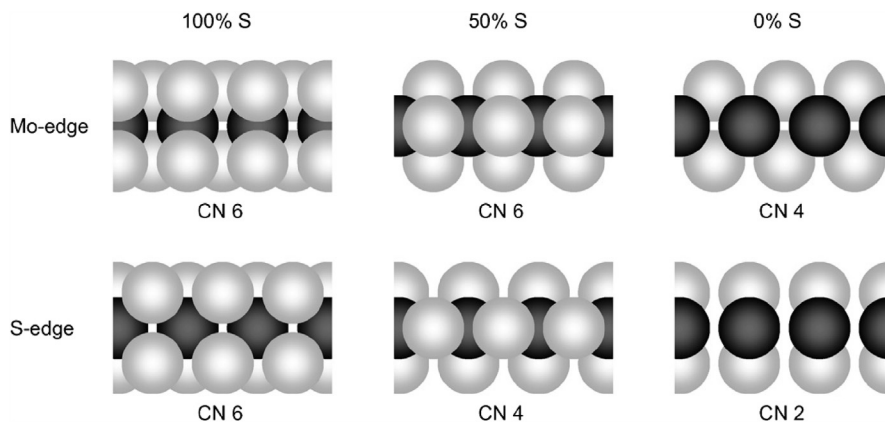
$\text{MoS}_2$  can also be prepared in poorly crystalline form, termed the “rag” structure, consisting of several stacked but highly folded and disordered S—Mo—S layers.<sup>89</sup> On the other hand, line defects and stacking faults as well as nanoindentations are currently observed in  $\text{MoS}_2$ .<sup>90</sup>

Molybdenum sulfide may also be prepared in the form of fullerene like particles as well as nanotubes, nanorods, nanostrips, nanowires, nanoflowers, nanoflakes, nanospheres and nanohexagonal plates.<sup>91,92</sup>

WS<sub>2</sub> occurs naturally as the rare mineral called tungstenite, with the same structure of molybdenite. It can also be prepared in the rhombohedral form, as well as microtubes, microribbons and nanotubes.<sup>93</sup>

Commercial unsupported sulfide-hydrotreating catalysts denoted as NEBU-LA™,<sup>94</sup> (New BULk Activity), developed jointly by Akzo Nobel, Nippon Ketjen and Exxon Mobil in 2001, are reported to be based on Ni-promoted (Mo,W)S<sub>2</sub>.<sup>95</sup> They are substantially more active than alumina-supported catalysts. After the development of these materials, many recent studies have been devoted to the preparation of unsupported molybdenum and tungsten sulfides. While the classical preparation of sulfides involves the reductive sulfidation of the oxides with H<sub>2</sub>S/H<sub>2</sub>, soft chemical methods have been developed to produce it nanosized, with high surface areas (>300 m<sup>2</sup>/g) and large pore volumes (>0.70 m<sup>3</sup>/g).<sup>96</sup> Some of these methods start from ammonium tetrathiomolybdate (ATTM) and do not need further sulfidation.

According to the most accepted theory, mostly developed for supported MoS<sub>2</sub> catalysts, the catalytic chemistry of these materials should mostly occur at the lateral termination (edges) of the MS<sub>2</sub> slabs. Two kinds of termination should exist for stoichiometric MoS<sub>2</sub>, the S edge ( $\bar{1}010$  face), where coordinatively unsaturated sulfur is located for stoichiometric MoS<sub>2</sub>, and the Mo- edge ( $10\bar{1}0$  face) where coordinatively unsaturated Mo species are expected in stoichiometric MoS<sub>2</sub> (see Figure 10.3 and Figure 10.4<sup>97</sup>). As said, hydrogen is supposed to adsorb with an oxidative mechanism at sulfur atoms<sup>78</sup> while organic sulfide molecules would adsorb through the sulfur lone pair on sulfur vacancies associated to Lewis acidity of unsaturated Mo centers.<sup>98</sup>



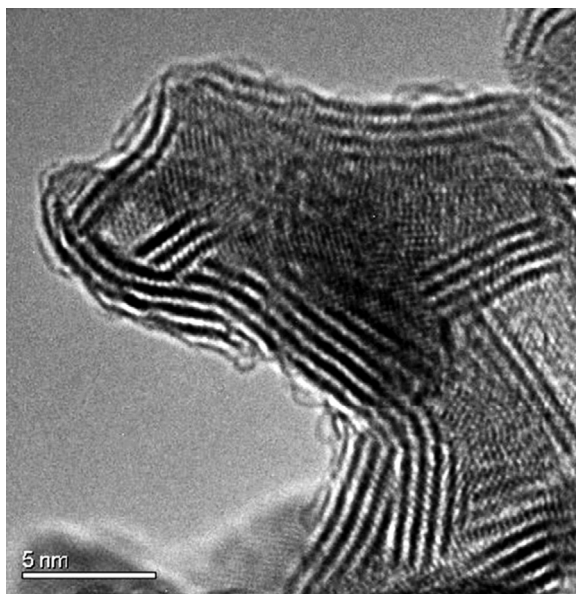
**FIGURE 10.4**

Ball model (side view) of the edges of a MoS<sub>2</sub> slab at different sulfur loadings. Dark spheres represent Mo, light spheres S atoms. Indicated are the total sulfur coordination (%) of the edge and the coordination number (CN) for Mo in each case. For theoretical stoichiometric MoS<sub>2</sub> the S edge has 100% sulfur, while the Mo edge has 0% sulfur.

*Reprinted with permission from Ref. 97.*

The promoters Ni and Co introduce further defects and disorder in the structure perturbing the stacking of the layered sulfides, introducing curvatures and nonstoichiometry. This is evident in Figure 10.5. Additionally, or more important, they are mostly supposed to locate at the edges decorating them, increasing edge reactivity. In particular, most authors suggest that the promoters substitute for Mo or W at the edges of the (Mo,W)S<sub>2</sub> slabs, producing the most active sites for reaction.

However, more recent studies suggested a different point of view. For unsupported Co-promoted MoS<sub>2</sub> catalyst, it has been reported<sup>99</sup> that the catalytic activity is directly proportional to the increase of surface area of the two separate sulfide phases, Co<sub>9</sub>S<sub>8</sub> and MoS<sub>2</sub>. This suggests that activity is directly connected with an increase of the contact surface area between the two sulfide phases. This has been achieved through the detailed characterization by X ray diffraction (XRD), X ray photoelectron spectroscopy (XPS) and high-resolution Transmission Electron Microscopy (HRTEM) of a highly active Co<sub>9</sub>S<sub>8</sub>/MoS<sub>2</sub> catalyst. This model was also subjected to a DFT analysis to determine a reasonable description of the surface contact region between the two bulk phases. Modeling of the interface shows the creation of open latent vacancy sites on Mo atoms interacting with Co and formation of direct Co–Mo bonds. Strong electron donation from Co to Mo also occurs through



**FIGURE 10.5**

HRTEM micrograph on unsupported mixed Ni–Mo sulfide showing a large curved MoS<sub>2</sub> stacks with numerous defects and intergrowths.

*Reprinted with permission from Ref. 85.*

the intermediate sulfur atom bonded to both metals while an enhanced metallic character is also found.

On the other hand, it has been underlined that for fully saturated MoS<sub>2</sub>, a metallic state extends over the slab basal (0001) plane generating possible “brim” sites.<sup>100,101</sup> In fact, unsaturated molecules such as butadiene, thiophene, benzothiophene, pyridine, quinoline, benzene and naphthalene may adsorb on the basal plane by van der Waals interactions.<sup>102</sup> Additionally, it has been shown recently that fully saturated MoS<sub>2+x</sub> without any coordinative unsaturation is able to activate hydrogen and catalyze hydrogenation.<sup>77</sup> Thus, it seems that the details of the reaction mechanisms on unsupported sulfides are still to be completely defined.

### 10.2.3 Supported bimetallic sulfides

Transition metal sulfide catalysts used in refineries for hydrotreatments are mostly molybdenum or tungsten sulfides supported on alumina and promoted by Co or Ni.<sup>103</sup> The optimal promoter atomic ratio: Co(Ni)/[Co(Ni) + Mo(W)] is between 0.2 and 0.4. CoMo/Al<sub>2</sub>O<sub>3</sub> catalysts are very efficient in the HDS process but are less active for hydrodenitrogenation (HDN) and aromatic hydrogenation. Conversely, NiMo phases are better HDN and hydrogenation catalysts and are preferred in order to treat feedstock with a high concentration of unsaturated compounds. NiW catalysts are highly effective for aromatic hydrogenation reactions but have higher cost.

The support is most commonly  $\gamma$ -Al<sub>2</sub>O<sub>3</sub>, supposed to disperse and stabilize the sulfide-based active phase. Alumina also serves the function of making the catalyst less expensive by diluting the metal. The most common preparation implies the deposition of the required elements in the form of oxides, followed by reductive sulfurization in H<sub>2</sub>–H<sub>2</sub>S gaseous mixture. At least two different CoMo phases are reported: type I (sulfided at 673 K) is not fully sulfided with still Al–O–Mo bonds, type II, sulfided at 873 K, is fully sulfided.

After sulfidation, crystallites of the MS<sub>2</sub> phase in form of slabs form on the alumina surface. These crystallites may have different shapes, such as hexagonal, triangular and truncated triangular. As said, promoter atoms (Co, Ni) are supposed to locate in substitution of Mo (W) atoms at the edges of the slabs. Whereas the edges expose only promoter atoms in highly sulfiding conditions, severe reductive conditions induce a segregation of the promoter atoms from the edges producing particles of Co (Ni) sulfides. Intermediately, in HDS reaction conditions, Co(Ni) MoS-active phases have been found to exhibit different behavior: whereas both NiMoS edges may be totally or partially promoted, the CoMoS S-edge will be totally promoted and its M-edge only partially promoted by Co.

Further studies have shown that the degree of staking in MoS<sub>2</sub> and Co–Mo–S structures can be controlled by carefully controlling support properties and preparation parameters and the formation of small stable single slabs of MoS<sub>2</sub> on alumina supports have been achieved. Bending MoS<sub>2</sub> slabs on alumina have also been observed by HRTEM, suggesting that they can lead to the creation of new active sites on basal planes with original catalytic properties.<sup>104</sup>

During the last decade, HT catalyst performances have been highly improved by increasing the amount of the active phase.<sup>98</sup> In the oxidized precursor, the MoO<sub>3</sub> amount is today in the 15–20% range wt/wt. The use of organic additives during impregnation was found to improve the final performances of the catalyst. For instance, glycol molecules such as diethyleneglycol monobutyl ether (DEGbe) or triethyleneglycol (TEG) have been proposed as suitable compounds, leading to significant gains in hydrodesulfurization activities. These gains were observed whenever the additive impregnation was performed: on the support prior to active phase precursor impregnation, simultaneous impregnation of the cobalt and molybdenum precursors and the additive, postimpregnation of dried or calcined catalysts.<sup>98</sup> Nevertheless, the origins of the activity enhancement remain controversial.

Alumina-supported Mo and W catalysts have indeed a large field of applications: as said they are mostly used in refineries to purify different flows such as naphthas, FCC gasoline, kerosene, gasoils etc. Additionally, they are used to hydrodesulfurize gases such as natural gas previous to steam-reforming<sup>16</sup> or coke oven gas. They are also used to clean Claus tail gases, by hydrogenating SO<sub>2</sub> to H<sub>2</sub>S,<sup>105</sup> as well as to perform water gas shift in sulfur-containing syngases.<sup>15</sup> Finally, they are also interesting catalytic materials for the conversion of syngas into higher alcohols, a potentially interesting gas to liquids reaction.<sup>106</sup> Composition varies being tuned for each application with the nature and the amount of the main element (Mo versus W) and of the promoter (Co versus Ni) but also with the addition, sometimes, of other elements such as Na, Mg, P, F, B etc. In particular, phosphorus improves selectivity toward hydrogenolysis versus hydrogenation.

According to literature data, catalysts for FCC gasoline desulfurization may contain 5–11% Mo, 2–3% Co on Al<sub>2</sub>O<sub>3</sub>, with 220–240 m<sup>2</sup>/g,<sup>107</sup> while those for diesel fuel desulfurization to Low-Sulfur Diesel may have 11–20% MoO<sub>3</sub>, 1.6–6.0% CoO or NiO or both, with 0.05–2.0% Na<sub>2</sub>O on alumina, with 230–250 m<sup>2</sup>/g.<sup>108</sup>

Water gas shift in S-containing syngases is becoming of high interest, for hydrogen and syngas production starting from unconventional carbon sources such as coal, biomass, waste and petcoke. It seems that the most common formulation is Co–Mo/Al<sub>2</sub>O<sub>3</sub> with addition of magnesium zinc and/or alkali. These catalysts can work at low temperature (200 °C) with very good CO conversion, require a minimum of 300 ppm of sulfur in the gas entering the reactor; however, if the catalysts are properly presulfided as low values as 35 ppm has been reported to maintain them in the sulfurized form, and also catalyze, simultaneously, the conversion of carbonyl sulfide (usually present in the sour gas) to hydrogen sulfide.<sup>109</sup> The additional presence of titania improves activity and stability.<sup>110</sup> A composition (wt%) reported for a commercial catalyst in the fresh conditions is CoO ≥ 2%, MoO<sub>3</sub> ≥ 8%; MgO ≥ 24%, Al<sub>2</sub>O<sub>3</sub> ≥ 50%, with an additional promoter.<sup>111</sup> The difficulty in maintaining the catalyst properly sulfided and the relatively low space velocities practically allowed (2000–3000/h) makes the use of sulfide-based WGS catalysts less likely in the small-scale production of hydrogen.<sup>112</sup> Theoretical studies suggest

that for these catalysts the redox mechanism is kinetically more preferable than mechanism via formate intermediates.<sup>113</sup> This is confirmed by kinetic studies.<sup>114</sup>

In recent years, efforts have been devoted to the conversion of renewable feedstocks into fuels. Among these techniques, the catalytic conversion of fats and oils in the presence of hydrogen is found to represent a promising option. ENI and UOP jointly developed the Ecofining process<sup>115,116</sup> and Neste Oil developed the NExBTL diesel-producing process, both consisting in the production of hydrocarbons in the diesel fuel range by total hydrogenation of vegetable oils. In patents,<sup>117,118</sup> typical hydrodesulfurization catalysts like sulfided Ni-Mo/Al<sub>2</sub>O<sub>3</sub> or alumina-supported noble metals (Pt, Pd) are cited as the catalysts. Hydrogenation conditions include a temperature of 200–300 °C and a hydrogen partial pressure of 35–70 bar. These systems are under deep investigation in recent years.<sup>119–121</sup>

#### 10.2.4 Other sulfide catalysts

A number of studies reported on the very high catalytic activity in hydroprocessing of heavy metal sulfides (Table 10.2), even higher than that of MoS<sub>2</sub> (Figure 10.6<sup>86</sup>). While few investigations have been published concerning rhodium<sup>122</sup> and iridium sulfides,<sup>123,124</sup> ruthenium and rhenium sulfides appear to have very interesting activities. RuS<sub>2</sub> crystallizes in the pyrite structure (Table 10.2) thus being a Ru(II) disulfide (with the S<sub>2</sub><sup>2-</sup> disulfide anion). Supported ruthenium sulfide has been the object of recent studies. Sulfidation of Ru/Al<sub>2</sub>O<sub>3</sub> with H<sub>2</sub>S(15%)/N<sub>2</sub> at temperatures between 573 and 973 K is reported to produce well-sulfided ruthenium phase (with S/Ru > 2), which contains crystallized ruthenium sulfide (RuS<sub>2</sub>-pyrite) and highly defective ruthenium sulfide RuS<sub>2</sub>. The relative proportion of the two phases was related to the sulfidation temperature, the pyrite-like phase being predominant at higher sulfidation temperature, 973 K. This phase is reported to be stable under HDS reaction while and to be responsible for the HDS activity. The amorphous ruthenium sulfide phase, instead, should convert into Ru metal. The HDS activity of RuS<sub>2</sub>/Al<sub>2</sub>O<sub>3</sub> catalysts increases with the sulfur content of the active phase during reaction (higher S/Ru ratio). RuS<sub>2</sub>/TiO<sub>2</sub> is even more active than RuS<sub>2</sub>/Al<sub>2</sub>O<sub>3</sub> at low temperature, and forms well-crystallized pyrite-like particles.<sup>125</sup> Supporting RuS<sub>2</sub> over SBA-15 mesoporous silica also gives rise to stable, well-sulfided and active catalysts in HDS and HDN.<sup>126</sup>

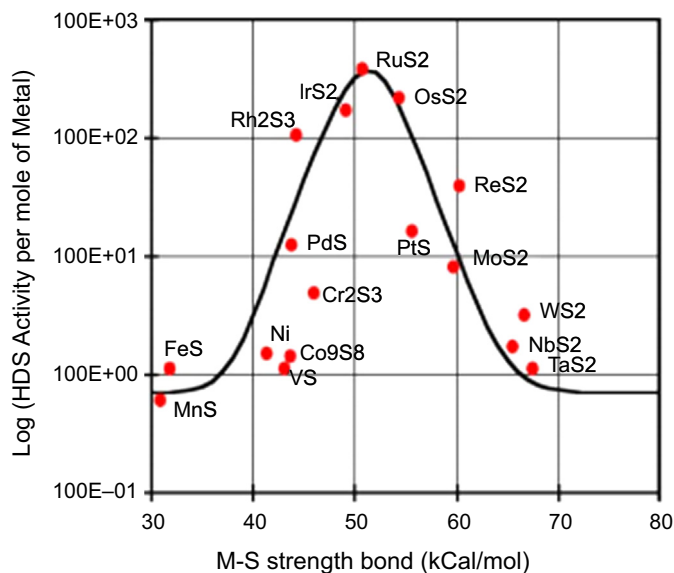
In a recent paper of Wang and Iglesia,<sup>127</sup> however, the instability of RuS<sub>2</sub> in H<sub>2</sub> at typical HDS temperatures (500–700 K) was emphasized. These authors measured turnover rates using 0.1–1.0% Ru/SiO<sub>2</sub> and found them to be unaffected by whether samples were treated in H<sub>2</sub> or H<sub>2</sub>S to form metal and sulfide clusters, respectively, before reaction. These data, taken together with the rate and extent of sulfur removal from used samples during contact with H<sub>2</sub>, suggested that active structures consist of Ru metal clusters saturated with chemisorbed sulfur at temperatures, pressures and H<sub>2</sub>S levels relevant to hydrodesulfurization catalysis.

Rhenium sulfide is also well known to be a very active hydrotreating catalyst. It presents a continuous series of phases between ReS<sub>4</sub> and ReS<sub>2</sub> differing from the

**Table 10.2** Crystal Structure of Bulk Metal Sulfides<sup>167</sup>

NiAs-type	Hexagonal $P6_3/mmc$ (194)	$Z = 2$	VS, CrS, FeS, CoS, NiS, NbS	TM octahedral
NaCl-type	Cubic $Fm\bar{3}m$ (225)	$Z = 4$	MnS	TM octahedral
Millerite NiS	Trigonal $R\bar{3}m$ (160)	$Z = 9$		Metal–metal neighbours
Braggite (Pt,Pd,Ni)S	Tetragonal $P4_2/m$ (84)	$Z = 8$	PdS	TM square planar
Cooperite PtS	Tetragonal $P4_2/mmc$ (131)	$Z = 2$		TM square planar
Troilite	Hexagonal $P\bar{6}2c$ (190)	$Z = 12$	FeS	Metal–metal neighbors
$Cr_2S_3$	Trigonal $R\bar{3}$ (148)			Metal–metal neighbors
Pyrite $FeS_2$	Cubic $Pa\bar{3}$ (205)	$Z = 4$	$MnS_2, CoS_2, NiS_2, RuS_2, OsS_2, IrS_2$	TM octahedral, disulfide
Marcasite $FeS_2$	Orthorhombic $Pn\bar{m}$ (58)	$Z = 2$		Disulfide
Pentlandite $(Ni,Fe,Co)_9S_8$	Cubic $Fm\bar{3}m$ (225)	$Z = 4$	$Co_9S_8$	TM oct, tetr, metal–metal neighbors
Hazelwoodite $Ni_3S_2$	Trigonal $R\bar{3}2$ (155)	$Z = 1$		Metal–metal neighbors
$\alpha$ - $MoS_2$	Hexagonal $P6_3/mmc$ (194)	$Z = 2$	$NbS_2, TaS_2, WS_2$	TM prismatic, layered
Molybdenite $\beta$ - $MoS_2$	Rhombohedral $R\bar{3}m$	$Z = 3$	$WS_2$	TM = prismatic, layered
$ReS_2$	Triclinic $P\bar{1}$ (12)	$Z = 8$	$TcS_2$	TM square planar
Kashinite $(Ir,Rh)_2S_3$	Orthorhombic $Pbcn$ (60)	$Z = 4$	$Rh_2S_3, Ir_2S_3$	TM octahedral
$PdS_2$	Orthorhombic $Pbca$ (61)	$Z = 8$		TM square planar

*TM = transition metal.*



**FIGURE 10.6**

Hydrodesulfurization (HDS) activity versus bond strengths for transition metal sulfides.

*Reprinted with permission from Ref. 86.*

amount of sulfide  $S^{2-}$  and disulfide  $S_2^{2-}$  anions. Indeed the structure of  $ReS_2$ , a Re(IV) sulfide, is still not completely ascertained.<sup>128</sup> Unsupported  $ReS_2$  is reported to have an extraordinarily high activity in hydrogenation.<sup>129</sup> The activity of supported rhenium sulfides in thiophene HDS was found to increase depending of the support in order:  $TiO_2 < \gamma-Al_2O_3 < ZrO_2$ . The presence of  $H_2$  in the sulfidation mixture has a negative effect on the catalytic activity. The catalysts with the highest activity have been obtained by a sulfidation under  $N_2-H_2S$  (15%) at 673 K.<sup>130</sup> Silica-supported  $RuS_2$  was claimed to have exceptionally high HDS activity attributed to its metallic character.<sup>131</sup> The much higher price of these catalysts with respect to the conventional ones, associated to the well-established high activity and stability of the lasts, discourages the industrial application of these catalytic materials.

### 10.2.5 Hydrocracking catalysts

Hydrocracking is usually performed on heavy gas oils and residues, to remove feed contaminants (nitrogen, sulfur, metals) and to convert them into lighter fractions including diesel gasoils.

The bottom fraction or residuum of distillates crude is typically processed in trickle-bed reactors at temperatures of 350–450 °C and pressures of 50–150 atm.<sup>132</sup> Under these conditions, much of the metals such as Ni, V and Fe, which are present as



porphyrin or chelating compounds, are deposited as metal sulfides ( $\text{Ni}_3\text{S}_2$ ,  $\text{V}_3\text{S}_2$  and  $\text{V}_3\text{S}_4$ , having 2–30 nm crystal size) over the catalyst. These deposited transition metal sulfides poison the catalyst by decreasing catalytic sites, hinder the transport of reacting molecule or eventually plugging the pores. The catalysts used for residue hydroprocessing are sulfides of Co-, Ni-, W- and Mo-supported catalysts, which have a variety of pore structure and active metal dispersion (active sites). Typical composition of the catalyst is 3–15 wt% Group VIB metal oxide and 2–8 wt% Group VIII metal oxide. The catalyst has to be sulfided before its use. The most important property for residue hydroconversion catalyst is pore diameter because feedstock contains large molecules of asphaltene, metal chelated, etc.

Several reactors are usually put in series with interstage hydrogen quenches, where different operations predominate. Hydrodemetallation, hydrodenitrogenation and hydrodesulfurization occur in the first catalytic beds, and hydrocracking predominates in the lasts.

Guard beds allow first large particles filtering and then hydrodemetallation with removal of Ni, V, as well as As and silica. Further pretreatment using NiMoS-based catalysts reduces nitrogen compounds through hydrodenitrogenation.<sup>133</sup> Finally, real hydrocracking is performed.

Hydrocracking catalysts are essentially polyfunctional materials with at least one acidic function mainly promoting catalytic cracking and a second component promoting hydrogenation. In the most common case, the acidity component is based on USY zeolite while the hydrogenating component is based on Co-MoS<sub>2</sub>/Al<sub>2</sub>O<sub>3</sub> for low-pressure operation, Ni-MoS<sub>2</sub>/Al<sub>2</sub>O<sub>3</sub> for high-pressure operation. Improvements can be obtained by increasing the vicinity and synergy of the two components, e.g., introducing a dehydrogenating function (Ni) into the zeolite component.<sup>134</sup>

Residue hydroprocessing is performed in the liquid phase using fixed-bed, slurry or ebullating reactors at 380–450 °C, 70–200 atm, which may allow continuous or intermittent deactivated catalyst replacement.<sup>132</sup> Slurry catalysts, typically molybdenum-based, are prepared.

### 10.2.6 Other catalytic materials for hydrotreatings

Metal nitrides, phosphides and carbides are becoming very interesting catalytic materials, mainly when transition metals are involved, due to their “metal-like” activity, e.g., in hydrogenation reactions.<sup>135</sup> Transition metal nitrides have been described as excellent hydrotreating catalysts,<sup>136,137</sup> but tend to deactivate due to sulfidation, nitrogen release and carbon deposition.<sup>138</sup> They are active in a number of hydrogenation reactions such as the hydrogenation of nitroaromatics to anilines,<sup>137</sup> as well as for hydrodenitrogenation.

Transition metal phosphide catalysts,<sup>139</sup> in particular, undoped and Fe-doped nickel phosphides, usually supported on oxide carriers, are also active catalysts with respect to hydrotreating:<sup>140</sup> HDS and HDN of hydrocarbon mixtures, but also hydrodeoxygenation (HDO) of bio-oils<sup>141</sup> and hydrodechlorination of chloroorganics.<sup>142</sup> Ni phosphide

catalysts are reported to display Lewis acidity attributed to Ni cations and Brønsted acidity attributed to phosphate species associate with uncomplete reduction.<sup>141</sup> During hydrodesulfurization, the active phase is reported to be a phosphosulfide species.<sup>143</sup> Other transition metal phosphide is have good catalytic properties: in HDO of bio-oils at 300 °C and 1 atm, the order of activity was Ni<sub>2</sub>P/SiO<sub>2</sub> > WP/SiO<sub>2</sub> > MoP/SiO<sub>2</sub> > CoP/SiO<sub>2</sub> > FeP/SiO<sub>2</sub> > Pd/Al<sub>2</sub>O<sub>3</sub>.

Transition metal carbides, such as those of molybdenum and tungsten, are also active catalysts in hydrotreating,<sup>144</sup> although it was found that they convert partially into sulfides by reacting with the sulfur feed.<sup>145,146</sup> Transition metal carbides, in particular Mo<sub>2</sub>C, are of interest for several hydrogenation reactions<sup>147</sup> such as, in particular CO hydrogenation to higher alcohols mainly when promoted by alkali or alkali-earth cations.<sup>148,149</sup> Theoretical studies suggest that the adsorption of hydrogen in Mo<sub>2</sub>C is similar to that occurring on metals; the most stable adsorption site for the H atom on fcc-Mo<sub>2</sub>C (100) is the hollow site, while on hcp-Mo<sub>2</sub>C (101), the H atom should preferentially adsorb at the step bridge site.<sup>150</sup>

In spite of the interesting data reported on the potentiality of transition metal nitrides, phosphides and carbides, in hydrotreating, according to Eijsbouts et al.<sup>71</sup> they are actually unstable in sulfur conditions, real catalysts becoming actually sulfided during reaction.

---

### 10.3 Olefin metathesis catalysts

Olefin metathesis is the disproportionation of olefins. This is a typical homogeneously catalyzed reaction, using which a large number of small scale processes have developed in the fine chemistry industry.<sup>151,152</sup> In the petrochemical industry, it has been applied mostly in the heterogeneous form.<sup>153,154</sup> Particular interest is devoted today to the production of propene from ethylene and butenes. This process can be integrated with Fluid Catalytic Cracking units or steam crackers for improving flexibility and performance. In fact, the demand of propene may increase more than that of ethylene and butenes. Other processes, such as those involving ring-opening polymerization of cycloolefins, based on their metathesis, as well as metathesis of cycloolefins with ethylene producing  $\alpha,\omega$ -diolefins, and the process producing neohexene are also of interest in petrochemistry. The most successful heterogeneous metathesis catalysts are those based on W, Mo and Re.

#### 10.3.1 Heterogeneous tungsten-based metathesis catalysts

Supported tungsten oxide catalysts are reported to be less active than Re- and Mo oxide-based ones for olefin metathesis. However, they are tolerant to various poisons commonly present in the industrial feed streams, and provide stable activity even in absence of cocatalysts, thus being largely applied practically.

The production of propene by converting butenes with ethylene is the object of the Olefin Conversion Technology process of ABB Lummus, the modern

version of the older Phillips Triolefin process. The former process was actually developed to produce the inverse reaction, the production of ethylene and butenes from propene. Two main equilibrium reactions take place together in the today configuration, i.e., metathesis and isomerization. Propylene is formed by the metathesis of ethylene and butene-2, and butene-1 is isomerized to butene-2 as butene-2 is consumed in the metathesis reaction. The catalyst is constituted by a mixture of  $\text{WO}_3/\text{SiO}_2$  metathesis catalyst with MgO isomerization catalyst, promoting both reactions simultaneously at 270 °C and 30 bar. The per-pass conversion of butylene is greater than 60%, with overall selectivity to propylene exceeding 90%.

A similar  $\text{WO}_3/\text{SiO}_2 + \text{MgO}$  catalytic systems is used in the Phillips “Neohexene” process that converts at 370 °C and 30 atm ethylene with 2,2,4-trimethyl-pentenes isomers (the dimers of isobutene) into neohexene and isobutene. Catalysts based on  $\text{WO}_3/\text{SiO}_2$  are reported to be used by Phillips for the production of  $\alpha,\omega$ -diolefins such as 1,9-decadiene and 1,5-hexadiene.<sup>155</sup>

A reported composition of a metathesis catalyst is 8%  $\text{WO}_3/\text{SiO}_2$  with 275 m<sup>2</sup>/g. In agreement with the poor dispersing ability of silica, both isolated wolframate centers and  $\text{WO}_3$  crystallite are found on the fresh catalysts; data show that the isolated centers on silica are those active in metathesis, and thus the better the dispersion (on silica) the better the catalyst. However, well-dispersed sites on alumina are less active. In recent studies, modifications of the catalyst are suggested. In particular, it seems that a silica-covered alumina can result in a better catalyst: the excellent catalytic activity obtained after pretreatment in situ at 873 K for 2 h under an Argon flow is related to the moderate dispersion of tungsten oxide and the suitable acidity of the support. The active  $\text{WO}_x$  species for metathesis are generated by partial reduction of the  $\text{WO}_x$  species interacting with substrate alkene.<sup>156</sup> In fact, carbene-like species involving tetravalent tungsten are supposed to act as intermediates. Another paper reports a different  $\text{WO}_3/\text{SiO}_2\text{--Al}_2\text{O}_3$  prepared by an aerosol technique as a very efficient one.<sup>157</sup> Tungsten hydride on alumina has been developed as a new catalyst allowing a stable good activity in propene synthesis by ethylene + butane at 150 °C.<sup>158</sup> The same catalytic system has been patented for neohexane synthesis.<sup>159</sup>

### 10.3.2 Heterogeneous rhenium-oxide metathesis catalysts

As said, supported rhenium oxides are reported to be even more active than tungsten-based catalysts for metathesis.<sup>160,161</sup> Some time ago, the Institut Français du Pétrole and the Chinese Petroleum Corporation (Taiwan) have jointly developed a continuous process, called Meta-4, applied for some years to produce propene from ethene and but-2-ene in the liquid phase producing in the presence of a  $\text{Re}_2\text{O}_7/\text{Al}_2\text{O}_3$  catalyst at 35 °C and 60 bar. The FEAST process from Shell for the production of  $\alpha,\omega$ -diolefins from metathesis of ethylene and cycloolefins is reported to apply  $\text{Re}_2\text{O}_7/\text{Al}_2\text{O}_3$  in very mild conditions, at 0–20 °C, 1–2 bar.<sup>155</sup> Rhenia-based catalysts are also of interest for metathesis of fatty acids and esters.<sup>162,163</sup>

Rhenium-based metathesis catalysts are composed of rhenium oxide dispersed over a high surface-area oxide support, usually alumina or silica–alumina. They have a high activity and high selectivity at low temperatures (20–100 °C), and are also active for the metathesis of functionally substituted olefins, but need a promoter or cocatalyst, usually a tetraalkyl-tin or–lead compound.

Typically, a  $\text{Re}_2\text{O}_7/\text{Al}_2\text{O}_3$  metathesis catalyst is prepared by impregnation of a  $\gamma$ -alumina support (surface area 180–200  $\text{m}^2/\text{g}$ ) with an aqueous solution of a rhenium salt such as  $\text{NH}_4\text{ReO}_4$  or perrhenic acid ( $\text{HReO}_4$ ), followed by drying at 110–120 °C and calcination at 500 °C or 550 °C in flowing air. During calcination, decomposition of this salt occurs and formally  $\text{Re}_2\text{O}_7/\text{Al}_2\text{O}_3$  is obtained, structured with three terminal  $\text{Re}=\text{O}$  bonds and one bridging  $\text{Re}-\text{O}-\text{Al}$  bond,<sup>164</sup> which should be referred to as the catalyst precursor. After introduction of the reactant, the initiation reaction leads to reduction of the heptavalent Re species ions and formation of the metal carbene complexes, the active sites in metathesis.

The catalytic performance of  $\text{Re}_2\text{O}_7/\text{Al}_2\text{O}_3$  in the region of lower rhenium loadings (<10 wt%  $\text{Re}_2\text{O}_7$ ) can be greatly improved by (1) the incorporation of a third metal oxide such as  $\text{V}_2\text{O}_5$ ,  $\text{MoO}_3$  or  $\text{WO}_3$ ; (2) the use of a mixed support, e.g.,  $\text{SiO}_2-\text{Al}_2\text{O}_3$  or  $\text{Al}_2\text{O}_3-\text{B}_2\text{O}_3$  or (3) the use of phosphated alumina.<sup>165</sup>

In particular, systems composed of highly loaded  $\text{Re}_2\text{O}_7$  supported on alumina or silica–alumina show promising initial activity and selectivity even at room temperature. However, these systems suffer from unknown deactivation processes, whose origin is still not known in detail.<sup>166</sup>

### 10.3.3 Molybdenum-based metathesis catalysts

Mo-based catalysts are reported to be applied industrially for higher olefins production from ethylene, in the Shell Higher Olefins Process. Supported molybdena or cobalt molybdate is used in the last metathesis step to produce linear detergent-type terminal olefins from ethylene.<sup>155</sup>

Silica or alumina-supported ones are reported to need relatively high temperatures and/or presence of cocatalysts for reaching a high catalytic activity and selectivity to the desired products. To improve Mo dispersion, various mono- and dinuclear Mo complexes with organic ligands reacting with surface OH groups were used as a source of Mo species and the Mo oxidation state was adjusted by catalyst pretreatment in reduction atmosphere or by photoreduction.<sup>154</sup>

---

## References

1. Ghiotti G, Chiorino A, Boccuzzi F. *Surf Sci* 1993;**287/288**:228.
2. French SA, Sokol AA, Bromley ST, Catlow CRA, Rogers SC, Sherwood P. *J Chem Phys* 2003;**118**(1):317–20.
3. Kiss J, Witt A, Meyer B, Marx D. *J Chem Phys* 2009;**130**(184706).

4. Frenzel J, Kiss J, Nair NN, Meyer B, Marx D. *Phys Status Solidi (B) Basic Res* 2013; **250**(6):1174–90.
5. Chauvin C, Saussey J, Lavalley JC, Djega-Mariadassou G. *Appl Catal C* 1986;**25**: 59–68.
6. Busca G. *J Catal* 1989;**120**:303–13.
7. Collins SE, Baltanás MA, Bonivardi AL. *Langmuir* February 1, 2005;**21**(3):962–70.
8. Kondo J, Sakata Y, Domen K, Maruya K, Onishi T. *J Chem Soc Faraday Trans* 1990;**86**: 397–401.
9. Ouyang F, Kondo JN, Maruya K-c, Domen K. *J Chem Soc Faraday Trans* 1996;**92**: 4491.
10. Syzgantseva O, Calatayud M, Minot C. *J Phys Chem C* 2010;**114**:11918–23.
11. Cavalleri M, Pelmenchikov A, Morosi G, Gamba A, Coluccia S, Martra G. *Stud Surf Sci Catal* 2001;**140**:131–9.
12. Doornkamp C, Poncer V. *J Mol Catal A Chem* 2000;**162**:19–32.
13. Vilé G, Bridier B, Wichert J, Pérez-Ramírez J. *Angew Chem Int Ed* August 20, 2012; **51**(34):8620–3.
14. Chen HT, Choi YM, Liu M, Lin MC. *ChemPhysChem* 2007;**8**:849–55.
15. Ratnasamy C, Wagner JP. *Catal Rev* 2009;**51**:325–440.
16. Aasberg-Petersen K, Dybkjær I, Ovesen CV, Schjødt NC, Sehested J, Thomsen SG. *J Nat Gas Sci Eng* 2011;**3**(2):423–59.
17. Lee DW, Lee MS, Lee JY, Kim S, Eom HJ, Moon DJ, et al. *Catal Today* July 1, 2013; **210**:2–9.
18. Cavani F, Trifirò F. *Appl Catal A General* 1995;**133**:219–39.
- 18b. Handbook of Petrochemicals Production Processes. In: Meyers RA, editor. McGraw-Hill; 2005. part 11.
19. Liu W, Addiego WP, Sorensen CM, Boger T. *Ind Eng Chem Res* 2002;**41**:3131–8.
20. <http://www.uop.com/objects/Smart%20SM.PDF>.
21. Jeffery C. *BrickerTop Catal* 2012;**55**:1309–14.
22. Kearby KK. Catalytic dehydrogenation. In: Emmett PH, editor. *Catalysis*, vol. 3. New York: Reinhold; 1955. pp. 453–91.
23. Baghalha M, Ebrahimpour O. *Appl Catal A General* 2007;**326**:143–51.
24. Rossetti I, Bencini E, Trentini L, Forni L. *Appl Catal A General* 2005;**292**:118–23.
25. Muhler M, Schütze J, Wesemann M, Rayment T, Dent A, Schlögl R, et al. *J Catal* 1990; **126**:339–60.
26. Kotarba A, Rozek W, Serafin I, Sojka Z. *J Catal* 2007;**247**:238–44.
27. Jiang K, Fan Q, Chen T, Miao C, Zhao Z, Yang X. *Hyperfine Interact* 2012;**205**:81–5.
28. Anikanova LG, Dvoretzkii NV. *Catal Industry* 2013;**5**(1):74–9.
29. Li Z, Shanks BH. *Appl Catal A General* 2011;**405**:101–7.
30. Sekine Y, Watanabe R, Matsukata M, Kikuchi E. *Catal Lett* 2008;**125**:215–9.
31. Watanabe R, Mukawa K, Kojima J, Kikuchi E, Sekine Y. *Appl Catal A General* 2013; **462–463**:168–77.
32. Tope BB, Balasamy RJ, Khurshid A, Atanda LA, Yahiro H, Shishido T, et al. *Appl Catal A General* November 4, 2011;**407**(1–2):118–26.
33. Vora BV. *Top Catal* 2012;**55**:1297–308.
34. Sanfilippo D. *Catal Today* 2011;**178**:142–50.
35. Marcilly C, Delmon B. *J Catal* 1972;**24**:336–47.
36. Gallardo Amores JM, Prieto MC, Sanchez Escribano V, Cristiani C, Trombetta M, Busca G. *J Mater Chem* 1997;**7**:1887–93.

37. Cavani F, Koutyrev M, Trifirò F, Bartolini A, Ghisletti D, Iezzi R, et al. *J Catal* 1996;**158**:236–50.
38. Sanfilippo D, Miracca I. *Catal Today* 2006;**111**:133–9.
39. Bashin MM, McCain JH, Vora BV, Imai T, Pujadó PR. *Appl Catal A General* 2001;**221**:397–419.
40. Miracca I, Piovesan L. *Catal Today* 1999;**52**:259–69.
41. Franck H-G, Stadelhofer JW, Germany. *Industrial aromatic chemistry, raw materials, process, products*. Berlin: Springer-Verlag; 1988. p. 122.
42. Chauvel A, Lefbvre G. *Petrochemical processes*, vol. 1. Technip; 1989. p. 276.
43. Karaduman A, Alp E, Yeniova H, Alibeyli R. *Pet Sci Technol* 2007;**25**(4):479–90.
44. Bhan A, Delgass WN. *Catal Rev Sci Eng* 2008;**50**(1):19–151.
45. Zhou L. BP-UOP Cyclar process. In: Meyers RA, editor. *Handbook of petroleum refining processes*; 2005. pp. 2.29-38.
46. Zheng B, Hua W, Yue Y, Gao Z. *J Catal* 2005;**232**:143.
47. Kazansky VB, Subbotina IR, Pronin AA, Schlögl R, Jentoft FC. *J Phys Chem B* 2006;**110**:7975.
48. Gabrienko AA, Arzumanov SS, Toktarev AV, Stepanov AG. *Chem Phys Lett* 2010;**496**:148–51.
49. Iezzi R, Bartolini A, Buonomo F. (Snamprogetti) IT, *Eur Pat Appl* 1995, 0 637 578 A1.
50. (WO2003053567) Catalytic composition for the dehydrogenation of alkylaromatic Snamprogetti S.p.A. Hydrocarbons.
51. Uma R, Kuriacose JC. *Z für Phys Chem* 1974;**89**(1–4):216–20.
52. Gulková D, Kraus M. *Collect Czech Chem Commun* 1992;**57**:2215–26.
53. Raizada VK, Tripathi VS, Lal D, Singh GS, Dwivedi CD, Sen AK. *J Chem Technol Biotechnol* 1993;**56**(3):265–70.
54. Sun J, Zhu K, Gao F, Wang C, Liu J, Peden CHF, et al. *J Am Chem Soc* 2011;**132**:356.
55. Nagamori N, Kawase M. *Micropor Mesopor Mater* 1998;**21**:439.
56. Li KT, Wang I, Wu JC. *Catal Surv Asia* 2012;**16**:240–8.
57. Yokoyama T, Setoyama T, Fujita N, Nakjima M, Maki T. *Appl Catal* 1992;**88**:149.
58. Yokoyama T, Yamagata N. *Appl Catal A General* 2001;**221**:227–39.
59. Yokoyama T, Fujita N. *Appl Catal A General* 2004;**276**:179–85.
60. de Lange MW, van Ommen JG, Lefferts L. *Appl Catal A* 2001;**220**:41.
61. Dury F, Clément D, Gaigneaux EM. *Catal Today* 2006;**112**:130.
62. Cheng D, Hou C, Chen F, Zhan X. *J Rare Earths* 2009;**27**(5):723–7.
63. Hakim SH, Shanks BH, Dumesic JA. *Appl Catal B Environ* 2013;**142–143**:368–76.
64. Martin A, Armbruster U, Gandarias I, Arias PL. *Eur J Lipid Sci Technol* 2013;**115**(1):9–27.
65. Gliński M. *Appl Catal A General* October 31, 2008;**349**(1–2):133–9.
66. Chia M, Dumesic JA. *Chem Commun* 2011;**47**(44):12233–5.
67. Battilocchio C, Hawkins JM, Ley SV. *Org Lett* 2013;**15**(9):2278–81.
68. Srivastava VC. *RSC Adv* 2012;**2**:759–83.
69. Bruneta S, Meya D, Pérota G, Bouchy C, Diehl F. *Appl Catal A General* 2005;**278**:143–72.
70. Stanislaus A, Marafi A, Rana MS. *Catal Today* 2010;**153**:1–68.
71. Eijsbouts S, Anderson GH, Bergwerf JA, Jacobi S. *Appl Catal A General* 2013;**458**:169–82.

72. Ferella F, Ognyanova A, De Michelis I, Taglieri G, Vegliò F. *J Hazard Mater* 2011;**192**(1):176–85.
73. Breyse M, Furimsky E, Kasztelan S, Lacroix M, Perot G. *Catal Rev Sci Eng* 2002;**44**(4):651–735.
74. Kogan VM, Nikulshin PA. *Catal Today* 2010;**149**:224–31.
75. Sundberg P, Moyes RB, Tomkinson J. *Bull Soc Chim Belg* 1991;**100**:967.
76. Lacroix M, Jobic H, Dumonteil C, Afanasiev P, Breyse M, Kasztelan S. *Studies in surface science and catalysis*, vol. 101; 1996. p. 117–126.
77. Drescher T, Niefind F, Bensch W, Grünert W. *J Am Chem Soc* 2012;**134**:18896–9.
78. Prodhomme PY, Raybaud P, Toulhoat H. *J Catal* 2011;**280**:178–95.
79. Alexiev V, Prins R, Weber T. *Phys Chem Chem Phys* 2001;**3**:5326–36.
80. Lacroix M, Yuan S, Breyse M, Dormieux-Morin C, Fraissard J. *J Catal* 1992;**138**:409.
81. Dumonteil C, Lacroix M, Geantet C, Jobic H, Breysey M. *J Catal* 1999;**187**:464–73.
82. Jiménez MV, Lahoz FJ, Lukešová L, Miranda JR, Modrego FJ, Nguyen DH, Oro LA, Pérez-Torrente JJ. *Chem – A Eur J* July 11, 2011;**17**(29):8115–28.
83. Donath EE. In: Anderson JR, Boudart M, editors. *Catalysis science and technology*, vol. 3. Berlin: Springer Verlag; 1982. pp. 1–38.
84. Bellussi G, Rispoli G, Molinari D, Landoni A, Pollesel P, Panariti N, et al. *Catal Sci Technol* 2013;**3**:176–82.
85. Eijsbouts S, Mayo SW, Fujita K. *Appl Catal A General* 2007;**322**:58–66.
86. Chianelli RR, Berhault G, Torres B. *Catal Today* 2009;**147**:275–86.
87. Cao T, Wang G, Han W, Ye H, Zhu C, Shi J, et al. *Nat Commun* 2012;**3**:887.
88. Elizondo-Villarreal N, Velázquez-Castillo R, Galván DH, Camacho A, Yacamán MJ. *Appl Catal A General* 2007;**328**:88–97.
89. Chianelli RR, Prestridge EB, Pecoraro TA, Deneufville JP. *Science* 1979;**203**:1105–7.
90. Stewart JA, Spearot DE. *Model Simul Mater Sci Eng* 2013;**21**:045003.
91. Enyashin A, Gemming S, Seifert G. *Eur Phys J Spec Top* 2007;**149**:103–25.
92. Castro-Guerrero CF, Deepak FL, Ponce A, Cruz-Reyes J, Del Valle-Granados M, Fuentes-Moyado S, et al. *Catal Sci Technol* 2011;**1**:1024–31.
93. Remkar M, Kraba Z, Regula M, Ballif C, SanjinØs R, LØvy F. *Adv Mater* 1998;**10**(3):246–9.
94. Plantenga FL, Cerfontain R, Eijsbouts S, van Houtert F, Anderson GH, Miseo S, et al. *Studies in surface science and catalysis*, vol. 145; 2003. p. 407–410.
95. Soled S, Miseo S, Krycak R, Vroman H, Ho TC, Riley K. *Nickel molybdenumstate hydrotreating catalysts*. US Patent No. 6299760 to Exxonmobil.
96. Yoosuk CB, Yoosuk B, Kim JH, Song C, Ngamcharussrivichai C, Prasassarakich P. *Catal Today* 2008;**130**:14–23.
97. Vogelaar BM, Kagami N, van der Zijden TF, Dick van Langeveld A, Eijsbouts S, Moulijn JA. *J Mol Catal A Chem* August 18, 2009;**309**(1–2):79–88.
98. Costa V, Guichard B, Digne M, Legens C, Lecour P, Marchand K, et al. *Catal Sci Technol* 2013;**3**:140–51.
99. Ramos M, Berhault G, Ferrer DA, Torres B, Chianelli RR. *Catal Sci Technol* 2012;**2**:164–78.
100. Bollinger MV, Lauritsen JV, Jacobsen KW, Norskov JK, Helveg S, Besenbacher F. *Phys Rev Lett* 2001;**87**:196803.

101. Lauritsen JV, Nyberg M, Nørskov JK, Clausen BS, Topsøe H, Lægsgaard E, et al. *J Catal* 2004;**224**:94.
102. Moses PG, Mortensen JJ, Lundqvist BI, Nørskov JK. *J Chem Phys* 2009;**130**:104709.
103. Toulhoat H, Raybaud P, editors. *Catalysis by transition metal sulfides*. Editions Technip, 2013.
104. Nogueira A, Znaiguia R, Uzio D, Afanasiev P, Berhault G. *Appl Catal A General* 2012;**429–430**:92–105.
105. <http://www.axens.net/product/catalysts-a-adsorbents/82/tg-103.html> [accessed 26.07.13].
106. Surisetty VR, Dalai AK, Kozinski J. *Appl Catal A General* 2011;**404**(1–2):1–11.
107. Hancsók J, Marsi G, Kasza T, Kallo D. *Top Catal* 2011;**54**:1102–9.
108. klimov OV, Pashigreva AV, Bukhtiyarova GA, Kashkin VN, Nioskov AS, Polunkin YM. *Catal Industry* 2010;**2**:101–7.
109. Topsoe, brochure Sulphur resistant/sour water-gas shift catalyst. [http://www.topsoe.com/business\\_areas/gasification\\_based/Processes/~media/PDF%20files/SSK/topsoe\\_SSK%20brochure\\_aug09.ashx](http://www.topsoe.com/business_areas/gasification_based/Processes/~/media/PDF%20files/SSK/topsoe_SSK%20brochure_aug09.ashx).
110. Liu B, Zong Q, Edwards PP, Zou F, Du X, Jiang Z, Xiao T, AlMegren H. *Ind Eng Chem Res* 2012;**51**:11674–80.
111. Hla SS, Duffy GJ, Morpeth LD, Cousins A, Roberts DG, Edwards JH. *Int J Hydrogen Energy* 2011;**36**(11):6638–45.
112. Hultberg C. *Int J Hydrogen Energy* 2012;**37**(5):3978–92.
113. Chen YY, Dong M, Wang J, Jiao H. *J Phys Chem C* 2012;**116**:25368–75.
114. de la Osa AR, De Lucas A, Romero A, Valverde JL, Sánchez P. *Int J Hydrogen Energy* 2011;**36**(16):9673–84.
115. Perego C, Bianchi D. *Chem Eng J* 2010;**161**:314–22.
116. Baldiraghi F, Di Stanislao M, Faraci G, Perego C, Marker T, Gosling C, et al. In: Centi G, Trifiró F, Perathoner S, Cavani F, editors. *Sustainable industrial chemistry*. Wiley; 2009. pp. 427–38.
117. Jakkula J, Niemi V, Nikkonen J, Purola V, Myllyoja J, Aalto P, et al. European Patent EP1396531 to Neste Oil; 2007.
118. Petri JA, Marker TL. European Patent Application EP1728844, to UOP; 2009.
119. Verma D, Kumar R, Rana BS, Sinha AK. *Energy Environ Sci* 2011;**4**:1667.
120. Kumar R, Rana BS, Tiwari R, Verma D, Kumar R, Joshi RK, et al. *Green Chem* 2010;**12**:2232.
121. Anand M, Sinha AK. *Bioresour Technol* 2012;**126**:148–55.
122. Hayes JR, Bowker RH, Gaudette AF, Smith MC, Moak CE, Nam CY, et al. *J Catal* 2010;**276**(2):249–58.
123. Vít Z. *Appl Catal A General* 2007;**322**:142–51.
124. Wajnert A, Wojciechowska M, Pietrowski M, Przystajko W. *Catal Commun* March 31, 2008;**9**(6):1493–6.
125. Castillo-Villalón P, Ramírez J. *J Catal* 2009;**268**:39–48.
126. Infantes-Molina A, Romero-Pérez A, Finocchio E, Busca G, Jiménez-López A, Rodríguez-Castellón E. *J Catal* 2013;**305**:101–17.
127. Wang H, Iglesia E. *J Catal* 2010;**273**:245–56.
128. Escalona N, Vrinat M, Laurenti D, Gil Llambías FJ. *Appl Catal A General* 2007;**322**:113–20.
129. Ho TC, She Q, McConnachie JM, Kliewer CE. *J Catal* 2010;**276**:114–22.
130. Laurenti D, Ninh Thi KT, Escalona N, Massin L, Vrinat M, Gil Llambías FJ. *Catal Today* 2008;**130**(1):50–5.



131. Sepulveda C, Garcia R, Escalona N, Laurenti D, Massin L, Vrinat M. *Catal Lett* 2011; **141**(7):987–95.
132. Rana MS, Sámano V, Ancheyta J, Diaz JAI. *Fuel* 2007;**86**:1216–31.
133. <http://www.uop.com/products/catalysts/hydrotreating/#hydrotreating-catalysts> [accessed 20.07.13].
134. Francis J, Gullon E, Bats N, Pichon C, Corma A, Simon LJ. *Appl Catal A General* 2011; **409–410**:140–7.
135. Alexander A-M, Hargreaves JSJ. *Chem Soc Rev* 2010;**39**:4388–401.
136. Furimsky E. *Appl Catal A General* 2003;**240**:1.
137. Hargreaves JSJ. *Coord Chem Rev* July 2013;**257**(13–14):2015–31.
138. Masatoshi Nagai. *Appl Catal A General* April 16, 2007;**322**:178–90.
139. Prins R, Bussell ME. *Catal Lett* 2012;**142**(12):1413–36.
140. Oyama ST, Gott T, Zhao H, Lee Y-K. *Catal Today* 2009;**143**(1–2):94–107.
141. Cecilia JA, Infantes-Molina A, Rodríguez-Castellón E, Jiménez-López A, Oyama ST. *Appl Catal B Environ* 2013;**136–137**:140–9.
142. Cecilia JA, Jiménez-Morales I, Infantes-Molina A, Rodríguez-Castellón E, Jiménez-López A. *J Mol Catal A Chem* March 2013;**368–369**:78–87.
143. Bando KK, Wada T, Miyamoto T, Miyazaki K, Takakusagi S, Koike Y, et al. *J Catal* February 2012;**286**:165–71.
144. Furimsky E. *Appl Catal A General* February 10, 2003;**240**(1–2):1–28.
145. Bui P, Antonio Cecilia J, Oyama ST, Takagaki A, Infantes-Molina A, Zhao H, et al. *J Catal* October 2012;**294**:184–98.
146. Villasana Y, Ruscio-Vanalesti F, Pfaff C, Méndez FJ, Luis-Luis MÁ, Brito JL. *Fuel* August 2013;**110**:259–67.
147. Zhu Q, Yang J, Ji S, Wang J, Wang H. *Prog Chem* 2004;**16**(3):382–5.
148. Woo HC, Park KY, Kim YG, Nam I, Chung JS, Lee JS. *Appl Catal* 1991;**75**:267–80.
149. Wu Q, Christensen JM, Chiarello GL, Duchstein LDL, Wagner JB, Temel B, et al. *Catal Today* 2013;**215**:162–8.
150. Qi KZ, Wang GC, Zheng WJ. *Surf Sci* 2013;**614**:53–63.
151. Hoveyda AH, Zhugralin AR. *Nature* 2007;**450**:243–51.
152. Michrowska A, Grela K. *Pure Appl Chem* 2008;**80**(1):31–43.
153. Mol JC. *J Mol Catal A Chem* 2004;**213**:39–45.
154. Fierro JLG, Mol JC. Metathesis of olefins on metal oxides. In: Fierro JLG, editor. *Metal oxides*. Taylor and Francis; 2006. pp. 517–42.
155. Lefbvre F. In: Khosravi E, Szymanska-Buzar T, editors. *Ring opening metathesis and related chemistry. NATO science series*. Kluwer; 2002. pp. 247–62.
156. Liu N, Ding S, Cui Y, Xue N, Peng L, Guo X, et al. *Chemical Engineering Research Design* 2013;**91**:573–80.
157. Debecker DP, Stoyanova M, Rodemerck U, Colbeau-Justin F, Boisèsre C, Chaumonnot A, et al. *Appl Catal A General* 2014;**470**:458–66.
158. Mazoyer E, Szeto KC, Merle N, Norsic S, Boyron O, Basset J-M, et al. *J Catal* May 2013;**301**:1–7.
159. Basset JM, Stoffelbach F, Taoufik M, Thivolle-Cazat J. *Process for manufacturing neo-hexene*. US Patent 8119852 B2.
160. Stoyanova M, Rodemerck U, Bentrup U, Dingerdissen U, Linke D, Mayer RW, et al. *Appl Catal A* 2008;**340**:242.
161. Phongsawat W, Netiworaruksa B, Suriye K, Praserttham P, Panpranot J. *J Ind Eng Chem* 2014;**20**:145–52.

162. Mol JC. *J Mol Catal* 1994;**90**:185–99.
163. Pillai SK, Hamoudi S, Belkacemi K. *Fuel* August 2013;**110**:32–9.
164. Wachs IE. In: Fierro JLG, editor. *Metal oxides*. Taylor and Francis; 2006. pp. 1–30.
165. Mol JC. *Catal Today* 1999;**51**:289–99.
166. Behr A, Schüller U, Bauer K, Maschmeyer D, Wiese K-D, Nierlich F. *Appl Catal A General* March 31, 2009;**357**(1):34–41.
167. Raybaud P, Kressey G, Hafnery J, Toulhoat H. *J Phys Condens Matter* 1997;**9**: 11085–106.

## CHAPTER OUTLINE

<b>11.1 Fundamentals of oxidation catalysis .....</b>	<b>376</b>
11.1.1 Oxidation reactions.....	376
11.1.2 The oxidant and the configurations of heterogeneously catalyzed oxidations.....	377
11.1.3 Mechanisms of the heterogeneously catalyzed oxidations .....	377
11.1.4 Adsorption/reaction/activation of oxygen on bulk metals.....	379
11.1.5 Supported metal catalysts.....	382
11.1.6 Adsorption/reaction/activation of oxygen on metal oxides.....	383
11.1.7 The activation of the substrate.....	384
<b>11.2 Transition-metal mixed oxides for selective and total oxidation reactions .....</b>	<b>385</b>
11.2.1 Metal molybdates for selective oxidations .....	385
11.2.1.1 <i>Iron molybdate for formaldehyde synthesis .....</i>	<i>387</i>
11.2.1.2 <i>Bismuth molybdates and multicomponent molybdates for oxidation and ammoxidations .....</i>	<i>387</i>
11.2.1.3 <i>Vanadium molybdate-based catalysts for acrylic acid synthesis and propane ammoxidation .....</i>	<i>389</i>
11.2.2 Antimony oxide-based catalysts .....	390
11.2.3 Vanadium oxide-based catalysts.....	391
11.2.3.1 <i>VPO catalysts for n-butane oxidation to maleic anhydride .....</i>	<i>391</i>
11.2.3.2 <i>Supported vanadia catalysts for selective oxidations and ammoxidations.....</i>	<i>392</i>
11.2.3.3 <i>Vanadia catalysts for NO<sub>x</sub> selective catalytic reduction.....</i>	<i>393</i>
11.2.3.4 <i>Vanadia catalysts for SO<sub>2</sub> oxidation to SO<sub>3</sub>.....</i>	<i>395</i>
11.2.4 Oxide catalysts for oxidative dehydrogenations .....	395
11.2.5 Heteropolyacids for selective oxidations.....	396
11.2.6 Zeolite catalysts for the abatement of NO <sub>x</sub> and N <sub>2</sub> O.....	397
11.2.7 Oxide catalysts for total oxidations .....	398
11.2.7.1 <i>Catalytic combustion for VOC abatement .....</i>	<i>398</i>
11.2.7.2 <i>Soot oxidation catalysts .....</i>	<i>398</i>
11.2.7.3 <i>Base-metal wet-oxidation catalysts.....</i>	<i>399</i>
<b>11.3 Metal catalysts for oxidation reactions .....</b>	<b>400</b>
11.3.1 Metal gauzes for selective oxidation catalysis.....	400

11.3.2	Silver catalysts for selective oxidations.....	401
11.3.3	Other noble metal-based catalysts for gas-phase selective oxidations of organics .....	402
11.3.4	Noble metal catalysts for selective oxidations in the liquid phase.....	402
11.3.5	Metal catalysts for ammonia selective catalytic oxidation to nitrogen .....	403
11.3.6	Metal catalysts for methane partial oxidation to syngas .....	403
11.3.7	Metal catalysts for CO oxidation.....	404
11.3.8	Combustion catalysts for energy generation.....	405
11.3.9	Noble metal catalysts for total oxidation for VOC abatement.....	406
11.3.10	Noble metals for catalytic wet oxidation .....	407
11.3.11	Catalysts for the aftertreatment of engines' waste gases.....	407
	11.3.11.1 Catalytic converters.....	407
	11.3.11.2 Catalysts for diesel engines aftertreatment .....	408
<b>11.4</b>	<b>Catalysts for oxidation reactions in the presence of chlorine .....</b>	<b>409</b>
11.4.1	Catalysts for the oxidation of HCl to Cl <sub>2</sub> .....	409
11.4.2	Catalysts for the oxychlorination of ethylene.....	409
11.4.3	Catalytic combustion of dioxins and other chlorinated organics.....	410
<b>11.5</b>	<b>Catalysts for the production and use of hydrogen peroxide .....</b>	<b>410</b>
11.5.1	The direct synthesis of hydrogen peroxide.....	410
11.5.2	Catalytic oxidations with H <sub>2</sub> O <sub>2</sub> .....	411
	<b>References .....</b>	<b>412</b>

---

## 11.1 Fundamentals of oxidation catalysis

### 11.1.1 Oxidation reactions

Catalytic oxidation reactions are largely used in industry.<sup>1,2</sup> According to basic chemistry, oxidation reactions are those when a substrate is oxidized by an oxidant so that atoms of the substrate increase their oxidation numbers while atoms of the oxidant are reduced. In industrial chemistry, two kinds of oxidation reactions can be distinguished, practically: (1) total oxidation or combustion; and (2) partial (or “selective”) oxidation. This nomenclature is particularly applied to oxidation of organic compounds, when organic molecules are converted either into carbon oxides, or into more (but still not completely) oxidized organics.

Total oxidation or combustion may be performed uncatalytically in air, but in this case high temperatures (>1000 °C) are produced and, in parallel, nitrogen oxides will be formed, thus polluting the waste gases. Catalytic combustion, i.e. total oxidation performed in the presence of solid catalysts, results in lower reaction temperatures (300–800 °C), thus avoiding the formation of substantial amounts of NO<sub>x</sub>.

In the case of partial oxidation,<sup>3</sup> catalysts are needed to make faster the wanted reaction with respect to total oxidation reaction and other possible partial oxidation

reactions of the same substrate. When possible, heterogeneous gas–solid catalysis is applied. In fact, such kinds of processes avoid needing of the use of solvents and of complex procedures to separate reactants and/or products from catalyst and solvents. Liquid–solid heterogeneous catalysis or liquid-phase homogeneous catalysis are second-choice processes, also depending on the oxidant chosen.

### 11.1.2 The oxidant and the configurations of heterogeneously catalyzed oxidations

Air is the cheapest oxidant in industrial processes. In most common configurations, air is fed in excess with respect to the substrate to be oxidized in order to fall below the lower explosion limit of the air–substrate mixture, for safety purposes. Catalytic burners are used as reactors of total oxidation. Multitubular cooled fixed-bed reactors are mostly used in selective partial catalytic oxidations to control a reaction temperature, the modern alternative being fluid bed-cooled reactors or transport-bed reactors (see Chapter 4). The use of air implies the presence of large amounts of nitrogen within the reaction medium, which sometimes gives rise to problems such as difficult separation from light selective oxidation products. The use of air makes also difficult working above the higher explosion limit of the mixture. In fact, nitrogen would dilute the unconverted reactants to be recycled to the reactor. The use of pure oxygen as the oxidant is a second choice, when the use of air generates drawbacks. In this case, the reaction may be performed easily above the mixture higher explosion limit, with full oxygen conversion, separation of the products and recycle of the unconverted reactant.

Both using air and pure oxygen as oxidants,  $O_2$  is the stoichiometric oxidant molecule. In less favorable cases, other conditions (e.g., liquid phase and homogeneous catalysis) and/or other oxidants, such as hydrogen peroxide, ozone, nitrous oxide ( $N_2O$ ), ..., must or can be applied.

### 11.1.3 Mechanisms of the heterogeneously catalyzed oxidations

As said, most of the heterogeneously catalyzed oxidations are performed in gas–solid reactors with oxygen or air fed together with the vaporized substrate. When working above the higher explosion limit of the reacting mixture, the environment is reducing and the catalyst tends to stay in a relatively low oxidation state. In contrast, when working below the lower explosion limit of the reacting mixture, the environment is oxidizing and the catalyst tends to stay in a relatively high oxidation state.

Upon catalysis, oxygen is supposed to adsorb and be “activated” over the catalyst surface, where it reacts with the substrate. According to the early literature, a number of different oxygen “adsorbed” or surface species can be obtained on solid surfaces,<sup>4</sup> which have been identified mostly by vibrational spectroscopies (IR, Raman, EELS) and Electron Spin Resonance: they are summarized in Table 11.1. Most of them are considered to be electrophilic, being less stable than the most reduced

Formula	Oxidation State	Name	Properties	Possible Structure
$O^{2-}$	-II	Oxide	Coordinationally unsaturated	
		Doubly bonded		
$O^-$	-I		Radical anion	
$O_2^{2-}$	-I	Peroxide		Side-on
				Bridging
$O_2^-$	-0.5	Superoxide	Radical anion	End-on, bent
				Bridging
$O_2$	0	Neutral dioxygen		
$O_2^+$	+0.5	Dioxygen cation	Radical cation	

species, the oxide anion  $O^{2-}$ . They were considered mainly involved in nonselective oxidations. The oxide ions  $O^{2-}$ , instead, are nucleophilic, and assumed to be involved mainly in selective oxidations.

This mechanism involving adsorbed oxygen species can be of the Eley–Rideal type (adsorbed oxygen reacting with gas-phase substrate) or of the Langmuir–Hinshelwood type (both species react being adsorbed at the catalyst surface).

In a mechanism usually attributed to Mars and Van Krevelen, the catalyst plays between two oxidation states. In a higher oxidation state, the catalyst acts as the oxidant for the substrate, reducing itself to a lower oxidation state. Oxygen reoxidizes *in situ* the catalyst from its lower to its higher oxidation state. The Mars–Van Krevelen mechanism (also called the redox mechanism) actually implies that oxygen is activated in the form of oxide anions. It is commonly associated to oxide catalysts.<sup>5</sup> It is generally thought to involve mostly reticular oxide species, mainly but not exclusively those located at the surface, which are removed by the substrate during its own oxidation, which results, in parallel, to a reduction of the oxidation state of the surface cationic species. The reaction with  $O_2$  molecules would result in the recovery of the higher oxidation state of the oxide surface. Also the Mars–Van

Krevelen mechanism may be of the Eley–Rideal type when the reacting substrate is in the gas phase or of the Langmuir–Hinshelwood type when the reacting substrate is previously adsorbed and “activated”.

#### 11.1.4 Adsorption/reaction/activation of oxygen on bulk metals

Transition metals and/or their oxides are typical catalysts in heterogeneously catalyzed oxidations. As said, oxidations can be produced in definitely oxidant conditions (excess air or oxygen) or, sometimes, in reducing conditions although an oxidant (mostly oxygen) is present. Thus, the question arises on what is the real state of the catalyst during reaction.

According to thermodynamics, metal oxides are stable at low temperature while they tend to decompose to the corresponding metals at high temperature, depending on oxygen pressure. In most cases, however, melting is expected by thermodynamics to occur in milder conditions than decomposition. Actually, base metals and most transition metal elements are stable as oxides even under high vacuum up to their melting point, frequently occurring at high temperature. Thus, when these oxides are charged to the oxidation reactor, they are stable as oxides and work as catalytic oxides. Some high oxidation-state transition metal oxides may undergo partial decomposition to lower oxides, at moderate temperature, before melting. This is the case of  $\text{Co}_3\text{O}_4$ , that may decompose into  $\text{CoO}$  at c.  $940^\circ\text{C}$  and of  $\text{CuO}$  that tends to decompose around  $1000^\circ\text{C}$  into  $\text{Cu}_2\text{O}$ , which last melts around  $1300^\circ\text{C}$ . Thus, different oxide phases may be active in oxidation catalysis at high temperature.

Few transition metal oxides, usually having high oxidation states, have quite low melting point. In few cases, the catalyst can work in a partially melt state. One of most interesting cases is  $\text{V}_2\text{O}_5/\text{SiO}_2$  catalysts for  $\text{SO}_2$  oxidation (see Chapter 11.2.3.4).

For noble metal oxides, instead, decomposition to the metal may occur at quite a low temperature also in oxidizing atmosphere, frequently well below melting. In Table 11.2, the approximate decomposition temperatures of noble metal oxides to the corresponding metals, as reported in the literature, are summarized. On the other hand, noble metals are charged, sometimes, after a previous reducing pretreatment, thus in a metallic form. Metal oxidation to the oxide is kinetically hindered at low temperature even when the oxide is the thermodynamically stable form. Thus, starting from a metal (previously produced by reduction of the oxide or other compounds using reductants such as hydrogen, CO, carbon, etc., or by decomposition of organometallics), it may remain in metallic stable or metastable state even at quite high temperature in oxidizing atmospheres or in the presence of oxidants. Thus, it is not always clear if the work catalyst is the metal or its oxide.

Metals may adsorb oxygen in a reactive form. Molecular and dissociative adsorption of oxygen has been revealed by vibrational spectroscopies such as IRAS and EELS over metal monocrystal faces. In most cases, molecular adsorption is found at low temperature producing superoxo- $\text{O}_2^-$  and peroxo- $\text{O}_2^{2-}$  molecular species. At higher temperature atomic or dissociative adsorption is found, producing surface

**Table 11.2** Decomposition Temperatures of the Most Common Noble-Metal Oxides<sup>4</sup>

Metal	Metal Oxide		
Ru	RuO <sub>2</sub>	1300 °C	Tetragonal
Os	OsO <sub>2</sub>	500 °C	Tetragonal
Rh	RhO <sub>2</sub>		Tetragonal
	Rh <sub>2</sub> O <sub>3</sub>	1100 °C	Orthorhombic, trigonal
Ir	Ir <sub>2</sub> O <sub>3</sub>	1000 °C	
	IrO <sub>2</sub>	1100 °C	Tetragonal
Pd	PdO	750 °C	Tetragonal
Pt	PtO <sub>2</sub>	450 (melt?)	Orthorhombic
	PtO	325 °C	Tetragonal
Ag	AgO	>100 °C	Monoclinic
	Ag <sub>2</sub> O	200 °C	Cubic
Au	Au <sub>2</sub> O <sub>3</sub>	150 °C	Orthorhombic
Re	Re <sub>2</sub> O <sub>7</sub>	327 (b.p. 360)	
	ReO <sub>3</sub>	400 °C	Cubic, hexagonal
	ReO <sub>2</sub>	900 °C	Orthorhombic

CRC handbook of chemistry and physics. 92nd ed. Online [Internet version 2012].

and subsurface oxide species, as a transition state toward the formation of the bulk oxide (Table 11.1).

Thus, for noble metal catalysts sometimes the structure during oxidation catalysis is certainly that of the metal with adsorbed oxygen species as active intermediates, while in other cases it is not clear if catalysis is done by the metal or by its oxide or by both.

Considering the elements most involved in oxidation catalysis, at least three different Rhodium oxide phases are reported: RhO<sub>2</sub> is apparently always a metastable phase, while two polymorphs of Rh<sub>2</sub>O<sub>3</sub> are reported. The hexagonal form  $\alpha$ -Rh<sub>2</sub>O<sub>3</sub>, corundum structure, transforms into an orthorhombic  $\beta$ -Rh<sub>2</sub>O<sub>3</sub> structure above 750 °C.<sup>6</sup> This phase is reported to be stable in oxygen up to decompose into Rh and O<sub>2</sub> only at 1133 °C.<sup>7</sup> In a reducing atmosphere, Rh<sub>2</sub>O<sub>3</sub> is reported to reduce to metallic Rhodium at about 100–150 °C.<sup>8</sup> Rh is very reactive, thus oxygen does not form a molecular state at low coverage on any of the clean low index surfaces, but dissociates into an atomic state. However, this atomic oxygen makes the surface less active for dissociation, so that molecular oxygen is then stable<sup>9</sup> over an oxidized surface. Actually, the existence of end-on bonded molecular oxygen on Rh(111) monocrystal face has been calculated to be stable but the energy barrier toward the decomposition oxygen is rather low. A minor extent of oxygen pre-occupation on a rhodium surface even enhances the ability of rhodium to decompose molecular oxygen. However, at higher initial oxygen coverages, this



ability is obstructed, supporting the suggestion that oxygen coverage stagnates.<sup>10</sup> The dissociation of O<sub>2</sub> on Rh(111) is definitely easier than on corresponding faces of less reactive metals such as Ag(111) and (even more) Au(111).<sup>11</sup> Also Ruthenium oxide RuO<sub>2</sub> is a stable phase also at high temperature, being reported to decompose into the metal at about 1400 °C. Dissociative adsorption of oxygen occurs on Ru monocrystal faces such as Ru(0001), which has been the object of several studies.<sup>12</sup>

For Pd, in 1 mbar O<sub>2</sub> the PdO  $\rightleftharpoons$  Pd + 1/2 O<sub>2</sub> transition is expected to occur at approximately 570 °C.<sup>13</sup> Accordingly, PdO is known to decompose in practice into Pd metal in the range 650–800 °C, depending on O<sub>2</sub> partial pressure<sup>14,15</sup> and reactive gas mixture composition. Molecular adsorption is observed over Pd(111) at 30 K producing two different species characterized by IR bands due to OO stretchings at 850 and 1035 cm<sup>-1</sup>.<sup>16</sup> These peaks are assigned to a peroxo-like state and a superoxo-like state, respectively. After saturation of these chemisorbed molecular states, a state of physisorbed oxygen with its vibrational frequency close to the gas-phase value of 1556 cm<sup>-1</sup> is populated. Upon warming the sample above 80 K, an additional loss feature at 650 cm<sup>-1</sup> develops, which is assigned to a second peroxo-like molecular species. The oxygen dissociation process is completed at  $T \approx 200$  K leaving a layer of atomic oxygen on the surface, which is characterized by a peak at 480 cm<sup>-1</sup> (Pd-O stretching) and by a 2 × 2 pattern in LEED.<sup>16</sup> Oxygen atoms are adsorbed on threefold hollow adsorption sites. At 250 °C, data show the formation of subsurface oxygen species on Pd(111) characterized by Pd-O stretching band at 326 cm<sup>-1</sup>.<sup>17</sup> At and above 330 °C, several surface oxide phases, like Pd<sub>5</sub>O<sub>4</sub>, may form<sup>18</sup> until Pd(111) converts into bulk PdO(101) face.<sup>19</sup> It seems that easier oxidation to PdO can occur with Pd(110) face, even below 300 °C.<sup>20</sup> The oxidation of Pd foils with both wet and dry oxygen is observed at relevantly lower temperature, being incipient already at 100 °C and extensive at 200 °C.<sup>21</sup>

A similar complex situation occurs with platinum and its oxides:  $\alpha$ -PtO<sub>2</sub> is the stable phase at low temperatures, metallic Pt is stable at high temperature, and in between there is a region of stability of Pt<sub>3</sub>O<sub>4</sub>. This region is c. 100 K wide and at 1 atm oxygen pressure it extends from 600–700 °C. Transition temperatures move to lower values at lower O<sub>2</sub> pressures, without qualitative changes. PtO is a metastable phase while other PtO<sub>2</sub> polymorphs are stable only at high temperatures and high oxygen pressures.<sup>22</sup> Accordingly, thermogravimetric studies in air showed the decomposition of platinum oxide via the transitions  $\alpha$ -PtO<sub>2</sub>  $\rightarrow$  Pt<sub>3</sub>O<sub>4</sub>  $\rightarrow$  Pt observed at 635 and 800 °C respectively.<sup>23</sup> O<sub>2</sub> adsorbs molecularly at low surface temperature (<100 K) also on Pt monocrystal faces producing peroxo- and superoxo-species.<sup>24,25</sup> Dissociation of adsorbed O<sub>2</sub> begins to occur above 135 K generating an atomic oxygen species while after annealing at 230–330 °C ordered surface oxide islands are observed to coexist with a chemisorption structure. From density functional theory calculations, on Pt(110) the PtO<sub>2</sub> phase is found to be metastable, and its presence is explained in terms of stabilizing defects in the chemisorption layer and reduced Pt mobility.<sup>26</sup> Oxidation of Pt foils also resembles that of Pd foils, being detectable already at 100–200 °C.<sup>21</sup>

The metal elements having the least stable oxides are gold and silver. Gold (III) oxide  $\text{Au}_2\text{O}_3$  is reported to be more stable than  $\text{Au}_2\text{O}$ , which is only metastable with respect to the  $\text{O}_2$  molecule and bulk Au.<sup>27</sup>  $\text{Au}_2\text{O}_3$  is reported to decompose to metallic gold at 160 °C.<sup>28</sup> Experiments have shown that room-temperature, gas-phase  $\text{O}_2$  does not readily chemisorb on macroscopic gold single crystals or supported gold clusters larger than  $\sim 1$  nm in diameter either dissociatively or molecularly. The adsorption of oxygen atoms on the surface assists in the molecular chemisorption of oxygen.<sup>29</sup> In any case, steps are reported to be more reactive, adsorption on plane faces being thermoneutral or even endothermic.<sup>30</sup>

The binary Ag–O system contains several defined compounds:  $\text{Ag}_2\text{O}$ ,  $\text{Ag}_3\text{O}_4$ ,  $\text{AgO}$ ,  $\text{Ag}_4\text{O}_3$  and  $\text{Ag}_2\text{O}_3$ , among which  $\text{Ag}_2\text{O}$  is the most stable.<sup>31</sup>  $\text{AgO}$  is reported to decompose into  $\text{Ag}_2\text{O}$  at low temperature (150–200 °C),<sup>32</sup> while different data are reported concerning the decomposition of  $\text{Ag}_2\text{O}$  (150–400 °C).<sup>33–37</sup> Thermodynamics forecasts stability of  $\text{Ag}_2\text{O}$  in oxygen up to ca 150 °C.<sup>38</sup> On silver monocrystal faces, molecular adsorption is observed at very low temperature. The study of the interaction of oxygen with silver at higher temperature (200 °C), i.e., at temperatures significant for heterogeneous catalysis, reported on the formation of different oxygen monatomic species. Actually, oxidation of silver gives rise to  $\text{Ag}_2\text{O}$ , which has an intermediate stability. It is reported that, thermodynamically, silver oxidation to  $\text{Ag}_2\text{O}$  is spontaneous below ca 200 °C.

Some authors suggested the formation of surface suboxide with an approximate stoichiometry of  $\text{Ag}_{1.8}\text{O}$ .<sup>39</sup> The situation, however, was found more recently to be more complex.<sup>40</sup> According to Rocha et al.<sup>41</sup> five different monoatomic oxygen species can be observed on silver at high temperature, parts of which are surface species others being subsurface species, interacting dynamically with each other.

Thus, if reaction conditions are fully oxidizing, only gold and, to a lesser extent, silver, as well as palladium and platinum only at very high temperatures, may act as metal catalysts. In fully oxidizing conditions, all other catalysts are expected to act as oxide catalysts. In contrast, for selective oxidations performed in partially reducing conditions, the real state of the catalyst may be doubtful.

### 11.1.5 Supported metal catalysts

As for the supported metal catalysts, the situation may be even more complex. Most literature concerning redox-properties of supported metal catalysts refer to the presence of metal particles of different sizes and oxide particles and their interconversions. This is in part because these species are those that can be detected with common techniques such as XRD and TEM, have parallelism with the surface science studies of monocrystals, and can be modeled by theoretical approaches. Also well-defined supported nanoparticles, however, may have significantly different properties than bulk particles. As for example, supported gold nanoparticles may be oxidized at least partially already at 150 K, while the temperature for total decomposition of the oxide depends from the support (30 °C on titania, 280 °C on silica),<sup>42</sup> a different behavior than for bulk gold. Small supported metal particles

differ for their properties significantly from bulk metals, having nonbulk properties such as, e.g., negative thermal expansion found for small supported Pt particles.<sup>43,44</sup> Particles with different shapes may be copresent on the same catalyst, such as e.g. on Pd/Al<sub>2</sub>O<sub>3</sub>,<sup>45</sup> where nanopolyhedra called multiply twinned particles (MTPs), appearing to be hexagonal at TEM analysis, are frequently observed to form together with rod-like nanocrystals.<sup>46</sup> These nanopolyhedra, according to Xiong et al.<sup>46</sup> and Berhault et al.,<sup>45</sup> are formed by six icosahedra subunits, covered only by (111) planes.

High-resolution microscopy studies of Pt on alumina systems provide evidence of the existence of atomically dispersed Pt metal and of Pt<sub>3</sub> clusters under reducing conditions.<sup>47</sup> According to Xiao and Schneider,<sup>48</sup> atomically dispersed Pd and Pt on supports ( $\alpha$ -Al<sub>2</sub>O<sub>3</sub>) can be quite easily oxidized and oxidation is also favored by support hydroxylation. Isolated zerovalent Pd centers can apparently be easily oxidized by oxygen to Pt<sup>2+</sup>, usually with the intermediacy of species like Cu<sup>+</sup>/Cu<sup>2+</sup> or heteropolyacids, in both homogeneous water solutions or heterogeneous solid/water and solid/vapor states at 300–400 K, as it occurs in the reoxidation step of the Wacker ethylene oxidation process.<sup>49</sup>

Theoretical studies reported on the stabilization of highly uncoordinated Pt and Pd metal centers by alumina, providing a relevant difference of alumina-supported catalysts with respect to bulk metal surfaces.<sup>50</sup> This work also confirmed on the effect of hydroxylation/dehydroxylation of the support on the states of Pt and Pd that become positively charged when deposited on hydroxylated alumina faces, while they are neutral or even negatively charged over dry surfaces. Other studies report the existence of Pd particles decorated with a thin layer of an aluminate phase on Pd/Al<sub>2</sub>O<sub>3</sub>-supported catalysts.<sup>51</sup> Indeed, individual cations of gold, platinum, palladium, rhodium, or other metals anchored to supports through M–O bonds can be formed using appropriate preparation techniques, sometimes favored by the presence of alkali and alkaline-earth metal ions. These sites can act in catalysis, as suggested for Au in the water-gas shift reaction.<sup>52</sup>

In practice, in the case of supported metals, the dispersing/nondispersing ability of the support plays a role, favoring the production of isolated atoms, clusters or particles of different shapes and sizes. Additionally, the redox properties of the supported metal species are strongly influenced by supports, some of which are insulating and nonreducible, as alumina and silica, others semiconducting and slightly reducible, as titania and zinc oxides, and others finally have significant oxygen storage capacity, typical of ceria. As a result of this, a number of different situations can exist and, frequently, several different species can coexist, simultaneously.

### 11.1.6 Adsorption/reaction/activation of oxygen on metal oxides

Also on metal oxides, adsorption of oxygen gives rise to molecular species as well as to atomic species. IR spectroscopy has been used to reveal the formation of molecular oxygen species adsorbed on metal oxide surfaces, as discussed in detail by Davydov and Sheppard.<sup>53</sup> Neutral weakly adsorbed dioxygen species

are observed e.g., on a  $\text{TiO}_2$  powder at 120 K, characterized by the O—O stretching at  $1550\text{ cm}^{-1}$ .<sup>54</sup> The position is the same as the Raman active (and IR inactive) mode of gas phase  $\text{O}_2$ , but the interaction with the surface caused its activation in IR. Indeed Davydov and coworkers reported already several years ago IR bands attributed to dioxygen adsorbed on metal oxide.<sup>53</sup> Over several metal oxides, such as  $\text{CeO}_2$  and  $\text{CeO}_2\text{—ZrO}_2$ <sup>55</sup> and  $\text{CoO—MgO}$ <sup>56</sup> solid solutions, bands due to dioxygen species in the region  $1000\text{—}1200\text{ cm}^{-1}$  have been well characterized and attributed to superoxide species  $\text{O}_2^-$ . Peroxide-like species,  $\text{O}_2^{2-}$ , absorbing in the region below  $1000\text{ cm}^{-1}$  have been reported to occur too, e.g., on chromia and ceria, but their characterization by IR is not easy due to the superimposition with bulk vibrations in several cases.

On the other hand, bulk or subsurface atomic oxide species ( $\text{O}^{2-}$ ) may be active in Mars—van Krevelen or redox mechanisms of catalytic oxidation reactions, as said above. In some cases, even full bulk reduction and reoxidation can occur, although during catalysis only the surface is supposed to be involved in the redox cycle. Experimental techniques (such as XPS and UV—vis spectroscopic studies of the catalysts, Temperature-Programmed Reduction experiments and IR spectra of adsorbed probe molecules such as CO) may provide evidence of the different oxidation states of the surface cations during reaction. Adsorption studies of oxidizable molecules give also information on the oxidation ability of the surface.

Metals and other elements in very high oxidation states can give rise to element-oxygen “double bonds” in their oxides, i.e., very short bonds. This is the case of vanadyl, niobyl, molybdenyl, chromyl and wolframyl groups. The existence of these species at the surface may be determined by IR and Raman studies, such as in the case of  $\text{V=O}$  bonds ( $1038\text{ cm}^{-1}$ ) at the surface of bulk  $\text{V}_2\text{O}_5$ ,<sup>57</sup>  $\text{Nb=O}$  bonds at the surface of niobic acid ( $\text{Nb}_2\text{O}_5 \cdot n\text{H}_2\text{O}$ ,  $995\text{ cm}^{-1}$ ),<sup>58</sup>  $\text{W=O}$  bonds at the surface of bulk  $\text{WO}_3$  ( $1040\text{ cm}^{-1}$ )<sup>59</sup>,  $\text{Cr=O}$  bonds at the surface of oxidized chromia<sup>60</sup> and chromia-based oxidation catalysts such as  $\text{CuCr}_2\text{O}_4$ ,  $\text{CoCr}_2\text{O}_4$ <sup>61</sup> and  $\text{MgCr}_2\text{O}_4$ <sup>62</sup> ( $800\text{—}1030\text{ cm}^{-1}$ ).

The reactivity of such species in oxidation catalysis has been well evidenced in the case of chromia and metal chromites, whose surface is covered by chromate species. Upon reduction the  $\text{Cr=O}$  stretching bands disappear, while they reappear by reoxidation.<sup>62</sup> IR spectra show the disappearance of the massive absorption at  $800\text{—}1000\text{ cm}^{-1}$ , due to the stretchings of multiple  $\text{Cr}^{6+}=\text{O}$  bonds of chromate species, that become reduced to  $\text{Cr}^{3+}\text{—O}$  by oxidizing hydrocarbons.

Cations with short  $\text{M=O}$  double bonds are usually considered to be active in oxygen insertion into the substrates, even if it has been determined that the oxygen atom inserted is not that involved in the double bond.

### 11.1.7 The activation of the substrate

Oxidation catalysts are generally thought not only to activate oxygen but also (or, maybe, alternatively) to activate the substrate to be oxidized. As for hydrocarbons, the most reactive toward oxidation are unsaturated molecules such as aromatics,

with the activation of both ring positions as well as of benzylic positions. Also oxidation of olefins are very relevant industrially, with the possibility of oxidation at the C=C double bond or at the allylic position. The activation of unsaturated C=C bonds is frequently obtained by  $\pi$ -bonding over noble metal centers or transition metal centers. Alternatively, they can be activated by electrophilic attacks. Activated saturated carbon atoms such as those in benzylic and allylic positions are activated by Lewis acid sites, which are able to abstract hydride species, or in a radical mode. Cations such as  $\text{Sb}^{3+}$ ,  $\text{Bi}^{3+}$ ,  $\text{Te}^{4+}$ , i.e., cations having nonbonding electron pairs, are generally thought to be active in H abstraction from allylic positions. The activation of nonactivated saturated positions of paraffins is supposed to occur by very basic centers or by noble and nonnoble metal centers.

Easier is the activation of heteroatom-containing molecules such as oxygenates, nitrogenated and halogenated compounds, that are in fact more reactive to oxidation. Activation likely involves the previous coordination of the molecules on Lewis and or Brønsted acid sites using the lone pairs on heteroatoms.

---

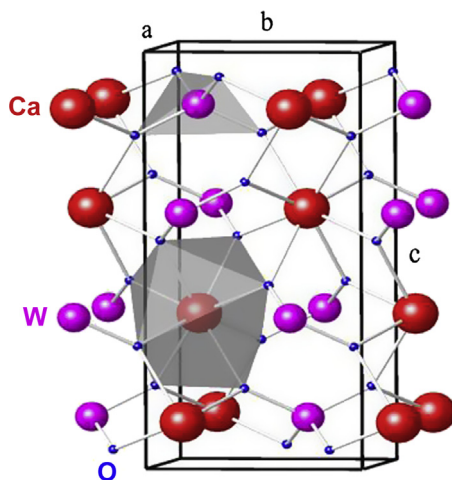
## 11.2 Transition-metal mixed oxides for selective and total oxidation reactions

A number of different mixed oxides, mostly but not exclusively based on high oxidation state elements such as molybdenum (VI), vanadium (V) and to a lesser extent antimony (V), tungsten (VI), niobium (V), have been developed for several specific industrial applications, in particular for selective oxidations. In many cases “multi-component” oxides, containing a large number of different elements, some of them in “doping” amounts have been the object of optimization studies. The crystal chemistry of several of such systems is very complex, different metastable phases being produced strictly depending on the particular preparation used. In many cases, several phases are present together and work synergistically in the optimized catalysts.

These materials, in particular when used for selective oxidation, have moderate-to-low surface area, in part due to the need for limiting products overoxidation and to resist quite high reaction temperatures. Deactivation may occur by further loss of surface area, structure modification and loss of volatile components.

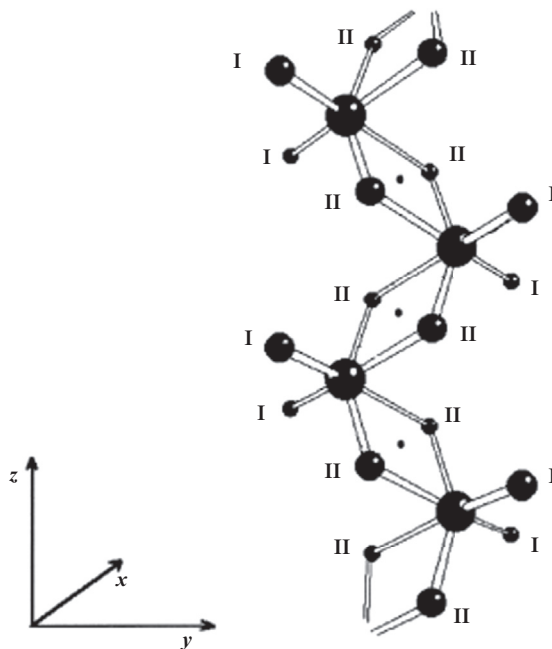
### 11.2.1 Metal molybdates for selective oxidations

Molybdates of divalent and trivalent transition metals represent a conspicuous class of selective oxidation catalysts. They have a variety of crystal structures. Most of them are defined as scheelite-type, when having the structure of scheelite  $\text{CaWO}_4$  (Figure 11.1<sup>63</sup>) or, in any case, containing the tetrahedral orthomolybdate anion. Others are denoted as “wolframite-type” (wolframite is the  $(\text{Fe},\text{Mn})\text{WO}_4$  mineral), when they contain the octahedral-based polymeric metamolybdate anions (Figure 11.2<sup>64</sup>).

**FIGURE 11.1**

Schematic view of the scheelite structure. Large circles represent the Ca atoms, middle-size circles correspond to the W atoms, and the small circles are the O atoms. The unit cell, Ca–O bonds, and W–O bonds are also shown together with  $\text{CaWO}_4$  tetrahedron and a  $\text{CaO}_8$  dodecahedron.

*Reprinted with permission from Ref. 63.*

**FIGURE 11.2**

View of the structure of the polymeric  $(\text{Mo}_2\text{O}_8)_n^{4-}$  anion in the wolframite-like structures. Bridging (II) and terminal (I) oxygens are distinct; the dots indicate inversion centers.

*Reprinted with permission from Ref. 64.*

### 11.2.1.1 Iron molybdate for formaldehyde synthesis

The selective oxidation of methanol is an important industrial process for the production of formaldehyde



One of the current industrial processes uses multitubular fixed-bed reactors cooled by a hydrocarbon liquid, at 300–350 °C.<sup>65</sup> The industrial catalyst consists of a ferric molybdate phase ( $\text{Fe}_2(\text{MoO}_4)_3$ ) with excess molybdena ( $\text{MoO}_3$ ) so that a typical molybdenum-to-iron atomic ratio is 2.2:1 instead of 1.5. The enhanced catalytic performance of bulk iron molybdate catalysts in the presence of excess  $\text{MoO}_3$  is reported<sup>66</sup> to be related to the formation of a surface  $\text{MoO}_x$  monolayer on the bulk  $\text{Fe}_2(\text{MoO}_4)_3$  phase. Thus, the catalytic active phase for bulk iron molybdate catalysts is the surface  $\text{MoO}_x$  monolayer on the bulk crystalline  $\text{Fe}_2(\text{MoO}_4)_3$  phase and the only role of the excess crystalline  $\text{MoO}_3$  is to replenish the surface  $\text{MoO}_x$  lost by volatilization during methanol oxidation. On the other hand it is known that the catalyst deactivates due to the volatilization of the  $\text{MoO}_3$  in excess.<sup>67</sup> Owing to the deactivation, the catalyst has to be replaced every 1–2 years depending on the operating conditions. The typical laboratory and industrial preparation method is a coprecipitation: the catalyst can be prepared by mixing iron nitrate solution ( $\text{Fe}(\text{NO}_3)_3$ ) with ammonium heptamolybdate ( $(\text{NH}_4)_6\text{Mo}_7\text{O}_{24}$ ) and adjusting the pH of the solution until both components coprecipitate. The precipitate is then filtered, washed, dried and calcined.

The complex, monoclinic room-temperature crystal structure of  $\text{Fe}_2(\text{MoO}_4)_3$  consists of an open framework of octahedral  $\text{FeO}_6$  and tetrahedral  $\text{MoO}_4$  building blocks, which are linked by Fe–O–Mo bonds. This monoclinic structure converts into orthorhombic  $\beta\text{-Fe}_2(\text{MoO}_4)_3$  at higher temperature but the connectivity of polyhedra remains the same.

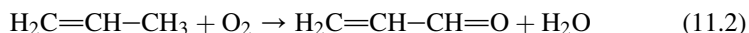
As said, although it is reported that the active phase of the catalysts is  $\text{Fe}_2(\text{MoO}_4)_3$ , industrial catalysts always have an excess of  $\text{MoO}_3$ , showing very high selectivity (>93%) at almost complete conversion of methanol.

On the other hand, two reduced phases,  $\alpha\text{-FeMoO}_4$  and  $\beta\text{-FeMoO}_4$ , are found in the aged catalysts, which are not catalytically active.  $\alpha\text{-FeMoO}_4$  and  $\beta\text{-FeMoO}_4$  can both exist at room temperature but interconvert if pure at higher temperatures (400 °C). In the  $\alpha\text{-FeMoO}_4$  phase, molybdenum is octahedrally coordinated, while in the  $\beta\text{-FeMoO}_4$  phase, it is tetrahedral, with a structure similar to that of scheelite.

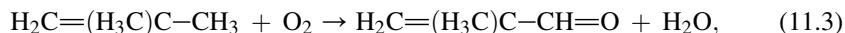
To reduce the problems associated to loss of  $\text{MoO}_3$ , catalysts based on spinel-type iron vanadate<sup>68</sup> and iron molybdeno-vanadate<sup>69</sup> are under investigation.

### 11.2.1.2 Bismuth molybdates and multicomponent molybdates for oxidation and ammoxidations

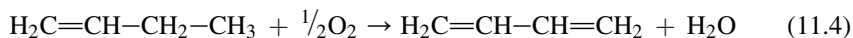
Bismuth molybdates have been developed as the catalysts for the selective oxidation of propene to acrolein



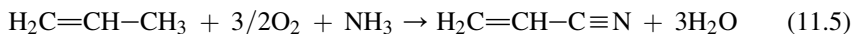
and are used today also for the oxidation of isobutene to methacrolein



and the oxidative dehydrogenation of butane to butadiene



Catalysts based on bismuth molybdates are used for ammoxidation of propylene to acrylonitrile,



the very important monomer for acrylic polymers.

The general chemical formula of bismuth molybdates is  $\text{Bi}_2\text{O}_3 \cdot n\text{MoO}_3$  where  $n = 3, 2$  or  $1$ , corresponding to the  $\alpha$ ,  $\beta$  and  $\gamma$  phases, respectively. These phases have all catalytic activities, but the relative activity and selectivity of these phases are different for each reaction. Unsupported bismuth molybdates have mainly been synthesized by precipitation and solid-state reaction. In the literature, different recipes for precipitation were used and the calcination was carried out at different temperatures. Pure phases were obtained under some given conditions. For example,  $\alpha$  and  $\gamma$  phases were usually synthesized at  $500\text{--}600^\circ\text{C}$ ,  $\beta$  phase— $\text{Bi}_2\text{Mo}_2\text{O}_9$  was only obtained above  $550^\circ\text{C}$  due to its decomposition at  $540^\circ\text{C}$  to  $\alpha$  and  $\gamma$  phases.

The crystal structure of  $\gamma$ -bismuth molybdate  $\text{Bi}_2\text{MoO}_6$  is composed of layers of octahedral  $[\text{MoO}_2]^{2+}$  (i.e. it is a metamolybdate) and five-coordinated  $[\text{Bi}_2\text{O}_2]^{2+}$  linked together by layers of  $\text{O}^{2-}$  ions (Aurivillius structure).  $\alpha$ -bismuth molybdate,  $\text{Bi}_2(\text{MoO}_4)_3$  is described as a defect scheelite structure containing three crystallographically distinct  $\text{MoO}_4$  units, while the presence of a fifth oxygen at  $2.29 \text{ \AA}$  from molybdenum atom means the coordination number of Mo is often considered to be five and the coordination polyhedron would be irregular trigonal bipyramid pairs of these polyhedra share edges.  $\beta$ -bismuth molybdate,  $\text{Bi}_2\text{Mo}_2\text{O}_9$ , has regularly tetrahedrally coordinated molybdenum (orthomolybdate) and can be considered as a defective fluorite structure. The structures of Bi molybdates are depicted in Figure 11.3.<sup>70</sup>

Most recent evolution of this catalytic system implies the preparation of “multi-component molybdates”. Industrial catalysts certainly containing Mo—Bi—Fe—Co—Ni and other elements are used for the acrolein synthesis from propene oxidation, performed in multitubular fixed-bed reactors at  $300\text{--}370^\circ\text{C}$ . Industrial catalysts for propylene ammoxidation are based on Bi, Fe, Cr, Ni, Co and Mg molybdates. According to the literature,  $\text{Bi}^{3+}$ ,  $\text{Sb}^{3+}$  and/or  $\text{Te}^{4+}$  play the role of H-abstraction sites from the allylic position of propene,  $\text{Mo}^{6+}$  and/or  $\text{Sb}^{5+}$  play the role of oxygen and nitrogen insertion sites, while the presence of couples such as  $\text{Fe}^{2+}/\text{Fe}^{3+}$  or  $\text{Ce}^{4+}/\text{Ce}^{3+}$  favor the diffusion of lattice oxygen. Two main phases are present in acrylonitrile catalysts: Bi/Fe/Cr trivalent scheelite-type tetrahedral molybdates (orthomolybdate) constitute the active phase while Ni/Co/Fe/Mg bivalent octahedral polymolybdates (metamolybdate) with the wolframite



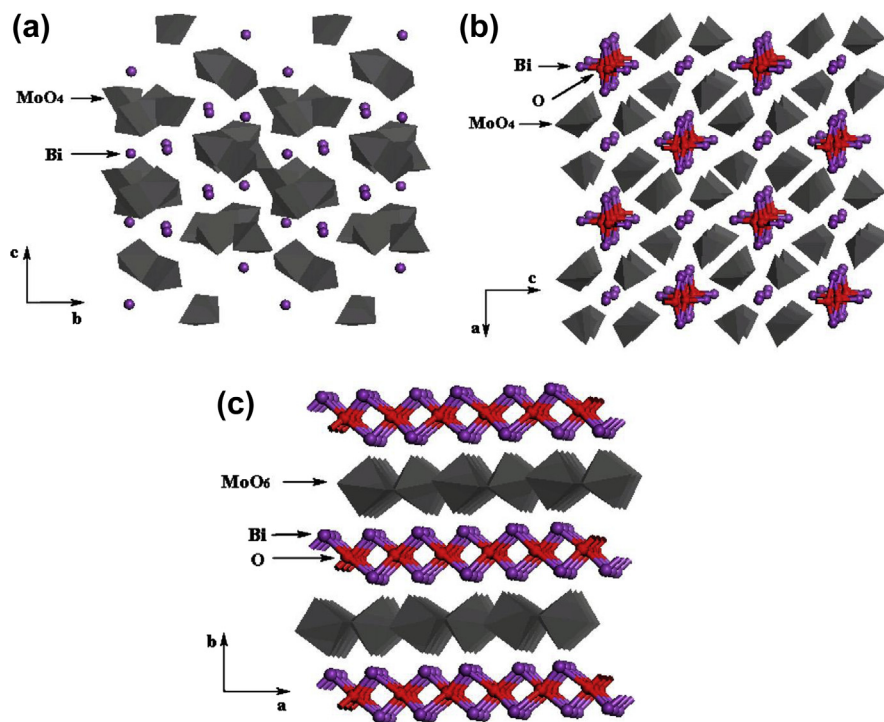


FIGURE 11.3

Crystalline structures of (a)  $\alpha$ - $\text{Bi}_2\text{Mo}_3\text{O}_{12}$ , (b)  $\beta$ - $\text{Bi}_2\text{Mo}_2\text{O}_9$  and (c)  $\gamma$ - $\text{Bi}_2\text{MoO}_6$ .

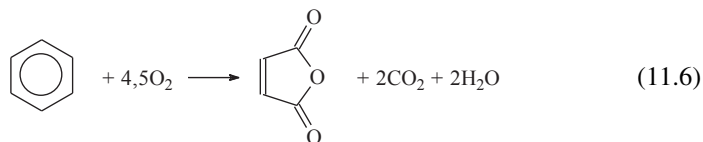
Reprinted with permission from Ref. 70.

structure act as catalysts of the reoxidation step. The catalysts are supported on silica and used in fluid bed reactor operating at 400–450 °C.

### 11.2.1.3 Vanadium molybdate-based catalysts for acrylic acid synthesis and propane ammoxidation

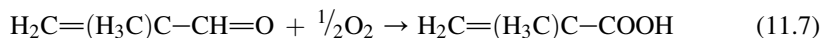
Catalysts based on molybdenum–vanadium oxides, with the addition of several other components, have been developed for selective oxidations and ammoxidations. This catalytic system has received much attention in recent years for the activation and the selective oxidation, in particular, of paraffins. The many phases obtained in these systems are mostly constituted by edge-sharing distorted  $\text{MO}_6$  octahedra, bonded with different crystal geometries.

Catalysts with compositions of  $\text{V}_2\text{MoO}_8$  to  $\text{V}_3\text{Mo}_2\text{O}_x$  ( $x \div 12$ –14), mostly supported on alumina or corundum, have been used in the past to produce maleic anhydride by selective oxidation of benzene with air at 400–450 °C, 2.5 bar, and a residence time of about 0.1 s, a process that has been abandoned in favor of that using n-butane as the feedstock.<sup>71,72</sup>



Poorly crystalline catalysts based on the system Mo/V/Nb oxides, containing also other components such as P, La, Ti and traces of noble metals (Pd, Au) have been patented for the selective oxidation of ethane to acetic acid, performed at 250–350 °C and 8–15 atm.

Catalysts based on Mo–W–V–Fe<sup>73</sup> are used for the selective oxidation of acrolein to acrylic acid at 260–300 °C, the main industrial process for producing such an important intermediate.



Catalysts based on Mo/V/Nb/Te oxides are reported to allow direct oxidation of propane to acrylic acid.<sup>74</sup> Complex catalysts have also been developed for propane ammoxidation, based on Mo/V/Nb/Te and Mo/V/Nb/Sb oxides.<sup>75</sup> The active catalysts belonging to these systems contain two predominant phases, the so-called M1 (orthorhombic) and M2 (pseudo-hexagonal). The M1 phase alone is capable of propane conversion, while the presence of the M2 phase may improve selectivity. M1 is a layered structure<sup>76</sup> (Figure 11.4<sup>77</sup>) giving rise to two sets of channels—one hexagonal and the other nearly heptagonal. In these channels, Te<sup>4+</sup> cationic sites carrying an electron lone pair possibly relevant for the ammoxidation reaction, may be located.

### 11.2.2 Antimony oxide-based catalysts

A number of antimonate-based catalysts have been found active for ammoxidation of olefins such as propylene to acrylonitrile.<sup>78</sup> In particular, uranyl antimonates based on USb<sub>3</sub>O<sub>10</sub> have been developed at the industrial level for ammoxidation of propene.<sup>79</sup>

Rutile-type antimonate catalysts, in particular the families of iron antimonates and vanadium antimonates, have also been developed at the industrial level for the production of acrylonitrile from propane ammoxidation.<sup>75</sup> The most relevant phase in the V/Sb oxide system is the so-called “*quasi* VSbO<sub>4</sub>”, which has the composition V<sub>0.92</sub>Sb<sub>0.92</sub>O<sub>4</sub> with pentavalent antimony balanced by some V<sup>3+</sup> and cationic vacancies with respect to the canonical tetravalency of cations in TiO<sub>2</sub> rutile structure. Materials based on this system, with the addition of a number of other elements (Ti, Sn, Al, Fe, W, Te) as activators, have been developed at the industrial level to produce acrylonitrile from propane ammoxidation (Eqn 11.5) at 450–500 °C. Recently, rutile-type Ga/V/Nb/Sb mixed oxide was found to give good performances.<sup>80</sup>

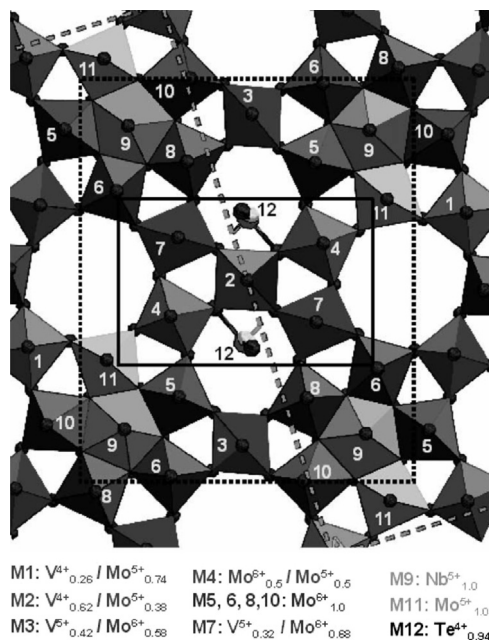


FIGURE 11.4

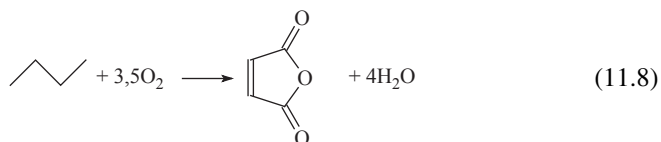
Structure and the proposed catalytically active center of  $\text{Mo}_{7.8}\text{V}_{1.2}\text{NbTe}_{0.94}\text{O}_{29}$  (M1) phase in [0 0 1] projection.

Reprinted with permission from Ref. 77.

### 11.2.3 Vanadium oxide-based catalysts

#### 11.2.3.1 VPO catalysts for *n*-butane oxidation to maleic anhydride

Vanadyl pyrophosphate catalysts  $(\text{VO})_2\text{P}_2\text{O}_7$  (VPO or VPP) are used industrially for the selective oxidation of *n*-butane to maleic anhydride (MA):



The reaction is performed at 350–450 °C with air and steam obtaining 75–85% conversion, 65–73% selectivity, with acetic and acrylic acids as byproducts besides  $\text{CO}_x$ . Thus, the system needs further improvement.<sup>81</sup>

A number of different vanadium phosphates exist with different vanadium oxidation states (V, IV, and III) taking different coordination states (tetrahedra, square pyramids, and distorted and regular octahedra), which can bound in different ways to  $\text{PO}_4$  tetrahedra.<sup>82</sup>

Among the many systems, the topotactic transformation from the vanadyl hydrogen phosphate hemihydrate  $(\text{VOHPO}_4 \cdot 0.5\text{H}_2\text{O})$  to the final vanadyl pyrophosphate

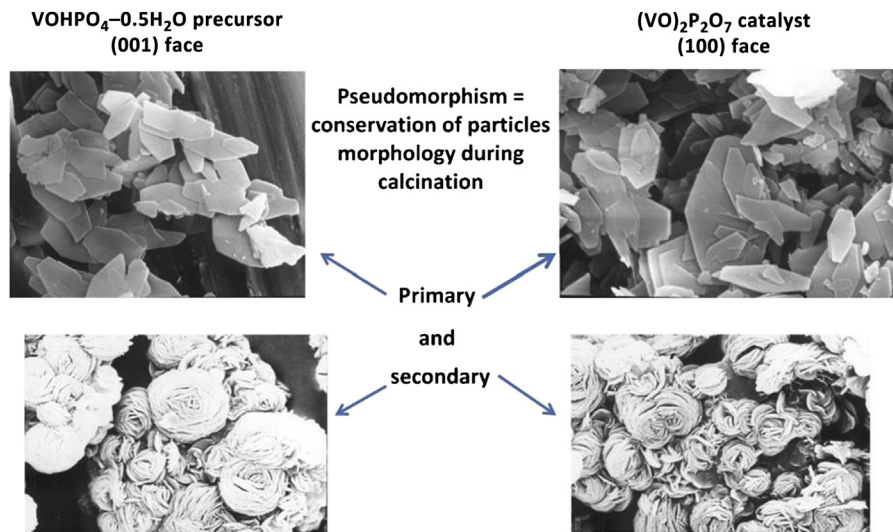
catalyst  $(VO)_2P_2O_7$  has been the object of many studies, Figure 11.5.<sup>83,84</sup> Various synthesis methods can be applied to obtain the precursor  $VOHPO_4 \cdot 0.5H_2O$  to convert it in active catalysts. Preparations using organics such as alcohols and glycols as solvent give rise to the more active catalysts. It was found that the alcohol used as a reducing agent can control the morphology introducing an optimal dose of defectivity.<sup>81</sup>

While the bulk vanadyl pyrophosphate constitutes the active phase, a slight excess of P with respect to the stoichiometric P/V ratio 1:1 is required for high catalytic activity and selectivity. The P/V atomic ratio in the most efficient catalysts may range from 1.10 to 1.20 giving rise to surface  $V^V$  species together with bulk  $V^{IV}$  species.

Another important factor governing the catalytic behavior of VPP is the presence of promoters. The promotional effect of Co and Fe, Bi, Nb, alkali metals and gold<sup>85</sup> has been reported.

### 11.2.3.2 Supported vanadia catalysts for selective oxidations and ammoxidations

The synthesis of phthalic anhydride (precursor of phthalate esters largely used as lubricants and plasticizers) is performed industrially over vanadia catalysts

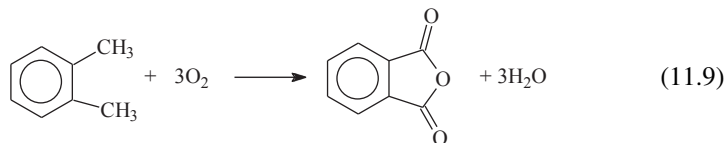


**FIGURE 11.5**

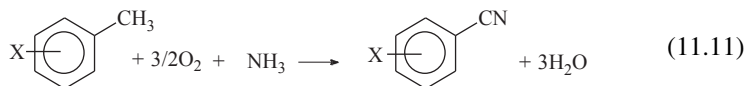
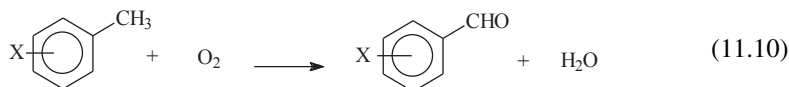
Pseudomorphism between primary particles (top) and secondary particles (bottom) of  $VOHPO_4 \cdot 0.5H_2O$  precursor (left) and  $(VO)_2P_2O_7$  catalyst (right) corresponding to a topotactic reaction driven by calcination. By controlling the morphology of the precursor, one can control the morphology of the final catalyst.

Reprinted with permission from Ref 83.

(4–10%  $V_2O_5$  wt/wt) supported on titania (anatase polymorph) with surface area 6–25  $m^2/g$ , alkali ions (K, Rb, Cs), Sb and P playing the role of promoters.<sup>86</sup> The temperature in the bed is 360–450 °C. Although this process is well established for decades, improvements are needed from several points of view, with the need, in particular, of improving catalyst selectivity.<sup>86–88</sup> Although the content of vanadium in industrial catalysts is generally quite high it has been shown that submonolayer  $V_2O_5$  on  $TiO_2$  catalysts may have also good activity and selectivity if the support area is sufficiently deactivated.<sup>89</sup>

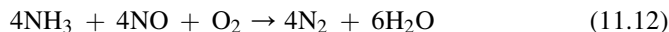


Reactions in similar conditions allow the syntheses of aromatic anhydrides and of aromatic nitriles by oxidation and ammoxidation of toluenes and xylenes over vanadia-based catalysts such as  $V_2O_5/TiO_2$  or  $V_2O_5/Al_2O_3$ .<sup>75</sup>



### 11.2.3.3 Vanadia catalysts for $NO_x$ selective catalytic reduction

Another example of oxides supported on oxide catalysts is that for the SCR of  $NO_x$  by ammonia. DeNO<sub>x</sub>ing of oxygen-containing waste gases from stationary sources (power plants, nitric acid plants) can be achieved efficiently by using the so-called Selective Catalytic Reduction (SCR) process,<sup>90</sup> i.e. the Selective Catalytic Reduction using ammonia as the reductant, which is actually a selective oxidation of ammonia to nitrogen by oxygen and  $NO_x$ :



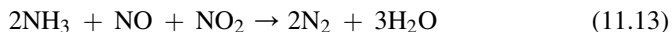
Industrial catalysts are constituted by  $V_2O_5-WO_3/TiO_2$  or  $V_2O_5-MoO_3/TiO_2$  monoliths.  $TiO_2$  in the anatase form supports a “monolayer” of  $V_2O_5$  and  $WO_3$  (or  $MoO_3$ ) deposited by impregnation. In general, the overall surface area of the catalysts is 50–100  $m^2/g$ , with  $V_2O_5$  virtual contents of 0.5–3% w/w and  $MoO_3$  or  $WO_3$  contents of 8–12% w/w. Typical reaction temperature is around 350 °C.

In all the cases, it has been found that the best catalysts contain nearly a full “monolayer” of vanadium-plus-tungsten (or molybdenum) oxides over the TiO<sub>2</sub>-anatase support. The amount of vanadium oxide is variable but generally very small (at least in the most recent catalyst formulations). Most authors believe that vanadium oxide species are nearly “isolated” and lie between polymeric tungsten or molybdenum oxide species.

The choice of TiO<sub>2</sub>-anatase as the best support for SCR catalysts seems to have at least two main reasons: (1) SO<sub>2</sub> is usually present in the waste gases of power stations, and in the presence of oxygen it can be oxidized to SO<sub>3</sub> and can give rise to metal sulfates by reacting with oxide catalyst supports. TiO<sub>2</sub> is only weakly and reversibly sulfated in conditions approaching those of the SCR reaction in the presence of SO<sub>2</sub> and the stability of sulfates on its surface is weaker than on other oxides such as alumina and zirconia. Consequently, TiO<sub>2</sub>-based industrial catalysts are partially and reversibly sulfated at their surface upon SCR reaction in the presence of SO<sub>2</sub>, and this sulfation even enhances the SCR catalytic activity; (2) It seems ascertained that supporting vanadium oxides on titania-anatase gives rise to very active oxidation catalysts, more active than those obtained with other supports. This has also been found for V<sub>2</sub>O<sub>5</sub>-TiO<sub>2</sub> (anatase) “monolayer” type catalysts for the selective oxidation of ortho-xylene to phthalic anhydride (see above). The reason for this activity enhancement can be found on the good dispersion of vanadium oxide on titania giving rise to “isolated” vanadyl centers and “polymeric” polyvanadate species and also on the semiconductor nature of titania, whose conduction band is not very far from the d-orbital levels of vanadyl centers, located in the energy gap. So, titania-anatase is an activating support, and gives rise to catalysts that are stable against sulphation or even improved upon sulphation.

Due to its high potential for NO<sub>x</sub> reduction under lean conditions, modification of the SCR process (using nontoxic urea instead of ammonia) is applied to mobile applications.<sup>91</sup> In this case, there are limitations to the catalyst volume that can be placed on-board. The operating conditions are also continuously changing in temperature and flow rate. Finally, the temperature window has to be enlarged with respect to stationary applications, in particular toward the low-temperature region.

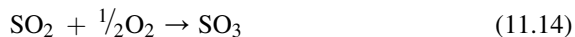
In relation to the last most challenging issue, it has been proposed to use the so-called Fast SCR reaction



in which NO<sub>2</sub> produced by oxidation of NO essentially substitutes for oxygen in the catalyst reoxidation step, allowing faster overall reaction rate, thus being applicable at much lower temperatures, such as 200–250 °C. This reaction is catalyzed efficiently by several materials like the same V<sub>2</sub>O<sub>5</sub>-WO<sub>3</sub>/TiO<sub>2</sub> catalyst, iron-exchanged zeolites and also purely acidic zeolites like H-ZSM5, and can be applied in particular to deNO<sub>x</sub>ing of automotive diesel engines' waste gases.<sup>92</sup>

### 11.2.3.4 Vanadia catalysts for SO<sub>2</sub> oxidation to SO<sub>3</sub>

The oxidation of sulfur dioxide to sulfur trioxide (sulfuric anhydride)



is performed industrially for many years mainly for the production of sulfuric acid in the so-called “contact process”.<sup>93</sup>

The reaction is moderately exothermic, being favored at low temperatures. With the best catalysts, reaction is carried out at 370–450 °C. At this temperature, the equilibrium is already very favorable, and thus operation at high pressures is not necessary. It then operates to 1.3–1.5 bar with dry air, so as to have excess oxygen (1:1 O<sub>2</sub>:SO<sub>2</sub>) to move to right the equilibrium but also to maintain the catalysts at oxidized state.

The modern industrial catalysts are based on V<sub>2</sub>O<sub>5</sub>–K<sub>2</sub>SO<sub>4</sub>/SiO<sub>2</sub>, which have an ignition temperature of 360 °C and normally operate at 400–430 °C, becoming unstable above 550 °C. A typical composition may be V<sub>2</sub>O<sub>5</sub> (6–8%) K<sub>2</sub>O (8–10%), Na<sub>2</sub>O (1–2%), SO<sub>3</sub> (20–30%), SiO<sub>2</sub> (55–65%), and is prepared by mixing a silica sol from potassium silicate with vanadyl sulfate and ammonia. The overall surface area is near 5 m<sup>2</sup>/g, with total pore volume of 0.5–0.6 ml/g. Commercial extrudates of these catalysts, whose shapes is optimized as a function of the reaction flow conditions to limit pressure drops, were shown in Figure 4.2. The more expensive Ce-containing catalysts V<sub>2</sub>O<sub>5</sub>–Cs<sub>2</sub>SO<sub>4</sub>/SiO<sub>2</sub> have a lower ignition temperature (320 °C) and operate continuously above 370 °C. The catalysts, whose active phase is liquid during the reaction, can work also for 10–15 years except for the first bed, which, by operating at higher temperatures (400–600 °C), should be replaced every 5 years. In the last bed (380–420 °C), the cesium-containing catalyst may be used to maximize conversion.

The process operates with several catalyst beds (usually four or five, 200–250 tons of catalyst) with intermediate cooling to dissipate the heat of reaction. The reactors are steel structures, of considerable size to allow high flow rates in spite of the reduced pressure. They are coated internally, in part, of brick, and with internal grids support the catalytic beds. The temperature of the beds decreases to follow the curve of the maximum speed. The heat exchangers are mostly external to the reactor, more rarely wedged in the structure of the reactor.

### 11.2.4 Oxide catalysts for oxidative dehydrogenations

Catalysts based on ferrite spinels, such as MgFe<sub>2</sub>O<sub>4</sub> and ZnFe<sub>2</sub>O<sub>4</sub> sometimes also containing Cr<sub>2</sub>O<sub>3</sub>, have been developed in the 1960s for the production of 1,3-butadiene by oxidative dehydrogenation of n-butenes, Eqn (11.4) (Oxo-D process developed by Petro-Tex<sup>94,95</sup>). The reaction is carried out at 550–600 °C in the presence of oxygen or air and steam, in an adiabatic fixed bed reactor. 65% conversion and a butadiene selectivity of 93% are obtained. The products mixture is quenched with water and butadiene is extracted with a solvent. Mg and Zn ferrites are medium acid–base catalyst. Iron ions at the surface of Fe<sub>2</sub>O<sub>3</sub>-based materials were found to be able to coordinate the π-type orbitals of the olefinic C=C double bonds. Allylic oxidation of

butene to methyl-allyl alkoxides on ferrite-based catalysts was facilitated by the stronger basicity arising from the MgO component, as well as by the reducibility of ferric ions. The elimination of such an intermediate produces 1,3-butadiene.<sup>96</sup>

The oxidative dehydrogenation (ODH) of light paraffins is more difficult, due to the lower reactivity of the CH bond in alkanes. ODH of paraffins separated by natural gas liquids (NGLs) is a way alternative to steam cracking to produce light olefins, allowing the use of natural gas instead of oil as the raw material. Isobutene, propene and ethylene can be produced from isobutane, propane and ethane.<sup>97,98</sup> The reaction temperature depends on the paraffin reactivity (350–550 °C). A typical redox element is present in most catalysts—frequently vanadium, but also molybdenum, chromium. However, elements that tend to moderate acidity are also frequently present such as magnesium in magnesium vanadate catalysts,<sup>99</sup> which have medium acido-basic properties, or potassium in V-K/Al<sub>2</sub>O<sub>3</sub> catalysts. Basic additives were found to decrease reactants conversion in selective oxidation reactions, sometimes strongly modifying the reaction path. Surface alkoxides are probably intermediate species also in this case, their generation being favored by the Lewis acidity of the redox metal site, which is moderated by alkali or alkali earth components. The moderating acidity component may increase selectivity, likely by decreasing the reactivity of the catalyst toward the olefin product. However, it has also some effect in favoring solid-initiated gas phase reactions.

Alternative catalysts for paraffin ODH do not contain redox elements. They are usually very basic materials (such as e.g., Li–Y<sub>2</sub>O<sub>3</sub>) working as initiators for gas phase radical reactivity.<sup>98</sup> The performances of light alkane ODH catalysts in terms of conversion/selectivity appear to be still too poor for developing industrial processes with ethane, propane and butane. Uhde commercialized an ODH process called STAR (Steam Active Reforming), which is actually a combination of steam dehydrogenation and oxidative dehydrogenation. The catalyst, both in the steam dehydrogenation step (without oxidant) and in the oxidative dehydrogenation step, is based on metals supported on Mg, Ca aluminates, promoted by a noble metal. The ODH step increases conversion and provides heat of reaction.<sup>100</sup>

### 11.2.5 Heteropolyacids for selective oxidations

Many polyoxometallates contain elements such as V, Mo or W, which are usually active in selective oxidation catalysis. They have indeed been studied for several oxidation reactions and are actually used in some industrial process. For several years, methacrylic acid can be produced commercially by oxidation of methacrolein (Eqn (11.7)) using catalysts based on CsH<sub>3</sub>PVMO<sub>11</sub>O<sub>40</sub>,<sup>101</sup> either unsupported or silica-supported, at ca 300 °C in the presence of steam.<sup>102</sup>

Quite recently, a process allowing the direct gas-phase selective oxidation of ethylene to acetic acid has been developed using a Pd- and Te-containing heteropolyacid catalyst based on silica-supported H<sub>4</sub>SiW<sub>12</sub>O<sub>40</sub>.<sup>103</sup>



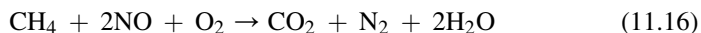


Typical reaction conditions are 130–230 °C, 0.1–1.0 MPa, and  $\text{C}_2\text{H}_4/\text{O}_2 = 5\text{--}15$ . Pure acetic acid is obtained after separation.

### 11.2.6 Zeolite catalysts for the abatement of $\text{NO}_x$ and $\text{N}_2\text{O}$

Zeolites containing transition metal centers have redox activities and find interesting catalytic activity in several oxidation reactions. They are practically used for several slightly different reactions for the abatement of  $\text{NO}_x$  (DeNOxing) in flue gases. Several metal-containing zeolites are used for the SCR of  $\text{NO}_x$  by ammonia in automotive waste gas treatments (Eqns (11.12) and (11.13)).<sup>92,104</sup>

The denitrification of waste gases can be obtained also using methane or other hydrocarbons as a selective reductant of  $\text{NO}_x$  to nitrogen:

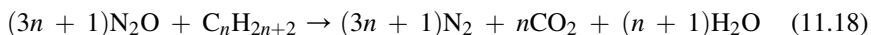


This reaction represents formally an oxidation of methane by  $\text{O}_2$  and  $\text{NO}_x$ . Co-containing zeolites, such as Co-MFI and Co-FER, were found by Armor<sup>105</sup> to be particularly active for this reaction. Parallel-flow reactor, IR and UV–vis characterization studies allowed to reveal a high complexity in active Co-FER, Co-MFI and Co-MOR catalysts,<sup>106–109</sup> with the presence of bivalent and trivalent cobalt and protonic sites both in the inner cavity and in the outer surfaces.

Iron zeolites have been found to be very efficient for the abatement of nitrogen oxides in a number of different configurations.<sup>110</sup> Fe-ZSM5 is active in the abatement of  $\text{NO}_x$  by reacting with ammonia catalyzing efficiently the so-called Fast SCR reaction, i.e. the reduction of  $\text{NO} + \text{NO}_2$  mixture by ammonia (Eqn (11.13)).<sup>111</sup> This reaction can be useful in deNOxing flue gas from diesel cars after a first step of oxidation of  $\text{NO}$  to  $\text{NO}_2$ .<sup>112</sup> Cu-ZSM5 is also active for this reaction.<sup>113</sup> However, Fe-ZSM5 can also catalyze the normal  $\text{NH}_3$ -SCR reaction, and used for this purpose in the so-called EnviNOx technology to abate  $\text{NO}_x$  from waste gases of nitric acid plants.<sup>114</sup> On the other hand, Fe-ZSM5 is also useful to abate  $\text{N}_2\text{O}$  in two different modes: simple decomposition at 425–525 °C, formally:

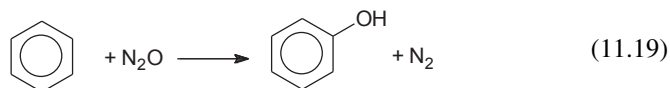


which is favored by the copresence of  $\text{NO}_x$  ( $\text{NO} + \text{NO}_2$ ), or reduction by hydrocarbons



at c. 350–400 °C (Uhde de $\text{N}_2\text{O}$  process), which is instead unfavored by the copresence of  $\text{NO}_x$ .<sup>115,116</sup>

The activity of Fe-zeolites in catalyzing reactions of  $\text{N}_2\text{O}$  as an oxidant were first discovered by Russian researchers<sup>117</sup> that collaborated to the development of an industrial process (AlphOx<sup>TM</sup><sup>118</sup>) for the hydroxylation of benzene to phenol



performed at 350 °C using Fe-ZSM5 catalysts. This reaction, useful when integrated with N<sub>2</sub>O by-production in adipic acid plants, may also be viewed as a reduction of N<sub>2</sub>O by benzene. The sites for N<sub>2</sub>O activation are reported to be the same in the two reactions, where two Fe<sup>2+</sup> species are oxidized to Fe<sup>3+</sup> and the oxygen of N<sub>2</sub>O is deposited on the surface in the form of an active oxide anion.<sup>119,120</sup> Fe-ZSM5, containing samples (both prepared by isomorphous substitution or post-synthesis ionic exchange), usually present a complex mixture of Fe sites with different nuclearity (from isolated to oxidic clusters, passing through dimers and small oligomers), different oxidation (Fe<sup>2+</sup>, Fe<sup>3+</sup> and maybe even Fe<sup>4+</sup>) and coordination state. This complexity is the main reason for the low reproducibility of the results reported in the open literature, and thus for the different conclusions about the nature of the active sites reached by different research groups.<sup>119,121</sup>

## 11.2.7 Oxide catalysts for total oxidations

### 11.2.7.1 Catalytic combustion for VOC abatement

In spite of their lower combustion activity with respect to noble metal-based catalysts, base metal-based catalysts, such as e.g., MnO<sub>x</sub>/Al<sub>2</sub>O<sub>3</sub>,<sup>122</sup> are commercially used for catalytic combustion of oxygenated VOCs. Manganese-based catalysts, such as unsupported Mn<sub>3</sub>O<sub>4</sub>, as well as Mn oxides supported on carriers such as titania, zirconia, silica, aluminate spinels, β-aluminas, perovskites, medium-low surface area alumina, the last being likely the preferred one.

While noble metals are normally used for hydrocarbons combustion, base metal oxides can be used when the VOC to be destroyed are organic oxygenates or N-compounds. Among oxides that are active in VOC catalytic combustion<sup>123,124</sup> manganese, copper and chromium-containing materials, and/or their combination, such as copper chromites, maybe doped with small amounts of Pt, seem to be the most active. Base metal oxides can also be used for CO catalytic oxidation, such as copper chromite catalyst.<sup>125</sup>

### 11.2.7.2 Soot oxidation catalysts

A number of nonnoble metal compositions were found to be active as catalysts for the oxidation of soot in catalyzed diesel filters. Among them, Cs-V mixed oxides (CsVO<sub>3</sub>, Cs<sub>4</sub>V<sub>2</sub>O<sub>7</sub>), LaCrO<sub>3</sub> perovskites as well as Co, Cr, Cu, Mn, Fe containing

spinels.<sup>126</sup> Ceria-based materials, such as ceria–zirconia doped with Nd, also act as combustion catalysts for soot.<sup>127</sup> It has been shown that  $\text{La}_{1-x}\text{Sr}_x\text{CoO}_3$  and  $\text{La}_{0.9}\text{Sr}_{0.1}\text{MnO}_3$  perovskites may substitute Pt both from catalytic Diesel Particulate Filters (DPF) and Lean  $\text{NO}_x$  Traps, allowing NO-to- $\text{NO}_2$  conversions and  $\text{NO}_x$  reduction with performance comparable to that of commercial platinum-based systems.<sup>128</sup>

### 11.2.7.3 Base-metal wet-oxidation catalysts

Considerable amount of research has been performed on Catalytic Wet Oxidation (CWO) including Catalytic Wet-Air Oxidation (CWAO) to overcome the other costly, high-pressure, energy-intensive technics for the abatement of organic pollutants in water. The number of different industrial waste/process streams requiring organics removal and the diversity of organic and inorganic compounds present in these streams has resulted in the investigation of a wide range of homogeneous and heterogeneous catalysts over the last three decades.<sup>129–131</sup> Homogeneous catalysts for CWAO are usually transition metal cations, such as Cu and Fe ions. Industrial homogeneous CWAO processes have been developed at the industrial level.<sup>131,132</sup> For practical reasons, solid catalysts are more useful to avoid the need of a separation step of the catalyst, and pollution of the waste. Most of the active catalysts proposed for CWAO are solids containing either noble metals (Pt, Ru) or transition metal cations (Cu, Co, Mn, Fe) as the active redox phases. Frequently, such active phases are supported on alumina or carbon carriers and may contain ceria additives.<sup>133</sup> Activated carbon may also act as a catalyst although it may be consumed by oxidation. Typical reaction conditions allowing, e.g., phenol conversion >90–95% and TOC or COD removal >80–90% are  $T = 100 \div 200$  °C and  $P_{\text{O}_2} = 0.3 \div 3.5$  MPa,  $t = 1 \div 3$  h.

A significant increase of toxicity has been observed during the early stages of phenol oxidation<sup>134</sup> caused by the formation of hydroquinone and *p*-benzoquinone as intermediates, the former showing the highest toxicity. Acetic acid is formed as a final intermediate during CWO of phenol using several different catalysts. Because acetic acid is a difficult compound to remove via CWO, it has a negative impact on phenol TOC conversions. First order in phenol has usually been obtained together with 0.5-order in oxygen.

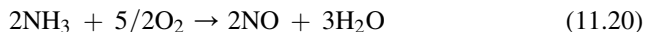
A relevant problem in heterogeneous CWAO is associated to the leaching of the active metal species, which can produce a heterogeneous/homogeneous catalysis. Leaching, however, pollutes the wastewater and results in the progressive loss of catalytic activity of the solid catalyst. This phenomenon is evident mostly for supported transition metal catalysts.

Metal oxide catalysts are very active but unstable (dissolution). In order to reduce leaching, the catalytically active compounds have to be incorporated into a lattice of catalyst support. If this is not feasible, the catalytic active phase should consist of precious metals.

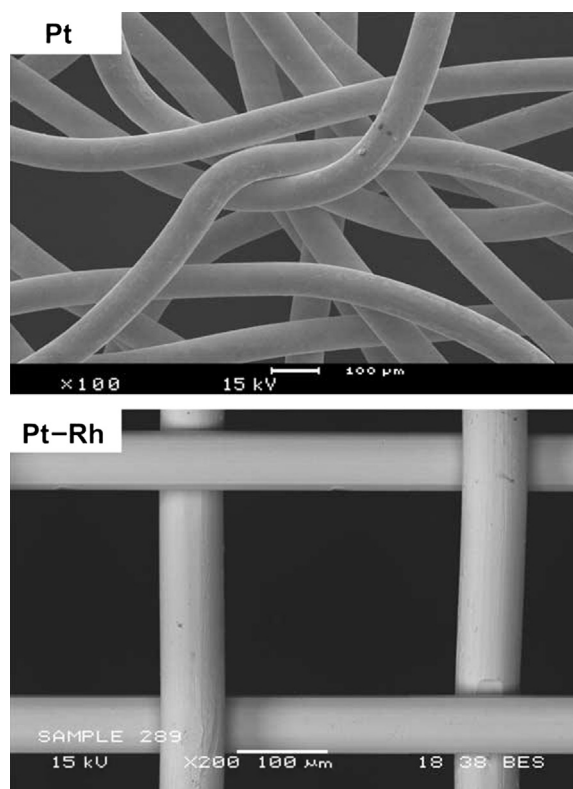
## 11.3 Metal catalysts for oxidation reactions

### 11.3.1 Metal gauzes for selective oxidation catalysis

While metal catalysts are most usually in the form of bulk or supported powders, in few cases they are used in form of gauzes.<sup>135</sup> Gauzes allow very short contact time and high-temperature applications. The most typical case is that of ammonia oxidation by air to nitrogen monoxide,



performed industrially as the first step in the production of nitric acid (Ostwald process).<sup>136,137</sup> The reaction is carried out at 800–1000 °C, 0.8–12 bar with 10–14% NH<sub>3</sub> in air using Pt-based gauze pads<sup>138</sup> (Figure 11.6<sup>139</sup>) in order to reduce the contact time to limit the further reaction of NO with ammonia and oxygen, to N<sub>2</sub>. To reduce Pt loss as volatile PtO, other metals such as Rh and Pd are usually alloyed to Pt.



**FIGURE 11.6**

Scanning electron micrographs of the knitted Pt gauze and woven Pt–Rh gauze.

*Reprinted with permission from Ref. 139.*

The typical composition may be 5–10% Rh, 0–15% Pd, sometimes 0.5% Ru. Micro-addition of other elements such as B and Y are reported to limit crystal growth, with a positive effect on catalytic activity.<sup>140</sup> The gauzes, of the woven- or the knitted type, are produced using 0.06–0.07 mm diameter wires. The same reaction is used as a first step of the synthesis of hydroxylamine, an intermediate in the production of Nylon 6.<sup>141</sup>

Similar catalysts and reactors are used for the Andrussow process for methane ammoxidation to hydrocyanic acid<sup>142,143</sup>:

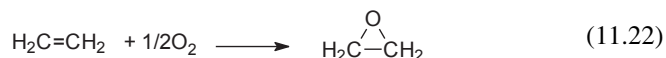


realized at c. 1100 °C using platinum–rhodium-based gauzes.

Silver gauzes may also be applied in the BASF process for the synthesis of formaldehyde (see next chapter).

### 11.3.2 Silver catalysts for selective oxidations

Several metal catalysts find application for selective oxidation of hydrocarbons. Among the largest productions, ethylene selective oxidation to ethylene oxide (EO)



is performed over silver-based catalysts. Typical industrial catalysts may contain 8–15% by weight of silver deposited over low surface-area alpha-alumina, 0.5–1.3 m<sup>2</sup>/g with a porosity of about 0.2–0.7 cc/g. The catalyst may contain several promoters such as 500–1200 ppm alkali metal (mostly cesium), 5–300 ppm by weight of sulfur as cesium or ammonium sulfate, 10–300 ppm of fluorine as ammonium fluoride or alkali metal fluoride.<sup>144</sup> Similar catalysts are used when oxidation is performed with air or with oxygen at 250–280 °C, ~20 bar.

The mechanism of the selective (ep)oxidation of ethylene to ethylene oxide has been the object of many studies. The subject has been reviewed by Ozbeck and Van Santen.<sup>145</sup> After original proposals that epoxidation might be due to molecular adsorbed species of the superoxide type,<sup>146</sup> today authors agree that a high oxygen loading is needed for high selectivity to EO, obtained when a surface oxide is formed. A weakly bound (electrophilic, O<sup>δ+</sup>) surface oxygen is suggested to enable selective epoxidation by attacking the C=C π-type electrons. In contrast, a strongly bound (nucleophilic, O<sup>δ-</sup>) surface oxygen is supposed to give rise to combustion to CO<sub>2</sub> by attacking the CH bonds. Selective ethylene epoxidation was proposed to follow an Eley–Rideal mechanism whereas the nonselective combustion follows a Langmuir–Hinshelwood mechanism, both belonging to the Mars–Van Krevelen type.

Actually, two different paths to EO should exist. One of them, less selective and prevailing at low oxygen coverage, should occur through an oxometallacycle surface

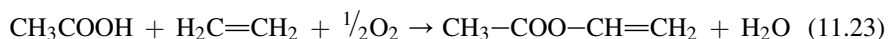
intermediate, formed by interaction of ethylene with both a silver and an electrophilic oxygen species: it should produce both EO and acetaldehyde (usually found as a minor byproduct). The other is a direct epoxidation mechanism, occurring by interaction of the ethylene with the electrophilic oxygen only, highly selective and found only at very high oxygen coverage.

Silver, either in the form of bulk crystals (granules with 30–35 cm<sup>2</sup>/g surface area<sup>147</sup>) or of gauzes (high purity silver, <100 ppm trace metals, with 0.1–2 mm sieve, 1.3–1.8 g/cm<sup>3</sup> bulk density<sup>148,149</sup>), is also used for methanol oxidative dehydrogenation to formaldehyde with high-temperature processes different from that considered in Chapter 11.2.1.1. The reaction, which is actually a combination of the oxidative dehydrogenation (Eqn (11.1)) and the pure dehydrogenation, takes place in the presence of oxygen and steam at 620–700 °C, the active species being considered to be adsorbed oxygen on silver metal.<sup>150</sup>

In the case of the BASF process, the reactor bed consists of a thin layer of electrolytic silver grains 2–3 mm thick sandwiched between silver gauzes.<sup>151</sup>

### 11.3.3 Other noble metal-based catalysts for gas-phase selective oxidations of organics

Vinyl acetate monomer is produced by the catalyzed, vapor phase reaction of acetic acid with ethylene and oxygen



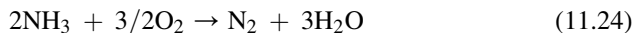
in a fixed-bed tubular reactor using a supported noble metal catalyst. The reaction is carried out at 175–200 °C and 5–9 bar pressure usually over silica supported Pd–Au bimetallic catalysts promoted with potassium acetate,<sup>152</sup> like Noblyst<sup>®</sup> EJK 3017 catalyst from Evonik.<sup>153</sup> More recently, a new catalyst with a similar composition has been developed by Johnson Matthey to be used in the new fluidized-bed ‘Leap Process’.<sup>154</sup>

### 11.3.4 Noble metal catalysts for selective oxidations in the liquid phase

A number of selective oxidation reactions are performed in the liquid phase with heterogeneous catalysts in the field of fine chemistry. They involve frequently quite complex organic molecules, sometimes containing several functional groups only one of which should be involved in the reaction. Most of the catalysts used in the industry are platinum-group metals (mainly Pt, Pd, Ru, frequently doped by Bi) supported on carbon, using few bars of oxygen, air or nitrogen-diluted air (depending, among other things, from solvent flammability) or even 30% hydrogen peroxide at 30–60 °C.<sup>155</sup> These catalytic systems in particular allow the selective oxidative dehydrogenation of alcohols to carbonyl compounds or to carboxylic acids, without oxidizing C=C double bonds.

### 11.3.5 Metal catalysts for ammonia selective catalytic oxidation to nitrogen

In recent years, the selective catalytic oxidation of ammonia to nitrogen



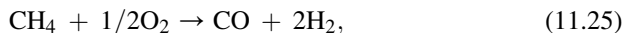
became an important reaction to limit ammonia slip from processes such as the Selective Catalytic Reduction of  $\text{NO}_x$  by ammonia (in the treatment of waste gases from power stations as well as from diesel engine aftertreatment) as well as from the combustion of biomass-derived gases. Several catalysts have been studied in the academic research, containing base and noble metal catalysts.<sup>156,157</sup> Roughly speaking, while some base metal oxide catalyst has activity only at high temperature but with very high selectivity to  $\text{N}_2$ , most platinum group metal catalysts have activity at very low temperature but low selectivity to  $\text{N}_2$ , with additional production of  $\text{N}_2\text{O}$  and  $\text{NO}_x$ . Haldor Topsøe<sup>158</sup> patented a process for catalytic low temperature oxidation of ammonia in an off-gas at a temperature of 200–500 °C. The catalysts used were silica supported Cu, Co and Ni oxides doped with small amount of noble metals (100–2000 ppm). The selectivity to nitrogen can be improved by sulfating the catalysts during or prior to contact with ammonia containing gas from 26–53% to 78–99%. On the other hand, in a recent publication of Topsøe<sup>159</sup> supported Pd and Pt “ammonia slip catalysts” were found to allow reducing ammonia slip and  $\text{N}_2\text{O}$  reduction from automotive diesel engine below 10 ppm.

A patent from BASF reports on a layered catalyst constituted by gamma-alumina (60–300  $\text{m}^2/\text{g}$ ) with 0.5–4% wt of Pt and 0.5–4% of vanadia all deposited over the surface of a monolytic structure, ceramic or metallic. The reactivity is studied with a 15 ppm  $\text{NH}_3$  containing feed, 70,000 VHSV at 275 °C.<sup>160</sup> A more recent patent from BASF concerns an ammonia selective oxidation catalyst containing a zeolite (including mordenite, ferrierite, zeolite Y or beta zeolite), from about 0.02 wt% to about 0.20 wt% of a precious metal, e.g., platinum, and a base metal, preferentially copper oxide. Typically, the amount of base metal compound added to the ammonia oxidation catalyst ranges from about 5 wt% to about 16 wt% when zeolite Y is used and from about 3 wt% to about 8 wt% when mordenite, beta, ferrierite or ZSM5 zeolites are used.<sup>161</sup>

To overcome the problem of low selectivity of noble metal catalysts, dual-layer catalysts have been developed,<sup>162</sup> where a noble-metal ammonia oxidation catalyst (e.g.,  $\text{Pt}/\text{Al}_2\text{O}_3$ ) is covered by an SCR catalyst. Thus,  $\text{NO}_x$  produced on the ammonia oxidation catalyst are reduced by the incoming ammonia in the SCR catalyst layer.

### 11.3.6 Metal catalysts for methane partial oxidation to syngas

The catalytic partial oxidation (CPO) of methane,



has received considerable attention for synthesis gas production<sup>163</sup> because it provides close to 100% methane conversion and >90% synthesis gas yields in

millisecond contact times.<sup>164</sup> Compared to contact times of seconds in a steam reformer, CPO reactors can be three orders of magnitude smaller processing the same amount of synthesis gas. In addition to reduced investment costs, methane CPO supplies a H<sub>2</sub>/CO ratio of 2/1, which is favorable for methanol or Fischer–Tropsch synthesis. Alternative applications are to produce hydrogen in refineries and filling stations.<sup>165</sup>

Ni- and Rh-based catalysts have been identified to be the most promising CPO catalysts,<sup>166,167</sup> the support being a refractory ceramic material such as  $\alpha$ -Al<sub>2</sub>O<sub>3</sub>, magnesia or zirconia. In contrast to supported Ni catalysts, however, Rh-based catalysts display both high activity and stability during the catalytic partial oxidation of methane to synthesis gas. Rh catalysts also show higher resistance to carbon deposition and to sulfur poisoning. However, due to the high cost of Rh, its use for commercial application is one of the key issues. Ni catalysts deactivate due to metal evaporation and formation of NiO and NiAl<sub>2</sub>O<sub>4</sub>. Pt and Ir also showed high stability, but significantly lower conversions and selectivities compared to Rh catalysts. Rapid deactivation was also observed in case of Pd coated monoliths as a result of coke deposition.

Results clearly pointed out that the final performances of the supported Rh catalysts are strongly influenced by the conditioning procedure. Important processes of reconstruction of Rh particles arising from their interaction with the reacting mixture and surface C-containing species certainly occur.<sup>168,169</sup> Data also suggest that several elements, such as cobalt, may act as promoters of Rh/MgO catalysts for CPO.<sup>170</sup> Several processes have been developed at the nearly industrial stage, such as CONOCO PHILLIPS COPOX™ and ENI SCT-CPO (Short Contact Time - Catalytic Partial Oxidation).<sup>165</sup>

### 11.3.7 Metal catalysts for CO oxidation

The oxidation of CO to CO<sub>2</sub>,



is applied in the purification of waste gases as well as in the purification of hydrogen. The preferential oxidation of CO in the presence of hydrogen (PROX) represents an important step in the synthesis of pure hydrogen for application in low temperature fuel cells.<sup>171</sup> Noble metals are active for this reaction at very low temperature (100–200 °C).

Commercial catalysts are typically based on Pt/ $\gamma$ -Al<sub>2</sub>O<sub>3</sub>. The commercial SELECTOXO™ process, developed in the early 1960s by Engelhard, uses a catalyst<sup>172</sup> containing from 0.3 to 0.5% platinum and 0.03% iron dispersed on alumina-support tablets or pellets by wet impregnation of the alumina with a solution of platinum and iron salts. The SELECTOXO™ catalyst material would be used at temperatures not higher than 125 °C and that a higher drying temperature would detrimentally affect the platinum. Mitsubishi Gas<sup>173</sup> disclosed the use of Pt with copper, as well as Pt with Mn, Ni or Co, for a PROX catalyst that is applied to fuel cells. In a more recent patent from Engelhard (now BASF), a catalyst suitable for a

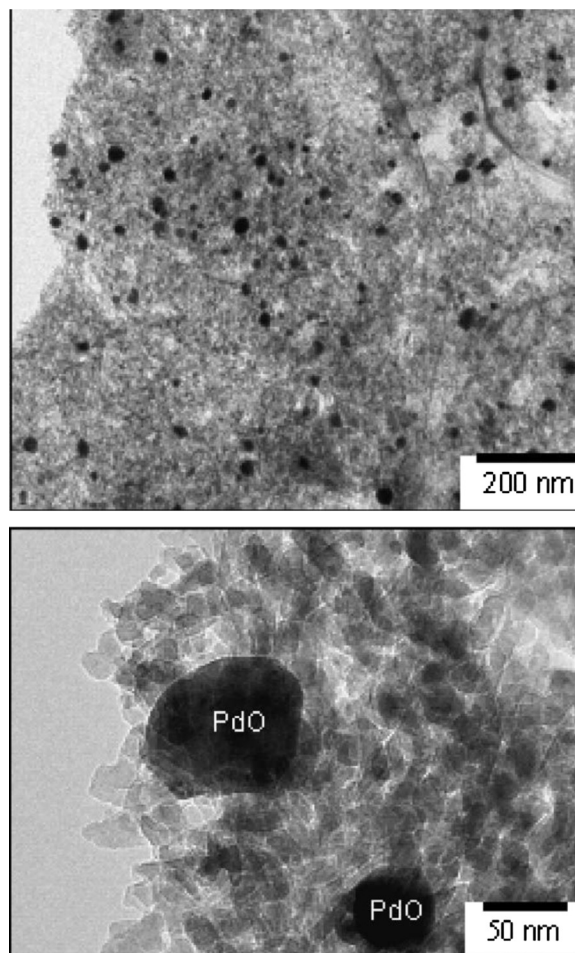


preferential oxidation is described where platinum is present in an amount of about 2%, copper is present in an amount of about 8%, and iron is present in an amount of 0.10–1.5% by weight.<sup>174</sup> K is also reported to act as a promoter of Pt/Al<sub>2</sub>O<sub>3</sub>.<sup>175</sup> Topsøe sells the DNO catalyst based on V<sub>2</sub>O<sub>5</sub>/WO<sub>3</sub>/TiO<sub>2</sub>/Pd for CO oxidation, working in the 200–450 °C temperature range. According to the producers, the synergy of vanadium and tungsten oxides and palladium provides the DNO catalysts with a uniquely high oxidation activity. The highly porous V<sub>2</sub>O<sub>5</sub>/WO<sub>3</sub>/TiO<sub>2</sub> combined with deep-impregnation of palladium furnishes the DNO catalysts with an unsurpassed stability, also when operating in sulfur- and chlorine-containing gases, e.g., flue gas from biomass-fired boilers or landfill- and digester gas.<sup>176</sup>

Supported gold was quite recently discovered to act as excellent catalyst for PROX as well as for the low temperature (200 K) CO oxidation in waste gases.<sup>177–179</sup> The very high catalytic activity appears when gold particles smaller than 30–50 Å are prepared, corresponding to a contraction of the Au–Au interatomic distance, and this seems to be independent from the support used.<sup>180</sup> In spite of this, it seems that the catalytic activity do strongly depend on the support. Au/TiO<sub>2</sub> seems to be the most active in CO oxidation while Au/Al<sub>2</sub>O<sub>3</sub> seems to be usually considered to be poorly active.<sup>181</sup> However, in the presence of hydrogen the activity of both Au/Al<sub>2</sub>O<sub>3</sub> and Au/TiO<sub>2</sub> are reported to be significantly promoted and may become similar.<sup>182,183</sup> Several other semiconducting supports besides titania such as zirconia, ceria and iron oxide and their mixtures have been tested and found acting as activators of gold with respect to isolating supports such as silica and alumina. Gold catalysts present a very high activity at low temperatures. These systems are strongly dependent on the preparation method and in general present deactivation problems and penalization of the selectivity by hydrogen oxidation at temperatures higher than 80 °C.

### 11.3.8 Combustion catalysts for energy generation

Methane, natural gas, syngas or hydrogen combustion for energy generation may be performed in the presence of a catalyst to reduce temperature as well as NO<sub>x</sub> formation. Palladium-based catalysts appear to be the most active catalysts in methane combustion.<sup>184–186</sup> Alumina is the most largely used support, although addition of ceria is reported to be beneficial.<sup>187</sup> Zirconia-<sup>188</sup> and zirconia–ceria<sup>189</sup>-supported catalysts have also been investigated. Despite there are still some divergences in literature concerning the most active state of the Pd-based catalysts for CH<sub>4</sub> oxidation, e.g., metallic Pd, PdO or a mixed-phase Pd<sup>0</sup>/PdO<sub>x</sub>, the active phase of Pd oxidation catalysts is mostly identified as PdO, which is known to decompose into Pd metal in the range 650–850 °C, depending on oxygen pressure and reactive gas mixture. In Figure 11.7<sup>190</sup> the Transmission Electron Microscopy images of a 5% Pd/Al<sub>2</sub>O<sub>3</sub> combustion catalyst, showing quite uniform PdO particles, are reported. The transformation of PdO into Pd is reported to negatively affect catalytic reaction by lowering conversion, CH<sub>4</sub> combustion activity being reversibly restored upon reoxidation of Pd to PdO. However, it is evident that Pd and PdO are not the

**FIGURE 11.7**

Transmission electron microscopy images of a 5% Pd/Al<sub>2</sub>O<sub>3</sub> methane combustion catalyst.

*Reprinted with permission from Ref. 190.*

only species present on the catalysts, and that Pd catalysts work also in conditions where Pd metal is the predominant species. Recent surface science studies showed that the chemistry of these systems is indeed very complex.<sup>189–192</sup> The combination of Pd/Al<sub>2</sub>O<sub>3</sub> with other active metallic component, such as e.g. Rh, Cu, Ni, may significantly improve low-temperature performances.

### 11.3.9 Noble metal catalysts for total oxidation for VOC abatement

Catalytic combustion<sup>193</sup> represents the alternative to thermal incineration to destroy highly concentrated VOC-containing streams, allowing heat recovery. The

advantages are represented by the lower  $\text{NO}_x$  emissions and the lower amount of fuel needed, both associated with the lower combustion temperature obtained in the presence of catalysts, i.e. 300–500 °C. However, also in this case, the heat can be recovered and utilized, but is obviously at lower temperature. The drawbacks are represented by a more complex reactor design, by the cost of the catalyst and sometimes by the relatively low catalyst lifetime. In fact, combustion catalysts can be deactivated in particular when the feed contains sulfur, nitrogen and chlorine. In this case, either regeneration procedures are needed, or the lifetime of the catalyst is low. Moreover, partial oxidation of the organic contaminants can occur and this can give rise to low concentration of partially oxidized species in the outstream that can be even more toxic than the original contaminant.<sup>194</sup> Catalyst producers propose different catalyst formulations for combustion of different contaminants.<sup>195</sup> Most of commercial combustion catalysts are based on supported noble metals,<sup>196</sup> which are needed to burn refractory compounds such as hydrocarbons. Alumina is the most frequent support, due to its stability at the required temperature. This is the case of the CK-304 and CK-307 catalysts (Pd/ $\text{Al}_2\text{O}_3$  and Pt/ $\text{Al}_2\text{O}_3$ , respectively, reported to be useful for most applications) from Topsøe.<sup>176</sup> Johnson Matthey PURAVOC catalysts contain 0.3–0.5% wt noble metal, Pt, Pd, Pt–Pd, or Rh, on alumina. The BASF RO-25 catalyst, specific for VOC combustion, is reported to contain 0.5% Pd on alumina, with 109  $\text{m}^2/\text{g}$ .<sup>197</sup>

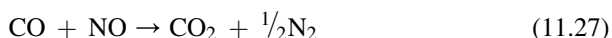
### 11.3.10 Noble metals for catalytic wet oxidation

As already said, catalysts based on supported ruthenium and platinum, on alumina, titania, ceria–zirconia, etc. are reported to be very active in the catalytic wet oxidation of organic pollutants, such as phenols, carboxylic acids, anilines and mixed pollutants in industrial wastewaters.<sup>133</sup> In fact, existing commercial processes employ supported noble metal catalysts.<sup>129–131</sup> It would be advantageous to design a catalyst that can be employed for the treatment in single-pass reactors with a minimum lifetime over 500 h. To improve the performances, a step constituted by an AC-adsorbing bed, where the organics are removed from the wastewater stream and preconcentrated, may be useful, as in the CALIPHOX process. In any case, the primary goal of CWAO should be to convert organics into products more amenable to biological treatment; complete oxidation may be too expensive.

### 11.3.11 Catalysts for the aftertreatment of engines' waste gases

#### 11.3.11.1 Catalytic converters

The aftertreatment of Otto-cycle gasoline engines is satisfactorily achieved by the so-called Three-Way Catalysts (TWC), a technology developed after the 1970s allowing the efficient abatement of unburnt hydrocarbons (HC), CO, and  $\text{NO}_x$ . As it is well known, such catalysts are active for the reactions of CO and hydrocarbon total oxidation and also for the reaction



The original TWC composition was Pt–Rh on alumina, deposited on ceramic monoliths. In recent years,<sup>198,199</sup> typical TWC formulations have included Pd as the active metal, ceria–zirconia as promoters according to the Oxygen Storage Capacity of ceria and the thermal stability of zirconia, and alumina as support as well as other minor components mainly present in order to enhance thermal stability. Perovskite materials can also be present to help limiting of noble metal sintering. The use of the different noble metal formulation (Pt–Rh, Pd–Rh, Pd only) is due in part to purely economic reasons, resulting from the high cost and scarcity of Rh and from the variable relative prices of Pd and Pt. The addition of gold could improve activity at low temperature.<sup>200</sup>

Improvements in catalyst technologies and optimized engine calibrations allowed a substantial reduction of noble metal content in the converter, now even less than 1 g. Zoning also allows to optimize the use of noble metals, with higher loading on the front of catalyst, to aid light-off, and lower amounts in the rear portion where mostly Rh is deposited.

### 11.3.11.2 Catalysts for diesel engines aftertreatment

Several different systems are under development to reduce the emissions of NO<sub>x</sub>, hydrocarbons and particulate matter from diesel and other lean burn engines. Among these, the SCR systems (Selective Catalytic Reduction of NO<sub>x</sub> by ammonia or urea), and ammonia slip catalysts have already been cited.

Pt-based or Pt-Pd-based porous ceramic wall-flow DPFs are largely used today to abate particulate matter from diesel engine waste gases.<sup>104,201</sup> At quite high car speeds, these systems allow “passive regeneration” behavior, where NO<sub>2</sub> is formed from NO and oxygen and oxidizes soot, by reducing to nitrogen. In general, periodical “active regeneration” steps are also needed, where oxygen is fed allowing particulate matter burning at 550–600 °C.

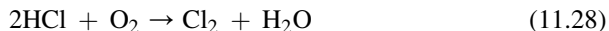
Pt-Ba/Al<sub>2</sub>O<sub>3</sub> or Pt-K/Al<sub>2</sub>O<sub>3</sub> sorbents-catalysts, typically containing ~1% Pt and ~8% Ba wt/wt, or ~8% K wt/wt, are used for “NO<sub>x</sub> storage-reduction” (NSR), a technology, first developed by Toyota in the early 1980s,<sup>202,203</sup> to reduce the NO<sub>x</sub> content in waste gases of lean-burn gasoline and diesel engines. A following evolution of this technology is the newer Diesel Particulate-NO<sub>x</sub> Reduction (DPNR) process, also developed by Toyota.<sup>204,205</sup> It allows the simultaneous abatement of both particulate and NO<sub>x</sub> due to the development of a new catalytic filter and a new diesel combustion technology.

The catalytic materials for both NSR and DPNR consist in porous ceramic filters coated with a catalytic layer constituted by a high surface-area support (typically  $\gamma$ -alumina), a noble metal (usually Pt) and an alkaline or alkali-earth metal oxide which presents a high NO<sub>x</sub>-storage capacity, most frequently Ba or K oxide. These catalytic systems work under cyclic conditions, alternating long lean phases (during which NO<sub>x</sub> are adsorbed on the catalyst in the form of nitrate/nitrites) with short phases in rich condition (during which the nitrate-nitrite species are reduced to molecular nitrogen). However, adsorption implies the conversion of NO into NO<sub>2</sub> catalyzed by Pt, which also catalyze the reaction to N<sub>2</sub> in the rich step.

## 11.4 Catalysts for oxidation reactions in the presence of chlorine

### 11.4.1 Catalysts for the oxidation of HCl to Cl<sub>2</sub>

Molecular chlorine is widely used for organic chlorinations. Aromatic and alkane chlorinations are substitution reactions with hydrogen, for which only half of the chlorine atoms are actually used to produce chloro-organics, the other half being lost as HCl and recovered as an aqueous solution hydrochloric acid. For this reason, it is useful to regenerate chlorine from hydrochloric acid. This has become urgent in recent years as the demand for chlorine is increasing significantly. There are different processes to do this. It can be done with an electrolytic process or via catalytic oxidation.



There are several versions of the catalytic oxidation process. The original version was the Deacon process, commercialized by Henry Deacon around 1870 using CuCl<sub>2</sub>/pumice in a fixed-bed reactor at 420–450 °C. A more recent version of this process, developed by Shell in the 1960s, was based on CuCl<sub>2</sub> on silica, to which alkali metal chloride and a rare-earth chloride are added, generating a molten salt in reaction conditions. In a later development from Mitsui Chemicals, Inc. (MT-Chlor process), a fluidized bed process for oxidation with pure oxygen that uses a Cr<sub>2</sub>O<sub>3</sub>/SiO<sub>2</sub> catalyst.

More recent processes were developed based on RuO<sub>2</sub> catalysts.<sup>206,207</sup> Sumitomo<sup>208</sup> developed RuO<sub>2</sub>/TiO<sub>2</sub> (rutile) catalysts working at 250–350 °C in a multi-tubular fixed-bed reactor cooled by a “heat transfer salt”, a liquid eutectic of salts. It operates with a ratio HCl/O<sub>2</sub> = 4, the unreacted HCl is recovered as hydrochloric acid or as hydrogen chloride (HCl dry gas), which can be recirculated in order to obtain complete conversion. Chlorine is dried with concentrated H<sub>2</sub>SO<sub>4</sub> and distilled to be separated by residual oxygen. Another recent process from Bayer uses RuO<sub>2</sub>/SnO<sub>2</sub>-cassiterite in an adiabatic reactor. The scientific literature reports about other oxide catalysts for this reaction.<sup>209</sup>

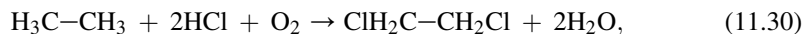
### 11.4.2 Catalysts for the oxychlorination of ethylene

The ethylene oxychlorination process to ethylenedichloride (EDC),



was born and is now used in the frame of the processes for the production of vinyl chloride monomer to recycle the hydrogen chloride produced in the cracking process of EDC. The catalyst used, CuCl<sub>2</sub>–KCl supported on γ-Al<sub>2</sub>O<sub>3</sub>,<sup>210</sup> is derived from that previously developed to produce chlorine from hydrochloric acid, Deacon process (see above). It may contain 5% copper with 100 m<sup>2</sup>/g. The reaction may be obtained with air or oxygen, in multitubular cooled reactors or in fluidized bed reactors.

A development in this area is the start of pilot plants of a new process of ethane oxychlorination



which has the advantage of a cheaper feedstock. The catalysts used at this stage are based on supported  $\text{CuCl}_2/\text{KCl}/\text{Al}_2\text{O}_3$  promoted by  $\text{LaCl}_3$  or  $\text{CeCl}_4$ .<sup>211</sup>

### 11.4.3 Catalytic combustion of dioxins and other chlorinated organics

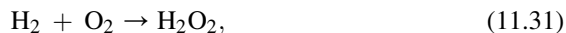
Particular care must be devoted to chlorided VOC's. In fact, chlorine is reported to poison noble-metal catalysts. The most common support for noble-metal VOC removal catalysts is alumina, although this support is often the cause for deactivation of the catalyst by halogen species, the formed aluminum halides blocking the active species. Therefore, much research has been made into the development of alternative supports for combustion catalysts. According to several authors, also base metals, including manganese, are poisoned by chlorine. In contrast to this, manganese based catalysts (such as the CK-395 catalyst from Topsøe,<sup>176</sup> and the HPM (Z-2) catalyst from Matrostech, which is >10%  $\text{Mn}_2\text{O}_3$  on alumina with 25–35  $\text{m}^2/\text{g}$ <sup>212</sup>), are suggested as special catalysts for chlorinated VOC destruction. Chromia-containing catalysts are reported to be specific for chloride hydrocarbons (e.g., the CK-305 catalyst from Topsøe<sup>176</sup>). Among the most important issues in this field, the catalytic combustion of chlorinated dioxins in waste incinerator waste gases. Catalytic dioxin abatement is usually performed<sup>213</sup> in the DeNOx SCR reactor. Typical SCR catalysts based on  $\text{V}_2\text{O}_5-\text{WO}_3-\text{TiO}_2$  are reported to be active for dioxin destruction. Vanadium-rich  $\text{V}_2\text{O}_5-\text{WO}_3-\text{TiO}_2$  catalysts (8% vanadium) are reported<sup>214</sup> to represent the catalyst component of Remedia<sup>®</sup> catalytic filters (W.L. Gore) working at 200 °C. Noble-metal based catalysts (such as CK-306 based on  $\text{Cr}-\text{Pd}/\text{Al}_2\text{O}_3$ ) from Topsøe<sup>176</sup> and EnviCat<sup>®</sup> HHC from Clariant (ex SüdChemie)<sup>215</sup> are also used to catalytically to destroy dioxins. These catalysts can be put as monolytic layers at the bottom of the downflow SCR reactor.<sup>216</sup>

---

## 11.5 Catalysts for the production and use of hydrogen peroxide

### 11.5.1 The direct synthesis of hydrogen peroxide

Hydrogen peroxide represents the most convenient alternative to oxygen or air to perform selective oxidations. The direct synthesis of hydrogen peroxide from hydrogen and oxygen,<sup>217</sup>



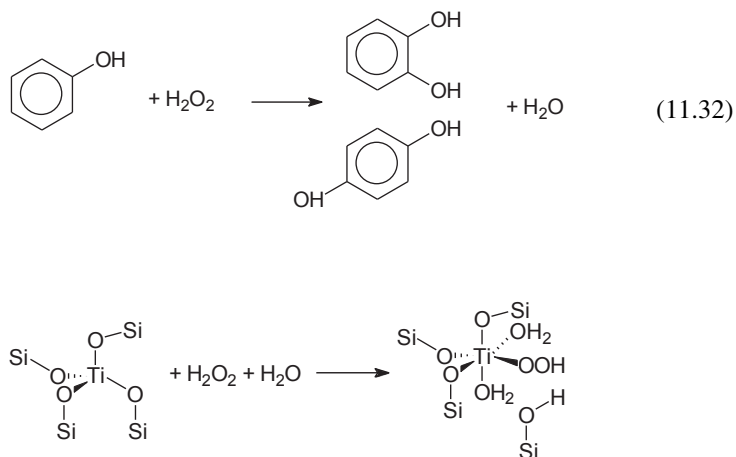
which could substitute the older anthraquinone-based process, may be performed over noble metal catalysts in a water or alcoholic medium. The reaction occurs in very

mild conditions, at room or even lower temperature and 1–20 bar. The catalysts described in the literature are based on noble metals or combinations thereof supported on a great variety of substrates such as alumina, silica, and carbon. Palladium is the most suitable active metal in most catalyst formulations. Acids are often incorporated into the reaction medium. According to Menegazzo et al.<sup>218</sup> in this case, metal dispersion is not a good property of the catalyst: the presence of less energetic Pd sites exposed at the surface of big particles allows better performances. Evonik–Headwaters developed a production plant for the direct synthesis of hydrogen peroxide coupled with propylene oxide production. The patents of these companies reveal that palladium nanoparticles deposited on carbon and an appropriate solvent (in general an alcohol), as well as the use of concentrations of hydrogen outside the flammability limits, are appropriate for industrial H<sub>2</sub>O<sub>2</sub> production.

### 11.5.2 Catalytic oxidations with H<sub>2</sub>O<sub>2</sub>

Some industrial processes allowing the selective oxidation of organics with H<sub>2</sub>O<sub>2</sub> as the oxidant and a heterogeneous catalyst have been developed after the synthesis by the ENI group of Ti-silicalite catalyst,<sup>219</sup> TS-1 is silicalite-1 (Al-free MFI zeolite) with Ti/(Ti + Si) c. 0.025, which is the maximum content to prevent segregation of TiO<sub>2</sub>. This material is an essentially hydrophobic molecular sieve with few hydrophilic Ti<sup>IV</sup> centers. This material is an excellent catalyst for the activation of H<sub>2</sub>O<sub>2</sub> toward selective oxidations. According to spectroscopic studies,<sup>219,220</sup> the activation of H<sub>2</sub>O<sub>2</sub> by TS-1 occurs with the formation of Ti-hydroperoxide species (Figure 11.8).

Ti-silicalite is used as the catalyst for the ENI process of hydroxylation of phenol to catechol and hydroquinone

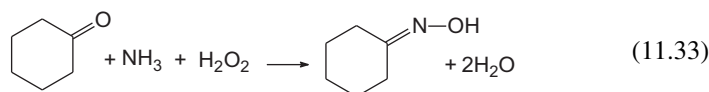


**FIGURE 11.8**

Activation of hydrogen peroxide at the Ti site of TS-1.

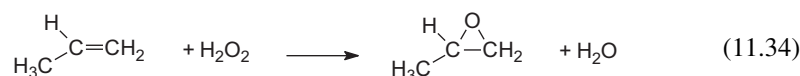
performed at c. 100 °C with excess phenol and hydrogen peroxide with TS-1 in slurry conditions.

An even more important application of TS-1 is in the process for production of cyclohexanone oxime (an intermediate in the synthesis of Nylon 6) by ammoximation of cyclohexanone with ammonia and hydrogen peroxide.<sup>221</sup>



The reaction is performed at 80–90 °C in aqueous tert-butanol in slurry conditions.

A third application of TS-1 catalyst is for the synthesis of propene oxide (Hydrogen Peroxide Propene Oxide, HPPO)<sup>222</sup>:



The industrial process developed by Uhde and Evonik performed <100 °C, propene at 30 bar and using methanol as solvent,<sup>223</sup> mainly with continuous stirred tank reactors. Very high conversion of hydrogen peroxide (>99%) and selectivities of H<sub>2</sub>O<sub>2</sub> to PO (95%) are obtained.

---

## References

1. Noritaka M, editor. *Modern heterogeneous oxidation catalysis design, reactions and characterization*. Wiley; 2009.
2. Duprez D, Cavani F, editors. *Advanced processes in oxidation catalysis*. World Scientific Pub Co Inc; 2014.
3. Centi G, Cavani F, Trifirò F. In: *Selective oxidation by heterogeneous catalysis*. 2nd ed. Springer London, Limited; 2012.
4. Bielanski A, Haber J. *Oxygen in catalysis*. New York: M. Dekker; 1991.
5. Doornkamp C, Ponc V. *J Mol Catal A Chem* 2000;**162**:19–32.
6. Šarić A, Popović S, Musić S. *Mater Lett* July 2002;**55**(3):145–51.
7. Jacob KT, Gupta P. *J Solid State Electrochem* 2013;**17**(3):607–15.
8. Bayer G, Wiedemann HG. *Thermochim Acta* 1976;**15**:213.
9. Comelli G, Dhanak VR, Kiskinova M, Prince KC, Rosei R. *Surf Sci Rep* 1998;**32**(5): 165–231.
10. Inderwildi OR, Lebedez D, Deutschmann O, Warnatz J. *J Chem Phys* 2005;**122**(3). art. no. 034710.
11. German E, Efremenko I. *J Mol Struct (Theochem)* 2004;**711**:159–65.



12. Takahashi S, Fujimoto Y, Teraoka Y, Yoshigoe A, Aruga T. *Chem Phys Lett* 2006;**433**: 58–61.
13. Warner JS. *J Electrochem Soc* 1967;**114**:68.
14. Werner JS. *J Electrochem Soc* 1967;**114**:68.
15. Kleykamp K. *Z Phys Chem NF* 1970;**71**:142.
16. Imbihl R, Demuth JE. *Surf Sci* 1986;**173**:395–410.
17. Leisenberger FP, Koller G, Sock M, Surnev S, Ramsey MG, Netzer FP, et al. *Surf Sci* 2000;**445**:380–93.
18. Klikovits J, Napetschnig E, Schmid M, Dubay O, Seriani N, Kresse G, et al. *Phys Rev B* 2007;**76**:045405.
19. Kan HH, Weaver JF. *Surf Sci* 2009;**603**:2671–82.
20. Westerström R, Weststrate CJ, Gustafson J, Mikkelsen A, Schnadt J, Andersen JN, et al. *Phys Rev B* 2009;**80**(125431):1–11.
21. Luo H, Park S, Chan HYH, Weaver MJ. *J Phys Chem B* 2000;**104**:8250–8.
22. Seriani N, Pompe W, Ciacchi LC. *J Phys Chem C* 2008;**112**:13623–8.
23. Punnoose A, Seehra MS, Wender I. *Fuel Process Technol* 2001;**74**:33–47.
24. Gorodetskii VV, Sametova AA, Matveev AV, Tapilin VM. *Catal Today* 2009;**144**: 219–34.
25. Elokhin VI, Matveev AV, Kovalyov EV, Gorodetskii VV. *Chem Eng J* 2009;**154**:94–106.
26. Li WX, Österlund L, Vestergaard EK, Vang RT, Matthiesen J, Pedersen TM, et al. *Phys Rev Lett* 2004;**93**:146104.
27. Shi H, Asahi R, Stampfl C. *Phys Rev B* 2007;**75**:205125.
28. Greenwood NN, Earnshaw A. *Chemistry of the elements*. 2nd ed. Butterworth–Heinemann; 1997, ISBN 0080379419.
29. Stiehl JD, Kim TS, McClure SM, Mullins CB. *J Phys Chem B* 2005;**109**(13): 6316–22.
30. De Bocarmé TV, Chau T-D, Tielens F, Andrés J, Gaspard P, Wang RLC, et al. *J Chem Phys* 2006;**125**(5). art. no. 054703.
31. Pierson J-F, Rousselot C. *Surf Coat Technol* 2005;**200**(1–4):276–9.
32. Shima T, Tominaga J. *Thin Solid Films* 2003;**425**(1–2):31–4.
33. Karakaya I, Thompson WT. *J Phase Equilibria* 1992;**13**:137–42.
34. Feng HL, Gao XY, Zhang ZY, Ma JM. *J Korean Phys Soc* April 2010;**56**(4):1176–9.
35. Gallardo OAD, Moiraghi R, MacChione MA, Godoy JA, Pérez MA, Coronado EA, et al. *RSC Adv* 2012;**2**(7):2923–9.
36. Roy R, Hoover MR, Bhalla AS, Slaweckil T, Dey S, Cao W, et al. *Mater Res Innovations* 2007;**11**:3–19.
37. Khayati GR, Janghorban K. *Trans Nonferrous Met Soc China* 2013;**23**:543–7.
38. Charles T. *Campbell Phys Rev Lett* 2006;**96**(066106).
39. Michaelides A, Bocquet M-L, Sautet P, Alavi A, King DA. *Chem Phys Lett* 2003;**367**: 344–50.
40. Michaelides A, Reuter K, Scheffler M. *J Vac Sci Technol A Vac Surf Films* 2005;**23**(6): 1487–97.
41. Rocha TCR, Oestereich A, Demidov DV, Hävecker M, Zafeiratos S, Weinberg G, et al. *Phys Chem Chem Phys* 2012;**14**(13):4554–64.
42. Ono LK, Cuenya BR. *J Phys Chem C* 2008;**112**(12):4676.
43. Kang JH, Menard LD, Nuzzo JH, Frenkel AI. *J Am Chem Soc* 2006;**128**:12068.
44. Sanchez SI, Menard LD, Bram A, Kang JH, Small MW, Nuzzo RG, et al. *J Am Chem Soc* 2009;**131**:7040.

45. Berhault G, Bisson L, Thomazeau G, Verdon C, Uzio D. *Appl Catal A Gen* 2007;**327**:32.
46. Xiong Y, McLellan IM, Yin YD, Xia YN. *Angew Chem Int Ed* 2007;**46**:790.
47. Nellist PD, Pennycook SJ. *Science* 1996;**274**:413.
48. Xiao Li, Schneider WF. *Chem Phys Lett* 2010;**484**:231–6.
49. Stobbe-Kreemers AW, van der Zon M, Makkee M, Scholten JFF. *J Mol Catal A Chem* May 6, 1996;**107**(1–3):247–53.
50. Hu CH, Chizallet C, Mager-Maury C, Corral-Valero M, Sautet P, Toulhoat H, et al. *J Catal* 2010;**274**:99–110.
51. Ivanova AS, Slavinskaya EM, Gulyaev RV, Zaikovskii VI, Stonkus OA, Dsnilova IG, et al. *Appl Catal B Environ* 2010;**97**:57–71.
52. Flytzani-Stephanopoulos M, Gates BC. *Annu Rev Chem Biomol Eng* 2012;**3**:545–74.
53. Davydov AA, Sheppard N. *Molecular spectroscopy of oxide catalyst surfaces*, Wiley, 2003, pp. 44–55.
54. Green IX, Yates Jr JT. *J Phys Chem C* 2010;**114**:11924–30.
55. Descorme C, Madier Y, Duprez D. *J Catal* 2000;**196**:167–73.
56. Giamello E, Sojka Z, Che M, Zecchina A. *J Phys Chem* 1986;**90**:6084–91.
57. Busca G, Ramis G, Lorenzelli V. *J Mol Catal* 1989;**50**:231–40.
58. Armaroli T, Busca G, Carlini C, Giuttari M, Raspolli Galletti AM, Sbrana G. *J Mol Catal* 2000;**151**:233–43.
59. Ramis G, Cristiani C, Elmi AS, Villa PL, Busca G. *J Mol Catal* 1990;**61**:319–31.
60. Hadjiivanov K, Busca G. *Langmuir* 1994;**10**:4534–41.
61. Busca G, Trifirò F, Vaccari A. *Langmuir* 1990;**6**:1440–7.
62. Finocchio E, Busca G, Lorenzelli V, Willey RJ. *J Catal* 1995;**151**.
63. Errandonea D, Javier Manjón F. *Prog Mater Sci* 2008;**53**:711–73. 204–215.
64. Daturi M, Busca G, Borel MM, Leclaire A, Piaggio P. *J Phys Chem B* 1997;**101**:4358–69.
65. Soares AP, Portela MF, Kiennemann A. *Catal Rev Sci Eng* 2005;**47**:125–45.
66. Routray K, Zhou W, Kiely CJ, Grunert W, Wachs IE. *J Catal* 2010;**275**:84–98.
67. Andersson A, Hernelind M, Augustsson O. *Catal Today* 2006;**112**(1–4):40–4.
68. Häggblad R, Hansen S, Wallenberg LR, Andersson A. *J Catal* 2010;**276**(1):24–37.
69. Massa M, Häggblad R, Hansen S, Andersson A. *Appl Catal A Gen* November 28, 2011; **408**(1–2):63–72.
70. Li HH, Li KW, Wang H. *Mater Chem Phys* 2009;**116**:134–42.
71. Bielanski A, Najbar M. *Appl Catal A Gen* 1997;**157**:223–61.
72. Uraz C, Atalay S. *Chem Eng Technol* 2007;**30**(12):1708–15.
73. Kampe P, Giebler L, Samuelis D, Kunert J, Drochner A, Haaß F, et al. *Phys Chem Chem Phys* 2007;**9**:3577–89.
74. Ishchenko EV, Popova GY, Kardash TY, Ishchenko AV, Plyasova LM, Andrushkevich TV. *Catal Sustain Energy*; 2013:75–81.
75. Cavani F, Centi G, Marion P. In: Jackson SD, Heargraves SJS, editors. *Metal oxide catalysis*. Wiley; 2009. pp. 771–818.
76. Sadakane M, Ueda W. *J Jpn Pet Inst* 2012;**55**(4):229–35.
77. Grasselli RK. *Catal Today* 2005;**99**:23–31.
78. Tway, CL. US Patent US6916763 B2, to Solutia; 2005.
79. Taylor SH. In: Jackson SD, Heargraves SJS, editors. *Metal oxide catalysis*. Wiley; 2009. pp. 539–60.
80. Castellia A, Ballarina N, Cavani F. *Catal Today* 2012;**192**:72–9.

81. Cavani F, Teles JH. *ChemSusChem* 2009;**5**:508–34.
82. Bartley JK, Dummer NF, Hutchings GJ. In: Jackson SD, Hearngraves SJS, editors. *Metal oxide catalysis*. Wiley; 2009. pp. 499–538.
83. Védrine JC, Hutchings GJ, Kiely CJ. *Catal Today* 2013;**217**:57–64.
84. Bordes E, Courtine P. *J Catal* 1979;**57**:237.
85. Luciani S, Cavani F, Dal Santo V, Dimitratos N, Rossi M, Bianchi CL. *Catal Today* 2011;**169**:200–6.
86. Rosowski S, Akltwasser S, Dobner CK, Storck S, Zühlke J, Hibst H. *Catal Today* 2010;**157**:339–44.
87. Becht S, Franke R, Geißelmann A, Hahn H. *Chem Eng Process Proc Int* 2009;**48**:329–32.
88. Guettel R, Turek T. *Chem Eng Sci* 2010;**65**:1644–54.
89. Luciani S, Ballarini N, Cavani F, Cortelli C, Cruzzolin F, Frattini A, et al. *Catal Today* 2009;**142**:132–7.
90. Forzatti P, Nova I, Castoldi L. *Chem Biochem Eng Q* 2005;**19**(4):309–23.
91. Brandenberger S, Kröcher O, Tissler A, Althoff R. *Catal Rev Sci Eng* 2008;**50**:492–531.
92. Johnson TV. *SAE Int J Engines* 2011;**4**(1):143–57.
93. Lloyd L. The first catalysts. In: *Handbook of industrial catalysts*. Springer; 2011. pp. 23–69.
94. Gibson MA, Hightower JW. *J Catal* 1976;**41**:420–30.
95. Satterfield CN. *Heterogeneous catalysis in industrial practice*. 2nd ed. New York: McGraw Hill; 1991. p. 290.
96. Busca G, Finocchio E, Lorenzelli V, Trombetta M, Rossini SA. *J Chem Soc Faraday Trans* 1996;**92**:4687–93.
97. Deo G, Cherioan M, Rao TVM. Oxidative dehydrogenation (ODH) of alkanes over metal oxide catalysts. In: Fierro JLG, editor. *Metal oxides: chemistry and applications*. Boca Raton, FL, USA: CRC Press; 2005. pp. 491–511.
98. Cavani F, Ballarini N, Cericola A. *Catal Today* 2007;**127**:113–31.
99. Kung HH. *Adv Catal* 1994;**40**:1–36.
100. *The Uhde-Star process, brochure*. www.uhde.com.
101. Marosi L, Cox G, Tenten A, Hibst H. *Catal Lett* 2000;**67**(2–4):193–6.
102. Bo1hnke H, Gaube J, Petzoldt J. *Ind Eng Chem Res* 2006;**45**:8801–6.
103. Kamiya Y, Okuhara T, Misono M, Miyaji A, Tsuji K, Nakajo T. *Catal Surv Asia* 2008;**12**(2):101–13.
104. Johnson T. *Platin Met Rev* 2008;**52**(1):23–37.
105. Armor JN. *Catal Today* 1995;**26**:147–58.
106. Resini C, Montanari T, Nappi L, Bagnasco G, Turco M, Busca G, et al. *J Catal* 2003;**214**:179–90.
107. Bagnasco G, Turco M, Resini C, Montanari T, Bevilacqua M, Busca G. *J Catal* 2004;**225**:536–40.
108. Montanari T, Bevilacqua M, Resini C, Busca G. *J Phys Chem B* 2004;**108**:2120–7.
109. Montanari T, Marie O, Daturi M, Busca G. *Appl Catal B Environ* 2007;**71**:216–22.
110. Shi X, Liu F, Xie L, Shan W, He H. *Environ Sci Technol* 2013;**47**(7):3293–8.
111. Colombo M, Nova I, Tronconi E, Schmeißer V, Bendl-Konrad B, Zimmermann L. *Appl Catal B Environ* 2012;**111–112**:106–18.
112. Schmeisser V, Weibel M, Sebastian Hernando L, Nova I, Tronconi E, Ruggeri MP. *SAE Int J Commer Veh* 2013;**6**(1):190–9. <http://dx.doi.org/10.4271/2013-01-1064>.

113. Colombo M, Nova I, Tronconi E. *Catal Today* 2012;**197**(1):243–55.
114. [http://uhde-ftp.de/cgi-bin/byteserver.pl/archive/upload/uhde\\_publications\\_pdf\\_en\\_15000012.00.pdf](http://uhde-ftp.de/cgi-bin/byteserver.pl/archive/upload/uhde_publications_pdf_en_15000012.00.pdf).
115. Hevia MAG, Pérez-Ramírez J. *Appl Catal B Environ* 2008;**77**:248–54.
116. EnviNOx. [http://www.thyssenkrupp-uhde.de/fileadmin/documents/brochures/uhde\\_brochures\\_pdf\\_en\\_5000028.pdf](http://www.thyssenkrupp-uhde.de/fileadmin/documents/brochures/uhde_brochures_pdf_en_5000028.pdf).
117. Panov GI, Kharitonov AS, Sobolev VI. *Appl Catal A* 1993;**98**:1–20.
118. Notté PP. *Top Catal* 2000;**13**:387–94.
119. Zecchina A, Rivallan M, Berlier G, Lamberti C, Ricchiardi G. *Phys Chem Chem Phys* 2007;**9**:3483–99.
120. Pirutko LV, Chernyavsky VS, Starokon EV, Ivanov AA, Kharitonov AS, Panov GI. *Appl Catal B Environ* 2009;**91**(1–2):174–9.
121. Rivallan M, Berlier G, Ricchiardi G, Zecchina A, Nechita M-T, Olsbye U. *Appl Catal B Environ* 2008;**84**(1–2):204–13.
122. Haldor Topsøe, brochure *Catalytic combustion technology for off-gas purification*. <http://www.topsoe.com>.
123. Dissanayake DP. Metal oxides. In: Fierro JLG, editor. *Chemistry and applications*. Taylor & Francis; 2006. pp. 543–68.
124. Li WB, Wang JX, Gong H. *Catal Today* 2009;**148**:81–7.
125. Prasad R, Singh P. *Catal Rev Sci Eng* 2012;**54**(2):224–79.
126. Fino D, Specchia V. *Powder Technol* 2008;**180**:64–73.
127. Hernández-Giménez AM, dos Santos Xavier LP, Bueno-López A. *Appl Catal A General* 2013;**462–463**:100–6.
128. Kim CH, Qi G, Dahlberg K, Li W. *Science* 2010;**327**:1624–7.
129. Luck F. *Catal Today* 1996;**27**:195–202.
130. Bhargava SK, Tardio J, Prasad J, Folger K, Akolekar DB, Grocott SC. *Ind Eng Chem Res* 2006;**45**:1221–58.
131. Levec J, Pintar A. *Catal Today* 2007;**124**:172–84.
132. Luck F. *Catal Today* 1999;**53**:81–91.
133. Kim K-H, Ihm SK. *J Hazard Mater* 2011;**186**:16–34.
134. Santos A, Yustos P, Quintanilla A, Garcia-Ochoa F, Casas JA, Rodriguez JJ. *Environ Sci Technol* 2004;**38**:133–8.
135. [http://heraeus-catalysts.com/media/webmedia\\_local/downloads/Heraeus\\_NitroTechnologies\\_brochure.pdf](http://heraeus-catalysts.com/media/webmedia_local/downloads/Heraeus_NitroTechnologies_brochure.pdf) [accessed 04.03.13].
136. <http://www.noble.matthey.com/pdfs-uploaded/10%20Tailored%20Catalyst.pdf> [accessed 04.03.13].
137. [http://www.thyssenkrupp-uhde.de/fileadmin/documents/brochures/uhde\\_brochures\\_pdf\\_en\\_4.pdf](http://www.thyssenkrupp-uhde.de/fileadmin/documents/brochures/uhde_brochures_pdf_en_4.pdf) [accessed 04.03.13].
138. Farrauto RJ, Lee HC. *Ind Eng Chem Res* 1990;**29**:1125–9.
139. Pérez-Ramírez J, Kondratenko EV, Kondratenko VA, Baerns M. *J Catal* 2004;**227**:90–100.
140. Rdzawski RM, Stobrawa JP, Szyrowski J. *JAMME* 2007; 24: 106–110. [www.journalamme.org](http://www.journalamme.org).
141. <http://www.noble.matthey.com/pdfs-uploaded/12%20Caprolactam.pdf> [accessed 04.03.13].
142. Kondratenko VA, Weinberg G, Pohl M-M, Su DS. *Appl Catal A Gen* June 15, 2010; **381**(1–2):66–73.
143. <http://www.noble.matthey.com/pdfs-uploaded/11%20HCN.pdf> [accessed 04.03.13].
144. Lauritzen AM. US Patent 4,833,261, to Shell; 1989.

145. Özbek MO, Van Santen RA. *Catal Lett* 2013;**143**(2):131–41.
146. Kilty PA, Sachtler WMH. *Catal Rev Sci Eng* 1974;**10**:1–16.
147. Twigg MW, Webster DE. In: Cybulski A, Moulijn JA, editors. *Structured catalysts and reactors*. Taylor & Francis; 2006. pp. 71–108.
148. [www.ka-rasmussen.no/docs/silver%20catalyst%202008.pdf](http://www.ka-rasmussen.no/docs/silver%20catalyst%202008.pdf).
149. <http://www.jm-metaljoining.com/applications-pages2.asp?pageid=11&id=113>.
150. Qian M, Liauw MA, Emig G. *Appl Catal A Gen* 2003;**238**:211–22.
151. Nagy A, Mestl G. *Appl Catal A Gen* 1999;**188**(1–2):337–53.
152. Thompson DT. *Platin Met Rev* 2004;**48**:169–72.
153. [http://catalysts.evonik.com/sites/dc/Downloadcenter/Evonik/Product/Catalysts/Brochures/112\\_Document.pdf](http://catalysts.evonik.com/sites/dc/Downloadcenter/Evonik/Product/Catalysts/Brochures/112_Document.pdf).
154. *Frontiers*, August 2002, p. 12 [http://www.bp.com/liveassets/bp\\_internet/globalbp/STAGING/global\\_assets/downloads/F/Frontiers\\_magazine\\_issue\\_4\\_Leaps\\_of\\_innovation.pdf](http://www.bp.com/liveassets/bp_internet/globalbp/STAGING/global_assets/downloads/F/Frontiers_magazine_issue_4_Leaps_of_innovation.pdf).
155. Johnson Matthey. *The catalyst technical handbook*, <http://www.jmcatalysts.com/pct/pdfs-uploaded/Pharmaceuticals%20Fine%20Chemicals/Catalyst%20Handbook%20EU.pdf>
156. Long RQ, Yang RT. *Chem Commun* 2000:1651–2.
157. Hung CM, Lai WL, Lin JL. *Aerosol Air Qual Res* 2012;**12**:583–91.
158. Dannevang F. US Patent 5,587,134, to Topsøe; 1996.
159. Folić M, Lemus L, Gekas I, Vressner A. *Selective ammonia slip catalyst enabling highly efficient NOx removal requirements of the future*. [http://www1.eere.energy.gov/vehiclesandfuels/pdfs/deer\\_2010/tuesday/presentations/deer10\\_folic.pdf](http://www1.eere.energy.gov/vehiclesandfuels/pdfs/deer_2010/tuesday/presentations/deer10_folic.pdf).
160. Harrison Tran P, Chen JMH, Lapadula GD, Blute T. US Patent 7410626 B2, to BASF Catalysts LLC; 2008.
161. Liu X, Tran P, Lapadula GD. Patent WO/2009/045833, to BASF Catalysts LLC; 2009.
162. Colombo M, Nova I, Tronconi E, Schmeißer V, Bandl-Konrad B, Rahel Zimmermann L. *Appl Catal B Environ* October–November 2013;**142–143**:337–43.
163. Christian Enger B, Lødeng R, Holmen A. *Appl Catal A Gen* August 31, 2008;**346**(1–2):1–27.
164. Hickmann DA, Schmidt LD. *Science* 1993;**259**:343–6.
165. Basini L. *Catal Today* 2006;**117**:384–93.
166. Tornaiainen PM, Chu X, Schmidt LD. *J Catal* 1994;**146**:1–10.
167. Enger BC, Lodeng R, Holmen A. *Appl Catal A Gen* 2008;**346**:1–27.
168. Bruno T, Beretta A, Groppi G, Roderi M, Forzatti P. *Catal Today* 2005;**99**:89–98.
169. Beretta A, Bruno T, Groppi G, Tavazzi I, Forzatti P. *Appl Catal B Environ* 2007;**70**:515–24.
170. Tanaka H, Kaino R, Nakagawa Y, Tomishige K. *Appl Catal A Gen* 2010;**378**:187–94.
171. Trimm D. *Appl Catal A Gen* 2005;**296**:1–11.
172. Choi Y, G Stenger H. *J Power Sources* 2004;**129**:246–54.
173. Takamura K, Hiramatsu Y. US Patent 6,548,034, (to Mitsubishi Gas Chem. Co.); 2000.
174. Shore L, Farrauto RJ. WO/2006/130574, to Engelhard Corporation; 2006.
175. Tanaka H, Kuriyama M, Ishida Y, Ito S, Tomishige K, Kunimori K. *Appl Catal A Gen* 2008;**343**:117–24.
176. [http://www.topsoe.com/business\\_areas/air\\_pollution\\_control/processes/catalytic\\_oxidation.aspx](http://www.topsoe.com/business_areas/air_pollution_control/processes/catalytic_oxidation.aspx).
177. Haruta M, Kobayashi T, Sano H, Yamada N. *Chem Lett* 1987:405–8.
178. Bond GC, Thompson DT. *Catal Rev Sci Eng* 1999;**41**:319–38.
179. Haruta M, Daté M. *Appl Catal A Gen* 2001;**222**:427–37.

180. Miller JT, Kropf AJ, Zha Y, Regalbuto JR, Delannoy L, Louis C, et al. *J Catal* 2006;**240**:222–34.
181. Schumacher B, Denkwitz Y, Plzak V, Kinne M, Behm RJ. *J Catal* 2004;**224**:449–62.
182. Quinet E, Morfin F, Diehl F, Avenier P, Caps V, Rousset JL. *Appl Catal B Environ* 2008;**80**:195–201.
183. Piccolo L, Daly H, Valcarcel A, Meunier FC. *Appl Catal B Environ* 2009;**86**:190–5.
184. Forzatti P, Groppi G. *Catal Today* 1999;**54**:165–80.
185. Ciuparu D, Lyubovsky MR, Altman E, Pfefferle LD, Datye A. *Catal Rev Sci Eng* 2002;**44**:593–649.
186. Gélín P, Primet M. *Appl Catal B Environ* 2002;**39**:1–37.
187. Colussi S, Trovarelli A, Groppi G, Llorca J. *Catal Commun* 2007;**8**:1263–6.
188. Ibashi W, Groppi G, Forzatti P. *Catal Today* 2003;**83**:115–29.
189. Specchia S, Finocchio E, Busca G, Palmisano P, Specchia V. *J Catal* 2009;**263**:134–45.
190. Persson K, Ersson A, Jansson K, Iverlund N, Järås S. *J Catal* 2005;**231**:139–50.
191. Schalow T, Brandt B, Laurin M, Schaueremann S, Guimond S, Kuhlenbeck H, et al. *Surf Sci* 2006;**600**:2528–42.
192. Schalow T, Brandt B, Laurin M, Schaueremann S, Libuda J, Freund H-J. *J Catal* 2006;**242**:58–70.
193. Everaert K, Baeyens J. *J Hazard Mater* 2004;**B109**:113–39.
194. Lintz HG, Wittstock K. *Appl Catal A Gen* 2001;**216**:217–25.
195. Berndt M, Landri P. *Catal Today* 2002;**75**:17–22.
196. Liotta LF. *Appl Catal B Environ* October 20, 2010;**100**(3–4):403–12.
197. Hurtado P, Ordóñez S, Vega A, Diez F. *Chemosphere* 2004;**55**:681–9.
198. Collins NR, Twigg MV. *Top Catal* 2007;**42–43**:323–32.
199. Twigg MV. *Catal Today* 2011;**163**(1):33–41.
200. Pattrick G, van der Lingen E, Corti CW, Hollyday TJ, Thompson DT. *Top Catal* 2004;**30–31**:273.
201. Twigg MT, Phillips PR. *Platin Met Rev* 2009;**53**:27–34.
202. Epling WS, Campbell LE, Yezerets A, Currier NW, Parks II JE. *Catal Rev Sci Eng* 2004;**46**:163–245.
203. Takahashi N, Shinjoh H, Lijima T, Suzuki T, Yamazaki K, Yokota K, et al. *Catal Today* 1996;**27**:63–9.
204. Nakatani K, Hirota S, Takeshima S, Itoh K, Tanaka T. SAE Paper SP-1674, 2002-01-0957; 2002.
205. Castoldi L, Artioli N, Matarrese R, Lietti L, Forzatti F. *Catal Today* 2012;**184**:271–8.
206. Over H. *J Phys Chem C* 2012;**116**(12):6779–92.
207. Over H. *Electrochimica Acta* 2013;**93**:314–33.
208. [http://www.sumitomo-chem.co.jp/english/rd/report/theses/docs/01\\_chlorine\\_production\\_e.pdf](http://www.sumitomo-chem.co.jp/english/rd/report/theses/docs/01_chlorine_production_e.pdf).
209. Amrute AP, Mondelli C, Hevia MAG, Perez-Ramírez J. *ACS Catal* 2011;**1**:583–90.
210. Kurta S. *Chem Chem Technol* 2012;**6**:1–8.
211. Cavani F. *Catal Today* 2010;**157**:8–15.
212. <http://www.matrostech.com/z-2.html>.
213. Finocchio E, Busca G, Notaro M. *Appl Catal B Environ* 2006;**62**:12–20.
214. Fino D, Specchia S, Specchia V, Saracco G. In: Cybulski A, Moulijn JA, editors. *Structured catalysts and reactors*. Taylor & Francis; 2006. pp. 553–78.

215. <http://www.catalysts.clariant.com/bu/Catalysis/internet.nsf/023cfbb98594ad5bc12564e400555162/509ec81c364718ddc1257b03001f5ba8?OpenDocument>.
216. Bassetti A, Bodini M, Denega M, Miglio R, Pistone L, Tirler W. *Organohalogen Compd* 1999;**40**:445.
217. Campos-Martin JM, Blanco-Brieva G, Fierro JLG. *Angew Chem Int Ed* 2006;**45**:6962–84.
218. Menegazzo F, Signoretto M, Frison G, Pinna F, Strukul G, Manzoli M, Bocuzzi F. *J Catal* 2012;**290**:143–50.
219. Clerici MG. In: Jackson SD, Heargraves SJS, editors. *Metal oxide catalysis*. Wiley; 2009. pp. 705–54.
220. Bordiga S, Damin A, Bonino F, Ricchiardi G, Zecchina A, Tagliapietra R, et al. *Phys Chem Chem Phys* 2003;**5**(20):4390–3.
221. Perego C, Carati A, Ingallina P, Mantegazza MA, Bellussi G. *Appl Catal A Gen* 2001;**221**:63–72.
222. Russo V, Tesser R, Santacesaria E, Di Serio M. *Ind Eng Chem Res* 2013;**52**:1168–78.
223. [http://www.thyssenkrupp-uhde.de/fileadmin/documents/brochures/uhde\\_brochures\\_pdf\\_en\\_10000032.pdf](http://www.thyssenkrupp-uhde.de/fileadmin/documents/brochures/uhde_brochures_pdf_en_10000032.pdf).

# Polymerization Catalysts and Heterogenized Homogeneous Catalysts

## CHAPTER OUTLINE

<b>12.1 Solid polymerization catalysts</b> .....	<b>421</b>
12.1.1 Ziegler–Natta-type catalysts.....	421
12.1.2 Phillips-type catalysts.....	423
12.1.3 Heterogenized “single-site” polymerization catalysts .....	423
<b>12.2 Supported or heterogenized homogeneous catalysts</b> .....	<b>426</b>
<b>References</b> .....	<b>426</b>

## 12.1 Solid polymerization catalysts

Stereoregular catalytic polymerization is performed mainly to produce High-Density PolyEthylene (HDPE), Linear Low-Density Polyethylene (LLDPE, a copolymer of ethylene and another terminal olefin such as 1-butene, 1-hexene, 1-octene) and Isotactic PolyPropylene (PP).<sup>1</sup> Other polyolefins (such as Poly-4-methyl-1-pentene (PMP)) as well as copolymers are produced with similar processes and catalysts. Three main families of industrial catalysts exist for the processes, the so-called Ziegler–Natta catalysts (ZN catalysts), the Phillips Catalysts and the so-called single site catalysts, the last being either homogeneous catalysts or immobilized.<sup>1,2</sup>

### 12.1.1 Ziegler–Natta-type catalysts

Ziegler–Natta catalysts based on titanium chlorides, developed from the later 1950s to the early 1960s by K. Ziegler and G. Natta, have been improved progressively during time, coming now to the fifth or sixth generation.<sup>3</sup> The modern catalysts<sup>4</sup> are constituted by  $\text{TiCl}_4$  supported on  $\text{MgCl}_2$  and treated with  $\text{Al}(\text{Et})_3$  as the cocatalyst. The catalytic system also contain a so-called “internal donor” (ID) and an “external donor” (ED). ID is a Lewis base (or electron donor, e.g., an organic ester, ether, alcohol or amine) whose presence increases the isotactic content of polypropylene by greatly diminishing the yield of the atactic one. The recent development of the catalyst is mostly associated with the choice of different ID molecules, being benzoate type, phthalate type (dibutyl- or diisobutyl-phthalate), “diether” (2,2-dialkyl-1,3-dimethoxy-propane) or succinate. The catalyst needs very little



amount of ED, usually dicyclopentylidimethoxy-silane, and in extreme cases it even works without any one.

In the preparation step, the support  $\text{MgCl}_2$  is impregnated with  $\text{TiCl}_4$  and the ID. According to theoretical studies, defects and corners of the  $\text{MgCl}_2$  support are likely anchoring sites for the catalytically active Ti-species,<sup>5</sup> while the ID coordinated in the proximity of the active Ti center confers a remarkable stereoselectivity. This catalyst is activated by  $\text{AlEt}_3$ , favoring the partial reduction of  $\text{Ti}^{4+}$  into  $\text{Ti}^{3+}$ , thus forming the “active”  $\text{TiCl}_3$  phase. The ED improves stereoregularity in the formation of isotactic PP by both activating the sites active in isotactic PP formation and by deactivating those that are active in the formation of the atactic polymer.<sup>6</sup>

The most broadly accepted mechanism for stereoregular polymerization on ZN catalysts is the so-called monometallic mechanism proposed by Cossee and Arlman (Figure 12.1). Polymerization would occur via two steps. First, coordination of the monomer to the active center occurs, followed by the stereospecific migratory insertion of the coordinated monomer into the titanium–carbon bond. In migratory insertion step, a vacant coordination site is regenerated, which enables further a chain propagation.<sup>7,8</sup>

The main features of the catalyst are high activity, excellent hydrogen response (i.e., ability to respond to the hydrogen pressure tailoring the chain length), narrow molecular weight distribution (MWD) and low Cold Xylene Soluble content (CXS, i.e., low atactic PP production) of the polymer.

Developed for the original Montecatini slurry processes, still performed using slurry Continuous Stirred Tank Reactors (CSTR) reactors operating at 5–10 bar, 75–85 °C in the presence of hydrogen and hexane as the solvent (HDPE Basell Hostalen process), catalysts belonging to this family can also work in loop reactors in supercritical propane at 65 bar and 85–100 °C (such as in the first step of the Borstar HDPE process) and in gas-phase fluidized bed processes at 80–90 °C, 20 bar (such as Basell’s Spherilene HDPE process and the second step of the Borstar HDPE process). Similarly, for isotactic PP production loop reactors in the Borstar technology work at 80–100 °C, 50–60 °C in supercritical propene while the second fluidized

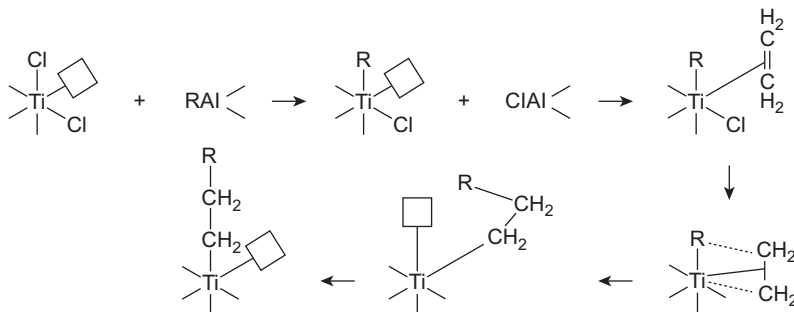


FIGURE 12.1

Cossee–Arlman mechanism of Ziegler–Natta polymerization catalysis.

bed gas-phase reactor works at 22–35 bar 80–100 °C. The Unipol PP process uses such kind of catalysts in two sequential gas-phase fluid bed reactors.

### 12.1.2 Phillips-type catalysts

The composition of Phillips catalysts is simpler<sup>9</sup>: they are constituted by chromium species on wide pore silica. The synthesis procedure implies first grafting of silica with Cr compounds or impregnation, followed by calcination producing mainly hexavalent chromate species.

The grafted Cr<sup>VI</sup> species are then reduced by ethylene (industrial process) or by CO (model laboratory process), yielding anchored isolated Cr<sup>II</sup> species, which are the species active in ethylene polymerization.

A number of different proposals have been done for ethylene and propylene polymerizations on such catalysts. Recent studies<sup>8</sup> support also for this catalyst a Cossee-Arlman-type mechanism similar to that is proposed for Ziegler–Natta catalysts.

However, the structure of the active sites at the molecular level is far from being understood and for this reason the Phillips catalyst continues to be one of the most studied and controversial system in the heterogeneous catalysis research. As a consequence of the high heterogeneity of the amorphous silica support, the Phillips catalyst allows a very broad molecular weight (MW) distribution for HDPE<sup>10</sup>, which gives to the polymer fine mechanical properties such as elasticity and impact resistance, and superior moldability due to its high melt viscosity.

Phillips-type catalysts are most commonly used in gas-phase fluidized bed reactors for bulk polymerization (e.g., Basell Lupotech G HDPE technology) at 20–25 bar, 85–116 °C, but are now also used in loop slurry reactors (Chevron Phillips process).

### 12.1.3 Heterogenized “single-site” polymerization catalysts

The so-called single-site catalysts are mononuclear metal complexes having stereoregular olefin polymerization activity. The ability of metallocene catalysts to produce stereospecific polymerization was already known by Natta, but found practical interest when Kaminski reported their very pronounced promotion when methylaluminoxanes (MAOs) are used as cocatalysts.<sup>11,12</sup> A number of substituted or nonsubstituted Zr,Ti and Hf cyclopentadienyl, indenyl or fluorenyl complexes were found to display excellent activity (Figure 12.2). After the Kaminsky discovery, a number of other nonmetallocene (or postmetallocene<sup>13</sup>) metal complexes (Figure 12.3) were found to display excellent stereospecific polymerization activity, in particular when used with activators. These metal complexes work in solution as homogeneous catalysts. Thus, liquid-phase solution polymerization processes were developed with these catalysts.

On the other hand, a further improvement was made when successful supporting of these “single-site” metal complexes was obtained, allowing the use of supported

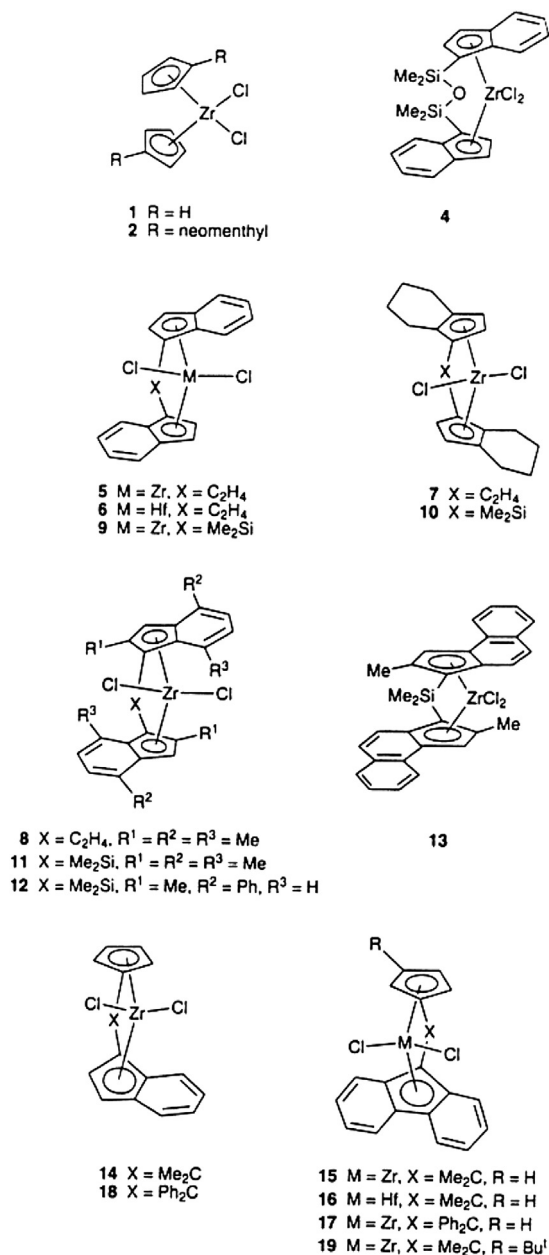


FIGURE 12.2

Structures of metallocenes used in olefin polymerization.

Reprinted with permission from Ref. 11.

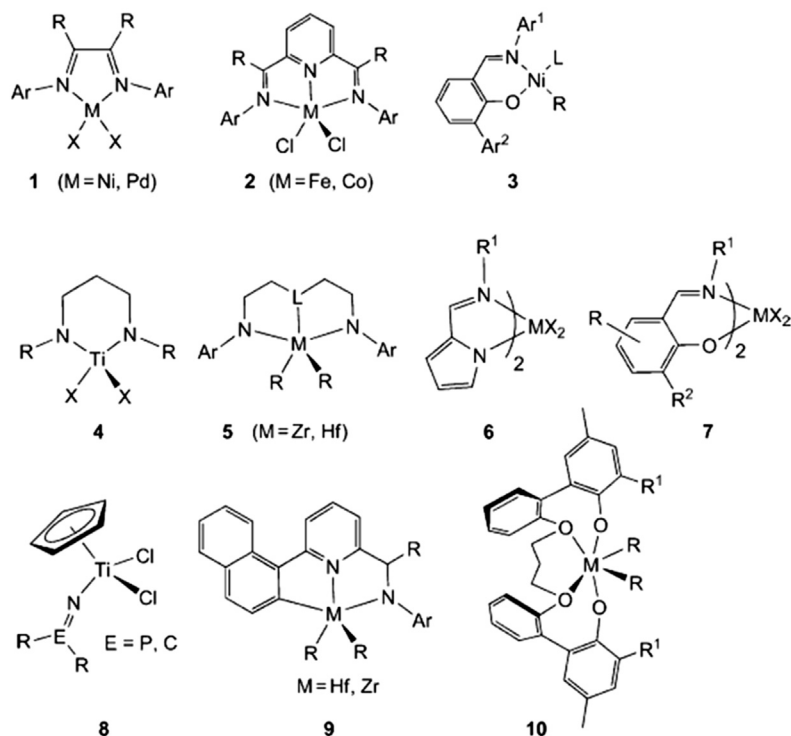


FIGURE 12.3

Postmetallocene polymerization catalysts.

Reprinted with permission from Ref. 13.

single-site catalysts to already existing typical gas-phase or slurry polymerization processes<sup>14</sup> in substitution of Ziegler–Natta and Phillips catalysts. In fact, most of the actual HDPE, LLDPE and iPP manufacture processes can today be applied using also supported single-site catalysts. According to the literature, silica and MgCl<sub>2</sub> are the most used supports for both metallocene and nonmetallocene catalysts. In fact, silica-supported zirconocenes are used industrially for the production of LLDPE.<sup>15</sup> However, a number of other supports have been cited in the open literature. Polymeric supports such as polysiloxanes and polystyrene-based materials are reported.<sup>16,17</sup> Some industrial processes such as Mitsui Evolve process are reported to work with supported metallocene catalysts,<sup>18</sup> using fluid-bed gas-phase reactors. Montmorillonite-supported metallocene catalysts have been developed at the industrial level for the production of isotactic polypropylene by Mitsubishi.<sup>19</sup> Among nonmetallocene catalysts, those based on salicylaldimines (also denoted as phenoxy-imine, FI) ligands have been studied and described in detail.<sup>20</sup> They can be heterogenized by supporting on silica and MgCl<sub>2</sub> or polymeric supports such as silicones, polystyrene and polyolefins. The Lyondell-Borstar Metocene

technology is apparently associated to the use of supported nonmetallocene catalysts<sup>21</sup> applicable in both gas-phase and slurry processes such as the Spheripol technology using a slurry loop reactor followed by a gas-phase fluid bed reactor.<sup>22</sup>

---

## 12.2 Supported or heterogenized homogeneous catalysts

As occurred for “single-site” polymerization catalysts, also for a number of other metal-based homogeneous catalysts, supporting on solid carriers has been attempted to make simpler separation steps in the process. A very large body of work has been done in a number of different fields.

A number of reactions usually performed with homogeneous catalysts, such as oxidations, hydrogenations, carbonylations, olefin metathesis, etc., have been tested also in heterogeneous conditions with immobilized metal complexes. Asymmetric synthesis is one of the fields where immobilization of homogeneous catalysts may be most interesting.<sup>23–25</sup> Unfortunately, immobilization is not always easily obtained and, after immobilization, the catalyst may lose significantly catalytic activity. Additionally, the immobilized catalyst may be even more expensive than the homogeneous one. On the other hand, among performances and costs, other factors such as disposal, toxicity and environmental harmfulness are relevant factors.<sup>26</sup>

A number of different supports have been studied for immobilization of catalysts, from the traditional ones, such as silica (which provides good results<sup>23</sup>), mesoporous solids,<sup>27,28</sup> polymers,<sup>16,29,30</sup> modified carbons,<sup>31</sup> hybrid solids<sup>32</sup> and Metal Organic Frameworks (MOF's).<sup>33</sup> Magnetic powders, such as those based on magnetite, can be used to make easy magnetic separation.<sup>34</sup>

Today, heterogenized homogeneous catalysts are available commercially<sup>35</sup> and processes based on them have been developed. One case is that of the Rh carbonyl iodide complex active in the methanol carbonylation reaction producing acetic acid. A polyvinyl-pyridine supported catalyst is applied in the ACETICA technology using a recycle slurry column reactor at 190 °C and 40 atm.<sup>19,36</sup> Polyurea-encapsulated Pd catalysts<sup>29,37</sup> (Pd EnCat™ catalysts, SigmaAldrich-Avecia) are available commercially to perform C–C bond forming reactions, carbonylations, hydrogenation, hydrogenolysis and dihydroxylations. FibreCat catalysts are polyolefin fiber-supported palladium complexes of electron-rich and bulky monodentate and bidentate ligands<sup>38,39</sup>, which can be applied as catalysts of a number of C–C forming reactions. SiliCat Pd heterogeneous catalysts are Pd complexes heterogenized in an ORMOSIL (Organically modified silica<sup>40,41</sup>). BASF (ex Engelhard) produces supported Rh catalysts active in chiral hydrogenations.<sup>42</sup>

---

## References

1. *Industrial Catalysts for Alkene Polymerization* Vaughan A, Davis DS, Hagadorn JR. *Polymer science: a comprehensive reference*, vol. 3; 2012. p. 657–672.
2. *Handbook of Transition Metal Polymerization Catalysts* (a cura di Ray Hoff, Robert T. Mather).

3. Gahleitner M, Resconia L, Doshev P. *MRS Bull* March 2013;**38**(03):229–33.
4. Bukatov GD, Sergeev SA, Zakharov VA, Echevskaya LG, Matsko MA. *Catal Ind* 2011;**3**(2):103–10.
5. Correa A, Credendino R, Pater JTM, Morini G, Cavallo L. *Macromolecules* 2012;**45**:3695–701.
6. Shen XR, Fu ZS, Hu J, Wang Q, Fan ZQ. *J Phys Chem C* 2013;**117**:15174–82.
7. Zhang HX, Zhang H, Zhang CY, Bai CX, Zhang XQ. *J Polym Sci Part A: Polym Chem* 2012;**50**:4805–8.
8. McGuinness DS, Davies NW, Horne J, Ivanov I. *Organometallics* 2010;**29**:6111–6.
9. McDaniel MP. *Advan. Catal.*, **53**; 2010. p. 123–606.
10. Tonosaki K, Taniike T, Terano M. *J Mol Catal A: Chem* April 23, 2011;**340**(1–2):33–8.
11. Kaminsky W. *Catal Today* 2000;**62**:23–34.
12. Kaminsky W. *Olefin polymerization catalyzed by metallocenes advances in catalysis*, vol. 46; 2001. p. 89–159.
13. Bryliakov KP. *Russ Chem Rev* 2007;**76**(3):253–77.
14. Choi Y, Soares JBP. *Can J Chem Eng* 2012;**90**(3):646–71.
15. Severn JR, Chadwick JC. *Dalt Trans* 2013;**42**:8979–87.
16. Polymer-supported Organometallic Catalysts Leadbeater NE. *Reference module in chemistry, molecular sciences and chemical engineering, from comprehensive organometallic chemistry III*, vol. 12; 2007. p. 663–753.
17. Heurtefeu B, Bouilhac C, Cloutet É, Tatona D, Deffleuxa A, Cramail H. *Prog Polym Sci* 2011;**36**:89–126.
18. <http://www.primepolymer.co.jp/evolve/english/technology/index.htm>.
19. Muroy T, Naojiri N, Deguchi T. *Appl Catal A Gen* 2010;**389**:27–45.
20. Makio H, Terao H, Iwashita A, Fujita T. *Chem Rev* 2011;**111**:2363–449.
21. <http://www.lyondellbasell.com/Technology/LicensedTechnologies/Metocene/>.
22. [http://www.lyondellbasell.com/NR/rdonlyres/55128077-776A-44E5-9799-BD51153BACB2/0/Spheripol\\_web\\_art.pdf](http://www.lyondellbasell.com/NR/rdonlyres/55128077-776A-44E5-9799-BD51153BACB2/0/Spheripol_web_art.pdf).
23. Trindade AF, Gois PMP, Afonso CAM. *Chem Rev* 2009;**109**:418–514.
24. Ding K, Uozomi Y, editors. *Handbook of asymmetric heterogeneous catalysis*. Wiley; 2008.
25. Pugin B, Blaser HU. In: Barbaro P, Liguori F, editors. *Heterogenized homogenous catalysts for fine chemicals production*. Springer; 2010. pp. 231–45.
26. Forte P, DeVos D. In: Barbaro P, Liguori F, editors. *Heterogenized homogenous catalysts for fine chemicals production*. Springer; 2010. pp. 361–84.
27. Zhao XS, Bao XY, Guo W, Lee FY. *Mater Today* March 2006;**9**(3):32–9.
28. Sahoo S, Bordoloi A, Halligudi SB. *Catal Surv Asia* 2011;**15**(3):200–14.
29. Akiyama R, Kobayashi S. *Chem Rev* 2009;**109**:594–642.
30. Anderson EB, Buchmeiser MR. *ChemCatChem* January 2, 2012;**4**(1):30–44.
31. Schaetz A, Zeltner M, Stark WJ. *ACS Catal* 2012;**2**(6):1267–84.
32. Zamboulis A, Moitra N, Moreau JJE, Cattoen X, Man MWC. *J Mater Chem* 2010;**20**:9322–38.
33. Genna DT, Womg-Foy AG, Matzger AJ, Sanford MS. *J Am Chem Soc* 2013;**135**:10586–9.
34. Gawande MB, Branco PS, Varma RS. *Chem Soc Rev* 2013;**42**(8):3371–93.
35. <http://www.strem.com/uploads/resources/documents/heterogeneouscatalysts.pdf>.
36. Hasono Y, Tasaki M. In: Meyers RA, editor. *Handbook of petrochemicals production processes*. McGraw Hill; 2005. 1.3–1.13.

37. <http://www.sigmaaldrich.com/chemistry/chemical-synthesis/technology-spotlights/reaxa/encats.html>.
38. Colacot TJ. *Top Catal* 2008;**48**:91–8.
39. <http://jmcct.com/docs/handbook-pharmaceutical-catalysis.pdf>.
40. Pagliaro M, Pandarus V, Béland F, Ciriminna R, Palmisano G, Carà PD. *Catal Sci Technol* 2011;**1**(5):736–9.
41. <http://www.silicycle.com/eu/applications/catalysis/use-of-siliacat-s-pd>.
42. Catalyst immobilization technology [http://apps-stage.catalysts.basf.com/Main/process/chemical\\_catalysts/pharma/catalyst\\_immobilization\\_agent.be1](http://apps-stage.catalysts.basf.com/Main/process/chemical_catalysts/pharma/catalyst_immobilization_agent.be1).

# Heterogeneous Catalysts and Biomass Conversion

# 13

## CHAPTER OUTLINE

<b>13.1 Heterogeneous catalysts and the future of industrial chemistry .....</b>	<b>429</b>
<b>13.2 Biomasses as raw materials for industrial chemistry .....</b>	<b>430</b>
<b>13.3 Heterogeneous catalysts and conversion of vegetable oils and animal fats.....</b>	<b>430</b>
13.3.1 Heterogeneous catalysts and biodiesel production .....	430
13.3.2 Heterogeneous catalysts and glycerol conversion to useful products .....	431
13.3.3 Hydrogenations of vegetable oils .....	432
13.3.4 Heterogeneous catalysts and pyrolysis of vegetable oils.....	433
13.3.5 Chemicals from triglycerides .....	433
13.3.6 Conversion of fatty acids and their salts.....	433
<b>13.4 Heterogeneous catalysts and the conversion of lignocellulosics .....</b>	<b>434</b>
13.4.1 Heterogeneous catalysts and the pyrolysis of lignocellulosic matter .....	434
13.4.2 Heterogeneous catalysts and upgrading of biooils .....	436
13.4.3 Heterogeneous catalysis and the gasification of lignocellulosic matter.....	437
13.4.4 Heterogeneous catalysis and the conversion of cellulose and hemicellulose .....	437
13.4.5 Heterogeneous catalysis and the conversion of lignin to chemicals .....	440
<b>13.5 Heterogeneous catalysts and industrial chemistry from renewables.....</b>	<b>441</b>
<b>References .....</b>	<b>443</b>

## 13.1 Heterogeneous catalysts and the future of industrial chemistry

Heterogeneous catalytic materials played a key role in the development of industrial chemistry based on coal first and on oil later. The future of industrial chemistry will be largely played on the conversion of renewable raw materials into renewable chemicals and biofuels. Heterogeneous catalysts do and will represent a precious tool also in this field. In this chapter we will give a short overview of the actual and potential application of heterogeneous catalysts for renewable and sustainable industrial chemistry.



## 13.2 Biomasses as raw materials for industrial chemistry

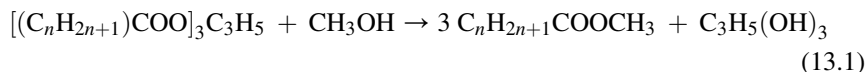
Raw materials for renewable industrial chemistry and energy production must be abundant and should not compete with alimentary agroindustrial productions. Thus, land for alimentary crops should not be limited by cultures intended for chemicals and biofuels productions. Nonedible starch and fatty materials grown in appropriate areas, lignocellulosics as well as wastes, are the candidates for this.

## 13.3 Heterogeneous catalysts and conversion of vegetable oils and animal fats

Both vegetable oils and animal fats are mostly constituted by triglycerides.<sup>1</sup> They are considered to be a promising family of raw materials for the production of renewable fuels by thermal processes.<sup>2,3</sup> Particularly interesting for industrial chemistry are the waste frying oils<sup>4</sup> and waste animal fats,<sup>5</sup> as well as the nonedible vegetable oils<sup>6</sup> and lipids from algae,<sup>7</sup> whose use can be not competitive with agri-food production.

### 13.3.1 Heterogeneous catalysts and biodiesel production

The commercial processes for the formation of biodiesel, i.e., fatty acids methyl esters (FAMES)

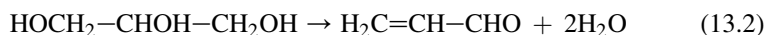


mostly imply the use of soda, potash or alkali methoxides as catalysts, which are mostly neutralized at the end, thus producing further waste materials. Solid catalyzed transesterification is expected to improve greatly the environmental impact of biodiesel manufacture. A number of solid catalysts,<sup>8,9</sup> including solid acids<sup>10,11</sup> and solid bases<sup>12,13</sup> have been investigated for solid-catalyzed transesterification to FAMES and find good opportunity.

Institut Francais du Petrole (IFP-Axens) has developed a process, already industrialized (denoted as EsterFipH) for the transesterification with a solid catalyst based on zinc aluminate.<sup>14</sup> The reaction operates at 200–300 °C at high pressures of gaseous methanol (30 bar). After the two reactors methanol is left to evaporate and thus allowing the separation of two phases: glycerin, rather pure, separates as the heavy phase from the biodiesel phase, lighter. This allows to produce a good glycerin coproduct (~98%), with additional few methyl ethers of glycerine. Also Refining Hydrocarbon Technologies (RHT) developed a biodiesel manufacture process with a first pretreating step where esterification of free fatty acids is performed with an acid solid-resin catalyst, and the main transesterification step performed over a fixed bed of a solid basic catalyst. Optionally, two swing reactors may be used to regenerate the catalyst.<sup>15</sup> A main problem in solid basic catalysis for biodiesel is catalyst leaching into glycerol.

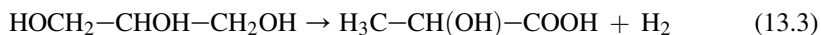
### 13.3.2 Heterogeneous catalysts and glycerol conversion to useful products

With the current technologies, about 100 kg of crude glycerol is produced per metric ton of biodiesel produced.<sup>16</sup> Over the last years, the demand of glycerol for food as well as cosmetic and pharmaceutical applications has not increased to the same extent as the production of biodiesel, thus glycerol becoming an interesting and low-price starting material for organic syntheses. A number of processes are under study to convert glycerol into useful products. One of the most interesting approaches is the conversion of glycerol into acrolein,



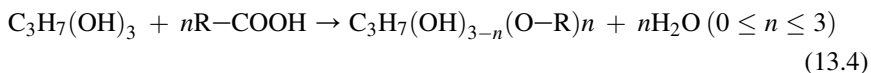
whose main use is to be further converted into acrylic acid and its esters, monomers for the production of polyacrylates.<sup>17</sup> Acrolein is also the intermediate for the manufacture of methionine, 1,3 propanediol, glutaraldehyde, pyridines, flavors, and fragrances.<sup>18</sup> A very large number of solid acids allow significant yields in the conversion of glycerol into acrolein, such as protonic zeolites, heteropolyacids (HPAs), bulk as well as supported phosphates, sulfonic-functionalized mesoporous silicas, supported tungsten oxide, pure and supported niobia etc. In general, activity is strongly dependent on the density of acid sites, whereas the selectivity to acrolein is related to the presence of Brønsted acid sites. Although the activity and the selectivity to acrolein can be optimized by finding the best combination of space velocity, reaction temperature and glycerol/water ratio in the feed, a main problem consists in the quite fast catalyst deactivation by coking. Deactivation rate can be significantly reduced by working in the presence of oxygen, while catalyst regeneration is possible by coke burning.<sup>19a</sup>

Dehydrogenation of glycerol at 290 °C over solid bases such as CaO allows the production of lactic acid with significant yields (>40%)<sup>20</sup>:



Lactic acid is a very significant intermediate for its applications in the food, pharmaceutical and cosmetic fields,<sup>21</sup> as well as for the production of polylactic acid,<sup>22</sup> a very promising biodegradable plastic already produced industrially.

Glycerol can be converted into its esters,



which have a wide variety of applications as solvents, as emulsifying and stabilizing compounds, as raw materials in food, and the cosmetic and pharmaceutical industries. In particular, acetyl esters find several applications: monoacetylglycerol (MAG) is used in the manufacture of explosives, in tanning, and as solvents for dyes; diacetylglycerol (DAG) is used as a plasticizer and softening agent and solvent. Triacetylglycerol (TAG) is used as a solvent, antimicrobial and emulsifying agent in cigarette filters, pharmaceuticals. DAG and TAG have also promising properties as fuel additives, as gasoline octane enhancer and as cold flow and viscosity

improving agent for biodiesel. A number of solid acids catalyze glycerol esterification such as zeolites, silica-alumina, acid sulfonated resins, niobic acid, sulfonated carbons, functionalized mesoporous silicas, zirconia based solid acids, hydroxylated magnesium fluorides, heteropolyacids.<sup>23–25</sup>

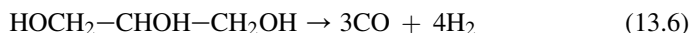
The conversion of glycerol in the presence of base-doped redox catalysts gives a mixture of products among which allyl alcohol, an important chemical intermediate in the production of resins, paints, coatings, silane coupling agents, and polymer crosslinking agents, etc., may be produced with near-30% selectivity.<sup>26</sup>

Hydrogenolysis of glycerol to 1,2-propanediol (propylene glycol)

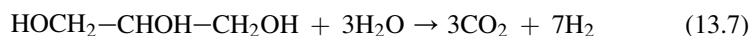


is another promising option. 1,2-propanediol has a number of applications to produce polyesters as well as a solvent, as an antifreeze in automobiles, as antifreeze in breweries and dairy establishments and deicing fluid for aircrafts, as an inhibitor of mold growth and as a mist to disinfect air, and has great potential for microbial processes.<sup>27</sup> The best catalysts appear to be based on supported copper and ruthenium.<sup>28</sup>

A main alternative to the production of chemicals is the conversion of glycerol to syngas and hydrogen.<sup>29,30</sup> Glycerol can undergo thermal and catalytic decomposition to syngas



at temperatures above 700 °C. The glycerol steam reforming



by different catalysts to produce hydrogen may be considered to occur first through glycerol dehydrogenation/decomposition followed by water-gas shift or methanation reaction. Catalysts similar to those active in methane and natural gas steam reforming as well as in ethanol steam reforming, such as those based on supported Ni and Co and on some noble metals (Pt, Rh, Ru) are also active for glycerol steam reforming at >400 °C, with high hydrogen yields (>90%) but also significant selectivity to CO (up to 10%), the performance being improved by CO<sub>2</sub> separation.<sup>31</sup> Partial oxidation and autothermal reforming have also been considered to reduce catalyst coking and to improve the thermal consumption.

Aqueous phase reforming (APR) is very interesting as an alternative to conventional gas-phase steam reforming.<sup>32</sup> It consists in the reaction of glycerol with water in liquid phase at moderate pressure (20–60 bar) and temperature (200–250 °C). The best catalysts are based on Pt and Ni,<sup>30</sup> allowing very low production of CO. In spite of the several problems, mainly due to catalyst poisoning by impurities and relatively low productivities, the system is under industrial development.

### 13.3.3 Hydrogenations of vegetable oils

Hydroprocessing of vegetable oils is already done industrially to reduce unsaturations in the production of margarine as well as to produce fatty alcohols useful mainly

for detergency. In the former case Ni/SiO<sub>2</sub> catalysts are mainly used (see Chapter 9.4.3.2), while in the latter copper-based catalysts are applied (see Chapter 9.4.4.4).

Full hydrogenation of fats to hydrocarbons has also been recently developed at the industrial level to produce high-performance “biodiesel”, using typical hydrotreating catalysts based on CoMo/Al<sub>2</sub>O<sub>3</sub><sup>33</sup> at 300–400 °C 10–50 bar likely in the presence of sulfur adding components to retain sulfided state of the catalyst (see Chapter 10.7.5.2). Due to the very high linearity of the paraffins obtained, the cetane number is very high (70–90) but the cold properties are bad. Thus a further hydroisomerization step using silicalumina-supported catalysts must be performed to reduce linearity. Investigations are very active in the field of hydrogenation of fats.<sup>34,35</sup>

### 13.3.4 Heterogeneous catalysts and pyrolysis of vegetable oils

The possibility to convert vegetable oils to hydrocarbons through catalytic decarboxylation/pyrolysis processes was initially proposed by the Mobil research group,<sup>36</sup> just a while later than the discovery of the particular properties of zeolite H-ZSM5, that they developed during a study on the “shape selectivity”. The term “catalytic cracking of vegetable oils” is generally used to indicate a process similar to the refining process performed with vacuum gasoils and deasphalted oils, denoted as Fluid Catalytic Cracking (FCC). Practically, solid acid catalysts, fluidized and entrained bed systems with catalyst regeneration and recycle (as it happens in the FCC process) and fixed bed reactors are used. The operative range for the temperature is 400–600 °C (thus lower than that used in the refinery FCC processes) but, as a consequence, the feed is essentially in a vapor phase.<sup>37</sup> Usually, the aim is to produce gasoline with a high octane number and/or fuel gases. With REY zeolite (Zeolite Y with rare earths), the optimal operative conditions to produce a gasoline rich in aromatics are 450 °C, residence time of 20 s, catalysts/oil ratio of 5 g/g.<sup>37</sup> Lower temperature and milder solid acids allow the conversion of vegetable oils into high quality Diesel liquids.<sup>38,35</sup>

### 13.3.5 Chemicals from triglycerides

Chemicals can be prepared from triglycerides using heterogeneous catalysts. Examples are the manufacture of fatty ethanolamides, used as ingredients for detergents, lubricants and other products, by catalytic aminolysis of fats using e.g., Zn–La oxycarbonates.<sup>39</sup> Epoxidated oils can act as raw materials for synthesis of variety of chemicals such as alcohols (polyols), glycols, olefinic compounds, lubricants, plasticizer and stabilizer for polymers. The use of heterogeneous catalysts for oils epoxidation is under study.<sup>40</sup>

### 13.3.6 Conversion of fatty acids and their salts

Fatty acids and salts can be produced as wastes of different technologies including biodiesel syntheses. Their conversion to hydrocarbons rich mixtures is possible.<sup>38,41</sup>

## 13.4 Heterogeneous catalysts and the conversion of lignocellulosics

The main “chemical” application of wood today is for the papermaking industry, together with burning to produce heat and energy and gasification. The papermaking industry separates the main components of wood, producing quite pure cellulose and a residue based on lignin, which today represents essentially a waste to be burnt, with few chemical applications.<sup>42</sup> In a conventional kraft cooking, hemicelluloses are dissolved into the cooking liquor and burned in the recovery boiler jointly with the lignin degradation products. Alternatively, hemicelluloses can be extracted by steam explosion or by steam treatment from wood prior to pulping.<sup>43</sup> Thus, the separation of the three main components of lignocellulosics and their exploitation separately can be easily done.

### 13.4.1 Heterogeneous catalysts and the pyrolysis of lignocellulosic matter

Three different biomass pyrolysis processes are generally mentioned<sup>33,44,45</sup>: (1) conventional pyrolysis performed at relatively low temperature with slow heating rate and long residence time, producing mostly charcoal; (2) fast pyrolysis, performed with higher heating rates (10–200 °C/s) up to 900 °C and short contact times (few seconds), aimed at producing biooils; and (3) flash pyrolysis, with very high heating rates (1000 °C/s) and low residence times (<0.5 s) producing liquids and gases.

Recently, several studies on the thermal conversion of different waste Lignocellulosic materials other than wood, such as seeds, sawdust, shells, hulls, husks, pits, kernels, straw, stalk and various residues, have been published. Many of these materials are mentioned, e.g., in the review of Neves et al.<sup>46</sup> These materials have intermediate compositions typically between those of cellulose and lignin, since cellulose, hemicellulose and lignin are their main components.

As it is reported by Huang et al.,<sup>47</sup> the behavior of several biomasses is properly interpreted as the sum of the behavior of the different compounds, such as cellulose, hemicellulose and lignin, the effects of their combination being usually quite limited.

Results about the conversion of wood materials have been reviewed by Mohan et al.<sup>48</sup> and Huber et al.<sup>44</sup> The wood starts to be reactive at about 190 °C and a rapid conversion already happens in the range 300–400 °C. In this range what really happens is the decomposition of cellulose microfibrils.<sup>49</sup> Afterwards, the reactivity of the aromatic nuclei of lignin starts, with the formation of graphene layers (graphite). The maximum amount of liquid products is achieved between 270 and 550 °C and it might be over 60% of the initial mass of the wood. The “biooils” obtained are full of aromatic and phenolic compounds.

In an inert atmosphere, lignin begins to lose weight above 200 °C, with a loss peak around 400 °C.<sup>50</sup> That peak has a tail till temperatures higher than 900 °C. This decomposition gives a residue of about 40% of the initial mass at 900 °C and of about 50% at 450 °C. In fast pyrolysis at 475 °C a gas with a yield higher

than 30%, an oil with a yield of 53% and a solid with a yield of 15% can be produced. In dependence of the main subunits composing lignin (Figure 13.1<sup>51</sup>), the main components of biooil are polyhydroxy- and/or polymethoxy-benzenes sometimes containing also C<sub>1</sub>–C<sub>3</sub> alkyl chains and aldehyde functions with the partial formation of oxygenated polycyclic aromatics.<sup>52</sup> Water, CO, CO<sub>2</sub>, methane, light alcohols including methanol, phenols and hydrogen are the main components of the pyrolysis gases.

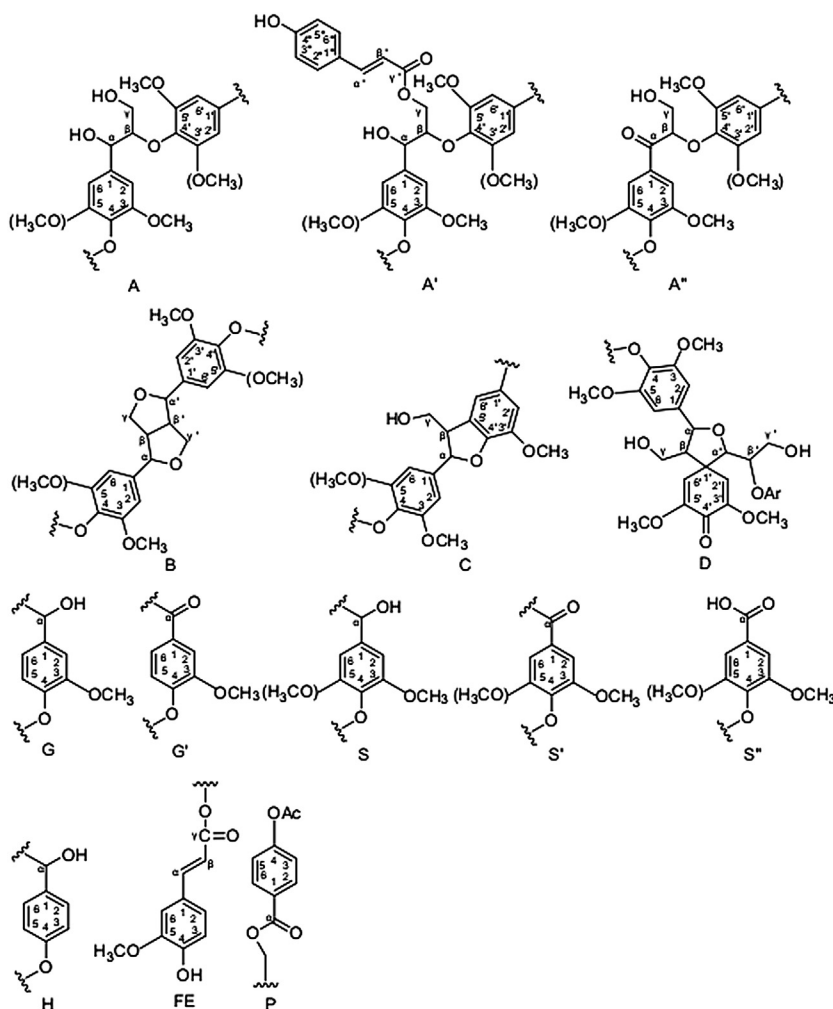


FIGURE 13.1

Main substructures of lignin.

In an inert atmosphere, at sufficiently high heating rates<sup>53</sup> cellulose starts to react just above 300 °C. In the range 300–380 °C there is a development of gaseous molecules with a weight loss higher than 80%. At temperatures above 400 °C, the further development of gas is of about 20–25% of the remaining mass, with a progressive evolution of a semisolid material (char) to a bituminous liquid (tar).<sup>54</sup> The biooil produced (tar) mainly contains the depolymerization product of levoglucosan (a highly oxygenated cyclic molecule with six carbon atoms; this molecule arises from glucose with loss of a water molecule by condensation of two hydroxy groups to a further C-O-C bridge) and other highly oxygenated compounds that derive from glucose. Lin et al.<sup>55</sup> investigated the transformation mechanism of cellulose. In an anhydrous atmosphere, the first stage of the reaction is the depolymerization, which produces levoglucosan. Subsequently, this compound isomerizes and/or partially dehydrates giving water vapor and other molecules belonging to the “anhydrosugars” family.

The anhydrosugars undergo a further dehydration to produce furfural and hydroxymethyl furan, which are oxygenated molecules with six carbon atoms and rings with five atoms. Those molecules start a decomposition producing three carbon atom molecules (glycol aldehyde, glyceraldehyde and hydroxyacetone), CO, CO<sub>2</sub> and decarbonylation and decarboxylation products. Some organic products begin a polymerization to produce carbonic species. Hemicellulose, which is mainly constituted by sugar oligomers with five carbon atoms, is even more reactive than cellulose: in fact it already decomposes in the range of 220–300 °C, producing an oily phase rich in anhydroxylopiranose (an anhydrosugar with five carbon atoms).<sup>53,54</sup>

Catalytic pyrolysis is mostly done at 400–650 °C with zeolites such as H-ZSM5.<sup>56–58</sup> Volatile products formed from the initial thermal decomposition of biomass, which are predominantly oxygenates (e.g., furans, acids, and phenolics), are then catalytically converted within the framework of the zeolites to aromatic hydrocarbons (e.g., benzene, toluene, and xylenes) via a series of reactions such as cracking, deoxygenation, oligomerization, and aromatization. Thus, the oxygen is largely removed with decarbonylation, decarboxylation, and dehydration reactions catalyzed by the zeolite. The resulting biooils have excellent octane numbers to be used as a gasoline.<sup>59</sup> It seems likely that problems arise from deactivation of catalysts by coking and poisoning.

### 13.4.2 Heterogeneous catalysts and upgrading of biooils

Biooils produced by pyrolysis of lignocellulosic mostly have big amounts of oxygen, poor stability, bad cool properties. Hydroprocessing (hydrodeoxygenation) of biooils allows their upgrading, using typical hydrotreating catalysts based on NiMo/Al<sub>2</sub>O<sub>3</sub> sulfides in the presence of sulfur adding components, or noble metal catalysts. The limit is the use and the huge consumption of hydrogen. The development of new non conventional catalysts is under study.<sup>60</sup> Upgrading of biooils to aromatics and light olefins can also be obtained by cracking with acid catalysts such as ZSM-5 zeolites.<sup>61</sup> Alternatively, deoxygenation may be obtained by catalytic treatments with less acidic materials less prone to coking such as metal oxides.<sup>59</sup>

### 13.4.3 Heterogeneous catalysis and the gasification of lignocellulosic matter

Gasification of biomasses represents a promising and already quite established approach to produce syngases,<sup>62</sup> whose combustion or conversion may give rise to renewable energy, biohydrogen and liquid biofuels. However, gasification technologies present a number of drawbacks, among which the production of tar<sup>63</sup> (1–50 g/Nm<sup>3</sup> depending mainly on the reactor type) and the presence of sulfur (20–600 ppmv H<sub>2</sub>S depending on the biomass<sup>64</sup>) and chlorine (up to some hundreds of ppm depending on the biomass<sup>65</sup>) as pollutants of the resulting syngas. Biomass tar is a complex mixture of quite heavy organic molecules produced together with other low volatility oxygenates.<sup>66</sup> These molecules can condense in the cold sections of the plant (like on heat exchangers) producing fouling, or may cause coking and deactivation of catalysts (such as for water gas shift) and anodes of fuel cells.<sup>67</sup> The uncomplete solution of the problem of tar abatement represents still a main obstacle to the industrial development of biomass gasification processes.<sup>68</sup>

Several approaches have been proposed to purify biomass-derived syngases from tar. Catalytic steam reforming appears to be one of the most interesting approaches,<sup>59,69,70</sup> being performed nearly at the same temperature of syngas coming out from the reactor. Ni-based conventional steam reforming catalysts appear to be active but noble metal based catalysts are even more active thus being applicable at lower temperature. However, low temperature steam reforming can be not useful depending on a reaction configuration. Noble metal catalysts, particularly Rh-based, are also less prone to coking and more sulfur-resistant than nickel catalysts.<sup>71,72</sup> In spite of this, catalysts commercialized as specific for biomass tar-steam reforming are based on Nickel–Magnesium–Silicate.<sup>73</sup> According to Topsøe, however, the best approach is tar hydrogenation.<sup>74</sup>

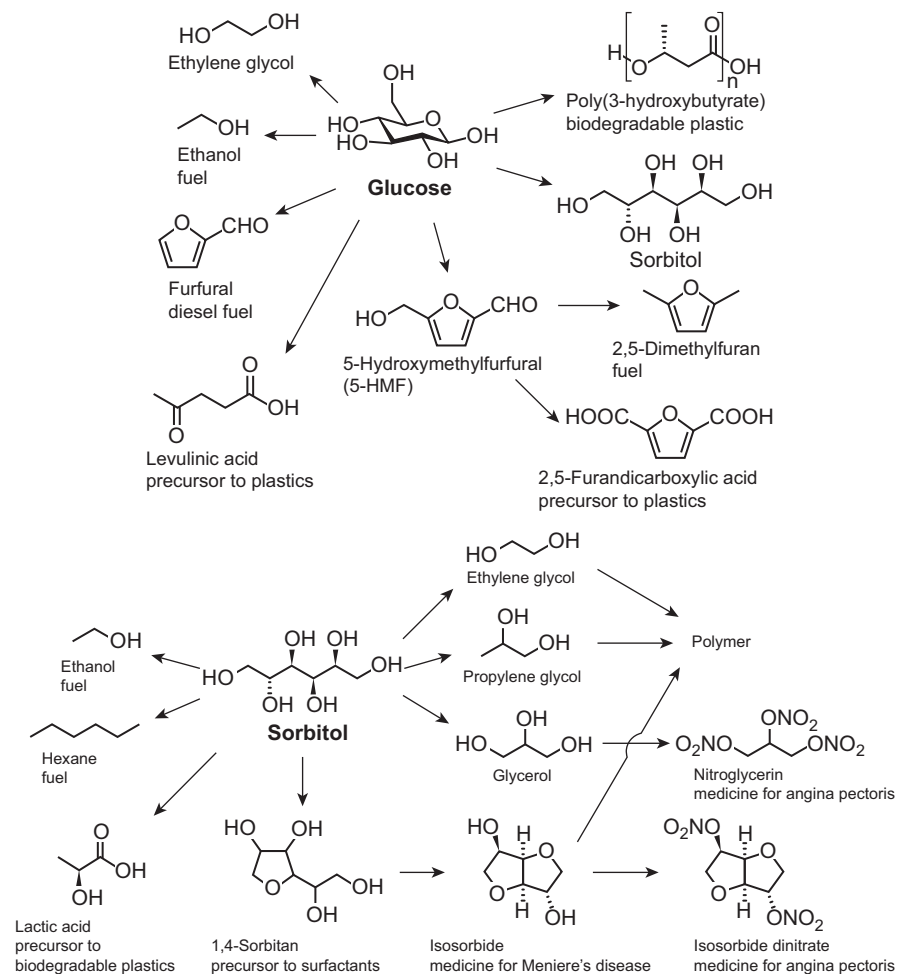
### 13.4.4 Heterogeneous catalysis and the conversion of cellulose and hemicellulose

Sugars, glucose first of all, can be the intermediates for the production of a number of oxygenated organic compounds. Starch is commonly at the origin of sugars chemistry. However, due to the edible character of starch and of most vegetables rich in starch, its large use for the production of chemicals and biofuels cannot be recommended. The nonedible nature of cellulose makes it a good raw material for industrial sugar nonfood chemistry. The hydrolysis of cellulose to glucose with enzymes has been applied for decades. Cellulose hydrolysis in the presence of liquid acid catalysts such as hydrochloric and sulfuric acid needs high temperature and usually high acid concentrations, with several drawbacks including starting of cellulose pyrolysis.<sup>75</sup> A number of solid acids can be applied to cellulose hydrolysis<sup>76–80</sup> including acid resins, sulfonated carbons, heteropolyacids, sulfonated silicas and oxides. The



selectivity to glucose using such solid acids as catalysts, without further conversion of it to degradation products is still matter of investigation.

Once produced, glucose may be converted into a number of products (Figure 13.2). Among these processes, the fermentative production of bioethanol represents a main process to gasoline biofuel. The cellulose separation and hydrolysis steps are indeed critical for sustainability of bioethanol production.



**FIGURE 13.2**

Chemicals derived from glycerol and sorbitol.

Reprinted with permission from 79

Glucose can also be converted by heterogeneous catalysis in a variety of intermediates (Figure 13.2). Hydrogenation to sorbitol, an alternative sweetener and a platform chemical for a wide variety of compounds, is obtained using solid metal catalysts.<sup>81</sup> Sorbitol can be later converted into other intermediates (Figure 13.2). One of these is isosorbide, another interesting intermediate, with acid catalysts such as niobium phosphate.<sup>82</sup>

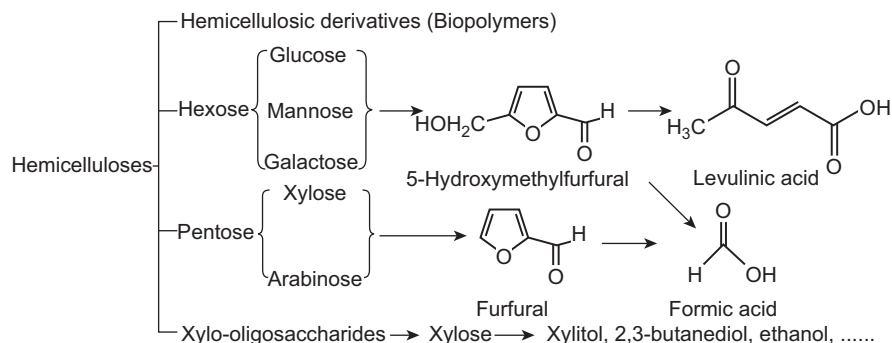
Glucose can be isomerized into fructose in water and further dehydrated to 5-hydroxy-methylfurfural (5-HMF), which is one of the most important platform molecules.<sup>83</sup> The conversion of glucose into 5-HMF can be realized in the presence of heterogeneous catalysts such as niobic acid, niobium phosphates and other Lewis acid catalysts.<sup>84</sup> The oxidation of glucose into gluconic acid with oxygen or air can be performed with metal catalysts such as supported gold and platinum. Gluconic acid, and its salts are used in the formulation of food, pharmaceutical and hygienic products.<sup>85</sup> Glucose can be converted into ethylene glycol over catalysts having a dual functionality, metallic and acidic, such as Ru-ammonium-metatungstate on carbon.<sup>86</sup> Glucose can also be converted into syngas by aqueous reforming with the intermediacy of sorbitol.<sup>87</sup>

Some of these products can also be obtained directly by conversion of cellulose. Cellulose can be converted by catalytic hydrolytic hydrogenation into hexitols (mainly sorbitol with low amounts of mannitol) in the presence of metal catalysts, such as carbon-supported Ru and Ni.<sup>79,88</sup> Methanolysis of glucose to methyl glucosides, useful to convert them into detergents, surfactants and cosmetics, can be performed in the presence of solid acid catalysts such as sulfonated carbons.<sup>79</sup> One-pot production of ethylene glycol and/or ethylene and propylene glycols or even mixtures including also butanediols and hexanediols from cellulose hydrogenation can be done using multifunctional catalysts including acid sites and hydrogenating components.<sup>79,89</sup>

Corma et al.<sup>90</sup> studied the conversion at 500 °C of an aqueous solution of sorbitol, a molecule that is quite similar to glucose and achievable through glucose hydrogenation, with different solid catalysts (with a variable acidity). With conversions of about 70% a gaseous yield of 40–50% can be obtained; moreover, with these operative conditions, a carbonic product (about 15%) and aromatics (18–20%) can be obtained. The main gaseous product is CO (yield of 20–25%), with 4–8% of propylene, 2–6% of yield both in CO<sub>2</sub> and ethylene, 2% of butenes, and finally methane, ethane and propane (less of 1% each of them).

Considering the high oxygen amount in cellulose (49% wt/wt) and the scant number of carbon atoms bonded between each other in glucose (the cellulose monomer), catalytic conversion of cellulose and sugars may predominantly result in the production of light and highly oxygenated fuel molecules (gasoline and gas).

Hemicelluloses have a wide variety of applications (Figure 13.3<sup>43,91</sup>). They can be easily hydrolyzed into pentoses (xylose and arabinose) and hexoses (glucose, galactose, and mannose), and can be fermented into bioethanol as well as converted to other value-added chemicals, such as 5-hydroxymethylfurfural (HMF), furfural,<sup>92</sup> levulinic acid and xylitol.



**FIGURE 13.3**

Potential products from hemicellulose.

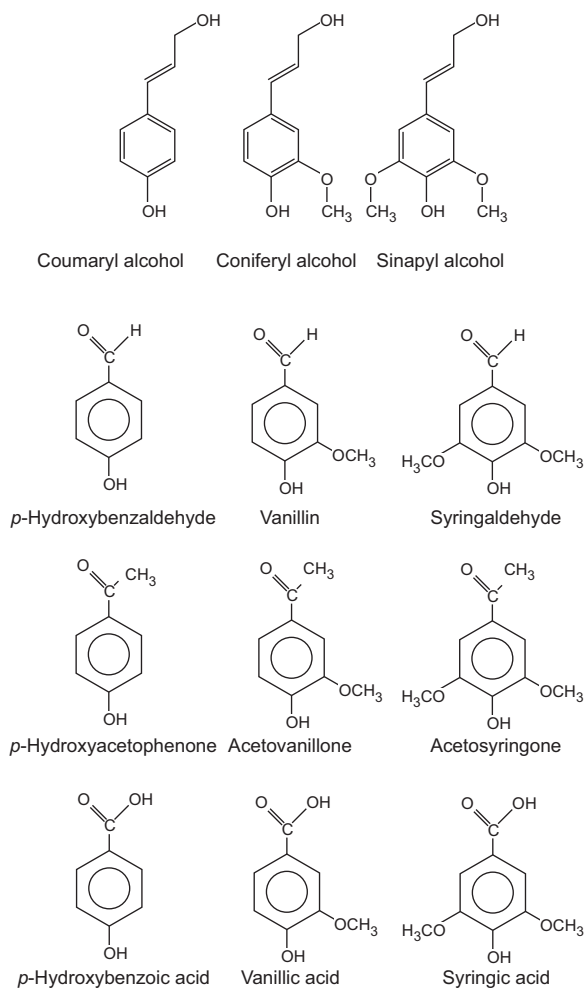
*Reprinted with permission from ref. 91*

### 13.4.5 Heterogeneous catalysis and the conversion of lignin to chemicals

Lignin is a polymeric matter containing methoxy-benzene units bonded through a carbon and through an oxygen to two different three-carbon chains. These chains contain an alcoholic group and bridge (through a direct C–C bond and through a C–O–C bond) two methoxybenzene units (Figure 13.1). The cracking of this structure can produce monoaromatic molecules such as the three monolignan molecules *p*-coumaryl-, coniferyl- and sinapyl- alcohols, and some additional fragmentation molecules (Figure 13.4). These molecules can be converted by conventional heterogeneous catalyzed process such as hydrodeoxygenation, cracking, transalkylation, oxidations into the main aromatic intermediates such as benzene, toluene, xylenes, phenol, benzoic acid, isophthalic acid, etc. Together, small-chain aliphatics can be produced by breaking of the three carbon chains.

The production of few chemicals from lignin has historical origin: among these, the production of methanol (also denoted as “wood alcohol”) from lignin acid hydrolysis was performed industrially at the beginning of the 20th century<sup>93</sup> while the extraction of vanillin from waste sulfite lye from pulp production in the papermaking industry has been performed until recently.<sup>94</sup>

The depolymerization of lignin can be performed using basic solids or liquid bases as catalysts. Hydrocracking can also be performed using solid catalysts such as iron sulfide catalysts to phenol (Naguchi process) or typical hydrocracking catalysts such as iron, cobalt, molybdenum or nickel, or combinations thereof, on a support comprising alumina, silica, zeolites or combinations thereof.<sup>95–97</sup> As said, catalytic lignin cracking produces biooils, i.e., complex mixtures of mainly aromatic oxygenates that can be, maybe after upgrading, used as fuel. The conversion to single molecules or simple mixtures of few molecules can be desirable. The conversion to monomeric units, mainly based on phenolic compounds, alkylaromatics and gaseous hydrocarbons depending on reaction temperature, could be attempted using zeolites and other solid acids. Hydrocracking can be performed similarly to produce aromatic mixtures—rich fuels using acid catalysts with metals or other hydrogenation components.

**FIGURE 13.4**

Molecules potentially deriving from lignin decomposition.

Lignin catalytic oxidation can give rise to oxygenated organic compounds. Liquid-phase oxidation with oxygen or hydrogen peroxide and solid catalysts can be studied.<sup>96,97</sup>

## 13.5 Heterogeneous catalysts and industrial chemistry from renewables

In Table 13.1 some possible ways to produce key industrial organic compounds from renewables are summarized. As it is evident, several of the needed steps are based on catalysis by solids.

<b>Table 13.1</b> Possible Ways to produce Industrial Chemicals from Biomasses					
Lignocellulosics	<u>Gasification to syngas</u>	<b>Methanol synthesis</b>	<b>Methanol to gasoline</b>		Gasoline
Fats	<b>Catalytic cracking</b>				
Lignocellulosics	<b>Catalytic cracking</b>		<b>Bioils refining</b>		
Cellulose	<u>Hydrolysis</u>	Glucose fermentation	Ethanol		
Lignocellulosics	<u>Gasification to syngas</u>	<b>Fischer Tropsch synthesis</b>	FT diesel		Diesel fuel
Fats	<b>Full hydrogenation</b>		<b>Waxes mild hydrocracking</b>		
	<b>Catalytic pyrolysis</b>		Mild hydrocracking		
	<u>Transesterification</u>		Biooil refining		
			Biodiesel (FAMES, FAEs)		
Biogas	Separation				Methane
CO <sub>2</sub>	<b>Hydrogenation</b>				
Cellulose	<u>Hydrolysis</u>	Glucose fermentation	Ethanol	<b>Ethanol dehydration</b>	Ethylene
Fats	Cracking				
Lignocellulosics	<u>Gasification to syngas</u>	<b>Methanol synthesis</b>	<b>Methanol to olefins</b>		Propylene
Lignocellulosics	<u>Gasification to syngas</u>	<b>Methanol synthesis</b>	<b>Methanol to propylene</b>		
Lignin	<u>Depolymerization</u>	Phenols	<b>Hydrogenation/cracking</b>		Aromatics
Fats	<b>Catalytic cracking</b>	Alkylphenols			
Cellulose	<u>Hydrolysis to glucose</u>	Fermentation to ethanol	<b>Steam reforming</b>	<b>Water-gas shift/CO<sub>2</sub> separation</b>	Hydrogen
Lignocellulosics	<u>Gasification to syngas</u>	<b>Water-gas shift</b>	CO <sub>2</sub> separation		
Biogas	<b>Dry reforming</b>	<b>Water-gas shift</b>	CO <sub>2</sub> separation		
Cellulose	Separation	<b>Methane steam reforming</b>			
	<u>Hydrolysis to glucose</u>	<b>Aqueous reforming</b>	<b>Water-gas shift</b>	CO <sub>2</sub> separation	
Fats	<u>Hydrolysis</u>	Glycerol	<u>Decomposition</u>	<b>Water-gas shift/CO<sub>2</sub> separation</b>	
	Saponification		<b>Steam reforming</b>		
	<u>Transesterification</u>		<b>Aqueous reforming</b>		

*Bold: heterogeneously catalyzed processes. Underline: processes that may involve heterogeneously catalyzed steps.*

The production of renewable gasoline can be obtained with the so-called Methanol to Gasoline process, or its variants, such as MTH, typically catalyzed by zeolites like H-ZSM5. At the origin, renewable methanol should be produced on Cu–ZnO–Al<sub>2</sub>O<sub>3</sub> catalysts from syngases arising from biomass gasification. This is one of the so-called BTL processes (biomass to liquids).

Gasolines can also be produced by catalytic cracking of fats or lignocellulosics, both catalyzed by solid acids such as zeolites, in particular if further refining is performed by catalytic hydrodeoxygenation processes. An additional component of renewable gasolines is certainly bioethanol mainly if produced by lignocellulosics with a cellulose hydrolysis step catalyzed by solid acids.

Excellent renewable diesel fuels can be prepared by another BTL technology based on the low-Temperature Fischer Tropsch process (Co/Al<sub>2</sub>O<sub>3</sub> catalysts) on syngases produced by biomass gasification. Another way to produce excellent renewable diesel fuels is the full hydrogenation of fats or vegetable oils on Co–Mo/Al<sub>2</sub>O<sub>3</sub> catalysts. These processes can be completed by the use of bio-gasolines produced by catalytic pyrolysis as well as by the use of conventional biodiesel.

The main gaseous olefins (mainly ethylene and propylene) can be produced by the so-called MTO (methanol to olefins) and MTP (methanol to propylene) processes performed on SAPO or on ZSM5 zeolites. Also in this case, renewable methanol coming from biomass gasification syngases should be used. Ethylene can also be produced by dehydration of bioethanol over alumina or zeolite catalysts.

Aromatics can be obtained by hydrogenation, dealkylation and/or transalkylation of the products of lignin depolymerization, using conventional catalytic technologies. Alternatively, also catalytic cracking of vegetable oils and lignocellulosics can produce aromatic mixtures.

Finally, renewable hydrogen can be obtained by separation of “biosyngases” such as those produced by biomass gasification, ethanol steam reforming, biooil and glycerol steam reforming and by aqueous reforming of glycerol, sugars and several other molecules.

Thus, although research and development in this field is still at the beginning, a number of technologies are set to be used in the future industrial organic chemistry based on renewables.

---

## References

1. Karmakar A, Karmakar S, Mukherjee S. *Bioresour Technol* 2010;**101**:7201–10.
2. Tian H, Li CY, Yang CH, Shan HH. *Chin J Chem Eng* 2008;**16**:394–400.
3. Demirbas A. *Energy Convers Manage* 2009;**50**:14–34.
4. Refaat AA. *Int J Environ Sci Technol* 2010;**7**(1):183–213.
5. Chakraborty R, Gupta AK, Chowdhury R. *Renew Sustain Energy Rev* 2014;**29**:120–34.
6. Atabani AE, Silitonga AS, Ong HC, Mahlia TMI, Masjuki HH, Badruddin IA, et al. *Renew Sustain Energy Rev* 2013;**18**:211–45.
7. Menetrez MY. *Environ Sci Technol* 2012;**46**:7073–85.

8. Mat R, Samsudin RA, Mohamed M, Johari A. *Bull Chem React Eng Catal* 2012;**7**(2): 142–9.
9. Islam A, Taufiq-Yap YH, Chu C-M, Chan E-S, Ravindra P. *Process Saf Environ Prot* 2013; **91**(1–2):131–44.
10. Sani YM, Daud WMAW, Abdul Aziz AR. *J Environ Chem Eng* 2013;**1**(3):113–21.
11. Sani YM, Daud WMAW, Abdul Aziz AR. *Appl Catal A Gen* 2014;**470**:140–61.
12. Lee DW, Park YM, Lee KY. *Catal Surv Asia* 2009;**13**:63–77.
13. Kouzu M, Hidaka J-S. *Fuel* 2012;**93**:1–12.
14. Bloch M, Bournay L, Casanave D, Chodorge JA, Coupard V, Hillion G, et al. *Oil Gas Sci Technol* 2008;**63**(4):405–17.
15. *Gulf Refining processes handbook, hydrocarbon processing*; 2008.
16. Zheng Y, Chen X, Shen Y. *Chem Rev* 2008;**108**:5235–77.
17. Ohara T, Sato T, Shimizu N, Prescher G, Schwind H, Weiberg O, et al. *Ullmann's encyclopedia of industrial chemistry*. 7th ed., vol. 17. Weinheim: Wiley-VCH; 2012. p. 348–364.
18. Arntz D, Fischer A, Höpp M, Jcobi S, Sauer J, Ohara T, et al. *Ullmann's encyclopedia of industrial chemistry*. 7th ed., vol. 17. Weinheim: Wiley-VCH; 2012. p. 329–346.
19. Massa M, Andersson A, Finocchio E, Busca G. *J Catal* 2013;**307**:170–84;  
a. Massa M, Andersson A, Finocchio E, Busca G, Lenrick F, Wallenberg LR. *J Catal* 2013;**297**:93–109.
20. Chen L, Shoujie Ren X, Philip Y. *Fuel Process Technol* 2014;**120**:40–7.
21. Castillo Martinez FA, Balcunas EM, Salgado JM, Domínguez González JM, Converti A, Oliveira RPDS. *Trends Food Sci Technol* 2013;**30**(1):70–83.
22. Pang X, Zhuang X, Tang Z, Chen X. *Biotechnol J* 2010;**5**(11):1125–36.
23. Gonçalves VLC, Pinto BP, Silva JC, Mota CJA. *Catal Today* 2008;**133**:673–7.
24. Patel A, Singh S. *Fuel* 2014;**118**:358–64.
25. Kim I, Kim J, Lee D. *Appl Catal B Environ* 2014;**148–149**:295–303.
26. Konaka A, Tago T, Yoshikawa T, Nakamura A, Masuda T. *Appl Catal B Environ* 2014; **146**:267–73.
27. Saxena RK, Anand P, Saran S, Isar J, Agarwal L. *Indian J Microbiol* March 2010;**50**(1): 2–11.
28. Vasiliadou ES, Eggenhuisen TM, Munnik P, de Jongh PE, de Jong KP, Lemonidou AA. *Appl Catal B Environ* 2014;**145**:108–19.
29. Vaidya PD, Rodrigues AE. *Chem Eng Technol* 2009;**32**:1463–9.
30. Lin Y-C. *Int J Hydrogen Energy* 2013;**38**(6):2678–700.
31. Dou B, Song Y, Wang C, Chen H, Xu Y. *Renew Sustain Energy Rev* 2014;**30**:950–60.
32. Dietrich PJ, Wu T, Sumer A, Dumesic JA, Jellinek J, Delgass WN, et al. *Top Catal* 2013; **56**(18–20):1814–28.
33. Perego C, Ricci M. *Catal Sci Technol* 2012;**2**:1776–86.
34. Furimsky E. *Catal Today* 2013;**217**:13–56.
35. Satyarthi JK, Chiranjeevi T, Gokak DT, Viswanathan PS. *Catal Sci Technol* 2013;**3**(1): 70–80.
36. Weisz PB, Haag WO, Rodewald PG. *Science* 1979;**206**:57–8.
37. Ong YK, Bhatia S. *Energy* 2010;**35**:111–9.
38. Sannita E, Aliakbarian B, Casazza AA, Perego P, Busca G. *Renew Sustain Energy Rev* 2012;**16**(8):6455–75.
39. de Almeida CG, de Souza IF, Sousa RA, Le Hyaric M. *Catal Commun* 2013;**42**:25–9.
40. Patil H, Waghmare J. *Discovery* 2013;**3**(7):10–4.
41. Lappi H, Alén R. *J Anal Appl Pyrol* 2009;**86**:274–80.

42. Vishtal A, Kraslawski A. *BioRes* 2011;**6**(3):3547–68.
43. Martin-Sampedro R, Eugenio ME, Moreno JA, Revilla E, Villar JC. *Bioresour Technol* 2014;**153**:236–44.
44. Huber GW, Iborra S, Corma A. *Chem Rev* 2006;**106**:4044–98.
45. Mu W, Ben H, Ragauskas A, Deng Y. *Bioenerg Res* 2013;**6**:1183–204.
46. Neves D, Thunman H, Matos A, Tarelho L, Gomez-Barea A. *Prog Energy Combust Sci* 2011;**37**:611–30.
47. Huang YF, Kuan WH, Chiueh PT, Lo SL. *Bioresour Technol* 2011;**102**:3527–34.
48. Mohan D, Pittman CU, Steele PH. *Energy Fuel* 2006;**20**:848–89.
49. Paris O, Zollfrank C, Zickler GA. *Carbon* 2005;**43**:53–66.
50. Shen DK, Gua S, Luo KH, Wang SR, Fang MX. *Bioresour Technol* 2010;**101**:6136–46.
51. Yang Q, Shi J, Lin L, Peng L, Zhuang J. *Bioresour Technol* November 2012;**123**:49–54.
52. Mullen CA, Boateng AA. *J Anal Appl Pyrol* 2011;**90**:197–203.
53. Van de Velden M, Baeyens J, Brems A, Janssens B, Dewil R. *Renew Energ* 2010;**35**:232–42.
54. Shen DK, Gu S, Bridgwater AV. *Carbohydr Polym* 2010;**82**:39–45.
55. Lin YC, Cho J, Tompsett GA, Westmoreland PR, Huber GW. *J Phys Chem C* 2009;**113**:20097–107.
56. Thring RW, Katikaneni SPR, Bakhshi NN. *Fuel Process Technol* 2000;**62**:17–30.
57. Carlson TR, Vispute TR, Huber GW. *ChemSusChem* 2008;**1**:397–400.
58. Li J, Li X, Zhou G, Wang W, Wang C, Komarneni S, et al. *Appl Catal A Gen* 2014;**470**:115–22.
59. Bulusheva DA, Ross JRH. *Catal Today* 2011;**171**:1–13.
60. Saidi M, Samimi F, Karimipourfard D, Nimmanwudipong T, Gates BC, Rahimpour MR. *Energy Environ Sci* 2014;**7**:103–29.
61. Rezaei PS, Shafaghat H, Wan Daud WMA. *Appl Catal A Gen* 2014;**469**:490–511.
62. Knoef HAM, editor. *Handbook biomass gasification*. The Netherlands: The Biomass Technology Group (BTG); 2005.
63. Wu W-G, Luo YH, Su Yi, Zhang YL, Zhao SH, Wang Y. *Energy Fuels* 2011;**25**:5394–406.
64. Cheah S, Carpenter DL, Magrini-Bair KA. *Energy Fuels* 2009;**23**:5291–307.
65. Calvo LF, Gil MV, Otero M, Morán A, García AI. *Bioresour Technol* 2012;**109**:206–14.
66. Milne TA, Evans RJ, Abatzoglou N. *Biomass gasifier “tars”: their nature, formation, conversion*, NREL/TP-570-25357, Available on internet; November 1998.
67. Lorente E, Millan M, Brandon NP. *Int J Hydrogen Energy* 2012;**37**:7271–8.
68. Asadullah M. *Renew Sustain Energy Rev* 2014;**29**:201–15.
69. Richardson Y, Blin J, Julbe A. *Prog Energy Combust Sci* 2012;**38**(6):765–81.
70. Aravind PV, De Jong W. *Prog Energy Combust Sci* 2012;**38**(6):737–64.
71. Torres W, Pansare SS, Goodwin Jr JG. *Catal Rev Sci Eng* 2007;**49**:407–56.
72. Yung MM, Jablonski WS, Magrini-Bair KA. *Energy Fuels* 2009;**23**:1874–87.
73. Long RQ, Monfort SM, Arkenberg GB, Matter PH, Swartz SL. *Catalysts* 2012;**2**:264–80.
74. Biomass gasification and tar reforming: the Topsøe approach. <http://bioenergi.di.dk/sitecollectiondocuments/6danskestyrkepositionerpoulerikhjoldordtopsoe.pdf>.
75. Wyman CE, Decker SR, Himmel ME, Brady JW, Skopec CE, Viikari L. In: Dumitriu S, editor. *Polysaccharides. Structural diversity and functional versatility*. 2nd ed. CRC Press; 2004 [Chapter 43].
76. Murzin DY, Simakova IL. *Catal Ind* 2011;**3**:218–49.



77. Huang YB, Fu Y. *Green Chem* 2013;**15**:1095–111.
78. Qian X, Lei J, Wickramasinghe SR. *RSC Adv* 2013;**3**(46):24280–7.
79. Yabushita M, Kobayashi H, Fukuoka A. *Appl Catal B Environ* 2013;**145**:1–9.
80. Gliozzi G, Innorta A, Mancini A, Bortolo R, Perego C, Ricci M, et al. *Appl Catal B Environ* 2014;**145**:24–33.
81. Zhang J, Wu S, Liu Y, Li B. *Catal Commun* 2013;**35**:23–6.
82. Xi J, Zhang Y, Ding D, Xia Q, Wang J, Liu X, et al. *Appl Catal A Gen* 2014;**469**:108–15.
83. Rosatella AA, Simeonov SP, Frade RFM, Afonso CAM. *Green Chem* 2011;**13**:754–93.
84. de Souza RL, Yu H, Rataboul F, Essayem N. *Challenges* 2012;**3**:212–32.
85. Ramachandran S, Fontanille P, Pandey A, Larroche C. *Food Technol Biotechnol* 2006;**44**(2):185–95.
86. Zhao G, Zheng M, Zhang J, Wang A, Zhang T. *Ind Eng Chem Res* 2013;**52**(28):9566–72.
87. Davda RR, Dumesic JA. *Chem Commun*; 2004:36–7.
88. Liang G, He L, Cheng H, Li W, Li X, Zhang C, et al. *J Catal* 2014;**309**:468–476s.
89. Cao Y, Wang J, Kang M, Zhu Y. *J Mol Catal A Chem* 2014;**381**:46–53.
90. Corma A, Huber GW, Sauvinaud L, O'Connor P. *J Catal* 2007;**247**(2):307–27.
91. Peng F, Peng P, Xu F, Sun RC. *Biotechnol Adv* 2012;**30**:879–903.
92. Agirrezabal-Telleria I, Requies J, Güemez MB, Arias PL. *Appl Catal B Environ* 2014;**145**:34–42.
93. Baskerville C. *J Ind Eng Chem* 1920;**12**:910–1.
94. Frank HG, Stadelhofer JW. *Industrial aromatic chemistry*. Berlin: Springer; 1988. p. 95.
95. Derk T, Huibers A, Hugh J, Parkhurst, Jr., *Lignin hydrocracking process to produce phenol and benzene*. US Patent 4,420,644, Lawrenceville (NJ): Assignee: Hydrocarbon Research, Inc.; 1983.
96. Zakzeski J, Bruijninx PCA, Jongerius AL, Weckhuysen BM. *Chem Rev* 2010;**110**:3552–99.
97. Azadi P, Inderwildi OR, Farnood R, King DA. *Renew Sustain Energy Rev* 2013;**21**:506–23.

# Index

*Note:* Page numbers with “f” denote figures; “t” tables.

## A

- AC. *See* Activated carbon
- Acid catalysts, 58
- acido-basicity in liquid phases, 58–62, 73–74
  - heterogeneous vs. homogeneous acid-base catalysis, 96
  - Lewis acids, 69–71, 71t
  - liquid superacids, 66t
  - protonic zeolites, 212–216
  - sulphuric acid, 63t
  - solid acids, 252–259, 265–267, 270–271
  - supported acids, 272–274
- Acidic oxides, 109
- Acido-basicity in liquid phases, 58–62
- Arrhenius theory, 58
  - Brønsted acidity and basicity, 59
    - acid strengths, 59
    - hydroxide ion, 61
    - pK<sub>a</sub> values, 63t
    - proton, 59–60
    - solvation of ion, 60
    - water autoprotolysis constant, 61
  - HSAB theory, 71–72
  - in concentrated water solutions, 62–66
  - in diluted water solutions, 58, 73–74, 96
  - in nonprotic solvents, 74
  - Lewis acidity and basicity, 69–71
  - in liquid phases, 58–62
- Acido-basicity in solids, 58–62
- acid-base catalytic materials, 252
  - calcareous minerals, 258–259
  - chemically modified clays, 255–256
  - clay minerals, 252–255
  - PILC, 256–258
  - silicate clays, 258–259
  - metal nitrides, phosphides and carbides, 265–266
  - metal sulphides, 265
  - metal oxides, 104
  - of supports for catalysts, 128–129
- Activated aluminas. *See* Transitional aluminas
- Activated carbon (AC), 277
- Adsorption, 18
- hydrogen on metals, 309–310
  - hydrogen on oxides, 346
  - hydrogen on sulphides, 355–356
  - organic substrates on metals, 310–311
  - organic substrates on oxides, 104–128
  - oxygen on metals, 379–382
  - oxygen on oxides, 383–384
- Aerogel preparation, 14–15
- Akdalaite, 137
- ALFOL process, 138–140
- Alkali
- cation zeolites, 204
  - fluorides, 264–265
  - oxides, 110, 121–122
  - phosphates, 271
  - zeolites, 210–211
  - supported alkali oxides, 129–131
- Alkaline-earth oxides, 131
- as adsorbents or absorbents, 136
  - basicity of, 131–132
  - as catalysts, 133–135
  - MgO and CaO, 133
  - MgO surface, 132f
  - as supports for catalysts, 135–136
  - surface hydroxy groups, 133
- Alkane dehydrogenation, 174, 321–322
- chromia-alumina interaction, 351–352, 357f
  - chromia-alumina catalysts, 352
  - copper catalysts, 321–322
  - gallium oxide-based catalysts, 352–353
  - platinum catalysts, 331–335
- AlkyClean process, 234
- $\alpha$ -Al<sub>2</sub>O<sub>3</sub>, 149
- $\alpha$ -methyl-styrene (AMS), 330
- AlPO. *See* Aluminophosphate
- Alumina, 304–305, 405–407
- alumina-rich silica-aluminas, 178–179
  - alumina-supported barium oxide, 134
  - aluminum hydroxides, 137, 138f
  - amorphous, 142
  - applications, 149–150
  - as catalysts, 148–150
  - corundum powders, 137–138
  - mesoporous, 142
  - polymorphism, 138f, 139t
  - preparation and solid-state chemistry, 136
  - stabilized, 142–143
  - structural data, 139t
  - as supports of catalysts, 149
  - surface chemistry, 143–148
  - transitional, 138–142

- Aluminated silicas, 179  
 Aluminophosphate (AlPO), 234  
 Aluminum compounds  
   alkyls, 138–140  
   ceria-zirconia-alumina, 179–180  
   chloride, 259–261  
   alumina-PILC, 257  
   fluoride, 262–263  
   hydroxides, 137, 138f  
   oxide, alumina, 137–138  
   phosphates, 234  
   silica–aluminas, 29  
   zeolites, 198–234  
 AM-n series titanosilicates, 238  
 Amberlyst<sup>®</sup> family, 284  
 Ammonium tetrathiomolybdate (ATTM), 358  
 Ammoxidations  
   bismuth molybdates, 387–388  
   multicomponent molybdates, 388–389  
   platinum gauzes, 400–401  
   supported vanadia catalysts, 392–393  
 AmoMax-10 catalyst, 313–314  
 Amorphous  
   aluminas, 142  
   silica, 128–129, 152, 159  
   solids, 25  
 Anatase. *See* Titania  
 Anhydrides. *See* Acidic oxides  
 Anionic exchange resins, 286  
 Antimony oxide-based catalysts, 390  
 Aqueous phase reforming (APR), 432  
 Atomic absorption, 24  
 Attapulgite, 254–255  
 ATTM. *See* Ammonium tetrathiomolybdate
- B**
- Backscattered electrons (BSE), 31  
 Baddeleyite. *See* Zirconia  
 Barium compounds  
   oxide, alumina supported, 134  
   sulphate, 271  
 Barrett-Joyner-Halenda method (BJH method), 30  
 Base-metal wet-oxidation catalysts, 399  
 Basic building unit (BBU), 198–199  
 Basic catalysts, 58  
   acido-basicity in liquid phases, 58–62  
   basicity strength scale, 70t  
   Brønsted basicity, 66–69  
   catalysis in liquid superbasic conditions, 78  
   hydrocarbons proton affinity, 77t  
   industrial conversion processes, 75t  
   industrial interest catalyzed reactions, 76t  
   industrial processes catalysts, 77t  
   Lewis bases, 69–71  
   metal oxides, 104–174  
   molecules activation, 74–78  
   nucleophilicity, 71–72  
   optical basicity, 86–88  
   reactant activation, 73–74  
 Basicity, 33, 88  
   and nucleophilicity, 71–72  
 Bauxite, 136  
 Bayer process, 136  
 BBU. *See* Basic building unit  
 BenSat process, 332  
 Benzene, toluene and xylenes (BTX), 333  
 BET method. *See* Brunauer, Emmet Teller method  
 Beta gallia structure, 113–114  
 Beta zeolite, 224–226  
 Bimetallic sulphides, 360–362  
 Biodiesel production, 430  
 Biomass  
   gasification, 134, 437  
   industrial chemicals from, 442t  
   pyrolysis, 434  
   as raw materials for industrial chemistry, 430  
 Bismuth  
   oxides, 115–116, 117f  
   molybdates, 387–388  
 Bivalent fluorides, 263–264  
 BJH method. *See* Barrett-Joyner-Halenda method  
 Boehmite, 137  
 Boiling water reactors. *See* Water-cooled reactors (WCRs)
- Boron  
   oxide, 116, 117f  
   trichloride, 264  
   trifluoride, 264  
 Brønsted acidity, 84, 169–170  
 Brunauer, Emmet Teller method (BET method), 30  
 BSE. *See* Backscattered electrons  
 BTX. *See* Benzene, toluene and xylenes  
 Bulk catalysts, 10  
   bulk metal catalysts, 302–304  
   bulk metal sulphide catalysts, 355t
- C**
- C5 isomplus process, 218  
 Calcareous minerals, 258–259  
 Calcium containing materials  
   aluminate, 320, 396  
   oxide, 86–87, 133–134, 168, 258  
   carbonate, 270–271

- phosphates, 271
- Calorimetric methods, 88–89
- Cancrinite (CAN), 210–211
- Carbides, 265–266
- Carbon-based materials, 276–277
  - ACs, 277, 278f
  - carbon blacks, 278
  - carbon gels, 279
  - carbon whiskers, 307–308, 316f
  - catalysts supports, 282–283
  - CN and nanofibers, 279–280, 281f
  - fullerenes and fullerene black, 280–281
  - GNS, 279
  - HSAG, 279
  - impregnated ACs, 277
  - ordered mesoporous carbons, 278–279
  - sulphonated carbon materials, 283–284
- Carboxylic acid hydrodeoxygenation, 353–354
- Catalysis, 2–3
  - catalyst producers, 6t
  - heterogeneous catalysis research, 5t
  - industrial catalysts, 4t
  - solid catalysts, 3
- Catalyst precursor, 368
- Catalytic hydrogen transfer reaction (CHTR), 354
- Catalytic material characterization
  - crystal size measurement, 31
  - electron microscopies, 31–32
  - FESEM micrograph, 40f
  - heterogeneous catalysts elemental composition, 24–25
  - inorganic materials, 25
  - MAS NMR, 29
  - porosity analysis, 30
  - real catalyst, 23–24
  - surface area measurement, 30
  - surface structure and composition analysis, 32–34
  - vibrational spectroscopies, 27–28
  - XAS, 28–29
  - XRD, 26
- Catalytic materials testing and application
  - activity laboratory evaluation, 53
    - gradientless laboratory testing reactors, 53
    - laboratory reactors, 54f
  - catalysts shaping, 38–41
  - catalyst extrudates, 38
  - transport phenomena, 38f
- Catalytic reactors, 41
  - burners, 377
  - catalytic distillation reactors, 45
  - catalytic membrane reactors, 46
  - combustion, 376, 398–399
  - converters, 407–408
  - fluidized bed reactors, 39, 46–47
  - gas/solid fixed-bed reactors, 41–45
  - gas/solid fluidized bed reactors, 46
  - liquid/solid fixed-bed reactors, 41–45
  - membrane reactors, 46
  - monolithic reactors, 45–46
  - polymerization reactor, 49f
  - raiser reactors, 46–47
  - slurry gas/liquid/solid reactors, 48
  - slurry liquid/solid reactors, 48
  - Operando spectroscopy, 53–55
  - reversibly deactivated catalysts regeneration, 51–52
    - solid catalysts deactivation, 48–51
- Catalytic Partial Oxidation (CPO), 312, 403–404
- Catalytic transfer hydrogenation (CTH), 354
- Catalytic transfer reduction (CTR), 354
- Catalytic Wet Oxidation (CWO), 399, 407
- Catalytic Wet-Air Oxidation (CWAO), 399
- Cation-deficient spinel, 114
- Catofin process, 352
- CBU. *See* Composite building unit
- ccp array. *See* cubic close packed array
- Ceria, 169, 171, 179–180, 305–306, 315–316, 354
- Cerium dioxide. *See* Ceria
- Cesium containing catalysts
  - cesium oxide, 206
    - supported cesium oxide, 130–131
  - Cs<sub>2</sub>SO<sub>4</sub>-V<sub>2</sub>O<sub>5</sub>/SiO<sub>2</sub> catalyst, 395
  - Cs in Ag catalyst, 401
  - Cs zeolites, 206
- CFA. *See* *cis* fatty acid
- CFB reactors. *See* Circulating fluidized bed reactors
- Chalcareous minerals, 258
- Charge transfer (CT), 86–87, 132–133
- Chemical activities, 2
- Chemical Reviews (ACS), 5–6
- Chemical Society Reviews (RSC), 5–6
- Chemical vapor deposition (CVD), 280
- Chevron Phillips Chemical Company LP (CPChem), 210–211
- Chimie douce approach, 13
- Chloride catalysts
  - aluminum trichloride, 11–12
  - boron trichloride, 262
  - chlorided alumina, 259–261
  - copper chloride, 149

- Chloride catalysts (*Continued*)  
 magnesium chloride, 261  
 metal chlorides, 261  
 silica chloride, 261–262  
 titanium chlorides, 162, 421
- Chlorine compounds  
 chlorine production, 409  
 hydrogen chloride oxidation, 409  
 chlorided VOCs combustion, 398  
 ethylene dichloride, 149, 328
- Chromia and chromites, 351  
 chromia-alumina, 351–352  
 copper chromite, 325–326, 398  
 zinc chromite, 321–322  
 fluorided chromia, 312  
 chromia combustion catalysts, 405–407
- CHTR. *See* Catalytic hydrogen transfer reaction
- Circulating fluidized bed reactors (CFB reactors), 46–47
- cis* fatty acid (CFA), 318
- Citrate autohocombustion method, 17–18
- Claus process, 148f
- Clay minerals, 252–255
- Clinoptilolite, 201–202
- Cloverite, 237
- CN. *See* Carbon nanotube
- Co-containing zeolites, 397
- Co-Mo-S structure, 360
- Cobalt-based metal catalysts, 314  
 Co-LTFT, 315  
 ethanol steam reforming, 315–316  
 oxides, 110–112, 379  
 sulphides, 354–366  
 Co-zeolites for DeNO<sub>x</sub>, 397
- COFs. *See* Covalent Organic Frameworks
- Coking catalysts, 50–51
- Colloid, 14
- Combustion synthesis, 12
- Composite building unit (CBU), 198–199
- Contact SO<sub>3</sub> process, 395
- Cooled fixed-bed reactors, 42–44
- Coordinatively unsaturated atoms (cus atoms), 86–87
- Copper-based catalysts, 321–322  
 CuAl<sub>2</sub>O<sub>4</sub> spinel, 51  
 chloride, 409  
 chromite, 325–326, 398  
 dehydrogenation of alcohols, 325–326  
 hydrogenation of nitrogenated compounds, 326  
 methanol decomposition, 324  
 methanol synthesis catalysts, 322–323  
 partial hydrogenations of oxygenates, 325  
 steam-reforming catalysts, 324  
 water–gas shift and RWGS, 323–324
- Coprecipitation, 13–14
- Corundum powders, 137–138
- Cossee–Arlman mechanism, 422f
- Covalent Organic Frameworks (COFs), 240
- CPChem. *See* Chevron Phillips Chemical Company LP
- CPO. *See* Catalytic Partial Oxidation
- Crop protection technology, 2
- Crystalline silicotitanate (CST), 238–239
- Crystalline solids, 25
- CST. *See* Crystalline silicotitanate
- CT. *See* Charge transfer
- CTH. *See* Catalytic transfer hydrogenation
- CTR. *See* Catalytic transfer reduction
- cubic close packed array (ccp array), 109
- Cubic fluorite structure, 118
- Cumene synthesis and diffusion, 226
- cus atoms. *See* Coordinatively unsaturated atoms
- CVD. *See* Chemical vapor deposition
- CWAO. *See* Catalytic Wet-Air Oxidation
- CWO. *See* Catalytic Wet Oxidation
- Cyclar process, 222
- ## D
- DAG. *See* Diacetylglycerol
- DEA. *See* Diethanolamine
- Deactivation of solid catalysts, 48–51  
 poisoning, 50  
 carbon whiskers, 307–308  
 coking, 50, 233, 272, 321, 352  
 sintering, 50  
 phase transitions and solid-state reactions, 51  
 breaking of extrudates, 51  
 erosion or breaking of monoliths, 51
- DEGbe. *See* Diethyleneglycol monobutyl ether
- Dehydrocyclodimerization, 352
- Dehydrogenation catalysts, 312  
 aromatization catalysts, 333  
 chromia-alumina catalysts, 351–352  
 copper based catalysts, 321–326  
 gallium oxide-based catalysts, 352–353  
 iron oxide-based catalysts, 348–351  
 K-Cr<sub>2</sub>O<sub>3</sub>-Al<sub>2</sub>O<sub>3</sub> catalysts, 351–352  
 metal oxides in, 346  
 oxide-based catalysts, 353–354  
 platinum based catalysts, 331–335  
 zinc oxide for, 353
- Density functional theory (DFT), 86–87
- Deposition/precipitation, 18
- Deprotonation energies (DPE), 72–73

DFT. *See* Density functional theory  
 Diacetylglycerol (DAG), 431–432  
 Diaspore, 137  
 Diatomaceous earth. *See* Kieselguhr  
 Diatomite. *See* Kieselguhr  
 Diesel engines aftertreatment, catalysts, 408  
 Diesel Particulate-NO<sub>x</sub> Reduction (DPNR), 131, 408  
 Diethanolamine (DEA), 223–224  
 Diethyleneglycol monobutyl ether (DEGbe), 361  
 Diffracted backscattered electrons (EBSD), 31  
 Dioctahedral, 252  
 Dioxygen species, 383–384  
 Direct solegel preparation, 15  
 Direct surface analysis, 33  
 Dolomite, 133  
 DPE. *See* Deprotonation energies  
 DPNR. *See* Diesel Particulate-NO<sub>x</sub> Reduction  
 Dry preparation, catalysts, 11–13  
 Dual-type methanol synthesis reactor, 44f  
 Dupont–KBR process, 282

## E

E<sub>1</sub>. *See* Elimination reactions  
 EBMax process, 229  
 EBSD. *See* Diffracted backscattered electrons  
 Ecofining process, 362  
 ED. *See* External donor  
 EDC. *See* Ethylene dichloride  
 Edge-shared MO<sub>6</sub> octahedra, 118f  
 EDX. *See* Energy-dispersive X-ray analysis  
 EELS. *See* Electron Energy Loss Spectroscopy  
 EF. *See* Extraframework material  
 EF-Al. *See* Extraframework aluminum  
 Electron diffraction, 26–27  
 Electron Energy Loss Spectroscopy (EELS), 302  
 Electron microscopies, 31–32  
 Electron paramagnetic resonance (EPR), 33  
 Elimination reactions (E<sub>1</sub>), 74–78  
 EMICT. *See* ExxonMobil Isomerization Catalyst Technology  
 Emission spectroscopies, 24  
 Emisupercages, 228  
 Endothermic equilibrium reaction, 3  
 Energy-dispersive X-ray analysis (EDX), 25  
 Eni Slurry Technology (EST), 356–357  
 Epoxidated oils, 433  
 EPR. *See* Electron paramagnetic resonance  
 Equilibrium constant, 66–67  
 Erionite, 204, 216  
 Erosion, 51  
 EST. *See* Eni Slurry Technology

EsterFipH. *See* Institut Francais du Petrole (IFP-Axens)  
 Ethylbenzene dehydrogenation, 349–351  
 Ethylbenzene disproportionation, 94  
 Ethylene dichloride (EDC), 328  
 EXAFS. *See* X-ray absorption fine structures  
 Exchangers/reactors, 44  
 Exothermic equilibrium reaction, 3  
 Exothermic reactions  
   cooled fixed-bed reactors, 42–45  
   dual-type methanol synthesis reactor, 44f  
   multitubular reactors, 45f  
   nonequilibrium reaction, 3  
   S-300 Topsøe ammonia converter, 43f  
 External donor (ED), 421–422  
 Extra-large pore zeolites, 199  
 Extraframework aluminum (EF-Al), 214–215, 225  
 Extrudates, 39, 40f  
   breaking, 51  
 ExxonMobil Isomerization Catalyst Technology (EMICT), 174

## F

Fast SCR reaction, 394  
 Fatty acids methyl ester (FAME), 430  
 FAU. *See* Faujasite  
 Faujasite (FAU), 207, 231–234  
 FBD. *See* Fluidized bed dehydrogenation  
 FCC. *See* Fluid catalytic cracking  
 FEAST process, 367  
 Ferrierite (H-FER), 217–219  
 FESEM. *See* Field Emission Scanning Electron Micrograph  
 Field Emission Scanning Electron Micrograph (FESEM), 31, 40–41  
 First-order Jahn–Teller effect (FOJT), 110  
 Fluid catalytic cracking (FCC), 40–41, 223, 253, 433  
 Fluidized bed dehydrogenation (FBD), 352  
 Fluorided chromia, 262  
 Fluorided inorganic solids, 262  
   alkali fluorides, 264–265  
   aluminum fluoride, 262–263  
   bivalent fluorides, 263–264  
   boron trifluoride, 264  
   fluorided alumina, 262–263  
   fluorided chromia, 262  
   fluorided silica–alumina, 264  
 FOJT. *See* First-order Jahn–Teller effect  
 Friedel–crafts catalysts, 259–260  
 Full width at half maximum (FWHM), 31

Fullerene, 280–281  
 black, 280  
 Fumed aluminas, 141  
 Fumed silicas, 154–155, 157f  
 FWHM. *See* Full width at half maximum

## G

Gallium oxide-based catalysts, 352–353  
 gallium oxide polymorphs, 347  
 Gas acidities (GA), 72–73  
 Gas-cooled reactor (GCR), 44  
 Gas-phase basicities (GB), 72–73  
 Gas/solid reactors  
 adiabatic fixed-bed catalytic reactors, 41–42  
 cooled fixed-bed reactors, 42–44  
 dual-type methanol synthesis reactor, 44f  
 fixed-bed reactors, 41  
 fluidized and transported bed reactors, 46, 48f  
 Haldor Topsøe reformer furnace, 42f  
 multitubular reactors, 45f  
 S-300 Topsøe ammonia converter, 43f  
 slurry gas/liquid/solid reactors, 48  
 Gasolines, 443  
 GB. *See* Gas-phase basicities  
 GCR. *See* Gas-cooled reactor  
 Gibbsite, 137  
 Glycerol conversion, 431–432  
 GNS. *See* Graphene nanosheets  
 GO. *See* Graphene oxide  
 Gold  
 gold oxides, 171, 282, 382  
 gold-based WGS catalysts, 335  
 gold based CO oxidation catalyst, 405  
 Grafting, 18–19  
 Graphene nanosheets (GNS), 279  
 Graphene oxide (GO), 279

## H

<sup>1</sup>H MAS NMR spectra, 90f, 157, 158f, 233  
 H-BEA. *See* Beta zeolite  
 H-FER. *See* Ferrierite  
 H-MAZ. *See* Zeolite. —. omega  
 H-MFI. *See* ZSM5 zeolite  
 H-MOR. *See* Mordenite  
 H-MWW zeolite. *See* MCM-22 zeolite  
 H<sub>+</sub> acidity function, 67  
 Halide salts, 259  
 fluorided inorganic solids, 262–265  
 solid chlorided catalytic materials, 259–262  
 Halloysite, 254  
 Hammett acidity function, 62–66  
 Hard acids, 71  
 Hard and soft acidity and basicity (HSAB), 71  
 Hausmannite (Mn<sub>3</sub>O<sub>4</sub>), 113  
 HC. *See* Hydrocarbons  
 hcp. *See* hexagonal close packed  
 HDN. *See* Hydrodenitrogenation  
 HDO. *See* Hydrodeoxygenation  
 HDPE. *See* High-Density PolyEthylene  
 HDS. *See* Hydrodesulphurization  
 Hectorite, 256  
 Hemicellulose  
 conversion, 437, 439  
 products from, 440f  
 Heterogeneous catalysis, 5–6, 5t  
 Heterogeneous catalysts  
 and biomass conversion, 429–443  
 metal catalysts, 302–309, 313–335  
 oxide catalysts, 354, 376–412  
 sulphide catalysts, 354–366  
 Heterogeneous metathesis catalyst  
 molybdenum-based, 368  
 rhenium-oxide, 367–368  
 tungsten-based, 366–367  
 Heterogenized homogeneous catalysts  
 metallocenes in olefin polymerization, 424f  
 montmorillonite-supported metallocene catalysts,  
 423–426  
 postmetallocene polymerization catalysts, 425f  
 supported or heterogenized homogeneous  
 catalysts, 426  
 Heteropolyacid (HPA), 109, 267, 396–397, 431  
 applications of, 269  
 phosphotungstic acid, 269  
 polyacid structures, 269–270  
 “pseudo-liquid” mechanism, 268  
 SAC, 267  
 solid HPAs and salts, 269  
 surface area of solid, 268  
 Walls–Dawson structures, 269  
 hexagonal close packed (hcp), 109  
 Hexamethyleneimine (HMI), 219  
 High oxidation state elements, 385  
 High steam-to-dry gas ratio, 349  
 High surface-area aluminum fluoride (HS-AlF<sub>3</sub>),  
 263  
 High surface-area graphite (HSAG), 279  
 High-Density PolyEthylene (HDPE), 421  
 High-resolution transmission electron microscopy  
 (HRTEM), 31–32  
 High-Temperature Fischer Tropsch process  
 (HTFT), 314  
 High-temperature water-gas shift (HTWGS),  
 348–349

- Higher Occupied Molecular Orbitals (HOMO), 109–110
- 5-HMF. *See* 5-hydroxy-methylfurfural
- HMI. *See* Hexamethylenimine
- HOMO. *See* Higher Occupied Molecular Orbitals
- Houdry DETOL process, 352
- Houdry technology. *See* Catofin process
- HPA. *See* Heteropolyacid
- HPPO. *See* Hydrogen Peroxide Propene Oxide
- HRTEM. *See* High-resolution transmission electron microscopy
- HS-AlF<sub>3</sub>. *See* High surface-area aluminum fluoride
- HSAB. *See* Hard and soft acidity and basicity
- HSAG. *See* High surface-area graphite
- HT. *See* Hydrotalcite
- HTFT. *See* High-Temperature Fischer Tropsch process
- HTWGS. *See* High-temperature water-gas shift
- Hydrocracking catalysts, 364–365
- Hydrodealkylation, 352
- Hydrodenitrogenation (HDN), 360
- Hydrodeoxygenation (HDO), 266, 365–366, 436
- Hydrodesulphurization (HDS), 265, 355–356  
bond strengths *vs.*, 364f
- Hydrogen peroxide  
activation, 411f  
catalytic oxidations with H<sub>2</sub>O<sub>2</sub>, 411–412  
direct synthesis for, 410
- Hydrogen Peroxide Propene Oxide (HPPO), 412
- Hydrogenation reactions and catalysts, 52, 309  
catalyst composition for hydrocarbon, 311  
cobalt-based metal catalysts, 314–316  
copper-based catalysts, 321–326  
gold-based catalysts, 335  
heterolytic dissociation of H<sub>2</sub>, 347  
iridium-based catalysts, 331  
iron-based metal catalysts, 313–314  
metal oxides in, 346–354  
nickel-based metal catalysts, 316–321  
oxide-based catalysts for carboxylic acid hydrodeoxygenation, 353–354  
palladium-based catalysts, 327–331  
platinum-based catalysts, 331–335  
rhenium metal in catalysis, 331  
rhodium-based catalysts, 327  
ruthenium-based catalysts, 326–327  
unsaturated hydrocarbons, 311
- Hydroprocessing, 436
- Hydrotalcite (HT), 180–181
- Hydrothermal synthesis, 16
- Hydrotreatment, 354–355, 360
- bulk metal sulphides, 355t
- catalytic activity in hydroprocessing, 362
- cobalt promoter, 359
- HDS *vs.* bond strengths, 364f
- hydrocracking catalysts, 364–365
- hydrogen adsorption, 353
- industrial processes using, 363t
- iron oxide-based catalysts, 348–351
- layered bulk sulphides, 356–360
- molybdenum sulphide, 357
- nickel promoter, 359
- rhenium sulphide, 362–364
- sulphide catalysts, 354–366
- supported bimetallic sulphides, 360–362
- tungsten sulphide, 357
- 5-hydroxy-methylfurfural (5-HMF), 439

## I

- ICDD. *See* International Centre for Diffraction Data
- ICP. *See* Inductively coupled plasma
- ICP-MS. *See* Inductively coupled plasma-mass spectrometry
- ICP-OES. *See* Inductively coupled plasma-Optical emission spectroscopy
- ID. *See* Internal donor
- Idemitsu Kosan Co., Ltd. (IKC), 210–211
- IFP-Axens. *See* Institut Francais du Petrole
- Impregnation method, 18
- Incipient wetness impregnation, 18
- Inductively coupled plasma (ICP), 24
- Inductively coupled plasma-mass spectrometry (ICP-MS), 24–25
- Inductively coupled plasma-Optical emission spectroscopy (ICP-OES), 24
- Industrial catalytic reaction  
catalysts shaping, 38  
catalytic distillation reactors, 45  
catalytic membrane reactors, 46  
circulating fluidized bed reactors, 46–47  
extrudates, 39, 40f  
FESEM micrograph, 40f  
fluid bed reactors, 39  
gas/solid fixed-bed reactors, 41–45  
gas/solid fluidized bed reactors, 46  
heterogeneous catalytic reactors, 41  
industrial catalytic reactors, 38  
liquid/solid fixed-bed reactors, 41–45  
monolithic reactors, 45–46  
polymerization reactor, 49f  
raiser reactors, 46–47



- Industrial catalytic reaction (*Continued*)  
 slurry gas/liquid/solid reactors, 48  
 slurry liquid/solid reactors, 48  
 temperature control, 41  
 transport phenomena, 38f
- Industrial chemistry, 1, 430  
 biomasses as raw materials, 430  
 catalysis, 2–3, 4t  
 chemical activities, 2  
 crop protection technology, 2  
 heterogeneous catalysts and, 429  
 industrial catalytic materials, 5–7  
 medicine development, 1–2  
 solid catalysts, 3
- Infrared spectroscopy (IR spectroscopy), 27,  
 91–92
- Inorganic acids  
 HPAs, 267–270  
 ionic liquids, 274  
 SPA, 272–273  
 SSA, 273–274  
 sulphuric acid, 63t  
 superacids, 66t  
 triflic acid, 274
- Inorganic materials, 25  
 electron diffraction, 26–27  
 MAS NMR, 29  
 neutron diffraction, 27  
 UV-vis spectroscopy, 29  
 vibrational spectroscopies, 27–28  
 XAS, 28–29  
 XRD, 26
- Institut Francais du Petrole (IFP-Axens), 430
- Internal donor (ID), 421–422
- International Centre for Diffraction Data (ICDD),  
 26
- International Union of Pure and Applied  
 Chemistry (IUPAC), 30
- International Zeolite Association (IZA), 199
- Inverse spinel, 113
- Ion exchange resins, 284  
 adsorption properties, 277t  
 anion exchangers, 286  
 anionic exchange resins, 286  
 application, 286–287  
 cationic exchange resins, 284–287  
   Hammett acidity function, 285–286  
 high surface-area mesoporous resins, 287  
 MTBE process, 284–285  
 Nafion<sup>®</sup>, 285–286  
 PDVB resins, 285
- Ionic liquids, 274
- Ionic network materials, 79
- Ionic oxide carriers, 128–129
- IR spectroscopy. *See* Infrared spectroscopy
- Iridium-based catalysts, 331
- Iron carbides, 349
- Iron molybdate, 387
- Iron oxide-based catalysts  
 Fe oxide-based catalysts for HTWGS, 348–349  
 K-Fe oxides for ethylbenzene dehydrogenation,  
 349–351  
   HREM micrograph, 350f  
   SEM micrograph, 351f
- Iron-based metal catalysts, 313  
 Fe-based ammonia synthesis, 313–314  
 HTFT, 314
- Irreversible poisoning, 50
- Isothermal reactors, 44
- IUPAC. *See* International Union of Pure and  
 Applied Chemistry
- IZA. *See* International Zeolite Association
- K**
- K-edge region, 28–29
- Kaolin, 253
- Keggin unit, 267
- Keggin-type homopolycation, 257
- Kellogg Advanced Ammonia Process (KAAP<sup>™</sup>),  
 283
- Kellogg Brown and Root (KBR), 283
- Kieselguhr, 155, 158, 160–161, 272
- Kraft cooking, conventional, 434
- L**
- LAB. *See* Linear-alkylbenzene
- Lactic acid, 431
- Lanthanum containing catalysts  
 Lanthana, 150–151, 169  
 Lanthanumoxysulphide (La<sub>2</sub>O<sub>2</sub>S), 265  
 La-H-ZSM-5 catalyst, 223–224  
 Rare earth Y zeolites for FCC, 149–150
- Large-pore zeolites, 199
- Layered bulk sulphides, 356–360
- Layered double hydroxide (LDH), 180
- LEED. *See* Low-Energy Electron Diffraction
- Lewis acid sites, 143–144
- Lewis acidity and basicity, 69–71
- Ligneocellulosic matter  
 gasification, 437  
 pyrolysis, 434–436
- Lignin  
 catalytic oxidation, 441

conversion, 440  
 depolymerization, 440  
 molecules from, 441f  
 Limestone, 258  
 Linde Type A code (LTA code), 206–207  
 Lindlar catalyst, 270–271  
 Linear Low-Density Polyethylene (LLDPE), 421  
 Linear-alkylbenzene (LAB), 256  
 Liquefied petroleum gas (LPG), 352  
 Liquid-phase partial saturation, 326  
 Liquid/solid reactors  
   fixed-bed reactors, 41–45  
   slurry, 48  
 LLDPE. *See* Linear Low-Density Polyethylene  
 Low Silica X (LSX), 207–208  
 Low-Energy Electron Diffraction (LEED), 302  
 Low-energy electron diffraction, 26–27  
 Low-temperature water–gas shift catalysts  
   (LTWGS catalysts), 323, 348  
 Lower Unoccupied Molecular Orbitals (LUMO),  
   109–110  
 LPG. *See* Liquefied petroleum gas  
 LSX. *See* Low Silica X  
 LTA code. *See* Linde Type A code  
 LTWGS catalysts. *See* Low-temperature  
   water–gas shift catalysts  
 LUMO. *See* Lower Unoccupied Molecular  
   Orbitals  
 Lyondell-Borstar Metocene technology, 423–426

## M

MA. *See* Maleic anhydride  
 MAG. *See* Monoacetylglycerol  
 Magic acid, 62–66  
 Magic angle spinning (MAS), 29, 86  
 Magnéli phases, 123  
 Magnesium containing materials  
   magnesium aluminate, 135, 180–181  
   magnesium oxide, magnesia, 133, 354  
   magnesium vanadates, 129  
 Maleic anhydride (MA), 391  
 MAO. *See* Methylaluminoxane  
 MAPO. *See* Metal heteroatom containing  
   aluminophosphate  
 Mars-van Krevelen mechanism, 347, 378–379  
 MAS. *See* Magic angle spinning  
 MBOH. *See* 2-methyl-3-butyn-2-ol  
 MCC. *See* Mitsubishi Chemicals Co  
 MCM-22 zeolite, 226–229, 227f  
 Medium-pore zeolites, 199, 219–220  
   clinoptilolite, 220  
   ZSM-22 zeolites, 220  
   ZSM-23 zeolites, 220  
   ZSM-48 zeolites, 220  
 Meervein-Ponndorf-Verley reaction, 354  
 MEK. *See* Methyl-ethyl-ketone  
 Mesityl oxide (MO), 330–331  
 Mesoporosity, 216  
 Mesoporous aluminas, 142  
 Mesoporous silicas, 153, 154t  
 Meta-4 process, 367  
 Metal aluminates, 305  
 Metal catalysts  
   for ammonia selective catalytic oxidation, 403  
   catalysts for aftertreatment of engines' waste  
     gases  
     catalytic converters, 407–408  
     diesel engines aftertreatment, 408  
   for catalytic wet oxidation, 407  
   for CO oxidation, 404–405  
   combustion catalysts for energy generation,  
     405–406  
   dehydrogenations, 301  
   for gas-phase selective oxidations of organics,  
     402  
   hydrogen and syngas production processes, 301  
   industrial reactions, 299t  
   knitted Pt gauze, 400f  
   metal gauzes for oxidation catalysis, 400–401  
   for methane partial oxidation to syngas, 403–404  
   Pd/Al<sub>2</sub>O<sub>3</sub> methane combustion catalyst, 406f  
   periodic table of elements, 301f  
   Raney metals, 302  
   for selective oxidations in liquid phase, 402  
   silver catalysts for selective oxidations, 401–402  
   surface science studies, 302–304  
   for total oxidation for VOC abatement, 406–407  
   unsupported metal nanoparticles, 304  
   water gas shift (WGS), 348–351  
   woven PteRh gauze, 400f  
 Metal chlorides, 261–262  
   flame hydrolysis, 11–12  
 Metal heteroatom containing aluminophosphate  
   (MAPO), 237  
 Metal molybdates for oxidations, 385  
   bismuth molybdates, 387–388  
   crystalline structures, 389f  
   iron molybdate for formaldehyde synthesis, 387  
   Mo/V/Nb/Te oxides, 390, 391f  
   multicomponent molybdates, 388–389  
   polymeric (Mo<sub>2</sub>O<sub>8</sub>)<sup>4-</sup><sub>n</sub> anion, 386f  
   scheelite structure, 386f  
   vanadium molybdate-based catalysts, 389–390  
 Metal nitrides, 265–266

- Metal Organic Framework (MOF), 239–240, 240f
- Metal oxide
- acidic oxides, 109
  - acidity and basicity, 69–73
  - alumina, 137–138
  - amorphous vs. crystalline metal oxides, 122
  - “bulk” acidity and basicity, 104
  - ceria, 171
  - covalent vs. ionic oxides, 121–122
  - crystal structures, 109, 111t, 117f
  - electronic conduction, 122–123
  - and hydroxides, 104, 108
  - hydrogen adsorption, 353
  - lanthana, 150
  - magnesia and alkaline-earth oxides, 131–136
  - magnetism, 122–123
  - niobia, 172–173
  - oxoacids, 108–109
  - oxygen adsorption/reaction/activation on, 383–384
  - particle size effect, 124
  - and properties, 105t
  - rare-earth oxides, 151
  - reactivity, 108
  - redox behavior, 122
  - silica, 151–161
  - structural chemistry, 109–121
  - supported alkali oxides, 129–131
  - thermal stability, 122, 124
  - titania, 161–165
  - tungsta, 173–174
  - zirconia, 166–171
- Metal sulphates, 271
- Metal sulphides.
- See also* Bimetallic sulphides
  - bulk sulphides, 356–360
  - HDS vs. bond strengths, 364f
  - hydrogen adsorption, 355–356
- Metal-based industrial catalysts, 306–307
- Metal-free Lewis acid catalysts, 69
- Metallic materials, 79
- Metallic species, 128
- Methanation, 320
- Methanol to Gasoline process (MTG process), 223
- Methanol to Olefin process (MTO process), 236, 443
- Methanol to propylene process (MTP process), 223, 443
- 2-methyl-3-butyn-2-ol (MBOH), 93–94
- Methyl-ethyl-ketone (MEK), 353
- Methyl-Isobutyl Ketone (MIBK), 330–331
- Methylaluminoxane (MAO), 423
- Mg aluminate ( $\text{MgAl}_2\text{O}_4$ ), 180–181
- $\text{Mg}_6\text{Al}_2(\text{OH})_{16}\text{CO}_3 \cdot 4\text{H}_2\text{O}$ . *See* Hydrotalcite (HT)
- MIBK. *See* Methyl-Isobutyl Ketone
- Micro/mesoporous materials, 219
- Microemulsion, 15–16
- Mitsubishi Chemicals Co. (MCC), 353
- Mitsubishi Gas, 404–405
- Mixed metal oxide
- alumina-rich silica–aluminas, 178–179
  - aluminated silicas, 179
  - calcined HT, 180–181
  - ceria and zirconia combination, 179–180
  - molybdates, 385
  - molybdeno-vanadate, 387
  - silica–aluminas, 174–178
  - silicated aluminas, 179
  - supported vanadia, 392–393
  - spinel, 180–181
  - titania and zirconia combination, 179
  - zinc aluminate, 182
- MO. *See* Mesityl oxide
- Mobil Selective DeWaxing process (MSDW), 223
- Mobil–Badger process, 222
- MOF. *See* Metal Organic Framework
- Molecular orbital theory, 87
- Molecular sieving effect, 198, 215
- Molecular weight (MW), 423
- Molecular weight distribution (MWD), 422
- Molybdenum based catalysts
- molybdate oxidation catalysts, 385–390
  - molybdenum oxide, 394
  - molybdenum sulphides, 357, 358f
  - molybdenum-based metathesis catalyst, 368
- Monoacetylglycerol (MAG), 431–432
- Monoclinic zirconia, 166
- Monolithic catalysts, 51
- Monolithic reactors, 45–46
- Monoliths breaking, 51
- Montecatini slurry processes, 422–423
- Montmorillonite catalysts
- montmorillonite, structure, 254, 255f
  - acid-treated clays, 256
  - pillared, 257
  - montmorillonite-supported metallocene catalysts, 423–426
- Mordenite, 229–230
- MPO. *See* Partial oxidation of methane
- MSDW. *See* Mobil Selective DeWaxing process
- MTG process. *See* Methanol to Gasoline process
- MTO process. *See* Methanol to Olefin process
- MTP process. *See* Methanol to Propylene process
- Multicomponent molybdates, 388–389

Multiply twinned particle (MTP), 307–308, 382–383

Multiply walled CN (MWNT), 279–280

Multitubular cooled fixed-bed reactors, 377

Multitubular reactors. *See* Exchangers/reactors

MW. *See* Molecular weight

MWD. *See* Molecular weight distribution

MWNT. *See* Multiply walled CN

n-bases, 74

## N

Nafion<sup>®</sup>, 285

Nanocrystalline hydrous oxyhydroxide, 138–140

Natural gas liquid (NGL), 396

Neutron diffraction, 27

NEw BULK Activity, 358

NEXBTL diesel-producing process, 362

NGL. *See* Natural gas liquid

NH sol–gel. *See* Nonhydrolytic sol–gel

Nickel-based materials.

*See also* Ruthenium-based catalysts

nickel oxide, 93, 403

nickel phosphides, 266

nickel-based metal catalysts, 316

carbon whiskers, 316f

Ni-alumina-and Ni-aluminate-based catalysts, 318–321

nickel raney and sponge nickel catalysts, 317–318

nickel/silica catalysts, 318

nickel traps, 40–41

Niobia, 119–120, 172–173

Nitrided carbon material, 284

Nitrides, metallic, 265–266

Nitro groups hydrogenation, 334

NMR spectroscopy. *See* Nuclear magnetic resonance spectroscopy

Noble metals, 124, 301

noble metal catalysts

for catalytic wet oxidation, 407

for selective oxidations in liquid phase, 402

for total oxidation for VOC abatement, 406–407

Nonaqueous sol–gel. *See* Nonhydrolytic sol–gel (NH sol–gel)

Nonhydrolytic sol–gel (NH sol–gel), 14

Nonporous ceramic crystalline silica powders, 156

Nonprotic solvents, Brønsted basicity in, 66–69

NO<sub>3</sub> storage-reduction (NSR), 131, 408

Nuclear magnetic resonance spectroscopy (NMR spectroscopy), 70, 92, 269

γ-Al<sub>2</sub>O<sub>3</sub> crystal structure, 94f

theoretical methods, 93

Nucleophilicity, 71–72

## O

ODH. *See* Oxidative dehydrogenation

Olefin metathesis, 366

heterogeneous rhenium-oxide, 367–368

heterogeneous tungsten-based, 366–367

molybdenum-based, 368

Olefins, 352, 421

olefin-modified site, 170

olefinic double bonds, 311

Operando spectroscopy, 53–55

Ordered mesoporous carbons, 278–279

Ordered solids. *See* Crystalline solids

Organic structure directing agents (OSDA), 201

Organo-inorganic hybrid materials, 275–276

Organoclays, 258

Organometallics, 275

Organosilanes, 153

OSDA. *See* Organic structure directing agents

Oxidation catalysis.

*See also* Transition-metal mixed oxides adsorption/reaction/activation of oxygen, 379–382

on metal oxides, 383–384

catalytic oxidations with H<sub>2</sub>O<sub>2</sub>, 411–412

direct synthesis for, 410

hydrogen peroxide activation, 411f

oxidation reactions, 376–377

mechanisms, 377–379

oxidant and process configurations, 377

substrate activation, 384–385

supported metal catalysts, 382–383

surface-oxygen species, 378t

Oxidation catalysts, 384–385

base-metal wet-oxidation catalysts, 399

chromia-based, 384

molybdates, 385

vanadium oxides, 391–395

noble metal based, 402

silver catalyst, 401–402

Oxidation reactions, 283

catalytic combustion of dioxins, 410

ethylene oxychlorination, 409–410

of HCl to Cl<sub>2</sub>, 409

soot oxidation, 398–399

Oxidative dehydrogenation (ODH), 396

Oxide catalysts

as acid-base catalysts, 128

for hydrogenations, 354

for oxidative dehydrogenations, 395–396

- Oxide catalysts (*Continued*)  
 for selective oxidations, 393–394  
 for total oxidations  
 base-metal wet-oxidation catalysts, 399  
 catalytic combustion for VOC abatement, 398  
 soot oxidation catalysts, 398–399
- Oxygen adsorption/reaction/activation  
 on bulk metals, 379–382  
 on metal oxides, 383–384
- Oxyhydroxides, 138–140
- P**
- PA. *See* Proton affinity
- Palladium-based catalysts, 327, 405–406  
 AMS, 330  
 C4-cuts treatment, 329  
 catalyst composition, 328  
 catalytic converters, 407–408  
 front-end hydrogenation configuration, 329  
 hydrogen adsorption on, 353  
 hydrogenation of acetylenic hydrocarbons,  
 327–328  
 for hydrogenation of oxygenated compounds,  
 330–331  
 for methanol synthesis and steam reforming,  
 330–331  
 oxidation catalysts, 376–385  
 oxygen adsorption on, 383–384  
 palladium oxide, 330–331
- Palygorskite. *See* Attapulgite
- Paraffin dehydrogenation, 46–47, 351–352
- Paraffin skeletal isomerization, 260
- Partial oxidation of methane (MPO), 159
- Partially Stabilized Zirconia (PSZ), 168
- Passive regeneration behavior, 408
- PBE-1 catalyst matrix, 225–226
- PCHs, 257–258
- PDVB. *See* Polydivinylbenzene
- Phase transitions, 51
- Phillips-type catalysts, 423
- Phosphides, 265–266
- Phosphotungstic acid, 269
- $\pi$ -basicity, 74–78
- Pillared clays (PILC), 256–257  
 catalytic activity, 257  
 Keggin-type homopolycation, 257  
 organoclays, 258
- Pillared montmorillonites (PILM), 257
- PILM. *See* Pillared montmorillonites
- Plasma-chemical synthesis. *See also*  
 Hydrothermal synthesis, 19
- Platinum group metals, 124
- Platinum-based catalysts, 331  
 for aromatic saturation, 332–333  
 aromatization, 333  
 carbon–carbon triple bonds, 331  
 for dehydrogenation of alkanes, 334  
 hydrogenation of olefins, 332  
 liquid-phase hydrogenation, 334  
 naphtha reforming, 333  
 water–gas shift and steam reforming, 334–335  
 oxygen adsorption on, 383–384  
 hydrogen adsorption on, 331–332  
 liquid phase oxidation, 333  
 platinum oxide, 381  
 total oxidation catalysts, 406–407
- PMP. *See* Poly-4-methyl-1-pentene
- Point of zero charge (PZC), 18, 19t
- Poisoning, 50
- Poly-4-methyl-1-pentene (PMP), 421
- Polydivinylbenzene (PDVB), 285
- Polymerization reactor, 49f
- Polyol process, 16–17
- Polyoxoacids, 109
- Polyoxometallates (POM), 267
- PolyPropylene (PP), 421
- Polytetrafluoroethylene, 264
- Polyvinyl chloride, 1–2
- POM. *See* Polyoxometallates
- POP. *See* Porous Organoc Polymer
- Porosity analysis, 30
- Porous materials, 17
- Porous Organoc Polymer (POP), 240
- Postmetallocene polymerization catalysts, 425f
- Potassium containing materials and catalysts  
 K-zeolites, 240  
 K-Cr<sub>2</sub>O<sub>3</sub>-Al<sub>2</sub>O<sub>3</sub>, 351–352  
 K-Fe oxides, 349–351  
 Pt-K-alumina, 408  
 Pt-K-LTL zeolite catalyst, 210–211  
 V-K/Al<sub>2</sub>O<sub>3</sub> catalysts, 396  
 K<sub>2</sub>SO<sub>4</sub>-V<sub>2</sub>O<sub>5</sub> catalysts, 395
- PP. *See* PolyPropylene
- Praseodymium oxysulphide (Pr<sub>2</sub>O<sub>2</sub>S), 265
- Precipitation, 13–14
- Preferential oxidation (PROX), 313
- Propene oligomerization, 273
- Proton, 59–60
- Proton affinity (PA), 72–73
- Protonic zeolites.  
*See also* Zeolite(s)  
 acidic protons, 213–214  
 beta zeolite, 224–226  
 bridging hydroxyl groups, 212

EF, 214–215  
 erionite, 216  
 external surface of, 215–216  
 ferrierite, 217–219  
 H-ZSM-5 zeolites, 213f  
 IR spectra, 212  
 MCM-22 zeolite, 226–229  
 medium-pore zeolites, 219–220  
 molecular sieving and shape selectivity, 215  
 mordenite, 229–230  
 porous zeolites, 216  
 zeolite omega, 230–231  
 ZSM-12 zeolite, 224  
 ZSM5, 220–224  
 PROX. *See* Preferential oxidation  
 Pseudoboehmite gel, 136  
 Pseudoionone, 286  
 Pseudomorphism, 392f  
 PSZ. *See* Partially Stabilized Zirconia  
 Pt-H-ferrierite, 219  
 Pyrogenic silicas, 154–155  
 Pyrrolidine (Pyr), 219  
 PZC. *See* Point of zero charge

## Q

*Quasi* VSbO<sub>4</sub> system, 390

## R

RAIRS. *See* Reflection Absorption Infrared Spectroscopy  
 Raiser reactors, 46–47  
 Raman spectroscopy, 27  
 Raney metals, 302  
 Rare-earth  
   rare earths oxides, 108, 114, 151  
   rare-earth sesquioxides, 114f  
   rare earth Y zeolite (REY), 149–150  
   lanthanum doped alumina, 142–143  
   lanthanum oxide, 150–151  
 Redox mechanism. *See* Mars-Van Krevelen mechanism  
 Refining Hydrocarbon Technologies (RHT), 430  
 Reflection Absorption Infrared Spectroscopy (RAIRS), 302  
 Regeneration of catalysts, 52  
 Rejuvenation. *See* Washing  
 Renewable Diesel fuels, 443  
 Reverse micelle method, 15–16  
 Reverse water–gas shift reaction (RWGS), 324  
 Reverse-Isomplus process, 218  
 Reversibly deactivated catalysts regeneration, 51–52

Rhenium based catalysts  
   metal in catalysis, 331  
   catalytic reforming catalysts, 333  
   rhenium-based metathesis catalysts, 368  
   sulphide, 362–364  
 Rhodium-based catalysts  
   rhodium oxides, 380–381  
   hydrogenation catalysts, 327  
   catalytic partial oxidation, 327, 403–404  
   catalytic converters, 407–408  
 RHT. *See* Refining Hydrocarbon Technologies  
 Rietveld analysis, 26  
 Routine analysis, 26  
 RSC. *See* Chemical Society Reviews  
 Ruthenium-based catalysts, 326–327  
   ruthenium oxide, 165, 380–381, 409  
   ammonia synthesis, 326  
   hydrogen chloride oxidation catalysts, 165, 409  
   liquid phase oxidation catalysts, 333  
   methanation, 320  
   ruthenium sulphide, 362  
 Rutile, 116, 165  
 Rutile-type antimonate catalysts, 390  
 RWGS. *See* Reverse water–gas shift reaction

## S

S-300 Topsøe ammonia converter, 43f  
 SA. *See* Silica–alumina  
 SAC. *See* Solid acid catalysts  
 SAED. *See* Selected area electron diffraction  
 SAPOs. *See* Silicoaluminophosphates  
 Scanning electron microscope (SEM), 31  
 Scanning transmission electron microscope (STEM), 32  
 Scanning tunneling microscopy (STM), 303  
 SCFs. *See* Supercritical fluids  
 SCW. *See* Supercritical water  
 SDA. *See* Structure Directing Agents  
 Second-order Jahn–Teller effect (SOJT), 109–110  
 Selected area diffraction (SAD). *See* Selected area electron diffraction (SAED)  
 Selected area electron diffraction (SAED), 26–27  
 Selective Hydrogenation Process (SHP), 319  
 Selective Hydrogenation Unit (SHU), 329–330  
 Selective ring opening (SRO), 331  
 Selective Toluene Disproportionation (STDP), 221–222  
 SELECTOXO™ catalyst material, 404–405  
 Self-propagating high-temperature synthesis. *See* Combustion synthesis  
 SEM. *See* Scanning electron microscope

- Semiregenerative naphtha-reforming process, 333
- Sepiolite, 259
- Sesquioxides, 114
- Shape-selectivity effect, 198
- SHP. *See* Selective Hydrogenation Process
- SHU. *See* Selective Hydrogenation Unit
- Silanol group, 128–129
- Silica
- aerogels, 153
  - as catalysts, 159–160
  - fumed or pyrogenic, 154–155, 157f
  - gels, 152, 157f
  - Kieselguhr, 155
  - mesoporous, 153, 154t
  - nonporous ceramic crystalline silica powders, 156
  - precipitated, 152
  - preparation and solid-state chemistry, 151–156
  - silicalites, 155–156
  - spherical, 153–154
  - Stöber, 153–154
  - as support of catalysts, 160–161
  - surface chemistry, 156–159
- Silica chloride ( $\text{SiO}_2\text{-Cl}$ ), 261–262
- Silica sulphuric acid (SSA), 273–274
- Silica–alumina (SA), 174–175
- acidity of pseudobridging OH, 177–178
  - bands, 175–176
  - as catalysts, 178
  - FT-IR spectra, 177f
  - Lewis acid sites, 175
  - surface hydroxy groups, 176–177
- Silicalites, 155–156
- Silicate clays, 258–259
- Silicated aluminas, 179
- Silicoaluminophosphates (SAPOs), 234–236
- Silver based materials
- oxygen adsorption on silver, 402
  - silver oxides, 382, 402
  - silver zeolites, 208–210
  - silver gauzes, 230
  - silver oxidation catalysts, 229
- Single wall carbon nanotubes (SWNT), 279–280
- Sintering, 50
- $\text{SiO}_2\text{-Cl}$ . *See* Silica chloride
- Slurry-phase preparation, 13
- adsorption, 18
  - aerogel preparation, 14–15
  - citrate auto-combustion method, 17–18
  - coprecipitation, 13–14
  - deposition/precipitation, 18
  - direct sol-gel preparation, 15
  - grafting, 18–19
  - hydrothermal synthesis, 16
  - impregnation method, 18
  - ion exchange, 18
  - metal oxides PZC, 19t
  - microemulsion, 15–16
  - plasma-chemical synthesis, 19
  - polyol process, 16–17
  - precipitation, 13–14
  - reverse micelle method, 15–16
  - sol-gel preparation, 14
  - solution combustion synthesis, 17
  - solvothermal synthesis, 16
  - template-driven hydrothermal preparation, 17
- Small-pore zeolites, 199
- Smectite clays, 254
- SMSI effect. *See* Strong Metal Support Interaction effect
- $\text{SN}_1$ . *See* Substitution reactions
- SNG. *See* Synthetic Natural Gas
- SNOW process, 353
- Sodium silicate, 11
- Soft chemistry. *See* Chimie douce approach
- SOJT. *See* Second-order Jahn–Teller effect
- Sol-gel chemistry, 14–15
- Sol-gel coordination chemistry, 14
- Solid acid catalysts (SAC), 267
- Solid catalysts, 3, 38, 134.
- See also* Monolithic catalysts
  - bulk catalysts, 10
  - catalytic materials components, 10–11
  - choice of starting compounds, 11
  - deactivation, 48–51
  - dry preparation procedure, 11–13
  - intermediate and treatments, 19–20
  - supported catalysts, 10
  - transesterification, 430
  - wet catalyst preparation, 13–19
- Solid phosphoric acid catalyst (SPA catalyst), 272–273
- Solid polymerization catalysts, 421
- heterogenized “single-site” polymerization catalysts, 423–426
  - Phillips-type catalysts, 423
  - ZN catalysts, 421–423
- Solid-state ion exchange, 12
- Solid-state reaction, 11, 51
- Solid-state wetting, 12
- Solids, surface acidity and basicity of
- calorimetric methods, 88–89
  - catalytic probe reactions, 93–95
  - characterization techniques, 80

- IR spectroscopy, 91–92  
<sup>1</sup>H MAS NMR spectra, 90f  
 molecular probes for, 80–84, 81t–82t, 83f  
 NMR spectroscopy, 92–93  
 probe molecules quantitative adsorption, 88  
 strength, amount, and distribution, 95  
 structural chemistry vs. surface chemistry, 79–80  
 surface basic sites, 86–88  
 surface hydroxyl groups direct detection, 80–84  
 Solution combustion synthesis, 17.  
   *See also* Hydrothermal synthesis  
 Solvay process, 258  
 Solvothermal synthesis, 16  
 Sonochemical treatments, 19  
 Soot oxidation catalysts, 398–399  
 SPA catalyst. *See* Solid phosphoric acid catalyst  
 Spectroscopic studies, 347  
 Spherical silica, 153–154  
 Spinel material, 180–181  
   defective spinel aluminas, 93  
   cobalt oxide, 314–316  
   magnesium aluminate, 180–182  
   copper aluminate, 51  
   copper chromite, 325–326, 398  
   magnetite, 313, 348  
   zinc chromite, 321–322, 353  
   zinc aluminate, 182  
 SRO. *See* Selective ring opening  
 SSA. *See* Silica sulphuric acid  
 Stabilized aluminas, 142–143, 149  
 STD. *See* Selective Toluene Disproportionation  
 Steam Active Reforming (STAR), 396  
 Steam reforming processes, 301  
 Steam-reforming, 312–313  
 STEM. *See* Scanning transmission electron microscope  
 Stishovite, 151  
 STM. *See* Scanning tunneling microscopy  
 Stöber silica, 153–154  
 Strong Metal Support Interaction effect (SMSI effect), 165, 305  
 Structure Directing Agents (SDA), 17  
 Substitution reactions (SN<sub>1</sub>), 74–78  
 Sulphated zirconia, 169–171  
 Sulphide catalysts, 165, 262  
   bulk sulphides crystal structure, 355t  
   hydrogen adsorption, 355–356  
   industrial processes using, 363t  
   layered bulk sulphides, 356–360  
   supported sulphides, 359  
 Sulphonated carbon materials, 283–284  
 Sulphur dioxide oxidation catalysts, 39f  
 Superacidity, 66, 66t  
 Superbasicity, 67–68  
 Supercritical drying process. *See* Aerogel preparation  
 Supercritical fluids (SCFs), 15  
 Supercritical water (SCW), 15  
 Supported catalysts, 10  
   supported alkali oxides, 129–131  
   supported homogeneous catalysts, 426  
   supported metal catalysts, 304–309  
   supported metal nanoparticles, 306–308  
   supported vanadium oxides, 392–393  
   supported metal sulphides, 128  
 Surface acidity, 33  
 Surface acido-basicity, 125–128, 127t  
 Surface area measurement, 30  
 Surface redox behavior, 34  
 Surface science studies, 302–304, 303f  
 Surface-oxygen species, 378t  
 SWNT. *See* Single wall carbon nanotubes  
 Synthetic Natural Gas (SNG), 320
- ## T
- TAG. *See* Triacetyl glycerol  
 TBOT. *See* Tetrabutyl titanate  
 Teflon. *See* Polytetrafluoroethylene  
 TEG. *See* Triethyleneglycol  
 TEM. *See* Transmission electron microscopy  
 Temperature-programmed desorption (TPD), 89–91  
 Temperature-programmed reduction (TPR), 34  
 Template-driven hydrothermal preparation, 17  
 TEOS. *See* Tetraethyl-orthosilicate  
 Tetrabutyl titanate (TBOT), 163  
 Tetraethoxysilane. *See* Tetraethyl-orthosilicate (TEOS)  
 Tetraethyl-orthosilicate (TEOS), 153, 179  
 Tetrafluoroethylene (TFE), 264  
 Tetragonal zirconia polycrystal (TZP), 168  
 Tetramethyl-orthosilicate (TMOS), 153  
 TFAs. *See trans* fatty acids  
 TFE. *See* Tetrafluoroethylene  
 Theoretical methods, 93  
 Thermal decomposition of precursors, 11  
 Thermodynamics, 3  
 Thin containing catalysts  
   Pt-Sn for dehydrogenation, 334  
   Pt-Re-Sn catalysts for catalytic reforming, 331  
   SnO<sub>2</sub> as catalyst support, 409  
 Three-Way Catalysts (TWC), 407  
 Ti-silicalite, 237–238, 411–412  
 Ti(OC<sub>4</sub>H<sub>9</sub>)<sub>4</sub>. *See* Tetrabutyl titanate (TBOT)



- Titania, 161–162, 305  
   anatase, 51, 118f, 124, 161, 305, 394  
   brookite, 118f, 161  
   as catalyst, 164  
   chloride process, 162  
   photocatalytic activity, 162–163  
   in rutile, 116, 117f, 161, 163  
   semiconducting behavior, 161  
   as support for catalysts, 164–165  
   surface chemistry, 163–164  
   TiO<sub>2</sub> (B), 161  
 Titration method, 88  
 TMOS. *See* Tetramethyl-orthosilicate  
 TOF. *See* Turnover frequencies  
 Toluene hydrodealkylation, 352  
 TPD. *See* Temperature-programmed desorption  
 TPR. *See* Temperature-programmed reduction  
*trans* fatty acids (TFAs), 318  
 Transition metal nitrides, 365  
 Transition-metal mixed oxides, 385.  
   *See also* Oxidation catalysts  
   antimony oxide-based catalysts, 390  
   heteropolyacids for selective oxidations, 396–397  
   metal molybdates for oxidations, 385–390  
   oxide catalysts for oxidative dehydrogenations,  
     395–396  
   oxide catalysts for total oxidations, 398–399  
   vanadium oxide-based catalysts, 391–395  
   zeolite catalysts, 397–398  
 Transitional aluminas, 138–142  
 Transmission electron microscopy (TEM), 26–27  
 Triacetyl glycerol (TAG), 431–432  
 Triethyleneglycol (TEG), 361  
 Triflic acid, 274  
 Triglycerides, 433  
 Trivalent “classical” carbocations, 74–78  
 Trivalent nonmetallic elements, 116  
 Trivalent rare-earth oxides, 114–115  
 Tungsta, 173  
   tungsta, tungsten oxides, 173–174, 366  
   tungsta as catalyst, 174  
   tungsta metathesis catalysts, 366–367  
   tungsta-zirconia as catalyst, 174  
   tungsten sulphides, 357, 358f  
 Tungstenite, 358  
 Turnover frequencies (TOF), 332–333  
 TWC. *See* Three-Way Catalysts  
 TZP. *See* Tetragonal zirconia polycrystal
- U**  
 Unsupported metal nanoparticles, 304  
 Uranyl antimonates, 390
- UV spectroscopy, 86–88  
 UV-vis spectroscopy, 29
- V**  
 Vanadium molybdate-based catalysts, 389–390  
 Vanadium oxide-based catalysts  
   vanadium oxides, 18–19, 119  
   vanadium pentoxide ( $\alpha$ -V<sub>2</sub>O<sub>5</sub>), 119  
   for NO<sub>x</sub> selective catalytic reduction, 393–394  
   pseudomorphism, 392f  
   for SO<sub>2</sub> oxidation to SO<sub>3</sub>, 395  
   supported vanadia catalysts, 392–393  
   VPO catalysts, 391–392  
 Vanadyl hydrogen phosphate hemihydrate  
   (VOHPO<sub>4</sub>·0.5H<sub>2</sub>O), 391–392  
 Vanadyl pyrophosphate catalysts (VPO), 391  
 VCM. *See* Vinyl chloride monomer  
 Vegetable oils  
   chemicals from triglycerides, 433  
   fatty acid conversion, 433  
   hydrogenations, 432–433  
   pyrolysis, 433  
 Verkade bases, 68  
 Vibrational spectroscopies, 27–28  
 Vinyl chloride monomer (VCM), 328  
 (VO)<sub>2</sub>P<sub>2</sub>O<sub>7</sub>. *See* Vanadyl pyrophosphate catalysts  
   (VPO)  
 VPO. *See* Vanadyl pyrophosphate catalysts  
 VPP. *See* Vanadyl pyrophosphate catalysts (VPO)
- W**  
 Walls–Dawson structures, 269  
 Washing, 52  
 Waste gas aftertreatment, catalysts for  
   catalysts for diesel engines aftertreatment, 408  
   catalytic converters, 407–408  
 Water autoprotolysis equilibrium, 58  
 Water gas-shift  
   HTWGS, 348–349  
   LTWGS, 348  
 Water solution, protonic acidity in, 62–66  
 Water-cooled reactor (WCR), 44  
 Water–gas shift processes, 301  
 WCR. *See* Water-cooled reactor  
 Weak basic molecule activation by acids, 74  
    $\pi$ -basicity, 74–78  
    $\sigma$ -basicity of saturated hydrocarbons, 78  
   proton affinity, 77t  
   carbenium ions, 72, 74–78, 93  
   carbonium ions, 78  
 Weight hourly space velocity (WHSV), 210–211  
 Wet catalyst preparation, 13

- adsorption, 18
  - aerogel preparation, 14–15
  - citrate auto-combustion method, 17–18
  - coprecipitation, 13–14
  - deposition/precipitation, 18
  - direct sol-gel preparation, 15
  - grafting, 18–19
  - hydrothermal synthesis, 16
  - impregnation method, 18
  - ion exchange, 18
  - metal oxides PZC, 19t
  - microemulsion, 15–16
  - plasma-chemical synthesis, 19
  - polyol process, 16–17
  - precipitation, 13–14
  - reverse micelle method, 15–16
  - sol-gel preparation, 14
  - solution combustion synthesis, 17
  - solvothermal synthesis, 16
  - template-driven hydrothermal preparation, 17
  - WHSV. *See* Weight hourly space velocity
- X**
- X-ray absorption fine structures (EXAFS), 28–29
  - X-ray absorption near-edge structure (XANES), 28–29
  - X-ray absorption spectroscopy (XAS), 28–29
  - X-ray diffraction spectrometry (XRD), 25
  - X-ray fluorescence (XRF), 24
  - X-ray photoelectron spectroscopy (XPS), 32–33, 86–88
  - X-rays (XR), 25
- Y**
- Yttria-stabilized zirconia (YSZ), 168
- Z**
- Zeolite(s), 198
    - adsorption of CO<sub>2</sub>, 206f
    - alkali cation zeolites, 204
    - alkali earth exchanged faujasites, 207–208
    - catalysts, 397–398
    - cationic siting in FAU and LTA, 203f
    - CO complex with Na<sup>+</sup> ions, 205f
    - co-containing, 397
    - EU-1, 231
    - faujasite, 231–234
    - HEU, 203f
    - K-Ferrierite, 205f
    - LTA zeolites, 206–207
    - mercury removal and drying section, 209f
    - omega, 230–231
    - preparation chemistry, 201
    - properties of natural, 202t
    - protonic, 198
    - Pt-KL zeolite, 211
    - silver zeolites, 208–210
    - structural chemistry, 198–199
    - and surface-related applications, 201–204
    - ZSM5 (H-MFI), 220–224
    - ZSM-12 (H-MTW), 224
  - Zeolite-like titanosilicates, 237–239
  - Zeolitic imidazole framework (ZIF), 239
  - Ziegler process, 138–140
  - Ziegler–Natta catalysts (ZN catalysts), 421–423
  - Zinc containing materials
    - copper-zinc oxide catalysts, 321–326
    - palladium-zinc oxide catalysts, 327–331
    - zinc aluminate, 182
    - zinc chromite, 146–147, 321–322
    - zinc oxide, 306, 353
    - ZnO/γ-Al<sub>2</sub>O<sub>3</sub>/H-ZSM-5 catalyst, 353
  - Zircon (ZrSiO<sub>4</sub>), 166
  - Zirconia, 166, 305
    - as catalyst, 168–169
    - ceria-zirconia, 179–180
    - crystal structure, 166f
    - preparation, 167–168
    - PSZ and TZP, 168
    - sulphated zirconia as catalyst, 169–171
    - as support for catalysts, 171
    - YSZ, 168
  - Zirconium phosphates, 271
  - ZSM-12 zeolite, 224
  - ZSM5 zeolite, 220–224